S
50 376
1999
401-2

THESE DE DOCTORAT DE L'UNIVERSITE DES SCIENCES ET TECHNOLOGIES DE LILLE

Spécialité : Océanologie Biologique

STATION MARINE DE WIMEREUX

CNRS UPRES-A 8013 ELICO

Présentée par

Laurent SEURONT

en vue d'obtenir le titre de

Docteur de l'Université de Lille 1

Hétérogénéité spatio-temporelle et couplage physique-biologie en écologie pélagique : implications sur les flux de carbone

Exemple d'un écosystème côtier à fort hydrodynamisme : la Manche Orientale

Volume 2 : Recueil des travaux

soutenue le 27 Octobre 1999 devant le jury composé de :

Prof.	**J. C. Dauvin**	**Université de Lille I**	**Président du jury**
Prof.	**P. Auger**	**Université de Lyon I**	**Rapporteur**
Prof.	**J.M. Redondo**	**Univ. Polytèch. Catalunya**	**Rapporteur**
Dr.	**F. Ibanez**	**Université de Paris VI**	**Examinateur**
Prof.	**Y. Lagadeuc**	**Université de Caen**	**Directeur de thèse**
Dr.	**D. Schertzer**	**Université de Paris VI**	**Codirecteur de thèse**
Prof.	**S. Frontier**	**Université de Lille I**	**Examinateur**

SCD LILLE 1
D 030 288894 1

tte 20 000 57

50376
1999
401-2

UNIVERSITÉ DES SC ET TECHN.
BIBLIOTHÈQUE UNIVERSITAIRE
LILLE

Ce sont les résultats qui importent, l'effort est salutaire et indispensable mais, sans résultats, il ne signifie rien

PAULO COELHO :
Le pélerin de Compostelle

74 1

A1 **Seuront L**, Schmitt F, Lagadeuc Y, Schertzer D, Lovejoy S & Frontier S (1996) Multifractal structure of phytoplankton biomass and temperature in the ocean. *Geophys. Res. Lett.*, **23**, 3591-3594.

A2 **Seuront L**, Schmitt F, Schertzer D, Lagadeuc Y & Lovejoy S (1996) Multifractal intermittency of Eulerian and Lagrangian turbulence of ocean temperature and plankton fields. *Nonlin. Processes Geophys.*, **3**, 95-104.

A3 **Seuront L** & Lagadeuc Y (1997) Characterization of space-time variability in stratified and mixed coastal waters (Baie des Chaleurs, Québec, Canada): application of fractal theory. *Mar. Ecol. Prog. Ser.*, **259**, 81-95.

A4 **Seuront L** (1997) Distribution inhomogène multi-échelle de la biomasse phytoplanctonique en milieu turbulent. *J. Rech. Océanogr.*, **22**, 9-16.

A5 **Seuront L** & Lagadeuc Y (1998) Spatio-temporal structure of tidally mixed coastal waters: variability and heterogeneity. *J. Plankton Res.*, **20**, 1387-1401.

A6 Lizon F, **Seuront L** & Lagadeuc Y (1998) Photoadaptation and primary production study in tidally mixed coastal waters using a Lagrangian model. *Mar. Ecol. Prog. Ser.*, **169**, 43-64.

A7 **Seuront L**, Schmitt F, Lagadeuc Y, Schertzer D & Lovejoy S (1999) Universal multifractal analysis as a tool to characterize multiscale intermittent patterns: example of phytoplankton distribution in turbulent coastal waters. *J. Plankton Res.*, **21**, 877-922.

A8 **Seuront L** (1999) Fractals et multifractals : nouveaux outils de caractérisation de l'hétérogénéité spatio-temporelle en écologie marine. *Oceanis* (sous presse).

A9 Ramat E, Preux P, **Seuront L** & Lagadeuc Y (1999) Modélisation multi-agents de systèmes naturels. Réflexions générales et application en biologie marine. *Proceedings JFIADSMA '98* (sous presse).

A10 **Seuront L**, Gentilhomme V & Lagadeuc Y (révisé) Do small-scale nutrient patches exist in tidally mixed coastal waters? *Limnol. Oceanogr.*

A11 Lagadeuc Y, **Seuront L** & Lizon F (en révision) Turbulence intermittency and diffusion around small organisms: a useful approach? *Mar. Ecol. Prog. Ser.*

A12 **Seuront L** & Lagadeuc Y (soumis) Variability, inhomogeneity and heterogeneity: dealing with scales in marine ecology. *J. Plankton Res.*

A13 Lagadeuc Y & **Seuront L** (soumis) Turbulence and small-scale phytoplankton patchiness: a new hypothesis on plankton feeding. *J. Plankton Res.*

A14 Lagadeuc Y, **Seuront L**, Ramat E, Preux P, Pitiot P, Denis V, Falk L & Vivier H (soumis) Microscale turbulence intermittency and zooplankton dynamics: how to include behavioural components? *Oceanol. Acta.*

A15 **Seuront L** (soumis) Small-scale processes in the coastal ocean: low order deterministic chaos or high order stochasticity? *J. Plankton Res.*

A16 **Seuront L**, Schmitt F & Lagadeuc Y (manuscrit) Eulerian and Lagrangian spatio-temporal patterns in a tidally mixed coastal ecosystem: a multiscale approach

A17 **Seuront L**, Schmitt F & Lagadeuc Y (soumis) Turbulence intermittency, small-scale phytoplankton patchiness and encounter rates in plankton: where do we go from here? *Deep-Sea Res. I.*

A18 Ramat E, Preux P, **Seuront L** & Lagadeuc Y (soumis) Multi-agent modeling of the physical/biological coupling—A case study in marine ecology. *ECAL.*

A19 **Seuront L**, Lizon F & Lagadeuc Y (manuscrit) Space-time heterogeneity of phytoplankton biomass in tidally mixed coastal waters: implication on primary production estimates.

A20 **Seuront L** & Lagadeuc Y (manuscrit) Multiscale horizontal distribution of the calanoid copepod *Temora longicornis* in a turbulent coastal sea.

A1

Multifractal structure of phytoplankton biomass and temperature in the ocean

Seuront L, Schmitt F, Lagadeuc Y, Schertzer D, Lovejoy S & Frontier S (1996)

Geophysical Research Letters, **23**, 3591-3594, 1996

GEOPHYSICAL RESEARCH LETTERS, VOL. 23, NO. 24, PAGES 3591-3594, DECEMBER 1, 1996

Multifractal analysis of phytoplankton biomass and temperature in the ocean

Laurent Seuront,[1] François Schmitt,[2] Yvan Lagadeuc,[1] Daniel Schertzer,[2] Shaun Lovejoy,[3] and Serge Frontier[1]

Abstract. Many attempts have been made to relate phytoplankton biomass ditributions to their turbulent environments. These studies have not taken the intermittent nature of turbulent processes into account, and hence poorly approximate inhomogeneous patterns. Since these oceanic fields are scaling for a wide range of scales, and scaling processes are believed to generically yield universal multifractal (characterized by three basic exponents), it is natural to analyse temperature and phytoplankton biomass in such a framework. Over the range 0.5s to 11h30', the temperature followed a single scaling regime, whereas the phytoplankton had both a low and high frequency regime (the break occurring at about 100s). We estimated the universal multifractal parameters finding that fluorescence was nearly dynamically passive (i.e. similar to temperature) on smaller scales but biologically active at larger scales.

Introduction

Marine systems exhibit intimate relationships between physical and biological processes (Legendre and Demers, 1984; Mackas *et al.*, 1985), as shown by the coupling between the distribution of phytoplankton populations and the structure of their physical environment over a wide range of spatial and temporal scales (Haury *et al.*, 1978). On small scales in fully turbulent flows, the fluctuations of phytoplankton biomass, estimated by Fourier power spectral analysis (Platt, 1972; Platt and Denman, 1975), are considered similar to those of a passive scalar. However, power spectral analysis is only adequate to characterize turbulent processes for homogeneous models. Contrary to classical theoretical concepts regarding turbulent events as homogeneous processes (Obukhov, 1949; Corrsin, 1951), it has been shown that the rate of energy transfer and the variance fluxes of passive scalars from large to small scales exhibit — at all scales — sharp fluctuations called intermittency which generate inhomogeneity (Batchelor and Townsend, 1949; Kolmogorov, 1962; Obukhov, 1962).

Indeed, the well-known "-5/3" power spectrum (i.e. a second order moment) associated with the behavior of a passive scalar only characterizes variability in a very limited way (except in the case of "quasi-Gaussian" statistics). Indeed the determination of the probability distribution require the determination of moments of all orders. With the assumption of scaling, this determination reduces to the estimation of an *a priori* infinite hierarchy of exponents which remain numerically indeterminable, especially for the highest orders corresponding to the most extreme variability. Multifractal fields then require an infinite hierarchy of exponents, rather than the single exponent of fractal patterns (Mandelbrot, 1983). However, in the framework of universal multifractals (Schertzer and Lovejoy, 1987, 1989), this hierarchy is characterized by only a few relevant exponents. In this letter we shall show how the intermittent distribution of temperature and phytoplankton biomass can be characterized with universal multifractals. We study a time series of temperature (a passive tracer of the fluid flow) and *in vivo* fluorescence (regarded as a phytoplankton biomass proxy) simultaneously recorded at an anchor station in a tidally mixed coastal water, the Southern Bight of the North Sea, using a CTD recorder (Sea-Bird 19) and a fluorometer (Sea Tech), respectively. The sampling frequency being 2 Hz, our analysis is based on a time series of 82,976 measurements.

Scaling and Multiscaling of Temperature and Phytoplankton fields

The estimation of the fluorescence power spectrum ($E(f)$, f is frequency) in a log-log plot shows two scaling regimes (Fig. 1). Over smaller scales (1s to 100s), the observed power law trend ($E(f) \propto f^{-\beta}$ with $\beta \approx 1.75$) shows that the temporal distribution (or spatial, *via* the classical Taylor's hypothesis) of phytoplankton and temperature are close to the expected Obukhov-Corrsin "-5/3 power law" for passive scalars. In

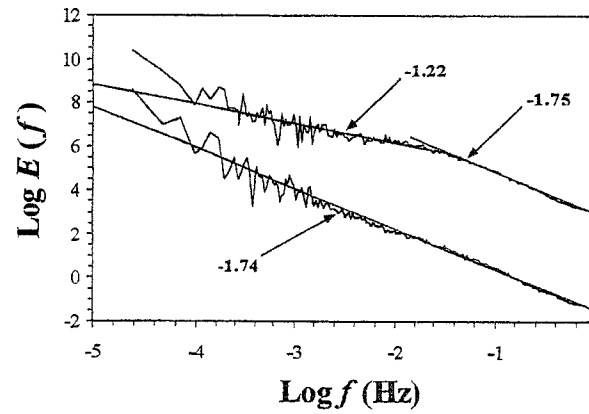

Figure 1. The power spectra $E(f)$ (f is frequency) of the fluorescence and the temperature data, shown in a log-log plot. The fluorescence data are scaling from 0.01 Hz to 1 Hz with a spectral slope $\beta \approx 1.75$ and for frequency smaller than 0.01 Hz with a spectral slope $\beta \approx 1.22$. The temperature data are scaling with $\beta \approx 1.74$.

[1]Station Marine, Université des Sciences et Technologies de Lille, France
[2]Laboratoire de Météorologie Dynamique du CNRS, Université P. et M. Curie, Paris, France
[3]Physics Department, McGill University, Montréal, Canada

Copyright 1996 by the American Geophysical Union.

Paper number 96GL03473.
0094-8534/96/96GL-03473$05.00

both cases, the spectra are slightly steeper than -5/3: this is expected in case of multifractal intermittency corrections (Frisch *et al.*, 1978; see below). On the other hand, over larger scales (> 100s), the scaling of the spectrum ($\beta \approx 1.22$) roughly agrees with theoretical and experimental studies predicting that the fluorescence spectrum will be flatter than the spectrum of a passive scalar, and supporting a predominant influence of biological factors on phytoplankton variability (Powell *et al.*, 1975; Denman and Platt, 1976; Denman *et al.*, 1977). Power spectral analysis corresponds to the second order structure function. It is generalized with the help of the q^{th} order structure functions $<(\Delta S_\tau)^q> = <|S(t+\tau) - S(t)|^q>$ (Kolmogorov, 1962; Obukhov, 1962) where for a duration τ the fluctuations of the scalar S are averaged over all available values ("$\langle\rangle$" indicates statistical or spatial averaging). For scaling processes, we consider the scale invariant structure functions exponents $\zeta(q)$ defined by $<(\Delta S_\tau)^q> = <(\Delta S_T)^q> (\tau/T)^{\zeta(q)}$, where T is the largest period (external scale) of the scaling regime (Monin and Yaglom, 1975). For simple (monofractal) processes such as Brownian motion, the scaling exponent of the structure function $\zeta(q) = qH$ is linear: $\zeta(q) = qH$ where $H = \zeta(1)$ is a parameter describing the scale dependence of the average fluctuations ($H = 1/3$ for a scalar passively advected by non-intermittent turbulence). For multifractal processes, $\zeta(q)$ is nonlinear and concave.

We performed this analysis for various moments of order from 0 to 5 (with an increment of 0.1) and showed the corresponding scaling in Fig. 2. These empirical curves also confirms the results of power spectral analysis and shows that there is a unique scaling regime for all scales for temperature, and two scaling regimes for fluorescence. We then plotted in Fig. 3 the functions $\zeta(q)$ — the slopes of the straight lines of Fig.2. The clear nonlinearity of this function is a first indication that variability in phytoplankton biomass and oceanic temperature can be characterized as multifractals. Moreover, the two curves corresponding to temperature and fluorescence on scales smaller than 100 seconds are very close to each other; within experimental error, they cannot be distinguished (we quantify this below with universal multifractal parameters). Thus, for all moments (and hence, all

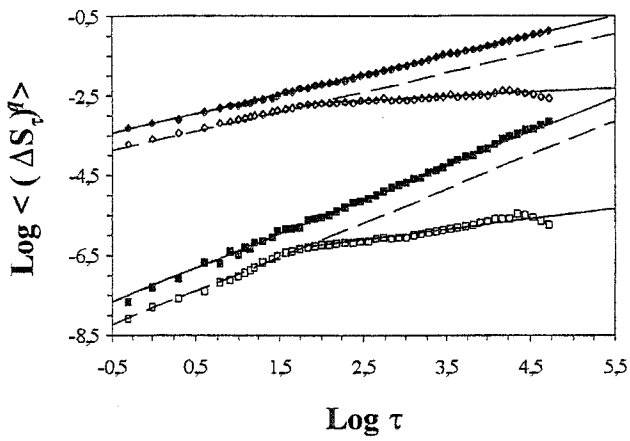

Figure 2. The structure functions $<(\Delta S_\tau)^q>$ vs. τ in a log-log plot for q = 1 and 3 (from top to bottom) for temperature (black symbols) and for fluorescence (open symbols). Linear trends are clearly visible for temperature for all orders of moments, whereas fluorescence exhibits two scaling tendencies.

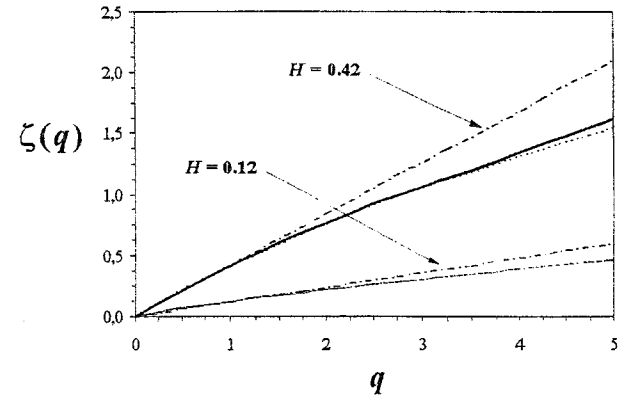

Figure 3. The empirical curves of scaling exponent structure functions $\zeta(q)$ for temperature (thick continuous line), small-scale (dashed line) and large-scale fluorescence (thin continuous line) compared to the theoretical monofractal linear curve $\zeta(q) = qH$ with $H = 0.42$ and $H = 0.12$ (discontinuous lines). The nonlinearity of the empirical curves indicates multifractality.

intensities), phytoplankton and temperature intermittencies have nearly the same probabilities. This confirms that small scale fluorescence is a passive scalar, as claimed by previous studies using only power spectra. On the other hand, the specific nonlinearity of the scaling exponent $\zeta(q)$ for *in vivo* fluorescence at scales greater than 100 seconds shows that phytoplankton variability can be regarded as a multifractal even for scales dominated by biological activities.

Universal Multifractal Parametrization

Universal multifractals are specific types of multifractals. They are likely to be ubiquitous, because they are stable and attractive limit classes obtained with continuous multiplicative scaling processes (Schertzer and Lovejoy, 1987, 1989). In this framework, $\zeta(q)$ depends only on three parameters in the following way: $\zeta(q) = Hq - K(q)$ where $K(q) = C_1(q^\alpha - q)/(\alpha - 1)$ ($\alpha \neq 1$) and the function $H = \zeta(1)$ defines the scaling of the mean field ($H = 0$ for a conservative field, i.e. its mean $<\phi_\tau>$ is strictly scale invariant) and $K(q)$ expresses intermittency. The first index C_1 ($0 \leq C_1$) measures the mean homogeneity of the field: the larger C_1, the more the mean field is inhomogeneous or fractal (C_1 is the fractal codimension of the mean of the process), C_1 is then the measure of the sparseness of the field. The index α ($0 \leq \alpha \leq 2$) expresses the deviation from the mean of the field values; as α decreases, the high values of the field do not dominate as much as for larger values of α. More precisely, α measures the "degree" of multifractality, i.e. how fast increases the inhomogeneity with the order of the moments. Indeed, $\alpha = 0$ corresponds to the monofractal β-model (Novikov and Stewart 1964; Mandelbrot 1974; Frisch *et al.*, 1978) and reaches its maximum ($\alpha = 2$) for the (misnamed) log-normal model (Kolmogorov, 1962; Obukhov, 1962). α, which characterizes the generator of the process, is called the Lévy index (see *e.g.* Feller (1971) for stable variables). First, taking $H = \zeta(1)$ gives $H_T = 0.42 \pm 0.02$ for temperature and $H_{FSS} = 0.41 \pm 0.02$ for small-scale fluorescence. These values are very close to each other, significantly larger than the 1/3 value for homogeneous Obukohv-Corrsin passive scalar turbulence, and

slightly larger than the value reported in Schmitt *et al.* (1996) for atmospheric temperature ($H = 0.38 \pm 0.02$). For large-scale fluorescence, we obtain $H_{FLS} = 0.12 \pm 0.01$. This is a small value but nevertheless shows that the mean of the fluctuations are scaling ($H = 0$ for scale-independent average fluctuations). We then estimate the values of α and C_1 by considering the field ϕ_τ obtained from the scalar field by performing a fractional differenciation of order H ($\phi_\tau = \Delta S_\tau / \tau^H$; see Schertzer and Lovejoy, 1987). The values of α and C_1 can be directly obtained from this field, by applying the Double Trace Moment analysis technique (Lavallée *et al.*, 1992): this consists of raising the field at the smallest scale to the η^{th} power, and then considering the q^{th} order of moments of the result at all scales. This gives a new scaling exponent function dependent on these two parameters: $K(q,\eta) = K(q\eta) - qK(\eta)$, $(K(q) \equiv K(q,1))$ and leads to $K(q,\eta) = \eta^{\alpha} K(q)$. Thus, $K(q,\eta)$ vs. η appear as a linear log-log plot with a slope of α. This is shown in Fig. 4, for q = 2, 2.5 and 3. Estimates of α are given by the slopes of the straight lines and C_1 is given by the value of $\log K(q)$, which is the intercept of the straight line. Using this method we find $\alpha_T = 1.7 \pm 0.05$ and $C_{1(T)} = 0.04 \pm 0.01$ for temperature data and $\alpha_{FSS} = 1.8 \pm 0.05$ and $C_{1(FSS)} = 0.04 \pm 0.01$ for fluorescence data at small scales. These values are very close to each other and confirm that the statistics of fluorescence at small scales are similar to those of a passive scalar. The values of α we obtain here for oceanic temperature are larger than previous reports of α for atmospheric turbulence (Schmitt *et al.*, 1993, 1996; Tessier *et al.*, 1993) within the range 1.3-1.5. It is nevertheless smaller than $\alpha = 2$ corresponding to log-normal statistics (Baker and Gibson, 1987; Gibson, 1991).

At small scales, the similarity of the universal multifractal parameters of temperature and fluorescence reflects profound couplings between the space-time structure of phytoplankton populations and the structure of their physical environment. In this multifractal framework, phytoplankton biomass then appears to be passive and inhomogeneously (i.e. non-randomly) distributed, contrary to the basic perception of small scale interactions in plankton ecology which is based on a passive but homogeneous distribution of phytoplankton. This inhomogeneity then may have important effects on concentration-dependent processes such as phytoplankton coagulation (e.g. Jackson and Lochmann, 1993). These findings also provide a complementary approach to previous theoretical studies of the effects of turbulence (regarded as a random process generating homogeneity) on contact rates between predators and preys (Rothschild and Osborn, 1988).

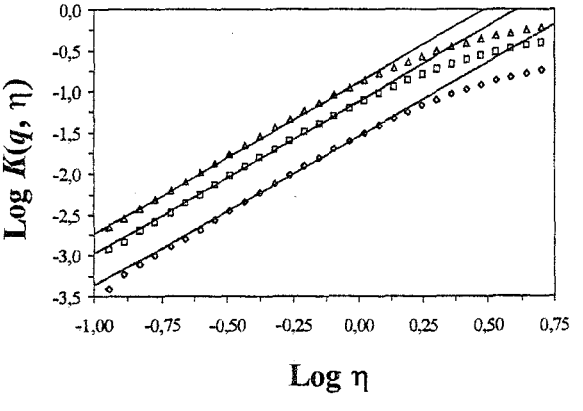

Figure 4. The curves $K(q,\eta)$ vs. η in a log-log plot for q = 2, 2.5 and 3 (from bottom to top) for temperature field. The slope and intercept of the lines give respectively estimates of α and C_1.

For large-scale fluorescence, we first averaged the data up to the scale of 100 s, to place it in what we identified as the second regime, and then applied the Double Trace Moment analysis technique. We obtained $\alpha_{FLS} = 0.8 \pm 0.02$ and $C_{1(FLS)} = 0.02 \pm 0.01$. These values show that the statistics of small-scale fluorescence differ significantly from those of large-scale: not only does the average of the fluctuations vary differently with scale (the value of H), but also with the parameters characterizing the type of intermittency. They indicate "lower" multifractality ($\alpha_{FLS} < \alpha_T$) and larger mean homogeneity ($C_{1(FLS)} < C_{1(T)}$) than temperature at the same scales. At these scales, the combination of biological processes — such as growth, sinking, or community interactions — provides an aggregative effect which dominates the dispersive effect of turbulence (Denman and Platt, 1975; Lekan and Wilson, 1978).

Conclusions

We have shown that the intermittency of phytoplankton and temperature fields in the Southern Bight of the North Sea are multifractal over the whole range of measurements scales. Furthermore, our analysis of the physical as well as the biological processes gives credence to the prediction that these stochastic processes are universal multifractals; we estimated the three fundamental parameters, which in this framework characterize all the statistics of the fields. Our analysis of temperature and phytoplankton biomass differs from the previous multifractal analysis of zooplankton data by Pascual *et al.* (1995) in several ways. First, the use of universal multifractals makes the analysis much more robust; only three basic parameters are needed to characterize the whole variability of the fields. Next, we directly analysed the data using structure functions as is usually done in turbulence studies (e.g. Monin and Yaglom, 1975), and estimated the slopes of their Fourier power spectra which are very suitable to make comparisons with other fields. Both approaches provide nevertheless a stochastic basis for multifractal simulations: this allows efficient simulation of intermittent fields on a wide range of space-time scales, contrary to the usual deterministic models which are restricted to specific scales. Furthermore, the universal multifractal framework is useful for simulations (Wilson *et al.*, 1989; Pecknold *et al.*, 1993), because it provides very precise control of the variability by the way of continuous multiplicative processes (with the help of the basic parameters). This approach then allows to include the multiscale detailed variability of natural processes and therefore opens a new perspective for modeling oceanic ecosystems.

These results show not only that biological as well as physical processes can be characterized by three universal exponents, but also that these exponents help to discriminate between a regime where physics is dominant (smaller scales, higher variability) and a regime where on the contrary biology is dominant, damping out variability of turbulent physical processes (larger scales, lower variability). The cross-over between passive and biologically active regimes for fluorescence (i.e. phytoplankton biomass) seems to intervene at a period of about 100 seconds. We have no clear

interpretation of this characteristic time scale to propose; it is indeed significantly smaller than the generation time of the phytoplankton populations (≈1 day).

Acknowledgments. We thank C. Luczak for supplying the temperature and fluorescence data set. We also thank M. Claerboudt, V. Gentilhomme, C. Marguerit, R. Nowak and Y. Tessier for stimulating discussions, and two anonymous referees for helpful suggestions.

References

Baker, M. A. and C. H. Gibson, Sampling turbulence in the stratified ocean: statistical consequences of strong intermittency, *J. Phys. Oceanogr., 17,* 1817-1836, 1987.

Batchelor, G. K. and A. A. Townsend, The nature of turbulent motion at large wavenumbers, *Proc. Roy. Soc., A 199,* 238, 1949.

Corrsin, S., On the spectrum of isotropic temperature in an isotropic turbulence, *J. Appl. Phys., 22,* 469-473, 1951.

Denman, K. L. and T. Platt, Coherences in the horizontal distributions of phytoplankton and temperature in the upper ocean. *Mem. Soc. Roy. Sci. Liege , 7,* 19-36, 1975.

Denman, K. L. and T. Platt, The variance spectrum of phytoplankton in a turbulent ocean, *J. Mar. Res., 34,* 593-601, 1976.

Denman, K. L., A. Okubo and T. Platt, The chlorophyll fluctuation spectrum in the sea, *Limnol. Oceano., 22,* 1033-1038, 1977.

Feller, W., *An Introduction to Probability Theory and its Applications*, vol. II, second ed., John Wiley&Sons, New York, 1971.

Frisch, U., Sulem, P.-L., and M. Nelkin, A simple dynamical model of intermittent fully developed turbulence, *J. Fluid. Mech., 87,* 719, 1978.

Gibson, C. H., Kolmogorov similarity hypotheses for scalar fields: sampling intermittent turbulent mixing in the ocean and galaxy, *Phil. R. Soc. Lond. A, 434,* 149-164, 1991.

Haury, L. R., J. A. McGowan and P. H. Wiebe, Patterns and processes in the time-space scales of plankton distributions, in *Spatial Pattern in Plankton Communities*, edited by J. H. Steele, pp. 277-327, Plenum, New York, 1978.

Jackson, G. A. and S. E. Lochmann, Modelling coagulation of algae in marine ecosystems, in Environmental particles, edited by J. Buffle, pp. 373-399, Lewis Publishers, 1993.

Kolmogorov, A. N., A refinement of previous hypothesis concerning the local structure of turbulence in viscous incompressible fluid at high Reynolds number, *J. Fluid Mech., 13,* 82, 1962.

Lavallée, D., S. Lovejoy, D. Schertzer and F. Schmitt, On the determination of universal multifractal parameters in turbulence, in *Topological aspects of the dynamics of fluids and plasmas*, edited by K. Moffat, Tabor, M. and G. Zaslavsky, pp. 463-478, Kluwer, Boston, 1992.

Legendre, L. and S. Demers, Towards dynamic biological oceanography and limnology, *Can. J. Fish. Aquat. Sci., 41,* 2-19, 1984.

Lekan, J. F. and R. E. Wilson, Spatial variability of phytoplankton biomass in the surface waters of Long Island. *Est. Coast. Mar. Sci., 6,* 239-251, 1978.

Mackas, D. L., K. L. Denman and M. R. Abbot, Plankton patchiness: biology in the physical vernacular, *Bull. Mar. Sci., 37,* 652-674, 1985.

Mandelbrot, B., Multiplications aléatoires itérées et distributions invariantes par moyenne pondérée aléatoire, *C. R. Acad. Sc. Paris, 278,* Série A, 289.

Mandelbrot, B., *The fractal geometry of nature*, Freeman, New York, 1983.

Monin, A. S. and A. M. Yaglom, *Statistical fluid mechanics: mechanics of turbulence*, vol. 2, 871 pp., MIT Press, Cambridge, 1975.

Novikov, E. A. and Stewart, R., Intermittency of turbulence and spectrum of fluctuations in energy dissipation, *Izv. Akad. Nauk. SSSR Geogr. I Geopfiz., 3,* 408-412, 1964.

Obukhov, A. M., Structure of the temperature field in a turbulent flow, *Izv. Akad. Nauk. S.S.S.R. Geogra. I Geopfiz., 13,* 55-69, 1949.

Obukhov, A. M., Some specific features of atmospheric turbulence, *J. Fluid Mech., 13,* 7, 1962.

Pascual, M., F. A. Ascioti and H. Caswell, Intermittency in the plankton: a multifractal analysis of zooplankton biomass variability, *J. Plankton Res., 17,* 1209-1232, 1995.

Pecknold, S., Lovejoy, S., Schertzer, D., Hooge, C. and J.-F. Malouin, The simulation of universal multifractals, in *Cellular Automata, Prospects in astrophysical applications*, eds. J. M. Perdang and A. Lejeune, World Scientific, Singapore, pp.228-267, 1993.

Platt, T., Local phytoplankton abundance and turbulence, *Deep-Sea Res., 19,* 183-187, 1972.

Platt, T. and K. L. Denman, Spectral analysis in ecology, *Annu. Rev. Ecol. Syst., 6,* 189-210, 1975.

Powell, T. M. et al., Spatial scales of current speed and phytoplankton biomass fluctuations in Lake Tahoe, *Science, 189,* 1088-1090, 1975.

Rothschild, B. J. and T. R. Osborn, Small-scale turbulence and plankton contact rates, *J. Plankton Res., 10,* 465-474, 1988.

Schertzer, D. and S. Lovejoy, Physically based rain and cloud modeling by anisotropic multiplicative turbulent cascades, *J. Geophys. Res., 92,* 9693-9714, 1987.

Schertzer, D. and S. Lovejoy, Nonlinear variability in geophysics: multifractal analysis and simulation, in *Fractals: Physical Origin and Consequences*, edited by L. Pietronero, pp.49-79, Plenum, New York, 1989.

Schmitt, F., Schertzer, D., Lovejoy, S., and Y. Brunet, Estimation of universal multifractal indices for atmospheric turbulent velocity fields, *Fractals, 1,* 568-575, 1993.

Schmitt, F., Schertzer, D., Lovejoy, S. and Y. Brunet, Multifractal temperature and flux of temperature variance in fully developed turbulence, *Europhys. Lett., 34,* 195-200, 1996.

Tessier, Y., Lovejoy, S., and D. Schertzer, Universal multifractals in rain and clouds: theory and observations, *J. Appl. Meteor., 32,* 223-250, 1993.

Wilson, J., Lovejoy, S.and D. Schertzer, Physically based cloud modelling by multiplicative cascade processes, in *Nonlinear Processes in Geophysics: scaling and fractals*, edited by D. Schertzer and S. Lovejoy, Kluwer Academic Press, Dordrecht-Boston, pp.185-208, 1991.

L. Seuront, Y Lagadeuc, S. Frontier, Station Marine, Université des Sciences et Technologies de Lille, BP 80, 62930 France. (e-mail: seuront@loalit.univ-littoral.fr; yvan@loalit.univ-littoral.fr)

F. Schmitt, D. Schertzer, Laboratoire de Météorologie Dynamique du CNRS, Université P. et M. Curie, 4 place Jussieu, 75252 Paris cedex 05, France. (e-mail: schmitt@lmd.jussieu.fr; schertze@lmd.jussieu.fr)

S. Lovejoy, Physics Department, McGill University, 3600 University Street, Montréal, Québec, H3A 2T8, Canada. (e-mail: lovejoy@physics.mcgill.ca)

(Received: June 3, 1996; revised: October 7; accepted: October 29, 1996.)

A2

Multifractal intermittency of Eulerian and Lagrangian turbulence of ocean temperature and plankton fields

Seuront L, Schmitt F, Schertzer D, Lagadeuc Y & Lovejoy S

Nonlinear Processes in Geophysics, **3**, 95-104, 1996

Nonlinear Processes in Geophysics (1996) 3: 236–246

Nonlinear Processes in Geophysics
© European Geophysical Society 1996

Multifractal intermittency of Eulerian and Lagrangian turbulence of ocean temperature and plankton fields

L. Seuront[1], F. Schmitt[2*], D. Shertzer[2], Y. Lagadeuc[1] and S. Lovejoy[3]

[1]Station Marine de Wimereux, CNRS-URA 1363, Université des Sciences et Technologies de Lille, 28 avenue Foch, BP 80, 62930 Wimereux, France
[2]Laboratoire de Météorologie Dynamique, CNRS-UPR 1211, Université Pierre et Marie Curie, Tour 15, BP 99, 4 \place Jussieu, 75252 Paris Cedex 05, France
[3]Physics Dept., McGill University, 3600 University St., Montréal, H3A 2T8, Canada
*now at the Institut Royal Météorologique, Section Climatologie Dynamique, 3 avenue Circulaire, 1180 Bruxelles, Belgium

Received 2 May 1996 - Accepted 11 November 1996

Abstract. In this paper, we present evidence that intermittency of Eulerian and Lagrangian turbulence of ocean temperature and plankton fields is multifractal and furthermore can be analysed with the help of universal multifractals. We analyse time series of temperature and *in vivo* fluorescence taken from a drifter in the mixed coastal waters of the eastern English Channel. Two analysis techniques are used to compute the fundamental universal multifractal parameters, which describe all the statistics of the turbulent fluctuations: the analysis of the scale invariant structure function exponent $\zeta(q)$ and the Double Trace Moment technique. At small scales, we do not detect any significant difference between the universal multifractal behavior of temperature and fluorescence in an Eulerian framework. This supports the hypothesis that the latter is passively advected with the flow as the former. On the one hand, we show that large scale measurements are Lagrangian and indeed we obtain for temperature fluctuations a ω^{-2} power spectrum corresponding to the theoretical scaling of a Lagrangian passive scalar. Furthermore, we show that Lagrangian temperature fluctuations are multiscaling and intermittent. On the other hand, the flatter slope at large scales of the fluorescence power spectrum points out that the plankton is at these scales a "biologically active" scalar.

1. Introduction

Scaling laws have been proposed in Eulerian (Kolmogorov, 1941a; Obukhov, 1941, 1949; Corrsin, 1951) and Lagrangian frameworks (Landau and Lifshitz, 1944; Inoue, 1950, 1951, 1952a, b; Lin, 1960; Monin and Yaglom, 1975) for velocity and passive scalar turbulence. In an Eulerian framework this general scaling picture has been confirmed with oceanic velocity (see e.g. Grant et al., 1962) and temperature data (Grant et al., 1968; Gargett et al., 1984) over a wide range of scales. However, we are not aware of any reports of scaling spectra of oceanic turbulent measurements of either velocity or passive scalars taken in Lagrangian frameworks. In this paper, we perform both Eulerian and Lagrangian analyses of the intermittency of temperature fluctuations and fluorescence data (which is a proxy of phytoplankton biomass; see below). This comparison between Eulerian and Lagrangian frameworks appears to be of main interest to understand the effect of a sampling procedure on the characterization of a given process, but also to provide information about living organisms' perception of their fluid medium.

In vivo fluorescence measurements are used to test the hypothesis that living particles in turbulent fluid motions behave as passive scalars (Platt, 1972; Denman and Platt, 1976) whose Fourier spectral statistics are — to within intermittency corrections — known theoretically. This comparison allows us to study the nature of the couplings between the structure of phytoplankton populations and the structure of their physical environment (Legendre and Demers, 1984; Mackas et al., 1985). The statistics of fluorescence data have been previously analysed using power spectral analysis (Platt and Denman, 1975). However, the power spectrum is a second order moment, and is only sufficient for characterizing the variability if the latter is quasi-gaussian. On the contrary we find that the variability is far from gaussian — in accord with cascade theories — and give it a precise scale-by-scale and intensity-by-intensity characterization using multifractals. In contrast to the single exponent which is sufficient to characterize the scaling properties of fractal sets, the multifractal formalism generally describes scaling relations with an infinite family of scaling exponents (e.g. the fractal dimensions associated with different levels of fluid activity). However, due to the existence of stable, attractive, multifractal generators, only certain aspects of the multifractal dynamics will be important; we expect to

Correspondence to: Y. Lagadeuc

obtain universal multifractals (Schertzer and Lovejoy, 1987, 1989), in which this hierarchy is characterized by only three fundamental exponents.

Our multifractal characterization of biomass improves on the multifractal analysis of Pascual et al. (1995) in several ways. First, the use of universal multifractals makes the data analysis much more robust; only three fundamental parameters need to be estimated and we can use an analysis technique specially designed for their study (the Double Trace Moment technique, see Lavallée (1991) and Lavallée et al. (1992)). Second, using the notions of sampling dimensions and multifractal phase transitions, we can quantify the range of statistical moments which can be accurately estimated given the limited sample size. Other improvements with respect to Pascual et al. (1995) concern the pre-processing of the data which is performed in their paper, taking the square of the difference of fluorescence data. While this processing can be somewhat justified for velocity turbulence — at least if it can be measured at dissipation scales for plankton biomass —, it becomes here quite *ad hoc*. Is is certainly better first to directly analyse the data using structure functions, as we do here, and as is usually done in turbulence studies (see e.g. Monin and Yaglom, 1975). Finally, we also estimate the slopes of the power spectra of our data, which is essential in making comparisons with other fields and experiments.

In this paper, we present evidence that temperature and fluorescence variability can be characterized as universal multifractals. Since our data were taken from a drifting platform, they have the interesting properties that they exhibit both Eulerian and Lagrangian regimes. In section 2 we present the theoretical scaling relations for velocity and passive scalar turbulent fluctuations in Eulerian and Lagrangian framework, and in section 3 the data analysis.

2. Scaling relations for turbulent fields in Eulerian and Lagrangian frames

2.1 Eulerian relations for turbulent velocity and passive scalar fields

Scaling relations in Eulerian turbulence (Kolmogorov, 1941a; Obukhov, 1941, 1949; Corrsin, 1951) can be expressed using the energy flux ε and the scalar variance flux χ :

$$\varepsilon_l \approx \frac{(\Delta V_l)^3}{l} \tag{1}$$

$$\chi_l \approx \frac{(\Delta\theta_l)^2 \Delta V_l}{l} \tag{2}$$

where $\Delta V_l = |V(x+l)-V(x)|$ and $\Delta\theta_l = |\theta(x+l)-\theta(x)|$ are the velocity and temperature shears at scale l, $\Delta V_l / l$ is the inverse of the local eddy turnover time, and "$\approx$" means equality of scaling laws, i.e. having the same scaling exponents (see below). Originally, these scaling relations where considered in the framework of homogeneous turbulence, i.e. the fluxes were considered as homogeneous, exhibiting no scale dependence. As a consequence, a unique exponent was required for the velocity and temperature, the famous 1/3 law in physical space, 5/3 for the energy or variance power spectra :

$$\Delta V_l \approx l^{1/3} \; ; \; E_v(k) \approx k^{-5/3} \tag{3}$$

$$\Delta\theta_l \approx l^{1/3} \; ; \; E_\theta(k) \approx k^{-5/3} \tag{4}$$

However, it is well known that this homogeneity assumption was theoretically and empirically untenable: fluxes are extremely inhomogeneous and scale dependent (therefore the subscript l in Eq. 1). But because the fluxes are conserved by the nonlinear terms of the equations of motion they are (on average) conserved during the cascade, i.e. their (ensemble) average should be strictly scale invariant :

$$\langle \varepsilon_l \rangle \approx \langle \varepsilon_1 \rangle \; ; \; \langle \chi_l \rangle \approx \langle \chi_1 \rangle \tag{5}$$

where the angle brackets "<.>" indicate statistical (ensemble) averaging. The corresponding (inhomogeneous) scaling relationship for the velocity field (Eq. 1) is often called the Kolmogorov refined similarity law (Kolmogorov 1962; Obukhov 1962) and the corresponding refining for the temperature fluctuations (Eq. 2) has been proposed for simulation and analysis of passive clouds (Schertzer and Lovejoy, 1987; Wilson et al., 1991; Pecknold et al.,1993).

In cascade models of turbulence, the highly inhomogenous fluxes are the results of a multiplicative process in which the variability is built up from large to small scales: larger structures are multiplicatively randomly modulated by smaller scales. In this case, this leads to multifractal fields, with the following multiscaling statistics (Schertzer and Lovejoy, 1987):

$$\left\langle (\varepsilon_l)^q \right\rangle \approx \lambda^{K_\varepsilon(q)} \tag{6}$$

$$\left\langle (\chi_l)^q \right\rangle \approx \lambda^{K_\chi(q)} \tag{7}$$

$$\left\langle \left[\Delta V_l\right]^q \right\rangle \approx \lambda^{-\zeta_V(q)} \tag{8}$$

$$\left\langle \left[(\Delta\theta_l)^2 \Delta V_l\right]^q \right\rangle \approx \lambda^{-\zeta_{V,\theta}(3q)} \tag{9}$$

with the relations, from Eqs. 1-2:

$$K_\varepsilon(q) = q - \zeta_V(3q) \; ; \; K_\chi(q) = q - \zeta_{V,\theta}(3q) \tag{10}$$

where L is a fixed outer scale and $\lambda = L/l$ is the corresponding scale ratio, $K_\varepsilon(q)$ and $K_\chi(q)$ are the scaling moment functions for the fluxes, $\zeta_V(q)$ is the scaling exponent of the (usual) velocity structure function and $\zeta_{V,\theta}(q)$ is the joint structure function scaling exponent of the product $(\Delta\theta_l)^2 \Delta V_l$. The strict scale invariance (Eq. 5) of the averaged fluxes yields $K_\varepsilon(1) = 0$

and $K_\chi(1)=0$. Such multifractal fields are called "conservative multifractals". On the contrary, Eqs. 3-4 point out already that V and θ are not conserved. We may note that the conservation of the fluxes implies $\zeta_V(3)=1$ and $\zeta_{V,\theta}(3)=1$, which corresponds to the exact relations for the small-scale dissipation fields given by Kolmogorov (1941) and Yaglom (1949).

These relations (Eqs. 6-9), giving the scaling moment functions $K(q)$ and $\zeta(q)$, characterize all the fluctuations of the fluxes of energy and scalar variances and the fluctuations of the wind shears. But they do not directly give the scaling moment function $\zeta_\theta(q)$ of the passive scalar fluctuations, defined as:

$$\left\langle (\Delta\theta_l)^q \right\rangle \approx \lambda^{-\zeta_\theta(q)} \tag{11}$$

Indeed, the corresponding flux $\varphi_l = \varepsilon_l^{-1/2}\chi_l^{3/2}$ is a mixed flux of energy and scalar variance, which is non conservative. Obviously the two fluxes ε_l, χ_l are strongly correlated, so that the assumption of independence of the fluxes, used in Benzi et al. (1992), is a very simplistic hypothesis. An alternative is to relate this mixed flux to the structure function of the velocity and the temperature, as is done in Schmitt et al. (1996), which obtained the following expression, assuming statistical independence of the velocity and passive scalar fluctuations:

$$\begin{aligned} \zeta_\theta(q) &= q/3 + K_\varepsilon(q/6) - K_\chi(q/2) \\ \zeta_\theta(q) &= \zeta_{V,\theta}(3q/2) - \zeta_V(q/2) \end{aligned} \tag{12}$$

This expression was tested by Schmitt et al. (1996) on atmospheric turbulence data, with simultaneous records of wind velocity and temperature fluctuations. Unfortunately, since our Eulerian data gives only the passive scalar field without simultaneous velocity fluctuations, Eq. 12 cannot be tested here.

Nevertheless, we can analyze Eulerian scaling moment functions for a passive scalar using for $\zeta_\theta(q)$ the general expression for universal multifractals. Universal multifractals are the stable and attractive classes which are obtained with continuous multiplicative scaling processes (Schertzer and Lovejoy, 1987, 1989). In this framework the scaling moment functions $\zeta(q)$ (or $K(q)$ [1]) have a precise theoretical shape:

$$\zeta(q) = Aq + Bq^\alpha \tag{13}$$

where A and B are constants and $0 \le \alpha \le 2$ is the Lévy index for stable variables (see e.g. Feller, 1971). This parameter is the most important, because, it describes the kind of multifractality of the field: for $\alpha = 0$, an inhomogeneous mono-fractal model is recovered (the β-model, see Frisch et al. (1978)), and for the other bound, $\alpha = 2$ corresponds to a lognormal multifractal (Kolmogorov, 1962; Obukhov, 1962; Yaglom, 1966). The condition of conservation of flux ($K(1)=0$) yields an expression which depends only on two parameters: C_1 is the codimension of the mean of the process, and verifies $0 \le C_1 \le 1$ (the larger is C_1, the more the field is inhomogeneous) and the Lévy index α:

$$K(q) = \frac{C_1}{\alpha - 1}\left(q^\alpha - q\right) \tag{14}$$

For the wind velocity field, the condition $\zeta_V(3)=1$ and Eqs. 1, 13 give:

$$\zeta_V(q) = \frac{q}{3} - \frac{C_1}{\alpha - 1}\left(\left(\frac{q}{3}\right)^\alpha - \frac{q}{3}\right) \tag{15}$$

This equation has been used to characterize the wind velocity field in atmospheric turbulence (Schmitt et al., 1993, 1996; Schertzer et al., 1995), giving the values: $\alpha = 1.5 \pm 0.05$ and $C_1 = 0.15 \pm 0.03$.

For a scaling field which has no known condition of normalisation (as for example a passive scalar), we can write Eq. 13 on the following way:

$$\zeta_\theta(q) = qH - \frac{C_1}{\alpha - 1}\left(q^\alpha - q\right) \tag{16}$$

The new parameter H is there the degree of non-conservation of the average field ($\zeta_\theta(1) = H$): $H \neq 0$ means that the fluctuations are scale-dependent ($H \approx 0.38$ for temperature in atmospheric turbulence, see Schmitt et al. (1996)). The second term expresses a deviation from homogeneity (in which case $\zeta_\theta(q) = qH$), and represents the intermittency corrections. We use Eq. 16 to test the scaling behaviour of the temperature and fluorescence data, and determine these three parameters (H, C_1 and α).

2.2 Lagrangian relations for turbulent velocity and passive scalar fields

In a Lagrangian framework, as one follows the motion of an element of fluid, the scaling relations (Eqs. 1-2) are now to be expressed as a function of the difference of time (t) of observations (usually between actual time and initial time) instead of difference of location in an Eulerian framework. One obtain by replacing $\Delta V_l / l$ by $1/t$ in Eqs. 1-2 (Landau and Lifshitz, 1944; Inoue, 1950, 1951, 1952a, b; Lin, 1960; Monin and Yaglom, 1975):

$$\varepsilon_t \approx \frac{(\Delta V_l)^2}{t} \tag{17}$$

$$\chi_t \approx \frac{(\Delta\theta_l)^2}{t} \tag{18}$$

where $\Delta V_t = |V(\tau+t) - V(\tau)|$ and $\Delta\theta_t = |\theta(\tau+t) - \theta(\tau)|$ are the velocity and temperature fluctuations for an element of fluid on a time scale t (τ being the initial time). The assumption of a Lagrangian cascade for these fluxes (Novikov, 1989, 1990) leads *formally* to simpler scaling relations than in an Eulerian framework, since in

[1] For conservative processes, we use the notation $K(q)$.

Eq. 18 the scalar variance flux no longer depends *explicitely*[2] on a cross-product of velocity and temperature fields:

$$\left\langle (\varepsilon_t)^q \right\rangle \approx \Lambda^{K_\varepsilon(q)} ; \left\langle (\Delta V_t)^q \right\rangle \approx \Lambda^{-Z_V(q)} \quad (19)$$

$$\left\langle (\chi_t)^q \right\rangle \approx \Lambda^{K_\chi(q)} ; \left\langle (\Delta \theta_t)^q \right\rangle \approx \Lambda^{-Z_\theta(q)} \quad (20)$$

with the relations, given by Eqs. 17-18:

$$K_\varepsilon(q) = q - Z_V(2q) ; \; K_\chi(q) = q - Z_\theta(2q) \quad (21)$$

where T is a fixed outer time-scale and $\Lambda = T/t$ is the corresponding time-scale ratio, $K_\varepsilon(q)$ and $K_\chi(q)$ are the Lagrangian scaling moment functions for the fluxes, $Z_V(q)$ is the Lagrangian velocity structure function scaling exponent and $Z_\theta(q)$ is the Lagrangian passive scalar structure function scaling exponent. The fluxes are still assumed to be conservative (i.e. their mean is scale-invariant): $K(1) = 0$. This implies $Z_V(2) = 1$ and $Z_\theta(2) = 1$.

Assuming universality (Eq. 14) for the (Lagrangian) flux of scalar variance, the (Lagrangian) structure functions' scaling exponents $Z_\theta(q)$ of a passive scalar depend only on the universal exponents (due to Eq. 21), whereas we pointed out that in the Eulerian framework the determination of the corresponding structure functions' scaling exponents is quite more involved and has not such a straightforward relationship with the scaling function of the variance flux. One may note that the transformations (for some other motivation) from space to space are somewhat discussed in Marsan et al. (1996).

2.3 Eulerian turbulent "biologically active" scalars

For chemically (Corrsin, 1961) or biologically (Denman and Platt (1976) and Denman *et al.* (1977)) active[3] scalars in turbulence, one usually assumes that there is a characteristic time, i.e. having a exponential decay (e.g. first order chemical reactions) or having an exponential population growth law. Due to this characteristic time, one expects a scalar variance spectrum with a slope -1 (as in the case of the Batchelor (1959) convective subrange, see below) for frequencies smaller than the corresponding characteristic frequency. The reason for this result is clear: for frequencies smaller than the characteristic frequency of the exponential law, the latter imposes its frequency, i.e. the flux of variance is no more ruled by turbulence, because it is too slow compared to the chemical reaction (here chlorophyll *a* synthesis) or population growth. Therefore, one must replace in Eq. 18 the inverse of the local eddy turnover time $1/t = \Delta V_l / l$ by this characteristic frequency ω_c, which gives:

$$\chi_{(F)l} \approx \left(\Delta F_l\right)^2 \omega_c \quad (22)$$

where F is the fluorescence concentration (which is a proxy of the phytoplankton concentration) and $\chi_{(F)}$ is the flux of scalar variance, as before. Then, the scalar variance being the Fourier transform of its spectrum, i.e.:

$$(\Delta F_l)^2 \approx E_F(k)k; \; k \approx l^{-1} \quad (23)$$

we obtain, for the Fourier power spectrum of the biologically active scalar (Denman and Platt, 1976):

$$E_F(k) \approx \left(\Delta F_l\right)^2 k^{-1} \approx \chi_{(F)l} \omega_c^{-1} k^{-1} \quad (24)$$

As mentioned this spectrum is similar to Batchelor (1959) convective-subrange, although the mechanism is rather different. In case of convection it corresponds to high wave numbers (or frequencies), contrary to the case of the active scalar, where it occurs for lower frequencies. More precisely, the convective subrange is the range of the wave numbers where the molecular viscosity is already effective, whereas the molecular diffusion is not yet effective. This obviously requires a high Prandtl number (this number being the dimensionless ratio of the molecular viscosity and diffusivity). The convection results from non-local interactions, it is therefore the eddy turn at the beginning of the viscous subrange which will rule the convection.

Furthermore, fluorescence as a measure of phytoplankton abundance is a very special active scalar. For scales where the biological activities have time to develop (and is not destroyed by the turbulent motion), the phytoplankton cannot be considered as isolated: there are continuous predator-prey interactions, and two fluxes of creation and destruction of phytoplankton. Therefore, at large scales (when the biological time scales are of the same order as turbulent time scales), we still expect a highly intermittent phytoplankton density, but with characteristics clearly different from a passive scalar. In a previous paper (Seuront et al., 1996), we empirically analysed the biological activity and its multifractal characteristics in an Eulerian framework and confirmed this picture. We can here interprete these previous empirical results (Seuront et al., 1996) and propose, using Eq. 22, for the structure function scaling exponent $\zeta_F(q)$ of a biologically active scalar the following expression:

$$\zeta_F(q) = -K_\chi\left(\frac{q}{2}\right) \quad (25)$$

where $K_\chi(q)$ is the scaling exponent of the flux of fluorescence scalar variance. Because this flux is conservative ($K_\chi(1) = 0$), the biologically active scalar is not conservative: $\zeta_F(1) = -K_\chi(1/2) \neq 0$. We may notice that, up until now, there have been no attempts to study even the average fluctuations of the plankton variability in a Lagrangian frame, to our knowledge.

[2] Indeed the velocity was used to define implicitely the time.

[3] However, there are still dynamically passive, i.e. not influencing the velocity field.

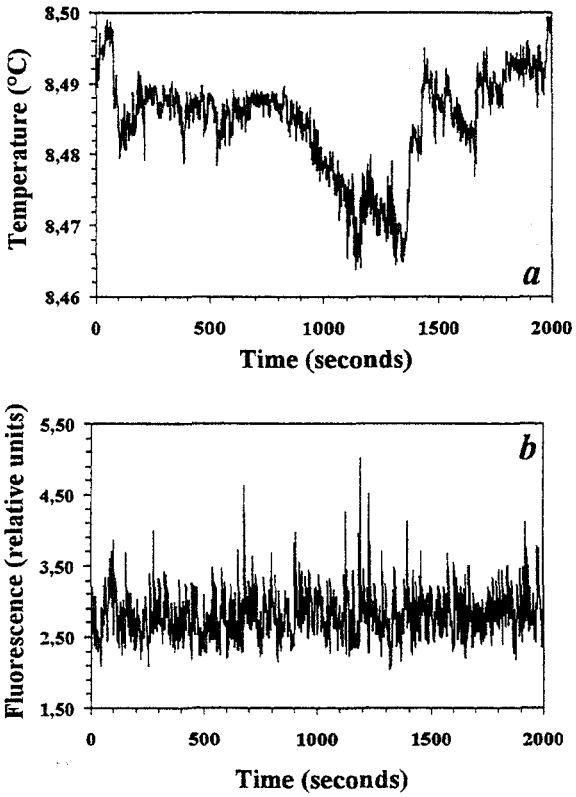

Fig. 1. A portion of temperature (*a*) and *in vivo* fluorescence (*b*) time series recorded in the Southern Bight of the North Sea. Sharp fluctuations occuring on all time scales are clearly visible, indicating the intermittent behaviour of the dataset.

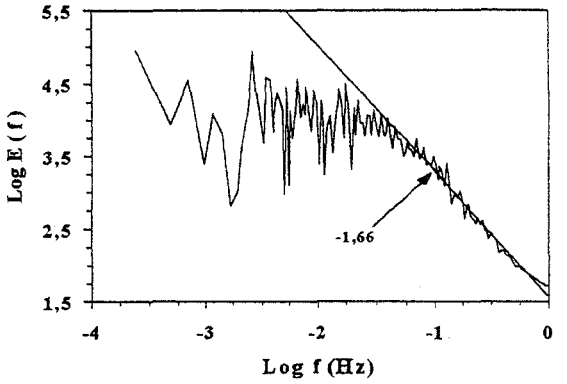

Fig. 2. The power spectrum of the turbulent fluorescence, shown in a log-log plot. The data are scaling from 0.04 to 1 Hz with a slope close to Kolmogorov power law trend of a passive scalar $E(f) \propto f^{-\beta}$ with $\beta \approx 1.66$. For lower frequencies, there is no evidence of a linear trend nor characteristic periods.

3. Empirical study of turbulent temperature and fluorescence

3.1 The data, their spectra and Eulerian/Lagrangian transition

The data were obtained as part as an experiment conducted adrift in tidally mixed coastal waters in the eastern English Channel, at the end of March 1995 during a period of spring tide. Temperature and *in vivo* fluorescence were simultaneously recorded during two hours at a 15m depth with a CTD recorder (Sea Bird 25) and a fluorometer (Sea Tech), respectively. The sampling frequency ω being 2 Hz, our analysis are based on a time series of 11082 measurements, presented as a typical case of the variability of the different datasets sampled in this period. Samples of the data are shown in Fig. 1. One may note that the variability observed in the data used in our computation is always greater than the resolution of the measurements in both cases, and then is independent of any instrumental uncertainties.

We computed the Fourier power spectra of temperature and *in vivo* fluorescence fluctuations. The fluorescence power spectrum is shown in Fig. 2. It follows a power-law behaviour from 0.04 to 1 Hz according to:

$$E(\omega) \propto \omega^{-\beta} \tag{26}$$

where the slope β is close to the Obukhov-Corrsin Eulerian value 5/3 given by Eq. 4 (using the usual Taylor hypothesis to transform frequencies into a distance). In the multifractal frame, the intermittencies are taken into account noting that:

$$\beta = 1 + \zeta_\theta(2) \tag{27}$$

with $\zeta_\theta(2)$ given by Eq. 16, but empirically the correction to 5/3 is small for this second order of moment. For frequencies less than 0.04 Hz, fluorescence fluctuations do not exhibit evidence of power law behaviour nor characteristic periods. This is likely due to the shortness of the data set; it has been shown (Seuront et al., 1996) from a longer time series (but taken in an anchor station), that fluorescence data are scaling over smaller frequencies. This may also be due to the transition from Eulerian to Lagrangian sampling — see below.

The temperature power spectrum presents a mixed behaviour with two scaling tendencies for frequencies from 0.038 to 1 Hz ($\beta \approx 1.65$), and for frequencies lower than 0.038 Hz ($\beta \approx 2$) (Fig. 3a). These tendencies being difficult to distinguish, we transformed the spectral density by a multiplicative factor ω^2, and the resulting spectrum exhibits a power law behaviour with an exponent 0.35 ($r^2 = 0.95, p < 0.001$) which clearly breaks for frequency of about 0.038-0.040 Hz, lower frequencies being assimilated to a "noisy background" (horizontal tendency, see Fig. 3b).

In order to interprete this change in behaviour of the power spectrum, let us recall that the measurements are taken from a boat adrift in the Channel. For the high frequency range of the measurements we can consider the boat as not moving, so the measurements correspond to a

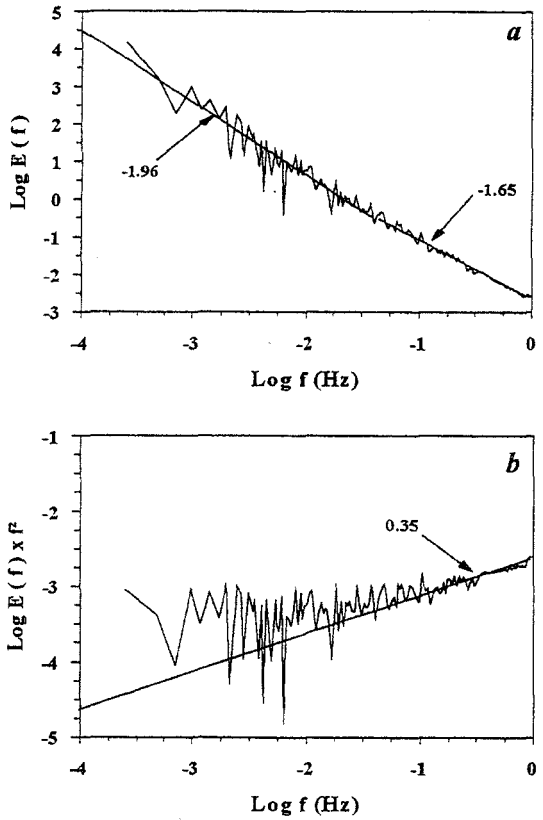

Fig. 3. The power spectrum of the turbulent temperature (*a*), shown in a log-log plot, exhibits a scaling behaviour for frequencies from 3.8 10^{-2} to 1 Hz with a spectral slope $\beta \approx 1.65$ and for frequencies greater than 3.8 10^{-2} Hz with a slope $\beta \approx 1.96$. The power spectrum, transformed by a factor ω^2 (*b*) confirms the scale breaking of the data, exhibiting a linear trend of 0.35 from 3.8 10^{-2} to 1 Hz.

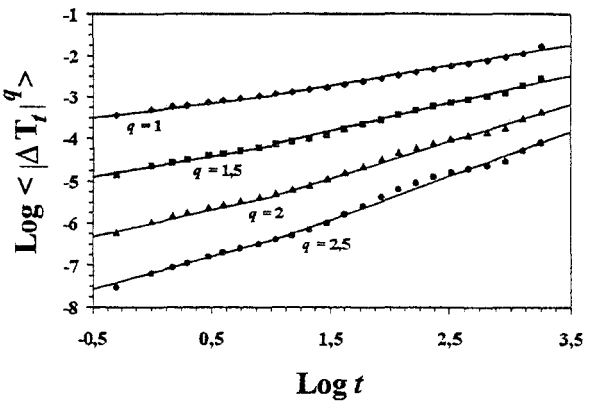

Fig. 4. The temperature structure functions vs. $<|\Delta\theta_t|^q>$ vs. t in a log-log plot for q = 1, 1.5, 2 and 2.5 (from top to bottom), were $<|\Delta\theta_t|^q> = <(\Delta\theta_T)^q> (t/T)^{\zeta(q)}$. Linear trends are clearly visible for all order of moments, from 0.5 to 13s, for Eulerian scales (less than 13 seconds) and Lagrangian time scales (greater than 13 seconds). The straight lines indicate the best regression over each range of scales for each value of q. This gives in particular: $H = \zeta(1) = 0.34 \pm 0.01$ and $\zeta(2) = 0.65 \pm 0.02$ for Eulerian temperature and $H = \zeta(1) = 0.51 \pm 0.01$ and $\zeta(2) = 0.96 \pm 0.03$ for Lagrangian temperature.

fix-point procedure, i.e. Eulerian sampling. This is confirmed by the two small-scale spectra, each of them close to a -5/3 slope. The scale break exhibited by the temperature field for frequencies of about 0.038 Hz is associated with a characteristic time scale of 13 seconds. Using the instantaneous tidal circulation of about 1 m.s^{-1} observed during the field experiment, we estimate that the associated length scale is ≈ 13 meters, which is close to the size (12.5m) of the ship used during the sampling experiment (N/O Sepia II, CNRS-INSU). This means that for frequencies smaller than 0.038 Hz, the inertia of the boat becomes negligible and the measurements are effectively taken following the flows, i.e. in a Lagrangian framework. This transition is also confirmed by the spectral analysis of the temperature data which exhibit a spectral slope close to -2 as given by Eqs. 20-21 and 27. We may note here that contrary to the Eulerian frame where there are intermittency corrections to the spectral slope, in the Lagrangian frame we do not expect any intermittent correction for this second order moment (because here, the second order moment has the same scaling as a conserved flux: $\beta = 1 + Z_\theta(2) = 2 - K_\chi(1) = 2$.

It is then possible to show that a time series recorded *a priori* in a oceanic Lagrangian framework can exhibit both Eulerian and Lagrangian components whose relative importance is determined by the size of the boat. We now determine the scale invariant properties of the intermittency of temperature and fluorescence fields, using direct multifractal analysis techniques.

3.2 Multifractal study of Eulerian intermittencies

We computed the structure functions $\langle(\Delta\theta_t)^q\rangle$ for the temperature field. Two power law regimes are visible in log-log plot (Fig. 4), consistent with the scale transition observed on the Fourier power spectrum. We obtain an Eulerian scaling over a range of scale from 0.5 s to 13 s (also observed for fluorescence field). We also estimated the structure functions for the fluorescence field.

In Fig. 5 we plotted the structure functions' scaling exponents $\zeta(q)$ obtained as the slopes of the straight lines for the range of scales 0.5 to 13 s. Here as below, the error bars come from the different portions of the dataset analysed separately: for example, with the scaling of Eulerian temperature and fluorescence up to 13 s and a database of 11082 points, we can estimate the exponents for 425 non-overlapping intervals. The scaling of the first exponents are very similar for temperature and fluorescence, respectively with $H = \zeta(1) = 0.34 \pm 0.02$ and $H = \zeta(1) = 0.36 \pm 0.02$, respectively. This is slightly smaller than the values obtained in Seuront et al. (1996) ($H = 0.42 \pm 0.02$ for temperature and 0.41 ± 0.02 for fluorescence), but nevertheless close to 1/3, the value corresponding to the Obukhov-Corrsin non-intermittent

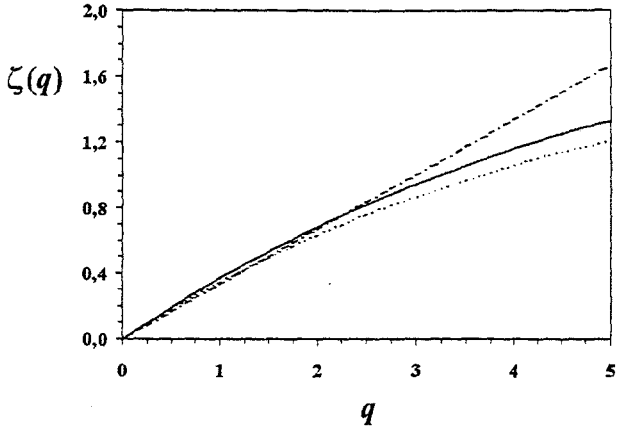

Fig. 5. Empirical values of $\zeta(q)$ obtained here for fluorescence (dashed line) and Eulerian (continuous line) temperature, compared to the homogeneous linear curve $\zeta(q) = q/3$ corresponding to Obukhov-Corrsin non-intermittent turbulence (discontinuous line). The nonlinearity of the empirical curves indicates multifractality.

passive-scalar turbulence. The scaling of the second order moments confirm the estimates from the power spectra ($\beta = 1 + \zeta(2)$), with $\zeta(2) = 0.66 \pm 0.02$ for fluorescence and $\zeta(2) = 0.65 \pm 0.02$ for temperature. More generally, for other orders of moments the non-linearity of the curves $\zeta(q)$ in Fig. 5 shows that these two fields can be considered as multifractals; the two curves corresponding to Eulerian sampling for temperature and fluorescence (i.e. phytoplankton biomass) are very close to each other. Within experimental error, they cannot be qualitatively considered as being different (we quantify is below). As shown in Seuront et al. (1996), this is a generalization of the result obtained by Denman and Platt (1976) who tested the assumption that the fluorescence was a passive scalar using only power spectra (a second order moment). Figure 5 shows that for all moments (and thus all intensities), fluorescence and temperature intermittencies have nearly the same probabilities. These multifractal statistics are compatible with the intermittent structure of the original time series (Fig. 1) which clearly exhibit numerous structures of different strengths and scales.

We now attempt to quantitatively characterize these intermittencies. Using Eq. (16) we have directly:

$$\begin{aligned} H &= \zeta(1) \\ C_1 &= H - \zeta'(1) \end{aligned} \tag{28}$$

This gives $H \approx 0.34 \pm 0.02$, $C_1 \approx 0.037 \pm 0.004$ for temperature, and $H \approx 0.36 \pm 0.02$, $C_1 \approx 0.035 \pm 0.004$ for fluorescence. The value of α can be estimated using the best nonlinear fit of Eq. 16 (for $0 \le q \le 6.5$ and using a simple least-square method) of the empirical curve: we obtain for both temperature and fluorescence $\alpha \approx 1.8 \pm 0.05$. These values are quite close to those reported in Seuront et al. (1996): $H \approx 0.42$, $C_1 \approx 0.04$ and $\alpha \approx 1.7$ for temperature, and $H \approx 0.41$, $C_1 \approx 0.04$ and

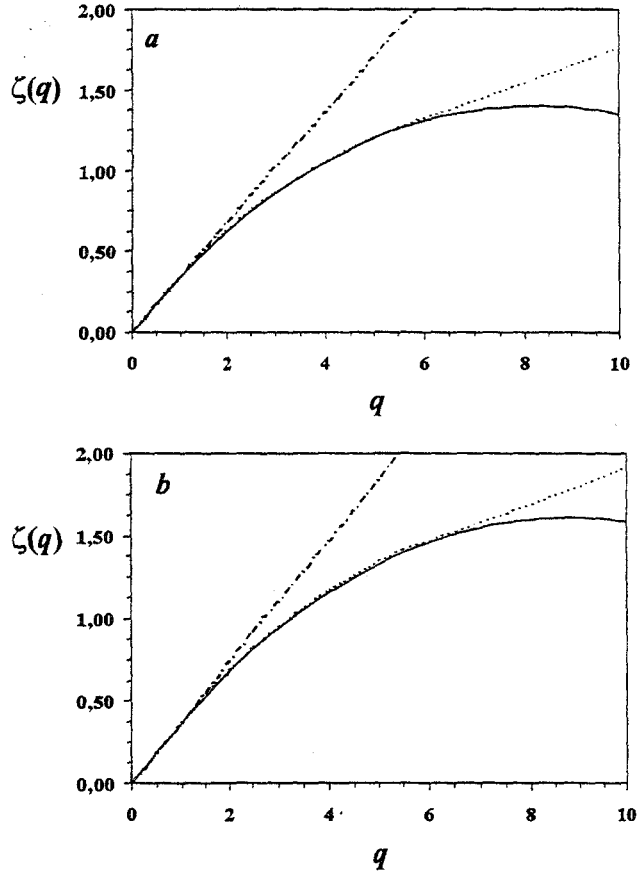

Fig. 6. The Eulerian scaling exponent structure function $\zeta(q)$ empirical curves (dashed line), compared to the homogeneous linear curve $\zeta(q) = q/3$ corresponding to Obukhov-Corrsin non-intermittent turbulence (discontinuous line), and to the universal multifractal functions obtain with H, C_1 and α in Eq. 16 (continuous line). The multifractal fit is excellent until moment order $q = 6.0 \pm 0.2$ for temperature (*a*) and $q = 6.2 \pm 0.2$ for fluorescence (*b*).

$\alpha \approx 1.8$ for fluorescence. The value of α we obtain shows that these fields are not lognormal multifractals ($\alpha = 2$), but also that the lognormal approximation for $\zeta(q)$ should not be too far from empirical estimates. The values of $C_1 \approx 0.04$ may seem to be quite small, but one must remember that this concerns the scalar field; if one considers the (non-conserved) flux (see Eq. 2):

$$\varphi_l = \varepsilon_l^{-1/2} \chi_l^{3/2} \approx \frac{(\Delta\theta)^3}{l} \tag{29}$$

then the value of C_1 must be transformed to $C_{1\varphi} = 3^{\alpha} C_{1\theta} \approx 0.27$. This values is larger than our latest estimate for the energy flux in the atmosphere (Schertzer et al., 1995; Schmitt et al., 1996): $C_1 \approx 0.15$; this shows that the scalar turbulence is more intermittent than the velocity turbulence.

Furthermore, within experimental error the values we obtain for temperature and fluorescence cannot be clearly

distinguished. We compared the empirical estimates with the theoretical curves in Fig. 6 (using Eq. 16 and the values above): the correspondence is excellent until moment order $q_T \approx 6.0 \pm 0.2$ and $q_P \approx 6.2 \pm 0.2$, after which the empirical curves are linear (Fig. 6). This linear behaviour of the empirical scaling exponent structure function $\zeta(q)$ is well-known for sufficiently high order moments (Schertzer and Lovejoy, 1989) and is due to sampling limitations (i.e. second order multifractal phase transition; see Schertzer and Lovejoy (1992)) or is associated with a divergence of statistical moments (i.e. first order multifractal phase transition; see Schertzer and Lovejoy (1992)) if substantiated by large enough sample size. Here with one realization of about 11,000 datapoints, the change in behaviour is likely to be due to sampling limitations. In this case, the critical moment q_s (for a scaling exponent structure function given by Eq. 16) is given by (Schertzer and Lovejoy, 1992):

$$q_s = \left(\frac{1}{C_1}\right)^{1/\alpha} \tag{30}$$

And in this case, the empirical $\zeta(q)$ follows:

$$\zeta(q) = 1 - \gamma_s q \quad ; \quad q \geq q_s \tag{31}$$

where γ_s is a maximum singularity associated to q_s. Here with the values estimated above, we obtain: $q_s \approx 6.2$ for temperature, and $q_s \approx 6.5$ for fluorescence, which are very close to the values previously proposed from the empirical curves. This critical moment is only linked to the sampling limitations; when more samples are taken into account in the statistics, it increases. In any case, most statistical parametrization basically dealing with maximum moment of order 3 (skewness), a critical moment greater than 6 then characterizes very rare events.

3.3 Multifractal study of Lagrangian intermittencies

As with Eulerian data above, we computed the structure functions for Lagrangian temperature which were shown to exhibit a scaling behaviour over scales greater than 13s. The corresponding behaviour of the fluorescence data is quite different, and it is not clear if there is some scaling or not (see Fig. 3); therefore, we do not proceed to the analysis of large-scales fluorescence field, leaving it to a future study. There is also an indetermination about the interpretation to give to this change of behaviour: is it due to Eulerian/Lagrangian transition, as for the temperature, or due to the biological activity, as obtained — for another dataset — in Seuront et al. (1996).

The scaling exponent for the first and second moments of the Lagrangian temperature are $Z_\theta(1) \approx 0.51 \pm 0.02$ and $Z_\theta(2) \approx 0.96 \pm 0.03$. The corresponding estimates for other moments gives the curve $Z_\theta(q)$, whose (slight) nonlinear behaviour (see especially the low order moments) is the signature of multifractal Lagrangian intermittency.

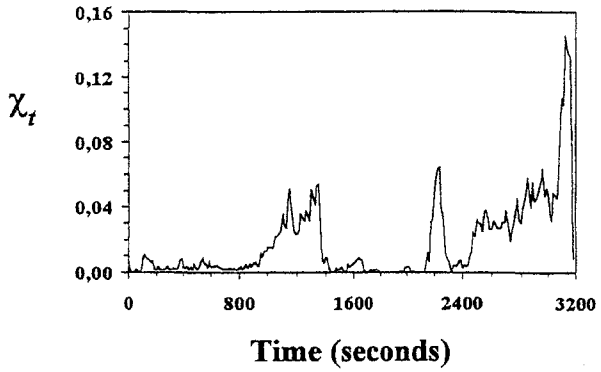

Fig. 7. Sample of the pattern of the rate of temperature variance transfert from large to small scales, showing intermittency.

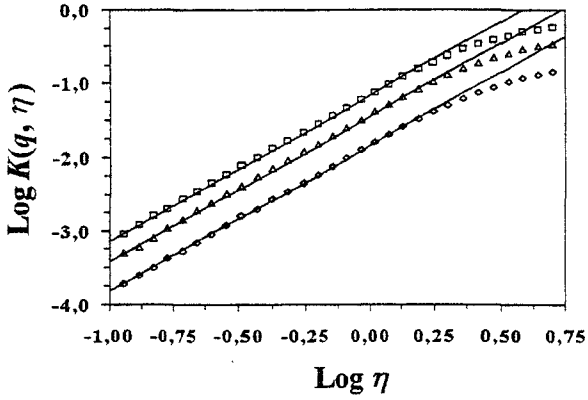

Fig. 8. The curves $K(q,\eta)$ vs. η in a log-log plot for $q = 2$, 2.5 and 3 (from bottom to top) for Lagrangian field χ_l, where $K(q,\eta) = \eta^\alpha K(q)$. The slopes of the straight lines then give the estimates of α: $\alpha \approx 1.8$ and C_1 is estimated by the intercept: $C_1 \approx 0.05$.

Let us recall here the simple expression for $Z_\theta(q)$, given by Eqs. 18, 20-21:

$$Z_\theta(q) = \frac{q}{2} - \frac{C_1}{\alpha - 1}\left(\left(\frac{q}{2}\right)^\alpha - \frac{q}{2}\right) \tag{32}$$

which directly gives the universal parameter C_1 as $C_1 = 1 - 2Z'(2)$. Here we obtain $C_1 \approx 0.05 \pm 0.01$. A simple way to estimate α is to take it as the best nonlinear fit of the data using Eq. 32. This gives $\alpha = 1.8 \pm 0.05$, the same value as what we obtain in the Eulerian case. We also verified these values by comparison with those obtained from the Double Trace Moment analysis (DTM) (Lavallée, 1991; Lavallée et al., 1992), which was applied on the data after a fractional differentiation of the temperature data of the order 1/2 (i.e. a $\omega^{1/2}$ multiplication in Fourier space, to remove the $t^{1/2}$ scaling of the first moment), and taking the square of the result, yielding an estimate of χ_l (see Eq. 18), whose pattern can be seen in Fig. 7.

The basic idea of the DTM technique is to generalize the application of statistical methods to the quantity

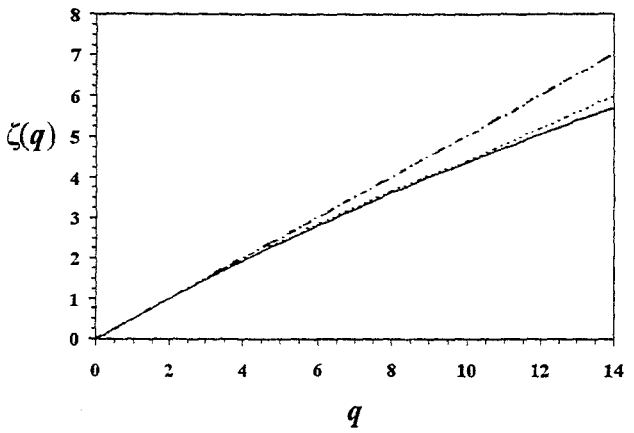

Fig. 9. The Lagrangian scaling exponent structure function $\zeta(q)$ empirical curves (dashed line) compared to the homogeneous Lagrangian turbulence linear curves $\zeta(q) = q/2$ (discontinuous line) and to the universal multifractal functions obtained with α and C_1 in Eq. 32 (continuous line). The universal multifractal fit is excellent until moment order $q \approx 10.4 \pm 0.5$ for temperature, corresponding to multifractal phase transition associated with sampling limitations.

$(\chi_\lambda)^\eta$. This is done by taking the η^{th} power of χ_{λ_0} at the scale ratio λ_0 (the ratio of the outer or largest scale of interest to the smallest scale of homogeneity), and then studying its scaling behaviour at decreasing values of the scale ratio $\lambda \leq \lambda_0$:

$$\chi_{\lambda,\lambda_0}(\eta) = \frac{(\chi_\lambda)^\eta}{\langle(\chi_\lambda)^\eta\rangle}\langle(\chi_{\lambda_0})^\eta\rangle \qquad (33)$$

The moments of this new field then have a multiple scaling behaviour, characterized by the new moment scaling function $K_0(q,\eta) = K(q\eta) - qK(\eta)$ (is a constant). For conservative universal multifractals, this gives, with the help of Eq. 14:

$$K_0(q,\eta) = \eta^\alpha K(q) \qquad (34)$$

Then, by keeping q fixed (but different from the special values 0 or 1), the slope of $K_0(q,\eta)$ as a function of η on a log-log graph gives the values of the index α, which with the help of the intersection with the line ($\eta = 1$) yields C_1 (Fig. 8). This again gives $\alpha \approx 1.8$ and $C_1 \approx 0.05$, which confirms the values estimated above.

We then compare the universal multifractal fit obtained with α and C_1 in Eq. 32, with the empirical estimates. The universal multifractal and empirical fits were excellent until moment of about 10.4 ± 0.5, after which the empirical curves exhibit a linear behaviour (Fig. 9) which can reasonably be associated with sampling limitation because of the small number of data considered (because we had to average the original time series up to the scale of 13s, in order to be in the Lagrangian scales). This critical moment is given here by the following expression, obtained using Eq. 32, (it replaces Eq. 30, which was obtained using Eq. 16):

$$q_s = 2\left(\frac{1}{C_1}\right)^{1/\alpha} \qquad (35)$$

We obtain $q_s \approx 10.5$, which is very close to the empirical value given above.

a

	Eulerian data ($f > 0.038$ Hz) H, C_1 and α from Eq. 16				Lagrangian data ($f < 0.038$ Hz) C_1 and α from Eq. 32			
	β	H	C_1	α	β	H	C_1	α
Temperature	1.65	0.34	0.037	1.7	1.96	0.51	0.05	1.8
Fluorescence	1.66	0.36	0.035	1.8	-	-	-	-

b

	Eulerian data passive scalar for $f > 0.01$ Hz				Eulerian data biologically active scalar for $f \cdot 0.01$ Hz			
	β	H	C_1	α	β	H	C_1	α
Temperature	1.74	0.42	0.04	1.7	-	-	-	-
Fluorescence	1.75	0.41	0.04	1.8	1.22	0.12	0.02	0.8

Table 1. The values of the universal multifractal parameters obtained here, according to Eq. 16 for Eulerian values and Eq. 32 for Lagrangian (*a*), compared to the values we previously obtained in Seuront et al. (1996) (*b*). The values of the slopes of the Fourier power spectra are also indicated.

4. Conclusion

It appears clearly from the present study that an *a priori* Lagrangian sampling may exhibit Eulerian and Lagrangian components separated by a length scale intimately linked to the size of the ship used to collect the field data. Indeed our results show that Eulerian and Lagrangian passive scalar turbulence exhibit multifractal statistics compatible with universal multifractals, in qualitative accord with the visual appearance of the time series. The values of the parameters are summarized in Tables 1a-b, which contain also the values reported in Seuront et al. (1996).

These analyses also provide an empirical confirmation of the ω^{-2} theory of the turbulent Lagrangian turbulent behaviour of a passive scalars. We obtained here a first evidence of Lagrangian multifractality, and we estimated the universal multifractal parameters (see also Table 1a-b), according to Eq. 32, which is a Lagrangian analogy of the refined similarity hypothesis for Eulerian turbulence. However, our Lagrangian study needed an averaging of the

dataset, which means that these results must be confirmed with much larger datasets, in order to be confident about the numerical values of the parameters.

On the other hand, *in vivo* fluorescence (a phytoplankton biomass proxy) appears to be a passive scalar on small scales (less than 13 seconds) associated with an Eulerian framework. Moreover, the commonality of the basic multifractal parameters of temperature and fluorescence reflects profound nonlinear coupings between the space-time structure of phytoplankton populations and the structure of their physical environment. As already noted in Seuront et al. (1996), this generalizes the results obtained in Denman and Platt (1976), with only a Fourier power spectrum analysis. In order to better understand the nature of the coupling between these fields, one direction for the future researches is to study their multifractal correlations; another is to analyze these fields in a vectorial multifractal framework.

Lastly, on larger scales (greater than 13 seconds) associated with a Lagrangian framework, the lack of scaling behaviour related to the small number of datapoints in the series does not allow us to explore the Lagrangian fluorescence variability, and to test Eq. 25: this will be done in future studies, using larger datasets.

Acknowledgements. We thank S. Frontier, Y. Teissier and R. Nowak for fruitful discussions and the "Sepia II" crew for their assistance during the cruise.

References

Batchelor, G.K., Small-scale variation of convected quantities like temperature in turbulent fluid, Part I. General discussion and the case of small conductivity, *J. Fluid Mech.*, 5, 113, 1959.

Benzi, R., Biferale, L. and Parisi, G., Intermittency correction to the Obukhov-Corrsin theory of a passive scalar, *Europhys. Lett.*, 18, 213, 1992.

Corrsin, S., On the spectrum of isotropic temperature fluctuations in an isotropic turbulence, *J. Appl. Physics*, *22*, 469-473, 1951.

Corrsin, S., The reactant concentration spectrum in turbulent mixing with a first-order reaction, *J. Fluid Mech.*, *11*, 407-416, 1961.

Denman, K. L. and Platt, T., The variance spectrum of phytoplankton in a turbulent ocean. *J. Mar. Res.*, *34*(3), 563-601, 1976.

Denman, K. L., Okubo, A. and Platt, T., The chlorophyll fluctuations spectrum in the sea, *Limnol. Oceanogr.*, *22*, 1033-1038, 1977.

Feller, W., *An introduction to probability theory and its applications*, vol. II, second ed., John Wiley&Sons, New York, 1971.

Frisch, U., Sulem, P.-L., and Nelkin, M., A simple dynamical model of intermittent fully developed turbulence. *J. Fluid Mech.*, 87, 719, 1978.

Gargett, A. E., Osborn, T. R. and Nasmyth, P. W., Local isotropy and the decay of fluid turbulence in a stratified fluid, *J. Fluid Mech.*, *144*, 231-280, 1984.

Grant, H., Stewart, R. and Moillet, A., Turbulent spectra from a tidal channel, *J. Fluid Mech.*, *12*, 241-268, 1962.

Grant, H., Hugues, B., Vogel, W. and Moillet, A., The spectrum of temperature fluctuations in turbulent flow, *J. Fluid Mech.*, *34*, 423-442, 1968.

Inoue, E., On the turbulent diffusion in the atmosphere, I, *Journal of the Meteorological Society of Japan*, *28*, N°12, 441-456, 1950.

Inoue, E., On the turbulent diffusion in the atmosphere, II, *Journal of the Meteorological Society of Japan*, *29*, N°7, 246-253, 1951.

Inoue, E., Turbulent fluctuations in temperature in the atmosphere and oceans, *Journal of the Meteorological Society of Japan*, *30*, N°9, 289-295, 1952a.

Inoue, E., On the Lagrangian correlation coefficient for turbulent diffusion and its application to atmospheric diffusion phenomena, *Geophysical Res. Pap.*, N°19, 397-412, 1952b.

Kolmogorov, A. N., The local structure of turbulence in incompressible viscous fluid for very large Reynolds number, *Dokl. Acad. Nauk SSSR*, *30*, 299-303, 1941a.

Kolmogorov, A. N., Energy dissipation in locally isotropic turbulence, *Dokl. Acad. Nauk SSSR*, *32*, 19, 1941b.

Kolmogorov, A. N., A refinement of previous hypothesis concerning the local structure of turbulence in incompressible viscous fluid for very large Reynolds number, *J. Fluid Mech.*, *13*, 82, 1962.

Landau, L. D. and Lifshitz, E. M., *Fluid mechanics*, Addison-Wesley, 1944 (first edition).

Lavallée, D., *Multifractal techniques: analysis and simulation of turbulent fields*, Ph.D. thesis, McGill University, Montréal, Canada, 1991.

Lavallée, D., Lovejoy, S. Schertzer, D. and Schmitt, F., On the determination of universal multifractal parameters in turbulence, in *Topological aspects of the dynamics of fluids and plasmas*, edited by K. Moffat, Tabor, M. and G. Zaslavsky, pp. 463-478, Kluwer, Boston, 1992.

Legendre, L. and Demers, S., Toward dynamic biological oceanography and limnology, *Can. J. Fish. Sci.*, *41*, 2-49, 1984.

Lin, C., On a theory of dispersion by continuous movements, *Proc. Nat. Acad. Sci. USA*, *46*, N°4, 556-570, 1960.

Mackas, D. L., Denman, K. L. and Abbot, M. R., Plankton patchiness: biology in the physical vernacular, *Bull. Mar. Sci.*, *37*, 652-674, 1985.

Marsan, D., Schertzer, D. and Lovejoy, S., Causal space-time multifractal processes; predictability and forecast of rain fields, *J. Geophys. Res.* (in press), 1996.

Monin, A. S. and Yaglom, A. M., *Statistical Fluid Mechanics: Mechanics of turbulence*, MIT Press, London, 1975.

Novikov, E. A., Two-particle description of turbulence, Markov property, and intermittency, *Phys. Fluids A* 1, 326, 1989.

Novikov, E. A., The effects of intermittency on statistical characteristics of turbulence and scale similarity of breakdown coefficients, *Phys. Fluids A* 2, 814, 1990.

Obukhov, A., Spectral energy distribution in a turbulent flow, *Dokl. Akad. Nauk. SSSR*, 32, N°1, 22, 1941.

Obukhov, A., Structure of the temperature field in a turbulent flow. *Izv. Akad. Nauk SSSR Geogr. I Jeofiz.*, *13*, 55-69, 1949.

Obukhov, A., Some specific features of atmospheric turbulence, *J. Geophys. Res.*, 67, 8, 3011, 1962.

Pascual, M., Ascioti, A. and Caswell, H., Intermittency in the plankton: a multifractal analysis of zooplankton biomass variability, *J. Plankton Res.*, *17*(6), 1209-1232, 1995.

Pecknold, S., Lovejoy, S., Schertzer, D., Hooge, C. and Malouin, J.-F., The simulation of universal multifractals, in *Cellular automata: prospects in astronomy and astrophysics*, eds. Perdang J.-M. and Lejeune A., World Scientific, 228, 1993.

Platt, T., Local phytoplankton abundance and turbulence, *Deep-Sea Res.*, *19*, 183-187, 1972.

Platt, T. and Denman, K. L., Spectral analysis in ecology, *Ann. Rev. Ecol. Syst.*, *6*, 189-210, 1975.

Schertzer, D. and Lovejoy, S., Physical modeling and analysis of rain and clouds by anisotropic scaling multiplicative processes. *J. Geophys. Res.*, *92*, 9693-9714, 1987.

Schertzer, D. and Lovejoy, S., Nonlinear variability in geophysics: multifractal analysis and simulation, in *Fractals: Physical Origin and Consequences*, edited by L. Pietronero, pp. 49-79, Plenum, New York, 1989.

Schertzer, D. and Lovejoy, S., Hard and soft multifractal processes, *Physica A*, *185*, 187-194, 1992.

Schertzer, D., Lovejoy, S. and Schmitt, F., Structures in turbulence and multifractal universality, in *Small scale structures in 3D hydro and MHD turbulence*, eds. M. Meneguzzi, A. Pouquet and P.L. Sulem, Springer, Lecture notes in physics vol. 462, 137, 1995.

Schmitt, F., Schertzer, D., Lovejoy, S. and Brunet, Y., Estimation of universal multifractal indices for atmospheric turbulent velocity fields, *Fractals*, 1, 3, 568, 1993.

Schmitt, F., Schertzer, D., Lovejoy, S. and Brunet, Y., Multifractal temperature and flux of temperature variance in fully developed turbulence, *Europhysics Letters*, 34, 3, 195, 1996.

Seuront, L., Schmitt, F., Lagadeuc, Y., Schertzer, D., Lovejoy, S. and Frontier, S., Multifractal analysis of phytoplankton biomass and temperature variability in the ocean, *Geophys. Res. Lett.* (in press), 1996.

Wilson, J., Lovejoy, S. and Schertzer, D., Physically based cloud modellling by multiplicative cascade processes, in *Nonlinear variability in geophysics: scaling and fractals*, eds. Schertzer D. and Lovejoy S., Kluwer Academic Press, Dordrecht-Boston, 185, 1991.

Yaglom, A. M., Local structure of the temperature field in a turbulent flow, *Dokl. Akad. Nauk SSSR*, *69*, 743, 1949.

Yaglom, A. M., The influence of fluctuations in energy dissipation on the shape of turbulent characteristics in the inertial interval, *Sov. Phys. Dokl.*, 2, 26, 1966.

A3

Characterisation of space-time variability in stratified and mixed coastal waters (Baie des Chaleurs, Québec, Canada): application of fractal theory

Seuront L & Lagadeuc Y

Marine Ecology Progress Series, **259**, 81-95, 1997

Vol. 159: 81–95, 1997 | MARINE ECOLOGY PROGRESS SERIES Mar Ecol Prog Ser | Published November 29

Characterisation of space-time variability in stratified and mixed coastal waters (Baie des Chaleurs, Québec, Canada): application of fractal theory

Laurent Seuront*, Yvan Lagadeuc

Université des Sciences et Technologies de Lille, URA CNRS 1363, Station Marine, BP 80, F-62930 Wimereux, France

ABSTRACT: The variability of *in vivo* fluorescence, temperature and salinity in the vertically stratified and well-mixed waters of the Baie des Chaleurs (Québec, Canada) was investigated as a continuous function of scale by applying the concept of fractal dimension to variogram analysis. Widely applied to the description of spatial heterogeneity, fractal dimension appears here to be a helpful descriptive tool in discriminating between homogeneity and heterogeneity in time series of both physical and biological parameters. In stratified waters, the structuration of *in vivo* fluorescence, temperature and salinity remains the same over time, in spite of mixing induced by the rise of a strong wind, and is shown to be associated with the global structure of the water column. In mixed waters, the situation is more complex, giving rise to specific behaviour of *in vivo* fluorescence and salinity. In both cases, the differences observed between the fractal dimensions can be explained in terms of different ranges of scales perceived in pattern variability and thus, in the complexity of the pattern structure. We also suggest that the departure from strict selfsimilarity which seems to be associated with the vertical structure of the residual circulation is an indicator of the transitional zone between different levels of system organisation.

KEY WORDS: Space-time variability · Homogeneity · Heterogeneity · Fractal dimension · Stratified and mixed waters

INTRODUCTION

Most processes in natural environments—physical forcings, population and community dynamics—are sources of heterogeneity and create space-time structures such as gradients, patches, trends or other complex patterns (Legendre & Fortin 1989, Dutilleul & Legendre 1993). These heterogeneous structures are particularly well developed in marine environments (Steele 1974, 1978, Haury et al. 1978) where resources such as plankton exhibit patchiness over a continuum of scales (Platt 1972, Mackas & Boyd 1979, Mackas et al. 1985). The multiscale variability of marine environments, outlined by Steele (1985, 1989), leads to a view of the ocean as a 'landscape' in the sense that it can be described by patterns of different temporal and spatial scales. Many physical and biological oceanographers have thus related their findings to the spectrum of physical processes, ranging from circulation patterns in oceanic basins to large gyres, to fine-scale eddies or rips (e.g. Denman & Powell 1984, Legendre & Demers 1984, Mackas et al. 1985, Platt & Sathyendranath 1988). Ecologists have also recognised spatial heterogeneity as a major factor regulating the distribution of species (Wiens 1976, Risser et al. 1984, Urban et al. 1987). Thus, as reviewed by Wiens (1989), ecology must deal with scale, because the objects it focuses on, the organisms and types of environment, are rarely found to be homogeneously distributed through time or space. Yet until recently no quantitative nor qualitative theory has described the origin, dynamics, and consequences of heterogeneity in ways that could increase the accuracy of predictions about ecological processes in complex environments. Dealing with scales has thus been required in order to overcome the difficulties generated by space-time dependencies associated with an heterogeneous distribution of ecological variables.

Mandelbrot (1983), who recognised the ubiquity of sets that violate basic assumptions of uniformity, introduced the concept of the fractal, a geometric form

*E-mail: seuront@loalit.univ-littoral.fr

© Inter-Research 1997
Resale of full article not permitted

which exhibits structure at all scales. In heterogeneous sets, where estimates of quantities such as biomass vary precisely with the scale at which measurements are made (Burrough 1981, 1983a, Milne 1988), fractal dimension then appears to be a useful measure of space-time complexity (Phillips 1985), and provides several advantages over other descriptive indices of ecological patchiness. Classical statistical theory works well in predicting change in variance due to different sizes of sampling units or different grains of sampling strategy when the sampling units are independent. The basic assumption of independence of replicates, however, is rarely verified in natural science and, therefore, the use of classical theory is questionable. Moreover, the more traditional, widely used mathematical descriptors, such as the variance-to-mean ratio (Taylor 1961, Frontier 1972, Downing et al. 1987), have little meaning in a multiscale spatial context (Palmer 1988, Hurlbert 1990). Furthermore, space-time dependence frequently prohibits rigorous statistical analyses of ecological data, while inferences based on autocorrelated observations are risky (Bivand 1980).

The primary goal of fractal analysis and similar techniques (i.e. spectral analysis) is to describe variability over a continuum of scales. Fractal geometry is thus becoming increasingly popular among scientists and has been successfully applied to a great variety of problems involving complex patterns in nature, including terrestrial (Burrough 1981, 1983a, Krummel et al. 1987) and Martian (Woronow 1981) landscapes, cloud shapes (Lovejoy 1982), rainfall time series (Olsson et al. 1992), breaking waves (Longuet-Higgins 1994), shoreline erosion rate (Phillips 1985), and distributions of nesting bald eagles in rugged landscapes (Pennycuick & Kline 1986). In ecology, insightful descriptions of various possible applications of fractals are given by Frontier (1987) and Sugihara & May (1990). Fractals have been used to describe habitat complexity (Bradbury & Reichelt 1983, Bradbury et al. 1984, Gee & Warwick 1994a, b), species diversity (Frontier 1985, 1994), movements of marine (Bundy et al. 1993, Erlandson & Kostylev 1995) and terrestrial (Wiens et al. 1995) invertebrates, shapes of marine snow (Li & Logan 1995, Logan & Kilps 1995) and growth processes (Kaandorp 1991, Kandoorp & Dekluijver 1992).

Basically, in ecology, 'variability' indicates changes in the values of a given quantitative or qualitative descriptor; it is distinct from 'heterogeneity' which refers to patterns and processes composed of parts of different kinds (Kolasa & Rollo 1991). This distinction is, however, not as sharp as may appear at first glance, and meanings essentially depend on the choice of approach (Downing 1991, Naeem & Colwell 1991, Shashak & Brand 1991). From a statistical viewpoint, however, 'heterogeneity', when applied to the distribution of the values taken by a random variable, is the opposite of 'homogeneity', which refers to sameness and similarity. The degree of similarity implied by the term 'homogeneity' may vary from a minimum of a single common attribute, as in the equality of means, to the extreme of total sameness, that is, equivalence of distributions, and thus refers—in the framework of time series analysis—to a pattern of variability characterised by the closeness of scales of variations. In this paper, 'homogeneity' and 'heterogeneity' are specifically associated with patterns remaining similar upon subdivision in time—at each scale, the pattern differs but always shows the same relative variability—as strictly defined in the framework of fractal theory (Mandelbrot 1977, 1983). In that way, fractal dimensions (D_F) appear to be helpful measures in discriminating between homogeneity and heterogeneity of space-time patterns. They reflect the balance of short-range and long-range variations and thus characterise homogeneous and heterogeneous patterns, respectively (Burrough 1981, He et al. 1994). A low D_F value means that the heterogeneity of the variable is high and there are dominant long-range effects. A high D_F characterises very complex processes where short-range, local variability is highly developed and tends to obfuscate long-range trends; the variable is thus more evenly distributed (i.e. less structured) in space and time. As an example, $D_F \approx 2$ in a bi-dimensional space characterises regular—or homogeneous—patterns, indicating that the variation within a sampling unit will be equal to the variation among sampling units, while $D_F < 2$ characterises more irregular—or heterogeneous—patterns.

In this paper, the concept of fractal dimensions is used in conjunction with variogram analysis, a geostatistical technique which is conceptually similar to the traditional block-size techniques of Pattern Analysis (Greig-Smith 1979), but offers the advantage of describing variation as a continuous function of scale (Palmer 1988). Fractal dimension D_F is thus regarded as an index of the complexity perceived in series of temperature, salinity and *in vivo* fluorescence recorded both in stratified and mixed waters in the Baie des Chaleurs (Québec, Canada).

MATERIAL AND METHODS

Sampling procedure. Sampling was conducted in the Baie des Chaleurs from 10 to 12 September 1991 at a stratified station (20 m depth) close to Caplan, located well inside the bay, and from 20 to 22 September at a vertically mixed water column (20 m depth) at Grande-Rivière, close to the entrance of the bay (Fig. 1). At each anchor station, measurements of physical parameters (temperature and salinity) and *in vivo* fluo-

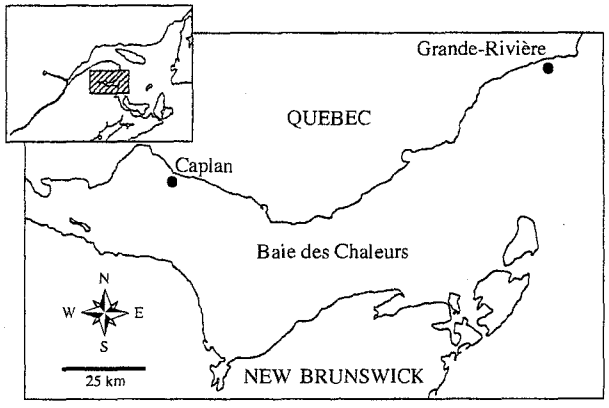

Fig. 1. Locations of the 2 anchor stations along the north shore of Baie des Chaleurs, eastern Canada

rescence (an index of phytoplankton biomass) were taken every hour from the surface to 20 m depth with a SBE 25 Sealogger CTD and a Sea Tech fluorometer over periods of 57 h at Caplan and 52 h at Grande-Rivière. Every 2.25 h, current speeds and directions were measured for 5 min at 2.5, 5, 7.5, 10, 12.5, 15, 17.5 and 20 m with an Aanderaa current meter, which was moored at 5 m during the times between profiles.

Data analysis. The vertical stratification of the water masses was calculated using the potential energy E_p (J m^{-3}), which corresponds to the amount of energy required to redistribute mass in a complete vertical mixing (Simpson et al. 1979, Pond & Pickard 1983):

$$E_p = \frac{1}{H}\int_{-H}^{0}(\rho - \bar{\rho})gz \cdot dz \quad (1)$$

where H, ρ, $\bar{\rho} = \frac{1}{H}\int_{-H}^{0}\rho z \cdot dz$, g and z are the height of the water column, the density, the mean density of the water column, the gravitational acceleration (m s^{-2}) and the depth, respectively.

The Richardson number, Ri, was used to estimate the dynamic stability of the water column (Vandevelde et al. 1987):

$$Ri = \frac{g}{\rho}\cdot\frac{d\rho/dz}{(du/dz)^2} \quad (2)$$

where ρ, g, u and z are the density, the gravitational acceleration, the horizontal component of the current velocity (m s^{-1}), and the depth, respectively. This number compares the stabilising effect of buoyancy forces (represented by the square of the Brunt-Väisälä frequency, $d\rho/dz$) to the destabilising influence of vertical shear in the horizontal velocity field (represented by the square of the velocity gradient, du/dz) over a given depth interval. Values under 0.25 indicate a potential instability, and larger values indicate a greater potential stability (Mann & Lazier 1991).

Missing data due to an inadequate (>1 m s^{-1}) descending speed of the CTD probe were estimated using the method proposed by Zagoruiko & Yolkina (1982), which is particularly adapted to the prediction of missing data in bi-dimensional data tables. Unlike 1-dimensional interpolation techniques, such as kriging, this method provides for each missing data value a predicted value which is not limited to an intermediate value of its surrounding data in a given series but takes into account the whole data table.

To detect dates, intensity and duration of any changes in the values of a given parameter, we used the cumulative sums method (Ibanez et al. 1993). The calculation consists of subtracting a reference value (here the mean of the series) from the data; then these residuals are successively added, forming a cumulative function. Successive negative residuals produce a decreasing slope, whereas successive positive residuals create an increasing slope (the value of the slope is proportional to the mean deviation). Values not very different from the mean show no slope.

Fractal analysis. The concept of fractals has been recently introduced to the description of natural systems (Mandelbrot 1983) and strictly refers to geometrical patterns in which the Hausdorff-Besicovitch dimension exceeds the topological (i.e. Euclidean) dimension. In less technical terms, fractals are temporal or spatial phenomena presenting a detailed structuration at all scales, i.e. they do not lose details upon repeated magnifications or reductions. We used a method (Burrough 1981, 1983a) based on geostatistics and regionalised variable (RV) theory (Matheron 1971, Journel & Huijbregts 1978) to calculate fractal dimensions of physical parameters and *in vivo* fluorescence for each of the profiles. RVs are continuous variables whose variations are too complex to be described by traditional mathematical functions (Phillips 1985). Patterns of variation in RVs can then be expressed by their semivariance $\gamma(h)$, defined as:

$$\gamma(h) = \frac{1}{2N(h)}\sum_{i=1}^{N(h)}[Z(i) - Z(i+h)]^2 \quad (3)$$

where $Z(i+h)$ is the value of the dependent variable $Z(i)$ at a point separated from point i by distance, or lag, h, and $N(h)$ is the number of pairs of data points separated by the lag h. The semivariogram is the plot of $\gamma(h)$ as a function of h. The semivariance has, under certain conditions (e.g. see Berry & Lewis 1980 for further developments on the variance properties of the Weierstrass-Mandelbrot fractal function), the form of a fractal function that scales with h^{4-2D} at the origin; the fractal dimension D of the RV $Z(i)$ can thus be estimated from the slope m of a log-log plot of the semivariogram of $Z(i)$ (Burrough 1981, 1983a):

$$D = (4 - m)/2 \quad (4)$$

Because semivariogram estimates tend to deteriorate with increasing lag h for finite-length sample series (i.e. greater distances are more affected by low sample sizes and spurious properties of the data; Journel & Huijbregts 1978), an objective criterion is needed for deciding upon an appropriate range of h to include in the regressions. We used the values of h which maximised the coefficient of determination (r^2) and minimised the total sum of the squared residuals for the regression.

Semivariogram analysis requires the assumption of at least reduced stationarity, i.e. the mean and the variance of a time series depend only on its length and not on the absolute time (Platt & Denman 1975, Legendre & Legendre 1984). Stationarity was tested by calculating Kendall's coefficient of rank correlation, τ, between the series and the x-axis values in order to detect the presence of a linear trend (Kendall & Stuart 1966) [Kendall's coefficient of correlation was used in preference to Spearman's coefficient of correlation ρ, although the latter was recommended in Kendall (1976), because Spearman's ρ gives greater weight to pairs of ranks that are further apart, while Kendall's τ weights each disagreement in rank equally; see Sokal & Rohlf (1995) for further developments]. We thus eventually detrended the time series by fitting regressions to the original data by least squares and used the regression residuals in further analysis.

RESULTS

Physical data

The structure of the current speed and direction at 5 m (where the greatest number of data values were collected) presented 2 distinct patterns associated with an increase of the wind speed at Caplan and with the rise of a heavy swell at Grande-Rivière.

At Caplan, the time series could be divided in 2 parts according to the wind speed, which ranged from 1.9 m s^{-1} during the first 27 profiles to 6.6 m s^{-1} on and after the 28th profile (Lagadeuc et al. 1997). For all the profiles, current speed and direction were tidally dependent (Lagadeuc et al. 1997). However, as current direction was always directed to the west-northwest during flood and to the east-southeast during ebb, current speed depended on wind. During the first 27 profiles, current speed was less than 5 cm s^{-1} during flood, and approximately 40 to 50 cm s^{-1} during ebb. During windy profiles, highest speeds were observed during flood (around 15 cm s^{-1}), while during ebb, current speeds were approximately half this value (Lagadeuc et al. 1997).

At Grande-Rivière, current speed and direction were not significantly tidally dependent (autocorrelation, $p < 0.05$). However, before the swell (i.e. the first 29 profiles) the current was consistently directed to the north-northeast with a speed around 6 to 8 cm s^{-1}, whereas during the swell (on and after the 30th profile), the speeds were slightly higher (around 15 cm s^{-1}) with a west-southwest direction.

The vertical structure of the water column also presented 2 distinct patterns. At Caplan, these 2 patterns are

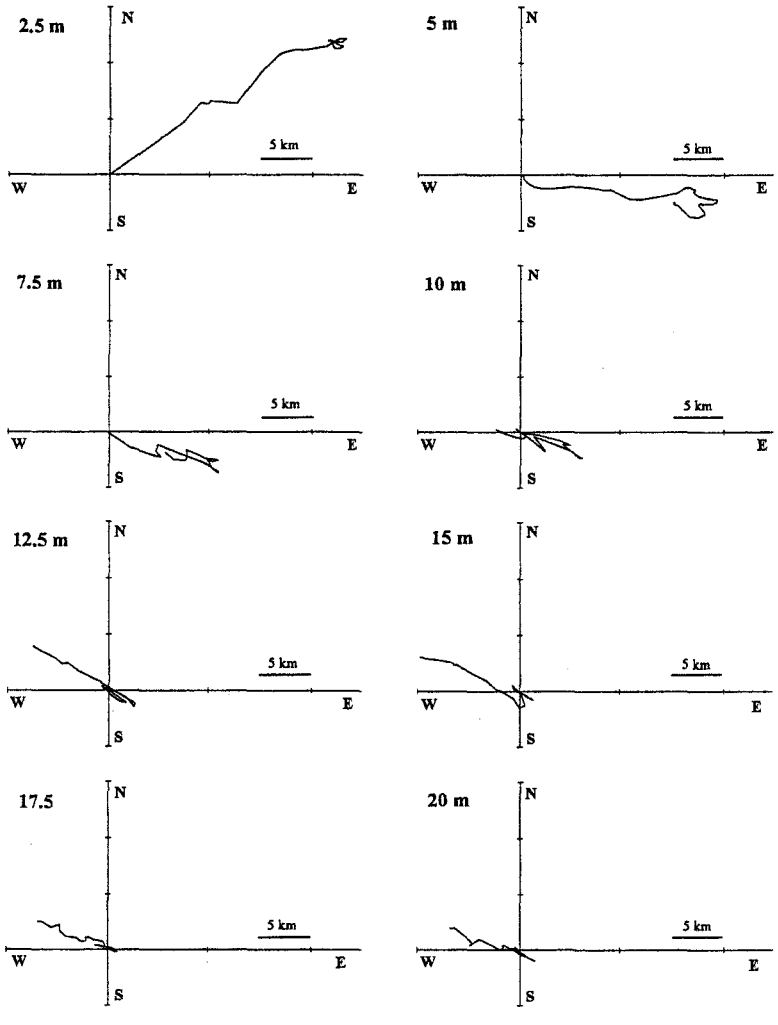

Fig. 2. Eulerian residual current in relation to depth at Caplan

perceptible from an unidirectional drift to the northeast which is stopped by the action of wind at 2.5 m (Fig. 2). For the other depths, a general pattern was observed for the effect of tide and wind on eulerian residual currents: southeastward drift followed by northwestward drift. Moreover, the magnitude of drift decreased near bottom, where the northwestward drift due to wind was stronger than the southeastward drift due to tide (Fig. 2). At Grande-Rivière, except at 2.5 m where the drift associated with the swell was west-northwest (Fig. 3), eulerian residual currents displayed similar patterns of variation whatever the depth: the north-northeast drift associated with tide before the swell was west-southwest thereafter (Fig. 3). As previously observed at Caplan, the amplitude of drifts decreased with depth, and the drift associated with the swell was always higher than the tidal drift (Fig. 3). In all cases, the drifts observed at Grande-Rivière were always 2 or 3 times smaller than those observed at Caplan.

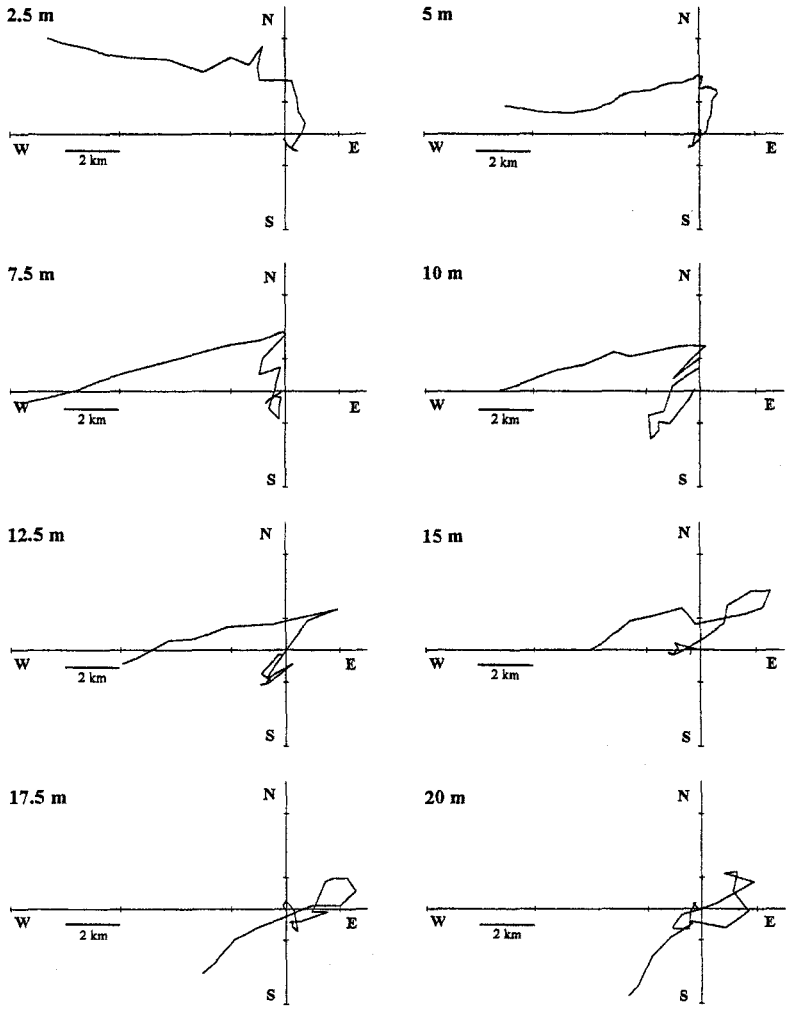

Fig. 3. Eulerian residual current in relation to depth at Grande-Rivière

During the first part of the cruise, alternative variations in intensity of stratification were tidally dependent at Caplan (Fig. 4a). Thereafter, progressive homogenisation was observed with the decrease of E_p. Dynamic stability Ri showed values less than 0.25 at the surface and near the bottom during windy profiles (Fig. 5a), which suggest a dynamic destabilisation (i.e. mixing) of the water column as opposed to the advection of mixed water. In contrast, at Grande-Rivière the water column was always homogeneous (i.e. mixed) with very low values of E_p (Fig. 4b) and values of dynamic stability Ri less than 0.25 at the surface during the 52 profiles and near the bottom, especially for profiles during swells (Fig. 5b).

In vivo fluorescence

In vivo fluorescence exhibited a vertical gradient at Caplan during the first part of the time series in relation to the stratification of the water column (Raby et al. 1994). During the second part of the time series, the vertical gradient was destroyed by water column mixing, and phytoplankton were evenly distributed. A fluorescence maximum was observed during the first part of the time series in the surface layer over the thermocline and was more than twice as large as the maximum observed at Grande-Rivière, where *in vivo* fluorescence was always homogeneously distributed.

Moreover, the computation of the cumulative sum series in both cases pointed out 2 distinct patterns of variability. At Caplan, except after profile 31 when the water column was homogenised by wind, we found the following recurrent trend: an increasing slope during flood which characterised a group of values lower than the mean, followed by a decreasing slope during ebb (Fig. 6a) that characterises some values higher compared to the whole series. Chlorophyll *a* (chl *a*) and *in vivo* fluorescence being highly correlated, as shown by Raby et al. (1994) on the same set of samples, *in vivo* fluorescence fluctuations can be related to the fluctuations of phytoplankton biomass.

In contrast, at Grande-Rivière, where hydrodynamic conditions were weaker, we found a diel periodicity,

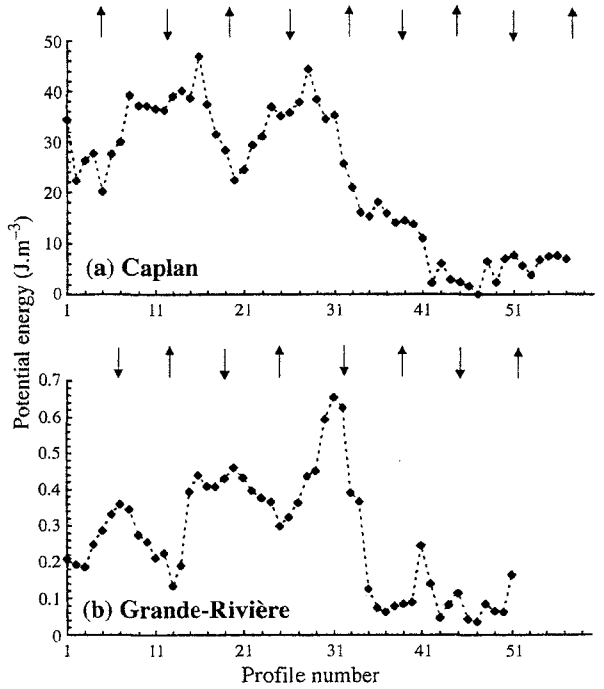

Fig. 4. Potential energy during the time series at (a) Caplan and (b) Grande-Rivière. ↑ and ↓ indicate high tide and low tide, respectively

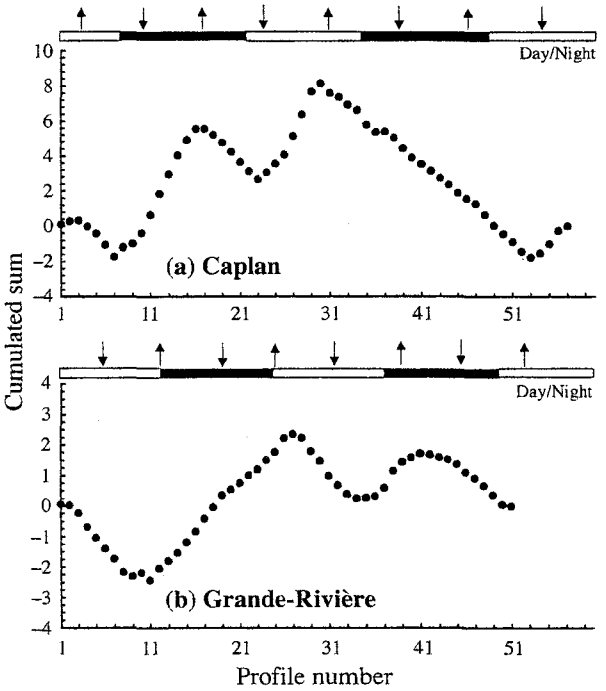

Fig. 6. Cumulative sum series of *in vivo* fluorescence at 4 m depth for (a) Caplan and (b) Grande-Rivière anchor stations. ↑ and ↓ indicate high tide and low tide, respectively

shown by an increasing slope during nighttime (i.e. from 2 h before sunset to 2 h before sunrise) and a decreasing slope during daytime (Fig. 6b). That behaviour might correspond to the decrease of *in vivo* fluorescence around the solar midday, corresponding to photoinhibition (Falkowski & Kiefer 1985), linked to a decrease of primary production as observed by Lizon et al. (1995) in low turbulent conditions and supported by the weak correlation between fluorescence and chl *a* (Raby et al. 1994).

Semivariogram analysis and fractal dimensions

The double logarithmic semivariograms for temperature, salinity and *in vivo* fluorescence time series at Caplan and Grande-Rivière together with their best fitting lines are given in Figs. 7 & 8, respectively. Only scales less than half of the total length of the data set are shown, because greater distances are more affected by low sample sizes and spurious properties of the data (Journel & Huijbregts 1978).

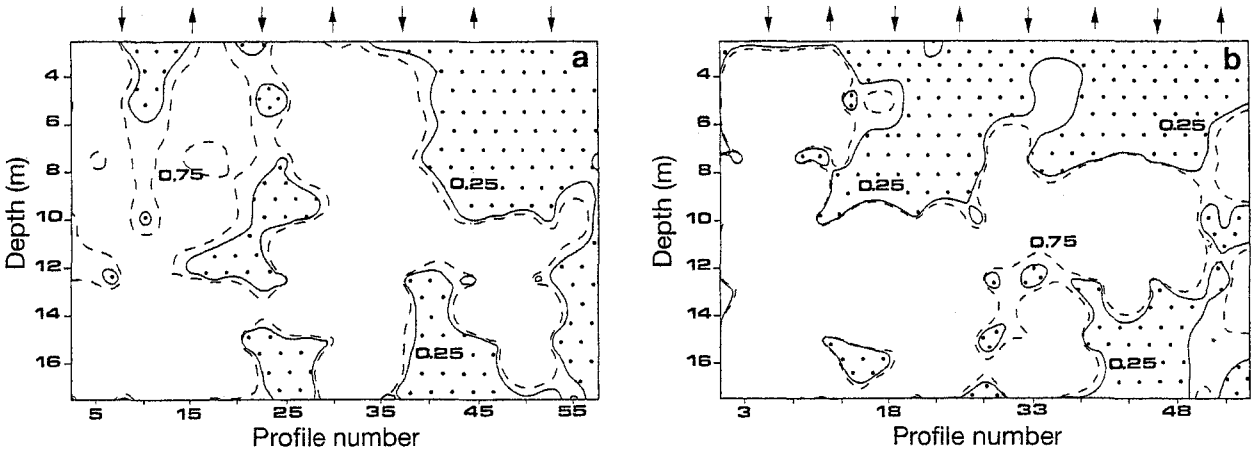

Fig. 5. Richardson number (*Ri*) in relation to depth and time at (a) Caplan and (b) Grande-Rivière. Hatched iso-*Ri* basins correspond to $Ri < 0.25$. ↑ and ↓ indicate high tide and low tide, respectively

At Caplan, temperature, salinity and *in vivo* fluorescence semivariograms exhibit similar behaviours. In the sub-surface (2 m; Fig. 7), their linearity over the whole range of time scales illustrates temporal dependence, suggesting that the same process can be regarded as the source of physical and biological patterns. This process can then be associated with the general drift to the northeast which clearly dominates the eulerian residual circulation pattern (cf. Fig. 2). From 5 to 11 m (Fig. 7); semivariograms exhibit a linear behaviour as the temporal lag increases up to 8 h. This behaviour is restricted to maximum time scales of 5 h for deeper layers. The scales of temporal dependence (i.e. semivariograms' linearity) can then be associated with characteristic time scales which are clearly depth-dependent (Fig. 7), and can be related to the progressive change in direction and intensity of the eulerian residual circulation (Fig. 2). The semivariograms are not influenced by that change of vertical structure, in spite of the transition observed between stratification and dynamic homogenisation of the water column due to the northwestward drift induced by the wind. Indeed, semivariogram analyses conducted separately on the stratified and the mixed part of the series revealed very similar linear behaviours (Fig. 9) which are indistinguishable from each other (*t*-test, $p > 0.05$; Zar 1984) and from the linear behaviour observed from the semivariogram analysis conduced on the whole series (covariance analysis, *F*-test, $p > 0.05$). These results thus suggest an extreme similarity—at a given depth—between the effects of different physical forcings such as wind or tide on the temporal structuration of variability of physical and biological parameters.

At Grande-Rivière, the situation is quite different (Fig. 8). Temperature semivariograms are clearly linear over the whole range of scales from the sub-surface to 15 m depth. At deeper layers the linearity is only observed for time scales increasing up to 5–6 h. Semivariograms of salinity are linear from the sub-surface to 15 m depth as the temporal lag increases up to about 16–18 h and linear deeper for time scales of about 6–8 h. As previously suggested at Caplan, the lost of scale dependence of semivariograms seems to be associated with the vertical structuration of the residual circulation in direction and intensity (Fig. 3). On the other hand, the differences observed in the time scales at which semivariograms of temperature and salinity lose linearity could be related to the specificity of salinity which, unlike temperature, is influenced by river discharge and mixing with water masses coming from outside the bay (Le Quéré 1992, Bonardelli et al. 1993) and exhibits a general temporal evolution more irregular than temperature, essentially deeper than 15 m (Le Quéré 1992). Semivariograms of *in vivo* fluorescence were linear for time scales of 6–8 h from the sub-surface to 17 m depth, and this specific behaviour of the fluorescence semivariograms can be related to the biological activity which is quite dominant (i.e. diel periodicity; cf. Fig. 6a), in comparison with the variability observed at Caplan which is mainly dominated by physical processes (i.e. tidal periodicity; cf. Fig. 6b).

In both cases, log-log linearity of scale-invariant parts of semivariograms is very strong, with coefficient of determination (r^2) ranging between 0.948 and 0.998 for temperature, 0.855 and 0.999 for salinity, and 0.905 and 0.999 for *in vivo* fluorescence at Caplan and 0.749 and 0.997 for temperature, 0.855 and 0.997 for salinity, and 0.959 and 0.999

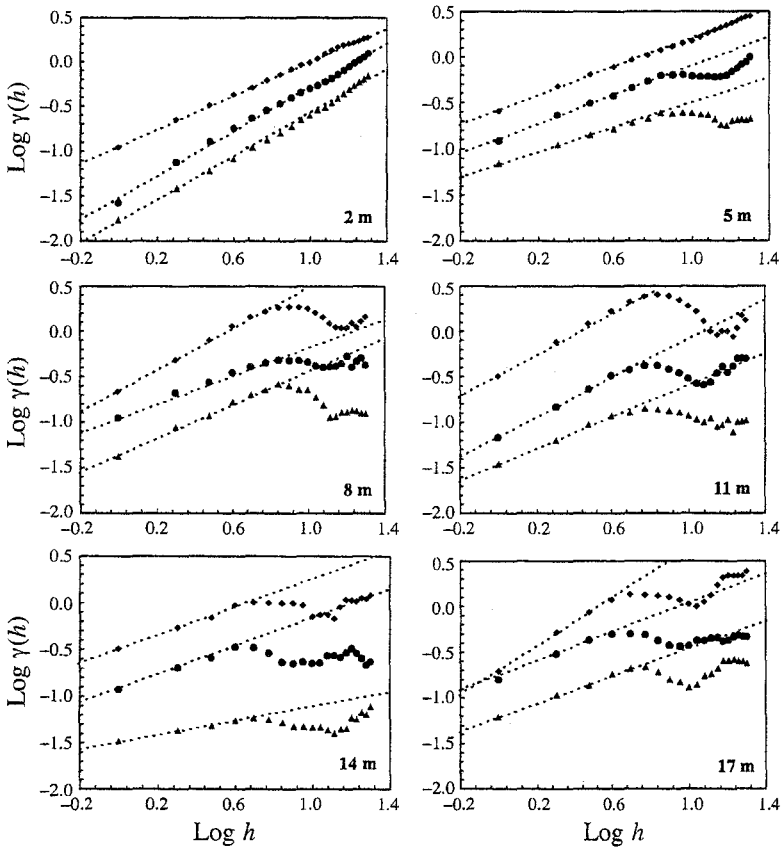

Fig. 7. Double logarithmic semivariograms of *in vivo* fluorescence (◆), temperature (●) and salinity (▲) for Caplan anchor station (curves have been vertically offset so as not to overlap). Straight dashed lines show the scaling range

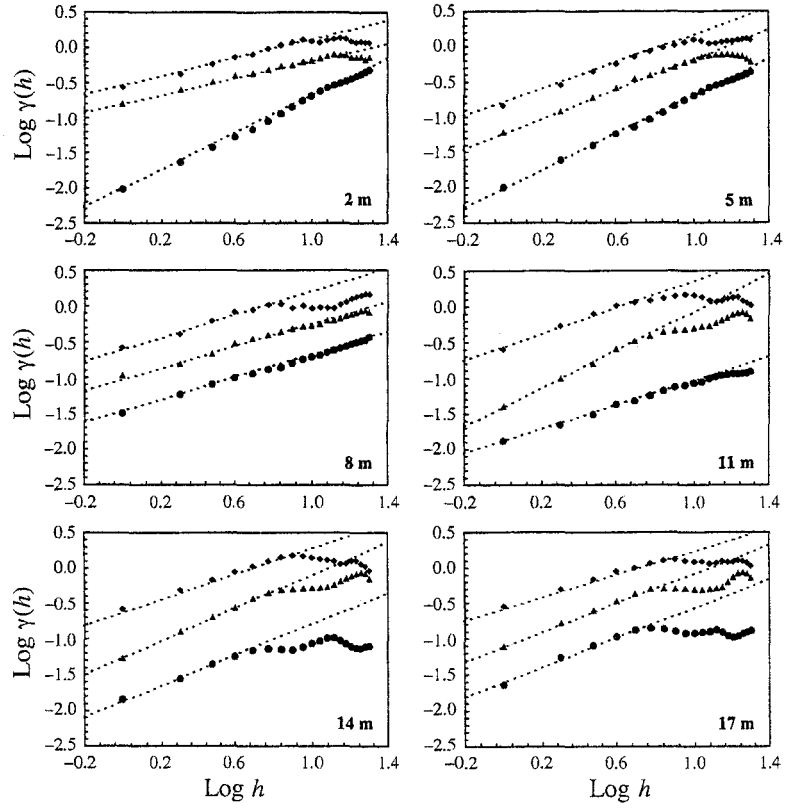

Fig. 8. Double logarithmic semivariograms of *in vivo* fluorescence (◆), temperature (●) and salinity (▲) for Grande-Rivière anchor station (curves have been vertically offset so as not to overlap). Straight dashed lines show the scaling range

for *in vivo* fluorescence at Grande-Rivière. The mean fractal dimensions of temperature, salinity and *in vivo* fluorescence were respectively 1.54 (± 0.02 SE), 1.69 (± 0.03 SE) and 1.48 (± 0.02 SE) at Caplan, and 1.5 (± 0.03 SE), 1.57 (± 0.02 SE) and 1.59 (± 0.01 SE) at Grande-Rivière. The mean empirical estimates of the fractal dimensions D_F of temperature, salinity and *in vivo* fluorescence exhibited different patterns of variation within stations and between stations. Thus, we showed that there were significant differences between salinity, temperature and *in vivo* fluorescence fractal dimensions for either station (Kruskal-Wallis test, $p < 0.05$). However, at Caplan mean fractal dimensions D_F of temperature, salinity and *in vivo* fluorescence were significantly different from each other (Jonckheere test, $p < 0.05$; Siegel & Castellan 1988), whereas at Grande-Rivière, mean fractal dimensions of salinity and *in vivo* fluorescence were not significantly different but were both significantly different from that of temperature (Jonckheere test, $p > 0.05$ and $p < 0.05$, respectively). On the other hand, mean fractal dimensions of salinity and *in vivo* fluorescence were significantly different between the 2 stations (Wilcoxon-Mann-Whitney *U*-test, $p < 0.05$), whereas there was no significant difference between mean fractal dimensions of temperature (Wilcoxon-Mann-Whitney *U*-test, $p > 0.05$). Fractal dimension D_F plotted as a function of depth (Fig. 10) leads to further conclusions. At Caplan (Fig. 10a), D_F of temperature, salinity and *in vivo* fluorescence exhibited similar patterns of variation, with a maximum value between 12 and 14 m depth, suggesting the influence of internal waves. In contrast, at Grande-Rivière the situation was quite different (Fig. 10b): fractal dimensions of temperature and *in vivo* fluorescence exhibit respectively maximum and minimum values around 10 m depth, while D_F of salinity exhibited a tendency to decrease from the sub-surface to bottom.

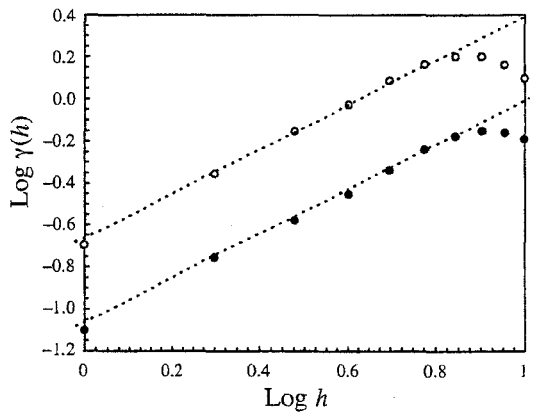

Fig. 9. Double logarithmic semivariograms of temperature at 4 m depth for Caplan anchor station before (○) and after (●) destratification by wind

DISCUSSION

The empirical estimates of the mean fractal dimensions D_F showed that the mean D_F of temperature is smaller than that of *in vivo* fluorescence and salinity at Caplan. This can be related with the processes likely to influence the variability of both temperature (T) and salinity (S). The T-S diagram (Fig. 11a) suggests an almost linear mixing of relatively warm ($T > 14°C$) and weakly saline ($27.5 < S < 29.5‰$) waters (A), with colder ($T < 14°C$) more saline ($S > 29.5‰$) waters (B), characteristic of the eastern part and to the mouth of

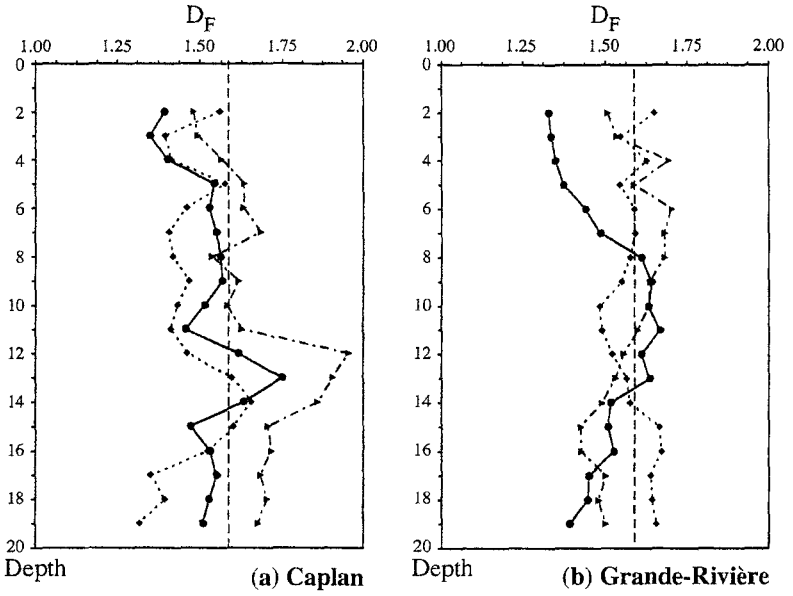

Fig. 10. Fractal dimensions (D_F) of in vivo fluorescence (♦), temperature (●) and salinity (▲) in relation to depth for (a) Caplan and (b) Grande-Rivière anchor stations. Straight broken lines correspond to the theoretical case $D_F = -5/3$

the bay, respectively (Legendre 1987). This distribution of water masses is associated with the cyclonic circulation of the Baie des Chaleurs observed during the sampling experiment (Le Quéré 1992) and has already been suggested to potentially modify the water mass properties of the Baie des Chaleurs by vertical mixing (Legendre & Watt 1970, Legendre 1987). Moreover, temperature fluctuations are mainly dependent on atmospheric (i.e. seasonal) warming and cooling whereas salinity is mainly influenced by river and precipitation runoffs leading to smaller scales variations. The intermediate value of the fractal dimension of *in vivo* fluorescence might then be regarded as a result of the interactions between these 2 different forcings. At Grande-Rivière the mean fractal dimension of temperature is smaller than those of salinity and *in vivo* fluorescence, which are not significantly different, indicating that variability of biological processes is mainly determined by salinity and is characterised by short-range variations in comparison with temperature. Indeed, the T-S diagram (Fig. 11b) shows the strong influence of weakly saline ($S < 29.5‰$) waters, different from the water masses typical of the mouth of the bay (B, Fig. 11a) and associated with the rise of a west-southwest heavy swell after the 30th profile (cf. Fig. 3) of the sampling experiment. The properties of these water masses (i.e. in terms of temperature and salinity) are roughly similar to those observed in the upper water masses of the Gulf of St. Lawrence, Canada (Lauzier 1957, Dickie & Trites 1983). The shift in the main current direction associated with the rising swell can then be suggested as being caused by the strengthening of the influence of the Gaspé current (Bugden 1981) on the northern coast of the Baie des Chaleurs, where it is usually weak, indeed lacking, as previously observed (Le Quéré 1992, Bonardelli et al. 1993). The associated time scales are then small compared with those associated with the seasonal forcing on temperature variability, leading to a perceived higher homogeneity.

The different fractal dimensions observed between stations lead to further conclusions. Mean fractal dimensions of temperature are not significantly different, whereas mean fractal dimensions of salinity and *in vivo* fluorescence are significantly different at Caplan to those at Grande-Rivière. This suggests that the physical forcings (i.e. mainly atmospheric) responsible for the temperature variability are on an equivalent space-time scale at Caplan and Grande-Rivière. On the other hand, salinity appears to be associated with more homogeneous space-time patterns at Caplan than at

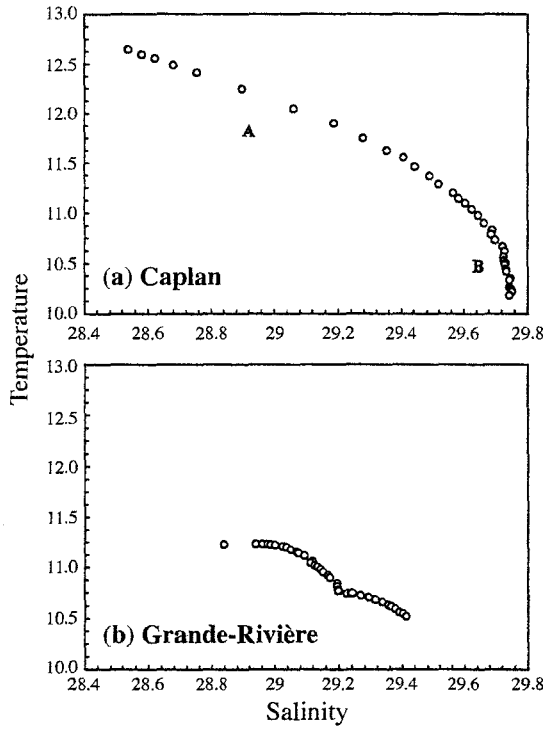

Fig. 11. Temperature-salinity diagrams for (a) Caplan (for explanation of A and B see 'Discussion') and (b) Grande-Rivière anchor stations

Grande-Rivière (i.e. D_F was greater at Caplan, showing the predominance of short-range processes at Caplan). This last observation agrees with our previous observations concerning the different forcing processes at Caplan and Grande-Rivière. In contrast, *in vivo* fluorescence shows a more heterogeneous structuration at Caplan than at Grande-Rivière (i.e. D_F greater at Grande-Rivière), indicating the prevalence of short-range variability and thus of biological processes when the hydrodynamical forcings are less developed (cf. Figs. 2 to 5).

Comparison of the estimated mean fractal dimensions of temperature, salinity and *in vivo* fluorescence with those of other environmental data shows that the variations of these variables are always more homogeneous than those of landform (Mandelbrot 1977), seismicity frequency (Khattri 1995), river discharge, geological sediment and climate data (Mandelbrot & Wallis 1969), and more heterogeneous than the variability perceived in soil properties (Burrough 1981, 1983a), spatial distribution of plant communities (Palmer 1988) and spatial distribution of marine birds and their zooplanktonic preys (Russel et al. 1992). We have no clear phenomenological explanation for these differences, though empirical D_F might be directly linked to the nature of the processes generating the observed patterns. Indeed, geological fluctuations associated with earthquake occurrence are associated with large-scale processes (in time or space; e.g. periods of about 100 yr; see e.g. Khattri 1995) and lead to low fractal dimensions corresponding to long-range trends and thus to a great heterogeneity. In contrast, fluctuating data associated with smaller-scale processes, such as turbulent motion, widely recognised as a controlling factor of plankton distribution (Legendre & Demers 1984, Mackas et al. 1985), are expected to lead to higher fractal dimensions (Burrough 1981, 1983a). Our empirical D_F can also be compared to the fractal dimension D_β estimated from the theoretical spectral exponent β ($\beta = 5/3$) characterising isotropic and homogeneous turbulent processes (Kolmogorov 1941, Obukhov 1941). D_β is estimated as $D_\beta = 2 - (\beta - 1)/2$ (Feder 1988, Schroeder 1991). From a statistical viewpoint, most D_F are significantly different from D_β (modified *t*-test; Scherrer 1984). Moreover, as previously suggested, D_F values reflect the balance of short- and long-range variations, and therefore the differences observed between D_F and D_β are associated with the theoretical spectral exponent β, as the differences observed in the empirical estimations of β might be related to the different space-time scales of the related external physical forcings (Platt 1972, Denman & Platt 1975, 1976, Platt & Denman 1975, Powell et al. 1975, Fasham & Pugh 1976, Denman et al. 1977, Horwood 1978, Lekan & Wilson 1978, Demers et al. 1979, Wiegand & Pond 1979, Seuront et al. 1996a, b, Seuront 1997).

At Caplan, no differences could be observed in the fractal dimensions of the data from the first and second day despite the increase in wind speed. Generally speaking, mixing processes in the ocean are responsible for the transfer of kinetic energy from the largest to the smallest scales, spanning several orders of magnitude from the basin scales down to the viscous scales (i.e. the Kolmogorov length scale, λ_k) at which turbulent energy is dissipated as heat by molecular viscosity (Denman & Gargett 1995). The range of spatial scales over which turbulence, or at least mixing, occurs is intrinsically linked to the dissipation rate of turbulent kinetic energy (ε) by the way of the Kolmogorov length and time scales λ_k and τ_k [$\lambda_k = (\nu^3/\varepsilon)^{1/4}$ and $\tau_k = (\nu/\varepsilon)^{1/2}$, where ν is the kinematic viscosity) and thus to the hydrodynamic conditions. The dissipation rate of wind turbulent kinetic energy ε ($m^2\ s^{-3}$) was estimated as $\varepsilon = (5.82 \times 10^{-9})W^3/z$, where W is the wind speed ($m\ s^{-1}$) and Z the depth (m) (MacKenzie & Leggett 1993). This dissipation rate, averaged over the water column for the 2 periods (i.e. before and after the increase in the wind speed), increased from 7.18×10^{-9} $m^2\ s^{-3}$ to 3.01×10^{-7} $m^2\ s^{-3}$, leading to a decrease in the Kolmogorov length and time scales λ_k and τ_k (from 3.43 to 1.35 mm and from 11.78 to 1.82 s, respectively) and thus to an increase in the range of time and space scales affected by turbulent motions. However, this increase in the range of turbulent space-time scales is far from being perceptible from our hourly sampling interval which can thus be proposed to explain the non significant differences between fractal dimensions before and after the destratification of the water column by wind (cf. Fig. 9) and thus does not allow any inferences about the effects of varying hydrodynamic conditions on the structure—in terms of homogeneity or heterogeneity, and thus in terms of short- or long-range variability—of this pelagic environment. Moreover, the structure of phytoplankton biomass appears to be independent of the concentration since a decrease of 40% of the total biomass between the first and the second part of the cruise (Raby et al. 1994) was not associated with a change in the estimated fractal dimension or the characteristic scale-breaking observed in the semivariograms. Furthermore, as the phytoplankton assemblage was very similar over the sampling period (Mingelbier 1995), we cannot test any potential specific effects on fluorescence fractal dimensions.

On the other hand, it is worth noting that the vertical distribution of the mean D_F of temperature, salinity and *in vivo* fluorescence at Caplan (Fig. 10a) can be related to the time-averaged vertical distribution of the Richardson number, *Ri* (Fig. 12a). The minimum and maximum values of D_F can be associated respectively with the least stable (i.e. low *Ri*, surface layers and near the bottom) and stable (i.e. high *Ri*, mid-depth)

water masses. Thus, in surface layers and near the bottom, where mixing processes are more developed, the low dynamic stability leads to low fractal dimensions showing—at the time-space scales of the study—the predominance patterns irregularly distributed in space and time and thus, characterised by long-range variations. On the other hand, at mid-depth, the greater dynamic stability tends to damp out any kind of fluctuations, leading to less structured patterns with close scales of variation, characterised by higher fractal dimensions and suggesting a potential aliasing of internal waves. The situation is quite different at Grande-Rivière (Fig. 10b), where the maximum value of the mean *Ri* (Fig. 12b) can be related to the maximum and minimum values of the fractal dimensions of temperature and *in vivo* fluorescence, respectively. This last observation shows that in weak hydrodynamic conditions *in vivo* fluorescence exhibits a very specific behaviour, far from physical control, showing that the biological activity and its associated variability are more developed in stable conditions (i.e. high *Ri*). In the case of salinity, we have no clear explanation to propose for the decreasing tendencies of the mean fractal dimension which can, however, be related to the interactions between the characteristic water masses of the mouth of the bay and the water masses advected by the west-southwest drift induced by the swell. Consequently, the differences observed between our low and high empirical D_F can be explained in terms of different range of scales perceived in pattern variability and thus in the complexity of the pattern structure.

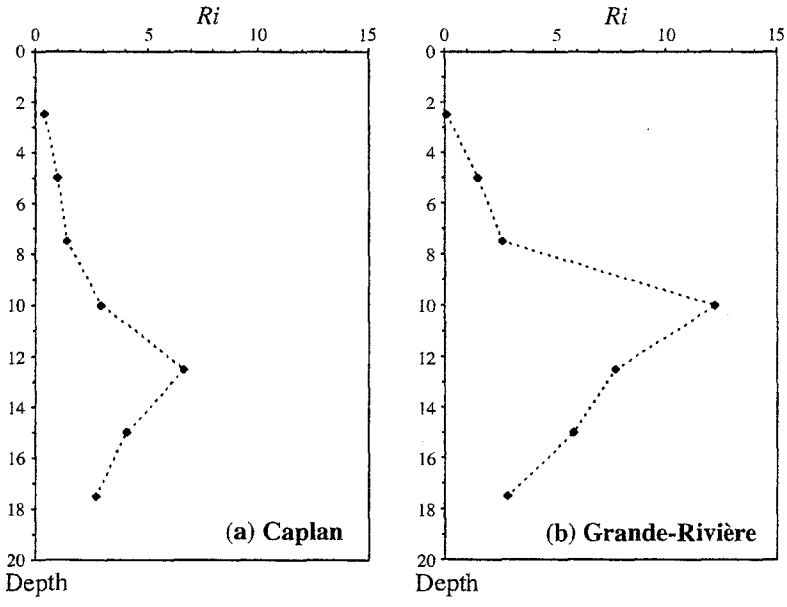

Fig. 12. Time-averaged Richardson number (*Ri*) in relation to depth for (a) Caplan and (b) Grande-Rivière anchor stations

Beyond the numerical values of fractal dimensions, semivariogram analysis can also provide information about the scaling behaviour of a given process. Thus, the fractal dimension is not necessarily a constant over varying sampling intervals (Palmer 1988). We cannot test the scale invariance of temporal patterns of temperature, salinity and *in vivo* fluorescence in that way because of the small number of data values available in the analysis and because the semivariance does not always increase monotonically with increasing lag (Fig. 7), but appears to increase in a series of steps (Figs. 7 & 8). In the case of ideal fractals, like Brownian fractal functions (Burrough 1983a, b), the semivariogram shows clear range and sill (e.g. see Phillips 1985 for further details), leading to the assertion that the data show at least local second-order stationarity (Journel & Huijbregts 1978). Increasing the size of the inter-sample distance, however, frequently leads to observation of increased semivariance (Burrough 1983a) implying that new scales of variation have been encountered. This stepwise behaviour (i.e. changes in fractal dimension when shifting between scales) implies that in place of true self-similarity, temperature, salinity and *in vivo* fluorescence show only partial self-similarity over limited range of scales separated by transition zones (Mandelbrot 1977, 1983), where the environmental properties or constraints acting upon organisms are probably changing rapidly (Frontier 1987; also e.g. the landscape patterns analysed by Krummel et al. 1987 and Palmer 1988). In the Baie des Chaleurs (i.e. at Caplan and Grande-Rivière), the departures from true self-similarity seem to be associated with the progressive change in the eulerian residual circulation with depth (cf. Figs. 2 & 3). Indeed, the change of direction of the eulerian residual circulation can be suggested as a possible source of scale breaking between scale dependence and scale independence, in so far as the loss of self-similarity of semivariograms seems to be associated with the depth, showing a reversal in the direction of the residual circulation of water masses (Figs. 2 & 3). These factors, their combinations and/or the interactions with water masses coming from river discharge or outside the bay can be proposed as possible sources of variability and thus could be responsible not only for the different time scales of temporal dependence of variogram analysis but also for the absence of scale-invariant structuration after the scale breaking. These departures

from true self-similarity, rather than the precise numerical values of the fractal dimension, may be of most interest to ecologists, because such departures indicate variation in the sources of biological patterns (Burrough 1983a, Bradbury et al. 1984, Russel et al. 1992). As an example, the critical range represented by the well-known 'Platt-knee' corresponds to the transition zone (at a scale between 0.2 and 20 km; Platt & Denman 1975, Denman & Platt 1976, Denman et al. 1977) between scales dominated by physical processes and larger scales dominated by the combination of biological activities, such as growth, sinking, or community interactions. However, unlike the previous case, our results do not show any characteristic scales which can be obviously related to a well-known physical or biological transition zone.

To date, most studies using fractal approaches have focused on phenomena which are temporally invariant over the scale of the study (e.g. vegetation patterns, Palmer 1988; coral reefs structure, Bradbury & Reichelt 1983, Bradbury et al. 1984; or geological formations, Burrough 1983a) and we are not aware of any reports of a temporal fractal approach. However, our sampling experiments have been conducted at anchor stations (i.e. an eulerian point of view), so that temporal and spatial components of variation are inextricably confounded in our data. This confounding of space and time has already been pointed out by Russel et al. (1992) in a study of the 'spatial' distributions of marine birds and their food and might be suggested as a possible source of bias in the estimation of fractal dimensions. Nonetheless, the estimated fraction dimensions are consistent with the global physical structure of both stations and can thus be regarded as a useful index of the complexity perceived in time series of temperature, salinity and *in vivo* fluorescence.

These results, suggesting relationships exist between the vertical structure of the water column (i.e. dynamic stability and residual circulation), fractal dimensions and the characteristic scale breaking between temporal dependence and independence thus lead us to consider a physical control of temperature, salinity and *in vivo* fluorescence variability at Caplan associated with high hydrodynamic conditions and a slightly more complex situation at Grande-Rivière, where, probably because of the weak hydrodynamism and the peculiar pattern of water masses circulation, temperature, salinity and *in vivo* fluorescence exhibit more specific patterns of variations. However, it can also be suggested that the differences observed between fractal dimensions may be caused by processes exhibiting very specific intermittent behaviours. Indeed, previous studies conducted on zooplankton data (Pascual et al. 1995), temperature and *in vivo* fluorescence (Seuront et al. 1996a, b) have shown that the best tool to describe intermittent fields is provided by multifractal theory. Multifractal analysis, inadequate in the present study because of the small number of data available, can be regarded as a statistical generalisation of fractal theory (Mandelbrot 1977, 1983) leading to the consideration of multifractal fields as a hierarchy of sets each with its own fractal dimension. Thus multifractal fields are described by scaling relations that require a family of different exponents, rather than the single exponent of 'traditional' fractal patterns, which then characterise variability in a very limited way. Furthermore, despite the apparent complexity induced by a multifractal framework, using the universal multifractal formalism (Schertzer & Lovejoy 1987, 1989)—recently successfully applied to oceanic fields (Seuront et al. 1996a, b, Seuront 1997)—the distribution of a scalar field can be wholly described with only 3 indices, which summarise the whole statistical behaviour from larger to smaller scales.

Nevertheless, fractals provide a workable middle ground between the excessive geometric order of Euclid and the geometric chaos of roughness and fragmentation (Mandelbrot 1989), and appear to be particularly well adapted to the study of multiscale environments such as pelagic ecosystems. However, even though the results of this fractal analysis should have probably been more illustrative by considering a finer grain and a greater extent, which are often regarded as some of the main aspects of the scales of a study (Legendre & Fortin 1989, Wiens 1989, Jarvis 1995), they are consistent with more classical techniques concerning the time-space physical structure of the studied environments, and thus appear to be quite satisfactory. Furthermore, the value of geostatistical analysis is that different and complex dynamics can be described in a common format that allows direct comparisons to be made among systems. One should be aware, however, that the generic name 'fractal dimension' deals with different concepts of dimensions: topological dimension, Hausdorff dimension, self-similarity dimension, box-counting dimensions and information dimension among others. They are all related, sometimes they are the same and sometimes different, and that can be confusing even for a research mathematician (Peitgen et al. 1992). Practically, for ecologists, this means that at present it is only possible to compare different estimates of fractal dimension when the same calculation technique is used. There is, therefore, a need to calibrate different methods of calculating fractal dimensions and until this is done, comparisons of D_F values of similar phenomena reported in the literature, obtained with different techniques, are of limited value.

Acknowledgements. We greatly acknowledge C. Luczak and F. Lizon for stimulating and constructive discussions on the subject. We are also thankful to V. Gentilhomme for her com-

ments on the manuscript and to D. Schertzer, F. Schmitt and 4 anonymous referees for their remarks and suggestions which greatly improved the manuscript.

LITERATURE CITED

Berry MV, Lewis ZV (1980) On the Weierstrass-Mandelbrot fractal function. Proc R Soc Lond A 370:459–484

Bivand R (1980) A Monte Carlo study of correlation coefficient estimation with spatially autocorrelated observations. Quaest Geogr 6:5–10

Bonardelli JC, Himmelman JH, Drinkwater K (1993) Current variability and upwelling along the North shore of Baie des Chaleurs. Atmos-Ocean 31:541–565

Bradbury RH, Reichelt RE (1983) Fractal dimension of a coral reef at ecological scales. Mar Ecol Prog Ser 10:169–171

Bradbury RH, Reichelt RE, Green DG (1984) Fractals in ecology: methods and interpretation. Mar Ecol Prog Ser 14:295–296

Bugden GL (1981) Salt and heat budgets for the Gulf of St-Lawrence. Can J Fish Aquat Sci 38:1153–1167

Bundy MH, Gross TF, Coughlin DJ, Strickler JR (1993) Quantifying copepod searching efficiency using swimming patterns and perceptive ability. Bull Mar Sci 53:15–28

Burrough PA (1981) Fractal dimensions of landscape and other environmental data. Nature 294:240–242

Burrough PA (1983a) Multiscale sources of spatial variation in soil. I. The application of fractal concepts to nested levels of soil variation. J Soil Sci 34:577–597

Burrough PA (1983b) Multiscale sources of spatial variation in soil. II. A non-Brownian fractal model and its application to soil survey. J Soil Sci 34:599–620

Demers S, Lafleur PE, Legendre L, Trump CL (1979) Short-term covariability of chlorophyll and temperature in the St. Lawrence Estuary. J Fish Res Bd Can 36:568–573

Denman KL, Gargett AE (1995) Biological-physical interactions in the upper ocean: the role of vertical and small scale transport processes. Annu Rev Fluid Mech 27: 225–255

Denman KL, Okubo A, Platt T (1977) The chlorophyll fluctuation spectrum in the sea. Limnol Oceanogr 22:1033–1038

Denman KL, Platt T (1975) Coherences in the horizontal distributions of phytoplankton and temperature in the upper ocean. Mém Soc R Sci Liège Collect 6:19–30

Denman KL, Platt T (1976) The variance spectrum of phytoplankton in a turbulent ocean. J Mar Res 34:593–601

Denman KL, Powell TM (1984) Effects of physical processes on planktonic ecosystems in the coastal ocean. Oceanogr Mar Biol Annu Rev 22:125–168

Dickie LM, Trites RW (1983) The Gulf of St-Lawrence. In: Ketchum BH (ed) Estuaries and enclosed seas. Elsevier, Amsterdam, p 403–425

Downing JA (1991) Biological heterogeneity in aquatic ecosystems. In: Kolasa J, Pickett STA (eds) Ecological heterogeneity. Springer Verlag, New York, p 160–180

Downing JA, Pérusse M, Frenette Y (1987) Effect of inter-replicate variance on zooplankton sampling design and data analysis. Limnol Oceanogr 32:673–680

Dutilleul P, Legendre P (1993) Spatial heterogeneity against heteroscedasticity: an ecological paradigm versus a statistical concept. Oikos 66:152–171

Erlandson J, Kostylev V (1995) Trail following, speed and fractal dimension of movement in a marine prosobranch, *Littorina littorea*, during a mating and a non-mating season. Mar Biol 122:87–94

Falkowski PG, Kiefer DA (1985) Chlorophyll a fluorescence in phytoplankton: relationship to photosynthesis and biomass. J Plankton Res 7:715–731

Fasham MJR, Pugh PR (1976) Observations on the horizontal coherence of chlorophyll *a* and temperature. Deep Sea Res 23:527–538

Feder J (1988) Fractals. Plenum, New York

Frontier S (1972) Calcul de l'erreur sur un comptage de zooplancton. J Exp Mar Biol Ecol 8:121–132

Frontier S (1985) Diversity and structure in aquatic ecosystems. Oceanogr Mar Biol Annu Rev 23:253–312

Frontier S (1987) Applications of fractal theory to ecology. In: Legendre P, Legendre L (eds) Developments in numerical ecology. Springer Verlag, Berlin, p 335–378

Frontier S (1994) Species diversity as a fractal property of biomass. In: Nowak MM (ed) Fractals in the natural and applied sciences (A-41). Elsevier, Amsterdam, p 119–127

Gee JM, Warwick RM (1994a) Body-size distribution in a marine metazoan community and the fractal dimensions of macroalgae. J Exp Mar Biol Ecol 178:247–259

Gee JM, Warwick RM (1994b) Metazoan community structure in relation to the fractal dimensions of marine macroalgae. Mar Ecol Prog Ser 103:141–150

Grey-Smith P (1979) Pattern in vegetation. J Ecol 67:755–779

Haury LR, McGowan JA, Wiebe PH (1978) Patterns and processes in the time-space scales of plankton distributions. In: Steele JH (ed) Spatial pattern in plankton communities. Plenum, New York, p 277–327

He F, Legendre P, Bellehumeur C (1994) Diversity pattern and spatial scale: a study of a tropical rain forest of Malaysia. Environ Ecol Stat 1:265–286

Horwood JW (1978) Observations on spatial heterogeneity of surface chlorophyll in one and two dimensions. J Mar Biol Assoc UK 58:487–502

Hurlbert SH (1990) Spatial distribution of the montane unicorn. Oikos 58:257–271

Ibanez F, Fromentin JM, Castel J (1993) Application de la méthode des sommes cumulées à l'analyse des séries chronologiques en océanographie. C R Acad Sci Paris 316: 745–748

Jarvis PG (1995) Scaling processes and problems. Plant Cell Environ 18:1079–1089

Journel AG, Huijbregts CJ (1978) Mining geostatistics. Academic Press, London

Kaandorp JA (1991) Modelling growth forms of the sponge *Haliclona oculata* (Porifera, Demospongiae) using fractal techniques. Mar Biol 110:203–215

Kaandorp JA, Dekluijver MJ (1992) Verification of fractal growth models of the sponge *Haliclona oculata* (Porifera) with transplantation experiments. Mar Biol 113:133–143

Kendall M (1976) Time-series, 2nd edn. Charles Griffin and Co Ltd, London

Kendall M, Stuart A (1966) The advanced theory of statistics. Hafner, New York

Khattri KN (1995) Fractal description of seismicity of India and inferences regarding earthquake hazard. Curr Sci 69: 361–366

Kolasa J, Rollo DC (1991) The heterogeneity of heterogeneity: a glossary. In: Kolasa J, Pickett STA (eds) Ecological heterogeneity. Springer Verlag, New York, p 1–23

Kolmogorov AN (1941) The local structure of turbulence in incompressible viscous fluid with very large Reynolds numbers. Dokl Akad Nauk SSSR 30:299–303

Krummel JR, Gardner RH, Sugihara G, O'Neill RV, Coleman PR (1987) Landscape patterns in a disturbed environment. Oikos 48:321–324

Lagadeuc Y, Boulé M, Dodson JJ (1997) Effect of vertical mixing on the vertical distribution of copepods in coastal

waters. J Plankton Res 19:1183–1204
Lauzier LM (1957) Variations of temperature and salinity in shallow waters of the southwestern Gulf of St-Lawrence. Bull Fish Res Bd Can 111:251–268
Legendre L (1987) Multidimensional contingency table analysis as a tool for biological oceanography. Biol Oceanogr 5: 13–28
Legendre L, Demers S (1984) Towards dynamic biological oceanography and limnology. Can J Fish Aquat Sci 41: 2–19
Legendre L, Fortin MJ (1989) Spatial pattern and ecological analysis. Vegetatio 80:1055–1067
Legendre L, Legendre P (1984) Ecologie numérique, Vol 2, 2nd edn. Masson, Paris
Legendre L, Watt WD (1970) The distribution of primary production relative to a cyclonic gyre in Baie des Chaleurs. Mar Biol 7:167–170
Lekan JF, Wilson RE (1978) Spatial variability of phytoplankton biomass in the surface waters of Long Island. Estuar Coast Mar Sci 6:230–251
Le Quéré C (1992) Physical oceanography of the Baie des Chaleurs, Gulf of St. Lawrence. MSc thesis, McGill University, Montréal
Li X, Logan BE (1995) Size distribution and fractal properties of particles during a simulated bloom in a mesocosm. Deep Sea Res I 42:125–138
Lizon F, Lagadeuc Y, Brunet C, Aelbrecht D, Bentley D (1995) Primary production and photoadaptation of phytoplankton in relation with tidal mixing in coastal waters. J Plankton Res 17:1039–1055
Logan BE, Kilps JR (1995) Fractal dimensions of aggregates formed in different fluid mechanical environments. Wat Res 29:443–453
Longuet-Higgins MS (1994) A fractal approach of breaking waves. J Phys Oceanogr 24:1834–1838
Lovejoy S (1982) Area-perimeter relation for rain and cloud areas. Science 216:185–187
Mackas DL, Boyd CM (1979) Spectral analysis of zooplankton spatial heterogeneity. Science 204:62–64
Mackas DL, Denman KL, Abbot MR (1985) Plankton patchiness: biology in the physical vernacular. Bull Mar Sci 37:652–674
MacKenzie BR, Leggett WC (1993) Wind-based models for estimating the dissipation rates of turbulence energy in aquatic environments: empirical comparisons. Mar Ecol Prog Ser 94:207–216
Mandelbrot B (1977) Fractals. Form, chance and dimension. Freeman, London
Mandelbrot B (1983) The fractal geometry of nature. Freeman, New York
Mandelbrot B (1989) Fractal geometry: what is it and what does it do? In: Fleischmann M, Tildesley DJ, Ball RC (eds) Fractals in the natural sciences. Princeton University Press, Princeton, NJ, p 3–16
Mandelbrot B, Wallis JR (1969) Some long-run properties of geophysical records. Wat Resour Res 5:321–340
Mann KH, Lazier JRN (1991) Dynamics of marine ecosystems. Biological-physical interactions in the ocean. Blackwell Scientific Publications, Boston
Matheron G (1971) La théorie des variables régionalisées et ses applications. Cah CMM Fontainebleau 5:1–212
Milne BT (1988) Measuring the fractal geometry of landscapes. Appl Math Comput 27:67–79
Mingelbier M (1995) Controle différentiel de la taille du phytoplancton marin dans les eaux côtières tempérées (Baie des Chaleurs, Golfe du St Laurent). PhD thesis, Université Laval
Naeem S, Colwell RK (1991) Ecological consequences of heterogeneity of consumable resources. In: Kolasa J, Pickett STA (eds) Ecological heterogeneity. Springer Verlag, New York, p 224–255
Obukhov AM (1941) Spectral energy distribution in a turbulent flow. Dokl Akad Nauk SSSR 32:22–24
Olsson J, Niemczynowicz J, Berndtsson R, Larson L (1992) An analysis of the rainfall time structure by box counting—some practical implications. J Hydrol 137:261–277
Palmer MW (1988) Fractal geometry: a tool for describing spatial patterns of plant communities. Vegetatio 75:91–102
Pascual M, Ascioti FA, Caswell H (1995) Intermittency in the plankton: a multifractal analysis of zooplankton biomass variability. J Plankton Res 17:1209–1232
Peitgen HO, Jügens H, Saupe D (1992) Chaos and fractal: new frontiers of science. Springer-Verlag, New York
Pennycuick CJ, Kline NC (1986) Units of measurement for fractal extent, applied to the coastal distribution of bald eagle nests in the Aleutian Islands, Alaska. Oecologia 68: 254–258
Phillips JD (1985) Measuring complexity of environmental gradients. Vegetatio 64:95–102
Platt T (1972) Local phytoplankton abundance and turbulence. Deep Sea Res 19:183–187
Platt T, Denman KL (1975) Spectral analysis in ecology. Annu Rev Ecol Syst 6:189–210
Platt T, Sathyendranath S (1988) Oceanic primary production: estimation by remote sensing at local and regional scales. Science 241:1613–1620
Pond S, Pickard GL (1983) Introductory dynamical oceanography, 2nd edn. Pergamon Press, Oxford
Powell TM, Richerson PJ, Dillon TM, Agee BA, Dozier BJ, Godden DA, Myrup LO (1975) Spatial scales of current speed and phytoplankton biomass fluctuations in Lake Tahoe. Science 189:1088–1090
Raby D, Lagadeuc Y, Dodson JJ, Mingelbier M (1994) Relationship between feeding and vertical distribution of bivalve larvae and mixed waters. Mar Ecol Prog Ser 130: 275–284
Risser PG, Karr JR, Forman RTT (1984) Landscape ecology: directions and approaches. Nat Hist Surv Spec Pub No. 2
Russel RW, Hunt GL, Coyle KO, Cooney RT (1992) Foraging in a fractal environment: spatial patterns in a marine predator-prey system. Landscape Ecol 7:195–209
Scherrer B (1984) Biostatitisques. Gaëtan Morin, Boucherville
Schertzer D, Lovejoy S (1987) Physically based rain and cloud modeling by anisotropic multiplicative turbulent cascades. J Geophys Res 92:9693–9714
Schertzer D, Lovejoy S (1989) Nonlinear variability in geophysics: multifractal analysis and simulation. In: Pietronero L (ed) Fractals: physical origin and consequences. Plenum, New York, p 49–79
Schroeder M (1991) Fractals, chaos, power laws. Minutes from an infinite paradise. Freeman, New York
Seuront L (1997) Distribution inhomogène multi-échelle de la biomasse phytoplanctonique en milieu turbulent. J Rech Océanogr 22:9–16
Seuront L, Schmitt F, Lagadeuc Y, Schertzer D, Lovejoy S, Frontier S (1996a) Multifractal analysis of phytoplankton biomass and temperature in the ocean. Geophys Res Lett 23:3591–3594
Seuront L, Schmitt F, Schertzer D, Lagadeuc Y, Lovejoy S (1996b) Multifractal intermittency of Eulerian and Lagrangian turbulence of ocean temperature and plankton fields. Nonlin Proc Geophys 3:236–246
Shachak M, Brand S (1991) Relations among spatiotemporal heterogeneity, population abundance, and variability in a

desert. In: Kolasa J, Pickett STA (eds) Ecological heterogeneity. Springer Verlag, New York, p 202–223
Siegel S, Castellan NJ (1988) Nonparametric statistics. McGraw-Hill, New York
Simpson, JH, Edelsten DJ, Edwards A, Morris NCG, Tett PB (1979) The Islay front: physical structure and phytoplankton distribution. Estuar Coast Mar Sci 9:713–726
Sokal RR, Rohlf FJ (1995) Biometry. The principles and practice of statistics in biological research. Freeman, San Francisco
Steele JH (1974) The structure of marine ecosystems. Harvard University Press, Boston
Steele JH (1978) Some comments on plankton patches. In: Steele JH (ed) Spatial patterns in plankton communities. Plenum Press, New York, p 1–20
Steele JH (1985) A comparison of terrestrial and marine systems. Nature 313:355–358
Steele JH (1989) The ocean 'landscape'. Landscape Ecol 3: 185–192
Sugihara G, May RM (1990) Applications of fractals in ecology. Trends Ecol Evol 5:79–86
Taylor LR (1961) Aggregation, variance and the mean. Nature 189:732–735
Urban DL, O'Neill VO, Shugart HH (1987) A hierarchical perspective can help scientists understand spatial patterns. BioScience 37:119–127
Vandevelde T, Legendre L, Therriault JC, Demers S, Bah A (1987) Subsurface chlorophyll maximum and hydrodynamics of the water column. J Mar Res 45:377–396
Wiegand RC, Pond S (1979) Fluctuations of chlorophyll and related physical parameters in British Columbia coastal waters. J Fish Res Bd Can 36:113–121
Wiens JA (1976) Population responses to patchy environments. Annu Rev Ecol Syst 7:81–120
Wiens JA (1989) Spatial scaling in ecology. Funct Ecol 3: 385–397
Wiens JA, Crist TO, With KA, Milne BT (1995) Fractal patterns of insect movement in microlandscape mosaics. Ecology 76:663–666
Woronow A (1981) Morphometric consistency with the Hausdorff-Besicovitch dimension. Math Geol 13:201–216
Zagoruiko NG, Yolkina VN (1982) Inference and data tables with missing values. Handb Stat 2:493–500
Zar JH (1984) Biostatistical analysis. Prentice-Hall International, Englewood Cliffs, NJ

Editorial responsibility: Otto Kinne (Editor), Oldendorf/Luhe, Germany

Submitted: July 8, 1997; Accepted: September 29, 1997
Proofs received from author(s): November 11, 1997

A4

Distribution inhomogène multi-échelle de la biomasse phytoplanctonique en milieu turbulent

Seuront L

Journal de Recherche Océanographique, **22**, 9-16, 1997

J. Rech.Océanographique, 1997, Vol. 22, n°1 : 9 à 16

DISTRIBUTION INHOMOGÈNE MULTI-ÉCHELLE DE LA BIOMASSE PHYTOPLANCTONIQUE EN MILIEU TURBULENT

Laurent SEURONT

Université des Sciences et de Technologies de Lille, CNRS URA 1363,
Station Marine, B.P. 80, F-62930 Wimereux, France

Mots clés : turbulence, inhomogénéité, phytoplancton, distribution spatio-temporelle

Résumé : La turbulence océanique est classiquement considérée comme génératrice d'homogénéité dans la distribution des paramètres physiques et biologiques, essentiellement aux petites échelles. Cependant, les nombreux travaux qui ont étudié la distribution de la biomasse phytoplanctonique en relation avec la structure de son environnement physique n'ont pas tenu compte de la nature intermittente des mouvements turbulents. Nous nous sommes donc intéressés à la description de tous les niveaux de variabilité de la température (un scalaire purement passif) et de la fluorescence (un estimateur de la biomasse phytoplanctonique) qui, par le biais de l'analyse multifractale universelle, peuvent être entièrement paramétrisés à l'aide de seulement trois paramètres fondamentaux. Les principes de la prise en compte de l'intermittence de la turbulence sont décrits le plus simplement possible et illustrés par une analyse d'une série temporelle de température et de fluorescence dont les résultats sont confrontés à ceux de la littérature.

MULTISCALE INHOMOGENEOUS STRUCTURATION OF PHYTOPLANKTON BIOMASS IN A TURBULENT ENVIRONMENT

Key words: *turbulence, inhomogeneity, phytoplankton, space-time distribution*

Abstract: *Usually, oceanic turbulent processes are regarded as a great factor of homogeneization of abiotic as well as biotic parameters, essentially on small scales. However, many attempts have been made to relate phytoplankton biomass distribution to their physical environment but without taking into account the intermittent properties of the turbulent fluid flows. We then consider here to describe each variability level of temperature (a purely passive scaar) and fluorescence (regarded as a phytoplankton biomass proxy) fields which can be wholly characterised with only three basic parameters by the way of universal multifractal analysis. Basis of our approach of intermittent turbulence are explained as simple as possible and illustrated by an analysis of a temperature and fluorescence time series which is compared with some published results.*

INTRODUCTION

En milieu océanique, globalement dominé par les processus turbulents (Yamazaki & Osborn, 1988), l'état actuel des connaissances tend à montrer que la distribution des organismes planctoniques résulte en grande partie des caractéristiques spatio-temporelles de leur environnement physique (Denman & Powell, 1984 ; Legendre & Demers, 1984). L'existence et la nature de ce couplage entre processus physiques et biologiques apparaissent aujourd'hui fondamentales dans les études écologiques du plancton en général et du phytoplancton en particulier (Mackas *et al.*, 1985 ; Davis *et al.*, 1991). En effet, les paramètres physiques et biologiques présentent une covariabilité spatio-temporelle très nette, depuis les échelles des bassins océaniques (Gargett, 1991) jusqu'à celles des couches mélangées de surface (Desiderio *et al.*, 1993), en passant par les échelles intermédiaires (Mackas *et al.*, 1991 ; Denman & Abbott, 1994).

Plus particulièrement, aux plus petites échelles, qui sont d'un intérêt majeur pour des processus biologiques et écologiques comme la dynamique phytoplanctonique (Estrada *et al.*, 1987, 1988) ou zooplanctonique (Costello *et al.*, 1990 ; Marrasé *et al.*, 1990), les processus turbulents sont considérés comme un facteur d'homogénéisation et introduits comme tels dans la modélisation de leurs effets biologiques (Rotschild & Osborn, 1988 ; Evans, 1989 ; Osborn *et al.*, 1990 ; Granata & Dickey, 1991; Yamazaki *et al.*, 1991 ; Kiørboe & Saiz, 1995).

Toutefois, contrairement à des concepts théoriques fondamentaux considérant la turbulence comme un processus homogène (Kolmogorov, 1941 ; Obukhov, 1941), des travaux ultérieurs (Batchelor & Townsend, 1949) ont montré que le taux de dissipation de l'énergie cinétique turbulente ε, classiquement utilisé pour décrire le degré de turbulence d'un fluide, présentait des variations brutales et très localisées incompatibles avec l'hypothèse d'homogénéité de la turbulence. Dès lors, il semble que la turbulence doive être considérée comme un processus générateur d'hétérogénéité à petite échelle (i.e. inhomogénéité), comme l'ont montré des analyses récentes de la distribution de la température en Manche orientale ou en Mer du Nord (Seuront, 1995).

La distribution de ces irrégularités, ou intermittences, de la turbulence ainsi que leurs effets sur la distribution des organismes planctoniques et sur le concept désormais

« classique » de passivité du phytoplancton (Platt, 1972) ayant été analysés en détail dans Seuront *et al.* (1996a, b), cet article se veut avant tout être une approche pédagogique du concept d'intermittence des processus, encore trop souvent méconnue de la communauté des océanographes biologistes. Par souci de clarté, toute formulation mathématique et détails des techniques d'analyse ont été évités et, à titre d'illustration, une série temporelle de température (traceur passif de la turbulence) et de fluorescence (estimateur de la biomasse phytoplanctonique) a été analysée à l'aide de ces techniques novatrices en sciences de la mer et ses résultats ont été comparés à ceux, plus généraux, présentés dans Seuront *et al.* (1996a, b).

PROBLÉMATIQUE : TURBULENCE, INTERMITTENCE ET INHOMOGÉNÉITÉ

Homogénéité et inhomogénéité d'un processus turbulent

De manière générale, aux plus petites échelles d'espace et de temps, l'étude de la distribution du phytoplancton repose essentiellement sur l'utilisation de l'analyse spectrale (Platt & Denman, 1975) qui permet d'exprimer la contribution relative de la variance locale à la variance totale d'un processus. Les différentes estimations des spectres de variance de l'abondance phytoplanctonique, estimée en terme de fluorescence, ont montré une loi de décroissance en -5/3 (Platt, 1972 ; Powell *et al.*, 1975 ; Fasham & Pugh, 1976 ; Lekan & Wilson, 1978). Ces résultats sont en accord avec des travaux essentiellement théoriques (Kolmogorov, 1941 ; Obukhov, 1941, 1949 ; Corrsin, 1951) qui ont montré, sous l'hypothèse d'isotropie locale (invariance par rotation) et d'homogénéité tridimensionnelles de la turbulence, que le spectre des fluctuations de vitesse (Kolmogorov, 1941 ; Obukhov, 1941) comme celui des fluctuations d'un scalaire passif (Obukhov, 1949 ; Corrsin, 1951), présentaient des lois de décroissance en -5/3, que la turbulence soit considérée d'un point de vue spatial ou temporel. Cette approche théorique est classiquement associée au concept de cascade d'énergie (Richardson, 1922), impliquant une hiérarchie infinie de tourbillons de taille décroissante, depuis les échelles de création de la turbulence jusqu'aux échelles où les effets de la viscosité n'étant plus négligeables, l'énergie cinétique turbulente se dissipe sous forme de chaleur (figure 1).

Cependant, une analyse spectrale étant associée à un moment statistique d'ordre 2 (i.e. la variance), elle ne fait que traduire le comportement moyen d'un processus et ne peut rendre compte des fluctuations brutales, perceptibles quelles que soient les échelles considérées, dans la distribution temporelle des flux de variance de données de température et de fluorescence (figure 2) ; le flux de variance exprimant la contribution de chaque donnée à la variance totale du processus.

L'apparition de ces irrégularités dans les champs turbulents correspond au phénomène d'intermittence, générateur d'inhomogénéité et, de fait, incompatible avec l'hypothèse d'homogénéité tridimensionnelle de la turbulence. Il est dès lors nécessaire de modifier la vision classique de la turbulence en y introduisant la notion d'inhomogénéité, traduisant le fait que les tourbillons à petite échelle remplissent de moins en moins d'espace, et ont une intensité de plus en plus grande, à mesure que

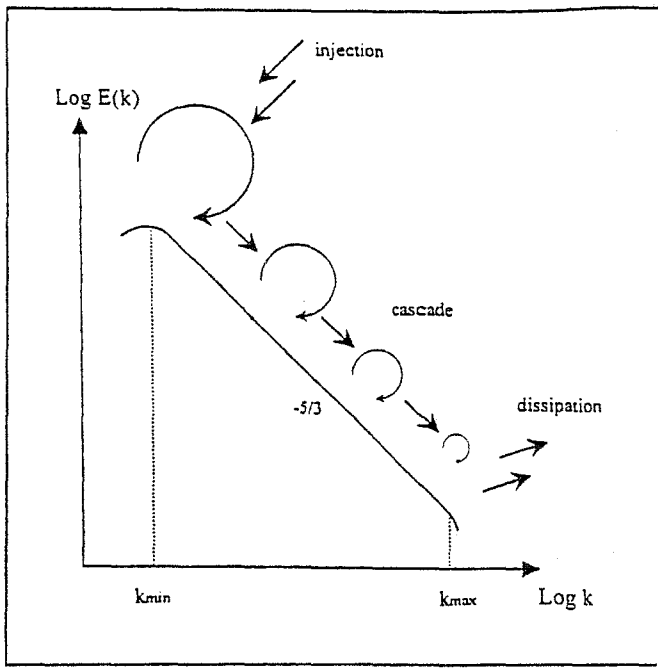

Figure 1 : Représentation schématique du spectre d'une cascade d'énergie, où $E(k)$ est la densité spectrale (unité de variance/k)² et k est indifféremment un nombre d'ondes ou une fréquence selon que la turbulence est considérée d'un point de vue spatial ou temporel. L'énergie cinétique, générée à grande échelle, cascade à travers une hiérarchie de tourbillons de taille décroissante jusqu'à l'échelle de la viscosité où elle est dissipée en chaleur. La variabilité du processus présente une invariance d'échelle en -5/3 conforme à la théorie de Kolmogorov-Obukhov. Les nombres d'ondes k_{max} and k_{min} correspondent respectivement aux échelles de création de la turbulence et aux échelles de dissipation visqueuse.

Figure 1: Schematic representation showing the form of the frequency spectrum of turbulent velocity cascade, where E(k) is the spectral density (variance units/k)² and k is indifferently a wavenumber or a frequency depending on whether turbulence is considered in a spatial or temporal framework. The kinetic energy generated by large scale processes (e.g. wind or tidal currents) cascades through a hierarchy of eddies of decreasing size to the viscous subrange where it is dissipated into heat. The change in variance with wavenumber (i.e. slope of spectrum) is scale-invariant with a -5/3 slope as predicted by the theoretical Kolmogorov-Obukhov power law. The wavenumbers k_{max} and k_{min} respectively show the largest scale of creation of turbulence and the smallest scale (Kolmogorov length scale) reached by turbulent eddies where turbulent motions are smoothed out by viscous effects.

l'échelle diminue. On remarquera que si classiquement les terminologies « variabilité » et « hétérogénéité » semblent devoir être appliquées à la description des fluctuations perceptibles dans les valeurs, respectivement d'un ou de plusieurs paramètres (Kolasa & Rollo, 1991 ; Shachak & Brand, 1991), il apparaît que dans leur utilisation, la distinction entre ces deux concepts n'est pas aussi nette (Downing, 1991 ; Pinel-Alloul, 1995). Nous avons donc introduit le terme « inhomogénéité », de préférence au terme générique « variabilité » et par opposition à « hétérogénéité », pour décrire les fluctuations perceptibles dans les valeurs d'un seul paramètre, ici la température ou la fluorescence.

Intermittence, fractals et multifractals

Ainsi, en considérant un processus de cascade élémentaire identique à toute échelle, il est possible de représenter un processus homogène (non-intermittent), comme un processus inhomogène (intermittent) (figure 3). Dans le premier cas de figure (figure 3a), à une échelle donnée, un tourbillon se résout, à l'échelle immédiatement inférieure, en quatre sous-tourbillons deux fois plus petits, ce qui conduit à un degré d'occupation totale de l'espace dans lequel se déploie la cascade, ici un espace bidimensionnel.

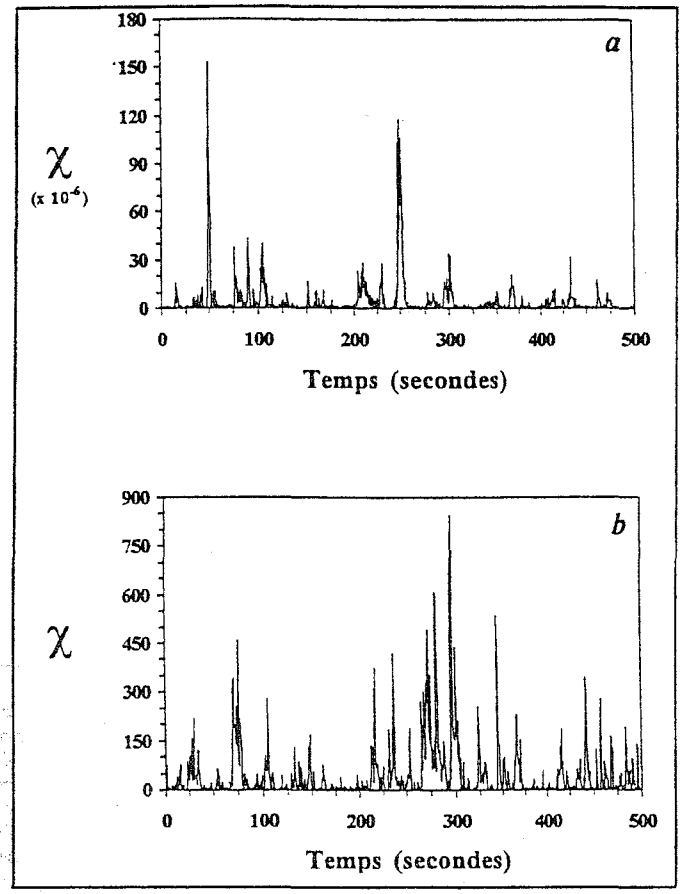

Figure 2 : Echantillons de la distribution temporelle de χ, le flux de variance de données temporelles de température (*a*) et de fluorescence (*b*) échantillonnées le 17 Juin 1991 dans le sud de la Mer du Nord, mettant en évidence le phénomène d'intermittence.
Figure 2: Samples of patterns of χ, the rate of variance fluxes of temperature (a) and fluorescence (b) time series recorded in the 17 June 1991 in the Southern Bight of the North Sea.

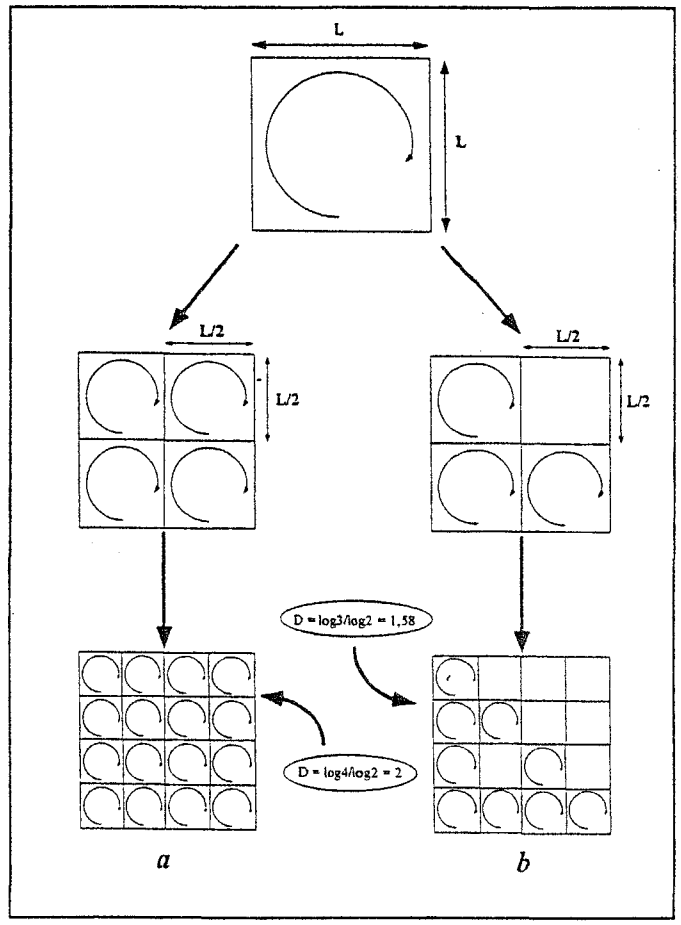

Figure 3 : Processus élémentaire de cascades isotropes : *a*, un processus de cascade homogène (non-intermittente) et *b*, un processus de cascade inhomogène (intermittente), ce dernier processus correspondant au "β-model". Dans les deux cas, la prise en compte d'un rapport d'échelle $\lambda = 2$ permet d'accéder à la dimension spatiale de la cascade, non entière (fractale) dans le cas de la cascade inhomogène (d'après Schertzer & Lovejoy, 1993).
Figure 3: Elementary processes of isotropic cascades : a, an homogeneous cascade process (non-intermittent) and b, an inhomogeneous cascade process (intermittent), which illustrates the "β-model". In both cases the scale ratio $\lambda = 2$ gives rise to the spatial dimension of the cascade which is non-euclidean (fractal) in the case of the inhomogeneous cascade (from Schertzer & Lovejoy, 1993).

En revanche, une manière d'introduire le concept d'intermittence est de considérer qu'un tourbillon se résout en sous-tourbillons actifs et inactifs, ce qui conduit à une dimension non entière, soit fractale, du support de la turbulence, représentée par le "β-model" (figure 3b) (Novikov & Stewart, 1964 ; Mandelbrot, 1974 ; Frisch *et al.*, 1978).
De manière générale le concept de dimension fractale découle de celui d'homothétie interne, ou autosimilarité, selon laquelle un objet peut être considéré comme un ensemble de copies de lui-même à différentes échelles. Ainsi, une transformation géométrique conduisant à « N objets n fois plus petits » introduit une dimension d :

$$d = \log N / \log n$$

L'introduction de la géométrie fractale dans les études des processus associés à la turbulence permet donc de rendre compte du degré d'occupation spatiale d'un processus. Le concept théorique de cascade homogène apparaît alors comme un cas particulier de cascade inhomogène.
Toutefois, un tel modèle, s'il permet d'accéder à une représentation inhomogène du concept de cascade d'énergie, présente l'inconvénient de réduire considérablement la représentation du degré d'intermittence d'un champ turbulent puisqu'il ne considère que deux niveaux d'énergie (ou plus généralement, deux niveaux d'activité), ce qui ne correspond pas à la multiplicité des intensités perceptibles au sein de processus turbulents, qu'ils soient d'origine biotique ou abiotique (figure 2). Dans ce cadre, il est préférable d'envisager un processus de cascade qui, au lieu de considérer des sous-tourbillons actifs ou inactifs, associe à un tourbillon des sous-tourbillons faibles ou forts, l' « α-modèle »" (Schertzer & Lovejoy, 1983, 1985), ce qui conduit à un champ inhomogène présentant différentes intensités, et donc à un plus grand réalisme (figure 4).
Au bout d'un grand nombre de pas de cascade de ce processus, il est possible de générer effectivement des champs intermittents en tous points similaires à ceux que nous avons pu observer à partir des données empiriques. Dans ce contexte, chaque degré d'intermittence est associé à une dimension fractale. L'intermittence de la turbulence est dès lors définie par une infinité de dimensions fractales, d'où la notion de multifractals qui apparaît comme une application du concept de fractal simple, développé à partir de la description d'objets géométriques (Mandelbrot, 1983), à la description de la variabilité temporelle et/ou spatiale de processus intermittents. En outre, les figures 3 et 4 illustrent la manière dont les concepts de fractals et de multifractals permettent d'étudier de manière continue un processus multi-échelle inhomogène par dégradation successive des échelles d'observation.

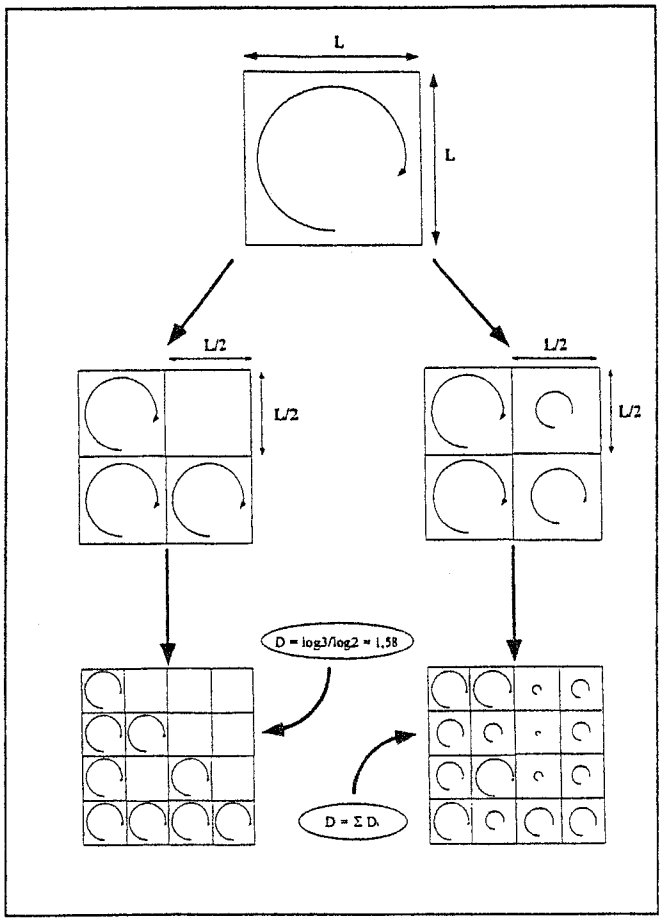

Figure 4 : Processus de cascade isotrope multifractale reposant sur une généralisation de la figure 3a par introduction de différents degrés d'intensité (i.e. intermittence) de la turbulence.
Figure 4: Processes of multifractal isotropic cascade based on a generalization of figure 3a introducing different turbulent intensity levels (i.e. intermittencies).

Vers une description multifractale universelle de l'intermittence

Notre prise en compte de l'intermittence des processus turbulents repose sur une généralisation du concept de multifractals géométriques qui consiste à associer un moment statistique à chaque intensité d'un processus turbulent, soit à chacun de ses degrés d'intermittence. Ainsi, les moments statistiques les plus faibles traduisent les propriétés moyennes d'un processus turbulent, comme peut le faire l'analyse spectrale par son association à un moment statistique d'ordre 2, alors que les moments statistiques les plus élevés traduiront les intermittences les plus fortes, qui sont aussi les plus rares et par conséquent les plus difficiles à détecter et à analyser.

Malgré l'apparente complexité induite par la multiplicité, voire l'infinité, des paramètres statistiques nécessaires à décrire la variabilité d'un champ inhomogène, l'utilisation des multifractals universels (Schertzer & Lovejoy, 1987, 1989) permet de caractériser pleinement les statistiques d'un champ turbulent à partir de trois paramètres : H, C_1 et α.

- H, estimé par combinaison non-linéaire de la pente du spectre de variance, traduit les propriétés moyennes du processus considéré.
- C_1 est la codimension fractale de la moyenne d'un processus, soit le degré d'hétérogénéité moyenne du processus. Plus C_1 est élevé, plus le degré d'intermittence, soit l'inhomogénéité sera important (C_1 = 0 pour un processus homogène tel que la cascade d'énergie de Kolmogorov et $C_1 = d$, d étant la dimension de l'espac euclidien considéré, pour un processus si hétérogène qu'i est de dimension fractale nulle).
- α représente un degré de multifractalité. Il exprim l'importance de la déviation à la moyenne des valeurs d champ; plus il est élevé, plus les valeurs s'écartant de l moyenne du champ sont nombreuses; $\alpha = 0$ dans le cas d modèle de turbulence monofractal (figure 3b).

La figure 5 présente une illustration des propriétés d'u champ intermittent hypothétique traduites par le paramètres C_1 et α. Dans le premier cas de figure (figur 5a), le paramètre C_1 est fixé et α varie: plus α augmente plus le nombre de valeurs du champ considéré s'écartan de sa moyenne est élevé (i.e. plus le nombr d'intermittences sera élevé et donc, la multifractalité) Dans le second cas de figure (figure 5b), le paramètre α est fixé et C_1 varie: plus C_1 augmente, plus l'expression d chaque intermittence est marquée par rapport au reste d champ, i.e. plus l'inhomogénéité est élevée.

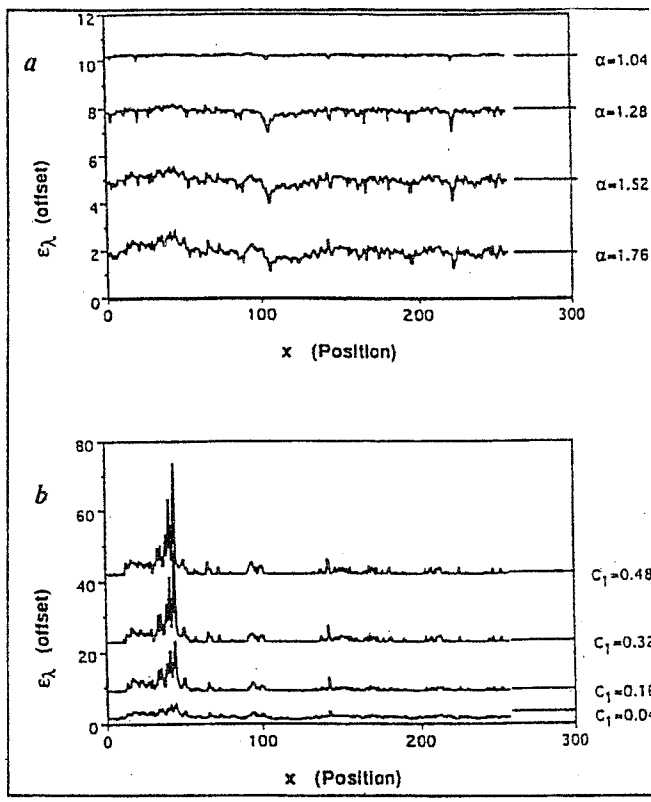

Figure 5 : Illustration des propriétés d'un champ turbulent (ε, le taux d dissipation de l'énergie cinétique) traduites par les paramètres multifractals universels C_1 et α quand α (*a*) et C_1 varient (*b*) (d'après Pecknold *et al.* 1993).
Figure 5: Illustration of turbulent field properties (ε, the turbulent kinetic energy dissipation rate) with the universal multifractal parameters C_1 and α for varying α (a) and C_1 (b) (from Pecknold et al., 1993).

MATÉRIEL ET MÉTHODES

Les données utilisées ici pour illustrer l'inhomogénéité de la turbulence océanique ont été obtenues le 17 juin 1991 lors d'un échantillonnage eulérien (i.e. au point fixe) de 4h55 réalisé en marée de mortes-eaux dans le sud de la Mer du Nord (51°01,30'N ; 02°04,90'E), caractérisée par son fort hydrodynamisme tidal. La température, considérée comme un scalaire purement passif, et la fluorescence, considérée comme un estimateur de la biomasse phytoplanctonique, ont été enregistrées simultanément, en continu, à une même profondeur (5 m),

respectivement à l'aide d'une sonde CTD Sea-Bird 19 et d'un fluorimètre Sea Tech. La fréquence d'échantillonnage étant de 2 Hz, nos analyses sont basées sur une série temporelle de 35400 données dont un échantillon est présenté sur la figure 6.

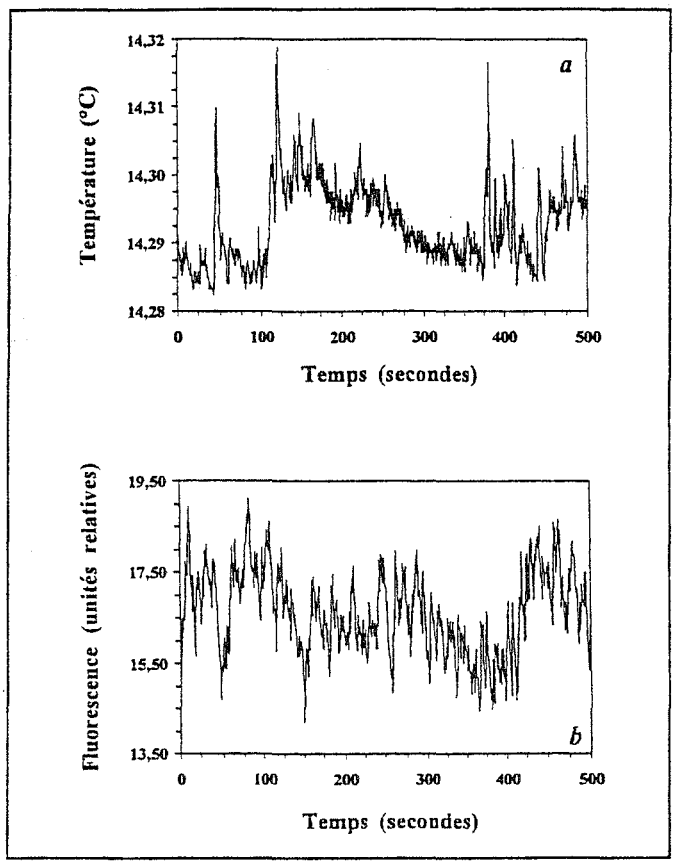

Figure 6 : Échantillons de données temporelles de température (*a*) et de fluorescence (*b*) prélevés dans le Sud de la Mer du Nord. Des fluctuations brutales et très localisées sont clairement visibles.
Figure 6: Samples of temperature (a) and fluorescence (b) time series from the Southern Bigh of the North Sea. Sharp fluctuations occurring on small time scales are clearly visible.

Notre caractérisation de la variabilité des champs de température et de fluorescence repose dans un premier temps sur l'analyse spectrale qui permet d'en résumer les caractéristiques moyennes, alors que leur caractérisation détaillée repose sur la paramétrisation de tous leurs niveaux de variabilité que nous autorise la technique d'analyse multifractale universelle, le DTM ("Double Trace Moment") (Lavallée, 1991 ; Lavallée *et al.*, 1992).

PARAMÉTRISATION MULTI-ÉCHELLE D'UN PROCESSUS INHOMOGÈNE

Si le spectre de variance E(f) de la température (figure 7), en représentation log-log, montre une loi de décroissance (i.e. invariance d'échelle) en -1,75 [$E(f) \propto f^{-\beta}$ avec β = 1,75] conforme au -5/3 théorique de Kolmogorov-Obukhov (1941) sur toute la gamme d'échelles considérées, le spectre de la fluorescence (figure 7), donc de la biomasse phytoplanctonique, présente un comportement sensiblement plus complexe (l'écart du β empirique au β théorique étant une expression de l'intermittence de la turbulence). Pour des fréquences s'étendant de $9{,}5.10^{-3}$ à 0,5 Hz (soit pour des échelles temporelles de 1 à 105 secondes), le spectre de fluorescence présente une loi de décroissance en -1,78 ce qui s'accorde avec l'hypothèse de passivité de la biomasse

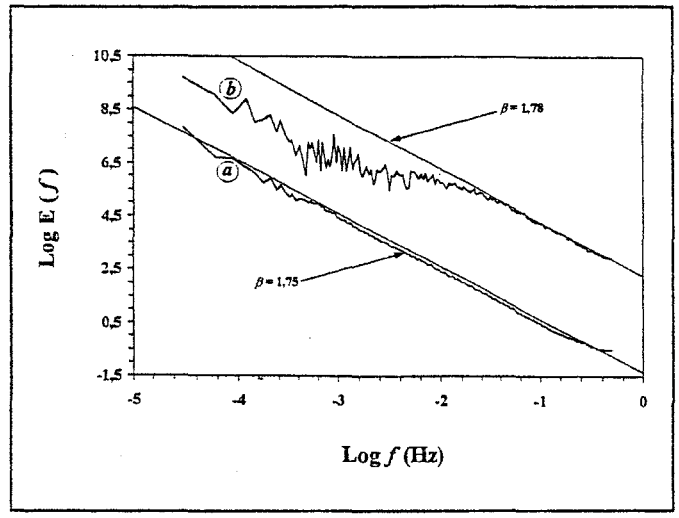

Figure 7 : Spectre de variance de la température (*a*) et de la fluorescence (*b*), en représentation log-log. La température présente une invariance d'échelle avec β = 1,75 à toutes les échelles, alors que la fluorescence est invariante d'échelle (β = 1,78) seulement de $9{,}5.10^{-3}$ à 0,5 Hz. Les différences observées avec le comportement spectral théorique d'un scalaire passif $E(f) = f^{-\beta}$ avec β = 5/3 sont dues aux intermittences
Figure 7: Variance spectrum E(f) (f is frequency) of the temperature (a) and fluorescence (b) data, shown in a log-log plot. The temperature data are scaling with β = 1,75 whatever the scale whereas fluorescence data are scaling only from $9{,}5.10^{-3}$ to 0,5 Hz with β = 1,78. The observed differences with the theoretical -5/3 power law trend of a passive scalar $E(f) = f^{-\beta}$ with β = 5/3 are due to intermittencies.

phytoplanctonique. En revanche, pour des fréquences inférieures à $9{,}5.10^{-3}$ Hz (soit pour des échelles temporelles supérieures à 105 secondes), le comportement spectral de la fluorescence présente une rupture d'échelle. L'insuffisance de données nous a empêché de déceler un comportement invariant d'échelle, observé dans le cas d'un enregistrement englobant un cycle de marée complet (β = 1,22 pour des échelles supérieures à 105 secondes) (Seuront *et al.*, 1996a). Dès lors, ce comportement peut être associé à des résultats théoriques et empiriques (Powell *et al.*, 1975 ; Denman & Platt, 1976 ; Denman *et al.*, 1977 ; Bennett & Denman, 1985 ; Steele and Henderson, 1992 ; Powell & Okubo, 1994) prédisant un aplatissement du spectre de fluorescence par rapport à celui d'un scalaire passif (e.g. la température) aux échelles où l'influence de la dynamique biologique sur la variabilité du phytoplancton devient prépondérante par rapport à celle des processus physiques.
De plus, la rupture d'échelle du champ de fluorescence pour des fréquences de l'ordre de $9{,}5.10^{-3}$ Hz peut être associée à une échelle temporelle de l'ordre de 105 secondes qui, en considérant la théorie de la turbulence gelée (Taylor, 1921) et une circulation moyenne instantanée de l'ordre de 0,3 $m.s^{-1}$, telle qu'observée durant l'échantillonnage, correspond à une échelle spatiale de l'ordre de 31 mètres.
Plus précisément, aux échelles inférieures à 105 secondes (i.e. 31 mètres), où le comportement de la fluorescence est similaire à celui de la température, l'application du DTM a montré que la distribution de la biomasse phytoplanctonique était analogue à celle de la température avec des paramètres multifractals sensiblement similaires : H = 0,41 ± 0,02 dans le cas de la température et 0,43 ± 0,02 dans le cas de la fluorescence et des valeurs de C_1 et α très proches dans les 2 cas : C_1 = 0,050 ± 0,01 et α = 1,75 ± 0,05 pour la température et C_1 = 0,045 ± 0,01 et α = 1,85 ± 0,05 pour la fluorescence. La

distribution du phytoplancton à petite échelle, qui est d'un intérêt écologique majeur (Davis *et al.*, 1991), semble donc passive dans la mesure où la grande similitude existant entre les estimations des paramètres universels de la fluorescence et de la température révèlent un couplage étroit entre la structure spatio-temporelle des populations phytoplanctoniques et celle de leur environnement physique. En outre, les techniques de simulation multifractale (Pecknold *et al.*, 1993) nous permettent d'accéder à une représentation encore inédite à ce jour de la structuration spatiale inhomogène de la biomasse phytoplanctonique (figure 8) en milieu turbulent.

En revanche, aux échelles où le comportement de la fluorescence diffère significativement de celui de la température, l'absence de comportement invariant d'échelle ne nous a pas permis d'appliquer une analyse multifractale.

Ces résultats confirment les résultats obtenus à petite échelle par Seuront *et al.* (1996a, b) à partir de séries temporelles enregistrées à la même station dans des conditions hydrodynamiques et hydrologiques similaires (marée de mortes-eaux, sud de la Mer du Nord ; Seuront *et al.*, 1996a) comme dans des conditions radicalement différentes en Manche orientale (marée de vives-eaux ; Seuront *et al.*, 1996b) (Tableau I) et dans l'estuaire du St Laurent (Teissier, com. pers.). D'autre part, Seuront *et al.* (1996a) ont montré à partir d'une série temporelle plus longue (11h30) qu'après une rupture d'échelle très nette se produisant autour de 30 mètres (≈ 100 secondes), la variabilité de la biomasse phytoplanctonique présentait une invariance d'échelle et des paramètres multifractals très spécifiques, indiquant une homogénéité plus grande et une multifractalité plus faible que dans le cas de la température (Tableau I).

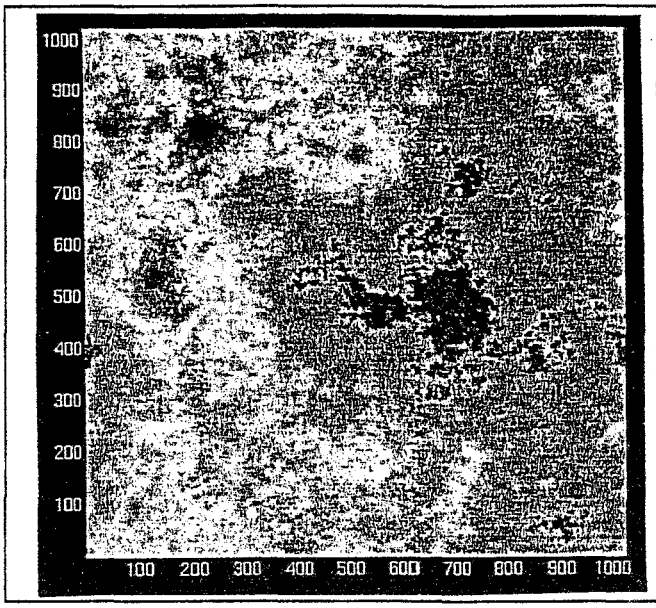

Figure 8 : Simulation bidimensionnelle d'un champ multifractal de phytoplancton avec $H = 0,40$; $C_1 = 0,045 \pm 0,01$ et $\alpha = 1,85 \pm 0,05$. Les structures perceptibles à différentes échelles illustrent la structure multifractale sous-jacente, responsable du phénomène d'intermittence observé dans les données empiriques. Les différents niveaux de gris correspondent aux intensités du champ (croissant du noir au blanc).

Figure 8: A bidimensional simulation of a multifractal turbulent field using $H = 0,40$; $C_1 = 0,045 \pm 0,01$ and $\alpha = 1,85 \pm 0,05$. Different structures dominate at different length scales, illustrating the underlying multifractal structure that produces the empirically observed intermittencies. The greyscale corresponds to the field intensities (increasing from black to white).

Tableau I : Valeurs des paramètres multifractals universels obtenus dans la présente étude, comparées aux valeurs obtenues par Seuront *et al.* (1996a, b), et valeurs des pentes β des spectres de Fourier.

Table I : The values of the universal multifractal parameters obtained here, compared to the values we previously obtained (Seuront et al., 1996a, b). The values of the slopes β of the Fourier power spectra are also indicated.

	scalaire passif												scalaire actif			
	pour f>0,01 Hz (Seuront *et al.*, 1996a)				pour f> 0,038 Hz (Seuront *et al.*,1996b)				pour f> 9,5 10^{-3} Hz présente étude				pour f< 0,01 Hz (Seuront *et al.*,1996a)			
	β	H	C1	α	β	H	C1	α	β	H	C1	α	β	H	Cl	α
Température	1,74	0,42	0,04	1,7	1,65	0,34	0,04	1,7	1,75	0,41	0,05	1,75	-	-	-	-
Fluorescence	1,75	0,41	0,04	1,8	1,22	0,12	0,02	0,8	1,78	0,43	0,045	1,85	1,22	0,12	0,02	0,8

CONCLUSION

Ces résultats nous ont permis de vérifier l'hypothèse de passivité moyenne de la biomasse phytoplanctonique en milieu turbulent telle qu'elle a été formulée dès les années 1970, mais aussi de confirmer sa validité en considérant la distribution des intermittences quelles que soient les échelles de variabilité. En effet, les analyses entreprises n'ont pas permis de déceler de différences significatives entre les distributions de la température et de la fluorescence, toutes deux inhomogènes, et ce, aux petites échelles d'espace et de temps (les échelles temporelles et spatiales considérées étant respectivement inférieures à une centaine de secondes et à une vingtaine de mètres), confirmant en cela des résultats récents (Seuront *et al.* 1996a, b).

En revanche, au delà d'une échelle critique qui a ici été estimée à une trentaine de mètres, et à la lumière de résultats antérieurs (Seuront *et al.*, 1996a), il semble que la dynamique des propriétés biologiques du phytoplancton prenne le pas sur les processus de dispersion turbulente et soit à l'origine d'une structuration très spécifique de la biomasse chlorophyllienne.

Contrairement aux résultats de Pascual *et al.* (1995) qui ne fournissent que des informations qualitatives (e.g. absence d'analyse spectrale, essentielle pour établir des comparaisons avec d'autres champs et un début de paramétrisation d'un processus sur la multifractalité du comportement statistique d'abondances zooplanctoniques), l'utilisation des multifractals universels a montré que la variabilité associée à des processus stochastiques, tels que la distribution de la température et de la fluorescence, pouvait être pleinement caractérisée par seulement trois paramètres et ce, quelles que soient les échelles spatiales ou temporelles considérées. De fait, ces résultats montrent que dans un milieu turbulent, considéré

classiquement comme étant générateur d'homogénéité, la distribution du phyto-plancton était particulièrement non uniforme, ou inhomogène. Cette inhomogénéité, inhérente à la structure des mouvements turbulents, retranscrite par l'outil de simulation multifractale, permet ainsi d'envisager, loin des statistiques gaussiennes classiques, la description multi-échelle du couplage fortement non-linéaire existant entre processus physiques et biologiques. Ces techniques, associées au concept de diffusion, processus influant directement sur la dynamique des populations planctoniques (Okubo, 1980), ont d'ailleurs permis d'élaborer un modèle de prospection alimentaire de copépodes dans un champ multifractal de phytoplancton (Marguerit, 1996) dont le développement semble aujourd'hui essentiel dans l'étude des flux de matière au sein de l'écosystème pélagique.

REMERCIEMENTS

L'auteur remercie tout particulièrement S. Frontier, initiateur de cette étude, pour sa confiance et ses précieux conseils, C. Luczak pour avoir fourni les séries temporelles de température et de fluorescence, Y. Lagadeuc pour sa relecture du manuscript et ses suggestions avisées, D. Marsan pour la réalisation de la simulation multifractale, D. Schertzer et F. Schmitt pour leur aide, plus que précieuse dans mon apprentissage des multifractals, S. Lovejoy, Y. Teissier, C. Marguerit et M. Claereboudt pour nos discussions stimulantes sur le sujet.

RÉFÉRENCES BIBLIOGRAPHIQUES

BATCHELOR, G. K. & TOWNSEND, A. A., 1949. The nature of turbulent motion at large wavenumbers. - *Proc. Roy. Soc. A*, **199** : 238.

BENNETT, A. F. & DENMAN, K. L., 1985. Phytoplankton patchiness: inferences from particle statistics. - *J. Mar. Res.*, **43** : 307-339.

CORRSIN, S., 1951. On the spectrum of isotropic temperature in an isotropic turbulence. - *J. Appl. Phys.*, **22** : 469.

COSTELLO, J.H., STRICKLER, J.R., MARRASE, C., TRAGER, G., ZELLER, R. & FREISE, A., 1990. Grazing in a turbulent environment: behavioral response of a calanoid copepod, *Centropages hamatus*. - *Proc. Natl. Acad. Sci. USA*, **87** : 1648-1652.

DAVIS, C. S., FLIERT, G.R., WIEBE, P.H.& FRANKS, P. J. S., 1991. Micropatchiness, turbulence and recruitment in plankton. - *J. Mar. Res.*, **49** : 109-151.

DENMAN, K. L. & PLATT, T., 1976. The variance spectrum of phytoplankton in a turbulent ocean. - *J. Mar. Res.*, **34** : 593-601.

DENMAN, K. L., OKUBO, A. & PLATT, T., 1977. The chlorophyll fluctuation spectrum in the sea. - *Limnol. Oceanogr.*, **22** : 1033-1038.

DENMAN, K. L. & POWELL, T. M., 1984. Effects of physical processes on planktonic ecosystems in the coastal ocean. - *Oceanogr. Mar. Biol. Ann. Rev.*, **22** : 125-168.

DENMAN, K. L. & ABBOTT, M. R., 1994. Time scales of pattern evolution from cross-spectrum analysis of advanced very high resolution radiometer and coastal zone color scanner imagery. - *J. Geophys. Res.*, **99** : 7533-7442.

DESIDERIO, R. A., COWLES, T. J. & MOUM, J. N., 1993. Microstructure profiles of laser-induced chlorophyll fluorescence spectra: evaluation of backscatter and forward-scatter fiber-optic sensors. - *J. Atmos. Ocean. Tech.*, **10** : 209-224.

DOWNING, J. A., 1991. Biological heterogeneity in aquatic ecosystems. In : *Ecological studies. Analysis and Synthesis.* (Billings, W. D. , Golley, F., Lange, O. L., Olson, J. S. & Remmert, H. eds.), Springer-Verlag : 160-180.

ESTRADA, M., ALCARAZ, M. & MARRASE C., 1987. Effects of turbulence on the composition of phytoplancton assemblages in marine microcosms. - *Mar. Ecol. Prog. Ser.*, **38** : 267-281.

ESTRADA, M., MARRASE, C. & ALCARAZ, M., 1988. Phytoplankton response to intermittent stirring and nutrient addition in marine microcosms. - *Mar. Ecol. Prog. Ser.*, **48** : 225-234.

EVANS, G. T., 1989. The encounter speed of moving predator and prey. - *J. Plankton Res.*, **11** : 415-417.

FASHAM, M.J.R. & PUGH, P.R., 1976. Observations on the horizontal coherence of chlorophyll *a* and temperature. - *Deep-Sea Res.*, **23** : 527-538.

FRISCH, U., SULEM, P. L. & NELKIN, M., 1978. A simple dynamical model of intermittency in fully developped turbulence. - *J. Fluid Mech.*, **87** : 719-724.

GARGETT, A. E., 1991. Physical processes and the maintenance of nutrient-rich euphotic zones. - *Limnol. Oceanogr.*, **36** : 1527-1545.

GRANATA, T. C. & DICKEY, T.D., 1991. The fluid mechanics of copepod feeding in a turbulent flow : a theoretical approach. - *Prog. Oceanogr.*, **26** : 243-261.

KIØRBOE, T. & SAIZ, E., 1995. Planktivorous feeding in calm and turbulent environments, with emphasis on copepods. - *Mar. Ecol. Prog. Ser.*, **122** : 135-145.

KOLASA, J. & ROLLO, C. D., 1991. The heterogeneity of heterogeneity: a glossary. In : *Ecological studies. Analysis and Synthesis.* (Billings, W. D., Golley, F., Lange, O. L., Olson, J. S. & Remmert, H. eds), Springer-Verlag : 1-23.

KOLMOGOROV, A. N., 1941. The local structure of turbulence in incompressible viscous fluid for very large Reynolds numbers. - *Dokl. Acad. Nauk. SSSR*, **30** : 299-303. -

LAVALLEE, D., 1991. *Multifractal techniques: analysis and simulations of turbulent fields.* Ph. D. Thesis., McGill Univ., Montréal, Canada.

LAVALLEE, D., LOVEJOY, S., SCHERTZER, D. & SCHMITT, F., 1992. On the determination of universal multifractal parameters in turbulence. In : *Topological aspects of the dynamics of fluids and plasmas* (Moffat, K.M., Tabor, G., Zaslavski, M., Tabov, M. & Comte, P. eds), Kluver : 463-478.

LEGENDRE, L. & DEMERS, S., 1984. Towards dynamic biological oceanography and limnology. - *Can. J. Fish. Aquat. Sci.*, **41** : 2-19.

LEKAN, J. F. & WILSON, R. E., 1978. Spatial variability of phytoplankton biomass in the surface water of Long Island. - *Est. Coast. Mar. Sci.*, **6** : 239-250.

MACKAS, D. L., DENMAN, K. L. & ABBOT, M. R., 1985. Plankton patchiness: biology in the physical vernacular. - *Bull. Mar. Sci.*, **37** : 652-674.

MACKAS, D. L., WASHBURN, L. & SMITH, S. L., 1991. Zooplankton community pattern associated with a California current cold filament. - *J. Geophys. Res.*, **96** : 781-797.

MANDELBROT, B., 1983. *The fractal geometry of nature*, Freeman, New York.

MANDELBROT, B., 1984. Multiplications aléatoires itérées et distributions invariantes par moyenne pondérée aléatoire. - *C. R. Acad. Sc., Paris*, **278**, Série A : 289.

MARGUERIT, C., 1996. *Modélisation de la prospection alimentaire d'un copépode dans un champ turbulent multifractal de phytoplancton.* - D.E.A. de Biomathématiques, Univ. P. & M. Curie, Paris VI, 20 pp.

MARRASE, C., COSTELLO, J.H., GRANATA, T. & STRICKLER, J.R., 1990. Grazing in a turbulent environment: energy dissipation, encounter rates, and efficacy of feeding currents in *Centropages hamatus*. - *Proc. Natl. Acad. Sci. USA*, **87** : 1653-1657.

NOVIKOV, E. A. & STEWART, R., 1964. Intermittency of turbulence and spectrum of fluctuations in energy dissipation. - *Izv. Akad. Nauk. SSSR Geogr. I Geofiz.*, **3** : 408-412.

OBUKHOV, A. M., 1941. Spectral energy distribution in a turbulent flow. - *Dokl. Acad. Nauk. SSSR*, **32** : 22-24.

OBUKHOV, A. M., 1949. Structure of the temperature field in a turbulent flow. - *Izv. Acad. Nauk. SSSR Ser. Geofiz.*, **3** : 408-412.

OKUBO, A., 1980. *Diffusion and ecological problems: mathematical models.* Springer-Verlag, New York.

OSBORN, T. R., YAMAZAKI, H. & SQUIRES, K. D., 1990. Direct calculation of the effect of turbulence on planktonic contact rates. In : *Large Marine Ecosystems.* (Sherman, K.,Alexander, L. M. & Gold, B. D. eds), American Association for Advancement of Science, Washington : 99-103.

PASCUAL, M., ASCIOTI, F. A. & CASWELL, H., 1995. Intermittency in the plankton: a multifractal analysis of zooplankton biomass variability. - *J. Plankton Res.*, **17** : 1209-1232.

PECKNOLD, S., LOVEJOY, S., SCHERTZER, D., HOOGE, C & MALOUIN, J. F., 1993. The simulation of universal multifractals. In : *Cellular Automata : Prospects in Astrophysical Applications.* (Perdang, J. M. & Lejeune, A. eds), World Scientific : 228-267.

PINEL-ALLOUL, B., 1995. Spatial heterogeneity as a multiscale characteristic of zooplankton community. - *Hydrobiologia*, 300/301 : 17-42.

PLATT, T., 1972. Local phytoplankton abundance and turbulence. - *Deep-Sea Res.*, **19** : 183-187.

PLATT, T. & DENMAN, K. L., 1975. Spectral analysis in ecology. - *Annu. Rev. Ecol. Syst.*, **6** : 189-210.

POWELL, T. M., RICHERSON, P. J., DILLON, T. M., AGEE, B. A., DOZIER, B. J., GODDEN, D. A. & MYRUP, L. O., 1975. Spatial scales of current speed and phytoplankton biomass fluctuations in Lake Tahoe. - *Science*, **189** : 1088-1090.

POWELL, T. M. & OKUBO, A., 1994. Turbulence, diffusion and patchiness in the sea. - *Phil. Trans. R. Soc. Lond. B*, **343** : 11-18.

RICHARDSON, L.F., 1922. *Weather prediction by numerical processes.* Cambridge Univ. Press (republished by Dover, New York, 1965).

ROTHSCHILD, B. J. & OSBORN, T. R., 1988. Small-scale turbulence and plankton contact rates. - *J. Plankton Res.*, **10** : 465-474.

SCHERTZER, D. & LOVEJOY, S., 1983. Elliptical turbulence in the atmosphere. In : *Proceedings of the 4 th symposium on turbulent shear flows*, Karlsrhule, West Germany.

SCHERTZER, D. & LOVEJOY, S., 1985. The dimension and intermittency of atmospheric dynamics. In : *Turbulent shear flows 4*, (Launder, B. ed.), Springer : 7-33.

SCHERTZER, D. & LOVEJOY, S., 1987. Physical modeling and analysis of rain and clouds by anisotropic scaling multiplicative processes. - *J. Geophys. Res., D,*. **92** : 9693-9714.

SCHERTZER, D. & LOVEJOY, S., 1989. Nonlinear variability in geophysics: multifractal analysis and simulation. In : *Fractals: Physical Origin and Consequences.* (Pietronero, L. ed.), Plenum, New York : 49-79.

SCHERTZER, D. & LOVEJOY, S., 1993. Nonlinear variability in geophysics 3. Scaling and multisfractal processes. E.G.S. Richardson memorial Conference, Cargèse (France) : Lectures notes.

SEURONT, L., 1995. *Analyses multifractales de la distribution du plancton en milieu turbulent.* - D.E.A. d'Océanologie Biologique, Univ. P. & M. Curie, Paris VI, 36 pp.

SEURONT, L., SCHMITT, F., LAGADEUC, Y., SCHERTZER, D., LOVEJOY, S. & FRONTIER, S., 1996a. Multifractal analysis of phytoplankton biomass and temperature variability in the ocean. - *Geophys. Res. Letters* , **23** : 3591-3594.

SEURONT, L., SCHMITT, F., SCHERTZER, D., LAGADEUC, Y. & LOVEJOY, S., 1996b. Multifractal intermittency of Eulerian and Lagrangian turbulence of ocean temperature and plankton fields. - *Nonlinear Processes in Geophysics* (sous presse).

SHACHAK, M. & BRAND, S., 1991. Relations among spatiotemporal heterogeneity, population abundance, and variability in a desert. In : *Ecological studies. Analysis and Synthesis.* (Billings, W. D., Golley, F., Lange, O. L., Olson, J. S. & Remmert, H. eds.),. Springer-Verlag : 202-223.

STEELE, J. H. & HENDERSON, E. W., 1992. A simple model for plankton patchiness. - *J. Plankton Res.*, **14** : 1397-1404.

TAYLOR, G.I., 1921. Diffusion by continuous movements. - *Proc. London Math. Soc.*, **20** : 196-212.

YAMAZAKI, H. & OSBORN, T. R., 1988. Review of oceanic turbulence: implications for biodynamics. In : *Towards a theory on biological-physical interaction in the world ocean.* (Rothschild, B. J. ed.). Dordrecht : 215-234.

YAMAZAKI, H., OSBORN, T. R. & SQUIRES, K. D., 1991. Direct numerical simulation of planktonic contact in turbulent flow. - *J. Plankton Res.*, **13** : 629-643.

A5

Spatio-temporal structure of tidally mixed coastal waters: variability and heterogeneity

Seuront L & Lagadeuc Y

Journal of Plankton Research, **20**, 1387-1401, 1998

Journal of Plankton Research Vol.20 no.7 pp.1387–1401, 1998

Spatio-temporal structure of tidally mixed coastal waters: variability and heterogeneity

Laurent Seuront and Yvan Lagadeuc

Station Marine de Wimereux, Université des Sciences et Technologies de Lille, CNRS-EP 1750, BP 80, 62930 Wimereux, France

Abstract. In the tidally mixed coastal waters of the eastern English Channel, the vertical properties of temperature, salinity, *in vivo* fluorescence, turbidity and light were investigated along an inshore–offshore transect, sampled in different tidal conditions. The vertical distribution of these parameters was then characterized in terms of mean value, variability (i.e. standard deviation) and heterogeneity (i.e. fractal dimension), regarded as a quantitative characterization of the structure of the vertical variability of both physical and biological parameters. These different estimates were then subjected to multivariate spatio-temporal analysis and showed a very specific spatio-temporal structure suggesting a differential control of the vertical properties of water masses associated with both inshore–offshore gradient and tidal advection. In particular, the fractal dimension (i.e. heterogeneity) of *in vivo* fluorescence is higher during ebb for offshore waters, suggesting a density dependence of the phytoplankton biomass structure. In contrast, the vertical variability of fluorescence is higher during flood for inshore waters, leading to an inverse relationship between variability and heterogeneity of the vertical distribution of phytoplankton biomass.

Introduction

The general importance of recognizing the causes and consequences of heterogeneity has frequently been emphasized both in marine and terrestrial ecology (Hutchinson, 1953; Levin and Paine, 1974; Wiens, 1976; Roughgarden, 1977; Southwood, 1977, 1988; Kolasa and Rollo, 1991; Levin, 1992). However, there is great confusion in the scientific literature about the relative meaning of 'variability' and 'heterogeneity', depending essentially on a choice of approach (Downing, 1991; Naeem and Colwell, 1991; Shachak and Brand, 1991). General measures of heterogeneity are sometimes not widely known (Kolasa and Rollo, 1991) and are usually associated with traditional descriptors, such as the variance-to-mean ratio (Taylor, 1961; Frontier, 1972; Downing *et al.*, 1987), or the variance associated with a mean abundance estimation, regarded as a primary measure to examine heterogeneity changes across scales (Greig-Smith, 1952; Kershaw, 1957; Goodall, 1974; Ripley, 1987). In this paper, 'variability' indicates changes in the values of a given quantitative or qualitative descriptor (Kolasa and Rollo, 1991), whereas 'heterogeneity' refers to the structure of its variability, estimated using the concept of fractal dimension. Initially introduced to describe the structure of patterns so irregular and fragmented that they present not simply a higher degree but an altogether different level of complexity, as compared with Euclidean approximations (Mandelbrot, 1977, 1983), the concept of fractal more generally characterizes patterns exhibiting structure at all scales. Fractal dimension then appears as a useful measure of spatial heterogeneity, offering the advantage of describing variability as a continuous function of scale (Palmer, 1988). Low and high fractal dimensions characterize heterogeneous and homogeneous patterns exhibiting strong and weak spatial dependence, respectively. Since the fractal

© Oxford University Press

dimension increases with an increase in complexity of a geometrical object, the fractal geometry therefore provides a method of gaining new insights into spatial patterns and heterogeneity. The applicability of these concepts to planktonology has recently been demonstrated (Seuront and Lagadeuc, 1997).

In the eastern English Channel, characterized by its megatidal regime, the fluvial supplies, distributed from the Bay of Seine to Cape Griz-Nez, generate a coastal water mass drifting nearshore, separated from the open sea by a frontal area (Brylinski and Lagadeuc, 1990; Lagadeuc *et al.*, 1997). This coastal flow ('fleuve côtier'; Brylinski *et al.*, 1991) is characterized by its freshness, turbidity (Dupont *et al.*, 1991) and phytoplankton richness (Brylinski *et al.*, 1984; Quisthoudt, 1987). Moreover, the dissipation of tidal energy is basically regarded to be responsible for the vertical homogenization of inshore and offshore water masses (50 m maximum depth). However, recent investigations have shown that the variability perceived in temperature and phytoplankton biomass fluctuations can be wholly characterized in terms of heterogeneity over a wide range of scales (Seuront *et al.*, 1996a,b; Seuront, 1997) and that this heterogeneity cannot be neglected. Indeed, considering the vertical and temporal heterogeneity of photosynthetic parameters, estimates of primary production are increased from 40 to 100% (Lizon *et al.*, 1995; Lizon, 1997; Lizon and Lagadeuc, 1998). The goal of the present paper is to focus on changes through time and space of the vertical patterns of both physical and biological parameters characterized in terms of variability and heterogeneity using a multivariate approach similar to the spatio-temporal analysis initially introduced by Ibanez (1973). Our main findings are: (i) that the variability perceived in vertical patterns of well-mixed waters can be quantitatively characterized as structurally homogeneous using the concept of fractal dimension; (ii) that there is a very specific structure in space and time of variability and heterogeneity associated with both inshore–offshore gradient and tidal forcing; (iii) that a multivariate spatio-temporal analysis, used in conjunction with fractal analyses, provides an appreciation of the nature and magnitude of the sources of variability, and appears to be critical for understanding the underlying biological and physical processes, and also for designing sampling strategies.

Method

Study area and sampling

Sampling was carried out in April 1993 during spring tide in the Dover straight (eastern English Channel), along a transect perpendicular to the coast and to the general drift of waters. The transect consisted of 15 equidistant stations (0.3 nautical mile) and was sampled four times from inshore to offshore waters (50°54'35N, 1°37'15E to 50°57'28N, 1°32'35E), leading to equivalent sampling of inshore and offshore water masses (Figure 1). It takes ~2.5 h to sample each transect, which was separated from the one after by ~30 min. At each station, measurements of physical parameters [temperature, salinity, transmission and photosynthetically active radiation (PAR)] and *in vivo* fluorescence (i.e. an index of phytoplankton biomass) were taken from the surface to bottom with an SBE 25 Sealogger CTD and a Sea Tech fluorometer, respectively.

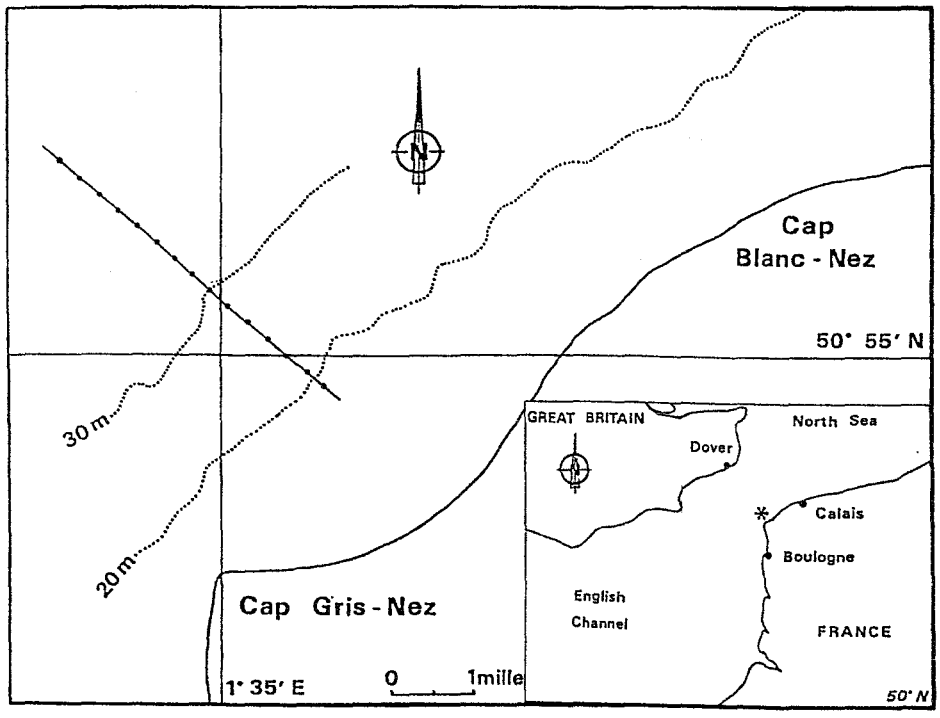

Fig. 1. Position of the stations along the transect, in the eastern English Channel in the Dover Strait.

Data analysis

Fractal dimensions were estimated using a method (Burrough, 1981, 1983) based on geostatistics and regionalized variables (RV) theory (Matheron, 1971; Journel and Huijbregts, 1978). Patterns of variation in RV can then be expressed by their semivariance $\gamma(h)$, defined as:

$$\gamma(h) = \frac{1}{2N(h)} \sum_{i=1}^{N(h)} [Z_{x+h} - Z_x]^2 \quad (1)$$

where $N(h)$ is the number of pairs of data separated by the distance, or lag h, and Z_x and Z_{x+h} are the observed values of a given variable at point x and $x + h$. The fractal dimension D was estimated from the slope m of a log–log plot of the semivariogram (Burrough, 1981, 1983):

$$D = (4 - m)/2 \quad (2)$$

It can be noticed that if the $\gamma(h)$ values estimated between two near samples are no more or less different than between two distant samples, the slope of the semivariogram will be 0, corresponding to a fractal dimension of 2. The slope of the

semivariogram m (and therefore the fractal dimension D), indicating the rate of change from one scale to another, can then be regarded as an index of the degree of spatial dependence of a given parameter. Only scales less than half of the total length of the data set are considered, because greater distances are more affected by low sample sizes and spurious properties of the data (Journel and Huijbregts, 1978).

Since our aim was to look for the spatio-temporal properties of our sampling, we applied a method similar to the spatio-temporal analysis developed by Ibanez (1973) to characterize sampling processes in plankton ecology. We selected variables related to the space–time scales of our sampling experiment and a principal component analysis (PCA) was performed on the observations (i.e. stations along each transect, Q mode) and the variables (R mode, *sensu* Legendre and Legendre, 1984). These variables are latitude, longitude, depth, sun elevation and tidal current direction. We take as an arbitrary origin for latitude and longitude a point located at the intersect between the transect extension and the coastline. Depth is expressed in metres, sun elevation reaches its maximum value around solar midday, and decreases before and after the solar midday at the same rate, and current direction is expressed as an alternance between northerly and southerly drifts during flood and ebb tides, respectively. Furthermore, the identification of the components of the multivariate analyses was carried out using the factor loadings of the variable in the R mode of PCA analysis since the factor loading of a given factor could be related to the variance explained by such a factor (Legendre and Legendre, 1984). Because a criterion is needed for deciding upon appropriate observations to group in the data space, a cluster analysis based on an unweighted centroid algorithm (Sokal and Michener, 1958) has been carried out on a (Euclidean) distance matrix calculated from the first two principal components of the multivariate analysis. Afterwards, we introduced additional variables related to both mean, variability and heterogeneity (i.e. mean, standard deviation and fractal dimension) of temperature, salinity, light transmission, PAR and *in vivo* fluorescence in order to characterize their organization in the spatio-temporal space associated with the sampling experiment. Wind speed and direction were also introduced as indicators of external physical forcing.

Results

Fractal dimensions were estimated for *in vivo* fluorescence, temperature and salinity which exhibited a scaling behaviour over the whole range of studied scales, for inshore as well as for offshore stations (Figure 2). Their linearity over the whole range of spatial scales illustrates spatial dependence, suggesting that the same process can be regarded as the source of physical and biological patterns. Indeed, the mean fractal dimensions of temperature, salinity and *in vivo* fluorescence, estimated for the whole data set as 1.495 (± 0.020 SE), 1.510 (± 0.017 SE) and 1.485 (± 0.019 SE), respectively, were not significantly different (Kruskal–Wallis test, $P > 0.05$). However, the mean fractal dimensions (Table I) and their spatial distribution along each transect (Figure 3) lead to further

Table I. The mean fractal dimensions of temperature (D_T), salinity (D_S) and *in vivo* fluorescence (D_F) for the four sampled transects, shown together with their standard error

Transect	Fractal dimension D		
	D_T	D_S	D_F
1	1.488 (0.032)	1.520 (0.024)	1.502 (0.044)
2	1.626 (0.025)	1.544 (0.034)	1.472 (0.030)
3	1.545 (0.016)	1.597 (0.018)	1.432 (0.034)
4	1.399 (0.032)	1.367 (0.048)	1.545 (0.040)

conclusions. First, except in the case of *in vivo* fluorescence, mean fractal dimensions were significantly different between transects (Kruskal–Wallis test, $P < 0.05$). Furthermore, except in the case of the first transect, mean fractal dimensions of fluorescence, salinity and temperature are significantly different for each transect (Kruskal–Wallis test, $P < 0.05$), the salinity and temperature fractal dimension being not significantly different (Dunn test, $P > 0.05$; Siegel and Castellan, 1988). Second, *in vivo* fluorescence fractal dimensions exhibit a significant tendency to increase for each transect (estimated by calculating the Kendall coefficient of rank correlation τ between the series and the x axis values; Kendall and Stuart, 1966), whereas temperature and salinity exhibit tendencies to increase for the first and fourth transects, and tendencies to decrease for the second transect. Furthermore, PAR and transmission did not exhibit even a partial scaling behaviour (i.e. their variability is independent of scale), and therefore were not subjected to fractal analysis (data not shown).

The results of PCA showed that two components explained 95.20% of the total variance. The first component (PC-1), which explained 58.95% of the variance, was significantly correlated to latitude, longitude and depth (Figure 4a; Table II). This component can then be considered representative of the transect from inshore to offshore waters. The second component (PC-2), which explained 35.25% of the variance, was significantly correlated to tidal current direction and sun elevation (Figure 4a; Table II). The significance of the latter component is essentially linked to the alternance of tidal current directions, the significant inverse correlation of this axis to sun elevation being associated with the solar midday occurrence during flood tide. The projections of the observations in a bidimensional plane defined by the first two components showed two distinct parts. The upper and lower parts characterize stations sampled during ebb and flood tides, respectively (Figure 4b). Furthermore, the unweighted centroid clustering showed four groups of observations (Table III; Figure 4b), which confirmed and specified the previous results. The nature of these clusters in the environmental space was related to the temporal and spatial discrimination shown by the PCA, highlighting both flood tide–ebb tide and inshore–offshore differences associated with the gradients shown by the two principal axes.

The additional variables (Table IV), shown in the space of the two first principal components, have been plotted considering their correlation with these axes

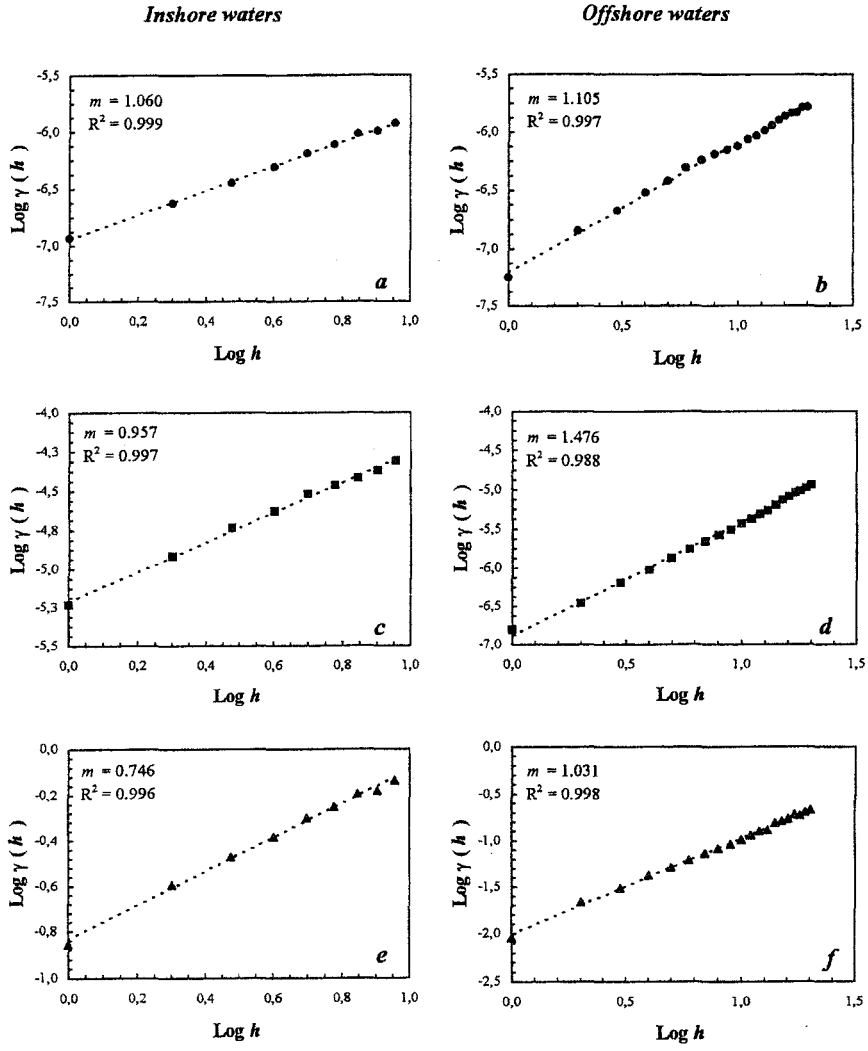

Fig. 2. Double logarithmic semivariograms of temperature, salinity and *in vivo* fluorescence (from top to bottom) for inshore (**a**, **c** and **e**) and offshore (**b**, **d** and **f**) stations of the first transect, shown together with their best fitting line. m is the slope of the empirical semivariance $\gamma(h)$ versus the lag h, in a log–log plot.

as coordinates; a central square indicates the 95% confidence limits (Figure 5). The coordinates of the initial five spatio-temporal variables were also plotted considering the values of their corresponding eigen vectors. The observed means, standard deviations and fractal dimensions exhibited very specific behaviours (Table IV). The behaviour of observed means can be divided into two different groups. First, the means of salinity, transmission and PAR showed a tendency to increase from inshore to offshore waters, whereas temperature and *in vivo*

fluorescence showed an inverse tendency. These results, in agreement with our previous clustering observations (cf. Figure 4b and Table III), can be related to the very specific hydrological structure observed in the eastern English Channel, characterized by an inshore–offshore gradient in terms of salinity, temperature, turbidity, phytoplankton and zooplankton biomass (Brylinski and Lagadeuc, 1990; Brylinski *et al.*, 1991).

The distribution of standard deviations (SD) and fractal dimensions (D) on the PCA plot leads to further conclusions. The standard deviations of temperature and salinity exhibit very similar behaviours, showing a higher vertical variability for inshore waters where mixing processes associated with tidal drift are more developed. On the contrary, the vertical variability of *in vivo* fluorescence and transmission is higher during flood and ebb tides, respectively, but is also slightly higher for inshore than offshore waters. These observations suggest a differential alteration of the mean vertical properties of water masses associated with both inshore–offshore gradient and tidal advection. Therefore, in the case of purely passive scalars (such as temperature and salinity), fluctuations are directly linked with tidal mixing processes, whereas in the case of transmission and fluorescence, other processes—related to physical and chemical properties of particulate matters or the species composition and physiological state of phytoplankton cells—get into action and should be taken into account very carefully. Only the fractal dimensions estimated for *in vivo* fluorescence are significantly correlated with the two first principal components in the case of fluorescence (Figure 5; Table IV). This last observation confirms the absence of systematic variations observed in the spatial distribution of temperature and salinity fractal dimensions, and the tendency to increase of fluorescence fractal dimensions along each transect (cf. Figure 3). *In vivo* fluorescence fractal dimension is then higher for offshore stations and during ebb tide.

Discussion

The empirical fractal dimensions, estimated over the whole range of considered scales for offshore and inshore stations, suggest that the scales of spatial dependence are very similar for *in vivo* fluorescence, salinity and temperature, indicating similar sources of physical and biological patterns. However, as shown by the spatio-temporal analysis, fractal dimensions of salinity and temperature are tidally and geographically independent, in opposition to fluorescence fractal dimensions, obviously higher in offshore waters (cf. Figure 5 and Table IV). The vertical structure of *in vivo* fluorescence is then more homogeneous, or less structured, in offshore locations where the mean observed values of fluorescence are low, suggesting a link between the structure and the strength of the fluorescence signal (i.e. phytoplankton biomass). Indeed, considering the absence of photoinhibition (i.e. a clear decrease of *in vivo* fluorescence around solar midday; Falkowski and Kiefer, 1985), phytoplankton biomass distribution in the eastern English Channel might then be strongly density dependent, whereas Prairie and Duarte (1996) found a weak density dependence in a set of various marine and freshwater phytoplankton populations. In that way, because of the strong

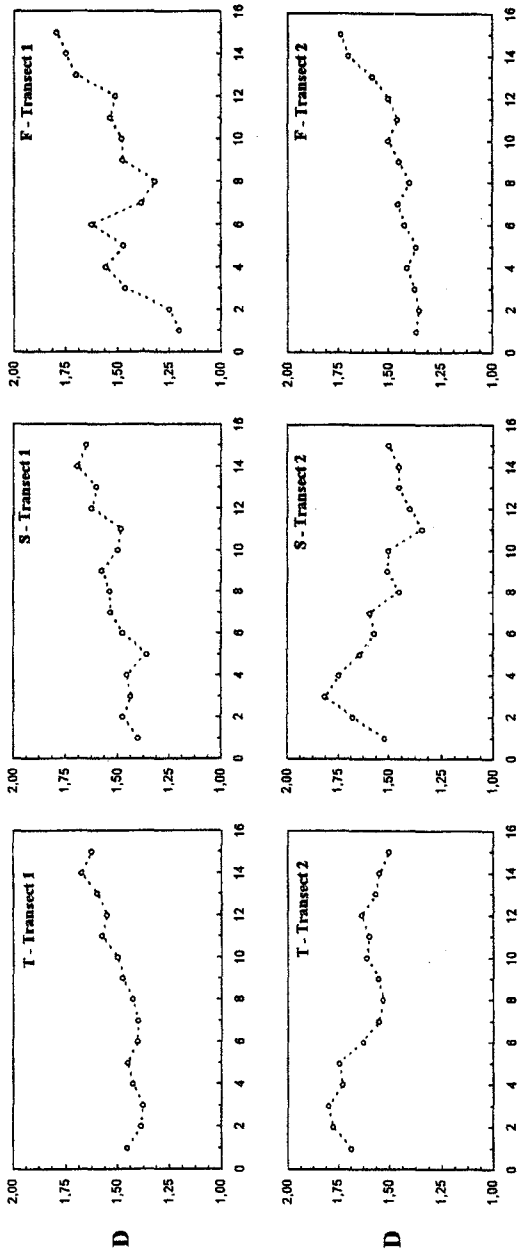
T - Transect 1
S - Transect 1
F - Transect 1
T - Transect 2
S - Transect 2
F - Transect 2
D
2,00
1,75
1,50
1,25
1,00
0
2
4
6
8
10
12
14
16

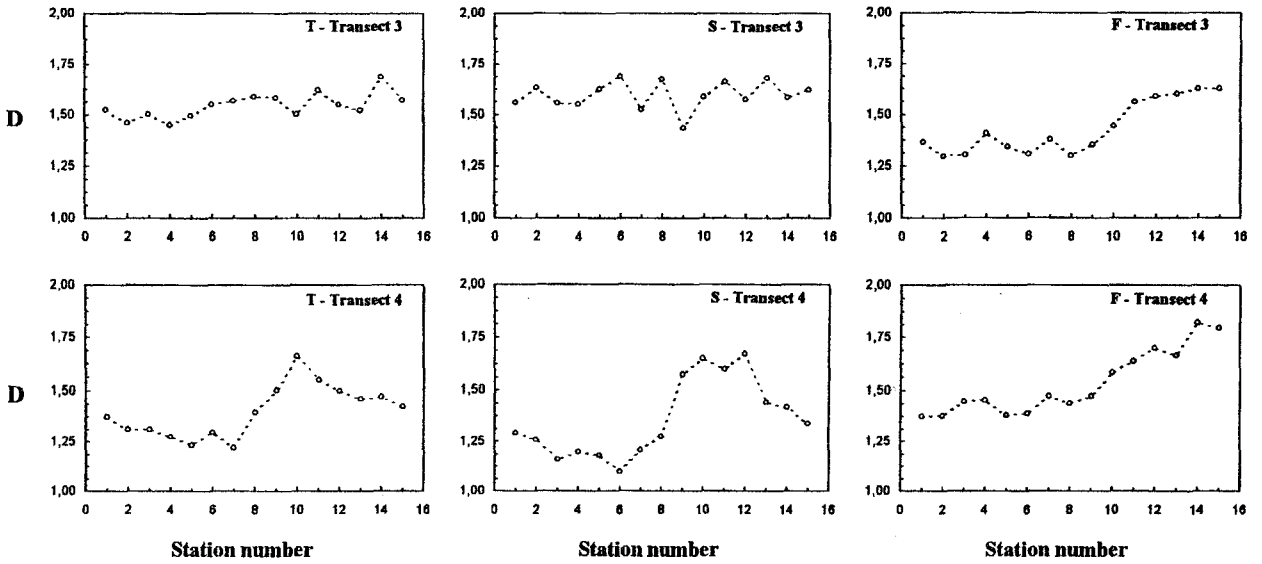

Fig. 3. Evolution of the fractal dimension D of temperature, salinity and *in vivo* fluorescence (from left to right) for each transect (from top to bottom), along the inshore–offshore transect.

Table II. The first two spatio-temporal eigen vectors (standardized after multiplication by the square root of the eigen vectors' corresponding eigen values) associated with the five spatio-temporal variables

	PC-1	PC-2
Latitude	–0.979	0.160
Longitude	0.981	–0.161
Depth	–0.977	–0.058
Sun elevation	–0.271	–0.906
Current direction	0.013	0.941

PC-1, first principal component; PC-2, second principal component.

Table III. Clusters of stations using the first two components of the PCA. Cluster analysis has been carried out on a Euclidean distance matrix calculated from the two first principal components of the PAC

C-I	C-II	C-III	C-IV
$T_{1\text{-}1}$–$T_{1\text{-}10}$	$T_{1\text{-}11}$–$T_{1\text{-}15}$	$T_{2\text{-}14}$–$T_{2\text{-}15}$	$T_{3\text{-}1}$–$T_{3\text{-}7}$
$T_{2\text{-}1}$–$T_{2\text{-}7}$	$T_{2\text{-}10}$–$T_{2\text{-}13}$	$T_{3\text{-}8}$–$T_{3\text{-}15}$	$T_{4\text{-}1}$–$T_{4\text{-}6}$
$T_{4\text{-}7}$–$T_{4\text{-}8}$	$T_{4\text{-}9}$–$T_{4\text{-}15}$		

C, cluster; $T_{i\text{-}j}$, transect number (i) and station number (j).

hydrodynamic conditions occurring in the eastern English Channel, the observed density dependence could be a consequence of the aggregation processes of phytoplankton cells, mainly driven by phytoplankton density and hydrodynamics (Riebesell, 1991a,b; Kiørboe, 1997). Fractal dimension of fluorescence also exhibits a tidal dependence, leading to an inverse relationship between fractal dimension and standard deviation of fluorescence (cf. Figure 5). Fractal dimension and standard deviation are then higher during ebb and flood, respectively. However, even if precise phenomenological arguments are still lacking to explain these differences, it can be suggested that horizontal advection processes associated with the semidiurnal M2 tidal component can be responsible for the advection of different water masses through the entire water column, and modify the biological structure of the water column, leading to a differential tidal control in terms of biological variability and heterogeneity between inshore and offshore waters. Whatever that may be, we showed that in tidally mixed coastal waters the vertical variability of both physical and biological parameters could be wholly characterized in terms of heterogeneity on small scales (i.e. the scale of the water column). Moreover, the vertical variability and its related heterogeneity present very specific patterns in time and/or in space on larger scales (i.e. scales related to the tidal cycle and to the inshore–offshore hydrological gradient).

Previous studies on the dynamics of plankton populations have generally underscored the importance of both temporal and spatial variability of biomass and population structure (e.g. Haury *et al.*, 1978). Our results indicate that the variability—in so far as it describes the amplitude of fluctuations around a mean value—is an insufficient parameter to characterize the structure of a given

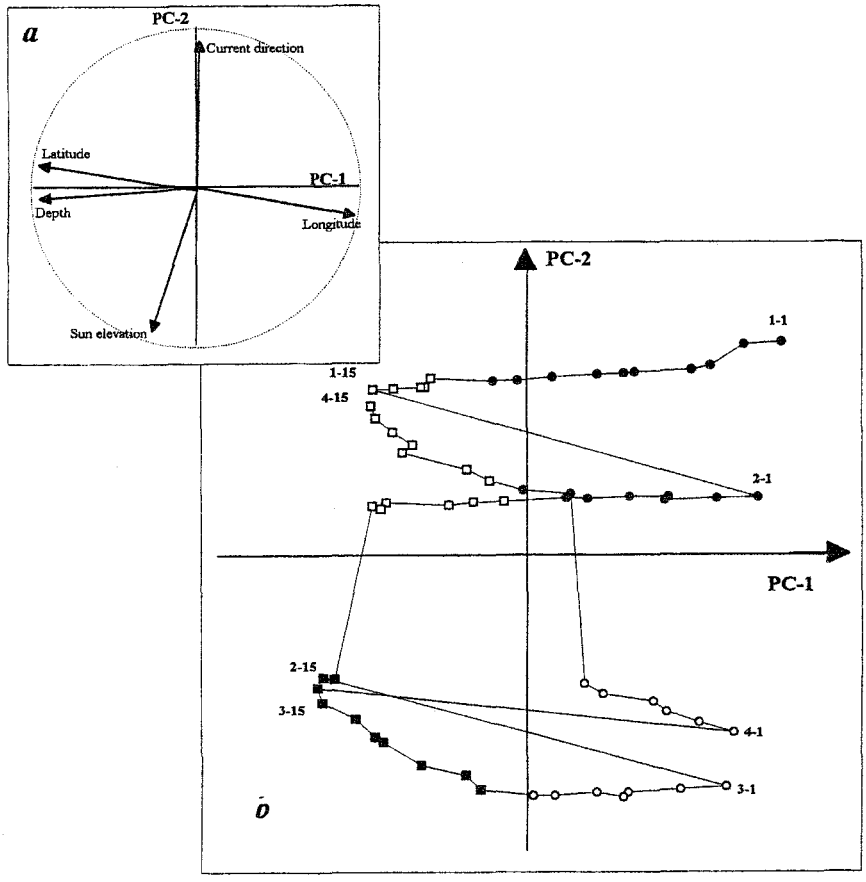

Fig. 4. Correlation circle showing (**a**) the position of the initial variables and (**b**) the position of the stations in the bidimensional space of the principal axes PC-1 and PC-2. Clusters are shown by dark circles (C-I), open squares (C-II), dark squares (C-III) and open circles (C-IV).

process. Describing and characterizing this variability is, however, a main problem in plankton ecology, especially given recent developments in methods for continuously recording at high spatial and temporal resolution (Dickey, 1988, 1991). In that way, the main contribution of semivariogram analysis and fractal dimensions is then to identify and to characterize the scales of spatial dependence—as well as the scales of temporal dependence (e.g. Seuront and Lagadeuc, 1997)—which are of main interest to appreciate the nature and magnitude of sources of variability, critical for understanding the underlying biological and physical processes. Moreover, quantitative characterization of patterns, as realized in the framework of fractal dimensions, provides a basis for comparing models to data, and biological to environmental fluctuations. Such an approach also has considerable implications for the design and evaluation of sampling schemes in coastal as well as in open ocean. Indeed, the accuracy of a regional

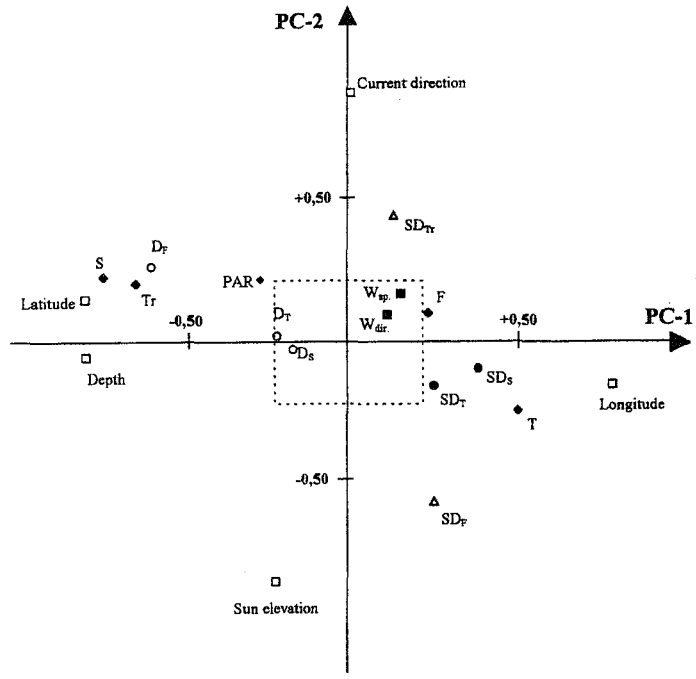

Fig. 5. Position of the 14 factors (for codes, see Table IV) in the bidimensional space of PC-1 and PC-2. The coordinates are the correlation coefficients with these axes. The five initial coordinates (no abbreviations) are placed with the corresponding elements of the eigen vectors (standardized after multiplication by the square root of the corresponding eigen values). Factors significantly correlated with PC-1 and/or PC-2 are located outside the central square, corresponding to the 95% confidence interval.

estimate of a spatially dependent parameter (i.e. temperature, salinity and *in vivo* fluorescence) will depend on both fractal dimension estimates and the scale at which measurements are taken. In contrast, the accuracy of a regional estimate of a spatially independent (e.g. transmission) parameter will depend only on the number of observations.

This paper has presented evidence for the potential of spatio-temporal analysis, used in conjunction with semivariogram and fractal analyses, to become an important descriptive tool in plankton ecology. Furthermore, distinguishing between variability and heterogeneity, such an approach provides new insights into the spatial and temporal structure of highly fluctuating patterns and processes, the understanding of which is actually a major issue in marine ecology. Indeed, both physical and biological small-scale variability experienced by planktonic organisms have been shown to have important implications for foraging, growth and population dynamics (Goldman, 1988; Costello *et al.*, 1990; Marrasé *et al.*, 1990; Davis *et al.*, 1991; Rothschild, 1992), while heterogeneity (i.e. a structured variability in space and/or in time) is increasingly regarded as an intrinsic property of ecosystems (Levin, 1976; Chesson, 1986; Chesson and Case, 1986; Naeem and Colwell, 1991). Future studies investigating the magnitude of key

Table IV. Names and codes of the 14 additional variables used in the PCA, together with their correlation with the two first components of the PCA. The codes are used on the graphs

Additional data	Code	PC-1	PC-2
Mean value			
Temperature	T	0.628	–0.259
Salinity	S	–0.912	0.244
Fluorescence	F	0.300	0.107
Transmission	Tr	–0.789	0.219
PAR	PAR	–0.327	0.232
Standard deviation			
Temperature	SD_T	0.320	–0.165
Salinity	SD_S	0.484	–0.102
Fluorescence	SD_F	0.320	–0.559
Transmission	SD_{Tr}	0.171	0.419
Fractal dimension			
Temperature	D_T	–0.267	0.022
Salinity	D_S	–0.205	–0.029
Fluorescence	D_F	–0.729	0.282
Wind speed	*Wsp.*	0.200	0.180
Wind direction	*Wdir.*	0.150	0.100

PC-1, first principal component; PC-2, second principal component.

fluxes (e.g. carbon or nitrogen cycles) in marine systems should then take advantage to focus on the ecological consequences of the spatio-temporal structure of variability and heterogeneity in order to provide the most precise understanding of a given system, critical to obtain robust estimates of stocks and fluxes (Platt *et al.*, 1989).

Acknowledgements

We would like to thank Bert Klein and one anonymous reviewer for their comments on an earlier version of the manuscript, and Fabrice Lizon for fruitful discussions. Thanks are also extended to the captain and crew of the N/O 'Sepia II' for their assistance during the cruise.

References

Brylinski,J.M. and Lagadeuc,Y. (1990) L'interface eau côtière/eau du large dans le Pas-de-Calais (côte française): une zone frontale. *C. R. Acad. Sci. Paris Sér. 2*, **311**, 535–540.

Brylisnki,J.-M., Dupont,J. and Bentley,D. (1984) Conditions hydrologiques au large du cap Griz-Nez (France): premiers résultats. *Oceanol. Acta*, **7**, 315–322.

Brylinski,J.-M. *et al.* (1991) Le 'fleuve côtier': un phénomène hydrologique important en Manche orientale. Exemple du Pas-de-Calais. *Oceanol. Acta*, **11**, 197–203.

Burrough,P.A. (1981) Fractal dimensions of landscape and other environmental data. *Nature*, **294**, 240–242.

Burrough,P.A. (1983) Multiscale sources of spatial variation in soil. I. The application of fractal concepts to nested levels of soil variation. *J. Soil Sci.*, **34**, 577–597.

Chesson,P.L. (1986) Environmental variation and the coexistence of species. In Diamond,J. and Case,T.J. (eds), *Community Ecology*. Harper & Row, New York, pp. 240–256.

Chesson,P.L. and Case,T.J. (1986) Nonequilibrium community theories: chance, variability, history,

and coexistence. In Diamond,J. and Case,T.J. (eds), *Community Ecology*. Harper & Row, New York, pp. 229–239.

Costello,J.H., Strickler,J.R., Marrasé,C., Trager,G., Zeller,R. and Freize,A. (1990) Grazing in a turbulent environment: Behavioral response of a calanoid copepod, *Centropages hamatus*. *Proc. Natl Acad. Sci. USA*, **87**, 1648–1652.

Davis,C.S., Flierl,G.R., Wiebe,P.H. and Franks,P.J.S. (1991) Micropatchiness, turbulence and recruitment in plankton. *J. Mar. Res.*, **12**, 3–24.

Dickey,T.D. (1988) Recent advances and future directions in multi-disciplinary *in situ* oceanographic measurement systems. In Rothschild,B.J. (ed.), *Toward a Theory on Biological–Physical Interactions in the World Ocean*. Kluwer, Dordrecht, pp. 555–598.

Dickey,T.D. (1991) The emergence of concurrent high-resolution physical and bio-optical measurements in the upper ocean and their applications. *Rev. Geophys.*, **29**, 383–413.

Downing,J.A. (1991) Biological heterogeneity in aquatic ecosystems. In Kolasa,J. and Pickett,S.T.A. (eds), *Ecological Heterogeneity*. Springer-Verlag, New York, pp. 160–180.

Downing,J.A., Pérusse,M. and Frenette,Y. (1987) Effect of interreplicate variance on zooplankton sampling design and data analysis. *Limnol. Oceanogr.*, **32**, 673–680.

Dupont,J.-P., Lafite,R., Huault,M.-F., Lamboy,M., Brylisnki,J.-M. and Guéguéniat,P. (1991) La dynamique des masses d'eau et matière en suspension en Manche orientale. *Oceanol. Acta*, **11**, 177–186.

Falkowski,P.G. and Kiefer,D.A. (1985) Chlorophyll a fluorescence in phytoplankton: relationship to photosynthesis and biomass. *J. Plankton Res.*, **7**, 715–731.

Frontier,S. (1972) Calcul de l'erreur sur un comptage de zooplancton. *J. Exp. Mar. Biol. Ecol.*, **8**, 121–132.

Goldman,J.C. (1988) Spatial and temporal discontinuities of biological processes in pelagic surface waters. In Rothschild,B.J. (ed.), *Toward a Theory on Biological–Physical Interactions in the World Ocean*. Kluwer, Dordrecht, pp. 273–296.

Goodall,D.W. (1974) A new method for analysis of spatial pattern by random pairing quadrats. *Vegetatio*, **29**, 135–146.

Greig-Smith,P. (1952) The use of random and contiguous quadrats in the study of the structure of plant communities. *Ann. Bot.*, **16**, 293–316.

Haury,L.R., McGowan,J.A. and Wiebe,P.H. (1978) Patterns and processes in the time-space scales of plankton distributions. In Steele,J.H. (ed.), *Spatial Pattern in Plankton Communities*. Plenum, New York, pp. 277–327.

Hutchinson,G.E. (1953) The concept of pattern in ecology. *Proc. Acad. Nat. Sci. Philadelphia*, **105**, 1–12.

Ibanez,F. (1973) Méthode d'analyse spatio-temporelle du processus d'échantillonnage en planctonologie, son influence dans l'interprétation des données par l'analyse en composantes principales. *Ann. Inst. Océanogr.*, **49**, 83–111.

Journel,A.G. and Huijbregts,C.J. (1978) *Mining Geostatistics*. Academic Press, London.

Kendall,M. and Stuart,A. (1966) *The Advanced Theory of Statistics*. Hafner, New York.

Kershaw,K.A. (1957) The use of cover and frequency in the detection of pattern in plant communities. *Ecology*, **38**, 291–299.

Kiørboe,T. (1997) Small-scale turbulence, marine snow formation, and planktivorous feeding. *Sci. Mar.*, **61**, 141–158.

Kolasa,J. and Rollo,D.C. (1991) The heterogeneity of heterogeneity: a glossary. In Kolasa,J. and Pickett,S.T.A. (eds), *Ecological Heterogeneity*. Springer-Verlag, New York, pp. 1–23.

Lagadeuc,Y., Brylinski,J.-M. and Aelbrecht,D. (1997) Temporal variability of the vertical stratification of a front in a tidal Region of Freshwater Influence (ROFI) system. *J. Mar. Syst.*, **12**, 147–155.

Legendre,L. and Legendre,P. (1984) *Ecologie numérique*, Vol. 2. Masson, Paris.

Levin,S.A. (1976) Population dynamic models in heterogeneous environments. *Annu. Rev. Ecol. Syst.*, **7**, 287–310.

Levin,S.A. (1992) The problem of pattern and scale in ecology. *Ecology*, **73**, 1943–1967.

Levin,S.A. and Paine,R.T. (1974) Disturbance, patch formation and community structure. *Proc. Natl Acad. Sci. USA*, **71**, 2744–2747.

Lizon,F. (1997) Photoadaptation et évaluation de la production photosynthétique du phytoplancton en relation avec les caractéristiques hydrodynamiques de la Manche orientale. PhD Thesis, University Paris 6.

Lizon,F. and Lagadeuc,Y. (1998) Comparisons of primary production values estimated from different incubation times in a coastal sea. *J. Plankton Res.*, **20**, 371–381.

Lizon,F., Lagadeuc,Y., Brunet,C., Aelbrecht,D. and Bentley,D. (1995) Primary production and

photoadaptation of phytoplankton in relation with tidal mixing in coastal waters. *J. Plankton Res.*, **17**, 1039–1055.
Mandelbrot,B.B. (1977) *Fractals. Form, Chance, and Dimension.* Freeman, San Francisco.
Mandelbrot,B.B. (1983) *The Fractal Geometry of Nature.* Freeman, San Francisco.
Marrasé,C., Costello,J.H., Granata,T. and Strickler,J.R. (1990) Grazing in a turbulent environment: Energy dissipation, encounter rates, and efficacy of feeding currents in *Centropages hamatus*. *Proc. Natl Acad. Sci. USA*, **87**, 1653–1657.
Matheron,G. (1971) *La théorie des variables régionalisées et ses applications. Cahiers du Centre de Morphologie Mathématique de Fontainebleau. Fasc 5.* ENSMP, Paris.
Naeem,S. and Colwell,R.K. (1991) Ecological consequences of heterogeneity of consumable resources. In Kolasa,J. and Pickett,S.T.A. (eds), *Ecological Heterogeneity*. Springer-Verlag, New York, pp. 224–255.
Palmer,M.W. (1988) Fractal geometry: a tool for describing spatial patterns of plant communities. *Vegetatio*, **75**, 91–102.
Platt,T., Harrison,W.G., Lewis,M.R., Li,W.K.W., Sathyendranath,S., Smith,R.E. and Vezina,A.F. (1989) Biological production of the oceans: the case for a consensus. *Mar. Ecol. Prog. Ser.*, **52**, 77–88.
Prairie,Y.T. and Duarte,C.M. (1996) Weak density-dependence and short-term perturbations as determinants of phytoplankton temporal dynamics. *Ecoscience*, **3**, 451–460.
Quisthoudt,C. (1987) Production primaire phytoplanctonique dans le détroit du Pas-de-Calais (France): variations spatiales et annuelles au large du cap Griz-Nez. *C. R. Acad. Sci. Paris*, **304**, 245–250.
Riebesell,U. (1991a) Particle aggregation during a diatom bloom. I. Physical aspects. *Mar. Ecol. Prog. Ser.*, **69**, 273–280.
Riebesell,U. (1991b) Particle aggregation during a diatom bloom. II. Biological aspects. *Mar. Ecol. Prog. Ser.*, **69**, 281–291.
Ripley,B.D. (1987) Spatial point pattern analysis in ecology. In Legendre,P. and Lengendre,L. (eds), *Developments in Numerical Ecology. NATO ASI Series Vol. 14.* Springer. Berlin, pp. 407–429.
Rothschild,B.J. (1992) Applications of stochatic geometry to problems in plankton ecology. *Philos. Trans. R. Soc. London Ser. B*, **336**, 225–237.
Roughgarden,J.D. (1977) Patchiness in the spatial distribution of a population caused by stochastic fluctuations in resources. *Oikos*, **29**, 52–59.
Seuront,L. (1997) Distribution inhomogène multiéchelle de la biomasse phytoplanctonique en milieu turbulent. *J. Rech. Océanogr.*, **22**, 9–16.
Seuront,L. and Lagadeuc,Y. (1997) Characterisation of space-time variability in stratified and mixed coastal waters (Baie des Chaleurs, Québec, Canada): application of fractal theory. *Mar. Ecol. Prog. Ser.*, **259**, 81–95.
Seuront,L., Schmitt,F., Lagadeuc,Y., Schertzer,D., Lovejoy,S. and Frontier,S. (1996a) Multifractal analysis of phytoplankton biomass and temperature in the ocean. *Geophys. Res. Lett.*, **23**, 3591–3594.
Seuront,L., Schmitt,F., Lagadeuc,Y., Schertzer,D. and Lovejoy,S. (1996b) Multifractal intermittency of Eulerian and Lagrangian turbulence of ocean temperature and plankton fields. *Nonlin. Proc. Geophys.*, **3**, 236–246.
Shachak,M. and Brand,S. (1991) Relations among spatiotemporal heterogeneity, population abundance, and variability in a desert. In Kolasa,J. and Pickett,S.T.A. (eds), *Ecological Heterogeneity*. Springer-Verlag, New York, pp. 202–223.
Siegel,S. and Castellan,N.J. (1988) *Nonparametric Statistics for the Behavioral Sciences*. McGraw-Hill, New York.
Sokal,R.R. and Michener,C.D. (1958) A statistical method for evaluating systematic relationships. *Univ. Kansas Sci. Bull.*, **38**, 1409–1438.
Southwood,T.R.E. (1977) Habitat, the templet for ecological strategies? *J. Anim. Ecol.*, **46**, 337–365.
Southwood,T.R.E. (1988) Tactics, strategies and templets. *Oikos*, **52**, 3–18.
Taylor,L.R. (1961) Aggregation, variance and the mean. *Nature*, **189**, 732–735.
Wiens,J.A. (1976) Population responses to patchy environment. *Annu. Rev. Ecol. Syst.*, **7**, 81–120.

Received on December 30, 1997; accepted on March 17, 1998

A6

Photoadaptation and primary production study in tidally mixed coastal waters using a Lagrangian model

Lizon F, Seuront L & Lagadeuc Y

Marine Ecology Progress Series, **169**, 43-64, 1998

Vol. 169: 43–54, 1998 | MARINE ECOLOGY PROGRESS SERIES Mar Ecol Prog Ser | Published August 6

Photoadaptation and primary production study in tidally mixed coastal waters using a Lagrangian model

F. Lizon*, L. Seuront, Y. Lagadeuc

Station Marine de Wimereux, Université des Sciences et Technologies de Lille, CNRS EP 1750, BP 80, F-62930 Wimereux, France

ABSTRACT: In theoretical and field primary production studies, much interest is currently focused on the influence of aperiodic vertical mixing generated at the surface by wind speed and/or heat flux. In the present work, a Lagrangian random walk model was used to study the interactions between periodic vertical tidal mixing and both photoadaptation and primary production of phytoplankton, in typical shallow coastal waters, such as the eastern English Channel. The model considers a depth-dependent diffusion coefficient fluctuating according to the high-low tidal cycles and neap-spring tidal cycles, water columns of different euphotic zone and mixed layer depths, and photoresponse time constants of natural phytoplankton populations collected in the eastern English Channel. Cells were allowed to light-shade adapt, according to the vertical mixing time scales, by altering their photosynthetic properties in response to variations in light. The simulation results indicate first that vertical tidal mixing could control photoadaptation processes at the scale of the high-low tidal cycles at spring tide, and at the scale of neap-spring tidal cycles in shallow coastal systems. Secondly, it appears that the decreasing vertical mixing intensity between spring and neap tide conditions is responsible for a significant increase in daily primary production rates, despite the occurrence of photoinhibition at neap tide. Therefore, primary production in coastal seas would be a function not only of light and nutrient concentrations, but also of photoadaptation processes in relation with vertical tidal mixing. In another way, the Lagrangian model suggests that the theory according to which cells are adapted to the mean light intensity of a water column in a turbulent regime is valid only from a populational point of view. From the model used, it appears also that our present knowledge on photosynthetic dynamic modeling is unsuited to generating pronounced vertical gradients of photosynthetic parameters in all water columns.

KEY WORDS: Models · Phytoplankton · Photosynthetic parameters · Photoadaptation kinetic · Primary production · Vertical tidal mixing · Coastal waters · Eastern English Channel

INTRODUCTION

In natural environments, phytoplankton cells experience light variations due to astronomical cycles, cloud cover, and also to vertical motion caused by turbulent mixing encountered in the water columns. Phytoplankton can respond to these light variations by photoadaptation processes (Harris 1980, Capblancq 1995).

Conceptual bases of phytoplankton photoadaptation in response to vertical mixing have been provided by studies by Marra (1978a, b), Falkowski (1980), Perry et al. (1981), Falkowski & Wirick (1981), Falkowski (1983) and Lewis et al. (1984a). These consist of an adaptation of cells to the vertical gradient of light when the time-scales of physiological processes are shorter than those of vertical mixing events. The photosynthetic characteristics of phytoplankton, such as the parameters of the photosynthesis versus irradiance curves, then display heterogeneities in the water column. In contrast, if vertical mixing takes place on lower time-scales than those of photoadaptation, photosynthetic properties of phytoplankton are expected to be more uniformly distributed with depth. In agreement with these theoretical considerations, it has recently been shown that photoadaptation of phytoplankton can take place at neap tide, in a shallow

*E-mail: lizon@loalit.univ-littoral.fr

© Inter-Research 1998
Resale of full article not permitted

coastal system like the eastern English Channel, influenced mostly by the tide (Lizon et al. 1995). In this area, the occurrence of photoadaptation processes was not obvious because the tidal range is one of the highest in the world (ranging from 3 to 9 m), and the physical structure of the waters, chlorophyll *a* and nutrient profiles are more generally homogeneous (Lizon et al. 1995). Furthermore, photoadaptation processes occurring in the eastern English Channel have noticeable ecological implications. If they are not considered at neap tide, substantial bias (on the order of 40%) can result in the daily primary production rate computations (Lizon et al. 1995).

Concurrently with field or experimental studies (Fortier & Legendre 1979, Marra 1980, Lewis et al. 1984a, b, Mallin & Paerl 1992, Kromkamp & Limbeek 1993, Grobbelaar 1994), several models (Falkowski & Wirick 1981, Woods & Onken 1982, Lande & Lewis 1989, Yamazaki & Kamykowski 1991, Kamykowski et al. 1994, Weissing & Huisman 1994, Woods & Barkmann 1994) have been formulated in order to carry out thorough studies of interactions between vertical mixing and photoadaptation. The previously mentioned biological-physical interactions have been modelled in 2 fundamentally different ways. The first approach describes the average values of photosynthetic properties of a cell population at a given depth, according to vertical mixing intensity. This type of model can be labelled Eulerian or bulk property model. The second approach describes vertical displacements and physiological responses of individual phytoplankton cells in a water column. This kind of model, called Lagrangian model, is primarily of interest because it considers variability in the photosynthetic characteristic of phytoplankton that may exist among cells at the same depth. Such a variability, resulting from different individual light exposure histories of cells in turbulent environments, matches with *in situ* measurements of the phytoplankton responses obtained, for example, by flow cytometry (Chisholm et al. 1986, Li & Wood 1988, Olson et al. 1991). Moreover, recent studies have shown — on the basis of innovative statistical techniques of analysis in oceanography — that phytoplankton biomass is heterogeneously distributed at microscale, though basically regarded as homogenised by turbulent fluid motions (Seuront et al. 1996a, b). Consequently, processes associated with primary production, or more generally processes encountered in marine environments, cannot be considered as average phenomena, but rather as a juxtaposition of many specific events such as individual photosynthetic responses. In this way, a Lagrangian approach along with the previous studies, leads to the characterization of each variability level rather than the description of an average process.

In the previous studies of photoadaptation in relation with turbulence, vertical mixing was always generated by an upper mixed-layer model forced by wind speeds, and sometimes by heat flux. Hydrodynamical regimes were generally constant throughout the day. No theoretical or field study has been conducted on the influence of periodic variations of vertical mixing — which is generated at the bottom of shallow waters by tidal currents (Simpson et al. 1990, 1991) — on photosynthetic processes and daily primary production rates of phytoplankton. Some theoretical studies have considered periodic variations of vertical tidal mixing, but with regard to phytoplankton biomass only (Cloern 1991, Koseff et al. 1993, Baretta et al. 1995, Skogen et al. 1995). Other studies on the interactions between turbulence and photosynthesis have been conducted *in situ*, but in deep waters or in wind-driven turbulent waters (Fortier & Legendre 1979, Demers & Legendre 1981, Lewis et al. 1984b, Vézina et al. 1995, Delgadillo-Hinojosa et al. 1997). Furthermore, the conclusions of field studies about the effect of vertical mixing on primary production rates (increase or decrease) are often inconsistent (Marra 1978b, Mallin & Paerl 1992, Delgadillo-Hinojosa et al. 1997). Thus, the aim of this paper is to conduct a theoretical study, using a Lagrangian model, on the interactions between vertical mixing (which changes according to high-low tidal cycles and neap-spring tidal cycles) and both photoadaptation processes and daily primary production rates in typical shallow coastal water columns. In this way, the variability of the environmental conditions involved in primary production control cannot hide a possible relationship between the previously mentioned physical and biological processes. Such a relationship is hypothesized here.

The model used in this study describes physiological properties of cells instead of cell concentrations. It takes into account both the photoresponse time constants of natural phytoplankton populations from the eastern English Channel and the tidal current speed measurements collected at the same place. For more clarity, non-mobile phytoplankton cells are considered in the present case. The sinking rate of cells and wind-driven turbulence are neglected. First, a detailed account of physical and biological aspects of our modelling is provided. Secondly, we focus on the relationships between vertical mixing related to tidal forcing and both photoadaptation and primary production processes.

MATERIALS AND METHODS

The physical model. In simple vertical transport models such as those used in some studies (Falkowski & Wirick 1981, Yamazaki & Kamykowski 1991, Koseff

et al. 1993, Kamykowski et al. 1994, McGillicuddy 1995), the effect of turbulence on vertical mixing is typically parameterized by a depth-dependent diffusion coefficient (K_v). Following Taylor (1954) and Koseff et al. (1993), eddy diffusivity is characterized by a turbulent velocity scale and a length scale which are respectively shear velocity u^* and the depth of the water column in shallow systems. Since we consider only the tide as a source of turbulence in the present study, the vertical distribution of K_v is parabolic (Koseff et al. 1993). Using the logarithmic law velocity profile, K_v ($m^{-2}\ s^{-1}$) at depth z and time t is given by (Fisher et al. 1979, Koseff et al. 1993):

$$K_v(z,t) = \left[\kappa \cdot u^*(t) \cdot H(t) \cdot \left(\frac{h(t)}{H(t)}\right) \cdot \left(1 - \frac{h(t)}{H(t)}\right)\right] + K_0 \quad (1)$$

where κ is the Von Karman constant (0.4), K_0 is a small value included so that the diffusivity is never equal to zero ($1 \times 10^{-5}\ m^{-2}\ s^{-1}$, a value higher than the molecular diffusivity; cf. Koseff et al. 1993), and $h(t)$ is the distance between the depth of a particle, $Z(t)$ (see Eq. 7), and the depth of the water column, $H(t)$ (see Eq. 4). The shear velocity u^* ($m\ s^{-1}$) is defined as (Dyer 1986):

$$u^*(t) = \frac{\kappa \cdot u(t)}{\log\left(\frac{30 \cdot d}{k_b}\right)} \quad (2)$$

where k_b is the average diameter of the grains of sediment (0.005 m), and $u(t)$ is the current velocity calculated for a depth d, near the bottom of the water column. In order to treat current velocity variations according to both the semidiurnal (M2) and the neap-spring (Mf) tidal cycles, current velocity $u(t)$ ($m\ s^{-1}$) was calculated by the standard following equation:

$$u(t) = \left[A + B \cdot \sin\left(\frac{2\pi t}{T_{Mf}}\right)\right] \cdot \sin\left(\frac{2\pi t}{T_{M2}}\right) \quad (3)$$

where A = 0.95 m s^{-1}, B = 0.43 m s^{-1}, T_{M2} = 12.4 h and T_{Mf} = 14 d. The 2 parameters A and B (the average and the range of current velocity variations at the scale of the neap-spring tidal cycles respectively) were calculated from *in situ* current velocity measurements made at a depth d in different tidal conditions in the eastern English Channel (Lizon 1997). The depth of the water column, $H(t)$ (m), a time-dependent parameter, also ranges according to both the M2 and Mf tidal cycles:

$$H(t) = \overline{H} + \zeta(t) \quad (4)$$

where $\overline{H}$ (m) is the average depth of a water column, and $\zeta(t)$ (m) is the range of the water elevation above the average depth of the water column. This last variable is defined from a model which depends on the semi-tidal range $a(t)$ (m) (G. Chapalain pers. comm.):

$$\zeta(t) = a(t) \cdot \cos\left(\frac{2\pi t}{T_{M2}}\right) \quad (5)$$

$$a(t) = 0.5\left[C + D \cdot \sin\left(\frac{2\pi t}{T_{Mf}}\right)\right] \quad (6)$$

where C = 5.9 m and D = 2 m. These 2 parameters were also calculated from *in situ* water column depth variations in different tidal conditions in the eastern English Channel (Lizon 1997).

The location of a particle $Z(t)$ (m) is parameterized by a random walk model which considers the vertical eddy diffusion coefficient K_v as (Pielou 1969, Falkowski & Wirick 1981):

$$Z(t) = Z(t-1) \pm [2\Delta t \cdot K_v(z,t)]^{1/2} \quad (7)$$

where Δt is the time interval (see below). A choice is made between the algebraical signs + and - with equal probability at each Δt. Following Falkowski & Wirick (1981), the surface and bottom of the mixed layers are treated as reflective boundaries.

The diurnal light incident upon a cell at depth z and time t is given by:

$$I(z,t) = I_M \cdot \sin\left(\frac{\pi t}{DL}\right) e^{[k_d Z(t)]} \quad (8)$$

where I_M is the light intensity on the water column surface at noon (850 µE $m^{-2}\ s^{-1}$), DL is the day length (12 h), and k_d the extinction coefficient. These last parameters are considered constant for the study of daily primary production rates at the scale of the neap-spring tidal cycles in a given water column.

The biological model. The biological model predicts the primary production rate (P) by the empirical model of Platt et al. (1980), as a function of the light incident upon a cell [$I(z,t)$ notated I in the following equation in order to simplify the expression], photosynthetic parameters and chlorophyll a concentration of a cell (B = 10 pg; Montagnes et al. 1994):

$$P(I; P_m^B, \alpha^B, \beta^B) = B \cdot P_m^B \cdot \left(1 - e^{(-\alpha^B I / P_m^B)}\right) \cdot e^{(-\beta^B I / P_m^B)} \quad (9)$$

where P_m^B is the photosynthetic capacity [maximum of the photosynthesis-irradiance (PE) curve], α^B is the photosynthetic efficiency (slope of the PE curve at low light intensity), and β^B a photoinhibition indice (slope of the PE curve at high irradiance).

According to the photoadaptation theory (Falkowski & Owens 1980), phytoplankton cells are assumed to adapt each of their photosynthetic parameters (Γ in abridged notation) after change in light towards fully adapted values Γ_i^*. Following Falkowski & Owens (1980) and Falkowski & Wirick (1981), Γ_i^* can be parameterized by linear functions of the logarithm of the light intensity incident upon a cell, as:

$$\Gamma_i^* = b_\Gamma + a_\Gamma \cdot \ln(I) \quad (10)$$

Table 1. Initial values of photosynthetic parameters [P_m^B is in mgC mg chl a^{-1} h^{-1}, α^B and β^B are in mgC mg chl a^{-1} h^{-1} (μE m^{-2} s^{-1})$^{-1}$] and cell-specific constants used in the biological model for each photosynthetic parameters: γ-LI (h^{-1}) are kinetic constants obtained from low to high light shift experiments on natural population of phytoplankton; γ-HI (h^{-1}), from the reciprocal light shifts; γ-inhib. (h^{-1}) is a kinetic constant determined when P_m^B decreases after a shift under saturating light intensity; a and b are the cell-specific constants of Eq. (10), deduced from the different light shift experiments

	P_m^B	α^B	β^B
Initial values	2.5	0.05	0.005
γ-LI	0.462	0.278	0.131
γ-HI	0.262	0.477	0.425
γ-inhib.	0.656		
a	1.2	−0.006	−0.001
a-inhib.	−0.4		
b	1.2	0.07	0.007

where a_Γ and b_Γ are cell-specific constants. The instantaneous values Γ_i of the photosynthetic parameters can then be calculated according to first-order reaction kinetics (Cullen & Lewis 1988):

$$\frac{d\Gamma_i}{dt} = \gamma_\Gamma \cdot (\Gamma_i^* - \Gamma_i) \quad (11)$$

where γ_Γ are first-order kinetic constants. The different cell-specific constants used (a_Γ, b_Γ and γ_Γ) are presented in Table 1. They have been determined from light shift experiments (cf. Cullen & Lewis 1988) of natural populations of phytoplankton collected in coastal waters of the eastern English Channel (Lizon 1997). Results are consistent with those of Cullen & Lewis (1988). Significant different kinetic constants have been obtained from low to high light shifts and from the reciprocal light shifts (high to low irradiance). Therefore, kinetic constants of each parameter determined from low to high light shift experiments are used when cells are displaced to the surface of the water column. In the opposite case, kinetic constants of each parameter determined from high to low light shifts are considered.

The photoinhibition process is well known to induce P_m^B decreases near the sea surface under high light intensity (Harris 1980, Vincent et al. 1984, Neale & Richardson 1987, Cullen & Lewis 1988, Ferris & Christian 1991). Such a process has been observed in our earlier works conducted in the eastern English Channel (Lizon et al. 1995) and during light shift experiments (Lizon 1997). Photoinhibition is therefore also taken into account in the present study. It is considered here as a photoadaptative process in agreement with Cullen & Lewis (1988). In order to parameterize photoinhibition, P_m^B values measured in the natural environment by Lizon et al. (1995) were fitted by Eqs. (10) & (11). For a light intensity higher than the photoinhibition threshold (450 μE m^{-2} s^{-1}) of photosynthesis, and with a particular kinetic constant (Table 1), we determined a specific value a_Γ for P_m^B. It appears that the best fit (r^2 = 0.703) of the measured data is obtained under high light, with a_Γ = −0.4 (Fig. 1).

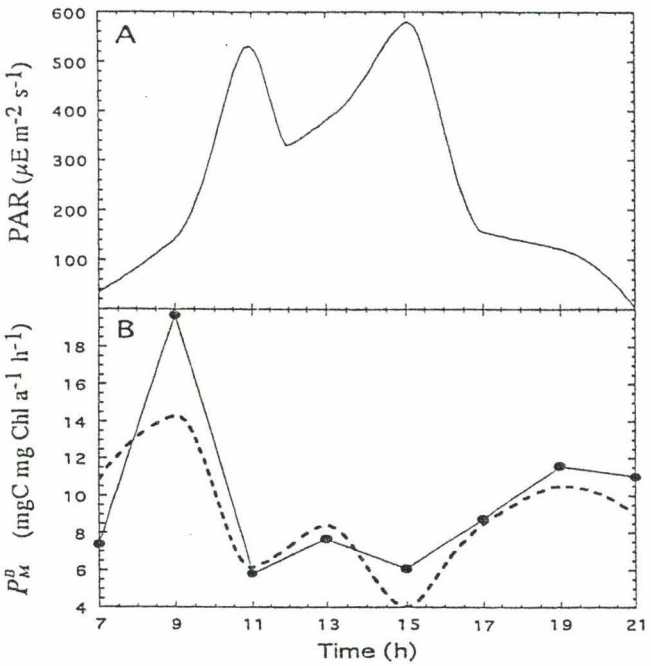

Fig. 1. (A) Irradiance and (B) P_m^B (continuous line) values (Lizon et al. 1995) used to determine a specific value a_Γ (cf. Eq. 10) for P_m^B, when light intensity induces photoinhibition processes. The best fit (r^2 = 0.703) of the measured data (dashed line) was obtained with a_Γ = −0.4. PAR: photosynthetically active radiation

Implementation of the model. The software STELLA, which has been demonstrated to be an efficient tool to transfer a conceptual dynamic model into a practical computer model (Costanza 1987, Richmond et al. 1987, Wu & Vankat 1991, Hannon & Ruth 1994), was used in the present work.

In all Lagrangian models, vertical displacements of organisms are a function of the vertical eddy diffusivity coefficient K_v, but also of the time step Δt (cf. Eq. 10). In the present case, K_v is parameterized from *in situ* measurements of current speeds, and therefore displays fluctuations according to the low-high and neap-spring tidal cycles (Fig. 2). The time step Δt is determined following McGillicuddy (1995) and Barkmann & Woods (1996), so that the mixed layer turnover times are consistent with measured values for mixing layers of similar extent. In this study, as for Barkmann & Woods (1996), a time step of 6 min was used. The turnover times of 20 and 40 m depth water columns — vertical extent of the largest eddies — are then on the order of 30 min and 1 h 30 min respectively at spring

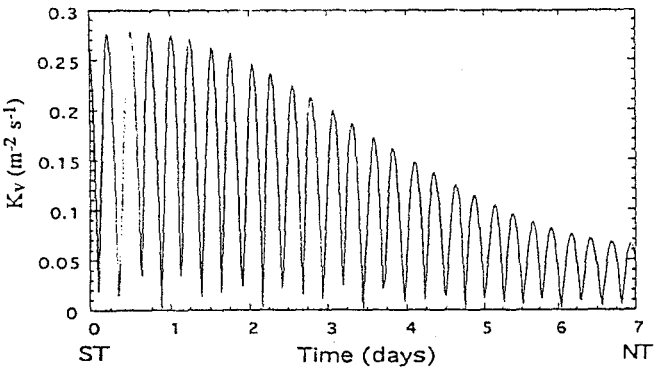

Fig. 2. Variations of the vertical eddy diffusivity coefficient K_v, at the scale of the semi-neap-spring tidal (NT-ST) cycle considered

tide, and on the order of 2 h 20 min and 7 h 30 min respectively at neap tide. Such turnover times are consistent with the values reported or used by many authors (Gargett et al. 1979, Denmann & Gargett 1983, Shay & Gregg 1986, McGillicuddy 1995, Barkmann & Woods 1996) for high and low turbulence regimes in shallow mixing layers. However, in order to compare primary production rates between neap tide conditions and very weak turbulent regimes, additional simulations were made for very small K_v values (10^{-3}, 10^{-4} and 10^{-5} m^2 s^{-1}), i.e. for turnover times up to 100 h.

The biological model considers only photoadaptation processes at short time-scales. It takes no account of processes such as ontogenic adaptations (Kirk 1983), which can occur at long time-scales, i.e. at the scale of the neap-spring tidal cycles. The physiological properties of cells were the same at the beginning of each daylight period (12 h) (Table 1). Therefore, the model was run independently for each simulated day, i.e. for each vertical mixing condition.

At sunrise of each simulated day, 100 cells with the same photosynthetic characteristics were randomly placed within the mixed layer. At each time step Δt, new depths, new light intensities and new photosynthetic parameter values were calculated for each cell. Instantaneous values of primary production were also calculated for each cell, and integrated over the daylight period with the 4th order Runge-Kutta method (Shampine & Watts 1977). Since 100 cells is too small a number for study of phytoplankton responses from a statistical point of view, 3 simulations with 100 cells were made for each tested vertical mixing condition. Thus, displayed daily primary production rates will square with the mean rates of the 3 simulations. Variation coefficients of the daily production rates will also be presented.

The interactions between vertical mixing intensity and daily primary production rates were studied at the scale of a semi-neap-spring tidal cycle (7 d) for different typical water columns found in the eastern English Channel, along an inshore-offshore transect. The extinction coefficients (k_d) and the average depths ($\overline{H}$) of the water columns were chosen from data collected in the coastal, offshore and intermediate waters of the eastern English Channel (Table 2; Lizon 1997). However, since the depths of the euphotic zones (Z_e) are all different from the depths of the mixed layers (Z_m) (i.e. depths of the water columns in the present case) in the 3 previous water masses (Table 2), additional simulations were made for waters where the Z_e/Z_m ratio is equal to the unit.

Table 2. Values of extinction coefficients (k_d), average depths ($\overline{H}$) of the coastal (CW), intermediate (IW) and offshore (OW) water columns considered in this study, and ratios between the euphotic zone and mixed layer depths (Z_e/Z_m) of the 3 water columns

	CW	IW	OW
k_d (m^{-1})	0.4	0.3	0.17
$\overline{H}$ (m)	20	30	40
Z_e/Z_m	0.49	0.53	0.68

RESULTS AND DISCUSSION

Photoadaptation versus vertical mixing

In Fig. 3, daily photosynthetic responses of some individual cells are presented for hydrodynamical regimes related to spring and neap tide. It appears that vertical heterogeneities of photosynthetic characteristics can take place both at neap and spring tide. At neap tide, such results are consistent with earlier studies conducted in the eastern English Channel (Lizon et al. 1995, Lizon & Lagadeuc 1998), whereas they are more surprising at spring tide. However, the results are relatively different between neap and spring tide conditions.

First, vertical gradients of photosynthetic responses match with the photoadaptation theory (Falkowski & Owens 1980), but only under neap tide conditions. The decreases in P_m^B and the increases of α^B and β^B with depth at neap tide indicate that phytoplankton cells adapt their photosynthetic properties to the vertical gradients of light for weak tidal forcing (Figs. 3 & 4). Pronounced photoinhibition processes also occur at neap tide, as shown by the weak values of P_m^B in surface waters in the middle of the day (Fig. 3). On the contrary, at spring tide, vertical heterogeneities of photosynthetic parameters are inconsistent with a photoadaptation to the decreasing vertical gradient of light. Such heterogeneities may be due to the fact that cells tend to continuously adjust their photosynthetic

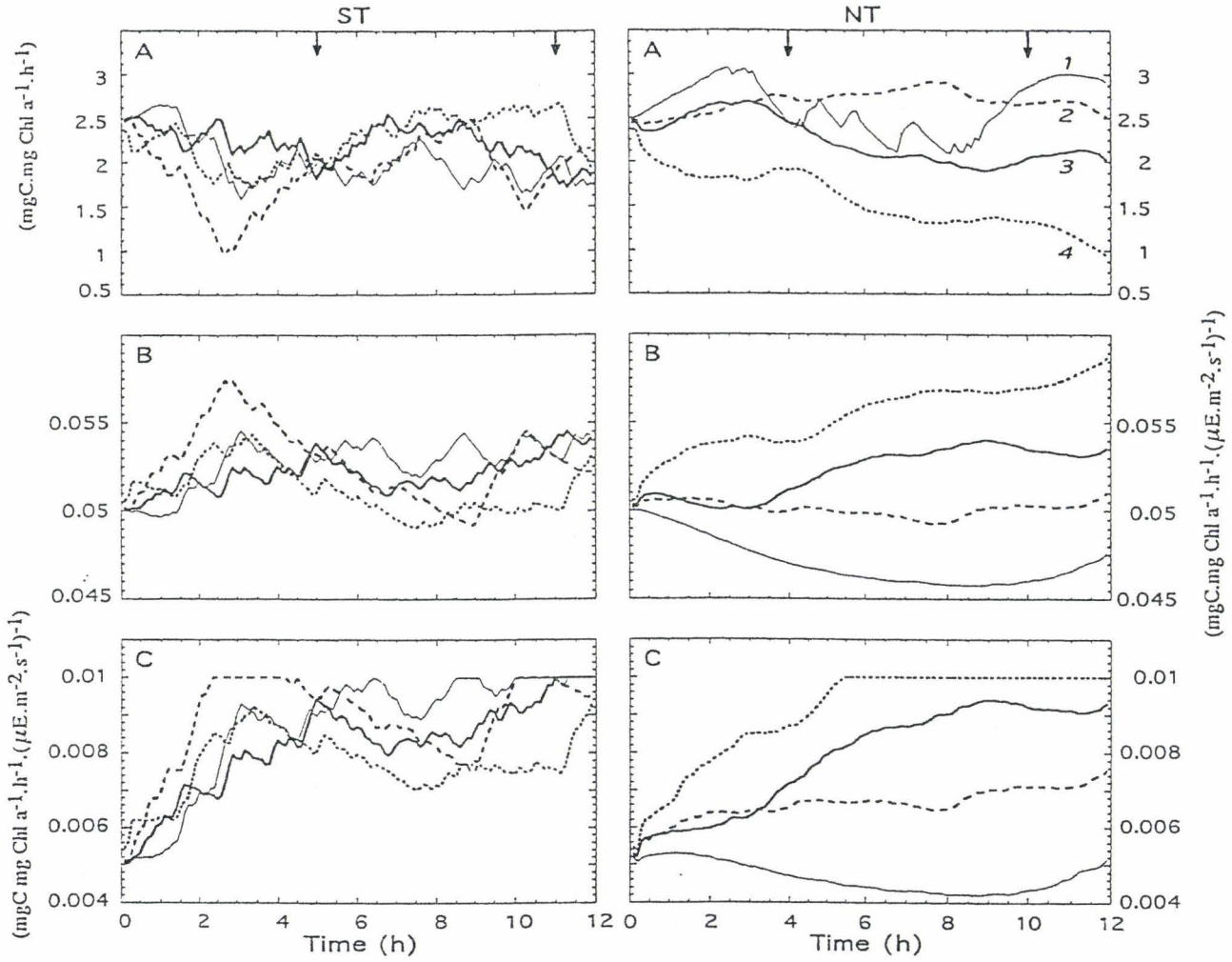

Fig. 3. Variations of the photosynthetic parameters (A) P_m^B, (B) α^B and (C) β^B for 4 individual cells, taken from 4 different depths (1, 5, 10 and 20 m) at spring tide (ST) and at neap tide (NT). Arrows indicate the maximum velocity of the tidal current

characteristics to light variations while they are exported rapidly through the water column. Since the time-scales of vertical mixing become shorter than those of the photoadaptation processes at spring tide, cells display only partial adaptations to the light environment. Actually, these photosynthetic parameter heterogeneities at spring tide reflect the large photosynthetic characteristic variability among phytoplankton cells located at the same depth (Fig. 4). Considering that eddy diffusivity is not homogeneously distributed in a water column (Koseff et al. 1993), each cell has its individual light exposure history, and therefore, different cells cannot show similar physiological properties at the same depth, or at different depths at spring tide. In brief, the difference between our results at spring tide and the photoadaptation theory (Falkowski & Owens 1980) can be explained by the fact that we consider here the individual cell properties and not the population properties, properties on which the photoadaptation theory is based.

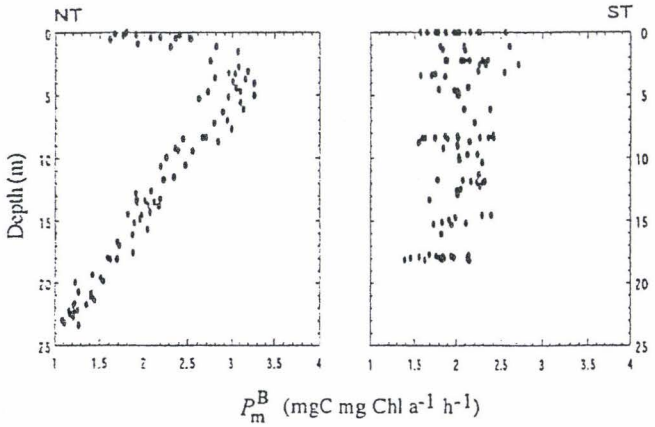

Fig. 4. Vertical gradients of P_m^B at neap tide (NT) and at spring tide (ST)

Second, vertical gradients of photosynthetic parameters are higher at neap tide than at spring tide (Figs. 3 & 5): the vertical variation coefficients (CV) of the pho-

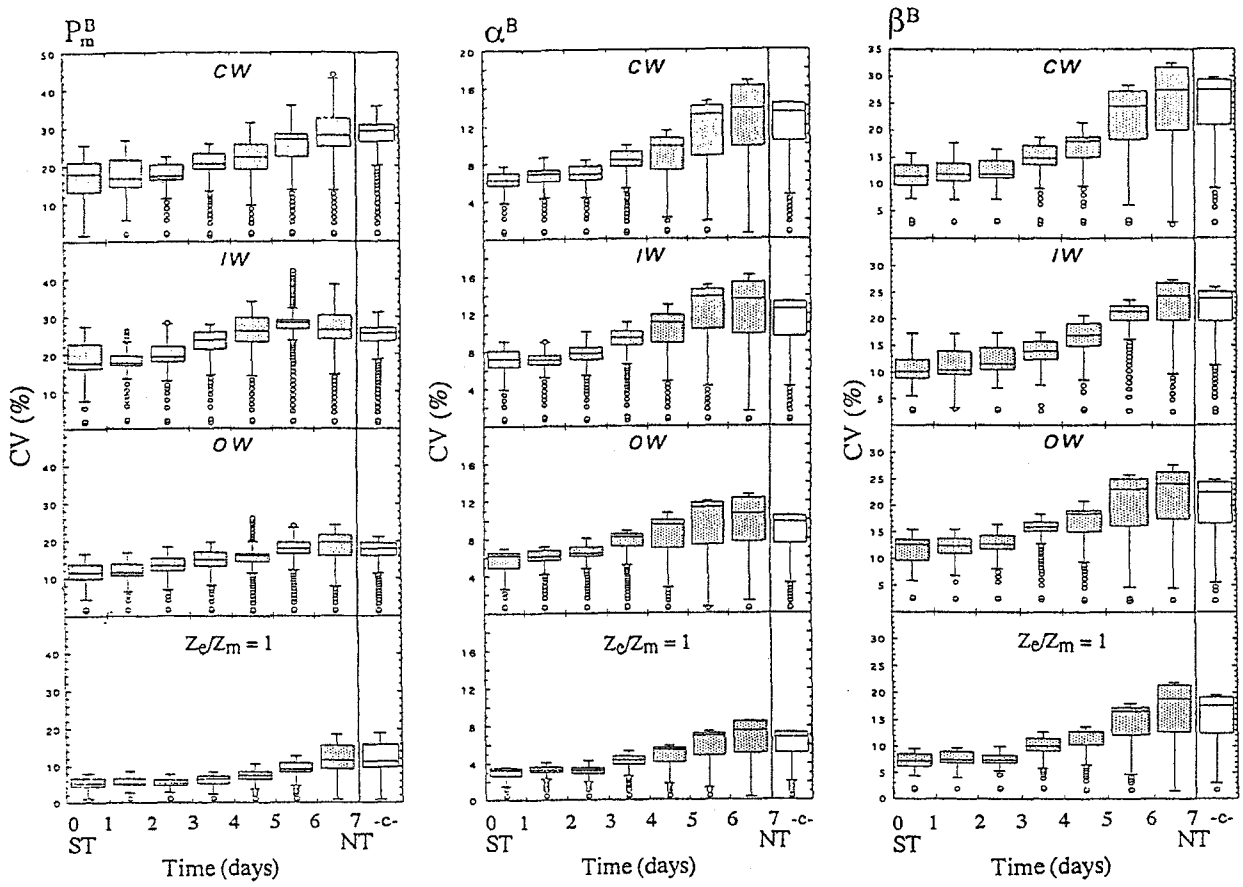

Fig. 5. Box plots showing the increase of the vertical variation coefficients (CV) of the 3 studied photosynthetic parameters (P_m^B, α^B and β^B) between spring (ST) and neap tide (NT) conditions, for coastal (CW), intermediate (IW), offshore (OW) and $Z_e/Z_m = 1$ water columns. In case c (-c-), CV of photosynthetic parameters resulting from simulations with a small K_v value of 10^{-5} m^2 s^{-1} are reported. Box plots show the median (horizontal line in the boxes), quartiles (boxes), and upper/lower 5th percentiles of all data

tosynthetic parameters display significant increases between spring and neap tide conditions in the 4 studied water columns (Fig. 5, Table 3). These results match with the simulations of Kamykowski et al. (1994) and the field studies of Lewis et al. (1984b). These authors showed, for the first time and from *in situ* collected data, the relationship between vertical heterogeneities of the phytoplankton photosynthetic parameters and the hydrodynamical regimes related to wind forcing. However, it appears from our simulation results that vertical heterogeneities of photosynthetic characteristics are continuous during the day at neap tide, whereas they tend to be reduced, especially for P_m^B when the current speeds are maximum at spring tide (Fig. 3). Therefore, the interactions between photoadaptation and vertical mixing at the scale of high-low tidal cycles can occur at spring tide in our model, in the same way as they occur in the eastern English Channel (Lizon et al. 1997).

Table 3. Kendall's coefficients of rank correlation (τ) calculated for the box plot medians (cf. Fig. 5) of the vertical variation coefficients (CV) of P_m^B, α^B and β^B, and for the daily primary production rates (P) corresponding to coastal (CW), intermediate (IW), offshore (OW) and $Z_e/Z_m = 1$ water columns, between spring and neap tide conditions (**$p < 1\%$, *$p < 5\%$). τ coefficients were calculated between the original data series and the data series and classified by increasing order (Legendre & Legendre 1984)

	CV P_m^B	CV α^B	CV β^B	P
CW	0.810**	0.905**	0.985**	0.970**
IW	0.820**	0.865**	0.901**	0.852**
OW	0.815**	0.880**	0.850**	0.335
$Z_e/Z_m = 1$	0.765*	0.810**	0.816**	0.231

It must be added that our simulation results show that the CV of P_m^B, α^B and β^B are higher in coastal than in $Z_e/Z_m = 1$ water columns, at neap tide as well as at spring tide (Fig. 5). The weak values of the CV for $Z_e/Z_m = 1$ water columns do not fit with the measurements of photosynthetic responses collected in the eastern English Channel waters. As a matter of fact, Lizon et al. (1995) have shown that vertical heterogeneity of photosynthetic parameters could be on the

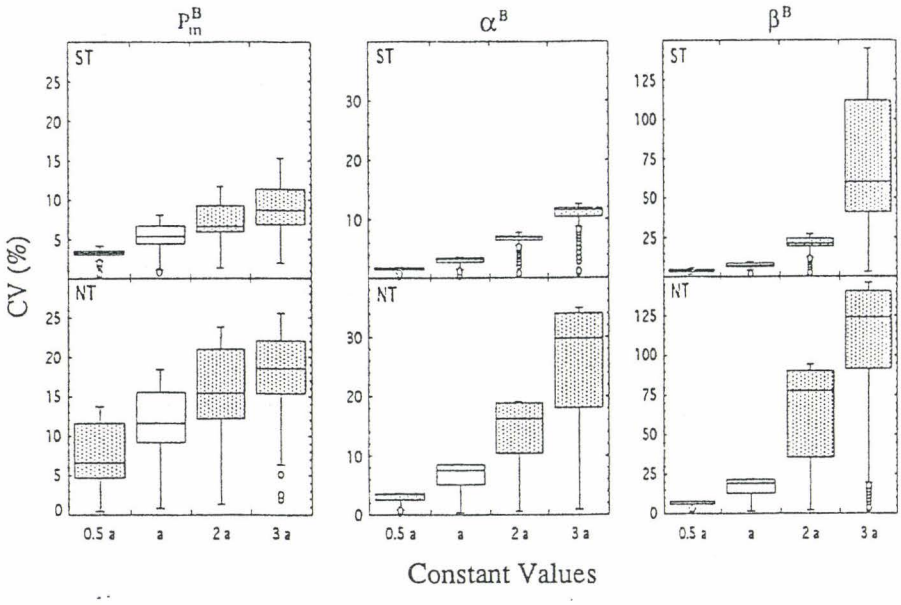

Fig. 6. Box plots showing the vertical variation coefficients (CV) of the 3 studied photosynthetic parameters (P_m^B, α^B and β^B) at spring (ST) and neap tide (NT), for cell-specific constants a_Γ (cf. Eq. 10 and Table 1) multiplied by the factors 0.5, 1, 2 and 3

order of 60% for water columns where $Z_e/Z_m = 1$. The photoadaptative dynamics used, which is based on our present knowledge of this subject, then is not adequate to generate pronounced vertical gradients of photosynthetic parameters in all water columns. The differences between *in situ* and modelling observations could be explained by only 1 measurement of the cell-specific constants of the photosynthetic parameters, and under only 1 hydrodynamical condition. Since taxonomic composition of phytoplankton community and cell pigment contents can change, owing to ontogenic adaptations at the scale of the neap-spring tidal cycles (Kirk 1983, Geider et al. 1996), it can be hypothesized that cell-specific constants, which are different with different species (Cullen & Lewis 1988), could also change at this time-scale and could be specific to water column physical characteristics. Lande & Lewis (1989) have also suggested that it could be interesting to reconsider the validity of some functions such as Eq. (10), which describe the fully adaptive state of cells (Γ_i^*). A non-linear relationship between Γ_i^* and the logarithm of the light intensity incident upon a cell could result in higher heterogeneity in photosynthetic responses between the top and the bottom of a water column. These remarks are supported here by a sensibility analysis of the cell-specific constants a_Γ. As a matter of fact, high values of a_Γ can induce high photosynthetic parameter heterogeneities in a $Z_e/Z_m = 1$ water column and higher differences in vertical heterogeneities of the photosynthetic parameters between neap and spring tide conditions (Fig. 6).

Given that variations of vertical tidal mixing intensity could control photoadaptation processes of phytoplankton at the scale of the neap-spring tidal cycles, and also at the scale of high-low tidal cycles at spring tide, the question now is: what is the effect of vertical mixing variations at the neap-spring tidal cycles on the daily primary production rates?

Primary production rates versus vertical mixing

First of all, the daily primary production rates are noticeably different between the 4 studied water columns, irrespective of the hydrodynamical conditions (Fig. 7A). At spring and neap tides, the higher the ratios between the euphotic zone depths and the mixed layer depths of a given water column, the higher the daily production rates (Fig. 7A). Such results are not surprising, since, when the euphotic zone depth increases, light incident upon the cells located at the bottom of the water column increases and the daily primary production rates of cells also increase. Therefore, the daily primary production rates of cell populations were divided by the average daily light intensities of each mixed layer in order to obtain a standardised index between the different studied water columns (Fig. 7B).

The overall result of our simulations then is an increase in the daily primary production rates between spring and neap tide conditions (Fig. 7B). However, the previous increases in the daily rates are related to the considered water columns, i.e. the values of the Z_e/Z_m ratios. Statistically significant increases, on the order of 40%, are observed in the course of the semi-neap-spring tidal cycle, for coastal and intermediate water columns (Table 3). In contrast, for offshore and $Z_e/Z_m = 1$ water columns, the tendency toward an increase in daily production rates is not significant from a statistical point of view (Table 3). In these last 2 cases,

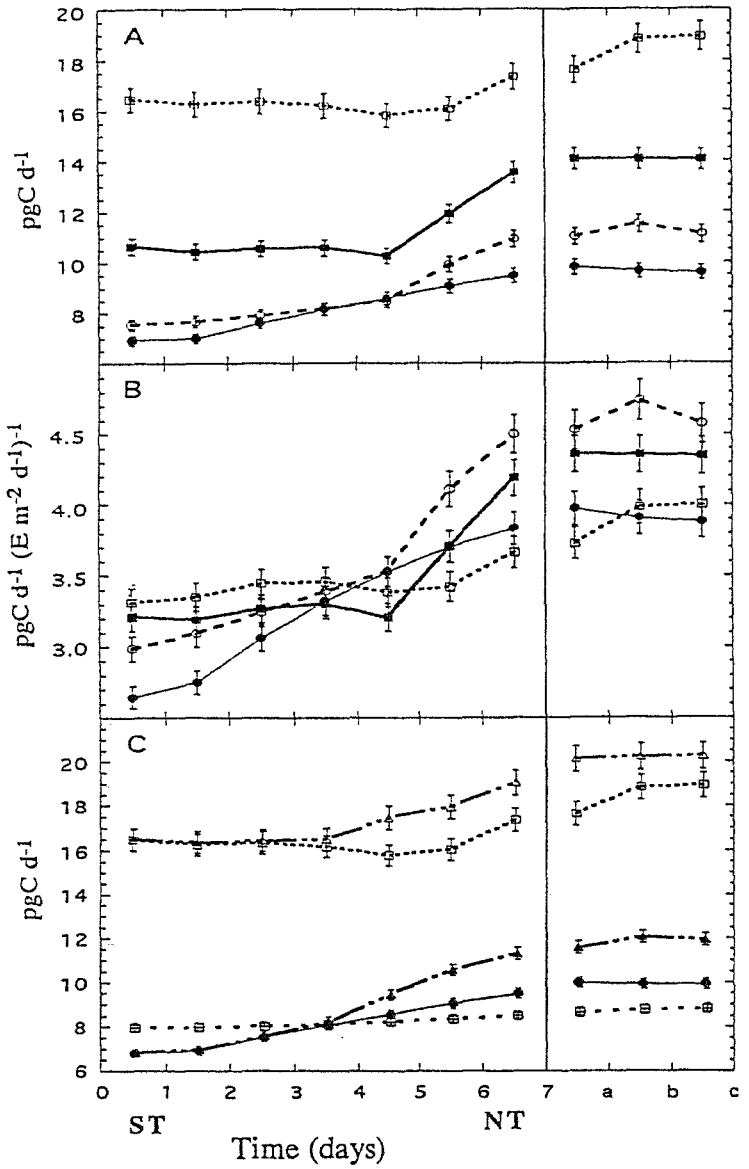

Fig. 7. (A) Daily primary production rates in coastal (●), intermediate (○), offshore (■) and Z_e/Z_m = 1 (□) water columns between spring (ST) and neap tide (NT) conditions. (B) Ratios between the daily production rates and the mean daily light intensities of each considered mixed layer. (C) Daily primary production rates considering photoinhibition processes (● and □) or not (▲ and △), in coastal (● and ▲) and Z_e/Z_m = 1 (□ and △) water columns, and daily primary production rates obtained by excluding photoadaptation processes (⊞) in our calculations in coastal waters. In the cases a, b and c, daily production rates resulting from simulations with small K_v values (10^{-3}, 10^{-4} and 10^{-5} m^2 s^{-1}) are reported

the increases in daily rates occur late in the course of the semi-neap-spring tidal cycle, and all the more weakly as the Z_e/Z_m ratios are close to unity (Fig. 7B). If a relationship between daily primary production rates and vertical mixing intensities was expected, the influence of the euphotic zone depth on this relationship was not because the vertical heterogeneity of 3 photosynthetic parameters decreases with an increase in the depth of the euphotic zone (Fig. 5). It can thus be hypothesized that the low CV of photosynthetic parameters in a Z_e/Z_m = 1 water column would be insignificant compared with the vertical gradients of light considered in the computation of the cell primary production rates. Thus, in a Z_e/Z_m = 1 water column, low photoadaptation processes would have a weak effect on the daily production rates between spring and neap tide conditions, for which the vertical gradients of light are similar.

Furthermore, the control of daily primary production rates by vertical mixing intensity is made *via* photoadaptation processes occurring at short time-scales. As a matter of fact, differences in daily primary production rates between spring and neap tide conditions are on the order of 40% when photoadaptation processes are taken into account in a coastal water column whereas they are on the order of only 4.2% if photoadaptation processes are not considered (Fig. 7C). Such results concerning the physical control of daily primary production rates *via* photoadaptation are in agreement with the simulation results of Barkmann & Woods (1996), and in disagreement with those of Lande & Lewis (1989) and Falkowski & Wirick (1981). As a matter of fact, Barkman & Woods (1996) also found higher production rates under stable conditions than in turbulent regimes, and differences on the order of 40% between daily production rates computed for the 2 above-mentioned hydrodynamical conditions. However, our results specify that production rate control can be exerted by vertical mixing generated by the tide (from the bottom of a shallow water column) and occurring periodically at short time-scales. In the Barkmann & Woods (1996) study, vertical mixing of deep water columns was induced by heat flux and wind stress, i.e. by physical processes occurring at longer time-scales than those of vertical tidal mixing, or those of photoadaptation processes. In contrast to our results, Lande & Lewis (1989) predicted weak production rate differences between low and high turbulent regimes, and Falkowski & Wirick (1981) concluded that turbulence has very little effect on phytoplankton primary productivity. The discrepancy between these studies and our simulations can be explained by the mixing time-scales considered. For example, Falkowski & Wirick (1981) used K_v values inducing turnover times of a 20 m depth water

column, ranging between 110 and 11000 h for high and low turbulent regimes, respectively. In such conditions, vertical eddy length scales can never be higher than 5 m, and differences in daily production rates between stable and turbulent environments cannot be displayed. Such explanations are supported here by daily primary production rates computed for weak eddy diffusivity values (10^{-3}, 10^{-4} and 10^{-5} m^2 s^{-1}) (Fig. 7A, B): daily production rates were not different between turbulent conditions resulting from these small K_v values and neap tide conditions.

From our simulation results, it appears that moderate vertical mixing, such as that encountered here some time before neap tide (1 or 2 d before), would not induce an increase in the daily primary production rates, irrespective of the water columns considered. There is no decrease in the daily production rates between the fifth and the seventh day of the semi-neap-spring cycle. Such results refute the hypothesis formulated by Gallegos & Platt (1985) and Mallin & Paerl (1992). These authors assert that moderate vertical mixing could stimulate phytoplankton production by tempering light limitation of cells located below the 10% incident irradiance or by reducing the photoinhibition effect in surface waters. Vertical mixing, however, would control photoinhibition processes, but at the scale of the semi-neap-spring tidal cycle according to the present study. As a matter of fact, Fig. 7C shows that for 2 different water columns, daily production rates, whether considering photoinhibition or not, are similar at spring tide whereas daily rates differ by about 10% at neap tide, irrespective of the Z_e/Z_m ratio values. These results then show, in contrast to the conclusions of Falkowski & Wirick (1981), that daily primary production rates can be a function of vertical mixing intensity, even if photoinhibition processes are not considered.

CONCLUSION

With reference to our hypothesis, we can conclude that vertical tidal mixing could control daily primary production rates at the scale of the neap-spring tidal cycles in shallow coastal water columns. As a matter of fact, from a simple Lagrangian model, it appears that the decreasing intensity of vertical mixing between spring and neap tide conditions is responsible for a significant increase in daily primary production rates (on the order of 40%), via photoadaptation processes occurring at short time-scales, with or without photoinhibition processes. If conclusions of field studies are often inconsistent with respect to the effect of turbulence on primary production rates (increase or decrease) (Marra 1978b, Mallin & Paerl 1992, Delgadillo-Hinojosa et al. 1997), this may be due to the competitive effect of light and nutrients in the context of vertical mixing and stratified waters. In the natural environment, vertical mixing can occur at different time-scales, and generate limitations in light, in nutrients, or in both light and nutrients (Huisman & Weissing 1995, Delgadillo-Hinojosa et al. 1997).

Therefore, primary production in coastal seas—such as the eastern English Channel—would not be only a function of light intensity and nutrient concentrations (Agoumi 1985, Moloney et al. 1986, Hoch 1995, Hoch & Ménesguen 1995, Ménesguen & Hoch 1995), but also of photoadaptation processes in relation with vertical tidal mixing intensity. Such processes should be considered in future work on primary production modelling at mesoscales, even if there is some difficulty in identifying this relationship at such scales and in coastal seas (Vézina et al. 1995). As a matter of fact, biological and physical fluctuations in coastal systems can occur faster than the biweekly neap-spring tidal cycles, owing to horizontal advection processes of different water masses (Lizon et al. 1995, Vézina et al. 1995, Brylinski et al. 1996), and can partially hide the relationship between primary production and vertical mixing. However, before conducting further modelling, new experiments must be carried out in order to study the cell-specific constants of photoadaptation processes, for water columns of different Z_e/Z_m ratios, and at the scale of the neap-spring tidal cycles.

Acknowledgements. The authors thank G. Chapalain, J. Steele and S. Monismith for their advice, and J. L. Sardin for a revision of the English of this manuscript. The authors are grateful to N. Esquerre and V. Gentilhomme for their assistance during the reciprocal light shift experiments with phytoplankton cells.

LITERATURE CITED

Agoumi A (1985) Modélisation de l'écosystème pélagique en Manche. Etude de l'influence des phénomènes physiques sur le système planctonique. PhD thesis, University of Paris 6

Baretta JW, Admiraal W, Colijn F, Malschaert JFP, Ruardij P (1995) Tidal flat estuaries. Simulation and analysis of the Ems estuary. Ecol Stud 71:77–104

Barkmann W, Woods JD (1996) On using a Lagrangian model to calibrate primary production determined from *in vitro* incubation measurements. J Plankton Res 17:767–787

Brylinski JM, Brunet C, Bentley D, Thoumlin G, Hilde D (1996) Hydrography and phytoplankton biomass in the eastern English Channel in spring 1992. Estuar Coast Shelf Sci 43:507–519

Capblancq J (1995) Production primaire autotrophe. In: Pourriot R, Meybeck M (eds) Limnologie générale. Masson, Paris, p 228–252

Chisholm SW, Armbrust EV, Olson RJ (1986) The individual cell in phytoplankton ecology: cell cycles and application of flow cytometry. Can Bull Fish Aquat Sci 214:343–369

Cloern JE (1991) Tidal stirring and phytoplankton bloom dynamics in an estuary. J Mar Res 49:203–221
Costanza R (1987) Simulation modeling on Macintosh using STELLA. BioSci 37:129–132
Cullen JJ, Lewis MR (1988) The kinetics of algal photoadaptation in the context of vertical mixing. J Plankton Res 10: 1039–1063
Delgadillo-Hinojosa F, Gaxiola-Castro G, Segovia-Zavala JA, Munoz-Barbosa A, Orozco-Bordon MV (1997) The effect of vertical mixing on primary production in a bay of the Gulf of California. Estuar Coast Shelf Sci 45:135–148
Demers S, Legendre L (1981) Mélange vertical et capacité photosynthétique du phytoplancton estuarien (estuaire du Saint-Laurent). Mar Biol 64:243–250
Denman KL, Gargett AE (1983) Time and space scales of vertical mixing and advection of phytoplankton in the upper ocean. Limnol Oceanogr 28:801–815
Dyer KR (1986) Coastal and estuarine sediment dynamics. John Wiley & Sons, New York
Falkowski PG (1983) Light-shade adaptation and vertical mixing of marine phytoplankton: a comparative field study. J Mar Res 41:215–237
Falkowski PG (1980) Light-shade adaptation in marine phytoplankton. In: Falkowski PG (ed) Primary production in the sea. Plenum Press, New York, p 99–119
Falkowski PG, Owens TG (1980) Light-shade adaptation: two strategies in marine phytoplankton. Plant Physiol 66: 592–595
Falkowski PG, Wirick CD (1981) A simulation model of the effects of vertical mixing on primary productivity. Mar Biol 65:69–75
Ferris JM, Christian R (1991) Aquatic primary production in relation to microalgal responses to changing light: a review. Aquat Sci 53:187–217
Fisher HB, List EJ, Koh RCY, Imberger J, Brooks NH (1979) Mixing in inland and coastal waters. Academic Press, New York
Fortier L, Legendre L (1979) Le contrôle de la variabilité à court terme du phytoplancton estuarien: stabilité verticale et profondeur critique. J Fish Res Bd Can 36:1325–1335
Gallegos CL, Platt T (1985) Vertical advection of phytoplankton and productivity estimates: a dimensional analysis. Mar Ecol Prog Ser 26:125–134
Gargett AE, Sanford TB, Osborn TR (1979) Surface mixing layer in the Sargasso Sea. J Phys Oceanogr 9:1090–1111
Geider RJ, Macintyre HL, Kana TM (1996) A dynamic model of photoadaptation in phytoplankton. Limnol Oceanogr 41:1–15
Grobbelaar JU (1994) Turbulence in mass algal cultures and the role of light/dark fluctuations. J Appl Phycol 6: 331–335
Hannon B, Ruth M (1994) Dynamic modeling. Springer-Verlag, New York
Harris GP (1980) The relationship between chlorophyll *a* fluorescence, diffuse attenation changes and photosynthesis in natural phytoplankton populations. J Plankton Res 2: 109–127
Hoch T (1995) Modélisation du cycle biogéochimique des éléments limitant la production biologique en Manche (N, P, Si). PhD thesis, University of Paris 7
Hoch T, Ménesguen A (1995) Modelling the biogeochemical cycles of elements limiting primary production in the English Channel. II. Sensitivity analyses. Mar Ecol Prog Ser 146:189–205
Huisman J, Weissing FJ (1995) Competition for nutrients and light in a mixed water column: a theoretical analysis. Am Nat 146(4):536–564
Janowitz GS, Kamykowski D (1991) An Eulerian model of phytoplankton photosynthetic response in the upper mixed layer. J Plankton Res 13:983–1002
Kamykowski F, Yamazaki H, Janowitz GS (1994) A Lagrangian model of phytoplankton photosynthetic response in the upper mixed layer. J Plankton Res 16:1059–1069
Kirk JTO (1983) Light and photosynthesis in aquatic ecosystems. Cambridge University Press, Cambridge
Koseff JR, Holen JK, Monismith SG, Cloern JE (1993) Coupled effects of vertical mixing and benthic grazing on phytoplankton populations in shallow, turbid estuaries. J Mar Res 51:843–868
Kromkamp J, Limbeek M (1993) Effect of short-term variation in irradiance on light harvesting and photosynthesis of the marine diatom *Skeletonema costatum*: a laboratory study simulating vertical mixing. J Gen Microbiol 139: 2277–2284
Lande R, Lewis MR (1989) Models of photoadaptation and photosynthesis by algal cells in a turbulent mixed layer. Deep Sea Res 36:1161–1175
Legendre L, Legendre P (1984) Ecologie numérique 2: la structure des données écologiques. Masson, Paris
Lewis MR, Cullen JJ, Platt T (1984a) Relationships between vertical mixing and photoadaptation of phytoplankton: similarity criteria. Mar Ecol Prog Ser 15:141–149
Lewis MR, Horne EPW, Cullen JJ, Oakley NS, Platt T (1984b) Turbulent motions may control phytoplankton photosynthesis in the upper ocean. Nature 311:49–50
Li WKW, Woods AM (1988) Vertical distribution of North Atlantic ultraphytoplankton: analysis by flow cytometry and epifluorescence microscopy. Deep Sea Res 35: 1615–1638
Lizon F (1997) Photoadaptation et évaluation de la production photosynthétique du phytoplankton en relation avec les caractéristiques hydrodynamiques de la Manche Orientale. PhD thesis, University of Paris 6
Lizon F, Lagadeuc Y (1998) Comparisons of primary production values estimated from different incubation times in a coastal sea. J Plankton Res 20:371–381
Lizon F, Lagadeuc Y, Brunet C, Aelbrecht D, Bentley D (1995) Primary production and photoadaptation of phytoplankton in relation with tidal mixing in coastal waters. J Plankton Res 17:1039–1055
Mallin MA, Paerl HW (1992) Effects of variable irradiance on phytoplankton productivity in shallow estuaries. Limnol Oceanogr 37:54–62
Marra J (1978a) Phytoplankton photosynthetic response to vertical movement in a mixed layer. Mar Biol 46:203–208
Marra J (1978b) Effect of short-term variations in light intensity on photosynthesis of a marine phytoplankter: a laboratory simulation study. Mar Biol 46:191–202
Marra J (1980) Vertical mixing and primary production. In: Falkowski PG (ed) Primary production in the sea. Plenum Press, New York, p 78–85
McGillicuddy DJ, Robinson AR, McCarthy JJ (1995) Coupled physical and biological modelling of the spring bloom in the North Atlantic (II): three dimensional bloom and post-bloom processes. Deep Sea Res 42:1359–1398
Ménesguen A, Hoch T (1995) Modelling the biogeochemical cycles of elements limiting primary production in the English Channel. I. Role of thermocline stratification. Mar Ecol Prog Ser 146:173–188
Moloney CL, Bergh MO, Field JG, Newell RC (1986) The effect of sedimentation and microbial nitrogen regeneration in a plankton community: a simulation investigation. J Plankton Res 8:427–445
Montagnes DJS, Berges JA (1994) Estimating carbon, nitro-

gen, protein, and chlorophyll *a* from volume in marine phytoplankton. Limnol Oceanogr 39:1044–1060
Neale PJ, Richardson PJ (1987) Photoinhibition and the diurnal variation of phytoplankton photosynthesis. I. Development of a photosynthesis-irradiance model from studies of in situ responses. J Plankton Res 9:167–193
Olson RJ, Zettler ER, Chisholm SW, Dusenberry JA (1991) Advences in oceanography through flow cytometry. In: Demers S (ed) Particule analysis in oceanography. Springer-Verlag, Berlin, p 351–402
Perry MJ, Talbot MC, Alberte RS (1981) Photoadaptation in marine phytoplankton: response of the photosynthetic unit. Mar Biol 62:91–101
Pielou EC (1969) An introduction to mathematical ecology. Wiley Interscience, New York
Platt T, Gallegos CL, Harrison WG (1980) Photoinhibition of photosynthesis in natural assemblages of marine phytoplankton. J Mar Res 38:687–701
Richmond B, Peterson S, Vescuso P (1987) An academic user's guide to STELLA. High Performance System, Lyme, NH
Seuront L, Schmitt F, Lagadeuc Y, Schertzer D, Lovejoy S, Frontier S (1996a) Multifractal analysis of phytoplankton biomass and temperature in the ocean. Geophys Res Lett 23:3591–3594
Seuront L, Schmitt F, Schertzer D, Lagadeuc Y, Lovejoy S (1996b) Multifractal intermittency of Eulerian and Lagrangian turbulence of ocean temperature and plankton fields. Nonlin Proc Geophys 3:236–246
Shay TJ, Gregg MC (1986) Turbulence in an oceanic convective mixed layer. Nature 310:282–285
Simpson JH, Brown J, Matthews J, Allen G (1990) Tidal straining, density currents, and stirring in the control of estuarine stratification. Estuaries 13:125–132
Simpson JH, Sharples J, Rippeth TP (1991) A prescriptive model of stratification induced by freshwater runoff. Estuar Coast Shelf Sci 33:23–35
Skogen MD, Svendsen E, Berntsen J, Aksnes D, Ulvestad KB (1995) Modelling the primary production in the North Sea using a coupled three-dimensional physical-chemical-biological ocean model. Estuar Coast Shelf Sci 41:545–565
Taylor GI (1954) The dispersion of matter in turbulent flow through a pipe. Proc R Soc Lond 223:446–448
Vézina AF, Gratton Y, Vinet P (1995) Mesoscale physical-biological variability during a summer phytoplancton bloom in the Lower St Lawrence estuary. Estuar Coast Shelf Sci 41:393–411
Vincent WF, Neale PJ, Richardson PJ (1984) Photoinhibition: alga responses to bright light during diel stratification and mixing in a tropical lake. J Phycol 20:201–211
Weissing FJ, Huisman J (1994) Growth and competition in a light gradient. J Theor Biol 168:323–336
Woods JD, Barkmann W (1994) Simulating plankton ecosystems by the Lagrangian Ensemble method. Phil Trans R Soc Lond B 343:27–31
Woods JD, Onken R (1982) Diurnal variation and primary production in the ocean-preliminary results of a Lagrangian Ensemble model. J Plankton Res 4:735–756
Wu J, Vankat JL (1991) An area-based model of species richness dynamics of forest islands. Ecol Model 58:249–271
Yamazaki H, Kamykowski D (1991) The vertical trajectories of motile phytoplankton in a wind-mixed water column. Deep Sea Res 38:219–241

Editorial responsibility: Otto Kinne (Editor), Oldendorf/Luhe, Germany

Submitted: December 22, 1997; Accepted: May 26, 1998
Proofs received from author(s): July 13, 1998

A7

Universal multifractal analysis as a tool to characterize multiscale intermittent patterns: example of phytoplankton distribution in turbulent coastal waters

Seuront L, Schmitt F, Lagadeuc Y, Schertzer D & Lovejoy S

Journal of Plankton Research, **21**, 877-922, 1999

Journal of Plankton Research Vol.21 no.5 pp.877–922, 1999

Universal multifractal analysis as a tool to characterize multiscale intermittent patterns: example of phytoplankton distribution in turbulent coastal waters

Laurent Seuront[1], François Schmitt[2,5], Yvan Lagadeuc[1,6], Daniel Schertzer[3] and Shaun Lovejoy[4]

[1]*Station Marine de Wimereux, Université des Sciences et Technologies de Lille, CNRS-UPRESA 8013 ELICO, BP 80, 62930 Wimereux, France,* [2]*Institut Royal Météorologique, Section Climatologie Dynamique, 3 avenue Circulaire, 1180 Brussels, Belgium,* [3]*Laboratoire de Modélisation en Mécanique, Université Pierre et Marie Curie, CNRS-UMR 7607, Case 162, 4 place Jussieu, 75252 Paris Cedex 05, France and* [4]*Physics Department, McGill University, 3600 University Street, Montréal, H3A 2T8, Canada*

[5]*Present address: Department of Fluid Mechanics, VUB, Pleinlaan 2, 1050 Brussels, Belgium*

[6]*To whom correspondence should be addressed*

Abstract. A multifractal method of analysis, initially developed in the framework of turbulence and having had developments and applications in various geophysical domains (meteorology, hydrology, climate, remote sensing, environmental monitoring, seismicity, volcanology), has previously been demonstrated to be an efficient tool to analyse the intermittent fluctuations of physical or biological oceanographic data (Seuront *et al.*, *Geophys. Res. Lett.*, **23**, 3591–3594, 1996 and *Nonlin. Processes Geophys.*, **3**, 236–246, 1996). Thus, the aim of this paper is, first, to present the conceptual bases of multifractals and more precisely a stochastic multifractal framework which among different advantages lead in a rather straightforward manner to universal multifractals. We emphasize that contrary to basic analysis techniques such as power spectral analysis, universal multifractals allow the description of the whole statistics of a given field with only three basic parameters. Second, we provide a comprehensive detailed description of the analysis techniques applied in such a framework to marine ecologists and oceanographers; and third, we illustrate their applicability to an original time series of biological and related physical parameters. Our illustrative analyses were based on a 48 h high-frequency time series of *in vivo* fluorescence (i.e. estimate of phytoplankton biomass), simultaneously recorded with temperature and salinity in the tidally mixed coastal waters of the Eastern English Channel. Phytoplankton biomass, which surprisingly exhibits three distinct scaling regimes (i.e. a physical–biological–physical transition), was demonstrated to exhibit a very specific heterogeneous distribution, in the framework of universal multifractals, over smaller (<10 m) and larger (>500 m) scales dominated by different turbulent processes as over intermediate scales (10–500 m) obviously dominated by biological processes.

Introduction

Marine systems, globally dominated by turbulent events in coastal as in offshore locations (Grant *et al.*, 1962; Oakey and Elliott, 1982; Mitchell *et al.*, 1985), exhibit an intimate relationship between the structure of phytoplankton populations and their physical environment (Steele, 1974, 1976, 1978; Denman and Powell, 1984; Legendre and Demers, 1984). This association of physical and biological processes occurs over a whole range of scales, as shown by the patterns of physical, chemical and biotic parameters which are strongly interrelated within a given time period or spatial region (Cassie, 1959a,b, 1960). Even if for many decades many

© Oxford University Press

investigators have shown that planktonic organisms are neither uniformly nor randomly distributed in the ocean (Hardy and Gunther, 1935; Cassie, 1963), these results are essentially related to spatial patterns associated with large- and coarse-scale physical processes (Mackas *et al.*, 1985). On the contrary, on fine and micro scales, which are of main interest for biological processes such as phytoplankton or zooplankton dynamics (Estrada *et al.*, 1987; Alcaraz *et al.*, 1988; Rothschild and Osborn, 1988; Sundby and Fossum, 1990; Thomas and Gibson, 1990; Granata and Dickey, 1991; Peters and Gross, 1994), very little is known about the effects of turbulent processes, basically regarded as a great factor of homogenization.

More specifically, physical processes, regarded as a main factor in structuring biological communities (Legendre and Demers, 1984; Mackas *et al.*, 1985; Daly and Smith, 1993), are intimately linked with the capability of organisms to aggregate (i.e. to create patches), at least in the case of phytoplankton communities. Plankton patchiness (variability at horizontal scales between 10 m and 100 km, and at vertical scales between 0.1 and 50 m; Mackas *et al.*, 1985) is then determined by the quasi-equilibrium which exists (or not) between biotic processes such as phytoplankton growth and hydrodynamism—basically estimated by the rate of kinetic energy ε—which was shown to be determinant in the size of patches which can maintain themselves in the face of diffusion (Skellam, 1951; Kierstead and Slobodkin, 1953; Denman and Platt, 1976; Wroblewski and O'Brien, 1976; Denman *et al.*, 1977; Okubo, 1978, 1980; Powell and Okubo, 1994) (e.g. the KISS length as defined by Okubo, 1980). Moreover, in addition to these theoretical investigations, the interactions between phytoplankton community dynamics and turbulent processes have been widely studied by numerous investigators (Platt *et al.*, 1970; Platt, 1972; Powell *et al.*, 1975; Denman, 1976; Fasham and Pugh, 1976; Steele and Henderson, 1977, 1992; Fortier *et al.*, 1978; Horwood, 1978; Lekan and Wilson, 1978; Demers *et al.*, 1979; Wiegand and Pond, 1979).

These pioneering approaches were essentially based on the assumption that turbulent processes can be regarded as homogeneous processes (Kolmogorov, 1941; Obukhov, 1941, 1949; Corrsin, 1951). However, it has been shown that not only turbulent fluid motions and the fluctuations of purely passive scalars such as temperature generate sharp fluctuations at all scales, but the distribution of these fluctuations, i.e. the activity of turbulence, is far from being homogeneous and rather extremely intermittent (Batchelor and Townsend, 1949; Kolmogorov, 1962; Obukhov, 1962). Thus, recent analysis conducted on zooplankton data (Pascual *et al.*, 1995), temperature and *in vivo* fluorescence (Seuront *et al.*, 1996a,b; Seuront, 1997) have shown that oceanic scalar fields were heterogeneously distributed over scales dominated by physical (i.e. turbulent) or biological processes.

Earlier statistical analysis techniques of plankton patchiness, such as models of point processes or power spectral analysis [see Fasham (1978) for a review] characterize variability in a very limited way. For instance, power spectral analysis, widely used in ecological applications (Platt and Denman, 1975), being only a second-order statistic, characterizes the variability very poorly by implicitly assuming 'quasi-Gaussian' statistics, which are not relevant for intermittent fields. For such fields, the best tool is provided by multifractal analysis, as shown by Pascual *et al.* (1995), Seuront *et al.* (1996a) and Seuront (1997) for planktonic fields.

Multifractals can be regarded as a rather considerable generalization of fractal geometry, essentially developed for the description of geometrical patterns (Mandelbrot, 1983). Indeed, fractal geometry has been introduced to describe the relationship—known as a scaling relationship—between patterns and the scale of measurement: the 'size' of a fractal set varies as the scale at which it is examined and raised to a (scaling) exponent, in this case given by the fractal dimension. The transition to the concept of multifractal fields (Grassberger, 1983; Hentschel and Procaccia, 1983; Schertzer and Lovejoy, 1983, 1985, 1987a; Lovejoy and Schertzer, 1985; Parisi and Frisch, 1985; Meneveau and Sreenivasan, 1987) leads to the consideration of multifractal fields as an infinite hierarchy of sets (loosely speaking, each of them corresponds to the fraction of the space where data exceed a given threshold) each with its own fractal dimension. Thus, multifractal fields are described by scaling relationships that require a family (even an infinity) of different exponents (or dimensions), rather than the single exponent of fractal patterns. Despite the apparent complexity induced by a multifractal framework, using the universal multifractal formalism (Schertzer and Lovejoy, 1987b, 1989), the distribution of a given scalar field can be wholly described by only three indices, which resume the statistical behaviour of turbulent fields from larger to smaller scales, as well as from extreme to mean behaviours.

Previous empirical and theoretical studies of phytoplankton patchiness (e.g. Platt, 1972; Denman and Platt, 1976; Denman *et al.*, 1977) have been able to quantify the scale of variation present in transects of chlorophyll, salinity and temperature, but have been able to say little about the precise variability associated with those scales. Herein, the goal of this paper is to provide to marine ecologists and oceanographers a detailed account of the universal multifractal techniques previously used for the description of phytoplankton biomass and temperature fluctuations (Seuront *et al.*, 1996a,b; Seuront, 1997) and their application to time series of *in vivo* fluorescence (i.e. phytoplankton biomass) and related physical parameters (i.e. temperature and salinity), taken from a fixed mooring in tidally mixed coastal waters of the Eastern English Channel. In that way, we provide an illustration of the applicability of these techniques in the characterization of the whole variability associated with specific scaling regimes identified with power spectral analysis: on small scales, where phytoplankton biomass distribution is controlled by turbulent processes, and at broader scales, where the variability in the biological and physical parameters such as cell growth and community structure, and horizontal processes, respectively, has an important role in shaping the phytoplankton distribution and overrides the local effects of turbulent mixing.

Background theoretical concepts in turbulence

Describing turbulent processes

Developed from 'intuitive' ideas (Richardson, 1922), a classical picture of turbulence treats it as a field of nested eddies of decreasing sizes, where turbulent kinetic energy 'cascades' with negligible dissipation from the largest energy-containing eddies to smaller and smaller eddies until it reaches Kolmogorov's length scale (i.e. viscous scale), where viscosity effects cannot be neglected and

start to smooth out turbulent fluctuations. Under the associated hypothesis of local isotropy and tri-dimensional homogeneity of turbulence, the velocity fluctuations of a given eddy can be described by the scaling relationships (Kolmogorov, 1941; Obukhov, 1949):

$$\Delta V_l \approx \varepsilon^{1/3} l^{1/3} \tag{1}$$

$$\Delta T_l \approx \varphi^{1/3} l^{1/3} \tag{2}$$

where $\Delta V_l = |V(x + l) - V(x)|$ and $\Delta T_l = |T(x + l) - T(x)|$ are the velocity and temperature shears at scale l, ε is the dissipation rate of turbulent kinetic energy and φ is the resulting flux of non-linear interactions of velocity and temperature fields given by $\varphi = \varepsilon^{-1/2}\chi^{3/2}$, where χ is the rate of temperature variance flux.

In Fourier space, the 1/3 law of velocity and temperature fluctuations in physical space [equations (1) and (2)] is associated with a power law for energy and variance power spectra (Figure 1) according to Obukhov (1941, 1949) and Corrsin (1951):

$$E_V(k) \approx \varepsilon^{2/3} k^{-5/3} \tag{3}$$

$$E_T(k) \approx \varphi^{2/3} k^{-5/3} \tag{4}$$

where k is a wavenumber.

However, contrary to the original proposal (Kolmogorov, 1941; Obukhov, 1941), it has been shown (Batchelor and Townsend, 1949; Kolmogorov, 1962; Obukhov, 1962) that the rate of energy flux ε and the rate of variance flux χ—respectively associated with velocity and temperature fluctuations—exhibit at all scales sharp fluctuations called intermittency (Figure 2). Turbulent velocity and temperature fluxes are intermittent in the sense that active regions occupy tiny fractions of the space available. Assumption of homogeneity is then untenable and turbulent fields have to be regarded as inhomogeneous and scale-dependent processes. Assuming the validity of the 'refined similarity hypothesis' (Kolmogorov, 1962; Obukhov, 1962), this leads to the introduction of the subscript l and to the modification of the relationships (1) and (2), respectively, as $\Delta V_l \approx \varepsilon_l^{1/3} l^{1/3}$ and $\Delta T_l \approx \varphi_l^{1/3} l^{1/3}$.

Modelling intermittent turbulence: from fractals to multifractals

Intermittent turbulence, fractal theory and multiplicative processes. Basically, the concept of eddies hierarchically organized in an isotropic cascade from large to small scales can be 'naturally' related to fractal properties in respect to the link existing between fractals and self-similarity (e.g. an object is called self-similar, or scale-invariant, if it can be written as a union of rescaled copies of itself, with the rescaling isotropic or uniform in all direction). However, the phenomenology of turbulent cascades is rather more complex than the expression 'eddy' would lead us to understand, since it becomes necessary to describe how the activity of

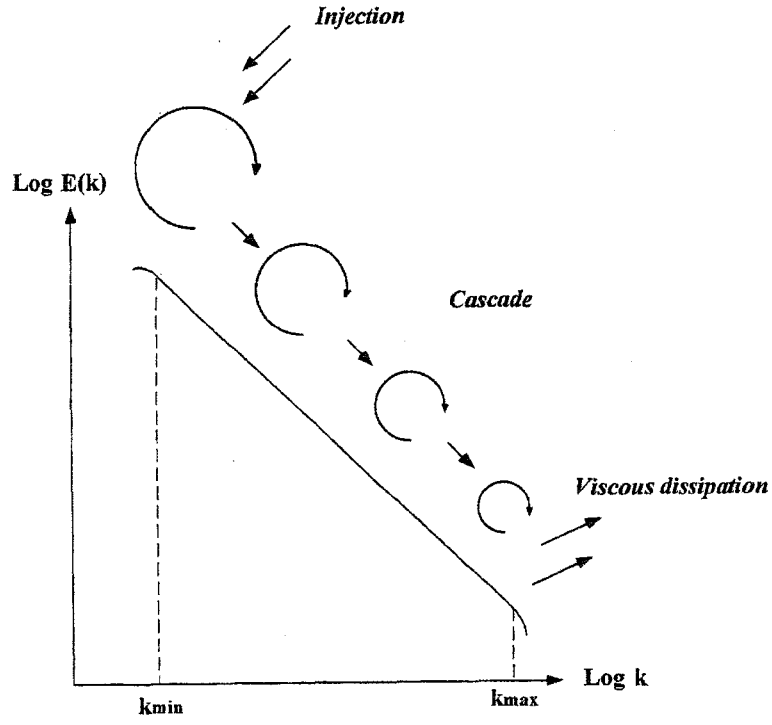

Fig. 1. Schematic representation showing the form of the frequency spectrum of turbulent velocity cascade, where $E(k)$ is the spectral density (variance units/k)^2 and k is a wavenumber (m^{-1}). The kinetic energy generated by large-scale processes (e.g. wind or tide) cascades through a hierarchy of eddies of decreasing size to the viscous subrange where it is dissipated into heat. The change in variance with wavenumber (i.e. slope of power spectrum) is scale invariant with a –5/3 slope as predicted by the theoretical Kolmogorov–Obukhov power law. The wavenumbers k_{max} and k_{min}, respectively, show the largest scale of creation of turbulence and the smallest scale (i.e. Kolmogorov length scale) reached by turbulent eddies where turbulent motions are smoothed out by viscous effects.

turbulence becomes more and more inhomogeneous at smaller and smaller scales. The simplest cascade model, the 'β-model' (Novikov and Stewart, 1964; Mandelbrot, 1974; Frisch *et al.*, 1978), takes the intermittent nature of turbulence into account by assuming that eddies are either 'dead' (inactive) or 'alive' (active). This cascade model has a discrete scale ratio between a parent structure and a daughter structure is introduced. For simplicity of implementation, this scale ratio is usually 2: one parent at scale l has 2 children at scale $l/2$. Using a notation including scale ratios $\lambda = L/l$ (where L is a fixed outer scale) associated to the scale l, we may write $\varepsilon_{2\lambda} = m.\varepsilon_{\lambda}$, where m is a multiplicative factor following the law:

$$\Pr(m = \frac{1}{\psi}) = \psi \qquad \text{'alive' sub-eddy} \tag{5}$$

$$\Pr(m = 0) = 1 - \psi \qquad \text{'dead' sub-eddy} \tag{6}$$

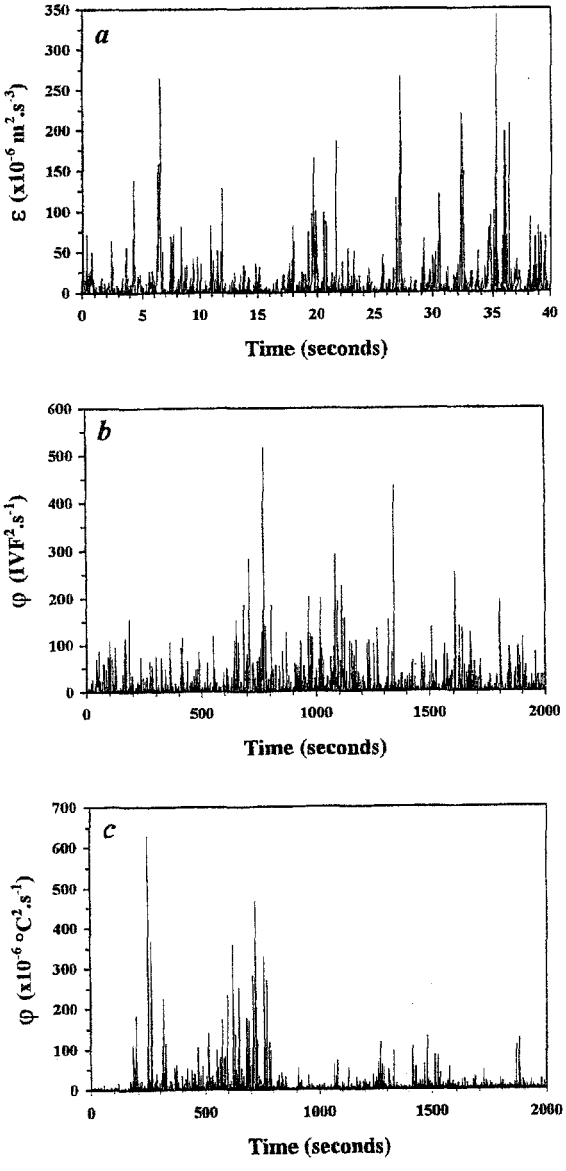

Fig. 2. Samples of the pattern of the rate of energy flux ε (**a**) estimated from grid generated turbulent velocity fluctuations recorded with a hot wire velocimeter, and the rates of variance fluxes φ estimated from *in vivo* fluorescence (**b**) and temperature (**c**) recorded in the Eastern English Channel with a Sea Tech fluorometer and a Sea-Bird 25 Sealogger CTD, respectively. Turbulent velocity, *in vivo* fluorescence and temperature fluxes exhibit at all scales sharp fluctuations called intermittency.

where ψ $(0 < \psi < 1)$ is the parameter of the model expressing the fraction of dead and alive eddies. This elementary process is then iterated n times until the total scale ratio $\lambda = 2^n$ is reached. If we denote $\psi = 2^{-c}$, then we have after n steps (if we take the first value $\varepsilon_1 = 1$):

$$\Pr(\varepsilon_\lambda = \lambda^c) = \lambda^{-c} \qquad \text{'alive' sub-eddy} \qquad (7)$$

$$\Pr(\varepsilon_\lambda = 0) = 1 - \lambda^{-c} \qquad \text{'dead' sub-eddy} \qquad (8)$$

In practice, this means that in an Euclidean space of dimension d, the 'β-model' (Figure 3) presents only λ^{-D} active sub-eddies, among λ^d potential sub-eddies (corresponding to the theoretical case of a homogeneous, or space-filling

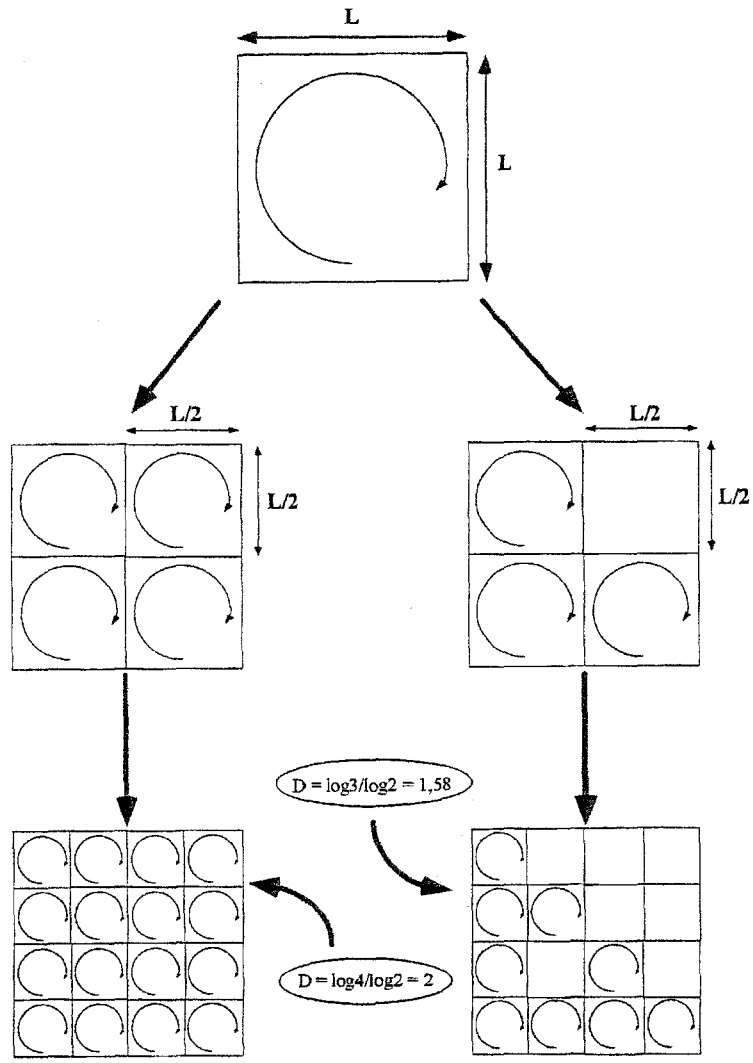

Fig. 3. Elementary isotropic cascades. The left-hand side shows a non-intermittent (i.e. homogeneous) cascade process corresponding to the hypothetical case of a space-filling turbulence. The right-hand side shows how intermittency can be modelled by assuming that not all sub-eddies are 'alive', leading to a (mono-) fractal description of turbulence. This is an implementation of the 'β-model' (adapted from Schertzer and Lovejoy, 1987b).

turbulence), c and D are, respectively, the fractal codimension and dimension characterizing the active eddies' activity, related as:

$$c = d - D \tag{9}$$

where d is the dimension of the space considered ($d = 1$ for time series, $d = 2$ for bi-dimensional fields). It is already essential to note (Schertzer and Lovejoy, 1992) that c measures intrinsically the fraction of the space occupied by active eddies, i.e. its relative sparseness. Equation (9) corresponds merely to the fact that at each step of the cascade process, the fraction of space filled with alive eddies decreases by the factor λ^{-c} and conversely their energy flux density increases by the same factor to ensure average conservation.

The discrete 'β-model' is, however, only a caricatural approximation since it involves only dead and alive structures, an eddy is killed within a step of the cascade. It was indeed expected that the (mono-) fractal nature of this approximation was inadequate considering the realistic perturbations which correspond to replace the alternative dead or alive structures by the alternative weak or strong structures.

Discrete multiplicative cascades and multifractals. Rather than only allowing eddies to be either 'dead' or 'alive', the 'α-model' (Schertzer and Lovejoy, 1983, 1985) considers a more realistic feature allowing them to be either 'more active' or 'less active' (Figure 4). Equations (7) and (8) are then modified according to the following binomial process:

$$\Pr(\varepsilon_\lambda = \lambda^{\gamma^+}) = \lambda^{-c} \qquad \text{'strong' sub-eddy} \tag{10}$$

$$\Pr(\varepsilon_\lambda = \lambda^{\gamma^-}) = 1 - \lambda^{-c} \qquad \text{'weak' sub-eddy} \tag{11}$$

where γ^+ and γ^- ($\gamma^- < 0 < \gamma^+$) are, respectively, the strongest (with associated codimension c) and weakest singularities of the turbulent field, each singularity corresponding to an intermittency level. Figure 5 illustrates this mechanism for one step of the 'α-model' cascade. For n steps of the cascade process, the scale ratio between the largest eddy and the smallest one is then $\lambda = 2^n$ and the final pattern obtained (Figures 6 and 7) is very similar to the one observed in the case of turbulent field data (cf. Figure 2). With larger and larger number n of steps, more and more 'mixed' singularities γ ($\gamma^- < \gamma < \gamma^+$) are generated by the two initial 'pure' singularities γ^+ and γ^-. One may note here that the 'β-model' corresponds to the particular and peculiar case $\gamma^+ = c$ and $\gamma^- = -\infty$, which explains why contrary to the general case of the 'α-model', the iteration of the elementary step does not introduce new singularities and therefore yields a 'black and white' outcome.

When n becomes very large, intermittency can then be characterized by the statistical distribution of singularities γ ($\gamma^- < \gamma < \gamma^+$):

$$\varepsilon_\lambda \approx \lambda^\gamma \tag{12}$$

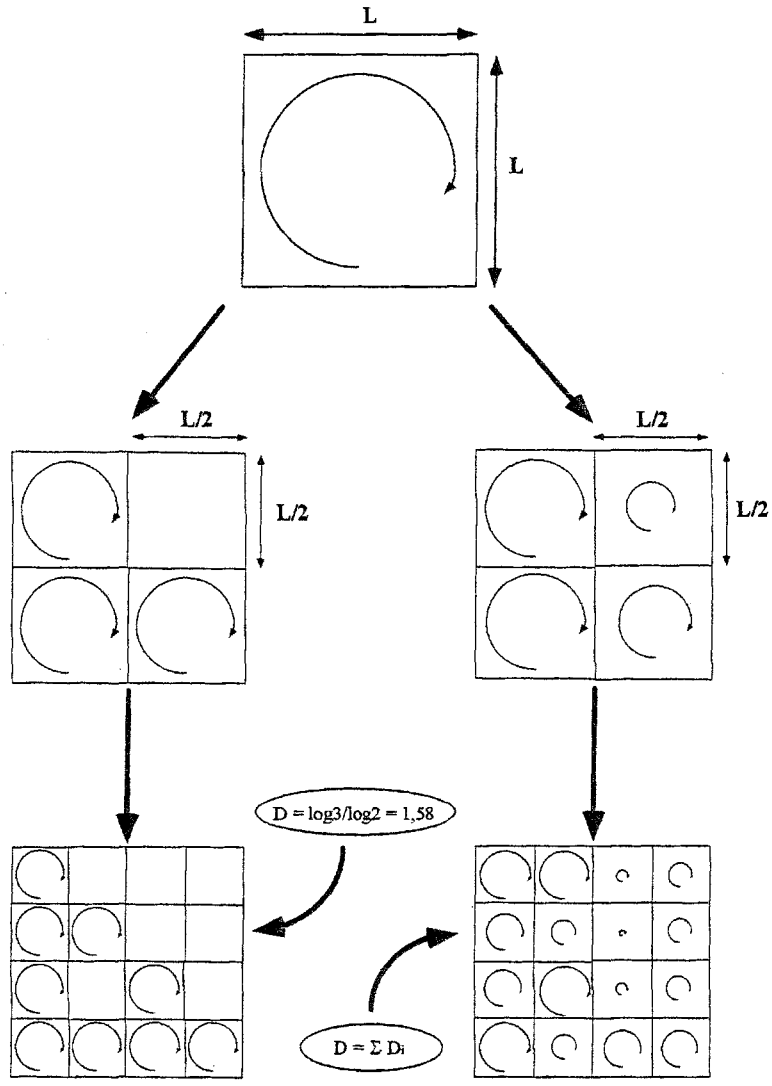

Fig. 4. These isotropic cascade processes show how the right-hand side multifractal 'α-model' generalizes the left-hand side monofractal 'β-model' by introducing a more realistic feature of intermittency. The 'α-model' allows eddies to be 'more active' or 'less active' rather than allowing them to be either 'dead' or 'alive', leading to a multifractal description of turbulence, each intermittency level being associated with its own fractal dimension.

and by the associated probability distribution (Schertzer and Lovejoy, 1987b):

$$\Pr(\varepsilon_\lambda \geq \lambda^\gamma) \approx \lambda^{-c(\gamma)} \tag{13}$$

where $c(\gamma)$ is a function characterizing the singularities' distribution. One may note here that for a multifractal, the value of the field depends on the scale of

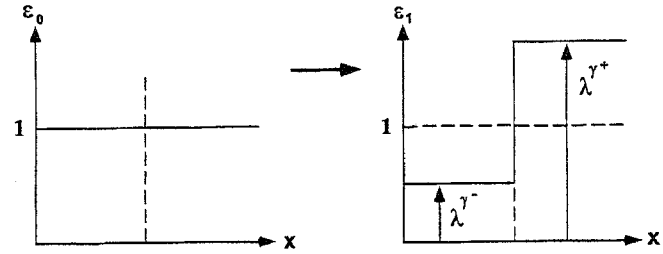

Fig. 5. Illustration of the 'α-model' for one step of cascade. The weak and strong sub-eddies have, respectively, an associated probability $Pr(\varepsilon_\lambda = \lambda^{\gamma-}) = 1 - \lambda^{-c}$ ($\lambda^{-c} < 0$) and $Pr(\varepsilon_\lambda = \lambda^{\gamma+}) = \lambda^{-c}$ ($\lambda^{-c} > 0$), rather than $Pr(\varepsilon_\lambda = 0) = 1 - \lambda^{-c}$ and $Pr(\varepsilon_\lambda = \lambda^c) = 1 - \lambda^{-c}$ expected in the case of inactive and active sub-eddies of the 'β-model'.

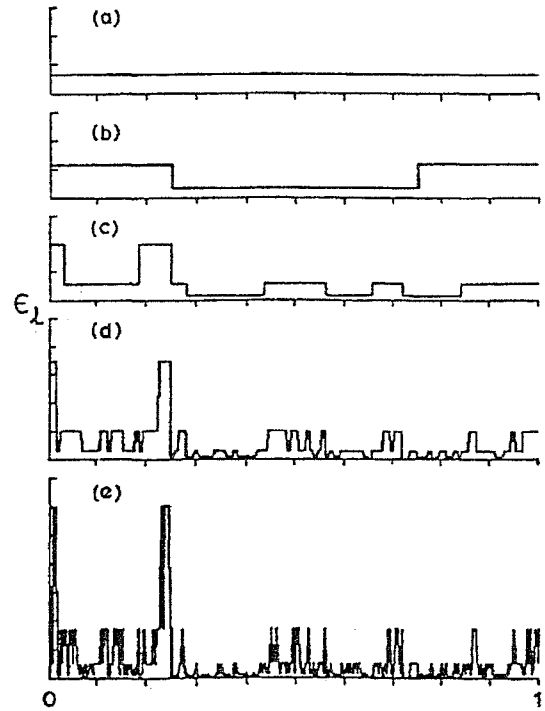

Fig. 6. A schematic representation of the 'α-model' generalizing Figure 5 for five steps of the cascade process. This shows a function which starts as homogeneous over the entire interval (**a**), whose scale of homogeneity is systematically reduced by a successive factor of 4 (**b**, **c**, **d** and **e**). Such a cascade model has the property of conserving the area under the curve (i.e. the energy flux to smaller scale), leading to a more and more sparse distribution of increasingly high peaks. The limit of the function when the scale of homogeneity goes to zero is dominated by singularities distributed over sparse fractal sets (redrawn from Schertzer and Lovejoy, 1987b).

observation, this is why λ is introduced here as a subscript. In practice, experimental data are recorded at the smallest available scale, and are then degraded through averaging, up to a given scale. As previously shown for c in the case of the monofractal 'β-model', $c(\gamma)$ is a codimension [for more discussion, see

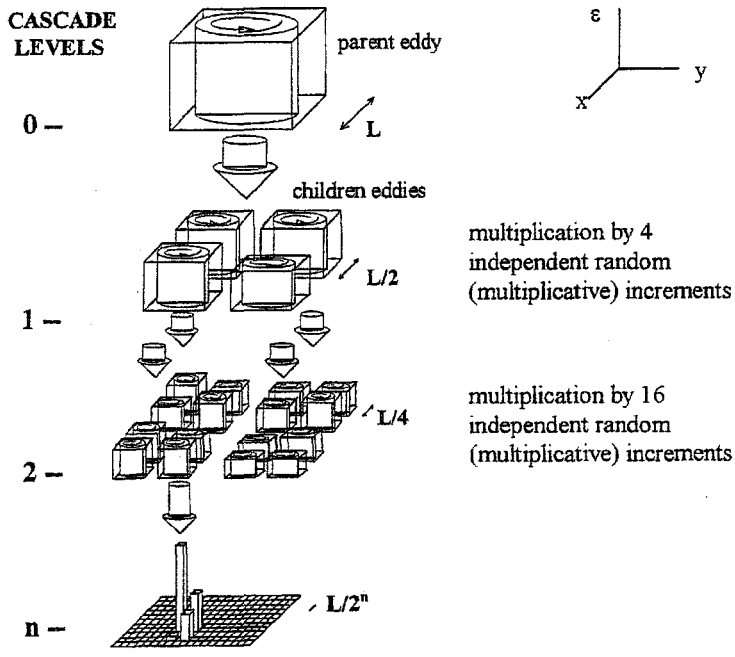

Fig. 7. A 2D schematic diagram showing a few steps of the discrete multiplicative cascade process of the 'α-model' with two orders of singularity γ^- and γ^+ (corresponding to the two values taken by the independent random increments $\gamma^{\gamma-} < 1$, and $\gamma^{\gamma+} > 1$), leading to the appearance of mixed orders of singularity γ ($\gamma^- \leq \gamma \leq \gamma^+$) (adapted from Schertzer *et al.*, 1998).

Schertzer and Lovejoy (1992)]. Considering that among λ^d potential sub-eddies (i.e. in the case of a hypothetical space-filling turbulence) there are $\lambda^{-D(\gamma)}$ sub-eddies of different intensity, $c(\gamma)$ is expressed as a generalization of equation (9):

$$c(\gamma) = d - D(\gamma) \tag{14}$$

where $D(\gamma)$ characterizes the hierarchy of fractal dimensions associated with the different intermittency levels (i.e. singularities). That leads to consideration that the support of turbulence is defined by an infinite hierarchy of fractal dimensions rather than the single dimension of the 'β-model'. A turbulent process can then be regarded as a multifractal field, characterized by highly varying fractal dimensions in space and time in accordance with the local intensity of turbulent fluid motions.

Under fairly general conditions, the properties of the probability distribution of a random variable are equivalently specified by its statistical moments. The latter corresponds to the introduction of the scaling moment function $K(q)$ which describes the multiscaling of the statistical moments of order q of the turbulent field which writes:

$$\left\langle (\varepsilon_\lambda)^q \right\rangle \approx \lambda^{K(q)} \tag{15}$$

where '$\langle . \rangle$' indicates statistical or spatial averaging.

The relationship existing between the two scaling functions $c(\gamma)$ and $K(q)$ reduces to the Legendre transform (Parisi and Frisch, 1985) for large scale ratios (i.e. $\lambda >> 1$):

$$K(q) = \max_{\gamma} \{q\gamma - c(\gamma)\} \Leftrightarrow c(\gamma) = \max_{q} \{q\gamma - K(q)\} \tag{16}$$

Equation (16) implies that there is a one-to-one correspondence (see Figures 8 and 9 for an illustration) between singularities and orders of moments: to any order q is associated the singularity which maximizes $q\gamma - c(\gamma)$ and is the solution of $c'(\gamma_q) = q_\gamma$. Similarly to any singularity γ is associated the order of moment q_γ which maximizes $q\gamma - K(q)$ and is the solution of $K'(q_\gamma) = \gamma_q \cdot c(\gamma)$ and $K(q)$ exhibits several general properties of multifractals such as convexity and non-linearity. In particular, for conservative multifractal processes (i.e. $<\varepsilon_\lambda> = <\varepsilon_1>$, $\forall\lambda$) since $K(1) = 0$ corresponds via the Legendre transform to the fact that the corresponding mean singularity of the process, $C_1 = K'(1)$ is a fixed point of $c(\gamma)$, and by consequence the latter is tangential to the first bissectrix line $[c(\gamma) = \gamma]$ in $\gamma_1 = c(\gamma) = C_1$, hence $c'(C_1) = 1$. The determination of the probability distribution would require the determination of moments at all scales. With the assumption of scaling, it reduces to the determination of a hierarchy of exponents which remains nevertheless a priori infinite, and therefore indeterminable, especially for the highest orders which correspond to the most extreme variability. However, in the framework of universal multifractals (Schertzer and Lovejoy, 1987b, 1989, 1997; Lovejoy and Schertzer, 1990), the calculation complexity induced by the hierarchy previously described is included in few relevant exponents, which determine the moderate variability as well as the extreme variability.

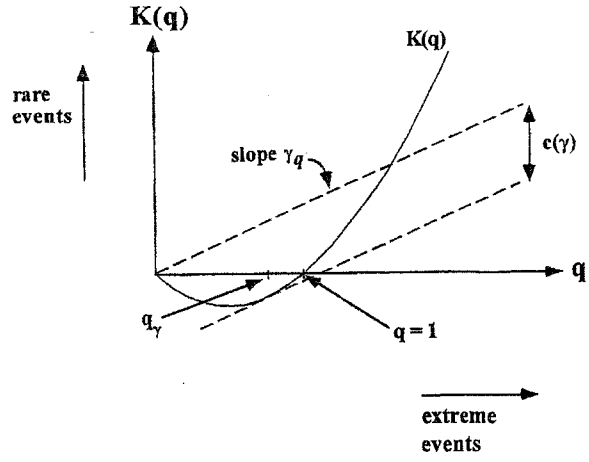

Fig. 8. $K(q)$ versus q showing the tangent line $K'(q_\gamma) = \gamma_q$. $K(q)$ exhibits several properties of multifractals such as convexity and non-linearity. One may note that the tangent line $K'(1) = C_1$ (not shown).

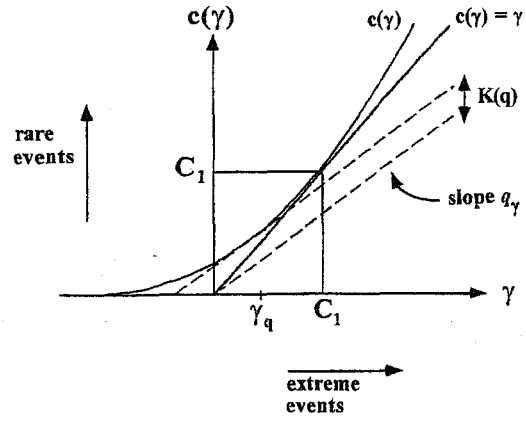

Fig. 9. $c(\gamma)$ versus γ showing the tangent line $c'(\gamma_q) = q_\gamma$. As $K(q)$, $c(\gamma)$ exhibits several properties of multifractals such as convexity and non-linearity. More precisely, $c(\gamma)$ is tangential to the first bissectrix line $[c(\gamma) = \gamma]$ in $\gamma_1 = c(\gamma_1) = C_1$.

Continuous multiplicative cascades and universal multifractals. The discrete cascade processes discussed up to now to simulate intermittency are quite unrealistic because of the fixed scale ratio (usually) used at each step of the cascade. The continuous multiplicative cascade processes (Schertzer and Lovejoy, 1987b, 1989, 1997), developed as a way to view cascade phenomenology as a continuous process, are associated with a densification of scales which consist on the one hand of studying the limit $\lambda_0 \to 1$ adding more and more intermediate scales with a fixed global scale ratio $\lambda = \lambda_0^n$ and on the other hand the limit $\lambda \to \infty$ (Figure 10). However, as theoretically demonstrated (Schertzer and Lovejoy, 1987b, 1989, 1997; Lovejoy and Schertzer, 1990; Schertzer *et al.*, 1991), the densification process converges on universal laws depending only on two fundamental parameters: C_1 and α, which describe the multiscaling behaviour of the scaling functions $K(q)$:

$$\begin{cases} K(q) = \dfrac{C_1}{\alpha - 1}(q^\alpha - q) & \alpha \neq 1 \\ K(q) = C_1 q \ln(q) & \alpha = 1 \end{cases} \tag{17}$$

and $c(\gamma)$:

$$\begin{cases} c(\gamma) = C_1 \left(\dfrac{\gamma}{C_1 \alpha'} + \dfrac{1}{\alpha} \right)^{\alpha'} & \alpha \neq 1 \\ c(\gamma) = C_1 \exp\left(\dfrac{\gamma}{C_1} - 1 \right) & \alpha = 1 \end{cases} \tag{18}$$

with $\dfrac{1}{\alpha} + \dfrac{1}{\alpha'} = 1$.

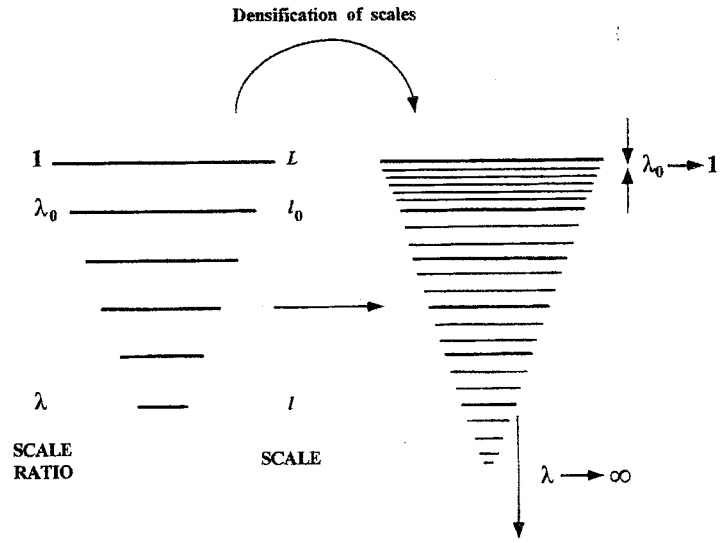

Fig. 10. Scheme of the densification of scales process, leading to the viewing of cascade phenomenology as a continuous process. This densification consists both of studying the limit $\lambda_0 \rightarrow 1$ adding more and more intermediate scales and the limit $\lambda \rightarrow \infty$, where λ_0 and λ are, respectively, the smallest scale ratio (i.e. the ratio between two successive measurements) and the global scale ratio [i.e. the ratio between the fixed outer scale L and the smallest scale of measurement l ($\lambda = L/l$)].

C_1 is the mean singularity of the process, and also, as already pointed out above the codimension of the mean singularity, and therefore measures the mean fractality of the process. It satisfies $0 \leq C_1 \leq d$ (d is the Euclidean dimension of the observation space): $C_1 = 0$ for a homogeneous process and $C_1 = d$ for a process so heterogeneous that the fractal dimension of the set contributing to the mean is zero. It then characterizes a mean inhomogeneity and can be regarded as the measure of the sparseness of a given field: the higher the C_1, the fewer the field values corresponding to any given singularity (Figure 11a). The index α, called the Lévy index, is the degree of multifractality bounded between $\alpha = 0$ and $\alpha = 2$ which correspond, respectively, to the monofractal 'β-model' and to the log–normal model. It defines how fast the fractality is increasing with higher and higher singularities: as α decreases, the high values of the field do not dominate as much as for larger values of α; there are more large deviations from the mean (Figure 11b).

It can be noticed here that the whole previous developments, conducted in the framework of turbulence, can be applied to a great variety of intermittent fields. Indeed, they do not depend on the fact that the governing equations are known or not: when these equations are known (e.g. in the framework of turbulence), one uses until now only their scaling symmetry, not the other ones [see Schertzer *et al.* (1998) for discussion on new alternatives to bridge this gap between phenomenology and governing equations]. This is the main reason that the following class of multifractal models, often called Fractionally Integrated Flux

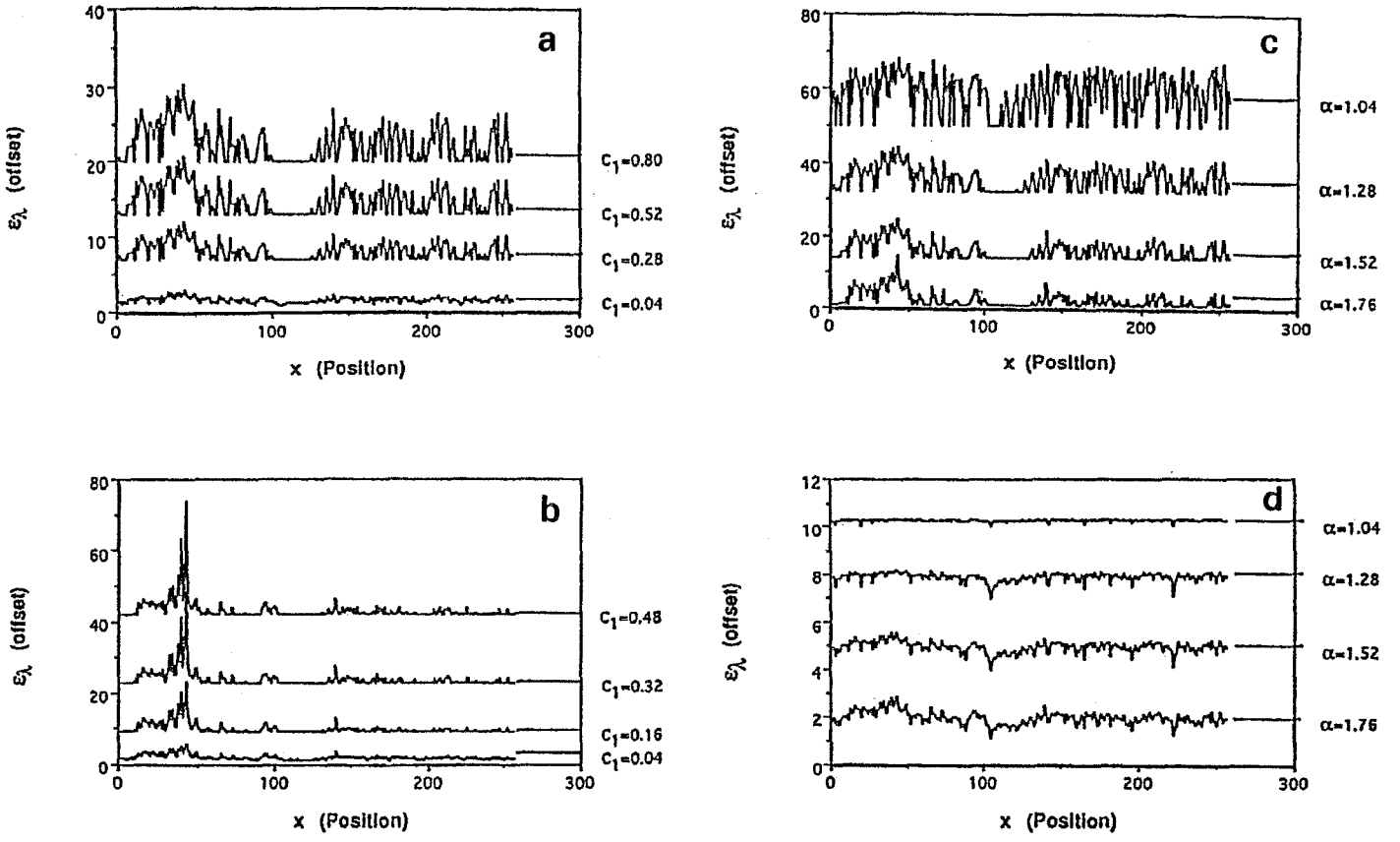

Fig. 11. Illustration of turbulent field ε_λ (i.e. the turbulent kinetic energy dissipation rate) properties described by the universal multifractal parameters C_1 and α using one-dimensional simulations of length 256, with $C_1 = 0.9$ (**a**) and $C_1 = 0.001$ (**b**) and varying α, and with $\alpha = 1.4$ (**c**) and $\alpha = 2.0$ (**d**) and varying C_1. These simulations have been vertically offset so as not to overlap (redrawn from Pecknold *et al.*, 1993).

models (FIF), became used in geophysical fields not related directly to turbulence: in analogy with turbulence, a flux ϕ_l, usually associated to some invariance or conservative property, is defined from a given intermittent scalar field S with a scaling relationship similar to those relating flux of energy ε and velocity shears, or flux φ and temperature gradients [equations (1) and (2)]:

$$\Delta S_l \approx \phi_l^a l^H \tag{19}$$

where H ($0 \leq H \leq 1$) is a parameter which characterizes in a general manner (and in a very precise manner when $a = 1$) the degree of non-conservation of the field ($H = 1/3$ for a scalar quantity passively advected by non-intermittent turbulence), whereas the power of the flux is often taken as $a = 1$ for simplicity (Schertzer and Lovejoy, 1987b; Teissier *et al.*, 1993a,b). However, the most important meaning of H corresponds to the fact that it is the order of fractional differentiation in order to obtain the flux ϕ_l from the field S [see Schertzer *et al.* (1998) for more discussion (in particular for space–time FIF models) and further details]. Let us mention briefly that an isotropic fractional differentiation corresponds to a multiplication by k^H in Fourier space equivalent to power law filtering.

Data analysis techniques

Spectral analysis. Basically applied to a variety of geophysical and ecological data (Platt and Denman, 1975; McHardy and Czerny, 1987; Ladoy *et al.*, 1991; Olsson *et al.*, 1993) to detect scaling behaviours, spectral analysis corresponds to an analysis of variance in which the total variance of a given process is partitioned into contributions arising from processes with different length scales or time scales in the case of spatially or temporally recorded data, respectively. A power spectrum separates and measures the amount of variability occurring in different wavenumber or frequency bands. When all or parts of the spectrum follow a power law like equations (3) and (4), i.e. $E(k) \approx k^{-\beta}$, the data are scaling in that range, i.e. the scaling regime. β is the exponent characterizing spectral scale invariance: for instance $\beta = 5/3$ in homogeneous turbulence. The absence of characteristic time scales and the presence of a scaling regime indicate that a multifractal analysis may prove to be successful.

Structure functions. A power spectrum being a second-order moment, it rather characterizes a mean variability, i.e. a mean scaling behaviour. Then, the previous spectral analysis is generalized with the help of the qth-order structure functions (Monin and Yaglom, 1975):

$$\left\langle (\Delta S_\tau)^q \right\rangle = \left\langle |S(t+\tau) - S(\tau)|^q \right\rangle \tag{20}$$

where for a given time lag τ the fluctuations of the scalar S are averaged over all the available values ('<.>' indicates statistical averaging). For scaling processes, one way (Monin and Yaglom, 1975; Anselmet *et al.*, 1984) to characterize intermittency statistically is based on the study of the scale invariant structure exponent $\zeta(q)$ defined by:

$$\left\langle (\Delta S_\tau)^q \right\rangle = \left\langle (\Delta S_T)^q \right\rangle \left(\frac{\tau}{T} \right)^{\zeta(q)} \tag{21}$$

where T is the largest period (external scale) of the scaling regime. The scaling exponent $\zeta(q)$ is estimated by the slope of the linear trends of $\langle (\Delta S_\tau)^q \rangle$ versus τ in a log–log plot. The first moment, characterizing the scaling of the average absolute fluctuations, corresponds to the scaling 'Hurst' exponent $H = \zeta(1)$, previously introduced in equation (19) to characterize the degree of non-conservation of a given field. The second moment is linked to the power scaling exponent β by $\beta = 1 + \zeta(2)$. For simple (monofractal) processes, the scaling exponent of the structure function $\zeta(q)$ is linear: $\zeta(q) = qH$ [$\zeta(q) = q/2$ for Brownian motion and $\zeta(q) = q/3$ for Obukhov–Corrsin non-intermittent turbulence]. For multifractal processes, this exponent is non-linear and concave.

Moreover, multifractal processes possessing stable and attractive generators (Schertzer and Lovejoy, 1987b, 1989; Schertzer *et al.*, 1995), in the universal multifractals framework, the departure from linearity of the scale invariant structure function exponent $\zeta(q)$ is then given by the universal multifractal parameters α and C_1:

$$\zeta(q) = qH - \frac{C_1}{\alpha - 1}(q^\alpha - q) \tag{22}$$

with $K(q) = \frac{C_1}{\alpha - 1}(q^\alpha - q)$ [see equation (17)]. The parameter H is the degree of non-conservation of the average field [$\zeta(1) = H$]: $H = 0$ and $H \neq 0$ mean that the fluctuations are, respectively, scale independent and scale dependent [H ranges from 0.34 to 0.42, and 0.36 to 0.43, respectively, for temperature and passive *in vivo* fluorescence, see Seuront *et al.* (1996a,b), Seuront (1997); and $H \approx 0.12$ for fluorescence over scales dominated by biological activity, see Seuront *et al.* (1996a)]. The second term expresses a deviation from homogeneity [in which case $\zeta(q) = qH$], and represents the intermittency effects.

Double Trace Moment. The Double Trace Moment analysis technique (Lavallée, 1991; Lavallée *et al.*, 1992) is a generalization of the expression given by equations (15) and (17) to a quantity $(\phi_\Lambda)^\eta$ by taking the ηth power of the field ϕ_Λ—which is the general field Φ_l defined by equation (19) at the scale ratio Λ—and then studying its scaling behaviour at decreasing value of the scale ratio $\lambda \leq \Lambda$. Hence, the new generated field has the following multiscaling behaviour:

$$\left\langle \left[\phi^\eta_{\lambda,\Lambda} \right]^q \right\rangle \approx \lambda^{K(q,\eta)} \tag{23}$$

where $K(q,\eta)$ is the double trace moment scaling exponent related to $K(q,1) \equiv K(1)$ by:

$$K(q,\eta) = K(q\eta) - qK(\eta) \tag{24}$$

which gives for universality classes [using equation (17)]:

$$K(q,\eta) = \eta^{\alpha} K(q) \tag{25}$$

The scaling exponent $K(q,\eta)$ is estimated by the slope of the linear trends of $\left\langle \left[\phi_{\lambda,\Lambda}^{\eta}\right]^{q} \right\rangle$ versus λ in a log–log plot. By keeping q fixed (but different from the special values 0 and 1), the slope of $|K(q,\eta)|$ as a function of η in a log–log graph gives the value of the index α and C_1 is estimated by the intersection with the line $\eta = 1$. Varying then allows a systematic verification of equation (25), and hence the universality hypothesis.

Case study: tidally turbulent coastal waters of the Eastern English Channel

Data sampling

Sampling experiments were conducted during 46 h and 24 min in a period of spring tide, from 2 to 4 April 1996, at an anchor station (Figure 12) located in inshore waters of the Eastern English Channel (50°47′300 N, 1°33′500 E). Temperature and salinity, regarded as passive scalars under purely physical control of turbulent motions, and phytoplankton biomass, estimated from measurements of *in vivo* fluorescence intensity, were simultaneously recorded from a single depth (10 m) with Sea-Bird 25 Sealogger CTD probe and a Sea Tech fluorometer, respectively. Our analyses are based on three time series recorded at 1 Hz (i.e. 167 040 data), which contain temperature, salinity and fluorescence data, labelled A, B and C, respectively. Samples of these data are shown in Figure 13. Every hour, samples of water were taken at 10 m depth to estimate chlorophyll *a* concentrations, which appear significantly correlated with *in vivo* fluorescence (Kendall's $\tau = 0.652$, $P < 0.05$).

Scaling and multiscaling of temperature, salinity and fluorescence fields

Power spectral analysis. We compute the Fourier power spectra of temperature, salinity and *in vivo* fluorescence fluctuations in order to estimate the mean scaling properties of those different fields (Figure 14). The temperature and salinity power spectra exhibit very similar scaling behaviours [i.e. $E(f) \propto f^{-\beta}$, where f is the frequency] over the whole range of studied scales (Figure 14a and b). Over smaller scales (1–1000 s), the observed power law trend gives $\beta \approx 1.72$ and $\beta \approx 1.67$ for temperature and salinity, respectively. Over larger scales (>1000 s), temperature and salinity power spectra both exhibit steeper power law trends with $\beta \approx 1.98$ and $\beta \approx 2.25$, respectively. The fluorescence power spectrum (Figure 14c) presents a slightly complex behaviour with three scaling tendencies for scales ranging from 1 to 20 s with $\beta \approx 1.77$, from 20 to 1000 s with $\beta \approx 0.66$ and for scales larger than 1000 s with $\beta \approx 1.96$. Those temporal transitional scales can be associated with spatial scales using probably the most cited and widely used method of relating time and space, 'Taylor's hypothesis of frozen turbulence' (Taylor, 1938), which basically states that temporal and spatial averages t and l,

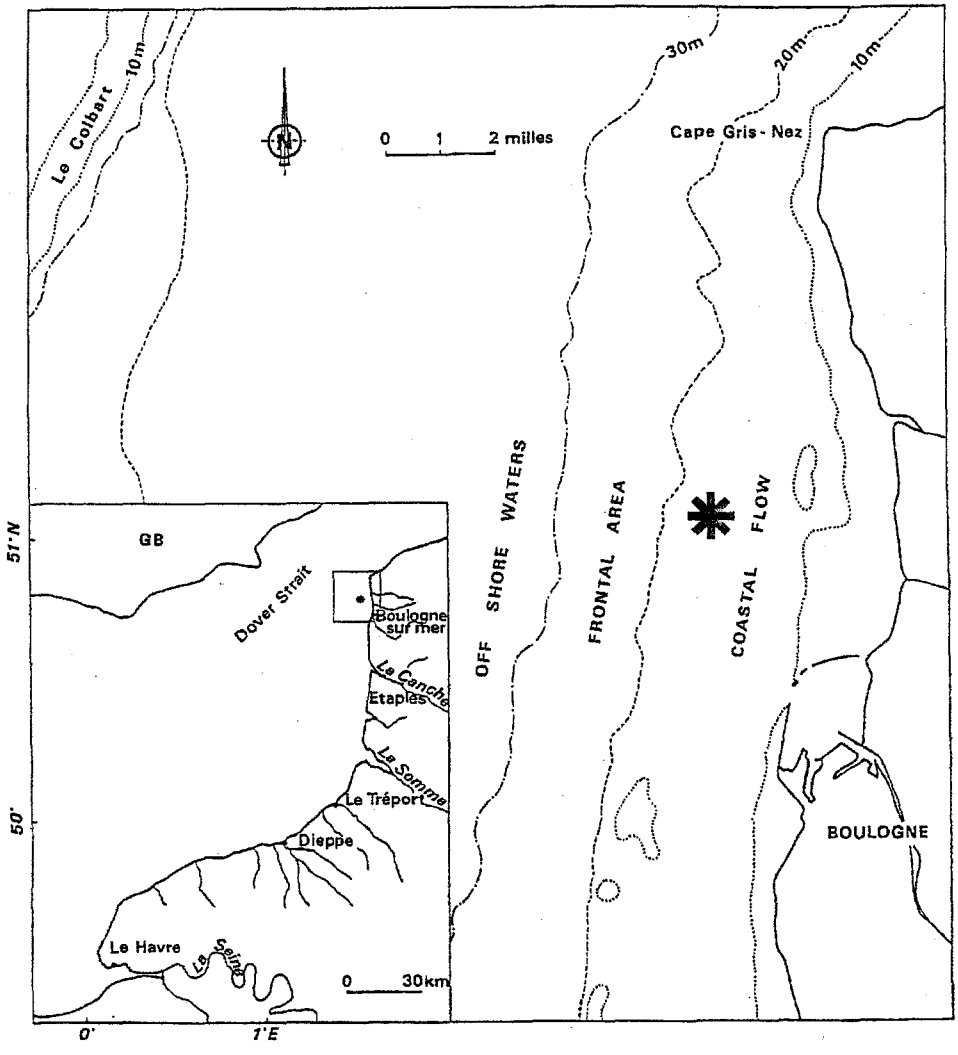

Fig. 12. Study area and location of the sampling station (*) along the French coast of the Eastern English Channel.

respectively, can be related by a constant velocity V, $l = V \cdot t$. Then, using the mean instantaneous tidal circulation of ~0.541 m s^{-1} (0.541 ± 0.126 SE), observed during the field experiment, the associated transitional length scales are around 12 and 540 m for *in vivo* fluorescence, and 540 m for temperature and salinity.

At small scales, the relative proximity between the spectral behaviour of temperature, salinity and fluorescence seems to confirm the hypothesis of passivity of phytoplankton biomass in a turbulent environment. Indeed, the departure from the expected theoretical value ($\beta \approx 5/3$) associated with the behaviour of a passive scalar in fully developed turbulence (Obukhov, 1949; Corrsin, 1951) is not

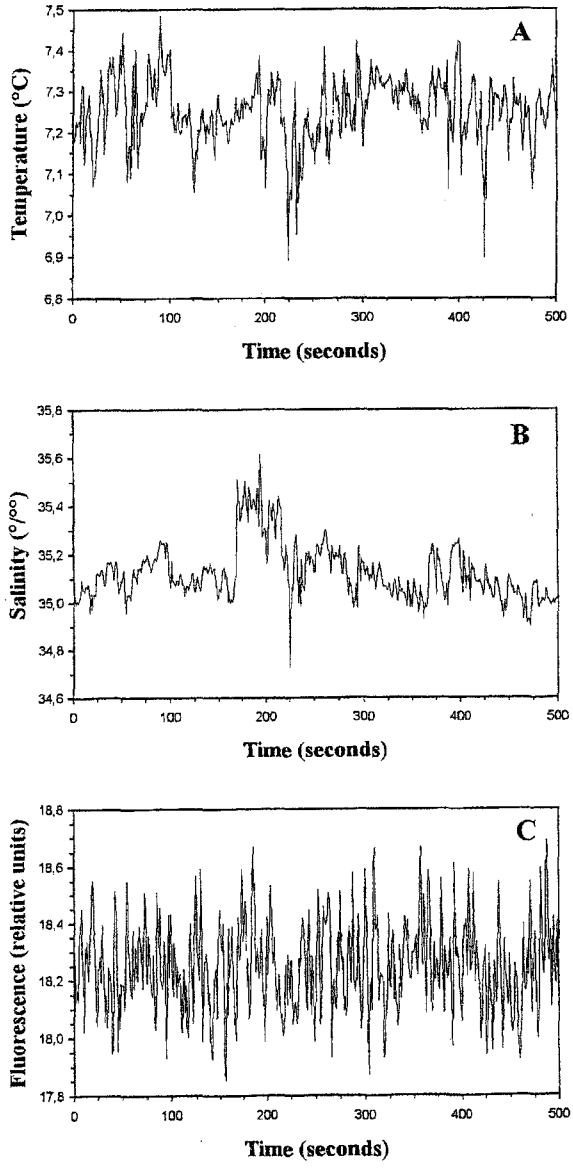

Fig. 13. A portion of temperature, salinity and *in vivo* fluorescence time series (from top to bottom) recorded in the Eastern English Channel. Sharp fluctuations occurring on all time scales are clearly visible, indicating the intermittent behaviour of the dataset.

significant (modified t-test, $P < 0.05$; Scherrer, 1984). These results, in agreement with previous field studies showing chlorophyll spectra which follow approximately the –5/3 power law (e.g. Platt, 1972; Powell *et al.*, 1975), seem to indicate that, over these small scales, the space–time structure of phytoplankton biomass is primarily influenced by the dynamics of the physical environment, rather than

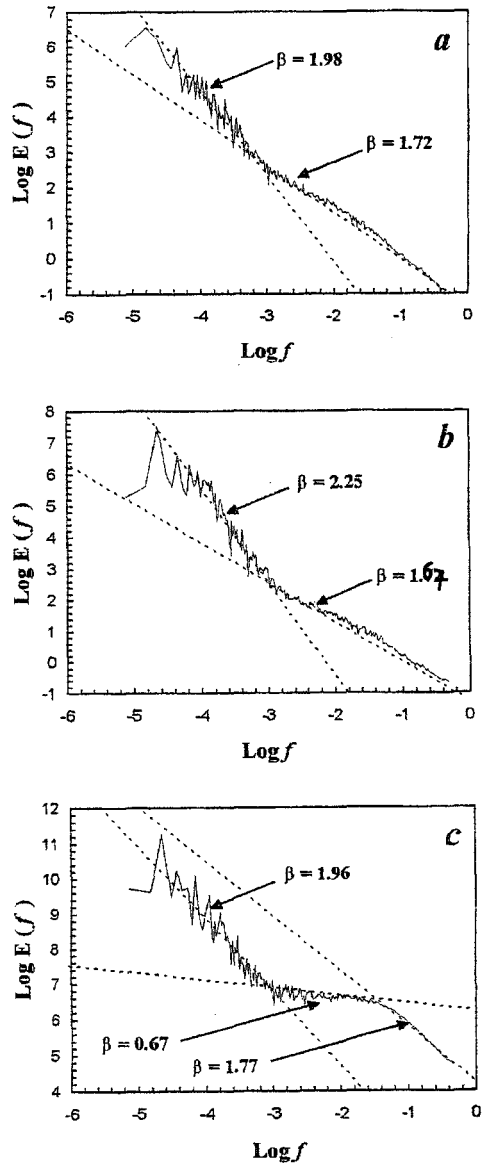

Fig. 14. The power spectra $E(f)$ (f is frequency) of temperature (**a**), salinity (**b**) and *in vivo* fluorescence (**c**), shown in log–log plots. Temperature and salinity power spectra exhibit two similar scaling regimes for scales ranging from 1 to 1000 s and for scales >1000 s, whereas *in vivo* fluorescence power spectrum exhibits a more complex behaviour with three scaling regimes for scales ranging from 1 to 20 s, 20 to 1000 s and for scales >1000 s.

the behaviour of the organisms themselves. On the other hand, over larger scales (i.e. 20 and 1000 s, or 12 and 540 m), fluorescence also exhibits a very specific spectral behaviour, independent of the physical forcings, with $\beta \approx 0.66$. This result roughly fits with theoretical and experimental results (Powell *et al.*, 1975;

Denman and Platt, 1976; Denman *et al.*, 1977; Bennett and Denman, 1985; Steele and Henderson, 1992; Powell and Okubo, 1994) predicting that the phytoplankton biomass spectrum will be flatter than the spectrum of a scalar contaminant of the flow field and indicating that in this region different processes contribute to the variance of phytoplankton biomass, i.e. that temporal variability in the biological parameters such as cell growth and community structure has an important role in shaping the phytoplankton biomass distribution.

On the other hand, for scales larger than 1000 s (or 540 m), the spectral exponents β are obviously larger than the theoretical $\beta \approx 5/3$ (modified *t*-test, $P > 0.05$; Scherrer, 1984) and the spectral exponent of salinity appears significantly larger than the exponents of temperature and the fluorescence, which cannot be distinguished (Tukey multiple comparison test, $P < 0.05$; Zar, 1996). This scaling behaviour, obviously independent of turbulent processes, may then qualitatively (we try a quantification latter) be related to the very specific structuration of the hydrological pattern of the Eastern English Channel. Indeed, the megatidal regime and the fluvial supplies distributed from the Bay of Seine to Cape Griz-Nez along the French coast generate a heterogeneous coastal water mass which drifts nearshore, separated from the open sea by a frontal area (Brylinski and Lagadeuc, 1990; Lagadeuc *et al.*, 1997)—known as the 'coastal flow' (Brylinski and Lagadeuc, 1990; Brylinski *et al.*, 1991)—and characterized by its freshness, turbidity (Dupont *et al.*, 1991) and phytoplankton richness (Quisthoudt, 1987; Brylinski *et al.*, 1991). The very specific scaling behaviour previously described can then be associated both with the coastal heterogeneity related to the progressive integration of freshwater inputs to marine waters (Brylinski *et al.*, 1991; Lagadeuc *et al.*, 1997) and with the influence of a frontal area, as suggested by the closeness of the scaling exponent β with the theoretical $\beta \approx 2$ expected in the case of frontal mixing (Kraichnan, 1967; Bennett and Denman, 1985).

Multifractality of oceanic turbulent fields. The computations of the temperature, salinity and *in vivo* fluorescence structure functions (i.e. $<(\Delta T_\tau)^q>$, $<(\Delta S_\tau)^q>$ and $<(\Delta F_\tau)^q>$, respectively) confirm the scaling regimes previously shown by spectral analysis for different orders of moments q (Figure 15). The slopes, fitted to the data by least squares over the range of scale values for which the data are scaling (i.e. the curves are linear), provide estimates of the exponents $\zeta(q)$.

The scaling of the first moment $\zeta(1)$ [$\zeta(1) = H$] for temperature, salinity (over scales smaller than 1000 s, or 540 m) and fluorescence (over scales smaller than 20 s, or 12 m) are not significantly different (Analysis of Covariance, $P < 0.05$; Zar, 1996), with $\zeta(1) = 0.40 \pm 0.01$, $\zeta(1) = 0.38 \pm 0.01$ and $\zeta(1) = 0.43 \pm 0.01$, respectively. Here, as below, the error bars come from the different portions of the dataset analysed separately: for example, with the scaling of temperature and salinity up to 1000 s and a database of 167 040 points, we can estimate the exponents for 167 non-overlapping intervals. For scales larger than 1000 s, the scaling exponents H (see Table I) appear significantly different for the temperature, salinity and fluorescence fields (Analysis of Covariance, $P > 0.05$; Zar, 1996), the scaling exponents being significantly larger for salinity than those related to temperature and fluorescence, which remain indistinguishable (Tukey multiple

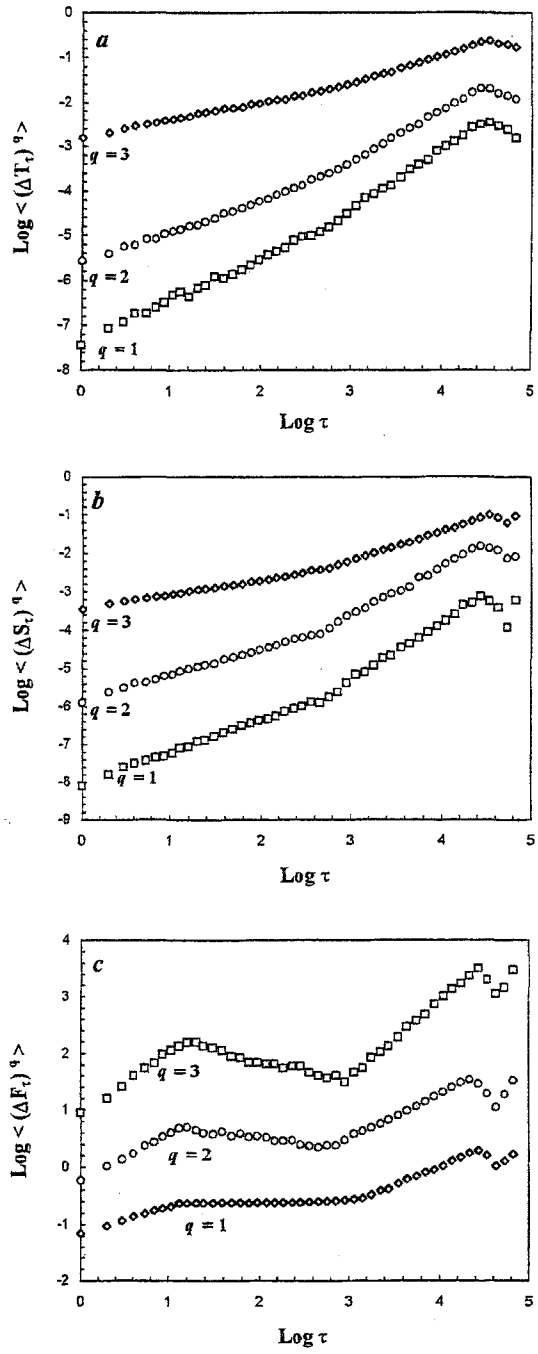

Fig. 15. The structure functions $<(\Delta T_\tau)^q>$, $<(\Delta S_\tau)^q>$ and $<(\Delta F_\tau)^q>$ versus τ in log–log plots for $q = 1$, 2 and 3 for temperature (**a**), salinity (**b**) and *in vivo* fluorescence (**c**). Two and three linear trends are clearly visible on the one hand for temperature and salinity, and on the other hand for *in vivo* fluorescence (see Table I for slope estimates).

Table I. Empirical estimates of the spectral exponent β, and the first and second moment scaling exponent $\zeta(1) = H$ and $\zeta(2)$ for temperature, salinity and *in vivo* fluorescence for the different scaling regimes encountered

	$t < 20$ s			$20 < t < 1000$ s			$t > 1000$ s		
	H	$\zeta(2)$	β	H	$\zeta(2)$	β	H	$\zeta(2)$	β
Temperature	0.40	0.71	1.72	0.40	0.71	1.72	0.64	0.97	1.98
Salinity	0.38	0.67	1.67	0.38	0.67	1.67	0.80	1.22	2.25
Fluorescence	0.43	0.75	1.77	0.00	-0.35	0.66	0.66	0.97	1.96

Table II. Empirical estimates of the universal multifractal parameters C_1 and α for temperature, salinity and *in vivo* fluorescence for the different scaling regimes encountered

	$t < 20$ s		$20 < t < 1000$ s		$t > 1000$ s	
	C_1	α	C_1	α	C_1	α
Temperature	0.05	1.90	0.05	1.90	0.24	1.35
Salinity	0.05	1.90	0.05	1.90	0.27	1.50
Fluorescence	0.06	1.80	0.20	1.60	0.24	1.37

comparison test, $P < 0.05$; Zar, 1996). Over intermediate scales (i.e. from 20 to 1000 s), *in vivo* fluorescence structure functions $<(\Delta F_\tau)^q>$ for the first order of moment show no slope, i.e. $\zeta(1) = H \approx 0$, indicating a conservative behaviour (i.e. fluctuations of fluorescence are scale independent). In the same way, the scaling of the second-order moments confirms the estimates of β from the power spectra [$\beta = 1 + \zeta(2)$] for each scaling regime (cf. Table II).

More generally, the non-linearity of the empirical curve $\zeta(q)$ in Figure 16 shows that these different fields can be considered as multifractals; the curves corresponding to temperature and *in vivo* fluorescence (i.e. phytoplankton biomass) are very close to each other for scales smaller than 1000 s and 20 s, respectively (Figure 16a and b), and for scales larger than 1000 s (Figure 16d and e). Within experimental error, they cannot be qualitatively (we try a quantification later) showed as being different. On the contrary, the empirical curves $\zeta(q)$ for salinity (Figure 16c and f) are slightly different, showing more convex behaviours, especially on large scales (Figure 16f), whereas *in vivo* fluorescence $\zeta(q)$ exhibits a very specific behaviour (Figure 17) over scales between 20 and 1000 s. It can be noticed that the empirical moment scaling exponent $K(q)$, obtained by the estimates of the slopes of the linear trend of $<(\Phi_l)^q>$ versus l in a log–log plot (Figure 18a) from equation (15), clearly exhibits multifractal properties previously described (Figure 18b; cf. Figure 8) and confirms the link existing between the exponents $K(q)$ and $\zeta(q)$ given by equations (17) and (22) (Figure 18b).

Universality of turbulent oceanic fields. We realize a quantitative description of scale invariant fields computing estimations of universal parameters and using the DTM analysis technique (Lavallée, 1991; Lavallée *et al.*, 1992), basically applied to a great variety of geophysical data (Schmitt *et al.*, 1992a,b, 1993; Teissier *et al.*,

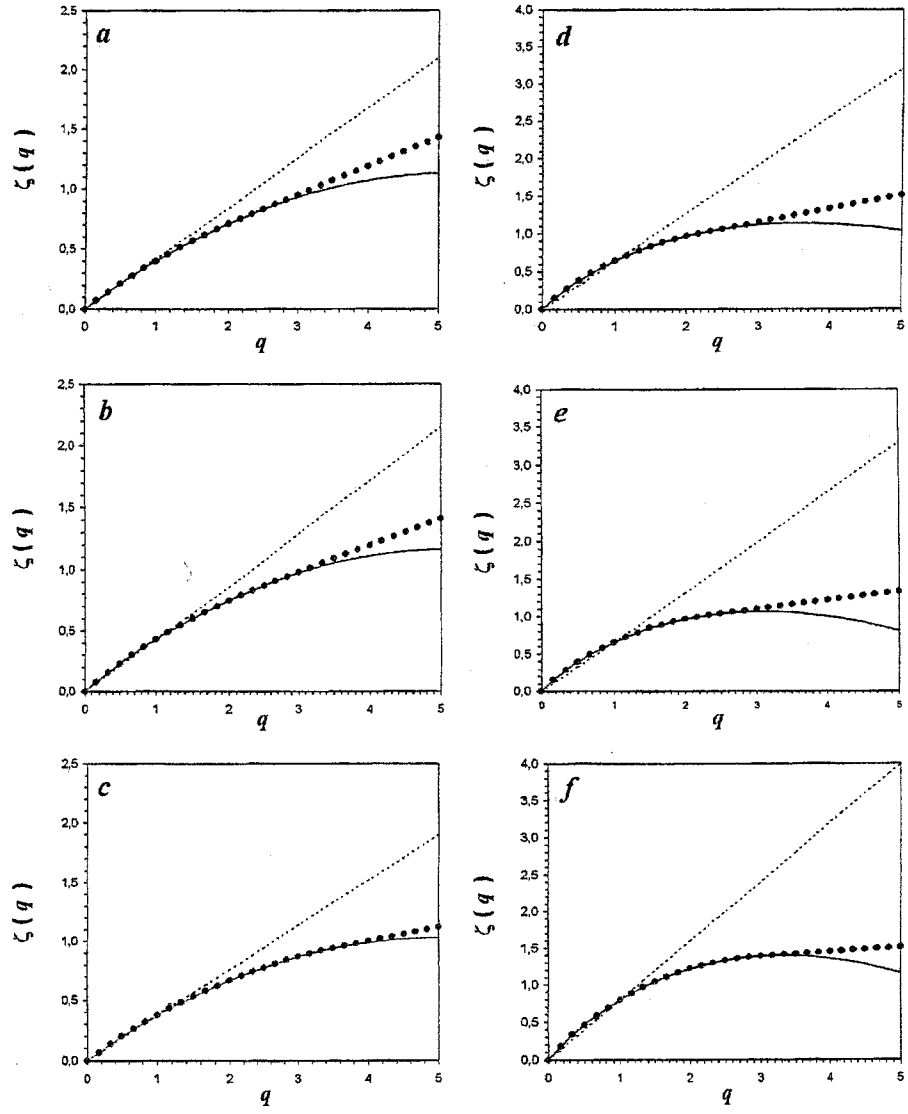

Fig. 16. The scaling exponent structure function $\zeta(q)$ empirical curves (dots), compared to the monofractal curves $\zeta(q) = qH$ (dashed line), and to the universal multifractal curves (continuous curve) obtained with C_1 and α (cf. Table II) in equation (22) for temperature, salinity and *in vivo* fluorescence over small scales (i.e. scales smaller than 1000 s for temperature and salinity, and smaller than 20 s for *in vivo* fluorescence) and large scales (i.e. scales >1000 s). The empirical curves are non-linear, indicating multifractality.

1993a,b; Chigirinskaya *et al.*, 1994, 1997; Lazarev *et al.*, 1994; Falco *et al.*, 1996), based on multiscaling properties of the intermittent fluxes Φ_λ (i.e. obtained by fractional differentiation of order H) of temperature, salinity and fluorescence fields as defined in equation (19). The scaling of the intermittent fluxes $<(\phi^{\eta}_{\lambda,\Lambda})^q>$ (Figure 19) is shown for $q = 2$ and different values of η. The slopes of $<(\phi^{\eta}_{\lambda,\Lambda})^q>$

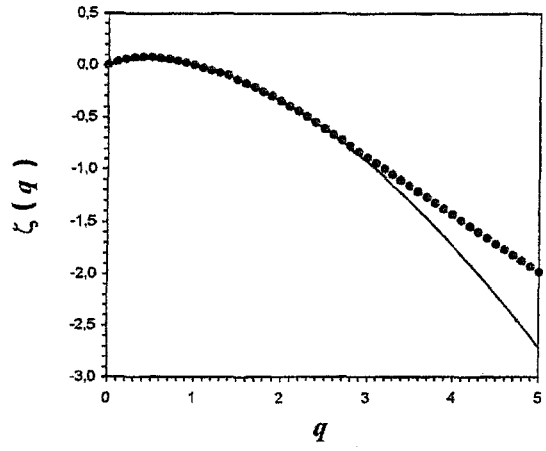

Fig. 17. The scaling exponent structure function $\zeta(q)$ empirical curves (dots), compared to the universal multifractal curve obtained with C_1 and α (cf. Table II) in equation (22) for *in vivo* fluorescence for scales bounded between 20 and 1000 s, where biological activity has an important role in shaping the phytoplankton biomass distribution.

versus λ in a log–log plot, fitted by least squares, are the estimates of $K(q, \eta)$. The linear trends of the curves $K(q, \eta)$ versus η, plotted in a log–log graph, show that equation (25) is well respected for a wide range of η values (Figure 20). Their slopes and the intercepts give, respectively, the estimates of α and C_1, wholly presented in Table II, and suggest an increasing heterogeneity and a decreasing multifractality from small to large scales for both physical and biological parameters, globally leading to view the distributions of these parameters as more patchy distributed on larger scales.

To test the validity of the estimates of α and C_1 of the intermittent fields, we fit the empirical scaling exponent $\zeta(q)$ with the theoretical universal multifractal expression given by α and C_1 (Table II) in equation (22). The universal multifractal and empirical fits are excellent until critical moment of order q_c (Table III), after which the empirical curves are linear (Figures 16 and 17). This linear behaviour of the empirical scaling exponent structure function $\zeta(q)$ is known for sufficiently high-order moments (Schertzer and Lovejoy, 1989) and is due to sampling limitations (i.e. second-order multifractal phase transition; Schertzer and Lovejoy, 1992) or is associated with a divergence of statistical moments (i.e. first-order multifractal phase transition; Schertzer and Lovejoy, 1992) if substantiated by large enough sample size. In both cases, for $q \geq q_c$, the empirical $\zeta(q)$ follows:

$$\zeta(q) = 1 - \gamma_{\max} q \tag{26}$$

where $\gamma_{\max}$ is the maximum singularity associated to q_c. In the case of a first-order phase transition, q_c corresponds specifically to maximum singularity measured, which is associated with the occurrence of very rare and violent singularities, whereas in the case of a second-order multifractal phase transition, q_c corresponds

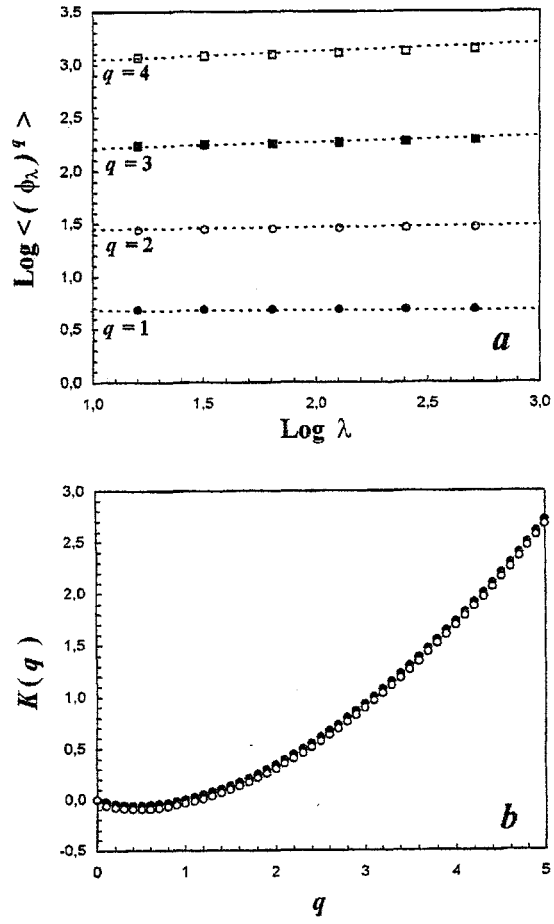

Fig. 18. The curves $<(\varphi_\lambda)^q>$ versus λ in a log–log plot for *in vivo* fluorescence for scales ranging from 20 to 1000 s (**a**). The slopes of straight lines indicating the best regression over the range of scales provide estimates of the empirical scaling exponent $K(q)$ [(**b**), dark circles; cf. equation (15)] which is compared to the $K(q)$ estimated following $K(q) = qH - \zeta(q)$ [open circles; cf. equation (22)].

to the maximum singularity effectively measurable from a finite sampling [see Schmitt *et al.* (1994) for further developments].

In order to differentiate between first and second multifractal phase transitions, we then compute the theoretical value of the critical moment q_s expected in the case of sampling limitations given by (Schertzer and Lovejoy, 1992):

$$q_s = \left(\frac{1}{C_1}\right)^{1/\alpha} \tag{27}$$

and compare it with the q_c estimated from the empirical $\zeta(q)$ (see Figures 16 and 17). With the values of α and C_1 estimated above (Table II), we obtain q_s values

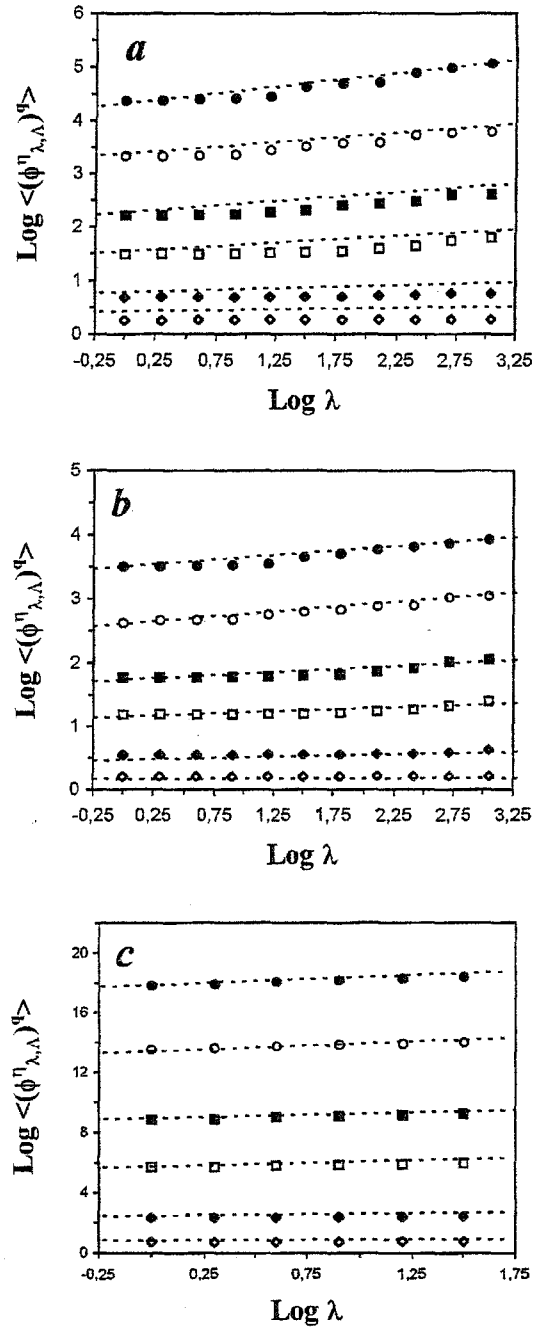

Fig. 19. The curves $<(\phi^{\eta}_{\lambda,\Lambda})^{q}>$ versus λ for temperature (**a**), salinity (**b**) and *in vivo* fluorescence (**c**) over small scales (i.e. scales smaller than 1000 s for temperature and salinity, and smaller than 20 s for *in vivo* fluorescence) shown in a log–log plot for $q = 2.5$ and for different values of η ($\eta = 0.2, 0.5, 1, 1.4, 2$ and 2.5 from bottom to top). The slope of the linear trends provides estimates of the double trace moment scaling exponent $K(q, \eta)$ [cf. equation (23)].

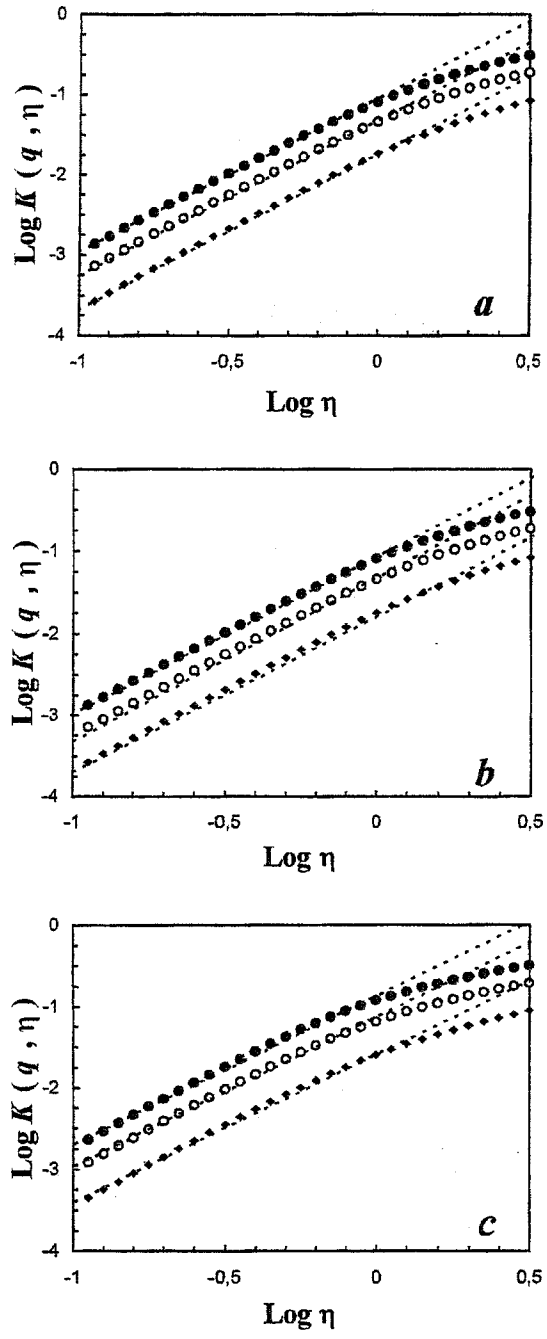

Fig. 20. The curves $K(q, \eta)$ versus η in a log–log plot for $q = 2.5$ and 3 (from bottom to top) for temperature (**a**), salinity (**b**) and *in vivo* fluorescence (**c**), where $K(q, \eta) = \eta^{\alpha} K(q)$. The slope of the straight lines then gives the estimates of α and C_1 is estimated by the intercept.

very close to the values estimated from the empirical curves $\zeta(q)$ for intermediate and large-scale fluorescence, but also for temperature and salinity for scales larger than 1000 s ($q_c \approx q_s$). Those critical moments are therefore only linked to sampling limitations (i.e. second-order multifractal phase transition), because we had to average the original time series up to the scale of 20 and 1000 s, in order to be in the appropriate ranges of scales. On the contrary, on smaller scales, the situation is obviously different with $q_c < q_s$, clearly indicating that the critical moments q_c are independent of sampling and characterizing the occurrence of very rare and violent singularities in our dataset (i.e. first-order multifractal phase transition).

Those results, showing the extreme similarity of temperature, salinity and fluorescence field on small scales (see Tables I, II and III), can be regarded as a quantitative verification of the hypothesis of small-scale fluorescence as being a purely passive scalar and generalization of previous works which tested the passivity assumption using only power spectra (i.e. a second-order moment). Furthermore, the very specific non-linear behaviour of the structure functions scaling exponent $\zeta(q)$ for *in vivo* fluorescence over scales ranging from 20 to 1000 s as the differences perceived in temperature, salinity and fluorescence distributions for scales larger than 1000 s indicate that variability can also be wholly described in a universal multifractal framework even over scales dominated by non-turbulent processes.

Discussion

Scales of patchiness for intermittent fields in turbulent coastal waters

Small scales. The present case study has shown that on small scales (i.e. < 20 s, or 12 m, for *in vivo* fluorescence and < 1000 s, or 540 m, for temperature and salinity), *in vivo* fluorescence, temperature and salinity spectral behaviours are statistically indistinguishable and closely follow the −5/3 power law derived by Kolmogorov (1941) for the inertial subrange of turbulent velocity fields. This is the region of the turbulence spectrum where energy transferred from larger eddies (i.e. large-scale eddies induced by external forcings such as wind and tidal patterns) to the smallest eddies which dissipate their energy into heat (i.e. viscous dissipation cannot be neglected and smooth out turbulent fluctuations). That implies that the distribution of phytoplankton was governed primarily by the turbulent environment, and not by the net growth rate (which includes division and predation) of cells themselves. One may note here that in the case of interacting species (i.e. intra- and interspecific interactions), the power spectrum of phytoplankton biomass fluctuations should have exhibited a steeper slope, even for the inertial subrange (i.e. $\beta = 3$; Powell and Okubo, 1994).

Subsequent multifractal analysis confirms and generalizes these observations. Indeed, the relative commonality of the estimates of the three basic universal multifractal parameters, H, C_1 and α—but also the critical moments q_c—of temperature, salinity and phytoplankton biomass, then reflects profound couplings between space–time structure of phytoplankton populations and the structure of their physical environment (see Tables II and III), as previously

Table III. Theoretical and empirical estimates of the critical moment q_s for temperature, salinity and *in vivo* fluorescence for the different scaling regimes encountered

	$t < 20$ s		$20 < t < 1000$ s		$t > 1000$ s	
	q_s (theoretical)	q_s (empirical)	q_s (theoretical)	q_s (empirical)	q_s (theoretical)	q_s (empirical)
Temperature	4.84	2.50	4.84	2.50	2.88	2.80
Salinity	4.84	3.20	4.84	3.20	2.39	2.50
Fluorescence	4.77	2.70	2.73	2.80	2.83	2.75

suggested by simple representations of the extreme intricacy between the space–time scales of physical and biological marine processes (Stommel, 1963; Haury *et al.*, 1978; Steele, 1978; Marquet *et al.*, 1993). Furthermore, the universal multifractal parameters H, C_1 and α obtained from the present study (cf. Table II) appear very similar to those obtained from previous studies conducted in different water masses and tidal conditions (Table IV). This suggests that the small-scale variability of phytoplankton biomass, wholly characterized in terms of multifractality, cannot be regarded as density dependent, as previously found by Prairie and Duarte (1996) in a various set of marine and freshwater phytoplankton distribution. One may also note that the difference between the estimates of H, C_1 and α observed during spring and neap tides (cf. Table IV) did not suggest any tidal dependence of the distribution of both physical and biological parameters. However, in a recent monofractal study of vertical phytoplankton variability also conducted in the coastal waters of the Eastern English Channel, Seuront and Lagadeuc (1998) showed both a density dependence and a tidal dependence of phytoplankton biomass distribution associated with the inshore–offshore hydrological gradient and the flood/ebb alternance, respectively. This study, involving narrower ranges of spatio-temporal scales, then cannot be directly compared with the present results. Further investigations are therefore still needed to identify the relative effects of different advection processes and hydrodynamics on the structuration of phytoplankton biomass variability, for instance by considering shorter datasets differentially distributed over a whole tidal cycle, but it was not the aim of this paper.

The examination of the critical moments q_c (Table III) led to further conclusions. Indeed, our results showed that during a period of spring tide $q_c < q_s$ [where q_c and q_s are the empirical moments after which the scaling exponent $\zeta(q)$ is linear, and the theoretical critical moment characterizing sampling limitations, respectively], while similar studies conducted during a period of neap tide (Seuront *et al.*, 1996a) rather suggest $q_c \approx q_s$ [$q_s \approx 6.0$, with $C_1 = 0.04$ and $\alpha = 1.80$ in equation (27) for phytoplankton biomass]. This could, therefore, suggest a differential intermittent behaviour of physical (i.e. temperature and salinity) and biological (i.e. phytoplankton biomass) variability in spring and neap tides. Spring tide physical and biological variability are characterized by more violent events than during neap tide. Such a difference in the occurrence of extreme events between different hydrodynamic conditions may be of prime interest in future studies in planktonology following the recent emphasis on understanding

Table IV. Values of the universal multifractal parameters H, C_1 and α obtained by Seuront *et al.* (1996b) in the Eastern English Channel at the end of March 1995 during a period of spring tide (a), by Seuront (1997) and Seuront *et al.* (1996a) in the Southern Bight of the North Sea in June 1991 during periods of neap tide (b and c, respectively), and compared to the values obtained in the present study (d). The values of the slopes of the Fourier power spectra β are also indicated

(a)

	$t < 13$ s			
	β	H	C_1	α
Temperature	1.65	0.34	0.035	1.70
Salinity	–	–	–	–
Fluorescence	1.66	0.36	0.035	1.80

(b)

	$t < 100$ s				100 s $< t <$ 6 h			
	β	H	C_1	α	β	H	C_1	α
Temperature	1.75	0.41	0.05	1.75	1.75	0.41	0.05	1.75
Salinity	–	–	–	–	–	–	–	–
Fluorescence	1.78	0.43	0.045	1.85	–	–	–	–

(c)

	$t < 100$ s				100 s $< t <$ 12 h			
	β	H	C_1	α	β	H	C_1	α
Temperature	1.74	0.42	0.04	1.70	1.74	0.04	0.05	1.70
Salinity	–	–	–	–	–	–	–	–
Fluorescence	1.75	0.41	0.04	1.80	1.22	0.12	0.02	0.80

(d)

	$t < 20$ s				20 $< t <$ 1000 s				1000 s $< t <$ 48 h			
	β	H	C_1	α	β	H	C_1	α	β	H	C_1	α
Temperature	1.72	0.40	0.05	1.90	1.72	0.40	0.05	1.90	1.98	0.64	0.24	1.35
Salinity	1.67	0.38	0.05	1.90	1.67	0.38	0.05	1.90	2.25	0.80	0.27	1.50
Fluorescence	1.77	0.43	0.06	1.80	1.66	0.00	0.20	1.60	1.96	0.66	0.24	1.37

detailed mechanisms that determine each individual feature (Yamazaki, 1993; Paffenhöfer, 1994). Moreover, one may note here that our multifractal approach provides a very precise statistical description of the studied processes (i.e. estimates of all moments, even non-integers, up to moment of order 5), while the characterization of other non-Gaussian empirical data or processes is basically limited to their three first moments (average, variance and skewness).

This demonstrated small-scale structured (i.e. non-random) distribution of phytoplankton biomass should therefore constitute an important subset in the growing field of determining the influence of turbulence on plankton ecosystems

(e.g. Costello *et al.*, 1990; Marrasé *et al.*, 1990; Granata and Dickey, 1991; Yamazaki and Kamykowski, 1991; Madden and Day, 1992; Kiørboe, 1993). Indeed, it is noteworthy that the present understanding of turbulence incorporated into most aspects of marine and freshwater biology is that turbulence has an essentially random effect on transport. This view is predicated on the assumption that transport in a turbulent flow is similar to molecular transport and diffusion, and is consequently reflected in plankton transport models (Okubo, 1986; Rothschild and Osborn, 1988; Yamazaki, 1993), as well as other areas in which turbulence is important (McCave, 1984; Davis *et al.*, 1991; Yamazaki and Haury, 1993). Moreover, heterogeneous particle distributions, such as the very specific phytoplankton distribution analysed here in the universal multifractal framework, may also have salient consequences, as demonstrated by Currie (1984) on the basis of Taylor approximations of the Michaelis–Menten function, on non-linear concentration-dependent processes such as phytoplankton coagulation (Riebesell, 1991a,b; Kiørboe *et al.*, 1994; Kiørboe, 1997), the encounter of a mate during sexual reproduction (Waite and Harrison, 1992), the encounter rates between a zooplanktonic predator and its prey (Rothschild and Osborn, 1988; Sundby and Fossum, 1990; MacKenzie *et al.*, 1994; Raby *et al.*, 1994; Kiørboe and MacKenzie, 1995; MacKenzie and Kiørboe, 1995), and then may provide new perspectives in the research on primary and secondary production.

Another salient consequence suggested by our results is that turbulent processes cannot be regarded as log-normally distributed, as propounded by many workers (Gregg *et al.*, 1973; Belyaev *et al.*, 1975; Osborn, 1978; Elliott and Oakey, 1979; Gregg, 1980; Wasburn and Gibson, 1984; Oakey, 1985; Osborn and Lueck, 1985a,b; Baker and Gibson, 1987; Gibson, 1991). Log–normal distribution being a particular case of multifractal distribution [i.e. $\alpha = 2$ in equations (17) and (22)], our universal multifractal characterization of small-scale temperature and salinity variability therefore indicates another level of structuration of turbulent fluid motions. Universal multifractal and log–normal distributions can be regarded as belonging to a particular family of skewed distributions reflecting a heterogeneous distribution with a few dense patches and a wide range of low-density patches. This means that occasionally we should expect stronger bursts, more often than in the Gaussian case, characterizing intermittent processes. The phenomenon of intermittency, which is discussed in more detail elsewhere (Jiménez, 1997; Jou, 1997), has recently been shown to be associated with the presence of strong coherent vortices, with diameter of the order of 10 times the Kolmogorov scale (i.e. the Kolmogorov length scale), but with much longer lengths and probably long lifetimes (Jiménez *et al.*, 1993; Jiménez and Wray, 1994).

Coarse scales. On coarser scales (i.e. 20–1000 s, or 12–540 m), the power spectrum of phytoplankton density fluctuations is flatter (i.e. 'whiter') than the –5/3 energy spectrum, i.e. the intensity of patchiness is less than that of environmental turbulence fluctuations. Denman and Platt (1976) and Denman *et al.* (1977) first described these relationships for the inertial subrange. They defined three distinct regions in the phytoplankton biomass power spectrum. If τ (s) represents the time

taken for a turbulent eddy to transfer its energy to an eddy half its size, and μ (s^{-1}) is the doubling rate of the phytoplankton, then for $\mu^{-1} >> \tau$, the growth rate of the phytoplankton is insufficient to produce a spatio-temporal distribution that is different from that of purely passive quantities such as temperature or salinity. The phytoplankton behave as passive tracers; thus, the slope of the power spectrum of phytoplankton density fluctuations is similar to that for environmental fluctuations, both in the inertial subrange ($\beta \approx 5/3$) and in two-dimensional turbulence ($\beta \approx 3$; Gower *et al.*, 1980; Deschamps *et al.*, 1981; Abraham, 1998). However, for $\mu^{-1} << \tau$, the phytoplankton are doubling sufficiently quickly for their spatio-temporal distribution to be no longer nullified by turbulence. The spatio-temporal structure of the community cannot be destroyed by the diffusive action of the eddies, and in this case theoretical curves indicate a flattening of the phytoplankton biomass spectrum, i.e. $\beta \approx 1$, both in the inertial subrange (Denman and Platt, 1976; Denman *et al.*, 1977) and in two-dimensional turbulence (Bennett and Denman, 1985; Powell and Okubo, 1994). For $\mu^{-1} \approx \tau$, a transitional regime where neither process dominates occurs, and the spatial patterns formed may be the result of a complex interaction between τ and μ. This transition zone corresponds to the minimum patch which can maintain itself in the face of diffusion, known as the KISS length (Okubo, 1978, 1980). The relationship between τ and μ has been further quantified by Denman *et al.* (1977), who proposed a critical patch size for phytoplankton in the open ocean of 5–10 km, while other theoretical studies have derived a characteristic patch size of 1–2 km for phytoplankton populations in bloom conditions (e.g. Okubo, 1980).

Yet, the interpretation of the proximal cause of small-scale plankton patchiness has then been in terms of population growth rather than aggregation of organisms which grew elsewhere. However, one may note here that the characteristic time and space scales associated with the flattening of our phytoplankton biomass spectrum (i.e. 1000 s, or 540 m) occurs for scales significantly smaller than the generation time of phytoplankton populations (i.e. $\approx$ 1 day) and the critical patch size found in the literature. In that way, comparisons of our universal multifractal distribution of phytoplankton biomass $\zeta(q)$ (cf. Figure 17) to the structure function scaling exponent $\zeta_F(q) = -K(q/2)$ of a biologically active scalar derived by Seuront *et al.* (1996b) from the previous theoretical results of Denman and Platt (1976) and Denman *et al.* (1977) then lead to further conclusions. Phytoplankton distributions observed in the Eastern English Channel and in the Southern Bight of the North Sea, respectively, over time scales ranging from 20 to 1000 s (i.e. 12–540 m) and for time scales >100 s (i.e. 30 m) (Table IV; Seuront *et al.*, 1996a), are obviously different from the theoretical curve $\zeta_F(q)$ (Figure 21). This suggests that aggregation processes occurring over these ranges of scales cannot be strictly associated with phytoplankton growth rates. Indeed, field studies frequently suggest that plankton aggregations can also be associated with hydrodynamic discontinuities such as fronts and eddies (Alldredge and Hammer, 1980; Mackas *et al.*, 1980; Herman *et al.*, 1981; Owen, 1981), while some theoretical studies proposed patch-generating mechanisms associated with Langmuir cells (Stommel, 1949; Stavn, 1971), internal waves (Kamykowski, 1974), tidal current shear (Riley, 1976), wind-driven currents (Verhagen, 1994) and grazing activity

(Evans, 1978). In the present case, plankton patches are obviously too small in spatial dimension and too transitory in duration to be the results of reproductive population increase. This suggests another level of complexity in the patch-generating mechanisms, such as complex interactions between the turbulence level of fluid motions (e.g. different tidal and wind conditions), the phytoplankton biomass concentration and the specific composition of phytoplankton assemblages, highly variable all along the year in the Eastern English Channel and in the Southern Bight of the North Sea (Martin-Jezequel, 1983; Gentilhomme and Lizon, 1998). This seems indeed to be the case following the differences observed in the universal multifractal parameters between exeriments conducted in the Eastern English Channel during a period of spring tide (i.e. $H = 0.00$, $C_1 = 0.20$ and $\alpha = 1.60$; present study), and the Southern Bight of the North Sea ($H = 0.12$, $C_1 = 0.02$ and $\alpha = 0.80$; Seuront *et al.*, 1996a). Phytoplankton biomass then appears to be more conservative (i.e. low H value, the mean of the fluctuations is then less scale dependent, indicating a reduced flux from large to small scales), more heterogeneously distributed (i.e. high C_1 value corresponding to sparse patches) and structured (i.e. high α value indicating a higher multifractality, that is to say the occurrence of numerous intermittency levels between maximum and minimum concentrations) in the Eastern English Channel than in the North Sea. Whatever that may be, further investigations are still needed to estimate the relative importance of hydrodynamic, hydrological, seasonal processes and their related populational, biological and physiological effects on the precise structure of phytoplankton fields.

At larger scales (i.e. >1000 s, or 540 m), the situation is quite different, phytoplankton biomass variability appearing essentially similar to temperature variability, suggesting a decoupling between phytoplankton and salinity dynamics.

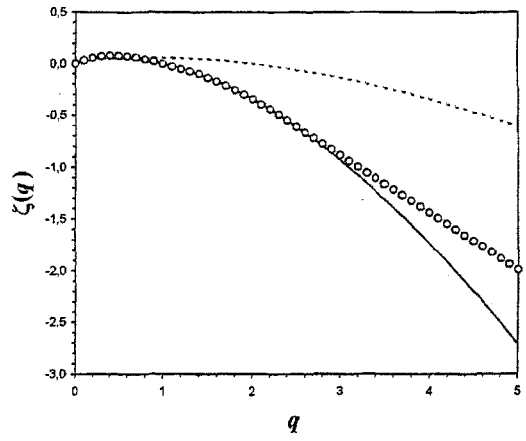

Fig. 21. The empirical structure function scaling exponent $\zeta(q)$ estimated for *in vivo* fluorescence for scales ranging from 20 to 1000 s (continuous curve) compared to the universal multifractal functions obtain with C_1 and α in equation (22) (open circles) and to the theoretical formulation for $\zeta(q)$ proposed by Seuront *et al.* (1996b) as an extension of previous spectral and dimensional theoretical works by Denman and Platt (1976) and Denman *et al.* (1977) (dashed curve).

Then, over this range of scales, river inflow cannot be directly regarded as a source of phytoplankton biomass variability, which seems to be rather controlled by mixing processes associated with the frontal area separating inshore and offshore waters, as suggested by the very specific spectral behaviour (i.e. $\beta \approx 2$; Kraichnan, 1967; Bennett and Denman, 1985) and the extreme similarity existing between the universal multifractal parameterization of temperature and *in vivo* fluorescence (cf. Table II). However, both the coastal heterogeneity in salinity related to the progressive integration of freshwater inputs to marine waters (Brylinski *et al.*, 1991; Lagadeuc *et al.*, 1997) and the haline stratification existing at the mouth of estuaries which maintains nutrient-rich waters favouring the initiation of phytoplankton blooms (Pingree *et al.*, 1986) can also be regarded as potential sources of heterogeneity in the coastal distribution of phytoplankton biomass in this area. In that way, one may also note that the occurrence of a joint transition zone for these three parameters demonstrates that the scales of the physics and biology were nearly coincident, even when the interactions are not necessarily closely coupled. This could suggest a differential physical control of phytoplankton biomass distribution, the precise nature of these interactions remaining unresolved. The values of the universal multifractal parameters, H, C_1 and α (see Table II), nevertheless indicate a more patchy distribution of temperature, salinity and phytoplankton biomass in comparison with the scales dominated by tri-dimensional turbulent processes (i.e. the inertial subrange) where heterogeneity was very low (i.e. C_1 values) and multifractality approached its upper limit (i.e. $\alpha \approx 2$).

Multifractal analysis: a new way of looking across scales for intermittent processes

The different transition zones separating the previously described partial scaling behaviours indicate characteristic scales where the environmental properties or constraints acting upon organisms, or more generally the structure of the variability of a given field, are changing rapidly (Frontier, 1987; Seuront and Lagadeuc, 1997). The concepts of 'scale' and 'pattern' being ineluctably intertwined (Hutchinson, 1953), the identification of scales, which is at the core of our thought process, then appears to be essential to the identification and characterization of patterns (Legendre and Fortin, 1989; Wiens, 1989; Jarvis, 1995). The problem of scale has fundamental applied importance in ecosystem modelling. Until now, the study of population variability has required the selection of an appropriate region of the space–time domain (Steele, 1988). For instance, the general circulation models that provide the basis for climate prediction (Hansen *et al.*, 1988), as well as the regional circulation models (Nihoul and Djenidi, 1991; Salomon and Breton, 1993), operate on spatial and temporal scales many orders of magnitude greater than the scales at which most ecological processes, such as physiological and behavioural responses of phytoplankton and zooplankton, occur. Moreover, the development of new observation techniques such as remote sensing, while providing very exciting images of surface patterns of both chlorophyll and temperature over a wide range of scales (Abbott and Zion, 1985, 1987;

Denman and Abbott, 1988), must also lump functional ecological classes, sometimes into very crude assemblages, suppressing considerable detail, whereas ecological studies require that we sample spatially and temporally as fully as possible (see, for example, Platt *et al.*, 1989). By interfacing individual-based models with fluid dynamics models, therefore, one seeks to interrelate phenomena acting on different scales (Billen and Lancelot, 1988; Sharples and Tett, 1994; Zakardjian and Prieur, 1994), but it is still necessary to have available a suite of models of different levels of complexity and to understand the consequences of suppressing or incorporating details. Actual key challenges in the study of ecological systems therefore involve ways to deal with the collective dynamics of heterogeneously distributed ensembles of individuals, and to understand how to relate phenomena across scales, i.e. to scale from small to large spatio-temporal scales (Auger and Poggiale, 1996; Levin *et al.*, 1997; Poggiale, 1998a,b).

However, the development of theoretical models which incorporate multiple scales and which will guide the collection and the interpretation of data is still lacking because of the insufficiency of techniques to look across scales (Steele, 1991). This is the major contribution of fractal geometry (Mandelbrot, 1977, 1983; Frontier, 1987; Milne, 1988; Sugihara and May, 1990a), which is recognized to be capable of describing how patterns change across scales. Then, basically assuming that there is no single scale at which ecosystems should be described, there is no single scale at which models should be constructed (Levin, 1992). Furthermore, Bellehumeur *et al.* (1997) showed that an ecological phenomenon spread out in space and time does not have discrete spatial scales, but a continuum of spatio-temporal structures whose perception depends on the size of the sampling units, an assumption which greatly agrees with our multiscale approach. Consequently, ecological processes seem to be better described by a continuum of scales rather than a hierarchy of overlapped scales (Allen and Starr, 1982; O'Neill, 1989; Allen and Hoekstra, 1991; O'Neill *et al.*, 1991). In such a background, universal multifractal formalism, leading to a very precise characterization of variability by the way of continuous multiplicative processes (with the help of the three basic empirical parameters), appears to be an efficient descriptive tool which should also allow the modelling of the multiscale detailed variability of intermittently fluctuating biological fields as the global properties of their surrounding physical environment. Indeed, multifractal approaches are much better than the usual approaches which give a description at a very limited range of scales. One may note that models or direct numerical simulations possess no way to change the scale upward (upscaling) or downward (downscaling). It is natural, on the contrary, for multifractal processes. In fact, to evaluate the effects of the statistics of the small-scale space–time patterns on the longer time scale global statistics, one requires simultaneous simulations of both. Such simulations are, however, now feasible using new multifractal techniques (Wilson *et al.*, 1989; Pecknold *et al.*, 1993; Marsan *et al.*, 1996, 1997), leading to the development of exploratory studies of zooplankton behaviour within multifractal phytoplankton fields (Marguerit *et al.*, 1998) which can be regarded as a new way to investigate the trophodynamics of zooplankton.

Multifractals and, in particular, universal multifractals then appear to be a

potential powerful tool in analysing multiscale space–time variability of any intermittent processes and improve on previous studies showing the applicability of non-linear algorithms (Sugihara and May, 1990b; Sugihara *et al.*, 1990; Ascioti *et al.*, 1993; Strutton *et al.*, 1996, 1997a,b) and multifractal analysis (Pascual *et al.*, 1995) to both spatial and temporal planktonic data in several ways. First, the use of universal multifractals provides three fundamental parameters characterizing the organization, or structure, of the whole variability of a given intermittent process, and then allows direct comparisons to be made between biological and physical fields. That is, universal multifractal analysis can be regarded as a way to delineate the relative contributions of the biological and physical processes to the patterns observed, a major issue in marine ecology (Haury *et al.*, 1978; Denman and Powell, 1984; Legendre and Demers, 1984; Mackas *et al.*, 1985; Daly and Smith, 1993). Moreover, even if spectral analysis methods and concepts have played a major role in previous work concerning the identification of the scales of plankton patchiness (Platt and Denman, 1975; Platt, 1978; Fasham, 1978; Harris, 1980), they are largely insufficient to characterize the precise distribution of phytoplankton biomass, which appears to be essential to provide accurate estimates of the magnitude of related key fluxes such as primary, new and export productions following the extreme sensitivity of numerical modelling even to minor changes in parameter values (Werner *et al.*, 1993). Second, the predictive efficiency of non-linear algorithms, based on interpolations of pre-existing data by a simplex procedure [see, for example, Sugihara and May (1990b) for further details on the nearest-neighbour algorithm] and essentially aimed to distinguish between determinist and stochastic components of a given dataset, is poor in comparison with the technique of simulating continuous multifractal cascades (Schertzer and Lovejoy, 1987b; Wilson *et al.*, 1991; Pecknold *et al.*, 1993; Schertzer *et al.*, 1998) which produce fields which are very good approximations—at all scales and intensities—of the statistics of the measured field, and determine the probability distribution of the field values. Finally, using the concept of first- and second-order multifractal phase transitions, we can characterize the strength of the very rare and violent events present in a given dataset and quantify the range of statistical moments which can be accurately estimated given the finite sample size, respectively. In the general background of spatio-temporal intermittency encountered in the ocean (Platt *et al.*, 1989), knowledge of the precise statistics of any intermittent field may avoid the bias introduced by chronic undersampling of an intermittent signal (Bohle-Carbonel, 1992). In that way, universal multifractals may have considerable implications for the design and evaluation of potential sampling schemes in coastal areas as in open ocean, but also to improve estimates of stocks and fluxes associated with heterogeneous distribution of resources and exploiters which will not be robust unless all processes are understood in detail.

These powerful applications of multifractals, which are still under development in a conceptual and modelling way (Marsan *et al.*, 1996, 1997; Schertzer *et al.*, 1998), can then provide new application fields to ecological sciences, opening a large perspective in understanding ecosystem structure, and then could be regarded as a new way to develop individual rather than global approaches in the apprehension of any intermittent pattern and process.

Acknowledgements

We are especially indebted to Dr T.Wyatt for stimulating this paper during our fruitful discussions at the Newton Institute Euroconference 'Modelling the role of zooplankton in marine food chain'. We are also grateful to Drs V.Gentilhomme and F.Lizon for stimulating discussions, and to three anonymous reviewers for helpful suggestions on improving the manuscript. Thanks are also extended to the captain and crew of the N/O 'Côte d'Aquitaine' for their assistance in collecting the data for this paper.

References

Abbott,M.R. and Zion,P.M. (1985) Satellite observations of phytoplankton variability during an upwelling event. *Cont. Shelf Res.*, **4**, 661–680.

Abbott,M.R. and Zion,P.M. (1987) Spatial and temporal variability of phytoplankton pigment of northern California during Coastal Ocean Dynamics Experiment. *J. Geophys. Res.*, **92**, 1745–1755.

Abraham,E.R. (1998) The generation of plankton patchiness by turbulent stirring. *Nature*, **391**, 577–580.

Alcaraz,M., Saiz,E., Marrasé,C. and Vaqué.D. (1988) Effects of turbulence on the development of phytoplankton biomass and copepod populations in marine microcosms. *Mar. Ecol. Prog. Ser.*, **49**, 117–125.

Alldredge,A.L. and Hammer,W.M. (1980) Recurring aggregation of zooplankton by a tidal current. *Estuarine Coastal Mar. Sci.*, **10**, 31–37.

Allen,T.F.H and Hoekstra,T.W. (1991) Role of heterogeneity in scaling of ecological systems under analysis. In Kolasa,J. and Pickett,S.T.A. (eds), *Ecological Heterogeneity*. Springer-Verlag, New York, pp. 47–68.

Allen,T.F.H. and Starr,T.B. (1982) *Hierarchy: Perspectives for Complexity*. Chicago University Press, Chicago.

Anselmet,F., Gagne,Y., Hopfinger,E.J. and Antonia,R.A. (1984) High-order velocity structure functions in turbulent shear flows. *J. Fluid Mech.*, **140**, 63–69.

Ascioti,F.A., Beltrami,E., Carroll,T.O. and Wirick,C. (1993) Is there chaos in plankton dynamics? *J. Plankton Res.*, **15**, 603–617.

Auger,P. and Poggiale,J.-C. (1996) Emergence of population growth models: fast migration and slow growth. *J. Theor. Biol.*, **182**, 99–108.

Baker,M.A. and Gibson,C.H. (1987) Sampling turbulence in the stratified ocean: statistical consequences of strong intermittency. *J. Phys. Oceanogr.*, **17**, 1817–1836.

Batchelor,G.K. and Townsend,A.A. (1949) The nature of turbulent motion at large wavenumbers. *Proc. R. Soc. A*, **199**, 238–250.

Bellehumeur,C., Legendre,P. and Marcotte,D. (1997) Variance and spatial scales in a tropical rain forest: changing the size of sampling units. *Plant Ecol.*, **130**, 89–98.

Belyaev,V.S., Gezentsvey,A.N., Monin,A.S., Ozmidov,R.V. and Paka,V.T. (1975) Spectral characteristics of small-scale fluctuations of hydrophysical fields in the upper layer of the ocean. *J. Phys. Oceanogr.*, **5**, 492–498.

Bennett,A.F. and Denman,K.L. (1985) Phytoplankton patchiness: inferences from particle statistics. *J. Mar. Res.*, **43**, 307–335.

Billen,G. and Lancelot,C. (1988) Modelling benthic nitrogen cycling in coastal ecosystems. In Blackburn,T.H. and Sorensen,J. (eds), *Nitrogen Cycling in Coastal Marine Environments*. Wiley & Sons, New York, pp. 343–378.

Bohle-Carbonel,M. (1992) Pitfalls in sampling, comments on reliability and suggestions for simulation. *Cont. Shelf Res.*, **12**, 3–24.

Brylinski,J.M. and Lagadeuc,Y. (1990) L'interface eau côtière/eau du large dans le Pas-de-Calais (côte française): une zone frontale. *C. R. Acad. Sci. Paris Sér. 2*, **311**, 535–540.

Brylinski,J.-M. *et al.* (1991) Le 'fleuve côtier': un phénomène hydrologique important en Manche orientale. Exemple du Pas-de-Calais. *Oceanol. Acta*, **11**, 197–203.

Cassie,R.M. (1959a) An experimental study of factors inducing aggregation in marine plankton. *N.Z. J. Sci.*, **2**, 339–365.

Cassie,R.M. (1959b) Some correlations in replicate plankton samples. *N.Z. J. Sci.*, **2**, 473–484.

Cassie,R.M. (1960) Factors influencing the distribution pattern of plankton in the mixing zone between oceanic and harbour waters. *N.Z. J. Sci.*, **3**, 26–50.

Cassie,R.M. (1963) Microdistribution in the plankton. *Oceanogr. Mar. Biol. Annu. Rev.*, **1**, 223–252.

Chigirinskaya,Y., Schertzer,D., Lovejoy,S., Lazarev,A. and Ordanovich,A. (1994) Unified multifractal atmospheric dynamics tested in the tropics: part I, horizontal scaling and self criticality. *Nonlin. Processes Geophys.*, **1**, 105–114.

Chigirinskaya,Y., Schertzer,D. and Lovejoy,S. (1997) Scaling gyroscopes cascade: universal multifractal features of 2-D and 3-D turbulence. In Giona,M. and Biardi,G. (eds), *Fractals and Chaos in Chemical Engineering*. World Scientific, Singapore, pp. 371–384.

Corrsin,S. (1951) On the spectrum of isotropic temperature in an isotropic turbulence. *J. Appl. Phys.*, **22**, 469.

Costello,J.H., Strickler,J.R., Marrasé,C., Trager,G., Zeller,R. and Freise,A. (1990) Grazing in a turbulent environment: behavioral response of a calanoid copepod, *Centropages hamatus*. *Proc. Natl Acad. Sci. USA*, **87**, 1648–1652.

Currie,D.J. (1984) Phytoplankton growth and the microscale nutrient patch hypothesis. *J. Plankton Res.*, **6**, 591–599.

Daly,K.L. and Smith,W.O. (1993) Physical-biological interactions influencing marine plankton production. *Annu. Rev. Ecol. Syst.*, **24**, 555–585.

Davis,C.S., Flierl,G.R., Wiebe,P.H. and Franks,P.J.S (1991) Micropatchiness, turbulence and recruitment in plankton. *J. Mar. Res.*, **49**, 109–151.

Demers,S., Lafleur,P.E., Legendre,L. and Trump,C.L. (1979) Short-term covariability of chlorophyll and temperature in the St. Lawrence estuary. *J. Fish. Res. Board Can.*, **36**, 568–573.

Denman,K.L. (1976) Covariability of chlorophyll and temperature in the sea. *Deep-Sea Res.*, **23**, 539–550.

Denman,K.L. and Abbott,M.R. (1988) Time evolution of surface chlorophyll patterns from cross-spectrum analysis of satellite color images. *J. Geophys. Res.*, **93**, 6789–6798.

Denman,K.L. and Platt,T. (1976) The variance spectrum of phytoplankton in a turbulent ocean. *J. Mar. Res.*, **34**, 593–601.

Denman,K.L. and Powell,T.M. (1984) Effects of physical processes on planktonic ecosystems in the coastal ocean. *Oceanogr. Mar. Biol. Annu. Rev.*, **22**, 125–168.

Denman,K.L., Okubo,A. and Platt,T. (1977) The chlorophyll fluctuation spectrum in the sea. *Limnol. Oceanogr.*, **22**, 1033–1038.

Deschamps,P.Y., Frouin,R. and Wald,L. (1981) Satellite determinations of the mesoscale variability of the sea surface temperature. *J. Phys. Oceanogr.*, **11**, 864–870.

Dupont,J.-P., Lafite,R., Huault,M.-F., Lamboy,M., Brylisnki,J.-M. and Guéguéniat,P. (1991) La dynamique des masses d'eau et matière en suspension en Manche orientale. *Oceanol. Acta*, **11**, 177–186.

Elliott,J.A. and Oakey,N.S. (1979) Average microstructure levels and vertical diffusion for phase III, GATE. *Deep-Sea Res.*, **26**, 279–294.

Estrada,M., Alcaraz,M. and Marrasé,C. (1987) Effects of turbulence on the composition of phytoplankton assemblages in marine microcosms. *Mar. Ecol. Prog. Ser.*, **38**, 267–281.

Evans,G.T. (1978) Biological effects of vertical-horizontal interactions. In Steele,J.H. (ed.), *Spatial Patterns in Plankton Communities*. Plenum, New York, pp. 157–179.

Falco,T., Francis,F., Lovejoy,S., Schertzer,D., Kerman,B. and Drinkwater,M. (1996) Universal multifractal scaling of synthetic aperture radar images of sea-ice. *IEEE Trans. Geosci. Remote Sensing*, **34**, 906–914

Fasham,M.J.R. (1978) The statistical and mathematical analysis of plankton patchiness. *Oceanogr. Mar. Biol. Annu. Rev.*, **16**, 43–79.

Fasham,M.J.R. and Pugh,P.R. (1976) Observations on the horizontal coherence of chlorophyll a and temperature. *Deep-Sea Res.*, **23**, 527–538.

Fortier,L., Legendre,L., Cardinal,A. and Trump,C.L. (1978) Variabilité à court terme du phytoplancton de l'estuaire du St-Laurent. *Mar. Biol.*, **46**, 349–354.

Frisch,U., Sulem,P.-L. and Nelkin,M. (1978) A simple dynamical model of intermittent fully developed turbulence. *J. Fluid Mech.*, **87**, 719–724.

Frontier,S. (1987) Application of fractal theory to ecology. In Legendre,P. and Legendre,L. (eds), *Developments in Numerical Ecology*. Springer-Verlag, Berlin, pp. 335–378.

Gentilhomme,V. and Lizon,F. (1998) Seasonal cycle of nitrogen and phytoplankton biomass in a well-mixed coastal system (Eastern English Channel). *Hydrobiologia*, **361**, 191–199.

Gibson,C.H. (1991) Kolmogorov similarity hypotheses for scalar fields: sampling intermittent turbulent mixing in the ocean and galaxy. *Proc. R. Soc. London Ser. A*, **434**, 149–164.

Gower,J.F.R., Denman,K.L. and Holyer,R.J. (1980) Phytoplankton patchiness indicates the fluctuation spectrum of mesoscale oceanic structure. *Nature*, **288**, 157–159.

Granata,T.C. and Dickey,T.D. (1991) The fluid mechanics of copepod feeding in a turbulent flow. A theoretical approach. *Prog. Oceanogr.*, **26**, 243–261.

Grant,H., Stewart,R. and Moillet,A. (1962) Turbulent spectra from a tidal channel. *J. Fluid Mech.*, **12**, 241–268.

Grassberger,P. (1983) Generalized dimensions of strange attractors. *Phys. Lett.*, **97**, 227–230.

Gregg,M.C. (1980) Microstructure patches in the thermocline. *J. Phys. Oceanogr.*, **10**, 915–943.

Gregg,M.C., Cox,C.S. and Hacker,P.W. (1973) Vertical microstructure measurements in the central North Pacific. *J. Phys. Oceanogr.*, **3**, 458–469.

Hansen,J., Fung,I., Lacis,A., Rind,D., Lebedeff,S., Ruedy,R., Russel,G. and Stone,P. (1988) Global climate changes as forecast by the Goddard Institute for Space Studies three dimensional model. *J. Geophys. Res.*, **93**, 9341–9364.

Hardy,L.R. and Gunther,E.R. (1935) The plankton of the South Georgia whaling grounds and adjacent waters, 1926–1927. *Discovery Rep.*, **11**, 1–456.

Harris,G.P. (1980) Temporal and spatial scales in phytoplankton ecology. Mechanisms, methods, models and management. *Can. J. Fish Aquat. Sci.*, **37**, 877–900.

Haury,L.R., McGowan,J.A. and Wiebe,P.H. (1978) Patterns and processes in the time-space scales of plankton distributions. In Steele,J.H. (ed.), *Spatial Pattern in Plankton Communities*. Plenum, New York, pp. 277–327.

Hentschel,H.G.E. and Procaccia,I. (1983) The infinite number of generalized dimensions of fractals and strange attractors. *Physica D*, **8**, 435–444.

Herman,A.W., Sameoto,D.D. and Longhurst,A.R. (1981) Vertical and horizontal distribution patterns of copepods near the shelf break south of Nova Scotia. *Can. J. Fish. Aquat. Sci.*, **38**, 1065–1076.

Horwood,J.W. (1978) Observations on spatial heterogeneity of surface chlorophyll in one and two dimensions. *J. Mar. Biol. Assoc. UK*, **58**, 487–502.

Hutchinson,G.E. (1953) The concept of pattern in ecology. *Proc. Natl Acad. Nat. Sci. Philadelphia*, **105**, 1–12.

Jarvis,P.G. (1995) Scaling processes and problems. *Plant Cell. Environ.*, **18**, 1079–1089.

Jiménez,J. (1997) Ocean turbulence at millimeter scales. *Sci. Mar.*, **61**, 47–56.

Jiménez,J. and Wray,A.A. (1994) Columnar vortices in isotropic turbulence. *Meccanica*, **29**, 453–464.

Jiménez,J., Wray,A.A., Safman,P.G. and Rogallo,R.S. (1993) The structure of intense vorticity in isotropic turbulence. *J. Fluid Mech.*, **255**, 65–90.

Jou,D. (1997) Intermittent turbulence: a short introduction. *Sci. Mar.*, **61**, 57–62.

Kamykowski,D. (1974) Possible interactions between phytoplankton and semi-diurnal internal waves. *J. Mar. Res.*, **32**, 67–89.

Kierstead,H. and Slobodkin,L.B. (1953) The size of water masses containing plankton blooms. *J. Mar. Res.*, **12**, 141–147.

Kiørboe,T. (1993) Turbulence, phytoplankton cell size and the structure of pelagic food webs. *Adv. Mar. Biol.*, **29**, 1–72.

Kiørboe,T. (1997) Small-scale turbulence, marine snow formation, and planktivorous feeding. *Sci. Mar.*, **61**, 141–158.

Kiørboe,T. and MacKenzie,B.R. (1995) Turbulence-enhanced prey encounter rates in larval fish: effects of spatial scale, larval behaviour and size. *J. Plankton Res.*, **17**, 2319–2331.

Kiørboe,T., Lunsgaard,C., Olesen,M. and Hansen,J.L.S. (1994) Aggregation and sedimentation processes during a spring phytoplankton bloom: a field experiment to test coagulation theory. *J. Mar. Res.*, **52**, 297–323.

Kolmogorov,A.N. (1941) The local structure of turbulence in incompressible viscous fluid for very large Reynolds numbers. *Dokl. Akad. Nauk SSSR*, **30**, 299–303.

Kolmogorov,A.N. (1962) A refinement of previous hypotheses concerning the local structure of turbulence in viscous incompressible fluid at high Reynolds number. *J. Fluid Mech.*, **13**, 82.

Kraichnan,R.H. (1967) Inertial ranges in two-dimensional turbulence. *Phys. Fluids*, **9**, 1937–1943.

Ladoy,P., Lovejoy,S. and Schertzer,D. (1991) Extreme variability of climatological data: scaling and intermittency. In Schertzer,D. and Lovejoy,S. (eds), *Non-linear Variability in Geophysics*. Kluwer, Norwell, pp. 241–250.

Lagadeuc,Y., Brylinski,J.-M. and Aelbrecht,D. (1997) Temporal variability of the vertical stratification of a front in a tidal Region of Freshwater Influence (ROFI) system. *J. Mar. Syst.*, **12**, 147–155.

Lavallée,D. (1991) Multifractal techniques: analysis and simulation of turbulent fields. PhD Thesis, McGill University, Montréal, Canada.

Lavallée,D., Lovejoy,S., Schertzer,D. and Schmitt,F. (1992) On the determination of universal multifractal parameters in turbulence. In Moffat,K., Tabor,M. and Zaslavsky,G. (eds), *Topological Aspects of the Dynamics of Fluid and Plasmas*. Kluwer, Boston, pp. 463–478.

Lazarev,A., Schertzer,D., Lovejoy,S. and Chigirinskaya,Y. (1994) Unified multifractal atmospheric dynamics tested in the tropics: Part II, vertical scaling and Generalized Scale Invariance. *Nonlin. Processes Geophys.*, **1**, 115–121.

Legendre,L. and Demers,S. (1984) Towards dynamic biological oceanography and limnology. *Can. J. Fish. Aquat. Sci.*, **41**, 2–19.

Legendre,P. and Fortin,M.J. (1989) Spatial patterns and ecological analysis. *Vegetatio*, **80**, 1055–1067.

Lekan,J.F. and Wilson,R.E. (1978) Spatial variability of phytoplankton biomass in the surface waters of Long Island. *Estuarine Coastal Mar. Sci.*, **6**, 239–251.

Levin,S.A. (1992) The problem of pattern and scale in ecology. *Ecology*, **73**, 1943–1967.

Levin,S.A., Grenfell,B., Hastings,A. and Perelson,A.S. (1997) Mathematical and computational challenges in population biology and ecosystems science. *Science*, **275**, 334–343.

Lovejoy,S. and Schertzer,D. (1985) Generalized scale-invariance in the atmosphere and fractal model of rain. *Water Resour. Res.*, **21**, 1233–1250.

Lovejoy,S. and Schertzer,D. (1990) Multifractals, universality classes and satellite and radar measurements of cloud and rain fields. *J. Geophys. Res.*, **95**, 2021–2034.

Mackas,D.L., Louttit,G.C. and Austin,M.J. (1980) Spatial distribution of zooplankton and phytoplankton in British Columbian coastal waters. *Can. J. Fish Aquat. Sci.*, **37**, 1476–1487.

Mackas,D.L., Denman,K.L. and Abbot,M.R. (1985) Plankton patchiness: biology in the physical vernacular. *Bull. Mar. Sci.*, **37**, 652–674.

MacKenzie,B.R. and Kiørboe,T. (1995) Encounter rates and swimming behavior of pause-travel and cruise larval fish predators in calm and turbulent laboratory environments. *Limnol. Oceanogr.*, **40**, 1278–1289.

MacKenzie,B.R., Miller,T.J., Cyr,S. and Leggett,W.C. (1994) Evidence of a dome-shaped relationship between turbulence and larval fish ingestion rates. *Limnol. Oceanogr.*, **39**, 1790–1799.

Madden,C.J. and Day,J.W. (1992) Induced turbulence in rotating bottles affects phytoplankton productivity measurements in turbid waters. *J. Plankton Res.*, **14**, 1171–1191.

Mandelbrot,B. (1974) Multiplications aléatoires itérées et distributions invariantes par moyenne pondérée aléatoire. *C. R. Acad. Sci. Paris Sér. A*, **278**, 289–292.

Mandelbrot,B. (1977) *Fractals. Form, Chance and Dimension*. Freeman, London.

Mandelbrot,B. (1983) *The Fractal Geometry of Nature*. Freeman, New York.

Marguerit,C., Schertzer,D., Schmitt,F. and Lovejoy,S. (1998) Copepod diffusion within a multifractal phytoplankton field. *J. Mar. Syst.*, **16**, 69–83.

Marquet,P.A., Fortin,M.-J., Pineda,J., Wallin,D.O., Clark,J., Wu,Y., Bollens,J., Jacobi,C.M. and Holt,R.D. (1993) Ecological and evolutionary consequences of patchiness: a marine-terrestrial perspective. In Levin,S.A., Powell,T.M. and Steele,J.H. (eds), *Patch Dynamics*. Springer-Verlag, New York, pp. 277–304.

Marrasé,C., Costello,J.H., Granata,T. and Strickler,J.R. (1990) Grazing in a turbulent environment: energy dissipation, encounter rates, and efficacy of feeding currents in *Centropages hamatus*. *Proc. Natl Acad. Sci. USA*, **87**, 1653–1657.

Marsan,D., Schertzer,D. and Lovejoy,S. (1996) Causal space-time multifractal processes: predictability and forecasting of rain fields. *J. Geophys. Res.*, **101**, 26333–26346.

Marsan,D., Schertzer,D. and Lovejoy,S. (1997) Predictability of multifractal processes: the case of turbulence. In Giona,M. and Biardi,G. (eds), *Fractals and Chaos in Chemical Engineering*. World Scientific, Singapore, pp. 465–475.

Martin-Jezequel,V. (1983) Facteurs hydrologiques et phytoplancton en Baie de Morlaix (Manche Occidentale). *Hydrobiologia*, **102**, 131–143.

McCave,I.N. (1984) Size-spectra and aggregation of suspended particles in the deep ocean. *Deep-Sea Res.*, **22**, 491–502.

McHardy,I. and Czerny,B. (1987) Fractal X-ray time variability and spectral invariance of the Seyfert galaxy NGC5506. *Nature*, **325**, 696–698.

Meneveau,C. and Sreenivasan,K.R. (1987) Simple multifractal cascade model for fully developped turbulence. *Phys. Rev. Lett.*, **59**, 1424–1427.

Milne,B.T. (1988) Measuring the fractal geometry of landscapes. *Appl. Math. Comp.*, **27**, 67–79.

Mitchell,J.G., Okubo,A. and Fuhrman,J.A. (1985) Microzones surrounding phytoplankton form the basis for a stratified marine microbial ecosystem. *Nature*, **316**, 58–59.

Monin,A.S. and Yaglom,A.M. (1975) *Statistical Fluid Mechanics: Mechanics of Turbulence*. MIT Press, London.

Nihoul,J.C.J. and Djenidi,S. (1991) Hierarchy and scales in marine ecohydrodynamics. *Earth-Science Rev.*, **31**, 255–277.

Novikov,E.A. and Stewart,R. (1964) Intermittency of turbulence and spectrum of fluctuations in energy dissipation. *Izv. Akad. Nauk SSSR Geogr. I Geofiz.*, **3**, 408–412.

Oakey,N.S. (1985) Statistics of mixing parameters in the upper ocean during JASIN Phase 2. *J. Phys. Oceanogr.*, **15**, 1502–1520.

Oakey,N.S. and Elliott,J.A. (1982) Dissipation within the surface mixed layer. *J. Phys. Oceanogr.*, **12**, 171–185.

Obukhov,A.M. (1941) Spectral energy distribution in a turbulent flow. *Dokl. Akad. Nauk SSSR*, **32**, 22–24.

Obukhov,A.M. (1949) Structure of the temperature field in a turbulent flow. *Izv. Akad. Nauk SSSR Geogr. I Geofiz.*, **13**, 55.

Obukhov,A.M. (1962) Some specific features of atmospheric turbulence. *J. Fluid Mech.*, **13**, 77.

Okubo,A. (1978) Horizontal dispersion and critical scales for phytoplankton patches. In Steele,J.H. (ed.), *Spatial Pattern in Plankton Communities*. Plenum Press, New York, pp. 21–42.

Okubo,A. (1980) *Diffusion and Ecological Problems: Mathematical Models*. Springer-Verlag, Berlin.

Okubo,A. (1986) Dynamical aspects of animal grouping: swarms, schools, flocks, and herds. *Adv. Biophys.*, **22**, 1–94.

Olsson,J., Niemczynowicz,J. and Berndtsson,R. (1993) Fractal analysis of high-resolution rainfall time series. *J. Geophys. Res.*, **98**, 265–274.

O'Neill,R.V. (1989) Perspectives in hierarchy and scale. In May,R.M. and Roughgarden,J. (eds), *Ecological Theory*. Princeton University Press, Princeton, pp. 140–156.

O'Neill,R.V., Gardner,R.H., Milne,B.T., Turner,M.G. and Jackson,B. (1991) Heterogeneity and spatial hierarchies. In Kolasa,J. and Pickett,S.T.A. (eds), *Ecological Heterogeneity*. Springer-Verlag, New York, pp. 85–96.

Osborn,T.R. (1978) Measurements of energy dissipation adjacent to an island. *J. Geophys. Res.*, **83**, 2939–2957.

Osborn,T.R. and Lueck,R.G. (1985a) Turbulence measurement from a towed body. *J. Atmos. Oceanic Technol.*, **2**, 517–527.

Osborn,T.R. and Lueck,R.G. (1985b) Turbulence measurement with a submarine. *J. Phys. Oceanogr.*, **15**, 1502–1520.

Owen,R.W. (1981) Fronts and eddies in the sea: mechanisms, interactions and biological effects. In Longhurst,A.R. (ed.), *Analysis of Marine Ecosystems*. Academic Press, London, pp. 197–233.

Paffenhöfer,G.-A. (1994) Variability due to feeding activity of individual copepods. *J. Plankton Res.*, **16**, 617–626.

Parisi,G. and Frisch,U. (1985) A multifractal model of intermittency. In Ghil,M., Benzi,R. and Parisi,G. (eds), *Turbulence and Predictability in Geophysical Fluid Dynamics and Climate Dynamics*. North Holland, Amsterdam, pp. 84–88.

Pascual,M., Ascioti,F.A. and Caswell,H. (1995) Intermittency in the plankton: a multifractal analysis of zooplankton biomass variability. *J. Plankton Res.*, **17**, 1209–1232.

Pecknold,S., Lovejoy,S., Shertzer,D., Hooge,C. and Malouin,J.F. (1993) The simulation of universal multifractals. In Perdang,J.M. and Lejeune,A. (eds), *Cellular Automata: Prospects in Astrophysical Applications*. World Scientific, Singapore, pp. 228–267.

Peters,F. and Gross,T. (1994) Increased grazing rates of microplankton in response to small-scale turbulence. *Mar. Ecol. Prog. Ser.*, **115**, 299–307.

Pingree,R.D., Mardell,G.T., Reid,P.C. and John,A.W.G. (1986) The influence of tidal mixing on the timing of the spring phytoplankton development in the southern of the North Sea, the English Channel and the northern Armorican Shelf. In Bowman,J., Yentsch,M. and Peterson,W.T. (eds), *Tidal Mixing and Plankton Dynamics*. Springer-Verlag, New York, pp. 164–192.

Platt,T. (1972) Local phytoplankton abundance and turbulence. *Deep-Sea Res.*, **19**, 183–187.

Platt,T. (1978) Spectral analysis of spatial structure in phytoplankton populations. In Steele,J.H. (ed.), *Spatial Pattern in Plankton Communities*. Plenum, New York, pp. 73–84.

Platt,T. and Denman,K.L. (1975) Spectral analysis in ecology. *Annu. Rev. Ecol. Syst.*, **6**, 189–210.

Platt,T., Dickie,L.M. and Trites,R.W. (1970) Spatial heterogeneity of phytoplankton in a near-shore environment. *J. Fish. Res. Board Can.*, **27**, 1453–1473.

Platt,T., Harrison,W.G., Lewis,M.R., Li,W.K.W., Sathyendranath,S., Smith,R.E. and Vezina,A.F. (1989) Biological production of the oceans: the case for a consensus. *Mar. Ecol. Prog. Ser.*, **52**, 77–88.

Poggiale,J.-C. (1998a) From behavioural to population level: growth and competition. *Math. Comput. Model.*, **27**, 41–49.

Poggiale,J.-C. (1998b) Predator-prey models in heterogeneous environments: emergence of functional response. *Math. Comput. Model.*, **27**, 63–71.
Powell,T.M. and Okubo,A. (1994) Turbulence, diffusion and patchiness in the sea. *Philos. Trans. R. Soc. London Ser. B*, **343**, 11–18.
Powell,T.M., Richerson,P.J., Dillon,T.M., Agee,B.A., Dozier,B.J., Godden,D.A. and Myrup,L.O. (1975) Spatial scales of current speed and phytoplankton biomass fluctuations in Lake Tahoe. *Science*, **189**, 1088–1089.
Prairie,Y.T. and Duarte,C.M. (1996) Weak density-dependence and short-term perturbations as determinants of phytoplankton temporal dynamics. *Ecoscience*, **3**, 451–460.
Quisthoudt,C. (1987) Production primaire phytoplanctonique dans le détroit du Pas-de-Calais (France): variations spatiales et annuelles au large du cap Griz-Nez. *C. R. Acad. Sci. Paris*, **304**, 245–250.
Raby,D., Lagadeuc,Y., Dobson,J.J. and Mingelbier,M. (1994) Relationship between feeding and vertical distribution of bivalves larvae in stratified and mixed waters. *Mar. Ecol. Prog. Ser.*, **103**, 275–284.
Richardson,L.F. (1922) *Weather Prediction by Numerical Processes*. Cambridge University Press, Cambridge.
Riebesell,U. (1991a) Particle aggregation during a diatom bloom. I. Physical aspects. *Mar. Ecol. Prog. Ser.*, **69**, 273–280.
Riebesell,U. (1991b) Particle aggregation during a diatom bloom. II. Biological aspects. *Mar. Ecol. Prog. Ser.*, **69**, 281–291.
Riley,G.A. (1976) A model of plankton patchiness. *Limnol. Oceanogr.*, **21**, 873–880.
Rothschild,B.J. and Osborn,T.R. (1988) Small-scale turbulence and plankton contact rates. *J. Plankton Res.*, **10**, 465–474.
Salomon,J.-C. and Breton,M. (1993) An atlas of long-term currents in the Channel. *Oceanol. Acta*, **16**, 439–448.
Scherrer,B. (1984) *Biostatistiques*. Morin, Boucherville.
Schertzer,D. and Lovejoy,S. (1983) The dimension and intermittency of atmospheric dynamics. In Launder,B. (ed.), *Turbulent Shear Flows 4*. Springer-Verlag, Karlsruhe, pp. 7–33.
Schertzer,D. and Lovejoy,S. (1985) Generalised scale invariance in turbulent phenomena. *Physico-Chem. Hydrodyn. J.*, **6**, 623–635.
Schertzer,D. and Lovejoy,S. (1987a) Physical modeling and analysis of rain and clouds by anisotropic scaling multiplicative processes. *J. Geophys. Res.*, **92**, 96–99.
Schertzer,D. and Lovejoy,S. (1987b) Physically based rain and cloud modeling by anisotropic multiplicative turbulent cascades. *J. Geophys. Res.*, **92**, 9693–9714.
Schertzer,D. and Lovejoy,S. (1989) Nonlinear variability in geophysics: multifractal analysis and simulation. In Pietronero,L. (ed.), *Fractals: Physical Origin and Consequences*. Plenum, New York, pp. 49–79.
Schertzer,D. and Lovejoy,S. (1992) Hard and soft multifractal processes. *Physica A*, **185**, 187–194.
Schertzer,D. and Lovejoy,S. (1997) Universal multifractals do exist! *J. Appl. Meteorol.*, **36**, 1296–1303.
Schertzer,D., Lovejoy,S., Lavallée,D. and Schmitt,F. (1991) Universal hard multifractal turbulence, theory and observations. In Sagdeev,R.Z., Frisch,U., Hussain,F., Moiseev,S.S. and Erokhin,N.S. (eds), *Nonlinear Dynamics of Structures*. World Scientific, Singapore, pp. 213–235.
Schertzer,D., Lovejoy,S. and Schmitt,F. (1995) Structures in turbulence and multifractal universality. In Meneguzzi,M., Pouquet,A. and Sulem,P.L. (eds), *Small-scale Structure in 3D Fluid and MHD Turbulence*. Springer-Verlag, New York, pp. 137–144.
Schertzer,D., Lovejoy,S., Schmitt,F., Chigirinskya,Y. and Marsan,D. (1998) Multifractal cascade dynamics and turbulent intermittency. *Fractals*, **5**, 427–471.
Schmitt,F., Lavallée,D., Shertzer,D. and Lovejoy,S. (1992a) Empirical determination of universal multifractal exponents in turbulent velocity fields. *Phys. Rev. Lett.*, **68**, 305–308.
Schmitt,F., Lavallée,D., Lovejoy,S., Schertzer,D. and Hooge,C. (1992b) Estimations directes des indices de multifractals universels dans le champ de vent et de température. *C. R. Acad. Sci. Paris Sér. II*, **314**, 749–754.
Schmitt,F., Schertzer,D., Lovejoy,S. and Brunet,Y. (1993) Estimation of universal multifractal indices for atmospheric turbulent velocity fields. *Fractals*, **1**, 568–575.
Schmitt,F., Schertzer,D., Lovejoy,S. and Brunet,Y. (1994) Empirical study of multifractal phase transitions in atmospheric turbulence. *Nonlin. Processes Geophys.*, **1**, 95–104.
Seuront,L. (1997) Distribution inhomogène multiéchelle de la biomasse phytoplanctonique en milieu turbulent. *J. Rech. Océanogr.*, **22**, 9–16.
Seuront,L. and Lagadeuc,Y. (1997) Characterisation of space-time variability in stratified and mixed

coastal waters (Baie des Chaleurs, Québec, Canada): application of fractal theory. *Mar. Ecol. Prog. Ser.*, **259**, 81–95.
Seuront,L. and Lagadeuc,Y. (1998) Spatio-temporal structure of tidally mixed coastal waters: variability and heterogeneity. *J. Plankton Res.*, **20**, 1387–1401.
Seuront,L., Schmitt,F., Lagadeuc,Y., Schertzer,D., Lovejoy,S. and Frontier,S. (1996a) Multifractal analysis of phytoplankton biomass and temperature in the ocean. *Geophys. Res. Lett.*, **23**, 3591–3594.
Seuront,L., Schmitt,F., Lagadeuc,Y., Schertzer,D. and Lovejoy,S. (1996b) Multifractal intermittency of Eulerian and Lagrangian turbulence of ocean temperature and plankton fields. *Nonlin. Processes Geophys.*, **3**, 236–246.
Sharples,J. and Tett,P. (1994) Modelling the effect of physical variability on the midwater chlorophyll maximum. *J. Mar. Res.*, **52**, 219–238.
Skellam,J.G. (1951) Random dispersal in theoretical populations. *Biometrika*, **38**, 196–218.
Stavn,R.H. (1971) The horizontal-vertical distribution hypothesis: Langmuir circulations and Daphnia distributions. *Limnol. Oceanogr.*, **16**, 453–466.
Steele,J.H. (1974) Spatial heterogeneity and population stability. *Nature*, **248**, 83.
Steele,J.H. (1976) Patchiness. In Cushing,D.H. and Walsh,J.J. (eds), *Ecology of the Sea*. Blackwell, London, pp. 98–115.
Steele,J.H. (1978) Some comments on plankton patches. In Steele,J.H. (ed.), *Spatial Patterns in Plankton Communities*. Plenum, New York, pp. 1–20.
Steele,J.H. (1988) Scale selection for biodynamics theories. In Steele,J.H. (ed.), *Spatial Patterns in Plankton Communities*. Plenum, New York, pp. 513–526.
Steele,J.H. (1991) Can ecological theory cross the land-sea boundary? *J. Theor. Biol.*, **153**, 425–436.
Steele,J.H. and Henderson,E.W. (1977) Plankton patches in the Northern North Sea. In Steele,J.H. (ed.), *Fisheries Mathematics*, Academic Press, London, pp. 1–19.
Steele,J.H. and Henderson,E.W. (1992) A simple model for plankton patchiness. *J. Plankton Res.*, **14**, 1397–1403.
Stommel,H. (1949) Trajectories of small bodies sinking slowly through convection cells. *J. Mar. Res.*, **8**, 24–49.
Stommel,H. (1963) Varieties of oceanographic experience. *Science*, **139**, 572–576.
Strutton,P.G., Mitchell,J.G. and Parslow,J.S. (1996) Non-linear analysis of chlorophyll a transects as a method of quantifying spatial structure. *J. Plankton Res.*, **18**, 1717–1726.
Strutton,P.G., Mitchell,J.G. and Parslow,J.S. (1997a) Using non-linear analysis to compare the spatial structure of chlorophyll with passive tracers. *J. Plankton Res.*, **19**, 1553–1564.
Strutton,P.G., Mitchell,J.G., Parslow,J.S. and Greene,R.M. (1997b) Phytoplankton patchiness: quantifying the biological contribution using Fast Repetition Rate Fluorometry. *J. Plankton Res.*, **19**, 1265–1274.
Sugihara,G. and May,R.M. (1990a) Applications of fractals in ecology. *Trends Ecol. Evol.*, **5**, 79–86.
Sugihara,G. and May,R.M. (1990b) Nonlinear forecasting as a way of distinguishing chaos from measurement error in time series. *Nature*, **344**, 734–741.
Sugihara,G., Grenfell,B. and May,R.M. (1990) Distinguishing error from chaos in ecological time series. *Philos. Trans. R. Soc. London Ser. B*, **330**, 235–251.
Sundby,S. and Fossum,P. (1990) Feeding conditions of Arcto-Norwegian cod larvae compared with the Rothschild–Osborn theory on small-scale turbulence and plankton contact rates. *J. Plankton Res.*, **12**, 1153–1162.
Taylor,G.I. (1938) The spectrum of turbulence. *Proc. R. Soc. London Ser. A*, **164**, 476–490.
Teissier,Y., Lovejoy,S. and Schertzer,D. (1993a) Universal multifractals: theory and observations of rain and clouds. *J. Appl. Meteorol.*, **32**, 223–250.
Teissier,Y., Lovejoy,S., Schertzer,D., Lavallée,D. and Kerman,B. (1993b) Universal multifractal indices for the ocean surface at far red wavelengths. *Geophys. Res. Lett.*, **20**, 1167–1170.
Thomas,W.H. and Gibson,C.H. (1990) Effects of small-scale turbulence on microalgae. *J. Appl. Phycol.*, **2**, 71–77.
Verhagen,J.H.G. (1994) Modeling phytoplankton patchiness under the influence of wind-driven currents in lakes. *Limnol. Oceanogr.*, **39**, 1551–1565.
Waite,A. and Harrison,P.J. (1992) Role of sinking and ascent during sexual reproduction in the marine diatom *Ditylum brightwelli*. *Mar. Ecol. Prog. Ser.*, **87**, 113–122.
Wasburn,L. and Gibson,C.H. (1984) Measurements of oceanic temperature microstructure using a small conductivity sensor. *J. Geophys. Res.*, **87**, 4230–4240.
Werner,F.E., Page,F.H., Lynch,D.R., Loder,J.W., Lough,R.G., Perry,R.I., Greenberg,D.A. and Sinclair,M.M. (1993) Influences of mean advection and simple behavior on the distribution of cod and haddock early life stages on Georges Bank. *Fish. Oceanogr.*, **2**, 43–64.

Wiegand,R.C. and Pond,S. (1979) Fluctuations of chlorophyll and related physical parameters in British Columbia coastal waters. *J. Fish. Res. Board Can.*, **36**, 113–121.
Wiens,J.A. (1989) Spatial scaling in ecology. *Funct. Ecol.*, **3**, 385–397.
Wilson,J., Lovejoy,S. and Schertzer,D. (1989) Physically based cloud modelling by scaling multiplicative processes. In Shertzer,D. and Lovejoy,S. (eds), *Scaling, Fractals and Non-linear Variability in Geophysics*. Kluwer, Dordrecht, pp. 185–208.
Wroblewski,J.S. and O'Brien,J.J. (1976) A spatial model of phytoplankton patchiness. *Mar. Biol.*, **35**, 161–175.
Yamazaki,H. (1993) Lagrangian study of planktonic organisms: perspectives. *Bull. Mar. Sci.*, **53**, 265–278.
Yamazaki,H. and Haury,L. (1993) A new Lagrangian model to study animal aggregation. *Ecol. Model.*, **69**, 99–111.
Yamazaki,H. and Kamykowski,D. (1991) The vertical trajectories of motile phytoplankton in a wind-mixed water column. *Deep-Sea Res.*, **38**, 219–241.
Zakardjian,B. and Prieur,L. (1994) A numerical study of primary production related to vertical turbulent diffusion with special reference to vertical motions of the phytoplankton cells in nutrient and light fields. *J. Mar. Syst.*, **5**, 267–295.
Zar,J.H. (1996) *Biostatistical Analysis*. Prentice-Hall International, Englewood Cliffs.

Received on June 22, 1998; accepted on December 17, 1998

A8

Fractals et multifractals : nouveaux outils de caractérisation de l'hétérogénéité spatio-temporelle en écologie marine

Seuront L

Oceanis, 1999 (sous presse)

Fractals et multifractals: nouveaux outils de caractérisation de l'hétérogénéité spatio-temporelle en écologie marine

Laurent Seuront

Station Marine de Wimereux, Université des Sciences et Technologies de Lille, CNRS-UPRESA 8013, BP 80, 62930 Wimereux

Mots clés : fractals, multifractals, multifractals universels, homogénéité, hétérogénéité, intermittence, variabilité spatio-temporelle, turbulence, mélange, phytoplancton

Résumé : Les concepts relatifs aux fractals et aux multifractals sont à l'heure actuelle encore méconnues et peu utilisés en écologie et *a fortiori* en écologie marine. Cet article propose donc une présentation succincte des concepts associés aux fractals et aux multifractales, dans un cadre purement géométrique comme probabiliste, et de quelques techniques d'analyses qui s'y rapportent. L'applicabilité et l'utilité de ces concepts en écologie marine seront ensuite illustrées à l'aide de quelques exemples tirés de travaux récents en écologie pélagique.

Fractals and multifractals : new tools to characterize space-time heterogeneity in marine ecology

Keywords : fractals, multifractals, universal multifractals, homogeneity, heterogeneity, intermittency, space-time variability, turbulence, mixing, phytoplankton

Abstract : Concepts related to fractals and multifractals are still misunderstood in ecological sciences and *a fortiori* in marine ecology. In that way, this paper proposed a brief overview of fractal and multifractal concepts, and some related analysis techniques are also discussed. The applicability and the usefulness of these concepts in marine ecology will then be illustrated using some concrete examples from the recent works in pelagic ecology.

1. Introduction

Mandelbrot (1975, 1977, 1978, 1983) a introduit le terme *fractal* pour désigner les objets qui manifestent un aspect extrêmement irrégulier et qui ne possèdent aucune échelle de longueur caractéristique. Historiquement, c'est dans les travaux de Cantor (1872) et Peano (1890) que l'on trouve les premières références à des ensembles "bizarres", souvent considérés comme des "monstres mathématiques" (Mandelbrot, 1975, 1977, 1983), comme les ensembles de Cantor (1872) ou de Koch (1904, 1906), le mouvement Brownien (Perrin, 1906) et la fonction continue non-différenciable de Weierstrass-Mandelbrot (Berry & Lewis, 1980) dont la géométrie est particulièrement complexe et structurée. La description de tels ensembles est très vite apparue comme incompatible avec le concept de dimension euclidienne, ou topologique, correspondant au nombre de coordonnées nécessaires pour caractériser la position d'un point dans cet ensemble.

En 1919, Hausdorff propose une nouvelle définition de la dimension d'un ensemble qui peut prendre des valeurs non-entières et qui permet de rendre compte du degré d'irrégularité de ces objets. Un des plus grands mérites de Mandelbrot (1975, 1977, 1978, 1983) est d'avoir su reconnaître que "l'exception est souvent la règle" et d'avoir montré que ces structures fracturées sont en fait très répandues dans la nature. Les profils de nos montagnes ou les découpages côtiers, les diverses géométries ramifiées que constituent les arbres, les rivières ou les imbrications des bronches dans les poumons sont autant d'exemples que l'on peut appréhender au sein du cadre fédérateur défini par Mandelbrot.

Dans ce cadre, le concept de fractals et sa généralisation multifractale apparaissent comme une alternative entre l'ordre excessif de la géométrie euclidienne et le désordre associé à la multiplicité de degrés de liberté des processus chaotiques (Mandelbrot 1989) et sont devenus quasi-incontournables dans l'étude des systèmes non-linéaires, dans le cadre de la théorie des systèmes dynamiques (Grassberger 1983; Hentschel & Procaccia 1983; Grassberger & Procaccia 1983), de la turbulence pleinement développée (Mandelbrot 1974; Frisch & Parisi 1985; Paladin & Vulpiani 1987), mais ont également trouvé un champ d'application considérable dans des domaines aussi variés que la morphologie des paysages terrestres (Burrough, 1981; Krummel *et al.*, 1987; Milne, 1988) et martiens (Woronow, 1981), la forme des nuages (Lovejoy, 1982), le déferlement des vagues (Longuet-Higgins, 1994), l'érosion des profils de côte (Phillips, 1985), les cours de la bourse (Ghashghaie *et al.*, 1996; Mandelbrot,

1997), la télédétection (Teissier *et al.*, 1993a, b), la climatologie (Schmitt *et al.*, 1995) ou l'astrophysique (McHardy and Czerny, 1987).

En écologie, une description détaillée des champs d'application de la théorie fractale a été réalisée par Frontier (1987) et Sugihara & May (1990). Ainsi, les fractals ont été utilisés pour décrire la complexité de différents habitats benthiques (Bradbury & Reichelt, 1983; Bradbury *et al.*, 1984; Gee & Warwick, 1994a, b), la diversité spécifique (Frontier, 1985, 1994), le déplacement des invertébrés marins (Bundy *et al.*, 1993; Erlandson & Kostylev, 1995) et terrestres (Wiens *et al.*, 1993, 1995), la structure de la neige marine (Li & Logan, 1995; Logan & Kilps, 1995) et les processus de croissance (Kandoorp, 1991; Kandoorp & Dekluijver, 1992). Toutefois en écologie marine, l'utilisation de tels concepts ne s'est développée que très récemment dans le cadre d'études de la structuration spatio-temporelle de l'écosystème pélagique, tant en terme de physique qu'en terme de biologie (Pascual *et al.*, 1995; Seuront, 1995, 1997; Seuront & Lagadeuc, 1997, 1998; Seuront *et al.*, 1996a, b).

Cet article ne prétend pas être un traité sur la géométrie fractale. Son objectif est d'introduire les aspects fondamentaux des concepts de fractals et de multifractals et de les illustrer par des applications relatives au milieu marin. Tant que faire se peut, cet article a été écrit et illustré de manière à être accessible à un lectorat aussi vaste que possible. Toutefois, le lecteur désireux d'obtenir plus de détails sur les concepts et les notations mathématiques relatifs aux fractals et aux multifractals pourra se reporter aux ouvrages de références de Mandelbrot (1975, 1977, 1983, 1997), Feder (1988), Crilly *et al.* (1991), Gouyet (1992), Peitgen *et al.* (1992), Falconer (1993), Hastings & Sugihara (1993) et Tricot (1993).

2. Ensembles et mesures fractales : dimensions, codimensions fractales et intermittence

2.1. Dimension fractale d'un ensemble géométrique : autosimilarité et autoaffinité

La notion usuelle de dimension coïncide avec le nombre de degrés de liberté qui caractérisent la position d'un point dans un ensemble. Cette dimension topologique d_T ne peut prendre que des valeurs entières strictement positives. D'un point de vue géométrique, cette définition est insuffisante dans la mesure où elle ne donne aucune information sur la mesure réelle (longueur, surface, volume) d'un ensemble et il est facile de construire des ensembles bornés de dimension topologique[1] (ou euclidienne) dont la longueur est infinie, par exemple

[1] La dimension topologique est, au sens strict, la dimension d'un objet nécessaire à en diviser une autre en deux augmenté d'une unité. Ainsi, une ligne est unidimensionnelle parce qu'elle peut être séparée en deux par

une spirale qui s'enroule sur un plan. C'est pour lever cette imprécision et donner une caractérisation plus fine d'un ensemble qu'une nouvelle définition de la dimension – la dimension fractale – a été introduite (Hausdorff, 1919).

La géométrie fractale permet de décrire des objets conceptuels ou concrets réalisant un certain degré d'occupation bi- ou tridimensionnel d'un espace euclidien, par exemple entre une courbe et une surface ou entre une surface et un volume. La dimension fractale doit être considérée comme une mesure de ce degré d'occupation, suivant une loi mathématique qui identifie les propriétés de cet indice à celle d'une dimension au sens usuel du terme. Une dimension entière ne sera ainsi qu'un cas particulier de dimension fractale généralisée.

L'accès au concept de dimension fractale se fait par analogie avec la dimension d'une figure euclidienne qui se présente comme un exposant. Si un segment d'un mètre de longueur est divisé en $N(1/N^1)$ segments de $(1/N^1)$ mètres, un carré d'un m² le sera en N^2 carré de $(1/N^2)\text{m}^2$ et un cube d'un m³ en N^3 cubes de $(1/N^3)\text{m}^3$. Les dimensions du segment, du carré et du cube correspondent aux exposants mis en jeu, soit respectivement 1, 2 et 3. La dimension fractale découle de cette notion d'homothétie interne, une transformation géométrique conduisant à 'N objets n fois plus petits', et la dimension fractale d_F est telle que:

$$N = n^{d_F} \tag{1}$$

ou encore

$$d_F = \log N / \log n \tag{2}$$

Une propriété de base de la géométrie fractale, l'autosimilarité est issue de ces considérations. Un objet est autosimilaire s'il peut être considéré comme un ensemble de copies de lui-même à différentes échelles, les changements d'échelle étant isotropes (ou uniformes) dans toutes les directions. Un objet autosimilaire est donc invariant d'échelle, sa structure étant la même quelle que soit l'échelle d'observation à laquelle on se trouve (Mandelbrot, 1975, 1977, 1983), comme la courbe de Koch (Koch, 1904, 1906; Fig. 1). Toutefois, la majorité des objets naturels présente une version affaiblie, statistique de l'autosimilarité, l'autoaffinité, propriété mise en évidence par la courbe de Koch aléatoire (Fig. 2). Pour de tels objets, les changements d'échelle entre leurs différentes parties sont anisotropes, ou dépendants de la direction de l'espace considérée. L'invariance d'échelle devient donc statistique, on ajoute en chaque point à l'image géométrique de l'objet fractal pris

---

un point,'zéro-dimensionnel'; un plan est bidimensionnel parce qu'il peut être séparé en deux par une ligne, unidimensionnelle; et ainsi de suite.

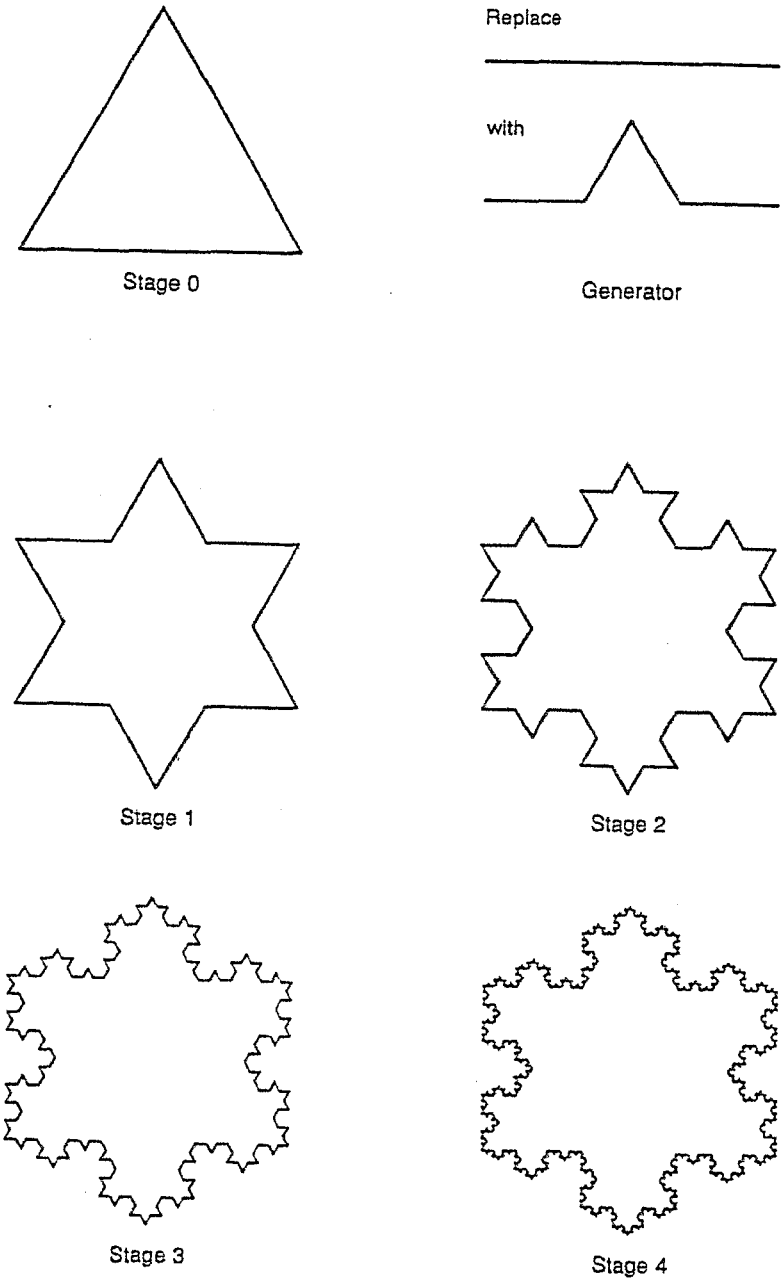

Fig. 1. Construction de la courbe de Koch. Partant d'un segment de droite de longueur 1, à chaque étape, on remplace le tiers médian par 2 segments de longueur 1/3 orienté à 60°. Le même processus est répété sur les 4 segments de longueur 1/3, donnant 16 segments de longueur 1/9 et ainsi de suite. A chaque étape, il y a 4 fois plus d'éléments 3 fois plus petits, d'où la dimension fractale $d_F = \log 4 / \log 3 \approx 1{,}262$.

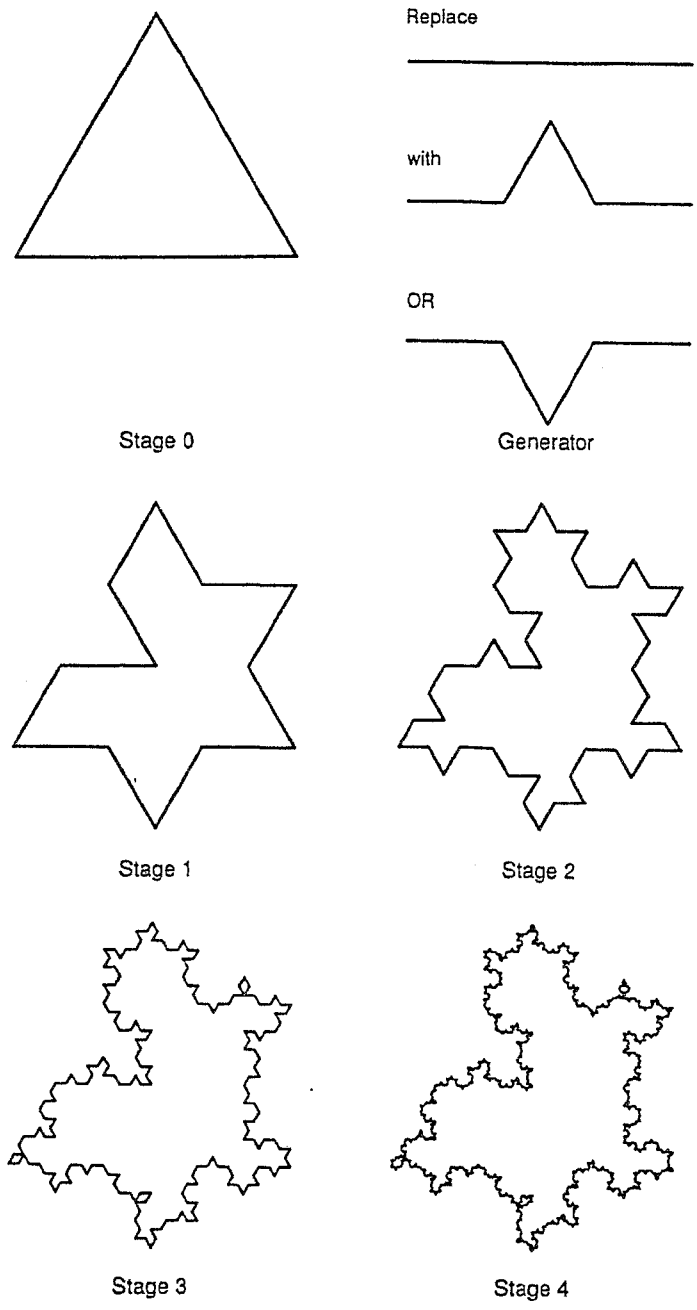

Fig. 2. Construction de la courbe de Cantor aléatoire. A chaque étape, on introduit un facteur aléatoire permettant de déterminer l'orientation des 2 nouveaux segments de longueur 1/3.

comme modèle un terme aléatoire faisant qu'une partie de l'objet n'est plus un modèle réduit du tout mais en possède seulement statistiquement les mêmes propriétés. Une excellente illustration de ce concept en écologie se trouve dans les modèles développés à partir du mouvement Brownien pour étudier la structure spatiale du déplacement d'un organisme (Mandelbrot, 1977, 1983).

Plus généralement, en considérant un ensemble A ($A \in \Re^n$) et $N(l)$ le nombre de boîtes de taille l nécessaire pour couvrir A, la dimension fractale de cet ensemble, d_F, est définie à partir du comportement en loi de puissance de $N(l)$:

$$N(l) \approx l^{d_F(A)} \tag{3}$$

où le symbole "≈" exprime un comportement asymptotique.

La dimension fractale quantifie donc comment la 'taille' d'un ensemble varie quand on prend une unité de mesure de plus en plus petite. En effet, si l'unité de mesure est l^p (pour p = 1, 2 ou 3 on mesure respectivement une longueur, une surface ou un volume), alors, à cette échelle l'ensemble 'mesure' $N(l)l^p \approx l^{p-d_F(A)}$ 'mètres à la puissance p'. Ainsi, on constate que A n'aura une surface finie que si $d_F(A) = 2$ alors que sa longueur ($p = 1$) sera infinie et son volume ($p = 3$) sera nul. Lorsque $d_F(A)$ prend des valeurs non entières, la longueur, la surface ou le volume ne permettent plus de caractériser l'ensemble A car ces quantités sont nulles ou infinies.

Exemple de construction d'une ensemble fractal

Si l'on considère un segment de droite ($[0,1]$) divisé en trois parties d'égale longueur, dont la partie centrale est retirée et que ce processus est répété sur les deux sous-intervalles restants, au bout d'un nombre infini d'itérations (Fig. 3), on obtient un ensemble de points ou ensemble de Cantor triadique (Cantor, 1883), plus prosaïquement appelé 'poussière de Cantor'. La règle de construction de cet ensemble permet un calcul simple des dimensions qui le caractérisent. A l'étape n de la construction, l'ensemble est constitué de 2^n intervalles de longueur 3^{-n} : sa longueur totale est donc $(2/3)^n$. La longueur du Cantor triadique obtenu à la limite $n \to +\infty$ est donc nulle et sa dimension topologique $d_T = 0$. Pour calculer sa dimension fractale, considérons un pavage $[0,1]$ par des segments de taille $l = 3^{-n}$. Par construction, seuls $N(l) = 2^n$ de ces segments contiendront une partie du Cantor. Il est alors possible d'introduire le rapport d'échelle λ, défini comme :

$$\lambda = l_n / l_{n-1} \tag{4}$$

où l_n et l_{n-1} sont respectivement la longueur des segments contenant une partie du Cantor aux étapes n et n-1 de la construction (dans le cas de l'ensemble de Cantor considéré ici, $\lambda = l_1 / l_0 = l_2 / l_1 = ... = l_n / l_{n-1} = 3$). A la limite $l \to 0^+$ ($n \to +\infty$), la relation (3) devient :

$$N(l_n) \approx l_n^{\,d_F(A)} \tag{5}$$

La dimension fractale du Cantor triadique devient $d_F(A) = \log N(l_n) / \log \lambda^n = \log 2^n / \log 3^n$ (soit $d_F = \log 2 / \log 3 = 0{,}631$ [2]) et représente un degré d'occupation relativement faible d'une ligne (ou ensemble euclidien de dimension 1) par un ensemble infini de points ($d_F < 1$).

Par la suite, pour plus de généralité dans le cadre d'une approche probabiliste, le rapport d'échelle λ sera défini comme :

$$\lambda = L / l \tag{6}$$

où L et l sont respectivement les échelles de résolution minimale et maximale considérées dans le cadre d'un processus invariant d'échelle.

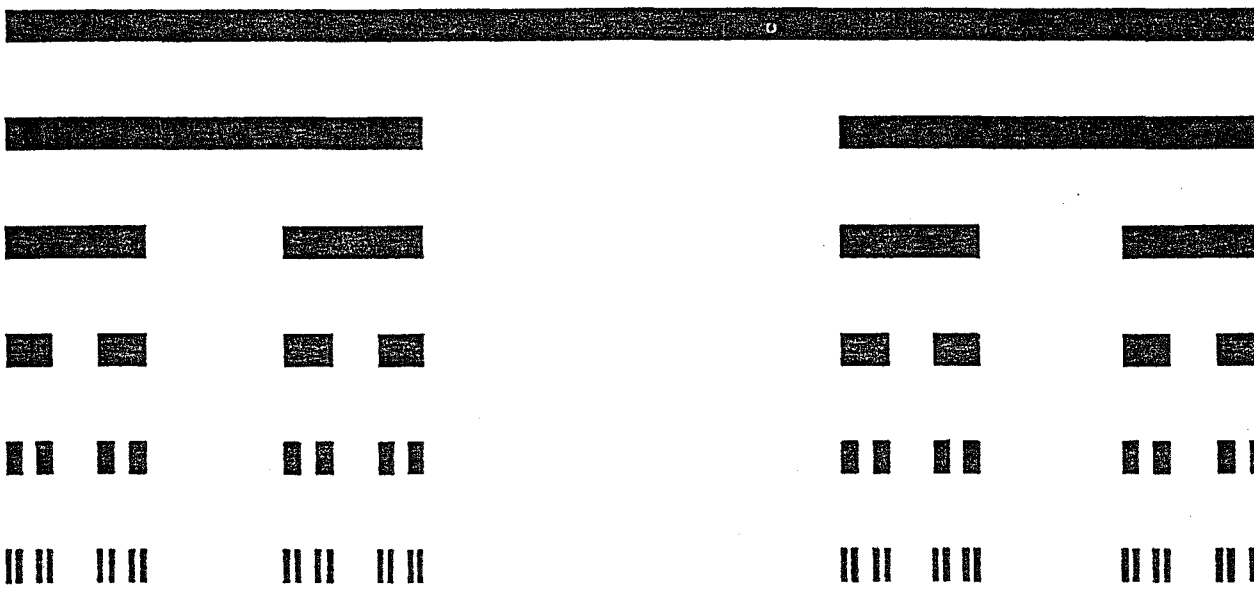

Fig. 3. Construction de l'ensemble de Cantor. A chaque étape, le tiers médian de chaque segment est supprimé; on a donc à chaque étape 2 éléments 3 fois plus petits, d'où la dimension fractale $d_F = \log 2 / \log 3 \approx 0{,}6309$.

[2] La dimensions fractales d_F de la courbe de Koch présentées (Fig. 1) est d_F = log4/log3 = 1,262. L'ensemble de Cantor est donc un objet fractal représentant un degré d'occupation partiel d'un espace à 2 dimensions.

Généralisation statistique

Les exemples considérés dans la section précédente portent essentiellement sur des ensembles géométriques. Il est toutefois possible d'estimer une dimension fractale d'un point de vue purement statistique, par exemple dans le cadre de l'étude de séries temporelles.

Cette approche est basée sur la répartition de la variance d'un processus donnée à différentes échelles d'observations.

$$\gamma(h) = \frac{1}{2N(h)} \sum_{i=1}^{N(h)} \left[Q_{x+h} - Q_x\right]^2 \tag{7}$$

où $N(h)$ est le nombre de couples de points séparés par la distance h, et Q_x et Q_{x+h} sont les valeurs prises par une quantité Q aux points x et $x+h$. La dimension fractale d_F est alors estimée comme la pente m de $\gamma(h)$ vs. h en cordonnées logarithmiques comme : $d_F = (4-m)/2$. Ainsi, plus la dimension fractale d_F sera élevée (i.e. m faible), moins les valeurs observées à 2 instants différents seront différentes.

Il convient ici de remarquer que la valeur informative du concept de dimension fractale est plus liée à la nature intrinsèque d'un objet, ou d'un processus, qu'à son degré de déploiement réel dans un espace à n dimensions. En effet, un ensemble de Cantor de dimension fractale $d_F = 0{,}631$ n'occupera pas de la même manière un espace bidimensionnel qu'un espace tridimensionnel. Ce type d'information est accessible à partir d'un autre exposant caractéristique de la théorie fractale, la codimension fractale.

2.2. Généralisation statistique : codimension fractale et dimension d'échantillonnage

2.2.1. Dimension et codimension fractales : dispersions absolue et relative

Soit un ensemble A de dimension fractale $d_F(A)$ inclus dans un espace E de dimension topologique (i.e. euclidienne) d_T, la codimension fractale de A, $c_F(A)$, s'exprime comme :

$$c_F(A) = d_T - d_F(A) \tag{8}$$

La codimension fractale apparaît comme une mesure de la dispersion relative de l'ensemble A, sa dimension fractale mesurant sa dispersion absolue. Ainsi, les ensembles de Cantor ou de Koch (réguliers ou statistiques) auront la même dimension fractale, qu'ils soient tracés (ou

projetés) dans un plan ou que leur structure se développe dans les 3 dimensions. Seule leur codimension augmente d'une unité. Le concept de codimension fractale peut donc être considéré comme plus fondamental que celui de dimension fractale, tout particulièrement dans un contexte probabiliste où il peut être introduit directement.

Ainsi, en considérant le nombre de boîtes de taille l ($l = L / \lambda$) nécessaires pour couvrir l'ensemble A, la probabilité $\Pr(B_l \cap A)$ qu'une boîte B_l a d'intersecter A est :

$$\Pr(B_\lambda \cap A) \approx \lambda^{-c_F(A)} \tag{9}$$

Cette probabilité variant en raison inverse de la codimension $c_F(A)$, de manière générale plus un événement sera rare, plus sa codimension fractale $c_F(A)$ sera élevée. Les formulations (4) et (5) pouvant être mises en relation par :

$$\Pr(B_\lambda \cap A) \approx \frac{N(B_\lambda \cap A)}{N(B_\lambda)} \approx \frac{\lambda^{-d_F(A)}}{\lambda^{-d_T}} \approx \lambda^{-c_F(A)} \tag{10}$$

où $N(B_\lambda \cap A)(N(B_\lambda \cap A) \approx \lambda^{-d_F(A)})$ est le nombre de boîtes B_l intersectant A et $N(B_\lambda)(N(B_\lambda) \approx \lambda^{-d_T})$ est le nombre total de boîtes B_λ considérées, il apparaît que les relations (8) et (9) sont équivalentes lorsque $c_F(A) \leq d_T$ (ou $d_F(A) \geq 0$). Par contre, la relation (9) n'impliquant aucune contrainte sur $c_F(A)$, si $c_F(A) > d_T$ les relations (8) et (9) conduisent à $d_F(A) < 0$. Ce dernier point est en parfaite contradiction avec le concept de dimension fractale définie comme une mesure strictement positive[3] (Mandelbrot, 1977, 1983; Falconer, 1993; Hastings & Sugihara, 1993). Une définition purement géométrique n'est donc plus suffisante dans un contexte probabiliste où la dimension effective de l'espace de probabilité est directement fonction de l'effort d'échantillonnage.

2.2.2. Caractérisation d'ensembles infinis : "dimension d'échantillonnage"

L'analyse statistique classique nous a habitué à utiliser des échantillons de taille finie. Cependant, le fait d'explorer un espace de probabilité en étudiant de plus en plus d'échantillons permet d'augmenter la dimension effective de cet espace (Fig. 4).

Soit N_S échantillons indépendants, tous de dimension d_T et λ le rapport d'échelle tel que défini par la relation (6), la quantité d'information tirée de l'échantillonnage sera de l'ordre de :

[3] Ce résultat se retrouve d'ailleurs de manière implicite dans les formulations de base du calcul d'une dimension fractale (relations (1) à (3)).

$$N.N_S = \lambda^{d_T+d_S} \tag{11}$$

où la 'dimension d'échantillonnage' d_S (Schertzer & Lovejoy 1989, Lavallée 1991) est définie comme :

$$d_S \approx \log N_S / \log \lambda \tag{12}$$

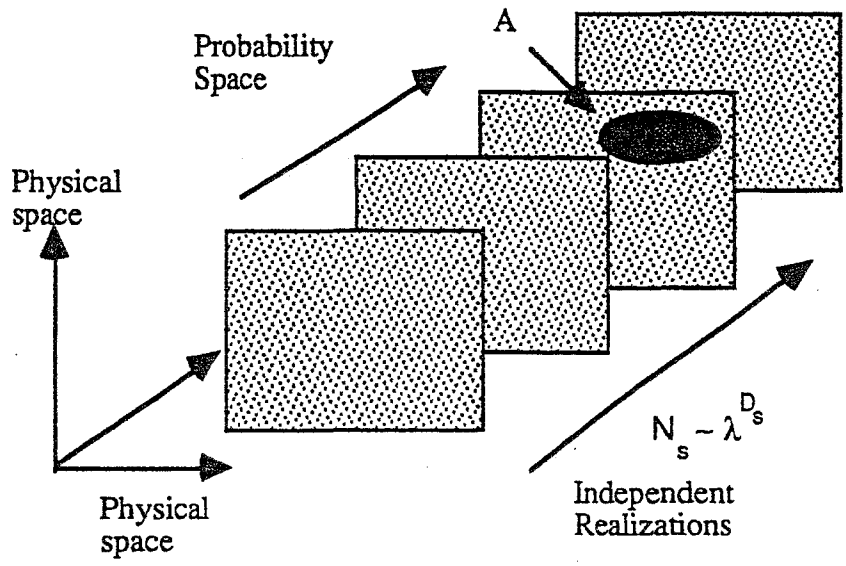

Fig. 4. Illustration de la manière dont il est possible d'augmenter la dimension effective de l'espace (d_T) en considérant de plus en plus de réalisations indépendantes (N_S). Quand $N_S \to \infty$, l'intégralité de l'espace de probabilité a été explorée.

Les relations (11) et (12) montrent ainsi que la dimension effective d'un espace de probabilité peut être augmentée au delà de d_T (un échantillon unique) et permettent de lever le paradoxe introduit au paragraphe précédent en rendant positive une dimension négative. Ainsi, en considérant un événement A suffisamment rare pour que $c_F(A) > d_T$, la relation (8) devient:

$$d_{F,S}(A) = d_T + d_S - c_F(A) > 0 \quad \text{pour} \quad d_S > c_F(A) - d_T \tag{13}$$

Le cas limite $d_{F,S}(A) = 0$ correspond à la présence de points isolés dans l'échantillon ; quand $d_S < c_F(A)$, A n'est pas présent dans l'échantillon, alors qu'il le sera quand $d_S > c_F(A)$.

La codimension fractale fournit une caractérisation intrinsèque d'un processus alors que la dimension fractale en fournit une caractérisation extrinsèque dépendant de la dimension de l'espace euclidien considéré.

De nombreux ensembles, ou plus généralement processus, aussi diversifiés que les découpages côtiers (Phillips, 1985), la forme des nuages (Lovejoy, 1982) et des reliefs (Burrough, 1981; Mandelbrot, 1977, 1983), les mouvements d'invertébrés terrestres (Wiens *et al.*, 1995) et marins (Erlandson & Kostylev, 1995) ou encore la diversité spécifique (Frontier, 1994) peuvent ainsi être caractérisés en terme de dimension fractale et d'invariance d'échelle. Toutefois, il apparaît clairement que la description de champs présentant différents niveaux d'intensité, comme c'est par exemple le cas pour les distributions temporelles de la température (Fig. 5a) ou de la biomasse phytoplanctonique (fig. 5b) dans l'océan, ne pouvait se résumer à une problématique essentiellement géométrique indissociable de la construction d'objets fractals 'classiques' tels que les ensembles de Cantor, Sierpinski ou Menger (e.g. Peitgen *et al.*, 1992; Falconer, 1993; Hastings & Sugihara, 1993). C'est la prise en compte de ces irrégularités, ou intermittences, perceptibles dans de nombreux champs géophysiques mais aussi biologiques (cf. Fig. 5) qui ont conduit à un abandon définitif du concept presque dogmatique de l'existence d'une dimension unique dans le contexte de la théorie des systèmes dynamiques (Grassberger, 1983; Grasberger & Procaccia, 1983; Henstchel & Procaccia, 1983; Halsey *et al.*, 1986) et de la turbulence (Schertzer & Lovejoy, 1983; Frisch & Parisi, 1985), et à l'avènement du concept de multifractals.

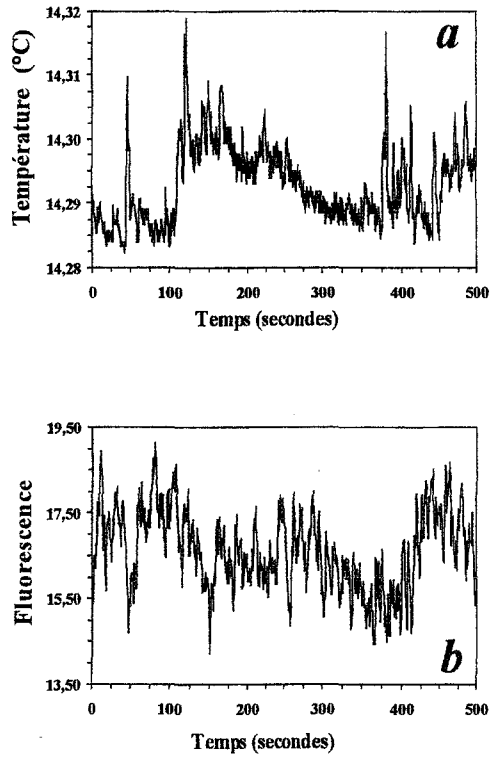

Fig. 5. Echantillons de données temporelles de température (***a***) et de fluorescence (***b***) prélevés dans le sud de la Mer du Nord. Des fluctuations brutales se produisant à toutes les échelles sont clairement visible, et indiquent un comportement intermittent (d'après Seuront, 1997).

2.3. Intermittence et mesures multifractales

Reprenons le formalisme développé au paragraphe 2.1 considérant le nombre $N(l)$ de boîtes de taille l nécessaire pour couvrir un ensemble A et associons une mesure μ[4] quelconque à cet ensemble, la dimension fractale d_F de cet ensemble est donnée par la relation (3), $N(l) \approx l^{d_F(A)}$. Toutefois, la dimension d_F ne fournit aucune information quantitative concernant la distribution de la mesure μ sur l'ensemble A. Dans ce cadre, se limiter à l'estimation de la dimension fractale d_F reviendrait à compter des pièces de monnaies sans prêter la moindre attention à leurs valeurs respectives (Evertsz & Mandelbrot, 1992).

Ainsi, soit μ une mesure quelconque de l'ensemble A, on appelle exposant de singularité en un point x_0 de l'ensemble A :

$$\alpha(x_0) = \frac{\log \mu(B_l(x_0))}{\log l} \tag{14}$$

où $B_l(x_0)$ désigne une boite de taille l centrée en x_0. L'exposant de singularité en un point rend compte du degré local de régularité de la mesure considérée. D'après la relation (14), on peut écrire :

$$\mu(B_l(x_0)) \approx l^{\alpha(x_0)} \tag{15}$$

avec $\alpha \geq 0$ a priori quelconque. Plus la valeur de $\alpha(x_0)$ est petite, moins la mesure μ est régulière autour de x_0.

Le spectre $f(\alpha)$ des singularités décrit la répartition des exposants α sur le support de la mesure. Ainsi, si l'on pave le support de la mesure de boîtes de taille l, alors le nombre de ces boîtes dont la mesure varie comme l^{α} pour un α donné (cf. Eq. 15), se comporte comme :

$$N_{\alpha}(l) \approx l^{-f(\alpha)} \tag{16}$$

ou

$$f_l(\alpha) = -\frac{\log N_l(\alpha)}{\log l} \tag{17}$$

[4] Une mesure permet d'associer des poids relatifs aux différentes parties d'un ensemble. On peut penser par exemple à des répartitions de charges, de masses, d'énergie, d'individus ou de toute distribution de probabilité.

Par analogie avec la relation (3), $f(\alpha)$ peut donc être considéré comme la fonction qui, à tout α, associe la dimension fractale de l'ensemble des points x_0 tels que $\alpha(x_0) = \alpha$.

A l'instar de la dimension fractale pour des ensembles irréguliers, le spectre $f(\alpha)$ des singularités peut être introduit comme une quantité qui donne une caractérisation relativement précise du degré d'irrégularités et d'homogénéité d'une mesure fractale.

Une mesure sera qualifiée d'homogène[5] (Halsey *et al.*, 1986) si son spectre des singularités est concentré en un seul point: un seule type de singularité permet de caractériser la mesure. Par contre, si le support de $f(\alpha)$ est large, la mesure considérée n'est pas homogène, l'exposant α fluctue d'un point à l'autre du support de μ, on parle alors de mesure multifractale.

Dans ce cadre, on comprend que la transition du concept de dimension fractale à celui, beaucoup plus général, de multifractals consiste à considérer un processus multifractal comme une hiérarchie *a priori* infinie d'ensembles fractals. Chacun de ces ensembles correspond à la fraction d'espace occupée par les parties du processus dépassant un certain seuil, et est donc caractérisé par une dimension fractale propre. Un processus multifractal sera ainsi caractérisé par un ensemble de relations invariantes d'échelle qui nécessitent un grand nombre (voire une infinité; cf. Eqs. 16 et 17) d'exposants (ou de dimensions) différents, plutôt que la dimension unique des ensembles fractals (cf. Eq. 3). Ce concept peut ainsi être parfaitement illustré par les modèles de cascades utilisés pour rendre compte de l'infinie hiérarchie de tourbillons de différentes intensités présents à une échelle donnée (Fig. 6).

Exemple de construction d'une mesure multifractale

Cet exemple consiste à construire une mesure multifractale distribuée sur un ensemble de Cantor triadique tel que défini au paragraphe 2.1 (Fig. 7a). A l'étape $n = 0$ de la construction, on affecte à l'intervalle $[0,1]$ la mesure $\mu_0 = 1$. A l'étape $n = 1$, on attribue un poids $\mu_1 = p$ à l'intervalle $[0,1/3]$ et $\mu_2 = q = 1 - p$ à l'intervalle $[2/3,1]$. A l'étape n de la construction, l'ensemble E_n est constitué de 2^n intervalles dont la mesure s'exprime comme la mesure binomiale :

$$\mu = p^m q^{n-m} \tag{18}$$

[5] Dans ce cas, la mesure considérée ne présente que des propriétés monofractales.

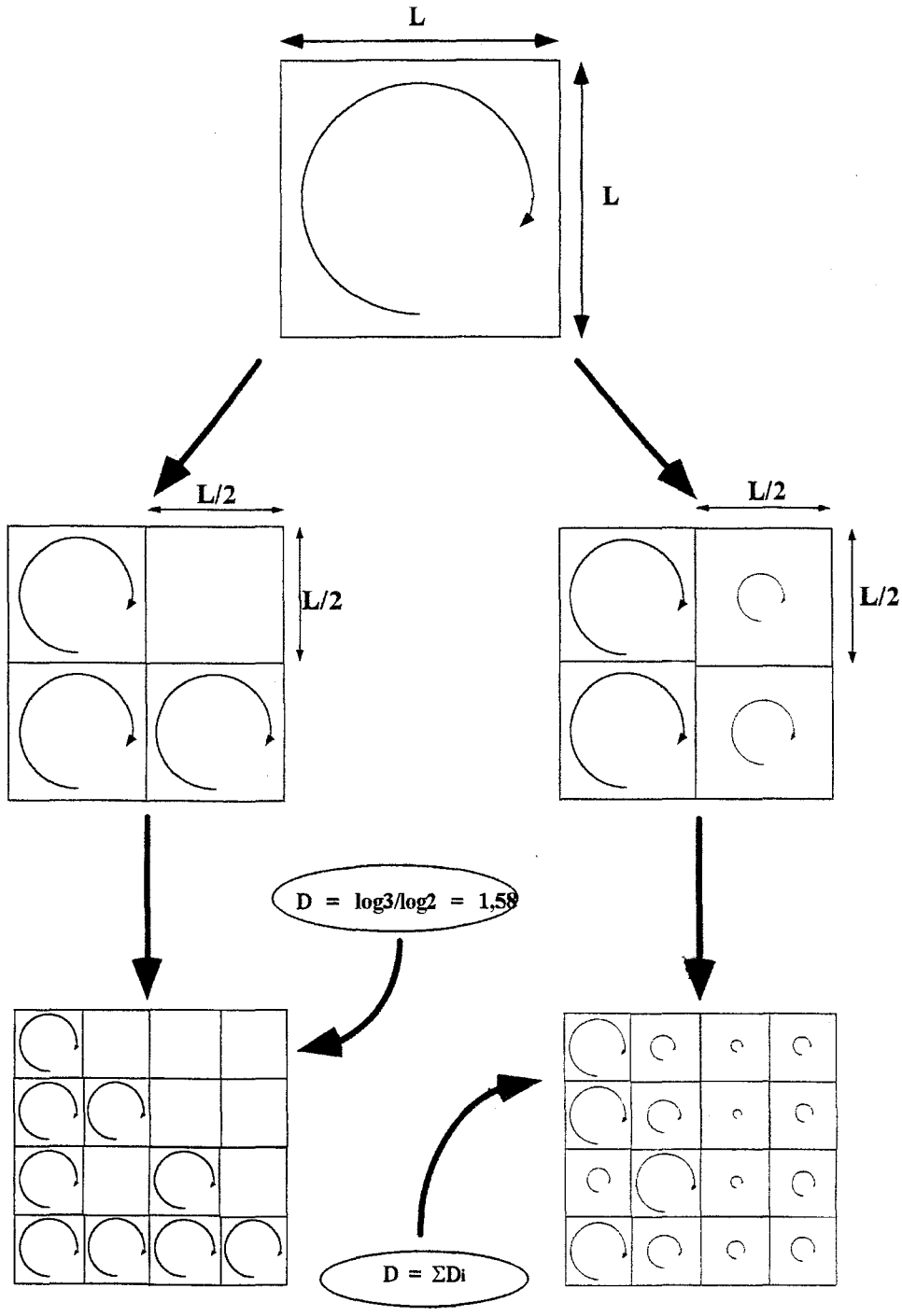

Fig. 6. Processus de cascade fractale (*a*) et multifractale (*b*) illustrant comment le concept de dimension fractale unique peut être généralisée en introduisant différentes intensités à chaque étape de la cascade (d'après Seuront, 1997).

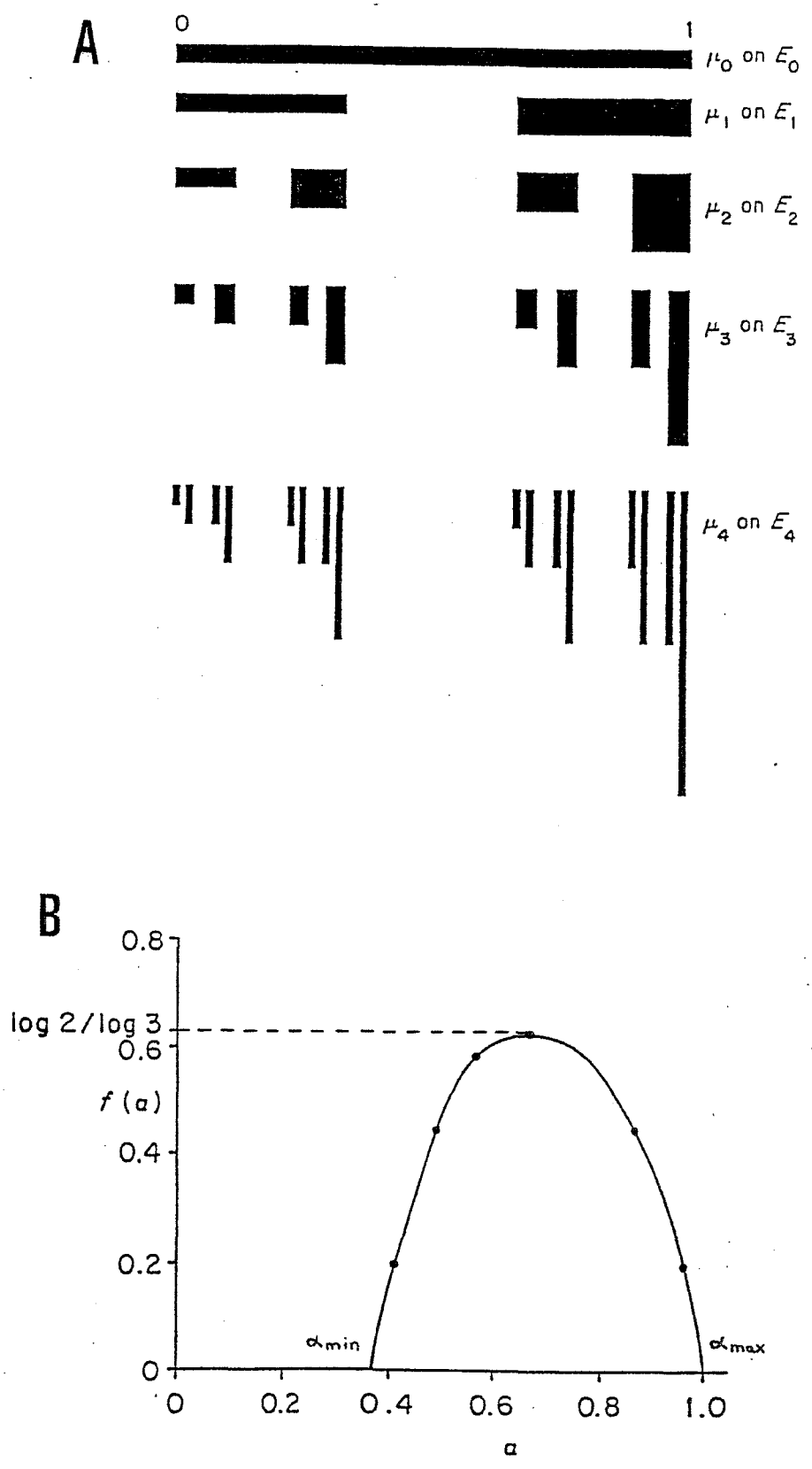

Fig. 7. Construction d'un ensemble de Cantor supportant une mesure multifractale (***a***). A chaque étape, la masse de chaque intervalle E_n, représentée par la surface du rectangle, est divisé en 2 sous-intervalles E_{n+1} suivant le rapport p:1-p (ici, $p = 1/3$). Au bout de n étapes de construction, on aboutit à une distribution de masse μ supportée par l'ensemble de Cantor et caractérisée par le spectre $f(\alpha)$ des singularités (***b***).

où m et $n-m$ représentent respectivement le nombre d'intervalles s'étant vu attribué les poids p et q. La longueur de chaque intervalle étant $l = 3^{-n}$, d'après la relation (14), il vient :

$$\alpha = \frac{\log p + (n/m - 1)\log(1-p)}{(n-m)\log(1/3)} \tag{19}$$

A l'étape n, α ne dépend donc que du rapport n/m, d'où :

$$f(\alpha) = f(n/m) = \frac{(n/m)\log(n/m - 1) - (n/m)\log(n/m)}{(n/m)\log(1/3)} \tag{20}$$

L'élimination de n/m dans les relations (19) et (20) permet alors d'obtenir le spectre $f(\alpha)$. Plus particulièrement, la relation (19) permet de calculer les bornes α_{min} et α_{max} du spectre $f(\alpha)$ telles que $f(\alpha) \geq 0$ pour $\alpha \in [\alpha_{min}, \alpha_{max}]$:

$$\begin{aligned} \alpha_{min} &= \min\left\{\frac{\log p}{\log(1/3)}, \frac{\log q}{\log(1/3)}\right\} \\ \alpha_{max} &= \max\left\{\frac{\log p}{\log(1/3)}, \frac{\log q}{\log(1/3)}\right\} \end{aligned} \tag{21}$$

Si $p = q = 1/2$, la mesure est répartie uniformement sur le Cantor et l'on retrouve le spectre d'une mesure homogène (ou monofractale) en $\alpha = \alpha_{min} = \alpha_{max} = \log 2 / \log 3$. D'après la relation (19), quelles que soient les valeurs de p et q, on peut vérifier que $f(n/m)$ est maximale pour $n/m = 2$, et dans ce cas, $f(\alpha) = \log 2 / \log 3$. Le maximum de la courbe $f(\alpha)$ correspond ainsi à la dimension fractale du support de la mesure (Fig. 7b).

Généralisation statistique

Les exemples considérés dans la section précédente portant essentiellement sur des ensembles géométriques, nous allons nous intéresser à la manière dont il est possible d'estimer les caractéristiques multifractales d'un processus d'un point de vue statistique, par exemple dans le cadre de l'étude de séries temporelles.

Ainsi, plutôt que de calculer la dimension fractale associée à chaque degré d'intermittence d'un processus dans le cadre du spectre $f(\alpha)$ des singularités, il est possible de généraliser l'approche statistique monofractale développée plus haut dans le cadre de moments d'ordre 2

(i.e. la variance) à des moments statistiques plus élevés. En d'autres termes, le moment statistique q permet de sélectionner les sous-ensembles correspondant à des intensités plus ou moins fortes du processus considéré : les moments les plus élevés caractériseront ainsi les intermittences les plus fortes qui sont aussi les plus rares et donc les plus difficiles à détecter (Fig. 8).

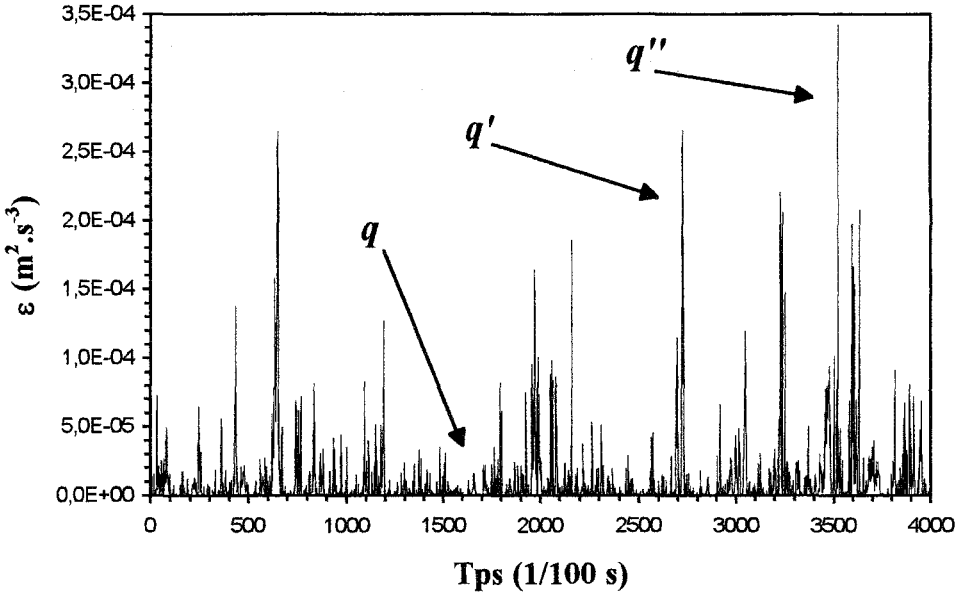

Fig. 8. Illustration schématique de la généralisation statistique des multifractals géométriques : chaque moment q est associé à un niveau d'intermittence. Les moments les plus grands caractériseront donc la distribution des intermittences les plus fortes qui sont aussi les plus rares et par conséquent les plus difficiles à détecter (ici, $q < q' < q''$).

Dans ce cadre, plusieurs approches sont possibles, basées sur les fonctions de partition (Halsey *et al.*, 1986), les dimensions fractales généralisées (Hentschel & Procaccia, 1983; Grassberger, 1983; Grassberger & Procaccia, 1984) et les fonctions de structure (Anselmet *et al.*, 1984). Seule l'approche par les fonctions de structure, qui est utilisée pour caractériser la structure de la distribution de la biomasse phytoplanctonique au paragraphe 3.3, sera développée ici (très brièvement), le lecteur désireux d'approfondir le sujet pourra se reporter aux références citées ci-avant, mais aussi aux ouvrages plus généraux de Gouyet (1992), Falconer (1993) et à l'article d'Evertsz & Mandelbrot (1992). Dans le cadre des fluctuations temporelles d'une quantité Q, les fonctions de structure s'expriment comme :

$$\left\langle (\Delta Q_\tau)^q \right\rangle = \left\langle \left| Q(t+\tau) - Q(\tau) \right| \right\rangle \approx \lambda^{\zeta(q)} \qquad (22)$$

où pour un décalage temporel τ les fluctuations de la quantité Q sont moyennés pour l'ensemble des valeurs disponibles. L'exposant $\zeta(q)$ est respectivement linéaire et non-linéaire pour les processus mono- et multifractals.

2.4. Intermittence et multifractals universels

Malgré l'apparente complexité induite par la multiplicité, voire l'infinité de dimensions nécessaires à la description d'un champ multifractal, l'utilisation des multifractals universels (Schertzer & Lovejoy, 1987, 1989) permet de décrire la distribution d'un processus intermittent à l'aide de seulement trois paramètres – H, C_1 et α – qui résument l'intégralité du comportement statistique du processus considéré et ce, quels que soient les échelles et le niveau de variabilité (Fig. 9) :

- H caractérise le degré de non-conservation du processus considéré, $H = 0$ pour un processus stationnaire, c'est à dire dont la variabilité moyenne est indépendante de l'espace ou du temps (Fig. 9a);

- C_1 est une codimension (comme définie au paragraphe 2.2.1) et caractérise donc l'hétérogénéité du processus : plus C_1 est fort, plus le processus est dominé par des valeurs fortes et faibles, alors que pour un C_1 plus faible, les niveaux de variabilité intermédiaire entre les valeurs les plus fortes et les valeurs les plus faibles sont mieux représentés numériquement. Dans ce sens, C_1 peut être considéré comme un analogue de la variance mais pour des distributions fortement non Gaussienne (Fig. 9b);

- α caractérise le degré de multifractalité, soit le degré de structuration du processus, c'est à dire le nombre de niveaux de variabilité intermédiaire entre les valeurs maximales et minimales du processus (Fig. 9c).

On remarquera que dans le cadre des multifractals universels, l'exposant $\zeta(q)$ des fonctions de structure prend la forme suivante :

$$\zeta(q) = qH - C_1(q^\alpha - q)/(\alpha - 1) \qquad (23)$$

Le premier paramètre multifractal est estimé comme $\zeta(1) = H$, alors que C_1 et α sont déterminés à partir du meilleur ajustement non-linéaire de la relation (22) au $\zeta(q)$ empirique.

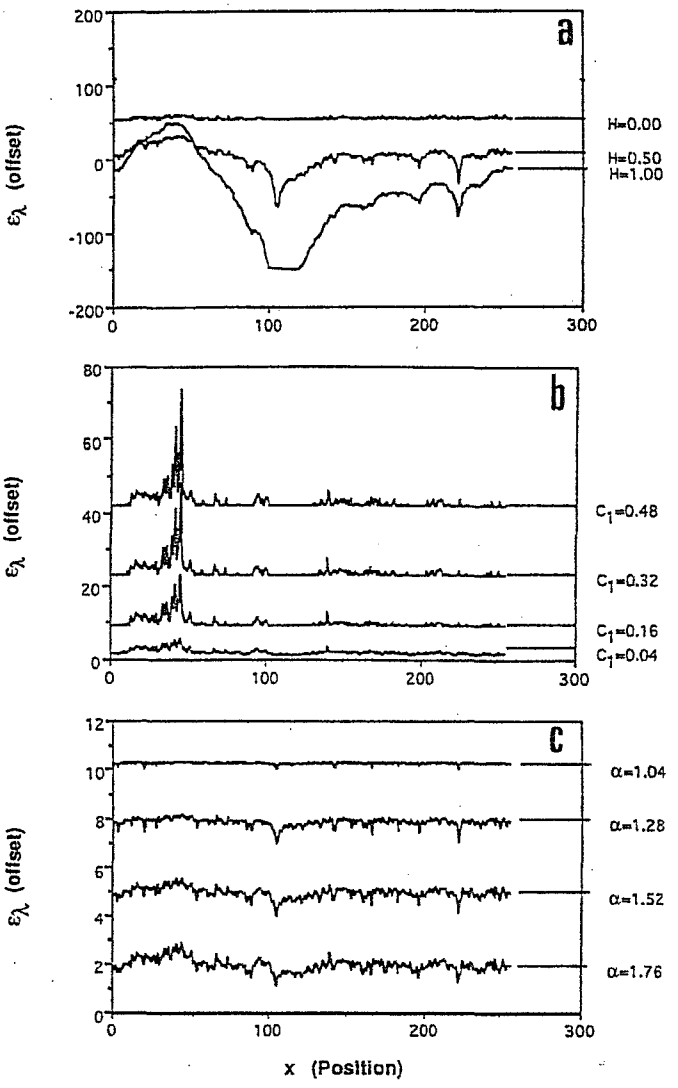

Fig. 9. Illustration des propriétés d'un champ turbulent décrites par les paramètres multifractals universels H, C_1 and α à l'aide d'une simulation unidimensionnelle de longueur 256, avec H variable (***a***), puis avec $H = 0$, $\alpha = 2$ et C_1 variable (***b***) et avec $H = 0$, $C_1 = 0{,}01$ et α variable (*c*).

3. Applications à la description spatio-temporelle de l'écosystème pélagique

Par souci de clarté, dans cette partie, l'auteur a volontairement omis toutes formulations mathématiques et détails des techniques d'analyses. Toutefois, le lecteur désireux d'obtenir de plus amples informations sur le mode de calcul associé aux différentes techniques d'analyses et à la détermination des différents paramètres dont il est question par la suite pourra se reporter aux nombreuses références bibliographiques qui jalonnent le texte. En outre, les concepts et résultats exposés dans ce paragraphe sont essentiellement basés sur les travaux de Seuront (1997), Seuront & Lagadeuc (1997, 1998) et Seuront *et al.* (1996a, b).

3.1. Variabilité, homogénéité et d'hétérogénéité

Ce paragraphe reprend brièvement des concepts développés de manière plus complète par Seuront & Lagadeuc (1997, 1998) et est destiné d'une part à lever toute ambiguïté sur l'utilisation des concepts associés aux termes "variabilité" et "hétérogénéité", et d'autre part à familiariser le lecteur avec la terminologie employée dans la suite du texte.

Il existe en effet dans la littérature une grande confusion entre les terminologies "hétérogénéité" et "variabilité". Ainsi, on parle presque indifféremment de la variabilité ou de l'hétérogénéité de la biomasse phytoplanctonique le long d'un gradient côte-large comme celui rencontré le long des côtes de la Manche orientale. Il apparaît également que la différence entre ces 2 terminologies est souvent liée au type d'approche (on parlera d'hétérogénéité des méandres du Gulf Stream alors qu'on parlera de microfluctuations de vitesse et non pas d'hétérogénéité à petites échelles pour caractériser les fluctuations associées à un enregistrement de vitesse turbulente). Dans la suite, nous ferons une distinction très nette entre ces 2 terminologies. La variabilité est ainsi considérée comme une mesure de l 'amplitude des fluctuations d'un descripteur quantitatif autour d'une valeur moyenne, alors que l'hétérogénéité fournira une description qualitative et quantitative de la structuration de cette variabilité dans le cadre des invariances d'échelle simples et multiples associées respectivement aux concepts de fractals et de multifractals. De plus, cette hétérogénéité sera plus ou moins forte selon la valeur prise par les paramètres de structuration que sont la dimension fractale et les paramètres multifractals universels H, C_1 et α.

3.2. Structuration spatio-temporelle monofractale de l'écosystème pélagique

Dans ce paragraphe, les dimensions fractales d_F sont calculées à partir de la pente m d'un semivariogramme en coordonnées logarithmiques comme : $d_F = (4-m)/2$. Le semivariogramme étant défini comme une expression de la variance en fonction de l'échelle d'observation, une valeur élevée de la pente m (i.e. une faible valeur de la dimension fractale d_F) traduit un processus hétérogène dans le sens où les différences de variabilité perceptibles d'une échelle à l'autre sont grandes. Réciproquement, un processus présentant une dimension fractale élevée sera beaucoup moins hétérogène (ou plus homogène) dans le sens où les

différences perceptibles d'une échelle à l'autre seront beaucoup plus faible (cf. Seuront & Lagadeuc, 1997, 1998) pour plus de détails).

3.2.1. Cas du détroit du Pas-de-Calais (Manche orientale)

A l'échelle de la Manche orientale, considérée comme un modèle de mer mégatidale, le régime marégraphique très particulier, constitué de courants alternatifs et parallèles à la côte avec une dérive résiduelle se dirigeant vers la Mer du Nord à une vitesse de l'ordre de 2,7 milles par jour, favorise la création d'une masse d'eau côtière permanente appelée "Fleuve côtier", dont l'individualité est sans cesse entretenue par les apports fluviatiles qui s'échelonnent de la Baie de Seine au détroit du Pas-de-Calais. La formation de cette structure côtière très spécifique se manifeste par un gradient côte-large très net en terme de salinité, température, charge particulaire, biomasse phyto- et zooplanctonique. De plus, dans le système Manche orientale, où la bathymétrie est faible et les courants de marées particulièrement forts, la marée est considérée comme le principal facteur de mélange vertical, responsable d'une homogénéisation verticale de la colonne d'eau. Ici, une colonne d'eau est qualifiée d'homogène essentiellement par opposition à une colonne d'eau stratifiée, il n'est donc pas possible d'en déduire a priori d'information sur la nature de la distribution verticale de la biomasse phytoplanctonique ou de la température en terme de variabilité ou d'hétérogénéité.

Dans ce cadre, nous nous sommes intéressés à la différence pouvant exister entre la perception de la variabilité et de l'hétérogénéité verticale de la colonne d'eau au sein d'une structure hydrologique hétérogène qu'est le détroit du Pas-de Calais. Nous avons réalisé 4 fois une radiale côte-large de 15 stations permettant d'échantillonner la masse d'eau côtière comme la masse d'eau du large. Nous nous sommes ensuite intéressés à la structuration spatio-temporelle de la structure verticale des différentes masses d'eau en termes de moyenne, de variabilité (caractérisée par un coefficient de variation, défini comme le rapport S/m) et d'hétérogénéité (caractérisée par une dimension fractale) de paramètres comme la température, la salinité, la fluorescence *in vivo* (considérée en tant qu'indicateur de la biomasse phytoplanctonique) et de la transmission (considérée en tant qu'indicateur de la charge de la masse d'eau en particules) échantillonnés à chaque station de la surface au fond.

L'analyse des semivariogrammes en coordonnées logarithmiques (Fig. 10) montre que si la température, la salinité et la fluorescence présentent une structuration qu'il est possible de caractériser en terme de dimension fractale, cette structuration est absente dans le cas de la

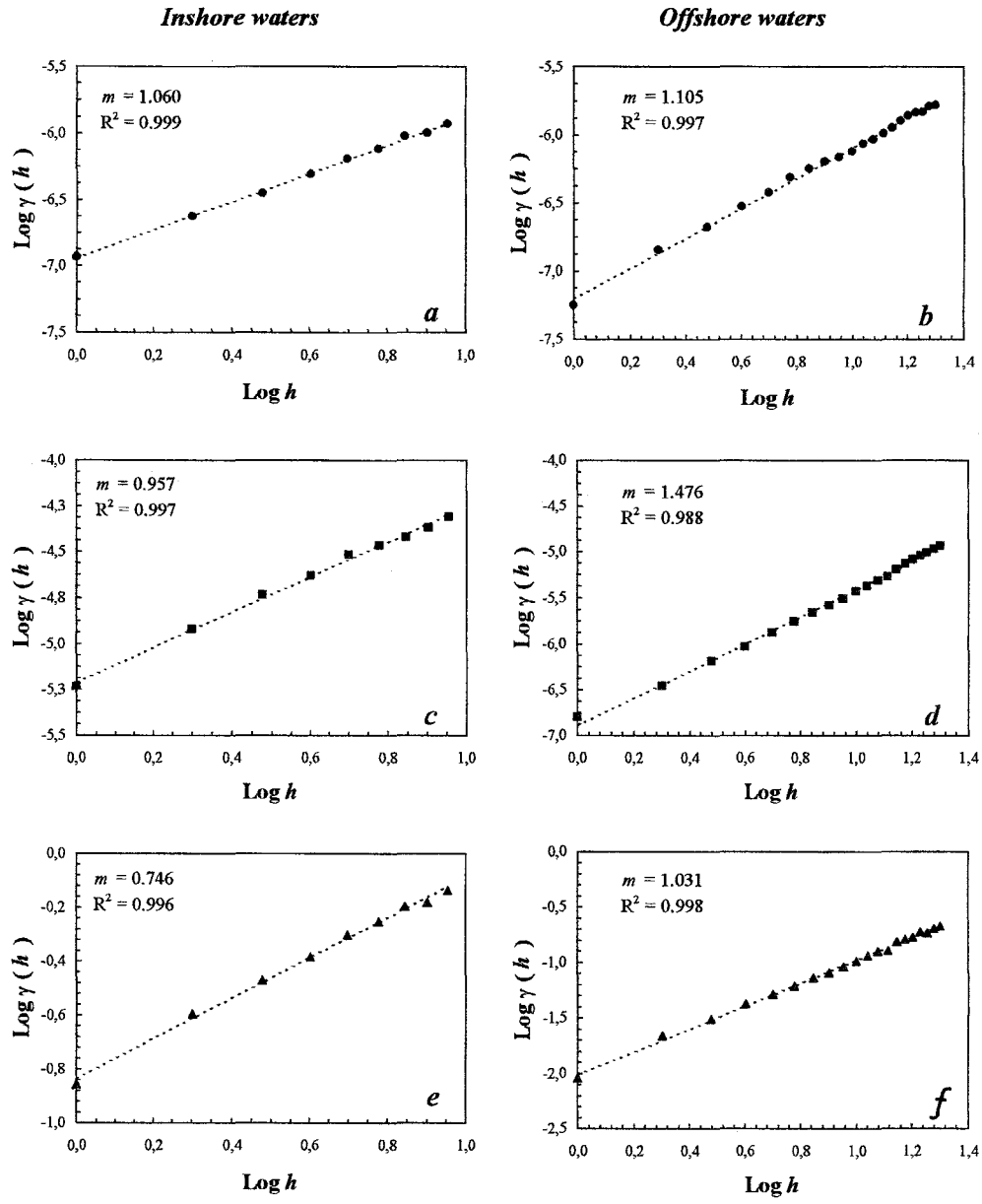

Fig. 10. Semivariogrammes de la température, la salinité et la fluorescence *in vivo* (de haut en bas) à la côte (***a***, ***c*** et ***e***) et au large (***b***, ***d*** et ***f***) en coordonnées logarithmiques, représentés avec leur meilleur ajustement linéaire de pente *m* (d'après Seuront & Lagadeuc, 1998).

charge particulaire. Ceci suggère que si les mêmes processus ou du moins des processus similaires vraisemblablement associés au mélange induit par la marée peuvent être considérés comme étant à l'origine de la structuration de paramètres tels que température, salinité et fluorescence, il en va tout autrement pour la teneur de la masse d'eau en matière particulaire, qui relève à la fois des propriétés physiques, chimiques et biologiques des particules d'origine biologique, qu'elles soient vivantes ou inertes, et minérales présentes dans la masse d'eau.

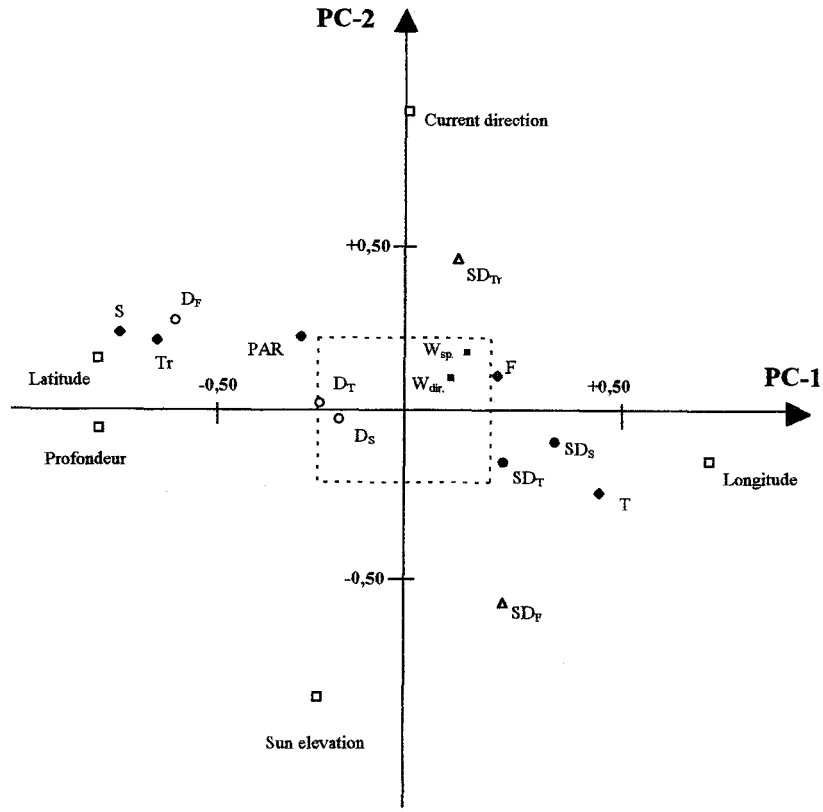

Fig. 11. Position des 14 variables (cf. Table 1 pour la signification des symboles) dans le plan principal de l'Analyse en Composantes Principales (d'après Seuront & Lagadeuc, 1998).

Nous avons ensuite introduit les différentes coordonnées spatio-temporelles de notre échantillonnage (latitude, longitude, profondeur, direction du courant de marée et hauteur solaire) dans une analyse en composantes principales (ACP) dans laquelle nous avons ajouté en tant que variables supplémentaires les paramètres relatifs à la moyenne, la variabilité et l'hétérogénéité verticale des paramètres physiques et biologiques (Fig. 11; Table 1). S'il apparaît que la moyenne verticale de ces paramètres se distribue classiquement dans le plan principal selon le gradient côte-large (salinité et température plus faibles à la côte, et biomasse phytoplanctonique plus forte à la côte), il en va tout autrement en ce qui concerne leur variabilité et leur hétérogénéité verticale.

Ces résultats nous montrent une organisation différentielle, dans l'espace et le temps, de la variabilité et de l'hétérogénéité en fonction de la nature, physique ou biologique, des paramètres considérés.

Additional data	Code	PC-1	PC-2
Mean value			
Temperature	**T**	0.628	-0.259
Salinity	**S**	-0.912	0.244
Fluorescence	**F**	0.300	0.107
Transmission	**Tr**	-0.789	0.219
PAR	**PAR**	-0.327	0.232
Standard deviation			
Temperature	$\mathbf{SD_T}$	0.320	-0.165
Salinity	$\mathbf{SD_S}$	0.484	-0.102
Fluorescence	$\mathbf{SD_F}$	0.320	-0.559
Transmission	$\mathbf{SD_{Tr}}$	0.171	0.419
Fractal dimension			
Temperature	$\mathbf{D_T}$	-0.267	0.022
Salinity	$\mathbf{D_S}$	-0.205	-0.029
Fluorescence	$\mathbf{D_F}$	-0.729	0.282
Wind speed	**Wsp.**	0.200	0.180
Wind direction	**Wdir.**	0.150	0.100

Table 1. Noms et codes des 14 variables supplémentaires utilisées dans l'Analyse en Composantes Principales, et leur corrélation avec les 2 premiers axes principaux. PC-1, premier axe principal; PC-2, deuxième axe principal.

3.2.2. Cas de la Baie des Chaleurs (Canada, Québec)

A une échelle toute autre (échantillonnage de la structure verticale de la masse d'eau toutes les heures pendant 57 heures) et dans un milieu très différent tant en terme d'hydrologie que d'hydrodynamisme, Seuront & Lagadeuc (1997) ont montré que la structuration temporelle de paramètres physiques et biologiques en terme de dimension fractale pouvait présenter 2 informations complémentaires.

La première correspond à la valeur de la dimension fractale, estimée à partir de la pente du semivariogramme en coordonnées logarithmiques. Ainsi, la distribution verticale des dimensions fractales de la température, la salinité et la fluorescence (Fig. 12) apparaît intimement liée à la structure hydrodynamique de la masse d'eau, les dimensions de tous ces

paramètres étant maximales aux profondeurs où le nombre de Richardson *Ri* est maximal (Seuront & Lagadeuc, 1997). Ces résultats indiquent donc une structuration temporelle différentielle de la colonne d'eau en fonction de l'intensité et de la nature du forçage physique qu'elle subit.

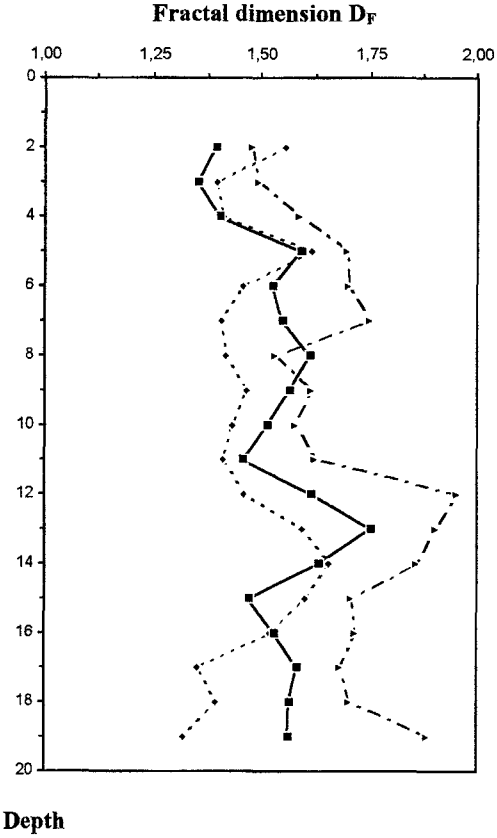

Fig. 12. Distribution verticale des dimensions fractales D_F de la fluorescence *in vivo* (losange), de la température (cercle) et de la salinité (triangle) (d'après Seuront & Lagadeuc, 1997).

La seconde correspond à la gamme d'échelles pour lesquelles le semivariogramme présente un comportement linéaire, donc une structuration fractale de la variabilité du processus considéré. Cette gamme d'échelle décroît en raison inverse de la profondeur (Fig. 13) et semble associée à la structure verticale de la circulation résiduelle (Seuront & Lagadeuc, 1997). Ces ruptures d'échelles suggèrent l'existence d'une zone de transition entre différents niveaux d'organisation d'un même système, ou entre 2 systèmes d'organisation différents. En effet, on peut penser que lorsque la dimension fractale varie brusquement ou, comme c'est la cas ici, n'est plus calculable, on passe d'une échelle de phénomènes à une autre. Inversement, tant que la dimension fractale ne change pas d'une échelle d'observation à une autre, le processus à l'origine de la structuration de la variabilité observée reste le même.

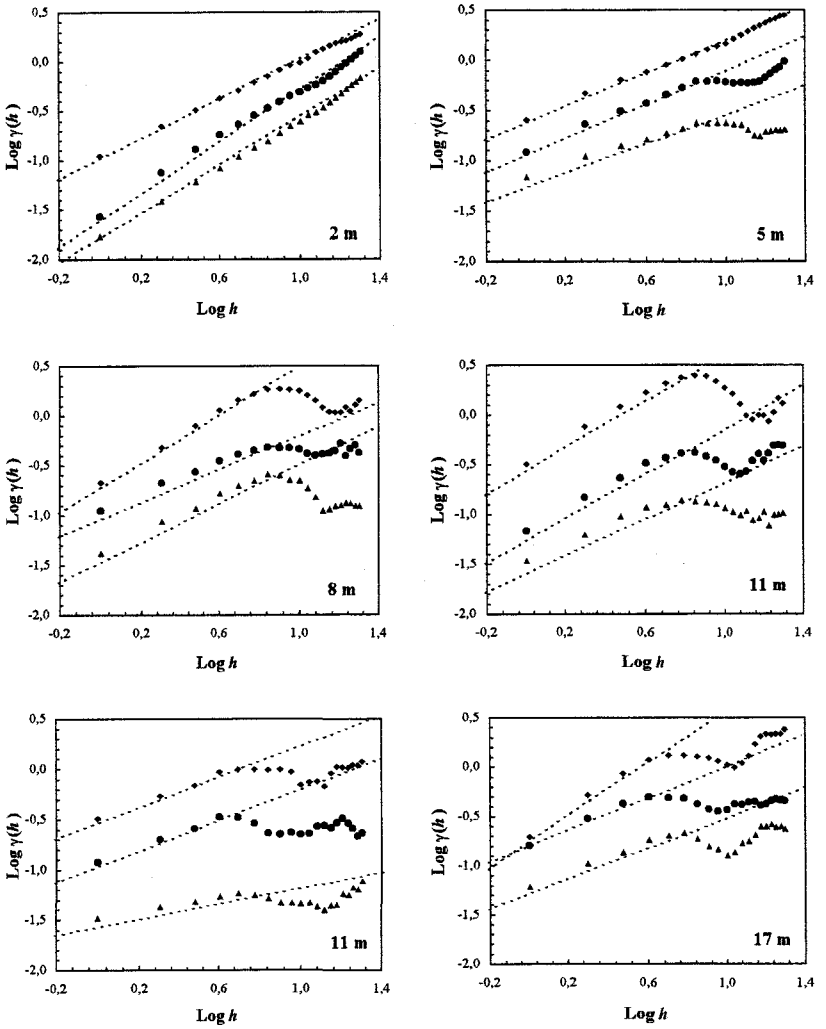

Fig. 13. Semivariogrammes de la fluorescence *in vivo* (losange), de la température (cercle) et de la salinité (triangle) en coordonnées logarithmiques, représentés avec leur meilleur ajustement linéaire de pente *m* (d'après Seuront & Lagadeuc, 1997).

Ces deux paragraphes ont présenté le potentiel des méthodes d'analyses fractales, d'un usage relativement récent en écologie et *a fortiori* en écologie marine, pour devenir un outil de description essentiel en écologie planctonique. De plus, la distinction des terminologies "variabilité" et "hétérogénéité" autorisée par de telles approches permet d'envisager de nouvelles avancées dans la description de la structuration spatio-temporelle du milieu dont la compréhension apparaît aujourd'hui essentielle en écologie marine.

3.3. Structuration multifractale de l'écosystème pélagique

De part son fort hydrodynamisme tidal, la Manche orientale est généralement considérée comme un milieu homogène. Cette homogénéité, remise en question à l'échelle de la colonne

d'eau (cf. § 3.1), l'a également été à plus petite échelle. En effet, Seuront *et al.* (1996a, b) et Seuront (1997) ont démontré que pour des échelles allant de 1 à 100 secondes, la distribution temporelle de la biomasse phytoplanctonique (exprimée en terme de fluorescence *in vivo*), bien que se comportant comme un scalaire purement passif, ne pouvait être considérée comme homogène mais présentait au contraire une structuration extrêmement complexe caractérisée en terme de multifractals. Aux échelles supérieures, la distribution de la biomasse phytoplanctonique présente une distribution multifractale très spécifique

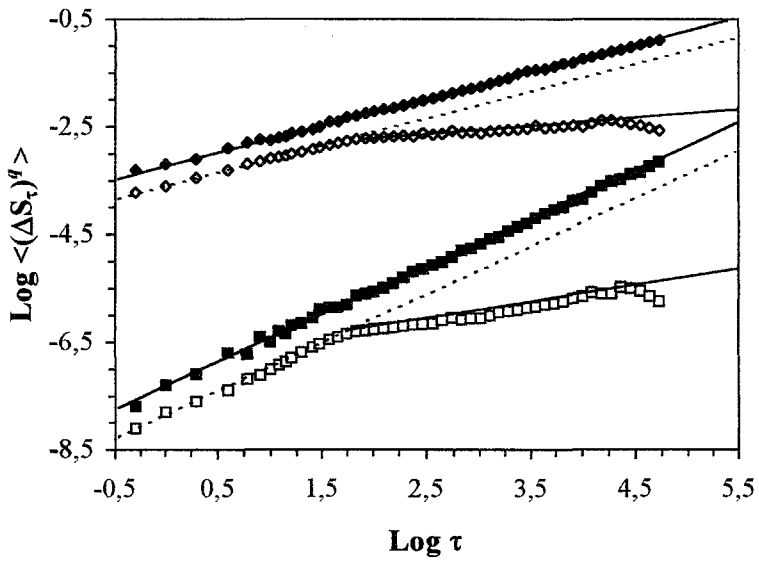

Fig. 14. Fonctions de structure $< (\Delta S_\tau)^q >$ vs. τ en coordonnées logarithmiques pour $q = 1$ and 3 (de haut en bas) pour la température (symboles noirs) et la fluorescence (symboles clairs). Un seul comportement linéaire est visible pour la température alors que la fluorescence présente de comportement invariants d'échelles (d'après Seuront *et al.*, 1996a).

Ainsi, les fonctions de structure de la température et de la biomasse phytoplanctonique (Fig. 14) présentent deux comportements distincts. La structuration de la température est la même des petites aux grandes échelles quel que soit le moment statistique considéré, suggérant qu'un seul et même processus (vraisemblablement ici le mélange turbulent) est à l'origine de la structuration de la variabilité observée. Par contre, la distribution de la biomasse phytoplanctonique présente deux comportements différents. Aux échelles inférieures à 100 secondes, la distribution de la biomasse phytoplanctonique est similaire à celle de la température, alors qu'aux échelles supérieures à 100 secondes les fonctions de structure de la biomasse phytoplanctonique présentent un aplatissement très net. Cet aplatissement n'est d'ailleurs pas sans rappeler les travaux de Platt & Denman (1976) et Denman *et al.* (1977) qui

prédisaient un aplatissement du spectre de variance de la biomasse phytoplanctonique aux échelles où des processus purement biologiques interféraient voire prenaient le pas sur les processus de dispersion turbulente. Dans ce cadre, les résultats de Seuront *et al.* (1996a) présentent une généralisation statistique à des moments d'ordre q de travaux antérieurs basés uniquement sur l'analyse spectrale associée à un moment d'ordre 2.

L'examen de la distribution des exposants $\zeta(q)$ en fonction de q montrent un comportement non-linéaire caractéristique d'une distribution multifractale (Fig. 15). Aux échelles inférieures à 100 secondes, les distributions de la température et de la biomasse phytoplanctonique ne peuvent être différenciées ($H = 0{,}42$, $C_1 = 0{,}04$ et $\alpha \approx 1{,}75$) alors qu'aux échelles supérieures à 100 secondes, la biomasse phytoplanctonique présente une distribution très spécifique avec des paramètres multifractals nettement différents ($H = 0{,}12$, $C_1 = 0{,}02$ et $\alpha = 0{,}8$).

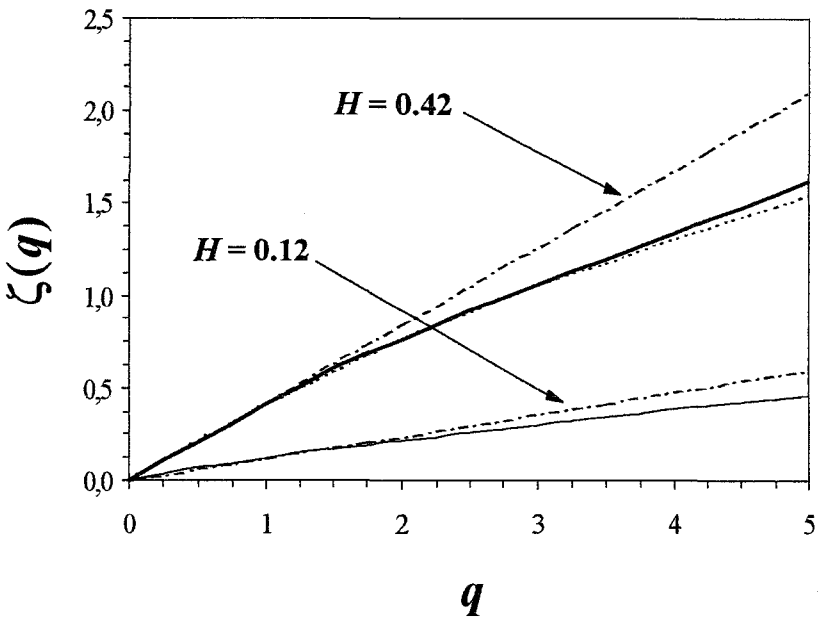

Fig. 15. Courbes empiriques de l'exposant invariant d'échelle des fonctions de structure $\zeta(q)$ pour la température (trait continu épais), la fluorescence à petite échelle (tirets) et à grande échelle (trait continu fin), comparées à la courbe monofractale théorique $\zeta(q) = qH$ avec $H = 0{,}42$ et $H = 0{,}12$. La non-linéarité des $\zeta(q)$ empiriques révèle un comportement multifractal (d'après Seuront *et al.*, 1996a).

Ces résultats montrent que la variabilité de la distribution de la température et de la biomasse phytoplanctonique peuvent être caractérisée en terme d'hétérogénéité dans le cadre des multifractals universels, et ce, quelles que soient les échelles considérées et les intensités du processus. De plus, la biomasse phytoplanctonique présente une structuration différentielle associée aux échelles considérées. On retrouve ici, une généralisation multifractale du concept

de rupture d'échelle discuté au paragraphe 3.2 dans le cadre monofractal. De plus, ces résultats nous ont permis de vérifier l'hypothèse de passivité moyenne de la biomasse phytoplanctonique en milieu turbulent telle qu'elle a été formulée dans les années 1970 (e.g. Platt, 1972), mais aussi et surtout de confirmer sa validité en considérant la distribution de tous les niveaux d'intensité quelles que soient les échelles considérées.

Enfin, l'utilisation des multifractals universels a montré que la variabilité associée à des processus stochastiques fortement non-Gaussien pouvait être pleinement caractérisée par seulement trois paramètres et ce, quelles que soient les échelles d'espace ou de temps considérées. De fait, ces résultats montrent que dans un milieu turbulent, considéré classiquement comme générateur d'homogénéité, la distribution de la biomasse phytoplanctonique était particulièrement hétérogène. Cette hétérogénéité, inhérente à la structure des mouvements turbulents, permet d'envisager, loin des statistiques gaussiennes classiques, une description multiéchelle du couplage fortement non-linéaire existant entre processus physiques et biologiques. La prise en compte de cette hétérogénéité dans le cadre d'une modélisation de la trophodynamique du zooplancton, actuellement en développement, semble aujourd'hui essentielle dans l'étude des flux de matière au sein de l'écosystème pélagique.

Références bibliographiques

Anselmet F., Gagne Y., Hopfinger E. J. & Antonia R.A., 1984.- " High-order velocity structure functions in turbulent shear flows ". *J. Fluid Mech.*, n° 140, p. 63-69.

Berry M. V. & Lewis, Z. V. 1980.- " On the Weierstarss-Mandelbrot fractal function ".- *Proc. Roy. Soc. London*, n° A370, p. 459-484.

Bradbury R. H. & Reichelt R. E., 1983.- " Fractal dimension of a coral reef at ecological scales ".- *Mar. Ecol. Prog. Ser.*, n° 10, p. 169-171.

Bradbury R. H., Reichelt R. E. & Green D. G., 1984.- " Fractals in ecology: methods and interpretation ".- *Mar. Ecol. Prog. Ser.*, n° 14: p. 295-296

Bundy M. H., Gross T. F., Coughlin D. J. and Strickler J. R., 1993.- " Quantifying copepod searching efficiency using swimming patterns and pzerceptive ability ".- *Bull. Mar. Sci.*, n° 53: p. 15-28

Burrough P. A., 1981.- " Fractal dimensions of landscape and other environmental data ".- *Nature*, n° 294, p. 240-242

Cantor G., 1872.- " Uber die Ausdehnung eines Satzes aus der Theorie der Trigonometrischen Reinhen ".- *Math. Annalen*, n°5, p. 123-132.

Crilly A. J., Earnshaw R. A. & Jones H., 1991.- *Fractals and chaos*.- New York : Springer-Verlag.

Denman K. L. & Platt T., 1976.- " The variance spectrum of phytoplankton in a turbulent ocean ".- *J. Mar. Res.*, n° 34, p. 593-601.

Denman K. L., Platt T. & Okubo A., 1977.- " The chlorophyll fluctuation spetrum in the sea ". *Limnol. Océanogr.*, n°22, p. 1033-1038.

Erlandson J. & Kostylev V., 1995.- " Trail following, speed and fractal dimension of movement in a marine prosobranch, *Littorina littorea*, during a mating and a non-mating season ".- *Mar. Biol.*, n° 122, p. 87-94.

Evertsz C. J. G. & Mandelbrot B. B., 1992.- Multifractal measures. *In* : *Chaos and Fractals. New Frontiers of Science* (Peitgen,H. O., Hartmut J. & Saupe D. eds.), 922-954.- New York : Springer-Verlag.

Falconer K., 1993.- *Fractal geometry. Mathematical foundations and applications.*- Chichester : Wiley.

Feder J., 1988.- *Fractals.*- New York : Plenum.

Frisch U. & Parisi G., 1985.- Fully developed turbulence and intermittency. *In* : *Turbulence and Predictability of Geophysical Flows and Climate Dynamics* (Ghil M., benzi R. & parisi G. eds.), 84.- New York : North Holland.

Frontier S., 1985.- " Diversity and structure in aquatic ecosystems ".- *Oceanogr. Mar. Biol. Ann. Rev.*, n° 23, p. 253-312

Frontier S., 1987.- Application of fractal theory to ecology. *In* : *Developements in Numerical Ecology* (Legendre P. & Legendre L. eds.), 335-378.- Berlin : Springer-Verlag.

Frontier S., 1994.- Species diversity as a fractal properties of biomass. *In* : *Fractals in the natural and applied sciences* (Nowak M. M. eds..), 119-127, North-Holland : Elsevier.

Ghashghaie S., Breymann W., Peinke J., Talkner P. & Dodge Y., 1996.- " Turbulent cascades in foreign exchange markets ".- *Nature*, n° 381, p. 767-770.

Gee J. M. & Warwick R. M., 1994a.- " Body-size distribution in a marine metazoan community and the fractal dimensions of macroalgae ". *J. Exp. Mar. Biol. Ecol.*, n° 178, p. 247-259.

Gee J. M. & Warwick R. M., 1994b.- " Metazoan community structure in relation to the fractal dimensions of marine macroalgae ".- *Mar. Ecol. Progr. Ser.*, n° 103, p. 141-150.

Gouyet J. F., 1992.- *Physique et structures fractales.*- Paris : Masson.

Grassberger P., 1983.- " Generalized dimensions of strange attractors ".- *Phys. Lett.*, n° 97, p. 227-230.

Grassberger P. & Procacia I., 1983.- " Characterization of strange attractors ".- *Phys. Rev. Lett.*, n° 50, p. 346-349.

Halsey T. C., Jensen M. H., Kadanoff L. P., Procaccia I. & Shraiman B. I., 1986.- " Fractal measures and their singularities: the characterization of strange sets ".- *Phys. Rev. A*, n° 33, p. 443-453.

Hastings H. M. & Sugihara G., 1993. *Fractals. A user's guide for the natural sciences.* Oxford : Oxford University Press.

Hausdorff F., 1919.- " Dimension und usseres Mass ".- *Math. Annalen*, n° 79, p. 157-179.

Hentschel H. G. E. & Procaccia I., 1983.- " The infinite number of generalized dimensions of fractals and strange attractors ". *Physica D*, n° 8, p. 435-444.

Kaandorp J. A., 1991.- " Modelling growth forms of the sponge *Haliclona oculata* (Porifera, Demospongiae) using fractal techniques ". *Mar. Biol.*, n° 110, p. 203-215.

Kaandorp J. A. & Dekluijver M. J., 1992.- " Verification of fractal growth models of the sponge *Haliclona oculata* (Porifera) with transplantation experiments ". *Mar. Biol.*, n° 113, p. 133-143.

Krummel J. R., Gardner R. H., Sugihara G., O'Neill R. V. & Coleman P. R., 1987.- " Landscape patterns in a disturbed environment ".- *Oikos*, n° 48, p. 321-324.

Lavallée D., 1991.- *Multifractal techniques: analysis and simulation of turbulent fields.* Ph.D. thesis, McGill University, Montréal, Canada.

Li X. & Logan B. E., 1995.- " Size distribution and fractal properties of particles during a simulated bloom in a mesocosm ".- *Deep-Sea Res. I*, n° 42, 125-138.

Logan B.E. & Kilps J. R., 1995.- " Fractal dimensions of aggreagates formed in different fluid mechanical environments ".- *Wat. Res.*, n° 29, p. 443-453.

Longuet-Higgins M. S., 1994.- " A fractal approach of breaking waves ". *J. Phys. Oceangr.*, n° 24, p. 1834-1838.

Lovejoy S., 1982.- " Area-perimeter relation for rain and cloud areas ".- *Science*, n° 216, p. 185-187.

Mandelbrot B. B., 1975, 1984, 1989, 1995.- *Les objets fractals.*- Paris : Flammarion.

Mandelbrot B. B., 1974.- " Multiplications aléatoires itérées et distributions invariantes par moyenne pondérée aléatoire ".- *C. R. Acd. Sci. Paris Série A*, n° 278, p. 289-292.

Mandelbrot B. B., 1977.- *Fractals. Form, chance, and dimension.*- San Francisco : Freeman.

Mandelbrot B. B., 1978.- " Les objects fractals ".- *La Recherche*, n°9, p. 1-13.

Mandelbrot B. B., 1983.- *The fractal geometry of nature.*- San Francisco : Freeman.

Mandelbrot B. B., 1989.- Fractal geometry: what is it and what does it do? *In* : *Fractals in the Nature Sciences* (Fleischmann M., Tidesley D. J. & Ball R. C. eds.), 3-16.- Princeton : Princeton University Press.

Mandelbrot B. B., 1997.- Fractals, hasard et finance.- Paris : Flammarion.

McHardy I. & Czerny B., 1987.- " Fractal X-ray time variability and spectral invariance of the Seyfert galaxy NGC5506 ".- *Nature*, n° 325, p. 696-698.

Milne B. T., 1988.- " Measuring the fractal geometry of landscapes ".- *Appl. Math. Comp.*, n° 27, p. 67-79.

Paladin G. & Vulpiani A., 1987.- " Anomalous scaling laws in multifractal objects ".- *Phys. Rep.*, n° 156, p. 145.

Palmer M. W., 1988.- " Fractal geometry: a tool for describing spatial patterns of plant communities ".- *Vegetatio*, n° 75, p. 91-102.

Pascual M., Ascioti F. A. & Caswell H., 1995.- " Intermittency in the plankton: a multifractal analysis of zooplankton biomass variability ".- *J. Plankton Res.*, n° 17, p. 1209-1232.

Peano G., 1890.- " Sur une courbe qui remplit une aire plane ".- *Math. Annalen*, n°36, p. 157-160.

Pecknold S., Lovejoy S., Schertzer D., Hooge C. & Malouin J. F., 1993.- The simulation of universal multifractals. *In* : *Cellular automata: prospects in astrophysical applications* (Perdang J. M. & Lejeune A. eds.), 228-267, Singapore : World Scientific.

Peitgen,H. O., Hartmut J. & Saupe D., 1992.- *Chaos and fractals. New frontiers of science.*- New York : Springer-Verlag.

Perrin J., 1906.- " La discontinuité de la matière ".- *Revue du mois*, n° 1, p. 323-344.

Phillips J. D., 1985.- " Measuring complexity of environmental gradients ". *Vegetatio*, n° 64, p. 95-102.

Platt T., 1972.- " Local phytoplankton abundance and turbulence ". *Deep-Sea Res.*, n° 19, p. 183-187.

Schertzer D. & Lovejoy S., 1983.- The dimension and intermittency of atmospheric dynamics. *In* : *Turbulent Shear Flows 4* (Launder B. ed.), 7-33.- Karlsruhe : Springer-Verlag.

Schertzer D. & Lovejoy S., 1987.- " Physically based rain and cloud modeling by anisotropic multiplicative turbulent cascades ". *J. Geophys. Res.*, n° 92, p. 9693-9714.

Schertzer D. & Lovejoy S., 1989.- Nonlinear variability in geophysics: multifractal analysis and simulation. *In* : *Fractals: physical origin and consequences* (Pietronero L. ed.), 49-79.- New York : Plenum.

Schertzer D. & Lovejoy S., 1993. Nonlinear variability in geophysics. 3. Scaling and multifractal processes. E. G. S. Richardson Memorial Conference, Cargèse : Lectures notes.

Schmitt F., Lovejoy S. & Schertzer D., 1995.- " Multifractal analysis of the Greenland ice-core project climate data ". *Geophys. Res. Lett.*, n°22, p. 1689-1392.

Seuront L., 1995.- *Analyses multifractales de la distribution du plancton en milieu turbulent.* DEA d'Océanologie biologique, Université P. & M. Curie.

Seuront L., 1997.- " Distribution inhomogène multiéchelle de la biomasse phytoplanctonique en milieu turbulent ". *J. Rech. Océanogr.*, n° 22, p. 9-16.

Seuront L., Schmitt F., Lagadeuc Y., Schertzer D., Lovejoy S. & Frontier S., 1996a.- " Multifractal analysis of phytoplankton biomass and temperature in the ocean ". *Geophys. Res. Lett.*, n° 23, p. 3591-3594.

Seuront L., Schmitt F., Lagadeuc Y., Schertzer D. & Lovejoy S., 1996b.- " Multifractal intermittency of Eulerian and Lagrangian turbulence of ocean temperature and plankton fields ". *Nonlin. Proc. Geophys.*, n° 3, p. 236-246.

Seuront L. & Lagadeuc Y., 1997.- " Characterisation of space-time variability in stratified and mixed coastal waters (Baie des Chaleurs, Québec, Canada): application of fractal theory ". *Mar. Ecol. Prog. Ser.*, n° 259, p. 81-95.

Seuront L. & Lagadeuc Y., 1998.- " Spatio-temporal structure of tidally mixed coastal waters: variability and heterogeneity ".- J. Plankton Res., n° 20 (sous presse).

Sugihara G. & May R. M., 1990.- " Applications of fractals in ecology ". *Trends Ecol. Evol.*, n° 5, p. 79-86.

Tessier Y., Lovejoy S. & Schertzer D., 1993a.- " Universal multifractals: theory and observations of rain and clouds ". *J. Appl. Meteor.*, n° 32, p. 223-250.

Tessier Y., Lovejoy S., Schertzer D., Lavallée D. & Kerman B., 1993b.- " Universal multifractal indices for the ocean surface at far red wavelengths ". *Geophys. Res. Lett.*, n° 20, p. 1167-1170.

Tricot C., 1993. *Courbes et dimension fractale.* Paris : Springer-Verlag.

Wiens J. A., Crist T. O. & Milne B. T., 1993.- " On quantifying insect movements ".- *Environ. Entomol.*, n° 22, p. 709-715.

Wiens J. A., Crist T. O., With K. A. & Milne B. T., 1995.- " Fractal patterns of insect movement in microlandscape mosaics ".- *Ecology*, n° 76, p. 663-666.

Woronow A., 1981.- " Morphometric consistency with the Hausdorff-Besicovitch dimension ".- *Math. Geol.*, 13, p. 201-216.

A9

Modélisation multi-agents de systèmes naturels.
Réflexions générales et application en biologie marine

Ramat E, Preux P, Seuront L & Lagadeuc Y

Proceedings JFIADSMA'98, 1999 (sous presse)

Modélisation multi-agents de systèmes naturels

Réflexions générales et application en biologie marine

E. RAMAT[(1)], P. PREUX[(1)], L. SEURONT[(2)] et Y. LAGADEUC[(2)]

(1) Laboratoire d'Informatique du Littoral (LIL)
B.P. 719
62228 Calais Cedex
France

e-mail : {ramat,preux}@lil.univ-littoral.fr

(2) Station marine de Wimereux - URA CNRS 1363
28 avenue Foch
BP 80
62930 Wimereux
France

e-mail : {seuront,lagadeuc}@loalit.univ-littoral.fr

Résumé

Dans le cadre d'un travail de recherche pluridisciplinaire, nous proposons une modélisation multi-agents d'un écosystème. Nous discutons d'aspects méthodologiques pour passer d'un modèle à base de bilans à une modélisation multi-agents. Nous justifions l'utilisation d'une modélisation multi-agents pour l'étude du comportement d'un organisme vivant ce qu'un modèle analytique ne peut rendre compte d'une manière pertinente. Nous présentons également la plate-forme que nous avons développé en cherchant la généricité afin de la réutilisée dans d'autres projets en cours.

Mots-clés

SMA, modélisation d'écosystèmes, biologie marine, laboratoire virtuel

1 Introduction les SMA dans les sciences de la nature

L'objet de nos travaux est la modélisation et la simulation de systèmes naturels à l'aide de systèmes multi-agents [4]. Ce travail est pluridisciplinaire : l'informaticien apporte sa connaissance de l'informatique, développe des travaux nouveaux pour répondre à des questions que se posent des chercheurs d'une autre discipline, une discipline des sciences naturelles dans notre cas. Notre travail repose sur un dialogue constant entre les disciplines.

Le choix des SMA pour l'étude de ce type de systèmes n'est pas un choix académique : c'est un choix de raison. En effet, notre objectif n'est pas, comme cela est généralement le but dans l'utilisation de l'informatique, de calculer une fonction ; l'objectif est d'étudier la dynamique d'un système. La modélisation consiste à transcrire un système dans un certain langage pour pouvoir l'étudier plus aisément. Ce peut-être le langage des équations différentielles. Cependant, nous pensons qu'il est beaucoup plus judicieux, parce qu'il se prête mieux à l'expression d'objets complexes, d'utiliser des agents dont le comportement est décrit algorithmiquement. Aussi, la modélisation multi-agents remplit-elle nos attentes. Notons bien que nous ne cherchons pas à « rendre tout agent », même s'il est intéressant de voir jusqu'où les SMA peuvent se substituer aux équations [7,10]. Si, dans le système que nous étudions, certaines parties de leur dynamique en est parfaitement décrite par des équations que l'on sait résoudre, nous l'utilisons.

D'un point de vue plus global, notre objectif est la réalisation de laboratoires virtuels [6]. Nous entendons par là un logiciel dans lequel un système est décrit et la dynamique simulée, les paramètres définissant le système modifiés dynamiquement, des capteurs placés à tout endroit du système pour collecter des mesures. Le but est de pouvoir tester des hypothèses en faisant jouer des

scénarii et d'observer et mesurer l'évolution du système. Cela permet également la visualisation des phénomènes émergeants que l'on ne peut pas imaginer/prévoir *a priori*. Cette visualisation aide à la compréhension du système et de sa dynamique.

1.1 Démarche pour la modélisation

D'une manière générale, les modèles rencontrés dans les sciences du type biologie, géologie, ... décrivent des flux de manière analytique. En modélisation MA, il faut décrire le comportement individuel des agents et leurs interactions. C'est un changement complet de perspective. Dans une modélisation multi-agents, les bilans sont émergeants : ce sont des résultats, et non plus des données. Généralement, le chercheur a un modèle de type bilans et une intuition concernant le comportement à un niveau plus fin et seul l'aspect bilan est utilisé effectivement, du fait qu'il est analytique. En renversant complètement le point de vue à l'aide d'une modélisation MA en mettant en avant le comportement individuel, nous mettons en question la cohérence des deux niveaux de « compréhension » du système : normalement, la simulation des comportements individuels doit naturellement déboucher sur l'observation des bilans censés décrire la dynamique du système (voir *infra*).

1.2 Validation

La validation du modèle est basée sur une comparaison entre les observations et la dynamique de la simulation. Après modélisation du comportement des agents et de leurs interactions, on paramètre le système et on simule des situations expérimentales connues. En fonction du décalage entre l'observation et la simulation, on cale le modèle.

Une fois calé, on extrapole en faisant jouer des scénarii nouveaux en supposant que le comportement du simulateur demeure fidèle à la réalité.

1.3 Impact des SMA dans un domaine particulier

Du point de vue de la mise en place d'un modèle multi-agents, la modélisation est intuitivement assez facile à réaliser en comparaison avec une modélisation analytique ; elle ne demande pas une aptitude pour les mathématiques et leurs applications ; elle évite les problèmes liés à la résolution effective d'un système d'équations différentielles.

Comme on l'a déjà souligné plus haut, elle permet de simuler les lois comportementales observées et d'en vérifier leur cohérence par rapport aux modèles de bilans classiques. On renverse donc la perspective entre les données et les résultats.

L'approche permet d'intégrer des modèles du comportement de plusieurs types d'agents dans une même simulation et de tester la cohérence de ces modèles entre eux. Cette possibilité est très originale et permet de se rendre compte des incohérences entre des modèles décrivant des processus différents et interagissants.

L'aspect visualisation de la dynamique du système est également fondamentale à nos yeux. Par essence, une émergence ne peut être prédite ; il est donc important de disposer d'un outil permettant de la voir, donc de mieux comprendre le système étudié.

1.4 Principes généraux de notre modélisation

Dans le reste de cet article, nous décrivons la modélisation que nous avons mise en place dans le cadre d'une collaboration informatique/biologie marine. Nous utilisons une modélisation multi-agents pour tester une hypothèse proposée par les biologistes sur la modélisation du milieu marin et sa pertinence pour rendre compte du comportement du zoo-plancton. Les agents représentant les organismes zoo-planctoniques sont des agents situés, réactifs, et percevant leur environnement. Ainsi, le modèle de leur environnement et de leur voisinage n'est pas fourni aux agents ; au contraire, les agents le construisent à chaque instant via leurs « sens ». C'est pour nous très important de modéliser la perception des agents sous cette forme « réaliste ». La perception de l'agent peut varier en fonction de son état physiologique et de son environnement ; sa situation (spatiale, dans l'espace des états physiologique...) intervient dans la perception qu'il a de son milieu. Notons également que le fait que les agents soient réactifs n'impliquent pas qu'ils n'ont pas une certaine forme de mémoire. Le comportement passé d'un agent rétro-agît sur son comportement à venir ; le comportement d'un agent à un instant est donc influencé par son histoire, qui lui est, par nature, individuelle.

Après avoir décrit le problème et le système biologique, nous présentons la modélisation qui a été réalisée. Nous montrons les résultats obtenus qui viennent confirmer les hypothèses des biologistes. Ce travail remet en cause une bonne partie des modélisations réalisées à ce jour dans ce domaine, ce qu'une approche de type analytique n'a pas permis de réaliser. Enfin, nous discutons des suites et perspectives de ce travail.

2 Modélisation multi-agents en biologie marine

L'objectif de ce travail est d'identifier les règles comportementales du copépode (cf. Figure 1) et les influences de l'environnement sur son comportement : l'hypothèse est que le copépode a un comportement actif de recherche de nourriture (phytoplanctons). Pour cela, nous nous proposons de croiser l'observation sur le vivant, les résultats des modèles analytiques et la modélisation par agents. La distribution du phyto-plancton est fortement hétérogène dans le milieu. Les résultats actuels [1] montrent que cette hétérogénéité influe sur le bilan énergétique du copépode. En mesurant la quantité d'azote absorbée lors de la nutrition, les observations montrent que le rendement du comportement du copépode (énergie dépensée/énergie ingérée) varie en fonction du type de distribution de la nourriture [1,3]. Par exemple, un milieu perturbé, propice aux échanges, favorise le taux de rencontre du copépode avec les particules de phyto-plancton et donc augmente son rendement. Il reste maintenant à montrer l'influence du comportement du copépode dans de telles situations. L'étude de ce comportement est incompatible avec une approche analytique, comme nous allons le voir. Aussi, nous étudions une approche SMA [4].

2.1 Le système étudié

A l'heure actuelle, le copépode (cf. Figure 1), petit organisme marin appartenant à la famille des zoo-planctons, est représenté par des modèles de type « boîte noire » (cf. Figure 2) ou analytiques (cf. Figure 3). Ces modèles cherchent à décrire chaque processus intervenant dans la vie de l'organisme en identifiant des flux d'entrée, des flux de sortie et une fonction de transfert.

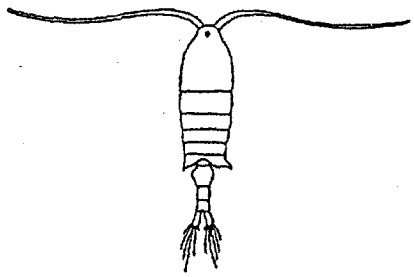

Figure 1. Copépode *Centropages hamatus*

Attardons nous sur le processus d'ingestion des proies dans le cas du phytoplancton (cf. Figure 2). Le copépode capture une proie (une particule de phytoplancton). Après un temps de manipulation, celle-ci est stockée dans l'estomac et entre dans le processus de digestion. L'estomac transforme son contenu soit en énergie utilisable (proies assimilées) que l'on exprime en azote, ou en déchets (pelotes fécales). Cette transformation est continue : à chaque Δt, une quantité Δq transite (cette quantité est proportionnelle à la quantité stockée dans l'estomac). L'énergie utilisable est soit consommée (métabolisme, digestion ou nage) soit stockée (pour la production d'œufs chez les femelles, par exemple). Quant aux déchets, ils sont éjectés.

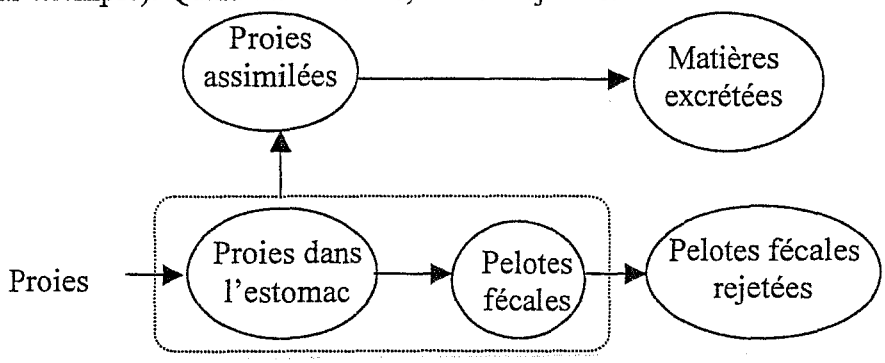

Figure 2. Modèle en boîte du processus d'ingestion

Il existe des modèles analytiques qui ont pour ambition de représenter, au mieux, les processus biologiques qui régissent les copépodes. [1] propose un modèle (cf. Figure 3) synthétisant les différents modèles développés jusqu'à présent. Il résume, à l'aide de cinq équations différentielles, l'activité de capture et de digestion.

$$\frac{dX_1}{dt} = I - A - F \qquad (1) \qquad \frac{dX_2}{dt} = A - \frac{C}{M_N} \qquad (2)$$

$$\frac{dX_3}{dt} = F - G \qquad (3) \qquad \frac{dX_4}{dt} = G \qquad (4)$$

$$\frac{dX_5}{dt} = C_{st} + C_{sda} + C_{sw} \qquad (5)$$

Figure 3. Modèle analytique du processus d'ingestion

X_1	Nombre de proies dans l'estomac
X_2	Nombre de proies assimilées
X_3	Nombre de pelotes fécales
X_4	Nombre de pelotes fécales évacuées
X_5	Energie dépensée exprimée en azote
I	Taux d'ingestion
A	Taux d'assimilation
F	Taux de formation de pelotes fécales
C	Energie dépensée par unité de temps
M_N	Masse en azote du copépode
G	Nombre de pelotes fécales évacuées par unité de temps
C_{st}	Energie dépensée pour le métabolisme par unité de temps
C_{sda}	Energie dépensée pour l'ingestion par unité de temps
C_{sw}	Energie dépensée pour le déplacement par unité de temps (nage + saut)

Table 1. Définition des variables et constantes du modèle analytique de la Figure 3

Prenons, à titre d'illustration, l'équation (1) qui décrit mathématique la variation du nombre de proies dans l'estomac de l'animal (X_1). Cette variable dépend de trois autres variables :

* le taux d'ingestion I qui mesure le nombre de proies rencontrées par le copépode en fonction de sa satiété[1] et du niveau de turbulence[2] du milieu,
* le taux d'assimilation A, proportion d'azote apporté par les proies qui devient utilisable,
* le taux de formation des pelotes fécales, proportion d'azote apporté par les proies qui n'est pas utilisé mais évacué en pelotes fécales.

Les deux dernières variables modélisent, *a priori* de manière correcte, la digestion. En revanche, la variable I est censée décrire le processus de capture du copépode en fonction de sa satiété et de l'environnement. A aucun moment, les équations mathématiques ne font mention du comportement du copépode. Pour s'en convaincre, développons un peu ce qui se cache sous I.

$$I = \left(\beta_{behaviour} + \beta_{turbulence}\right) N_p F_A$$

I est directement lié à la capacité de rencontre du copépode. Dans le modèle analytique proposé, cette capacité de rencontre est fonction de quatre paramètres :

* $\beta_{behaviour}$ la contribution du « comportement », celle-ci est fonction du rayon de perception du copépode, du rayon des proies et la différence de vitesse de nage entre le copépode et les proies,
* $\beta_{turbulence}$ la contribution de la turbulence,
* N_p la densité des proies dans le milieu,
* F_A une mesure de l'activité de nutrition dépendant de la quantité de nourriture dans l'estomac du copépode et, selon le mode de prédation (en suspension ou en embuscade), la densité des proies dans le milieu.

Ce modèle rend bien compte du processus de capture mis à part, de notre point de vue, la contribution du comportement. En effet, si l'on peut mettre en équation le fait que l'activité de nutrition du copépode est fonction de la densité des proies, du niveau de turbulence du milieu, du mode de prédation et de la quantité de nourriture dans l'estomac, il est, en revanche, délicat de

[1] Le niveau de satiété est proportionnelle à la quantité de nourriture contenue dans l'estomac. Plus l'estomac du copépode est plein, moins il cherche à capturer de nourriture.

[2] Plus le milieu est turbulent, plus la probabilité de rencontre entre le copépode et les cellules de phytoplancton est grande.

résumer le comportement par une relation qui fait seulement intervenir le rayon de perception, la taille des proies et la vitesse de nage du copépode relativement à celle de ses proies.

2.2 La modélisation multi-agents

Le système étudié est composé d'une masse d'eau (qui représente le milieu des autres agents) dans laquelle sont immergés des « patches[3] » de phytoplanctons et des copépodes. Chacun des agents est situé et possède ses propriétés parmi lesquelles son comportement. Les patches de phytoplanctons ont une certaine dimension et sont soumis aux courants et à la turbulence. Le copépode possède différentes caractéristiques (sa masse en azote, le volume de son estomac, sa vitesse de nage...). Son comportement, objet de l'étude pour le biologiste, est défini par un réseau de Pétri pour permettre la description de comportements sophistiqués avec un outil standard et simple. On se place dans une perspective d'agent réactif (cf. Figure 4) : l'état interne de l'agent et les stimuli auxquels il est sujet à un certain instant entraînent (de manière non nécessairement déterministe) un certain comportement et un nouvel état interne.

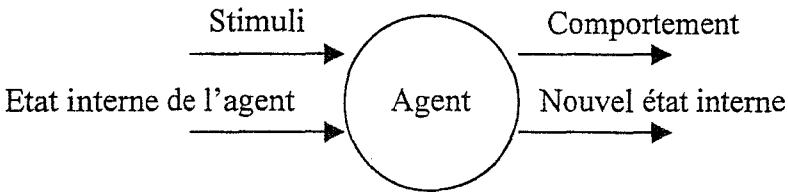

Figure 4. Agent réactif

2.2.1 *L'outil de modélisation*

Il existe une multitude d'outils de modélisation plus ou moins généraliste (Swarm [13], Manta [12]...). Dans la majorité des cas, ce sont des plates-formes soit adaptées à un ou à une famille de problèmes, soit génériques. A notre connaissance, la généricité entraîne, dans tous les cas, une dépendance vis à vis d'un environnement informatique ou d'un langage de développement mais surtout ces plates-formes sont à base de primitives réutilisables et il faut donc écrire du code ! Toutes ces raisons nous ont poussés à concevoir un nouvel outil de modélisation et de simulation d'agents réactifs, perceptifs et situés.

Nous utilisons un langage objet (Java) dans lequel nous retrouvons tous les concepts du paradigme objet ainsi qu'une arborescence de classes avancées (*thread*, *stream*...). Cette hiérarchisation des classes nous a permis de définir nos classes d'agents (cf. Figure 5). Dans un premier temps, ces classes d'agents ont été accessibles par un langage avec lequel on peut décrire une catégorie d'agents par l'intermédiaire de leur comportement, de leurs propriétés et de leurs moyens de communication. Un second langage rend possible la description de l'environnement. L'ensemble compose une plate-forme où l'on peut décrire les agents, les créer et les activer.

A l'heure actuelle, les deux langages sont partiellement[4] encapsulés dans une interface graphique écrite en Java (donc portable et accessible sur Internet) et accompagnés d'outils de définition de l'environnement, de représentation de déplacements d'agents situés et de tracé des variations des propriétés des agents.

Les familles d'agents

Notre approche repose sur quatre familles d'agents (cf. Figure 5). Les agents spatiaux sont les briques de base pour la construction de l'environnement en les juxtaposant et en les connectant.

[3] Agrégat

[4] Les actions sont toujours exprimées à l'aide de ce langage (cf. Figure 6 et Figure 9)

Selon le mode de connexion, il est possible de définir des environnements toriques ou bornés. Comme nous le verrons par la suite, l'interconnexion des agents spatiaux entre eux est aussi à la base des canaux de communication entre agents situés et spatiaux.

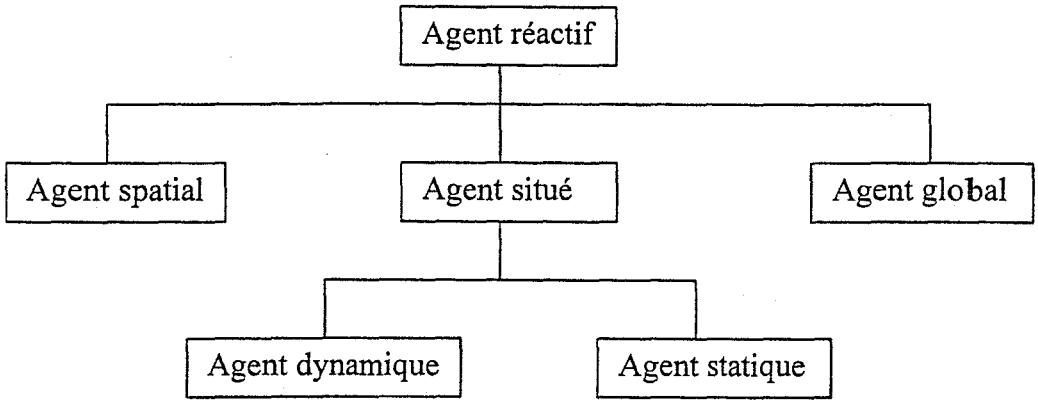

Figure 5. Hiérarchie des familles d'agents dans notre simulateur

Les agents situés constituent la deuxième grande famille. Un agent situé se trouve en relation avec un et un seul agent spatial. Cette relation permet de définir sa position dans l'espace. On distingue deux sous-familles : les agents dynamiques et les agents statiques. La différence fondamentale réside dans le fait que les agents dynamiques ont la faculté de se déplacer par leur propre initiative. En revanche, les agents statiques sont fixes ou peuvent être déplacés par d'autres agents.

Les agents globaux, comme leur nom l'indique, sont des entités communes à l'ensemble des autres agents. Tous les agents peuvent y faire référence.

Les états internes

Malgré leurs différences conceptuelles, tous les agents sont construits autour de l'idée d'agent réactif. Les états internes précisent des valeurs telles que masse en azote, volume de l'estomac, vitesse de nage, fréquence des sauts... , c'est-à-dire toute valeur caractéristique de l'agent susceptible d'intervenir dans son comportement. Ces valeurs sont strictement privées à l'agent et donc, lui seul, en fonction de ce qu'il perçoit et de son comportement, modifie ces valeurs. On peut imaginer, par exemple, qu'après l'absorption d'une cellule de phyto-plancton par un copépode, celui-ci augmente sa masse en azote d'une certaine quantité (une fois assimilée).

La dynamique

La dynamique, directement liée au comportement que l'on cherche à tester, fait appel aux réseaux de Pétri (cf. Figure 6). Celui-ci a pour objectif de modéliser les changements d'état. On retrouve dans cet outil mathématique les notions d'état (stable) ou de place et de transition. A un état (ou place) est associé un ensemble d'actions (déplacement, mise à jour de l'état interne, envoi de message...) réalisées lors de l'activation de cet état. L'état est activé à chaque réception de jetons. Une transition, quant à elle, marque le passage d'un état stable à un autre. Ce passage s'effectue si le nombre de jetons nécessaires est atteint dans les places amonts, si la condition associée à la transition est valide et après une durée de temporisation déterministe ou stochastique. En d'autres termes, pour qu'il y ait changement d'état, il faut que les conditions de franchissement de la transition soient validées et, après une certaine attente, le nouvel état stable est activé.

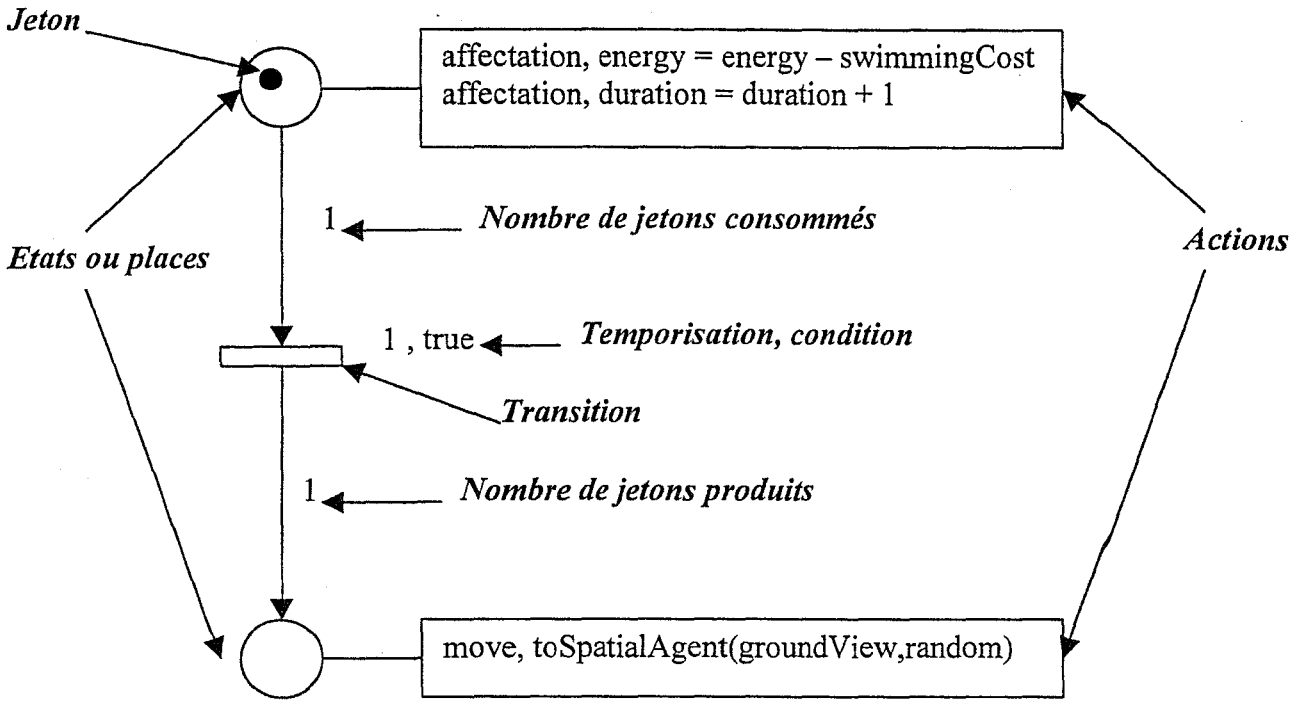

Figure 6. Réseau de Pétri temporisé modifié

L'introduction de durée de temporisation rend les modèles dépendant de la variable temps, si nécessaire. En effet, l'exécution des réseaux de Pétri temporisés construit dynamiquement un échéancier.

La perception

Par analogie avec les entités biologiques, tout agent est doué de sens plus ou moins développés. Dans notre modèle, un agent possède plusieurs sens et chacun d'eux est défini par trois paramètres : le type d'agents perçu, le secteur (selon l'orientation de l'agent) et la distance jusqu'à laquelle ces agents sont perçus. Par ce biais, on peut tester différents scénarii selon les perceptions possibles du copépode (par exemple, perception des cellules de phytoplancton situées dans un secteur de 90 degrés et à une distance inférieure à 1mm [2] – cf. Figure 7). De plus, un agent peut ne percevoir qu'une partie des caractéristiques d'un autre agent. On précise dans ce cas les caractéristiques perçues. Un agent peut aussi disposer de plusieurs sens. C'est lors d'actions que l'agent précisera le sens utilisé.

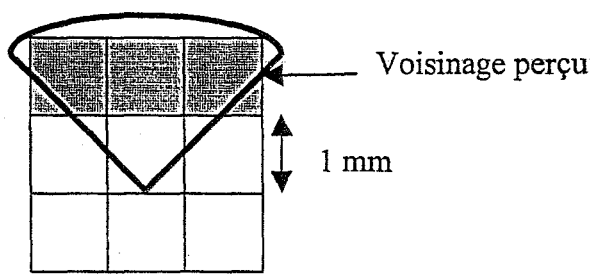

Figure 7. Distance de vision = 1 et secteur = 2

Les sens sont aussi, dans cette approche, à la base du réseau de connaissances des agents. Dynamiquement, l'agent construit son voisinage en fonction de sa position dans l'espace et de ses sens.

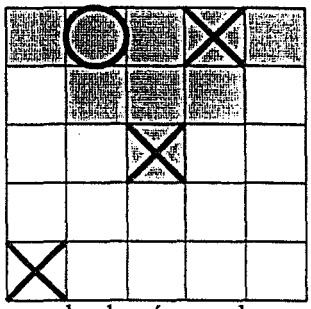

Figure 8. Exemple de réseau de connaissance par voisinage

A titre d'exemple (cf. Figure 8), considérons les agents « croix ». Ils perçoivent totalement leurs congénères et les agents spatiaux comme indiqué sur la Figure 8. Les cases grises représentent les agent spatiaux perçus (section de 90° et distance de 2). En revanche, les agents « croix » ne perçoivent pas les agents « rond ». Il en résulte que l'agent situé au centre de la grille ne perçoit qu'un seul agent (l'agent « croix » de la première ligne) et l'ensemble des agents spatiaux grisés.

Indirectement, les sens définissent aussi les possibilités de déplacement des agents dynamiques. Si l'environnement se compose de différents types d'agents spatiaux, l'un de ces agents peut ne pas être perçu par un agent dynamique. Prenons l'exemple d'un labyrinthe, il est composé de couloirs et de murs. Les agents qui se déplace dans ce labyrinthe ne peuvent pas se positionner sur les murs. On interdit donc la perception des murs par les agents mobiles. Lors d'une action de déplacement, l'agent va construire l'ensemble des futures positions possibles en fonction de ses perceptions et choisir parmi elles.

Les messages

La quatrième caractéristique concerne les communications entre agents. Les agents ont la possibilité d'envoyer des messages aux seuls agents qu'ils perçoivent. Ces messages se présentent sous la forme d'un vocabulaire que les agents peuvent émettre (ou non) et entendre (ou non) selon leur type. La réception d'un message par un agent le conduit à effectuer une ou plusieurs actions. Le mécanisme d'envoi de messages est le seul moyen pour un agent de modifier les caractéristiques d'un autre agent (à condition que celui-ci l'accepte). L'envoi d'un message est considéré comme une action au même titre qu'un déplacement. A titre d'exemple, la place n°3 de la Figure 9 contient un exemple d'envoi de message (*send,toSpatialAgentWhereIsIt(Init)*). Ce message est envoyé à l'agent spatial où l'agent expéditeur se situe ; il se nomme *Init* et ne possède pas de paramètres. Lorsque le message est reçu par l'agent spatial, destinataire du message, celui-ci effectuera les actions associées au message.

2.2.2 Le modèle

Nous sommes partis de l'hypothèse que le copépode adopte deux comportements distincts : une nage orientée à la recherche de nourriture et des sauts aléatoires. Ces comportements ont une influence directe sur le processus d'ingestion des cellule de phytoplancton. Nous allons donc nous intéresser exclusivement à ce processus et laisser de côté la partie digestion qui, néanmoins, n'est pas à négliger pour obtenir un modèle complet.

Généralités

Le système se compose de trois entités : la masse d'eau, les cellules de phytoplancton et les copépodes. Dans un premier temps, nous ne considérons qu'un seul copépode à la fois. La masse

d'eau constitue l'environnement (ou le milieu) dans lequel évolue les autres entités. La taille du copépode (1 mm) sert de longueur de base pour la discrétisation de ce milieu. Le milieu est considéré, pour l'instant, en deux dimensions et découpé en parcelles d'1 mm^2. Chaque parcelle est pris en charge par un agent spatial. Les cellules de phytoplancton sont très nombreuses (de 10 cellules par litre à 10^8 cellules par litre soit au maximum 10^4 cellules par parcelle). Il n'est donc pas raisonnable de modéliser chaque cellule par un agent. La solution retenue consiste à définir, au niveau des agents spatiaux, une propriété « Nombre de cellules ». On délègue la gestion de la nourriture aux agents spatiaux c'est-à-dire à l'environnement. Quant au copépode, il est représenté par un agent dynamique dont on va décrire la dynamique dans la partie suivante.

Le pas de temps de la simulation est noté u. t. Celui-ci est fixé par la durée correspondant au temps nécessaire à la plus petite action, c'est-à-dire la manipulation d'une cellule de phytoplancton par le copépode soit 1/20 s.

La dynamique du copépode.

Le réseau de Petri modélisant la dynamique de déplacement du copépode (cf. Figure 9) se divise en quatre parties :

* dès que l'on atteint la fin d'un cycle de 75 u. t.[5], le copépode effectue un saut sans considérer ce qu'il l'entoure[6] - **place n°3**,
* pendant 20 u. t. (le temps de traverser une parcelle du milieu), le copépode explore l'espace où il se trouve et si de la nourriture s'y trouve, il peut, à chaque unité de temps, capturer une cellule de phytoplancton – **place n°9**,
* en revanche, s'il n'y a pas de nourriture, il continue à nager pour atteindre la parcelle suivante –**place n°8**,
* au bout des 20 u. t. nécessaires à la traversée d'une parcelle, le copépode choisit une nouvelle parcelle à explorer et s'y rend – **place n°6**.

Intéressons-nous à la phase active de capture de nourriture. A l'exception des sauts aléatoires (place n°3), le copépode nage et parcourt une parcelle toutes les 20 u. t. Lorsqu'il a atteint ce délai, il change de parcelle (place n°6). Ce changement est fonction de la stratégie que l'on teste. Dans le cas de la Figure 9, la parcelle disposant de plus de nourriture aura plus de chance d'être choisie ce qui se traduit par l'instruction *move,toSpatialAgent(groundView,true,random(currentQuantity)*. Cette instruction fait partie de l'ensemble des actions disponibles et permet le déplacement d'un agent dynamique vers un des agents spatiaux perçu par un sens, ici *groundView*, et sélectionné par tirage aléatoire proportionnel à la valeur d'une variable (*currentQuantity*, dans notre cas).

Localement, le copépode capture les cellules de phytoplancton. S'il n'a pas encore tout consommé, on vérifie s'il a « envie » de manger (place n°7). En effet, nous avons vu que le copépode diminue la quantité de nourriture qu'il absorbe en fonction de son niveau de satiété, lui-même directement lié, pour l'instant, au nombre de cellules de phytoplancton présentes dans l'estomac. La fonction de satiété est la suivante :

$$C_g = 1 - \left(\frac{V_{proie} X_1}{\frac{2}{3} V_{estomac}} \right)^2$$

où $V_{proie}X_1$ présente le volume des proies non digérées et $V_{estomac}$ le volume de l'estomac du copépode.

Si le tirage aléatoire de la place n°7 est favorable alors il capture la cellule sinon cette cellule disparaît de son champ de vision.

[5] 75 u. t. est une valeur moyenne issue d'une campagne d'observations.

[6] pour l'instant, c'est l'hypothèse retenue car on ne sait absolument pas pourquoi il saute.

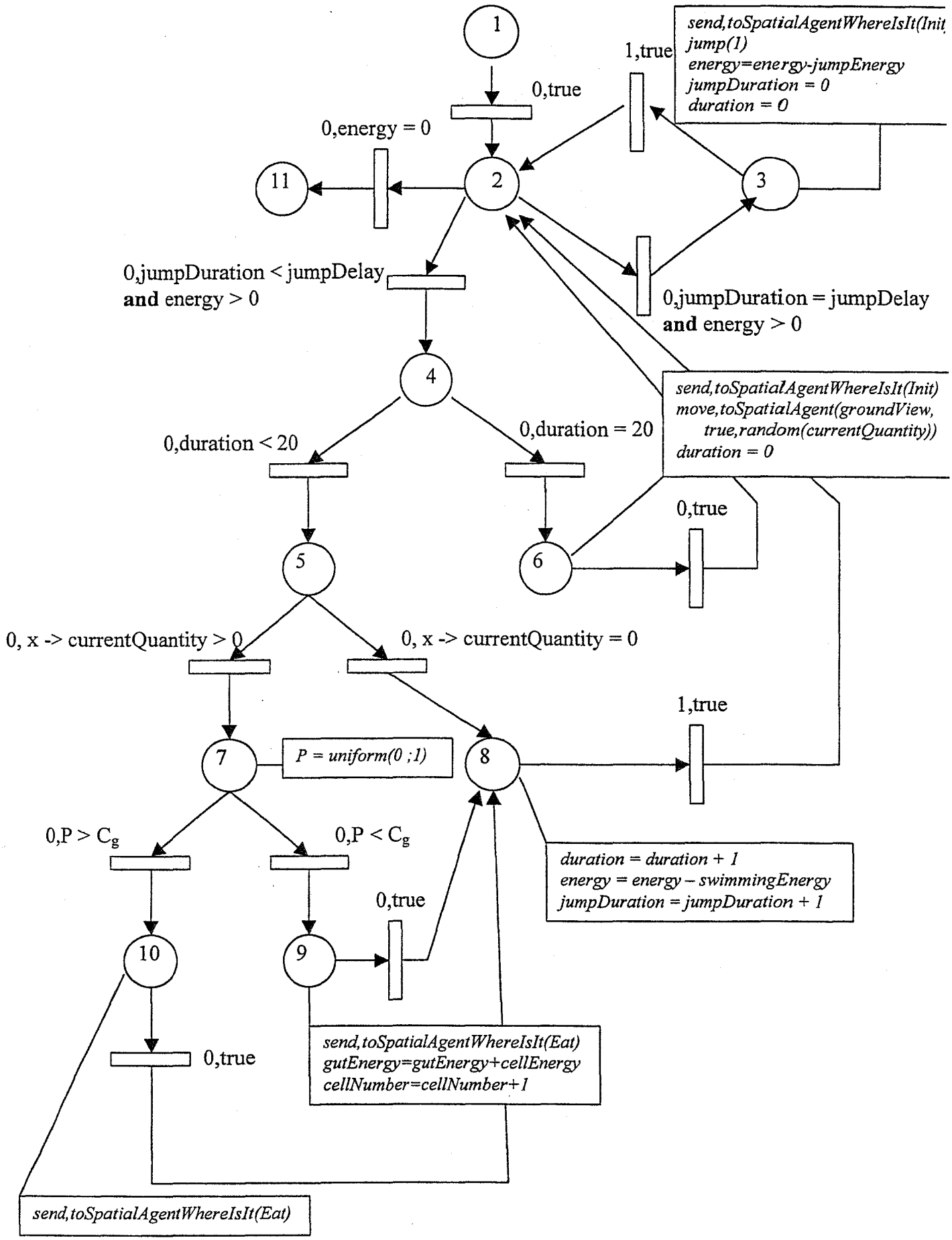

Figure 9. Dynamique de déplacement

Ce premier modèle est une traduction algorithmique du modèle analytique. On y retrouve des valeurs moyennes issues de bilans et des processus aléatoires, tel que celui de la satiété. La même remarque est valable pour la partie digestion. Le seul élément nouveau est la prise en compte du comportement au niveau de la nage. Il faut néanmoins souligné que la construction des agents est nettement plus simple et fait intervenir un nombre réduit de paramètres par rapport au modèle analytique.

Nous nous intéressons maintenant à décomposer les processus « énigmatiques », tels que les sauts aléatoires ou la vitesse de nage constante. Il est évident que derrière ces actions se cachent des règles de décision ou des processus plus complexes. Par exemple, l'observation montre que la vitesse de nage n'est pas constante et que ces variations sont dues à des interactions avec l'environnement. Il reste, aux biologistes, à les définir ou à les imaginer.

2.3 *Résultats expérimentaux*

Nous avons défini deux types de copépode en fonction de leur stratégie de nage : aléatoire ou orientée. L'environnement se compose d'une grille 2D de 2500 parcelles carrées (50x50). Chaque parcelle est un agent spatial et est connectée à ces 8 voisines. Les cellules de phytoplancton sont réparties soit par patches (cf. Figure 10 – tâches grises) soit uniformément. Dans les deux cas, la densité globale est identique (1 cellule par parcelle). Pour les patches, différentes densités sont utilisées (représentées par des niveaux de gris différents).

A l'aide des variables définies au niveau des agents *Copépode*, on mesure à chaque pas de la simulation : l'énergie, exprimée en pg[7] d'azote, contenue dans l'estomac (*gutEnergy*), l'énergie utilisable (*energy*), le nombre de cellules de phytoplancton capturées (*cellNumber*) et quatre variables du modèle analytique (X_3, X_4, T_g et C_a).

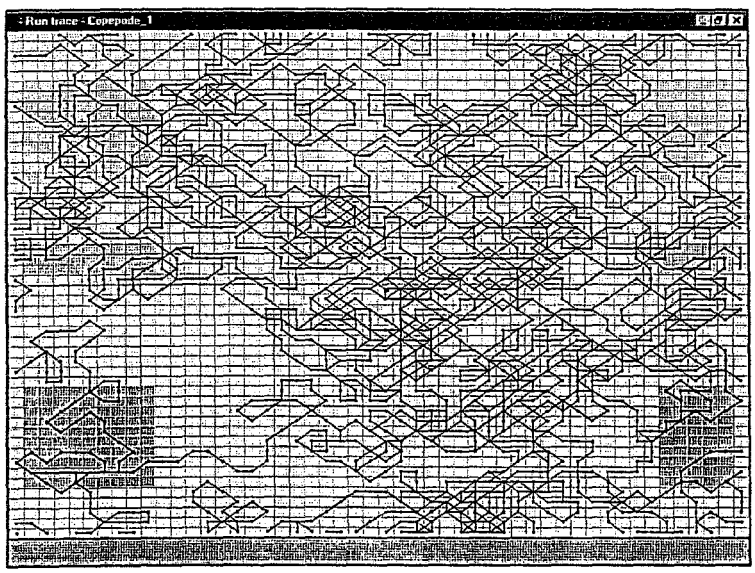

Figure 10. Trajectoire du copépode (nage aléatoire)

Nous disposons d'un outil de visualisation de trajectoire. Il permet de tracer le chemin parcouru par un agent situé durant la simulation. En superposant la trajectoire du copépode étudié et la distribution des cellules de phytoplancton, on montre que dans le cas d'une distribution des cellules

[7] picogramme

de phytoplancton par patch, la stratégie de la nage orientée est plus efficace. La Figure 11 est là pour en témoigner.

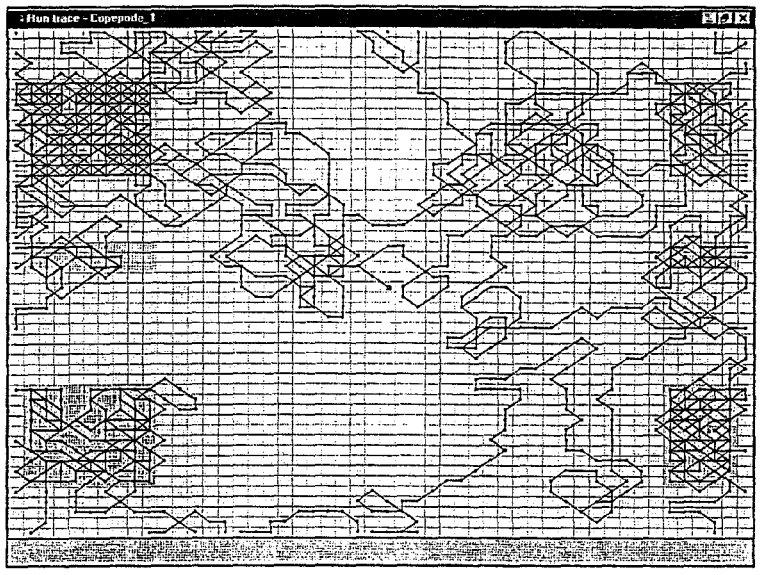

Figure 11. Trajectoire du copépode (nage orientée)

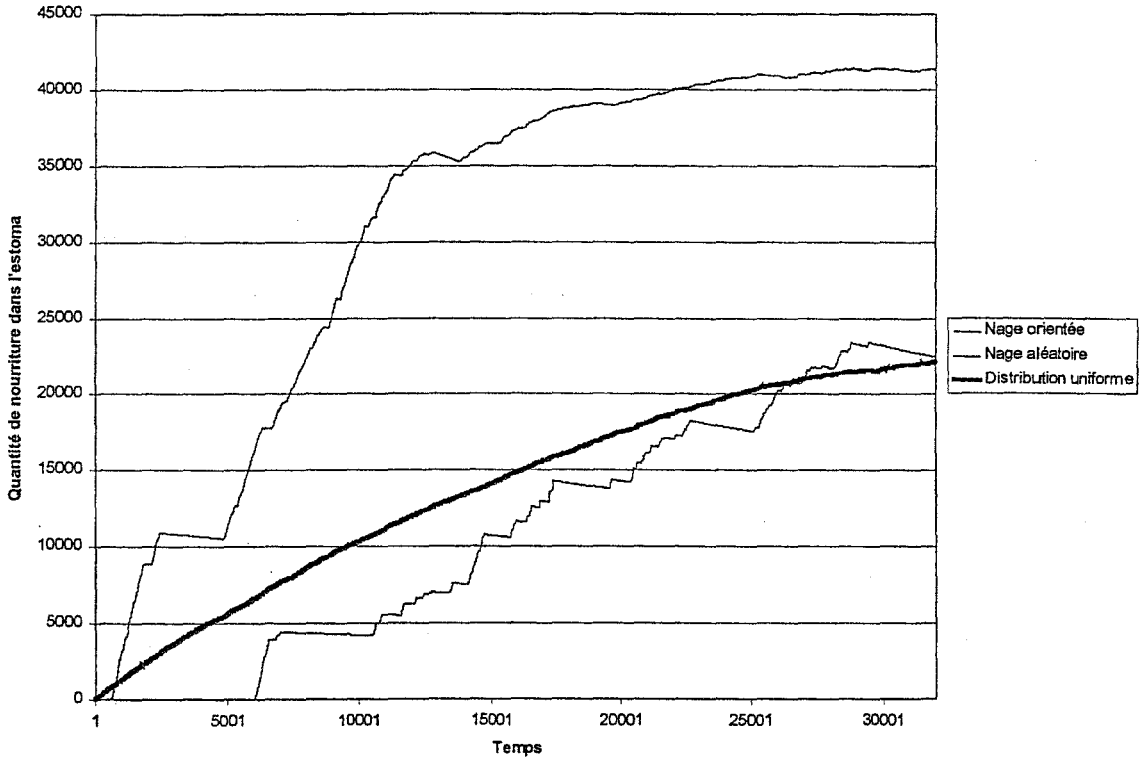

Figure 12. Quantité de nourriture (en pg d'azote) dans l'estomac du copépode en fonction du temps

Si on superpose les courbes représentant la quantité de nourriture dans l'estomac du copépode en fonction du temps et selon la distribution des cellules de phytoplancton et la stratégie de nage, il apparaît très rapidement que la nage orientée est favorable à l'alimentation du copépode du point de vue énergétique.

Si le copépode est plongé dans un champ homogène, la stratégie de nage n'a aucune influence sur l'alimentation puisqu'il trouvera de la nourriture dans toutes les directions en même quantité. En revanche, dans un champ hétérogène, la stratégie aléatoire conduit le copépode à tomber par hasard

sur un patch de cellules de phytoplancton et surtout d'en sortir sans chercher à en profiter. Donc cette stratégie est moins efficace.

En conclusion, on retrouve les principaux résultats énoncés dans [1] pour une configuration de champ uniforme et de nage aléatoire. Il reste à effectuer des comparaisons avec des résultats d'expériences *in vivo* mais qui restent pour l'instant difficile à réaliser. Les seuls points de comparaison possible concerne l'aspect des trajectoires selon la densité de nourriture (cf. [3]).

3 Discussion

Nous avons présenté la démarche et les premiers résultats d'un travail reposant sur une collaboration informatique/biologie qui a pour objectif d'étudier le comportement d'un organisme zoo-planctonique, le copépode. Nos résultats sur un champ de phytoplanctons hétérogène sont les premiers obtenus. Ils montrent clairement la différence par rapport au champ uniforme, qui aura des conséquences importantes sur le comportement, donc sur la dynamique de l'écosystème marin. En effet, si le phytoplancton est distribué de manière hétérogène, le copépode a un comportement qui tend à les concentrer dans des zones où le phytoplancton se trouve. Le copépode étant lui-même la nourriture de certains poissons, ceux-ci auraient à leur tour une répartition différente dans les eaux...

Ce travail réalisé, de nombreuses voies de poursuite sont possibles. Tout d'abord, le passage à un système 3D est envisagé. Ce passage du 2D au 3D ne devrait pas remettre en cause les conclusions de ce travail au niveau biologie. Par contre, pour l'informaticien, le passage à la troisième dimension soulève des problèmes en terme de charge de calcul. Ce problème lié au nombre d'objets et au nombre d'interactions à simuler est plus général que celui du passage au 3D ; c'est un problème que l'on rencontre partout, dès que le système est un peu compliqué. Nous travaillons actuellement sur l'agrégation d'agents pour faire face à ce problème.

Les temps de calcul sont également dus au fait que la plate-forme a été développée en Java pour permettre, notamment, une compatibilité avec Internet. Par ailleurs, le développement d'une application à l'aide d'agents « propres » peut entraîner des surcharges de traitements.

Ce travail conceptuel et cette plate-forme sont actuellement en cours de réutilisation dans le cadre d'une collaboration avec un laboratoire de géologie où l'aspect laboratoire virtuel séduit également beaucoup les chercheurs.

L'utilisation d'un modèle multi-agents nous semble être indispensable pour autoriser l'étude fine d'un comportement, ce qu'un modèle analytique ne nous aurait pas permis.

Au niveau méthodologique de modélisation, nous avons dû étudier le passage d'un modèle reposant sur des bilans à un modèle orienté individu ; nous retrouvons le même type de changement de paradigme dans notre travail avec des géologues. Les variables habituellement manipulées dans les modèles dans ces sciences sont en effet collectives, émergeantes de l'activité des individus. Nous pensons que l'approche multi-agents oblige à se concentrer sur les « vraies » questions. Dans le travail décrit ici, le comportement en moyenne d'un copépode n'a aucun sens : le copépode n'a jamais ce fameux comportement moyen, et ce lissage masque les véritables comportements, altérant finalement l'étude du système en se concentrant sur de faux problèmes et en ignorant les bonnes questions.

4 Références

1. Caparroy P. et Carlotti F., *A model for Acartia tonsa : effect of turbulence and consequences for the related physiological processes*, Journal of Plankton Research, vol. 18, n° 11, pp. 2139-2177, 1996

2. Tiselius P. et Jonsson P. R., *Foraging behaviour of six calanoid copepods : observations and hydrodynamic analysis*, Marine ecology progress series, vol. 66, pp. 23-33, 1990
3. Bundy M. H., Gross T. F., Coughlin D. J. et Strickler J. R., *Quantifying copepod searching efficiency using swimming pattern and perceptive ability*, Bulletin of Marine Science, vol 53, n°1, pp. 15-28, 1993
4. Ferber J., *Les systèmes multi-agents, vers une intelligence collective*, InterEditions, 1995
5. Pavé A., *Modélisation en biologie et en écologie*, ed. Aléas, 559 p., 1994
6. Cambier Ch., *Simdelta --- Un système multi-agents pour simuler la pêche sur le delta central du Niger*, Thèse de doctorat, Université de Paris 6, 1994
7. Cambier Ch., Perrier E., Treuil J-P. et Preux Ph., *Action physique et géométrique, Contribution à une réflexion sur l'utilisation des processus physiques, Application RIVAGE*, poster, 5ième JFIADSMA, avril 1997
8. Marcenac P., *Modélisation et simulation par agents --- Application aux systèmes complexes*, mémoire d'habilitation à diriger des recherches, Université de la Réunion, 1997
9. Marcenac P., *Modélisation de systèmes complexes par agents*, Techniques et Sciences Informatiques, TSI, vol. 16, n°8, pp. 1013-1037, octobre 1997
10. Perrier E., Cambier Ch., *Une approche multi-agents pour simuler les interactions entre des acteurs hétérogènes de l'infiltration et du ruissellement d'eau sur une surface de sol*, Journées CNRS « Tendances nouvelles en modélisation pour l'environnement » du programme environnement, vie et sociétés, janvier 1997
11. Treuil J-P., Perrier E., Cambier Ch., *Directions pour une approche multi-agents de la simulation de processus physiques spatialisés*, 5ième JFIADSMA, avril 1997
12. Drogoul A. et Ferber J., *Multi-Agent Simulation as a Tool for Modeling Societies: Application to Social Differentiation in Ant Colonies*, Actes du Workshop MAAMAW'92, Viterbo, 1992
13. Minar N., Burkhart R., Langton C. et Askenazi M., *The SWARM simulation system : a toolkit for building multi-agent simulations*, 1996

A10

Do small-scale nutrient patches exist in tidally mixed coastal waters?

Seuront L, Gentilhomme V & Lagadeuc Y

Limnology and Oceanography (révisé)

Do small-scale nutrient patches exist in tidally mixed coastal waters?

Laurent Seuront, Valérie Gentilhomme and Yvan Lagadeuc

Station Marine de Wimereux, CNRS-UPRESA 8013 ELICO, Université des Sciences et Technologies de Lille, BP 80, 62930 Wimereux, France

Acknowledgements

We acknowledge the captain and the crew of the NO 'Côte d'Aquitaine' for their cooperation, N. Esquerre for her help in the data processing and measuring out of nitrite and nitrate concentrations, D. Hilde for the extraction of chlorophyll *a*, as well as N. Jobert, and B. Vignolle for excellent assistance during the cruise. We enjoyed conversation with F. Schmitt and acknowledge his helpful advice on multifractals. We also thank the two anonymous reviewers for their critical reviews of the manuscript.

Abstract

In the Eastern English Channel, characterized by its megatidal regime and the resulting very high hydrodynamic conditions, recent studies have demonstrated—on the basis of innovative statistical analyses in marine ecology—that phytoplankton biomass but also purely passive scalars such as temperature were heterogeneously distributed at small-scale, though basically regarded as homogenized by turbulent fluid motions. Thus, we extended these concepts to dissolved nitrogen (NO_2^-), and we first demonstrated the validity of our high resolution (3-sec temporal resolution) procedure of continuously measuring nitrite concentration. Second, we described how these time series recorded at different times of four tidal cycles can be characterized as heterogeneously distributed using fractal and multifractal parameters, and then can be described in terms of small-scale patches. Moreover, these parameters showed very specific temporal patterns revealing the absence of density-dependence of nitrite distribution. In contrast, nitrite distributions clearly appeared to be less heterogeneously distributed in higher hydrodynamic conditions, suggesting a physical control of small-scale nutrient patchiness. Nevertheless, taking into account the differential structure of nitrite distributions between high and low hydrodynamic conditions, we suggested that the observed small-scale nutrient patches could also be the results of complex interactions between hydrodynamic conditions, biological processes related to phytoplankton and bacterial populations.

The ecological importance of space-time heterogeneity in phytoplankton populations has been pointed out by several authors (e.g. Hutchinson 1961; Margalef 1967, 1976; Platt 1975) and widely investigated both in marine and freshwater ecology (e.g. Platt 1972; Powell et al. 1975; Abbott et al. 1982; Weber et al. 1986; Denman and Abbott 1994). However, in spite of the intensive investigations conducted on the nutrient dependence of phytoplankton growth (Jickells 1998; McCarthy et al. 1998) that provided direct evidence for nutrient control of photosynthesis in the ocean (Platt et al. 1992; Falkowski et al. 1998), studies concerning the small-scale heterogeneity of nutrients were still scarce (Estrada and Wagensberg 1977; Steele and Henderson 1979).

The small-scale distribution of nutrient in the sea is nevertheless a particular salient issue in marine ecology. Indeed, if small-scale heterogeneity in the distribution of nutrients was really more prevalent than previously thought, for instance, new production by phytoplankton might have been biased in many environments, especially at the continental margins of the ocean where spatio-temporal variability of both physical and biological processes is usually very developed (see e.g. Mackas et al. 1985, and references therein). Moreover, while large scale studies can provide informations on population dynamics and regional and global scale estimates of primary production (e.g. Longhurst et al. 1995), and micro-scale data (i.e. 10^{-2}-1m) might reveal details of nutrient uptake (Lehman and Scavia 1984; Currie 1984), small-scale studies (i.e. 1-10^3 m, Mackas et al. 1985) could bridge the gap and provide a better understanding of general behavior. The scarcity of studies in this range of scales is, to our knowledge, actually evident, especially when hydrodynamic conditions—basically regarded as a great factor of homogenization—are high.

In the Eastern English Channel and the Southern Bight of the North Sea, characterized by their megatidal regime and the resulting very high hydrodynamic conditions, recent studies have nevertheless shown that phytoplankton biomass was not randomly, nor homogeneously distributed but rather exhibited a very structured small-scale patchy distribution similar to the one of purely passive scalars such as temperature and salinity (Seuront et al. 1996*a* , *b*, 1999). The question is then now to know whether dissolved nitrogen exhibits a structured distribution purely driven by physical forcings (i.e. similar to the one observed in the case of temperature, salinity and phytoplankton biomass) or whether exhibits another kind of distribution, suggesting an altogether level of complexity in the structuration of nutrient variability. Indeed, while some studies have been dedicated to spatio-temporal distributions of phyto- and zooplankton (Brylinski et al. 1984, 1988; Quisthoudt 1987; Brunet et al. 1993; Seuront et al. 1996*a*, *b*; Seuront and Lagadeuc 1998), results concerning the spatio-temporal distribution of

nutrient are still scarce in this area (Bentley et al. 1993; Gentilhomme and Lizon 1998), especially on smaller scales.

However, such studies still raise many unresolved difficulties, all the more because of both technical and statistical limitations. Small-scale patches with elevated nitrogen content then cannot be observed with present day techniques, the faster response nutrient analyzer allowing, to our knowledge, only a 2-mn temporal resolution (Sakamoto et al. 1996) and was still insufficient to work in the coastal ocean where spatio-temporal variability is high relative to the open ocean (Mackas et al. 1985). Previous statistical study of plankton patchiness, mainly based on spectral analysis (see e.g. Platt and Denman 1975; Fasham 1978), have allowed inferences to be made as to when biological processes are likely to be a significant contributor of phytoplankton spatial structure, at spatial scales ranging from tens of meters to tens of kilometers. However, while able to quantify the variance as a function of both spatial and temporal scales, these techniques were able to reveal little concerning both the precise variability associated with those scales and the mechanism of the physical-biological interactions, particularly at small scales (i.e. meters, and seconds), as this is in the range where physical forces obviously dominate biological processes (e.g. Seuront et al. 1996*a*, *b*, 1999). Herein the goal of this paper is: (i) to demonstrate the validity of a high resolution (i.e. a 3-sec temporal resolution) dissolved nitrogen analysis technique; (ii) to show how high resolution nitrogen time series can be wholly characterized in terms of structured variability in the powerful frame of fractal and multifractal analyses; and (iii) how the organization of this structured variability can be regarded as being mainly dependent of hydrodynamic conditions.

Materials and methods

Sampling experiment—Sampling was conducted during 48 h (ca. four tidal cycles) in a period of spring tide, from 2 to 4 April 1996, at an anchor station (Fig. 1) located in the coastal waters (i.e. the "Coastal Flow"; Brylinski et al. 1991) of the Eastern English Channel (50°47'300 N, 1°33'500 E). Measurements of physical parameters (temperature and salinity) and *in vivo* fluorescence were taken every hour from the surface to the bottom with a SBE 25 Sealogger CTD and a Sea Tech fluorometer, respectively. Every 5 minutes, current speed and direction were measured at 3, 6 and 9 m with Anderra current meters. Every hour, wind data were collected with the on board anemometer. Every 2 h, water samples were taken at 2, 6, 10 and 16 m, using Niskin bottles. Dissolved inorganic nitrogen concentrations (5 ml frozen samples, analyzed using a Technicon autoanalyzer II; Treguer and Le Corre 1971) and chlorophyll *a* concentrations (1 l filtered frozen samples, extracted with 90% acetone, assayed

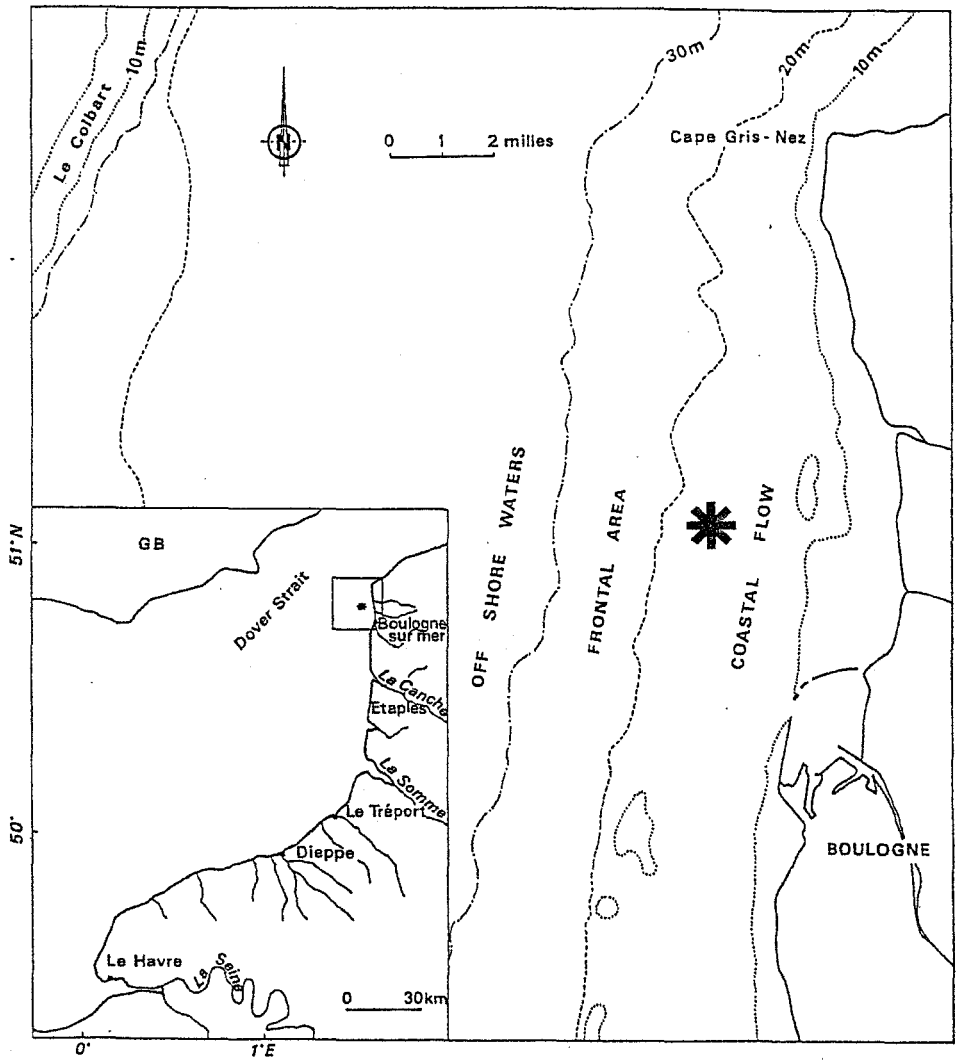

Fig. 1. Study area and location of the sampling station (*) along the French coast of the Eastern English Channel.

in a spectrophotometer and the chlorophyll *a* concentration calculated following Strickland and Parson 1972) were estimated for each sampled depth.

High resolution nitrogen sampling design—We focused on nitrite (NO_2^-) rather than nitrate (NO_3^-) or ammonium (NH_4^+) concentration for both conceptual and technical reasons. Nitrite is indeed the nutrient which is *a priori* the most conservative, and then could be expected to behave as a purely passive scalar. In that way, one may hope that the observed variability would be little or none aliased by biological processes such as phytoplankton uptake and release as nitrate and ammonium can be. Moreover, nitrite also allows a higher temporal resolution—and then more direct comparisons with the 0.5-sec resolution reached by Seuront et al. (1996*a*, *b*, 1999)—than nitrate because of the substantial smoothing introduced by the reduction process associated with nitrate quantity determination (see Treguer and Le Corre 1971 for further details).

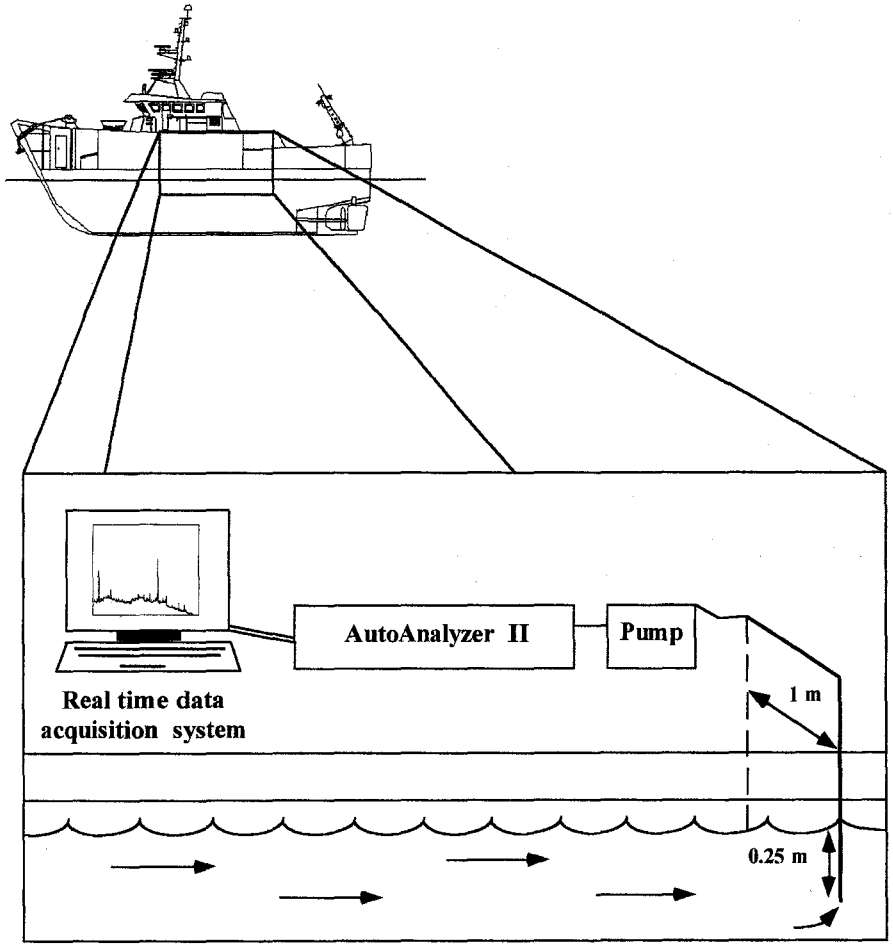

Fig. 2. Side view shematic diagram of the experimental set-up used to continuously sample subsurface water.

In order to continuously investigate the small-scale distribution of nitrite (NO_2^-) water was continuously taken from a depth of 0.25 m through a sea-water intake mounted on a suspended hose at 1m of the hull of the vessel, and directly brought through a Technicon autoanalyzer II (Treguer and Le Corre 1971) by means of a railwheel pump with an approximate output of 0.80 $ml.mn^{-1}$, connected to 1.5 mm diameter plastic tubing (Fig. 2). The temporal resolution (i.e. 3-sec) has been chosen as the minimum time interval allowed by the Technicon autoanalyzer II between two nitrite quantity determinations. One may note here that such an approach, while suggested by Treguer and Le Corre (1971) has, to our knowledge, never been used in that way except by Estrada and Wagensberg (1977) but with a lower temporal resolution (1 minute) and an important smoothing of the output signal associated with the dimension of the pumping apparatus.

In more practical terms, the Reynolds number associated with our pumping apparatus was very low (i.e. Re ~ 18.75), indicates that no turbulent processes occur during the pumping in the plastic tubing. We then subsequently estimated the characteristic length scale, L, covered by the nitrite molecules because of molecular diffusion occurring in the plastic tubing during

pumping following $L = \sqrt{D.t}$ (Mann and Lazier 1991), where D is the molecular diffusion ($D = 10^{-9}$ $m^2.s^{-1}$) and t the diffusion time scale (i.e. the time taken by the water to be brought through the Technicon autoanalyzer II; $t = 20$ min). This led to a characteristic diffusion length scale $L = 10^{-3}$ m which is about five orders of magnitude lower than the intersample bubbling used by the a Technicon autoanalyzer II. We can then state that our pumping apparatus cannot be responsible for any aliasing associating with turbulent nor molecular diffusion. Finally, our sampling cannot be aliased by the boundary layer occurring around the hull of the vessel because of the 1-m distance chosen for our sea water intake. Indeed, the thickness of a boundary layer, δ, increases with increasing distance from the leading edge (i.e. the ship prow) according to $\delta = (x\nu / u)^{1/2}$ (Prandtl 1969), where x (m) is the distance from the leading edge (i.e. the distance from the ship prow) where water has been continuously taken (i.e. $x = 15$ m), ν the kinematic viscosity (10^{-6} $m^2.s^{-1}$) and u ($m.s^{-1}$) the free-stream velocity. We then estimated δ for the range of free-stream velocity (i.e. 10-104 $cm.s^{-1}$) experienced during the sea water pumping experiment as being in the range 0.40-1.20 cm. The potential influence of such minute boundary layer thickness in the temporal patterns in the nitrite measurements can then be obviously neglected in the present case.

We then recorded 11 time series of nitrite concentrations of approximately one hour duration at a sampling frequency of 0.33 Hz; data were directly recorded on a PC by means of a data logger system interfaced with the Technicon autoanalyzer II. Between each time series, the whole plastic tubing was rinsed with HCl 10%, Milli-Q water and the Technicon autoanalyzer II was calibrated using a standardized nitrogen solution.

Data analysis—The dynamic stability of the water column was calculated using the total shear squared (Lizon et al. 1995):

$$S^2 = (\Delta u / \Delta z)^2 + (\Delta v / \Delta z)^2 \quad (1)$$

where Δz is depth variation, Δu and Δv are variations in the speed of the two orthogonal components u (cross-channel) and v (along-channel). One may note here that the vertical stability of the water column cannot be estimated by the Richardson number (Ri), or static stability (N^2), when there is no vertical gradient of density.

The dissipation rate of turbulent energy induced by tide ε_t ($m^2.s^{-3}$) was calculated following MacKenzie and Leggett (1993):

$$\varepsilon_t = \phi u^3 / h \quad (2)$$

where ϕ, u and h are the fraction of the tidal energy which is used for vertical mixing ($\phi = 0.006$, Bowers and Simpson 1987), the M_2 depth-averaged tidal velocity ($m.s^{-1}$) and the water column height (m), respectively. Values of ε_t exceeding 2.4×10^{-5} $m^2.s^{-3}$ (i.e. values of $(u^3 / h) > 0.004$ $m^2.s^{-3}$) are typical of tidally mixed area (MacKenzie and Leggett 1991).

The effect of wind events being of main interest in structuring the whole water column (Raby et al. 1994; Lagadeuc et al. 1997; Seuront and Lagadeuc 1997), we especially focused on the relative effects of dissipation rates of turbulent energy induced by wind on the sub-surface small-scale distribution of nitrite. Thus, we estimated the dissipation rates of wind-generated turbulent kinetic energy ε_w ($m^2.s^{-3}$) using the formulation of the boundary layer model used by MacKenzie and Leggett (1991) as:

$$\varepsilon_w = (5.82 \times 10^{-9}) W^3 / z \tag{3}$$

where W and z are the wind speed ($m.s^{-1}$) and the sampling depth (m), respectively.

Fractal and multifractal analyses—In this study we have used two related but conceptually different analysis methods to investigate the temporal structuration of nitrite concentrations. The first method is based on a monodimensional fractal approach, thus assuming that the process can be described by a single fractal dimension, D. In general, fractal dimensions (Mandelbrot 1977, 1983) characterize patterns remaining similar upon subdivision in time, i.e. at each scale, the pattern differs but always shows the same relative variability. A fractal dimension may then be interpreted as a characteristic degree of heterogeneity of the series, independent of scale, arising from underlying properties of a given process and characterizing the distribution of the variability. Thus the dimension of a nitrite time series would be a characteristic value of the heterogeneity of the nitrite distribution at all scales within the series, originating from the nitrite generating mechanisms (Seuront and Lagadeuc 1997, 1998). Assuming that a process can be described by a single fractal dimension D allows one to use power spectral analysis, a widely used method in ecology to separates and measures the amount of variability (i.e. the variance, S^2) occurring at different frequencies (Platt and Denman 1975; Fasham 1978). When all or parts of the spectrum $E(f)$ obeys a power-law form:

$$E(f) \approx f^{-\beta} \tag{4}$$

where f is frequency, this indicates absence of characteristic time-scale in the range of the power law, i.e. a scaling behavior. Thus fluctuations at all scales within the range are related to

each other by the same scale-dependent relationship. The power law form will manifests itself as an approximately straight-lined behavior of the power spectrum when plotted in a double-logarithmic diagram. For time series, the exponent β and the fractal dimension D are related according to (Feder 1988; Schroeder 1991):

$$D = d + 1 - (\beta - 1)/2 \tag{5}$$

where d is the Euclidean dimension of the observation space ($d = 1$ for time series). For time series, the fractal dimension D takes values between 1 and 2. A low D value means that the heterogeneity is high (strong autocorrelation both in weak and high values of h) and there may be dominant long-range effects, while high D value indicates that the variable is randomly distributed in time (weak or not autocorrelation) and that only weak short-range effects exit (see e.g. Seuront and Lagadeuc (1997) for further details). In this paper, the fractal dimension is regarded as a measure of the degree of temporal dependence of a variable. So the relation of D to the sampling scale indicates the trend of the temporal structure of the variable.

The second method employed is related to the recently developed universal multifractal framework (Schertzer and Lovejoy 1987), which is based on a multidimensional fractal approach, i.e. that the variability of the distribution at different scales is connected through a dimension function instead of one single dimension. Indeed, contrary to the previously described monodimensional approach, based on a power spectrum (i.e. a second order moment characterizing a 'mean' variability), the multidimensional approach leads to consider the variability of a given process as a hierarchy of sets characterized by different intensity levels, each with its own fractal dimension. Multifractal models then require an infinite number of parameters for their specification. However, Schertzer and Lovejoy (1987) showed that multifractals processes generally lead to universal multifractal characterized by only three fundamental parameters. Their so called universal properties arise in part from the generalized central limit theorem that applies to stable distribution (Feller 1971; Schertzer and Lovejoy 1987; Samorodnitsky and Taqqu 1993). Concepts of universal multifractals may be presented in different ways. In this communication, we will use the so-called structure functions—recently successfully applied to the small-scale distribution of temperature, salinity and phytoplankton biomass (Seuront et al. 1996*a*, *b*, 1999)—which can be regarded as a generalization in the real domain of the power spectrum (i.e. a second order moment proportional to the square of the amplitude of a given frequency fluctuations). For time series of a given quantity Q, q^{th} order structure function can be defined as:

$$<(\Delta Q(\tau))^q> = <|Q(t+\tau) - Q(t)|^q> \tag{6}$$

where <.> indicates statistical averaging and $(\Delta Q(\tau))^q$ is the statistical moments of the fluctuations of the quantity Q at scale τ. For scaling processes, the scale invariant structure functions exponents $\zeta(q)$ which characterize all the statistics is defined as:

$$< (\Delta Q(\tau))^q > \approx \tau^{\zeta(q)} \tag{7}$$

The scaling exponent $\zeta(q)$ is then estimated by the slope of the linear trends of $< (\Delta Q(\tau))^q >$ vs. τ in a log-log plot. The first moment gives the scaling exponent $H = \zeta(1)$ corresponding to the scale dependency of the average absolute fluctuations: indeed, if $H \neq 0$ the latter will depend on the time scale τ, it therefore characterizes the degree of nonconservation (i.e. nonstationarity) of the process. The second moment is linked to the power spectrum scaling exponent by $\beta = 1 + \zeta(2)$. For simple scaling (monofractal) processes, the scaling exponent of the structure function $\zeta(q)$ is linear ($\zeta(q) = q/2$ for Brownian motion and $\zeta(q) = q/3$ for Obukhov-Corrsin homogeneous turbulence). For multifractal processes, this function is nonlinear and concave.

Theoretically, the function $\zeta(q)$ could depend on a very large number of parameters, therefore a very large number of its estimates for different values of q would be necessary. However, in the framework of universal multifractals (Schertzer and Lovejoy 1987) $\zeta(q)$ can be determined by only 3 parameters as:

$$\zeta(q) = qH - \frac{C_1}{\alpha - 1}(q^\alpha - q) \tag{8}$$

C_1 is the codimension that characterizes the sparseness (i.e. heterogeneity) of the process, and satisfies $0 \leq C_1 \leq d$ (d is the Euclidean dimension of the observation space, $d = 1$ for time series): $C_1 = 0$ for a homogeneous process and C_1 is all the more high as the process is sparse, indicating that the field values corresponding to any given level of variability are more scarce. The Lévy index α is the degree of multifractality, bounded between $\alpha = 0$ and $\alpha = 2$ corresponding to the monofractal case and to the maximum, or log-normal, multifractal case, respectively. In other words, the second term of Eq. 8 expresses the multifractal deviation from monofractality, in which case $\zeta(q) = qH$. The distance between monofractality and multifractality is then of function of α and C_1. The knowledge of these parameters is enough to characterize all the statistics of the field. C_1 is given by:

$$\zeta'(1) = H - C_1 \tag{9}$$

and α is estimated as the best non-linear fit of Eq. 8, for values between 0 and 2, using a simplex procedure (O'Neill 1971). More details on the universal multifractal theoretical

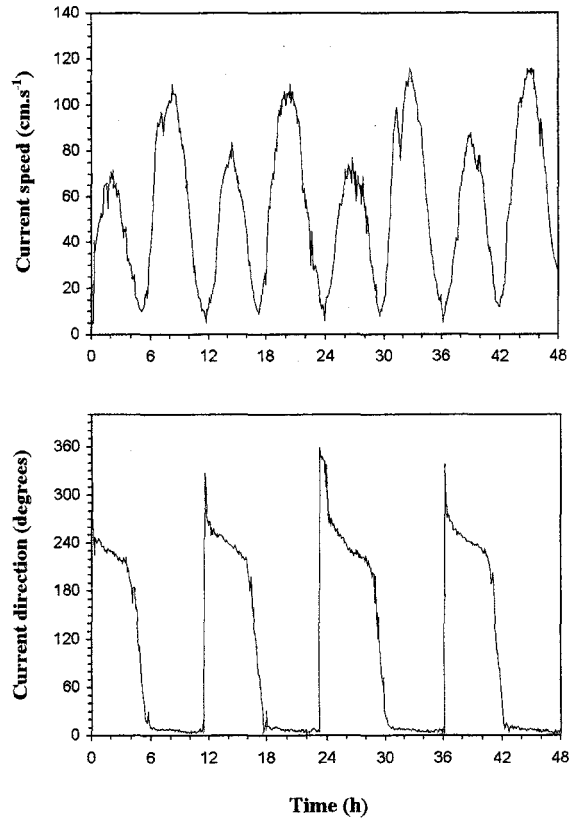

Fig. 3. Time series of current velocity (A) and direction (B) at 3 m depth.

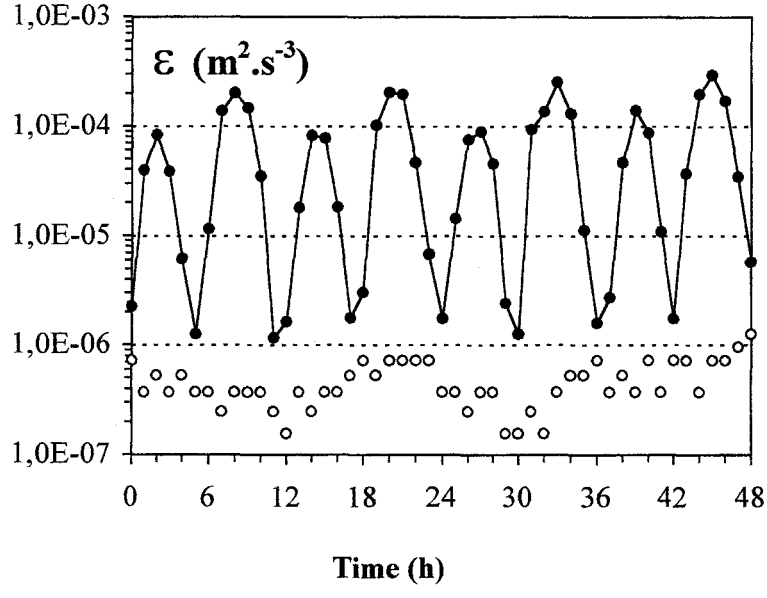

Fig. 4. Temporal patterns of the dissipation rates of turbulent energy induced by tide ε_t (balck dots) and by wind ε_w (open dots).

background can also be found in Schertzer and Lovejoy (1983, 1985, 1987, 1989), and in a recent review (Seuront et al. 1999) wholly devoted to the introduction of multifractal concepts and their related analysis techniques to marine ecology. Finally, for a detailed discussion of what can be ecologically conclude from the use of fractal and multifractal algorithms, one may respectively refer to Seuront and Lagadeuc (1997, 1998), and Seuront *et al.* (1999).

Because an objective criterion is needed for deciding upon an appropriate range of scales to include in the regressions to determine both the spectral exponents β and the structure function scaling exponent $\zeta(q)$, we used the values of the frequencies and the time scales which maximized the coefficient of determination (r^2) and minimized the total sum of the squared residuals for the regression, as proposed by Seuront and Lagadeuc (1997). Before performing the calculations, the measured time series must be detrended and normalized. This is done, first, by calculating Kendall's coefficient of rank correlation, τ, between time series and the x-axis values in order to detect the presence of a linear trend (Kendall and Stuart 1966). We thus eventually detrended the time series by fitting linear regressions to the original data by least squares and used the regression residuals in further analysis, a common remedial procedure in time-series analysis (Fuller 1976). Second, the measured time series were normalized (nondimensionalized) by dividing all values by the average of the total series.

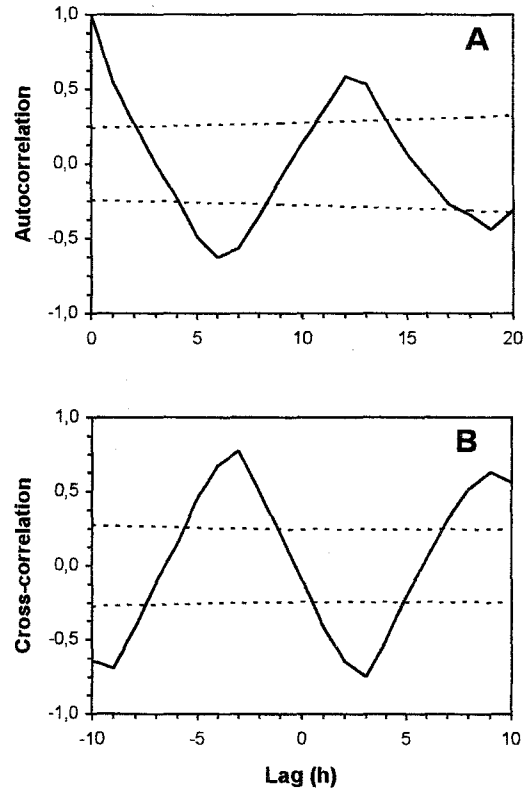

Fig. 5. Autocorrelation of salinity at 3 m depth (A) and cross-correlation between current direction and salinity at 3 m depth (B). Dashed lines indicate 5% confidence limits.

Results

Environmental conditions— The values of the vertical shear activity, S^2, (0.005 ± 0.004 s^{-1} SD) which can generate turbulence were always greater than 2.4×10^{-4} s^{-1}, a low shear effect according to Itsweire et al. (1989), indicating an elevated shear activity in the whole water column. At all depths, current vectors showed wide variations (Fig. 3) which were related to the semidiurnal M2 (12.4 h) tidal component. It resulted in variations of 6 h periodicity in the current speed, which ranged from 5 to 116 $cm.s^{-1}$ at 3 m depth (Fig. 3). A moderate NNE wind (4.35 ± 0.20 $cm.s^{-1}$) blowed during the whole sampling experiment, leading to a dissipation rate of 5.24×10^{-7} $m^2.s^{-3}$ at 1 m depth (Fig. 4). Moreover, the depth-average mean dissipation rate of tidally induced turbulent energy, ε_t, was 6.85×10^{-5} $m^2.s^{-3}$, significantly higher than the wind-generated turbulent dissipation rate ε_w ($\varepsilon_w = 5.24 \times 10^{-7} m^2.s^{-3}$ at 1 m depth), characterizes a tidally mixed area and indicates a negligible effect of wind-induced turbulent kinetic energy on the water column (Fig. 4). Autocorrelation of salinity (Fig. 5A), and cross-correlation between current direction and salinity (Fig. 5B), show that this parameter also varied with a periodicity of 12 h, and was negatively correlated with current direction.

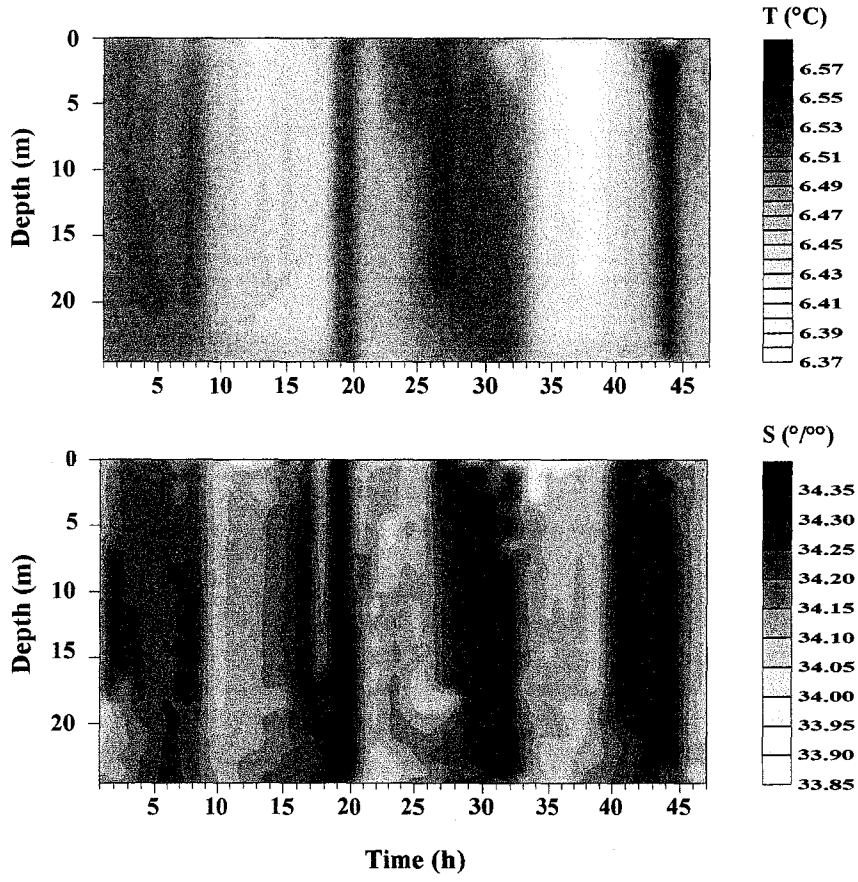

Fig. 6. Distribution of temperature (up) and salinity (down) during the 48 hours sampling experiment.

Temperature exhibit a slightly complex behavior, showing a light-dark cycle (sinusoidal regression, $r^2 = 0.678$) surimposed on a significantly autocorrelated ($p < 0.05$) 12 h tidal cycle. In both cases, the water column always has no vertical structure (Fig. 6). These observations then suggest that horizontal advection associated with the M2 tidal component can be responsible for the advection of different water masses through the entire water column which was wholly homogenized since salinity and temperature was uniformly distributed vertically.

Nutrients and phytoplankton biomass—The mean nitrite and nitrate concentrations were respectively 0.17 ± 0.02 and 0.71 ± 0.14 $\mu mol.l^{-1}$, while mean chlorophyll *a* concentration was 17.91 ± 1.10 $\mu g.l^{-1}$. There were clear systematic variations in nutrient and chlorophyll *a* concentrations (Fig. 7), and no statistical differences between mean values at the four sampled depth, as shown by autocorrelation analyses ($p < 0.05$) and Kruskal-Wallis test ($p > 0.05$), respectively. Nutrients and chlorophyll *a* concentrations exhibited significant negative correlation for the whole water column (Spearman's ρ, $p < 0.001$). No decrease of *in vivo* fluorescence was observed in the surface layers during the daylight period, indicating the absence of photoinhibition (Falkowski and Kiefer 1985), linked to a decrease of primary production (Lizon et al. 1995); *in vivo* fluorescence and chlorophyll *a* were highly significantly correlated over the whole water column (Spearman's ρ, $p < 0.01$).

Nitrite time series—The time series of nitrite exhibit a very intermittent behavior, where sharp fluctuations occurring on small scales are clearly visible (Fig. 8). Results of descriptive analysis, including skewness and kurtosis estimates, for the 11 nitrite time series are presented in Table 1. The different time series of nitrite concentrations are obviously not normally distributed (Kolmogorov-Smirnov test, $p < 0.01$; Lilliefors 1967) and their frequency distribution then exhibit a skewed behavior (Table 1), reflecting a heterogeneous distribution with a few dense patches and a wide range of low density patches. This last observation agrees with the observations realized both at smaller and larger scales concerning the clustering of bacteria around phytoplankton cells (Azam and Ammerman 1984), and the log-normal distribution of zooplankton (Cassie 1963; Frontier 1973; Fasham 1978), such a distribution describing one particular family of skewed variables.

In order to validate our continuous use of the Technicon autoanalyzer II, we compute the mean of each time series and plotted them together with the evolution curves of the hourly

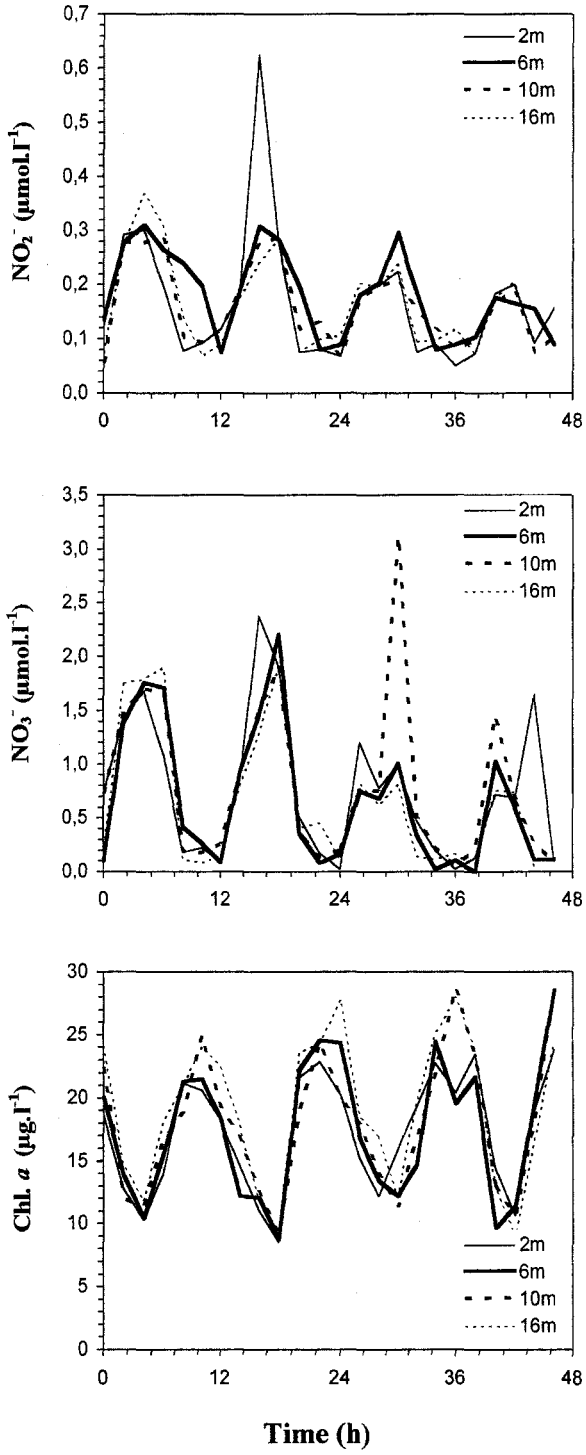

Fig. 7. Time series of NO_2^- (µmol.l^{-1}), NO_3^- (µmol.l^{-1}) and chlorophyll *a* (µg.l^{-1}) concentrations at 2, 6, 10 and 16 m.

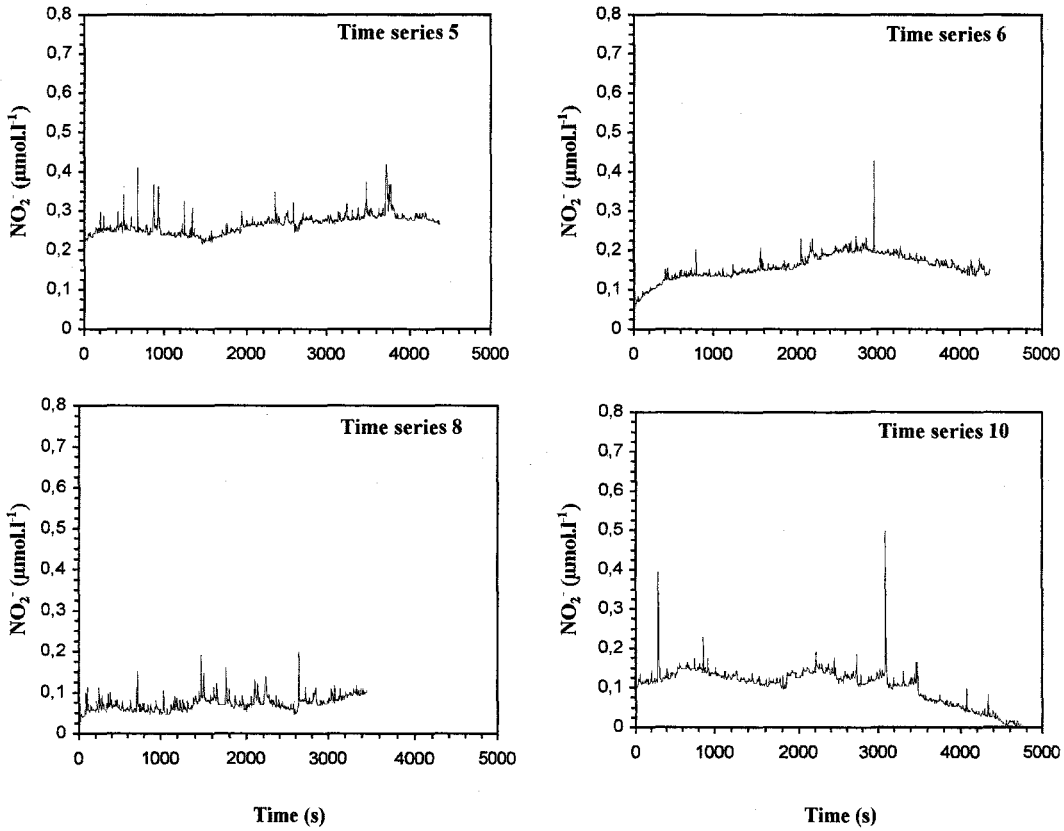

Fig. 8. Samples of high resolution (0.33 Hz) nitrite concentration time series recorded in the Eastern English Channel in low (time series 6 and 11) and high (time series 5 and 8) current speed conditions.

			Nitrite concentration (µmol.l^{-1})					
Time series	**N**	**T**	**Mean**	**Min**	**Max**	**SD**	**Skewness**	**Kurtosis**
1	999	3	0.10	0.05	0.29	0.03	1.97	5.80
2	604	6	0.29	0.21	0.41	0.04	0.58	2.85
3	659	6	0.11	0.03	0.31	0.05	0.39	3.83
4	613	6	0.26	0.19	0.50	0.03	2.69	17.65
5	1454	3	0.27	0.21	0.42	0.03	1.94	8.52
6	1455	3	0.16	0.05	0.43	0.03	0.30	7.18
7	1167	3	0.20	0.09	0.77	0.07	2.57	11.52
8	1157	3	0.07	0.03	0.20	0.02	1.86	7.94
9	1207	3	0.20	0.14	0.27	0.02	0.10	4.89
10	1241	3	0.20	0.13	0.45	0.02	16.19	45.94
11	1579	3	0.11	0.04	0.50	0.05	0.17	6.58

Table 1. Descriptive analysis of the 11 nitrite concentration time series. T: temporal resolution; SD: standard deviation.

estimates of nitrite concentrations (Fig. 9). Thus, means of the continuously recorded time series clearly appear to be very well integrated in the 12 h tidal cycle of the nitrite concentrations corresponding to our discrete sampling scheme at 2 m depth. More precisely, means of the different time series cannot statistically be regarded as being different from the closest discrete estimate of nitrite concentration (Binomial test, $p > 0.05$; Siegel and Castellan 1988), except in the case of the time series 4.

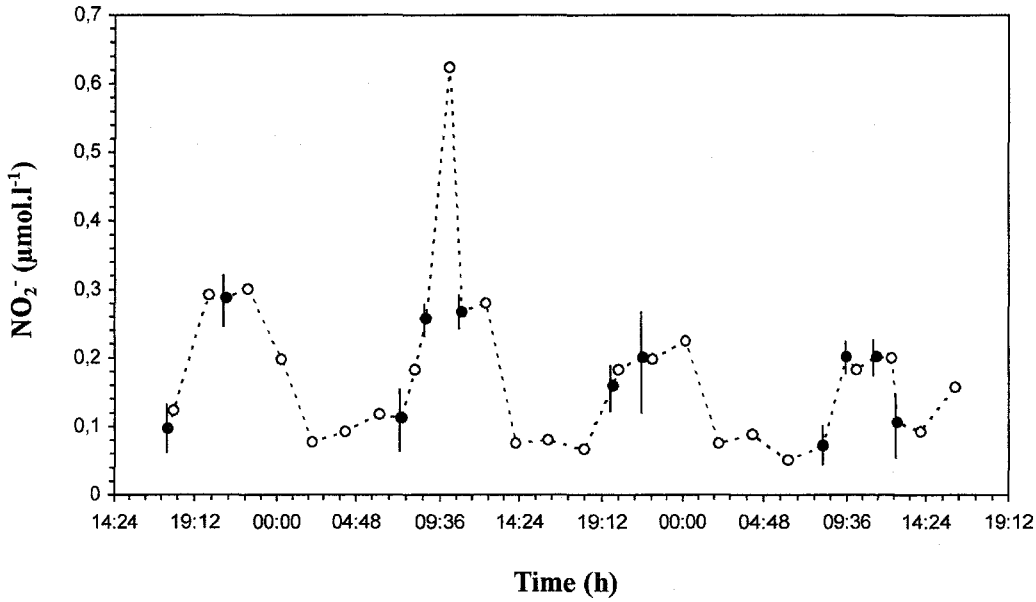

Fig. 9. Time series of nitrite concentrations (open dots) estimated from a 2 m depth sampling using Niskin bottles, shown together with the means (black dots) and standard deviations (vertical bar) of the 11 high resolution nitrite time series continuously recorded at 0.50 m depth. Time in local hours.

The double logarithmic power spectra for the nitrite time series together with their best fitting lines are given in Fig. 10. Log-log linearity of power spectra is very strong for the whole range of scales considered—with coefficient of determination (r^2) ranging from 0.76 to 0.95—suggesting that the same process could be at the origin of the temporal distribution of nitrite. Those temporal scales can be associated with spatial scales using probably the most cited and widely used method of relating time and space, 'Taylor's hypothesis of frozen turbulence' (Taylor 1938), which basically states that temporal and spatial averages t and l, respectively, can be related by a constant velocity V, $l = V \cdot t$. Then using the mean instantaneous tidal circulations observed during the sampling of the different nitrite time series (Table 2), the associated spatial resolutions and extents associated with our sampling experiments ranges respectively from 0.3 to 4 m, and from 362 to 4926 m (Table 2). The spectral exponents β (i.e. the slope of the power spectra in a log-log plot; $\beta = 1.40 \pm 0.05$ SE)

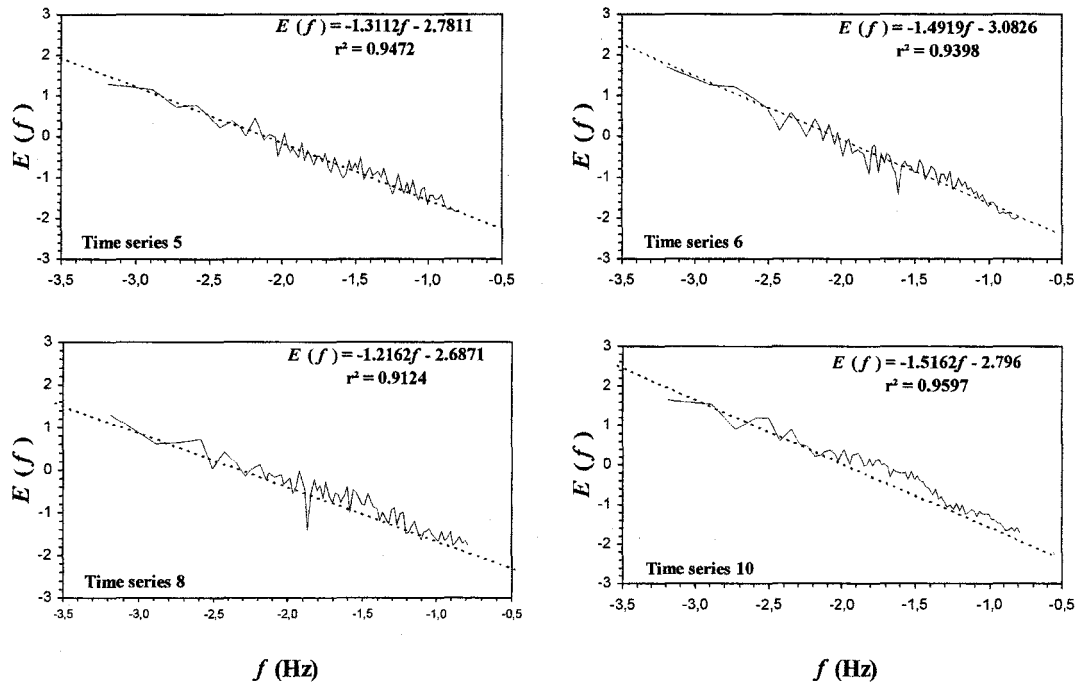

Fig. 10. The power spectra $E(f)$ (f is frequency) of the nitrite time series 5, 6, 8 and 11, shown together with their best fitting lines in a log-log plot. The clear linearity of the power spectra indicates a scaling behavior over the whole range of scales.

Time series	C_{Speed} (m.s^{-1})	Resolution (m)	Extent (m)
1	0.55	1.65	1648.35
2	0.10	0.60	362.40
3	0.33	1.98	1304.82
4	0.62	3.72	2280.36
5	0.98	2.94	4274.76
6	0.30	0.90	1309.50
7	0.11	0.33	385.11
8	0.87	2.61	3019.77
9	0.73	2.19	2643.33
10	0.18	0.54	670.14
11	1.04	3.12	4926.48

Table 2. Mean instantaneous tidal circulations (C_{Speed}) observed during the sampling of the nitrite time series, and the associated spatial resolution and extent.

lead to further conclusions (Fig. 11A). Indeed, an analysis of covariance concluded that the 11 spectral exponents β were not all equal ($p < 0.05$). We then conducted a multiple comparison procedure based on the Tuckey test (Zar 1984) to determine which β was different from the others, and showed that the slopes of the series 2, 3, 6, 7 and 11 on the one hand and the slopes of the series 1, 4, 5, 8, 9 and 10 on the other hand cannot be statistically distinguished ($p > 0.05$). This result leads to consider two groups of β values, with the following mean

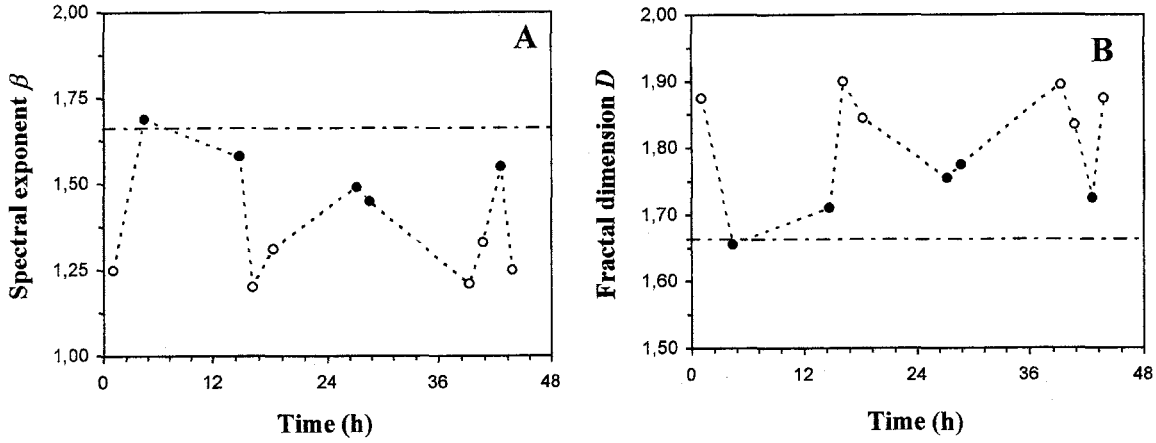

Fig. 11. Temporal patterns of the spectral exponent β (A) and the fractal dimension D (B). Straight broken lines correspond to the theoretical cases $\beta = 5/3$ and $D = 5/3$ (estimated with $\beta = 5/3$ in Eq. 5). Black and open dots are respectively associated with the time series 2, 3, 6, 7, 11, and 1, 4, 5, 8, 9, 10 identified by the subscript 1 and 2 in the text.

properties: $\beta_1 = 1.55 \pm 0.04$ SE and $\beta_2 = 1.26 \pm 0.02$ SE. Here as below, the subscripts 1 and 2 always refer to the time series 2, 3, 6, 7, 11, and 1, 4, 5, 8, 9, 10, respectively. The fractal dimensions D ($D = 1.80 \pm 0.02$ SE), estimated from Eq. 5, then exhibit an inverted pattern (Fig. 11B), where $D_1 = 1.72 \pm 0.02$ SE and $D_2 = 1.87 \pm 0.01$ SE are statistically different (Wilcoxon-Mann-Whitney U-test, $p < 0.05$). The generalization of this spectral approach to higher orders of moment with the help of the q^{th} order structure functions confirm the scaling previously shown by spectral analysis (i.e. a second order moment). Indeed, the nitrite structure functions, $< (\Delta NO_2(\tau))^q >$, clearly exhibit a linear behavior as a function of scale in a log-log plot for different orders of moments (Fig. 12). Their slope, fitted by least squares over the range of scale values for which the data are scaling (i.e. the curves are linear), provide estimates of the exponents $\zeta(q)$, whom nonlinearity (Fig. 13) indicates that the small-scale distributions of nitrite can be considered as multifractals. More specifically, the scaling of the first moments $\zeta(1) = H$ ($H = 0.30 \pm 0.04$ SE) lead to a behavior very similar to the one observed in the case of the spectral exponents β (Fig. 14A); an analysis of covariance and an appropriate multiple comparison procedure also lead to statistically distinguish two groups of H values, with $H_1 = 0.42 \pm 0.02$ SE and $H_2 = 0.20 \pm 0.01$ SE (Wilcoxon-Mann-Whitney U

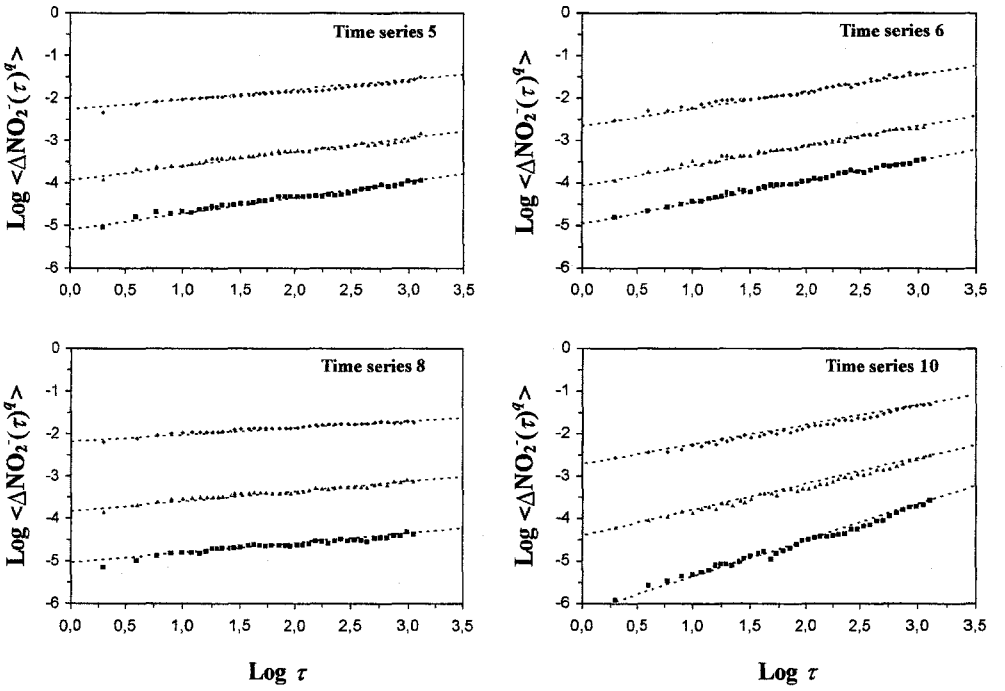

Fig. 12. The structure functions $< (\Delta NO_2^-(\tau))^q >$ vs. τ in log-log plots for $q = 1$, 2 et 3 (from top to bottom) for time series 5, 6, 8 and 11. As shown in the case of power spectral analysis, the data are scaling over the whole range of scales. The slopes of the straight dashed lines provide estimates of the first, second and third moment scaling exponent $\zeta(1) = H$, $\zeta(2)$ and $\zeta(3)$.

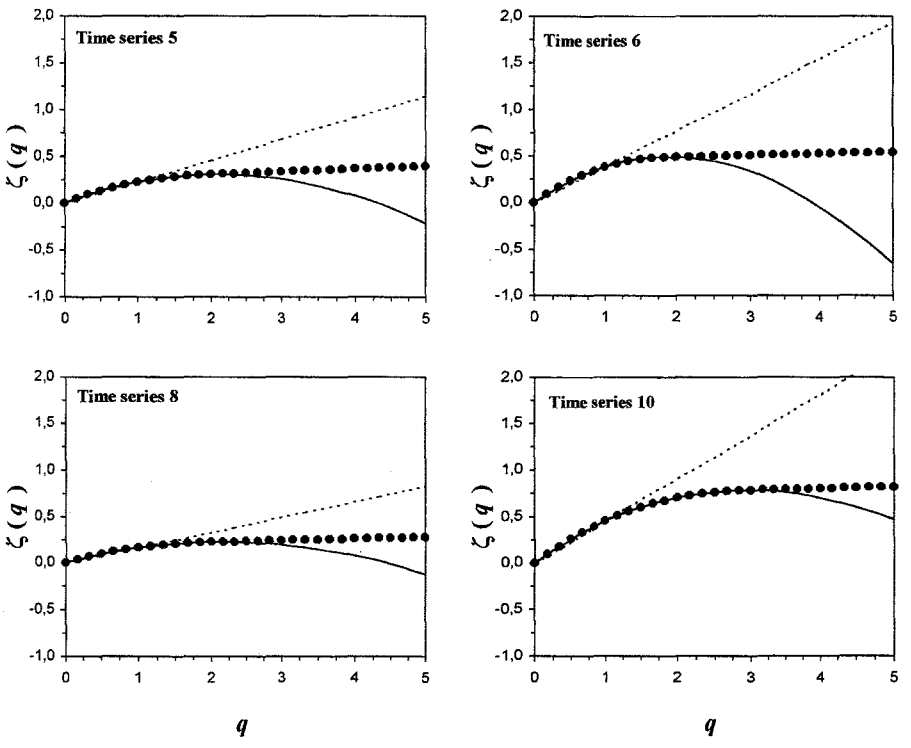

Fig. 13. The scaling exponent structure function $\zeta(q)$ empirical curves (dots), compared to the monofractal curves $\zeta(q) = qH$ (dashed line), and to the best non-linear fits of Eq. 8 (continuous curve) leading to the estimates of the multifractal parameters C_1 and α. The empirical curves are obviously non-linear, indicating multifractality.

-test, $p < 0.05$). Moreover, the scaling of the second order moment (i.e. $\zeta(2)$) confirms the estimates of the power spectral exponents β ($\beta = 1+\zeta(2)$) for each time series (Table 3). One may note here that in the monofractal case, H and β are related as $H = (\beta - 1)/2$, hence $H = 2 - D$ in Eq. 5, which is obviously not the case in our dataset (cf. Table 3). The universal multifractal parameters C_1 ($C_1 = 0.095 \pm 0.01$ SE) and α ($\alpha = 1.87 \pm 0.01$ SE), estimated as the best non-linear fit of Eq. 8, also exhibit a variable behavior from one time series to another (Fig. 14B, C), suggesting a differential control of the organization of the NO_2^- variability over time. However, one may note that C_{1_1} and C_{1_2} ($C_{1_1} = 0.14 \pm 0.01$ SE and $C_{1_2} = 0.07 \pm 0.01$ SE) are significantly different, whereas α_1 and α_2 ($\alpha_1 = 1.89 \pm 0.02$ SE and $\alpha_2 = 1.84 \pm 0.02$ SE) cannot be statistically distinguished (Wilcoxon-Mann-Whitney U-test, $p < 0.05$ and $p > 0.05$, respectively). One may finally note that the observed differences between the spectral exponents β as the structure function scaling exponents $\zeta(q)$—and consequently between the values of the multifractal parameters H, C_1 and α—cannot be associated with the different spatial resolutions associated with each nitrite time series (see Table 2). In this particular case, we should have observed any scale-breakings (i.e. a transition between two different scaling regimes) respectively for high frequencies and small scales of power spectra and structure functions log-log plots, which is obviously not the case here (see Fig. 10 and 12, respectively).

	Time series										
	1	**2**	**3**	**4**	**5**	**6**	**7**	**8**	**9**	**10**	**11**
H **(multifractal case)**	0.33	0.48	0.37	0.18	0.23	0.39	0.40	0.17	0.24	0.45	0.20
$H = (\beta - 1)/2$ **(monofractal case)**	0.13	0.35	0.29	0.10	0.16	0.25	0.23	0.11	0.17	0.26	0.13
β	1.25	1.69	1.58	1.20	1.31	1.49	1.45	1.21	1.33	1.51	1.25
$1+\zeta(2)$	1.28	1.70	1.59	1.22	1.31	1.49	1.52	1.23	1.33	1.70	1.24

Table 3. Empirical estimates of the spectral exponent β, and the first and second moment scaling exponents $\zeta(1) = H$ and $\zeta(2)$ for nitrite time series. The first moment scaling exponent $\zeta(1) = H$ is compared to the monofractal estimate $H = (\beta - 1)/2$, and the second moment scaling exponent $\zeta(2)$ to the power spectra exponent estimate following $\beta = 1 + \zeta(2)$.

In order to determine the factors influencing the magnitude of the differential structuration levels of nitrite time series represented by the fractal dimension D, and the universal multifractal parameters H, C_1 and α, we realized correlation analyses between these parameters, the sum of the nitrite spectra (i.e. an estimate of the total variation in a given record; Bendat and Piersol 1986), the means of the nitrite time series and chlorophyll *a* concentrations estimated from 2 m depth water samples during each time series recording, and the current speed and direction, as an indicator of the physical forcings (Table 4). Then, it was found that the structuration of nitrite variability (i.e. fractal dimension, D, and multifractal parameters, H, C_1 and α) was not correlated with the mean nitrite and chlorophyll *a* concentrations nor with the sum of the nitrite spectra (Spearman's ρ, two-tailed, 90% level, $p > 0.05$; see Table 4), indicating the absence of density-dependence in the structuration of nitrite variability, but also an independence between the concept of variability and heterogeneity, as already noticed by Seuront and Lagadeuc (1998) in the case of a monofractal analysis of the spatio-temporal structuration of the water column in the Eastern English Channel. Moreover, the absence of correlation between fractal and multifractal parameters and current direction also indicates that the structuration of nitrite variability cannot be associated with the horizontal advection processes associated with the M2 tidal component. On the contrary, fractal and multifractal parameters were significantly correlated with current speed (Spearman's ρ, two-tailed, $p < 0.05$; see Table 4), suggesting a differential hydrodynamical control of the structuration of nitrite variability.

Discussion

Small-scale nutrient patches exist in turbulent coastal waters—The empirical estimates of the vertical shear activity (S^2), and the tidal energy dissipation rates ε_t (Fig. 4), which are typically in the range of values occurring in highly energetic coastal environments (i.e. 10^{-7}-10^{-4} $m^2.s^{-3}$; Grant et al. 1962), are a common feature of tidally-energetic shallow seas in which water mass properties remain vertically well-mixed (e.g. Schumacher et al. 1979; Bowman et al. 1983). Both physical and biological variability is then mainly associated with horizontal advection processes associated with the M2 tidal component which can be responsible for the advection of different water masses because of the very specific hydrological structure observed in this area, characterized by an inshore-offshore gradient in terms of salinity, temperature, turbidity, phytoplankton and zooplankton biomass (Brylinski and Lagadeuc 1990; Brylinski et al. 1991).

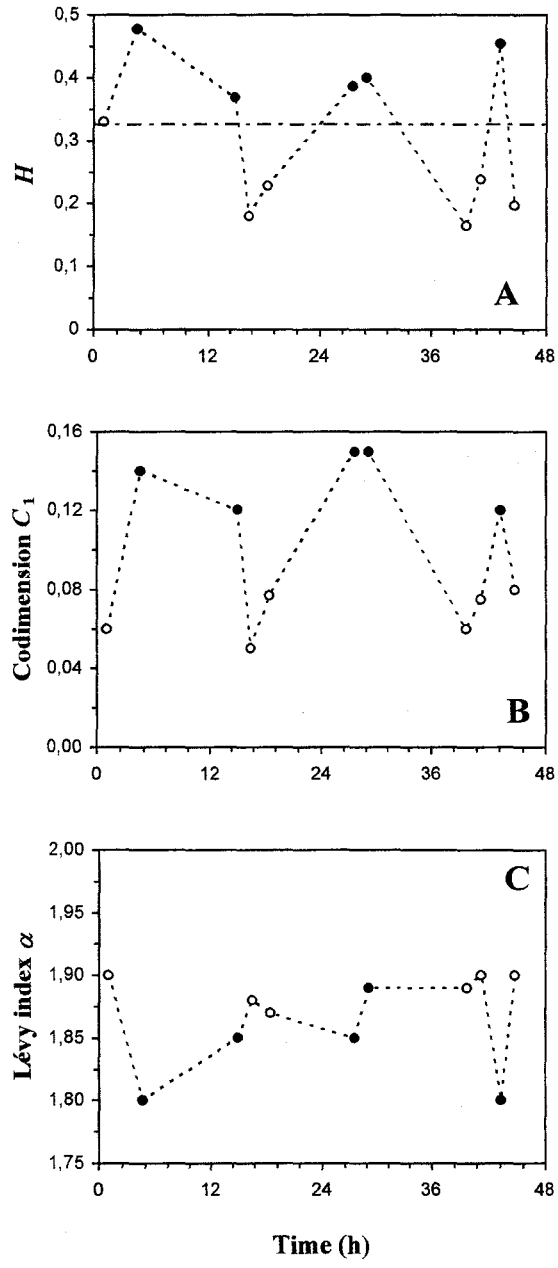

Fig. 14. Temporal patterns of the universal multifractal parameters H (A), C_1 (B) and α (C). Black and open dots are respectively associated with the time series 2, 3, 6, 7, 11, and 1, 4, 5, 8, 9, 10 identified by the subscript 1 and 2 in the text.

In such well-mixed environments where turbulent processes are fully developed—as indicated by the high values of ε_t—previous theoretical and empirical works have demonstrated that the fluctuations of biological parameters (e.g. phytoplankton biomass) could follow a spectral power law behavior characterized by a characteristic exponent β ($\beta = 5/3$) over a wide range of time and space scales (e.g. Platt 1972; Powell et al. 1975; Seuront et al. 1996*a*, *b*, 1999), as theoretically expected in the case of purely passive scalars (i.e. temperature

or salinity) advected by turbulent processes (Kolmogorov 1941; Obukhov 1941). However, except in the case of the time series 2, our empirical estimates of the spectral exponent β are significantly different from the previously defined theoretical value ($\beta = 5/3$) (modified *t*-test; Scherrer 1984), indicating that the small-scale variability of NO_2^- time series cannot be regarded as to be purely passively driven by turbulent fluid motion and that there could exist an altogether level of complexity in the origin of the structuration of NO_2^- variability. Moreover, fractal dimensions D, as previously suggested by the values of the spectral exponents β, appear to be highly variable in time (Fig. 11A) and significantly positively correlated with current speed (cf. Table 4). This suggests that the physical and/or biological forcings responsible for the NO_2^- variability are on smaller time scales in higher hydrodynamic conditions. Indeed, the high fractal dimensions associated with strong current speeds (i.e. that range between 55 and 104 $cm.s^{-1}$, and lead to tidal energy dissipation rates ε_t ranging from 4×10^{-5} to 2×10^{-4} $m^2.s^{-3}$) characterize very complex processes where short-range, local variability is highly developed and tends to obfuscate long-range trends perceptible from lower fractal dimensions, associated with weak current speed (i.e. that range between 10 and 33 $cm.s^{-1}$, and associated with ε_t ranging from 1×10^{-6} to 6×10^{-6} $m^2.s^{-3}$); NO_2^- is thus more evenly distributed (i.e. less structured) in space and time in high hydrodynamic conditions. Furthermore, the negative correlation between H and the fractal dimensions D confirms the results of the monofractal analysis. Indeed, the first universal multifractal parameter H characterizing the degree of nonstationarity of the process, the lower is H, the more conservative is the corresponding process, i.e. the mean of the fluctuations is less scale dependent, indicating a reduced flux of variance from large to smaller scales, and then the prevalence of local variability. Moreover, the values of the second universal multifractal parameter C_1, negatively correlated with current speed (cf. Table 4), show that NO_2^- distribution is all the more sparse (i.e. higher C_1 values) as the current speed is low, indicating a potential homogenization (i.e. a decreasing heterogeneity) effect of mixing processes in high turbulent conditions. Indeed, the higher values of C_1 (i.e. $C_{1_1} = 0.12 \pm 0.01$ SE) associated with low current speed indicate the occurrence of sparse patches of high NO_2^- concentrations that are several orders of magnitude above the background levels, while in higher hydrodynamic conditions the lower C_1 values (i.e. $C_{1_2} = 0.07 \pm 0.01$ SE) lead to view the different NO_2^- variability levels as being more regularly distributed. Here the so-called

Table 4. Correlation matrix of variables relative to the structure of nitrite time series. $NO_{2\,mean}^{-}$ and NO_{2}^{-}spectral: mean concentration of nitrite time series and sum of the nitrite power sepctra; Chl. *a*: mean chlorophyll *a* concentration; *D*: fractal dimension; *H*, C_1 and α: universal multifractal parameters; C_{Speed} and $C_{Direction}$: current speed and direction.

	$NO_{2\,mean}^{-}$	$NO_{2\,spectral}^{-}$	D	H	C_1	α	C_{Speed}	$C_{Direction}$
$NO_{2\,mean}^{-}$	1.000	-	-	-	-	-	-	-
$NO_{2\,spectral}^{-}$	-0.150	1.000	-	-	-	-	-	-
D	-0.347	-0.187	1.000	-	-	-	-	-
H	0.489	0.169	-0.927 **	1.000	-	-	-	-
C_1	0.177	0.380	-0.805 **	0.846 **	1.000	-	-	-
α	-0.512	0.097	0.690 *	-0.648 *	-0.509	1.000	-	-
C_{Speed}	-0.305	-0.191	0.724 *	-0.815 **	-0.654 *	0.610 *	1.000	-
$C_{Direction}$	-0.509	-0.124	0.184	-0.401	-0.370	0.234	0.014	1.000

* : 5% significance level

** : 1% significance level

homogenization effect is then mainly perceptible from the disruption of these patches (see Fig. 8), NO_2^- distribution remaining nevertheless heterogeneous (i.e. structured) whatever the hydrodynamic conditions. Finally, the mean value of α (i.e. the hierarchy of variability levels present in the NO_2^- distribution; $\alpha = 1.87 \pm 0.01$ SE) indicates that NO_2^- cannot be regarded as log-normally distributed, in which case $\alpha = 2$. On the contrary, this value is typically in the range of α values estimated for phytoplankton biomass, temperature and salinity distribution over similar ranges of scales (see Seuront et al. 1996*a*, *b*, 1999). The positive correlation between α and the current speed nevertheless indicate a differential NO_2^- structure characterized by a greater complexity in the hierarchy of its variability levels in high hydrodynamic conditions.

Moreover, mean NO_2^- and chlorophyll *a* concentrations were not correlated to the structure of NO_2^- variability (i.e. fractal dimension D, and multifractal parameters H, C_1 and α; Table 4). The organization of NO_2^- variability then cannot be regarded as density-dependent, whereas Seuront and Lagadeuc (1998) have found a strong density-dependence of phytoplankton biomass structuration (estimated on the basis of a monofractal analysis) in relation with both the inshore-offshore gradient and the horizontal advection processes characterizing the coastal waters of the Eastern English Channel. However, a source of NO_2^- in marine waters being its release by phytoplankton populations that are growing on nitrate (McCarthy et al. 1984), the observed heterogeneity in the NO_2^- distributions could be connected to the occurrence of the prymnesiophyceae *Phaeocystis* sp. which reaches high concentration during the whole sampling experiment (Truffier et al. 1997). This species being known for its highly developed swarming capacities along the English coast of the Eastern English Channel (Tyler 1977; Lennox 1979), we could then suggest two non-conflicting hypotheses for the observed nitrite heterogeneous distributions:

(i) The aggregative properties of *Phaeocystis* and its associated potential release of nitrite can then be regarded as a direct source of heterogeneity for nitrite concentrations.

(ii) The presence of *Phaeocystis* aggregates could provide highly favorable microhabitats for microplankton populations (Azam and Ammerman 1984; Mitchell et al. 1985; Mitchell and Fuhrman 1989) and then represent a source of patchiness for nutrient distributions.

The observed heterogeneous distributions of nitrite concentrations would then be on the one hand a direct consequence of the heterogeneous distribution of *Phaeocystis* (NO_2^- release)

and on the other hand the result of the interactions between the heterogeneous distribution of phytoplankton cells and the associated clustering of bacteria. In that way, the degradation of *Phaeocystis* can also be regarded as a potential secondary source of nutrient patchiness. Indeed, the degradation of phytoplankton cells has been widely shown to be a source of patchiness and taxonomic diversity for bacterioplankton populations (Wilcox Silver et al. 1978; Blight et al. 1995), and then a likely patchy nutrient resource. In both case, an increase in hydrodynamic conditions leads to the disruption of *Phaeocystis* aggregates—as suggested by previous works on phytoplankton coagulation (Riebesell 1991*a*, *b*)—and/or the disruption of the bacterial clusters existing around phytoplankton cells (Bowen et al. 1993) and then could be regarded as a potential source of homogenization, as previously shown from the values of the universal multifractal parameter C_1 (see also Fig. 8). Under the previously suggested role of nitrifying and/or denitrifying bacteria in the NO_2^- structuration, one may furthermore note the absence of any circadian periodicity in the mean nitrite concentration and the structuration of nitrite variability. That could indicate that contrary to previous studies which demonstrated photoinhibition of nitrification in field samples from marine (Herndl et al. 1993) and freshwater (Lipschultz et al. 1985) environments, NO_2^- nitrifying bacterial production was not photoinhibed—as previously demonstrated by Gentilhomme (1993) and Gentilhomme and Raimbault (1995)—during the whole sampling experiment.

Comparison of the estimated fractal and multifractal parameters with those of other marine environmental data leads to further comments. Thus, the fractal dimensions D ($D = 1.80 \pm 0.02$ SE) are obviously higher than those found for phytoplankton biomass distribution by Seuront and Lagadeuc (1998) and Seuront et al. (1996*a*) in neap tide, and by Seuront et al. (1996*b*, 1999) in spring tide (fractal dimensions were estimated using the β values reported by Seuront et al. (1996*a*, *b*, 1999) in Eq. 5). That indicates that the processes generating the nitrite variability could be associated with smaller-scale variability than the processes responsible for the small-scale distribution of phytoplankton biomass, whatever the hydrodynamic conditions. These observations are confirmed by the values of the first universal parameter H ($H = 0.30 \pm 0.04$ SE) which are slightly smaller than the values reported by Seuront et al. (1996*a*, *b*, 1999), indicating the prevalence of a more local variability than for phytoplankton biomass and passive tracers distributions (i.e. temperature and salinity). Moreover, the values of the universal multifractal parameters C_1 ($C_{1_1} = 0.14 \pm 0.01$ SE and $C_{1_2} = 0.07 \pm 0.01$ SE) for nitrite time series are always larger than those found for both

phytoplankton biomass and passive scalars, such as temperature and salinity, in spring and neap tides in the coastal waters of the Eastern English Channel and the Southern Bight of the North Sea (Seuront et al. 1996*a*, *b*, 1999). The small-scale distribution of nitrite is then always more heterogeneous than phytoplankton biomass, temperature and salinity distributions over similar ranges of scales. This then indicates the very specific structure of nitrite variability, whatever the external physical and/or biological forcings. In that way, the differences in sampling techniques could be important when comparing the variability of temperature, salinity or phytoplankton biomass from previous studies (Seuront et al. 1996*a*, *b*, 1999) to that of nitrite seen here. However, the temporal and spatial resolutions of these studies (i.e. 0.5-1 second, and 0.3-1 meter, respectively), as the minute scales of the temperature, conductivity and *in vivo* fluorescence sensors lead to sampling conditions very similar to those reached in the present case.

Whatever that may be, the hypotheses related to the origin of the differential temporal structure of nitrite variability need to be tested both in the field and by the way of numerical experiments. Simultaneous measurements of nitrite and phytoplankton concentration, bacterial abundance and activity in different hydrodynamical conditions, known to influence the bacterial production rates (Confer and Logan 1991; Logan and Kirchman 1991), could then be helpful in determining what are the sources of the nutrient patches. On the other hand, numerical simulations of the differential aggregative properties of phytoplankton and bacterial populations relative to physical forcing of turbulent processes could lead to a better understanding of the small-scale patches formation and maintenance. Indeed, while Blackburn et al. (1998) demonstrated that spherical patches a few millimeters in diameter could sustained swarms of bacteria for about 10 minutes, such informations are, to our knowledge, still not available in turbulent environments.

Small-scale nutrient patchiness: ecological perspectives—The previously demonstrated small-scale heterogeneity of nitrite distribution presents several implications concerning the structuration of the pelagic food-web. Small-scale nutrient patchiness is indeed of prime interest in the estimates of phytoplankton growth. Some authors then outlined the importance of nutrient 'surge uptake' by phytoplankton in the presence of ephemeral point sources of nutrients (McCarthy and Goldman 1979; Glibert and Goldman 1981; Goldman and Glibert 1982; Collos 1983; Raimbault and Gentilhomme 1990). Indeed, the nitrogen uptake rates for marine phytoplankton can exceed the nitrogen uptake required for population growth (McCarthy and Goldman 1979). In that way, small-scale patchiness will have a positive effect

on phytoplankton growth as so far as a phytoplankton cell need only to be exposed to intermittent pulses of nitrogen to acquire its daily ration of nutrient. On the other hand, there exists some empirical evidence that uptake is less efficient at higher nutrient concentrations than at low ones (see e.g. Dugdale 1977), suggesting a negative effect of nutrient patchiness on phytoplankton growth. This conclusion was supported by experiments by Lehman and Scavia (1982) who compared nutrient uptake under homogeneous and heterogeneous conditions and found that the average uptake was lower in the patchy treatment than in the homogeneous one. It has also been shown that Michaelis-Menten kinetics—widely used to describe uptake rates of both bacteria and phytoplankton as a function of nutrient concentration—lead to lower estimates of average uptake rate in a patchy environment than by assuming a homogeneous nutrient distribution (Currie 1984), and do not adequately describe uptake when nutrient concentrations fluctuate with time (Goldman and Glibert 1982; Harrison et al. 1989). Finally, one may note the absence of any adequate model of uptake under non-steady state conditions and of any convergent empirical evidence of the effect of a heterogeneous nutrient distribution on phytoplankton uptake and growth. Further extensions of these ideas and observations are then still needed to achieve a more complete understanding of the small-scale spatio-temporal couplings between a heterogeneous nutrient supply and utilization of the different components of the oceanic nitrogen cycling by phytoplankton populations.

Heterogeneous nutrient distribution, or more generally small-scale heterogeneity of resources and consumers in the ocean—which has been widely demonstrated elsewhere (see e.g. Pascual et al. 1995; Seuront et al. 1996*a*, *b*, 1999)—could provide a potential phenomenological explanation to the persistence of local high phytoplankton diversity in highly energetic areas (Hutchinson 1961) referred as the 'paradox of the plankton'. Indeed, heterogeneous distributions could be regarded as a source of patchiness for higher and lower trophic levels, such as detritus and marine snow for microbial communities (Azam 1998). One may also note that the differential structuration in time of nutrient distribution—as revealed by our fractal and multifractal parameters—indicate that the size of the elemental structures of the pattern was very much related to the available energy, as proposed by Margalef (1979), but also to the biological response to physical forcing as to the interactions of biological and physical processes.

It is now well-known that primary production is very far from being constant in space and time, so that the way it is averaged has a profound effect on the results (Platt and Harrison 1985; Lizon et al. 1995). Moreover, the results will not be robust unless all processes are

understood in details (Platt et al. 1989; Yamazaki 1993), which is actually clearly not the case, especially for small-scale processes (Haury et al. 1978; Davis et al. 1991). Indeed, because of the general background of spatial variability and temporal intermittency, chronic undersampling is a fact of life in oceanography (Bohle-Carbonel 1992), and leads to biased estimates of means and confidence limits (Baker and Gibson 1987). In that way, the precise knowledge of the whole statistics of any intermittent field allowed by fractal and multifractal approaches could provide new insights into the apprehension of the variability of any ecological process whatever the scales and the intensity. These novative techniques in marine ecology then could be regarded as a new way to develop individual rather than global approaches to improve estimates of key fluxes, such as primary, new and regenerated productions, which are still disputed to within a factor of 10 (see e.g. Platt et al. 1989), mainly because of our limited capacity to harmonize the different measurement procedures and their implied time and space scales (Berger 1989; Platt et al. 1989) but also because of the extreme sensitivity of actual numerical modeling even to minor changes in parameter values (Werner et al. 1993).

References

Abbott, M. A., E. Beltrami, and P. J. Richerson. 1982. The relationship of environmental variability to the spatial patterns of phytoplankton biomass in Lake Tahoe. J. Plankton Res. **4:** 927-941.

Azam, F. 1998. Microbial control of oceanic carbon flux: the plot thickens. Science **280:** 694-696.

Azam, F., and J. W. Ammerman. 1984. Cycling of organic matter by bacterioplankton in pelagic marine ecosystems: microenvironmental considerations, p. 345-360. *In* M. J. R. Fasham et al. [eds.], Flows of energy and materials in marine ecosystems. Plenum.

Baker, M. A., and C. H. Gibson. 1987. Sampling turbulence in the stratified ocean: statistical consequences of strong intermittency. J. Phys. Oceanogr. **17:** 1817-1836.

Bendat, J. S., and A. G. Piersol. 1986. Random data: analysis and measurement procedures, 2nd ed. Wiley.

Bentley, D., R. Lafite, N. H. Morley, R. James, P. J. Statham, and J. C. Guary. 1993. Flux de nutriements entre la Manche et la Mer du Nord. Situation actuelle et évolution depuis dix ans. Oceanol. Acta **16:** 599-606.

Berger, W. H. 1989. Global maps of ocean productivity, p. 429-455. *In* W. H. Berger et al. [eds.], Productivity of the ocean: present and past. Wiley.

Blackburn, N., T. Fenchel, and J. Mitchell. 1998. Microscale nutrient patches in planktonic habitats shown by chemotactic bacteria. Science **282:** 2254-2256.

Blight, S. P., T. L. Bentley, D. Lefevre, C. Robinson, R. Rodrigues, J. Rowland, and P. J. Williams. 1995. Phasing of autotrophic and heterotrophic plankton metabolism in a temperate coastal ecosystem. Mar. Ecol. Prog. Ser. **128:** 61-75.

Bohle-Carbonel, M. 1992. Pitfalls in sampling, comments on reliability and suggestions for simulation. Cont. Shelf Res. **12:** 3-24.

Bowen, J. D., K. D. Stolzenbach, and S. W. Chisholm. 1993. Simulating bacterial clustering around phytoplankton cells in a turbulent ocean. Limnol. Oceanogr. **38:** 36-51.

Bowers, D. G., and J. H. Simpson. 1987. Mean position of tidal fronts in Europen-shelf seas. Cont. Shelf Res. **7:** 35-44.

Bowman, M. J., A. C. Kibblewhite, S. M. Chiswell, and R. A. Murtagh. 1983. Shelf fronts and tidal stirring in Greater Cook Strait, New Zealand. Oceanol. Acta **6:** 119-129.

Brunet, C., J. M. Brylinski, and Y. Lemoine. 1993. In situ variations of the xanthophylls dioxanthin and diadinoxanthin: photoadaptation and relationships with a hydrodynamical system in the eastern English Channel. Mar. Ecol. Prog. Ser. **102:** 69-77.

Brylinski, J. M., D. Bentley, and C. Quisthoudt. 1988. Discontinuité écologique et zooplancton (copépodes) en Manche orientale. J. Plankton Res. **10:** 503-513.

Brylinski, J. M., J. Dupont, and D. Bentley. 1984. Conditions hydrologiques au large du cap Griz-Nez (France): premiers résultats. Oceanol. Acta **7:** 315-322.

Brylinski, J. M., and Y. Lagadeuc. 1990. L'interface eau côtière/eau du large dans le Pas-de-Calais (côte française): une zone frontale. C. R. Acad. Sc. Paris **311:** 535-540.

Brylinski J. M., Y. Lagadeuc, V. Gentilhomme, J. P. Dupont, R. Lafite, P. A. Dupeuple, M. F. Huault, Y. Auger, E. Puskaric, M. Wartel, and L. Cabioch. 1991. Le "fleuve côtier": un phénomène hydrologique important en Manche orientale. Exemple du Pas-de-Calais. Oceanol. Acta **11:** 197-203.

Cassie, R. M. 1963. Microdistribution of plankton. Oceanogr. Mar. Biol. Ann. Rev. **1:** 223-252.

Collos, Y. 1983. Transient situations in nitrate assimilation by marine diatoms. 4. Non-linear phenomena and the estimation of the maximum uptake rate. J. Plankton Res. **5:** 677-691.

Confer, D. R., and B. E. Logan. 1991. Increased bacterial uptake of macromolecular substrates with fluid shear. Appl. Environ. Microbiol. **57:** 3093-3100.

Currie, D. J. 1984. Phytoplankton growth and the microscale nutrient patch hypothesis. J. Plankton Res. **6:** 591-599.

Davis, C. S., G. R. Flierl, P. H. Wiebe, and P. J. S. Franks. 1991. Micropatchiness, turbulence and recruitment in plankton. J. Mar. Res. **49:** 109-151.

Denman, K. L., and M. R. Abbott. 1994. Time scales evolution from cross-spectrum analysis of advanced very high resolution radiometer and coastal zone color scanner imagery. J. Geophys. Res. **99:** 7433-7442.

Dugdale, R. C. 1977. Modelling, p. 789-806. *In* E. D. Goldberg et al. [eds.], The sea: ideas and observations on progress in the study of the seas. Wiley.

Estrada, M., and M. Wagensberg. 1977. Spectral analysis of spatial series of oceanographic variables. J. Exp. Mar. Biol. Ecol. **30:** 147-164.

Falkowski, P. G., R. T. Barber, and V. Smetacek. 1998. Biogeochemical controls and feedbacks on ocean primary production. Science **281:** 200-206.

Falkowski, P. G., and D. A. Kiefer. 1985. Chlorophyll *a* fluorescence in phytoplankton: a comparative field study. J. Mar. Res. **7:** 715-731.

Fasham, M. J. R. 1978. The statistical and mathematical analysis of plankton patchiness. Oceanogr. Mar. Biol. Ann. Rev. **16:** 43-79.

Feder, J. 1988. Fractals. Plenum.

Feller, W. 1971. An introduction to probability theory and its application. Wiley.

Frontier, S. 1973. Etude statistique de la dispersion du zooplankton. J. Exp. Mar. Biol. Ecol. **12:** 229-262.

Fuller, W. A. 1976. An introduction to statistical time series. Wiley.

Gentilhomme, V. 1993. Quantification des flux d'absorption et de régénération de l'azote minéral (nitrate, nitrite et ammonium) et organique (urée) dans la couche euphotique des océans oligotrophes. PhD Thesis, University of Aix-Marseille II.

Gentilhomme, V., and F. Lizon. 1998. Seasonal cycle of nitrogen and phytoplankton biomass in a well-mixed coastal system (Eastern English Channel). Hydrobiol. **361:** 191-199.

Gentilhomme, V., and P. Raimbault. 1995. Absorption et régénération de l'azote dans la zone frontale du courant Algérien (Méditerranée Occidentale): réévaluation de la production nouvelle. Oceanol. Acta **17:** 555-562.

Glibert, P. M., and J. C. Goldman. 1981. Rapid ammonium uptake by marine phytoplankton. Mar. Biol. Lett. **2:** 25-31.

Goldman, J. C., and P. M. Glibert. 1982. Comparative rapid ammonium uptake by four species of marine phytoplankton. Limnol. Oceanogr. **27:** 814-827.

Grant, H. L., R. W. Stewart, and A. Moillet. 1962. Turbulence spectra from a tidal channel. J. Fluid Mech. **12:** 241-263.

Harrisson, P. J., J. S. Parslow, and H. L. Conway. 1989. Determination of nutrient uptake parameters: a comparison of methods. Mar. Ecol. Prog. Ser. **52:** 301-312.

Haury,L.R., J. A. McGowan, and P. H. Wiebe. 1978. Patterns and processes in the time-space scales of plankton distributions, p. 277-327. *In* J. H. Steele [ed.], Spatial pattern in plankton communities. Plenum.

Herndl, G. J., G. Müller-Niklas, and J. Frick. 1993. Major role of ultraviolet-B in controlling bacterioplankton growth in the surface layer of the ocean. Nature **361:** 717-719.

Hutchinson, G. E. 1961. The paradox of the plankton. Am. Nat. **95:** 137-146.

Itsweire, E. C., T. R. Osborn, and T. P. Stanton. 1989. Horizontal distribution and characteristics of shear layers in the seasonal thermocline. J. Phys. Oceanogr. **10:** 301-320.

Jickells, T. D. 1998. Nutrient biogeochemistry of the coastal zone. Science **281:** 217-222.

Kendall, M., and A. Stuart. 1966. The advanced theory of statistics. Hafner.

Kolmogorov, A. N. 1941. The local structure of turbulence in incompressible viscous fluid with very large Reynolds number. Dokl. Akad. Nauk. SSSR. **30:** 299-303.

Lagadeuc, Y., M., Boulé, and J. J. Dodson. 1997. Effect of vertical mixing on the vertical distribution of copepods in a coastal water. J. Plankt. Res. **19:** 1183-1204.

Lehman, J. T., and D. Scavia. 1982. Microscale patchiness of nutrient in plankton communities. Science **216:** 729-730.

Lehman, J. T., and D. Scavia. 1984. Measuring the ecological significance of microscale nutrient patches. Limnol. Oceanogr. **29:** 214-216.

Lennox, A. J. 1979. Studies of the ecology and physiology of *Phaeocystis*. PhD Thesis, University of Wales.

Lilliefors, H. W. 1967. On the Kolmogorov-Smirnov test for normality with mean and variance unknown. J. Am. Stat. Assoc. **64:** 387-389.

Lipschultz, F., S. C. Wofsy, and L. E. Fox. 1985. The effects of light and nutrients on rates of ammonium transformation in an eutrophic river. Mar. Chem. **16:** 329-341.

Lizon, F., Y. Lagadeuc, C. Brunet, D. Aelbrecht and D. Bently. 1995. Primary production and photoadaptation of phytoplankton in relation with tidal mixing in coastal waters. J. Plankton Res. **17**: 1039-1055.

Logan, B. E., and D. L. Kirchman. 1991. Uptake of dissolved organics by marine bacteria as a function of fluid motion. Mar. Biol. **111:** 175-181.

Longhurst, A., S. Sathyendranath, T. Platt, and C. Caverhill. 1995. An estimate of global primary production in the ocean from satellite radiometer data. J. Plankton Res. **17:** 1245-1271.

Mackas,D.L, K. L. Denman, and M. R. Abbott. 1985. Plankton patchiness: biology in the physical vernacular. Bull. Mar. Sci. **37:** 652-674.

MacKenzie, B.R., and W. C. Leggett. 1991. Quantifying the contribution of small-scale turbulence to the encounter rates between larval fish and their zooplankton prey : effects of wind and tide. Mar. Ecol. Prog. Ser. **73:** 149-160.

MacKenzie, B.R., and W. C. Leggett. 1993. Wind-based models for estimating the dissipation rates of turbulence energy in aquatic environments : empirical comparisons. Mar. Ecol. Prog. Ser. **94:** 207-216.

McCarthy, J. J., and J. C. Goldman. 1979. Nitrogenous nutrition of marine phytoplankton in nutrient-depleted waters. Science **203:** 670-679.

McCarthy, M. D., J. I. Hedges, and R. Benner. 1998. Major bacterial contribution to marine dissolved organic nitrogen. Science **281:** 231-234.

McCarthy, M. D., J. J. Kaplan, and J. L. Nevins. 1984. Chesapeake Bay nutrient and plankton dynamics. 2. Sources and sinks of nitrite. Limnol. Oceanogr. **29:** 84-98.

Mandelbrot, B. 1977. Fractals. Form, chance and dimension. Freeman.

Mandelbrot, B. 1983. The fractal geometry of nature. Freeman.

Mann, K.H., and J.R.N. Lazier (1991) Dynamics of marine ecosystems. Biological-Physical interactions in the oceans. Blackwell.

Margalef, R. 1967. Some concepts relative to the organization of plankton. Oceanogr. Mar. Biol. Ann. Rev. **5:** 257-289.

Margalef, R. 1976. Distribucion horizontal del fitoplancton marino a escala media (1 a 10 km), illustrada con un ejemplo del area de afloramiento del NW de Africa. Mem. Real Acad. Cienc. Artes Barcelona **43:** 131-148.

Margalef, R. 1979. The organization of space. Oikos **33:** 152-159.

Mitchell, J. G., and J. A. Fuhrman. 1989. Centimeter scale vertical heterogeneity in bacteria and chlorophyll *a*. Mar. Ecol. Prog. Ser. **54:** 141-148.

Mitchell, J. G., A. Okubo, and J. A. Fuhrman. 1985. Microzones surrounding phytoplankton form the basis for a stratified marine microbial ecosystem. Nature **316:** 58-59.

O'Neill, R. 1971. Function minimization using a simplex procedure. Applied Stat. **21:** 338-343.

Obukhov, A. M. 1941. Spectral energy distribution in a turbulent flow. Dokl. Akad. Nauk. SSSR. **32:** 22-24.

Pascual, M., F. A. Ascioti, and H. Caswell. 1995. Intermittency in the plankton: a multifractal analysis of zooplankton biomass variability. J. Plankton Res. **17:** 1209-1232.

Platt T. 1972. Local phytoplankton abundance and turbulence. Deep-Sea Res. **19:** 183-187.

Platt T. 1975. The physical environment and spatial structure of phytoplankton populations. Mém. Soc. R. Sci. Liège **7:** 9-17.

Platt T., and K. L. Denman. 1975. Spectral analysis in ecology. Annu. Rev. Ecol. Syst. **6:** 189-210.

Platt, T., and W. G. Harrisson. 1985. Biogenic fluxes of carbon and oxygen fluxes in the upper ocean. Deep-Sea Res. **33:** 273-276.

Platt,T., W. G. Harrison, M. R. Lewis, W. K. W. Li, S. Sathyendranath, R. E. Smith, and A. F. Vezina. 1989. Biological production of the oceans: the case for a consensus. Mar. Ecol. Prog. Ser. **52:** 77-88.

Platt, T., S. Sathyendranath, O. Ulloa, W. G. Harrison, N. Hoepffner, and J. Goes. 1992. Nutrient control of phytoplankton photosynthesis in the Western North Atlantic. Nature **356:** 229-231.

Powell,T.M., P. J. Richerson, T. M. Dillon, B. A. Agee, B. J. Dozier, D. A. Godden, and L. O. Myrup. 1975. Spatial scales of current speed and phytoplankton biomass fluctuations in Lake Tahoe. Science **189:** 1088-1089.

Prandtl, H.L. (1969) The essentials of fluid dynamics. Blackie.

Quisthoudt, C. 1987. Production primaire phytoplanctonique dans le détroit du Pas-de-Calais (France): variations spatiales et annuelles au large du cap Griz-Nez. C. R. Acad. Sci. Paris **304:** 245-250.

Raby D., Y. Lagadeuc, J. J. Dodson, and M. Mingelbier. 1994. Relationship between feeding and vertical distribution of bivalve larvae and mixed waters. Mar. Ecol. Prog. Ser. **130:** 275-284.

Raimbault, P., and V. Gentilhomme. 1990. Short- and long-term responses of the marine diatom Phaeodactylum tricornutum to spike additions of nitrate at nanomolar levels. J. Exp. Mar. Biol. Ecol. **135:** 161-176.

Riebesell, U. 1991*a*. Particle aggregation during a diatom bloom. I. Physical aspects. Mar. Ecol. Prog. Ser. **69:** 273-280.

Riebesell, U. 1991*b*. Particle aggregation during a diatom bloom. II. Biological aspects. Mar. Ecol. Prog. Ser. **69:** 281-291.

Sakamoto, C. M., G. E. Friederich, S. K. Service, and F. P. Chavez. 1996. Development of automated surface seawater nitrate mapping systems for use in open ocean and coastal waters. Deep-Sea Res. I **43:** 1763-1775.

Samorodnitsky, G., and M. S. Taqqu. 1993. Stable non-gaussian random processes: stochastic models with infinite variance. Chapman-Hall.

Scherrer, B. 1984. Biostatistiques. Morin.

Schertzer, D., and S. Lovejoy. 1987. Physically based rain and cloud modelling by anisotropic, multiplicative turbulent cascades. J. Geophys. Res. **92:** 9693-9714.

Schroeder, M. 1991. Fractals, chaos, power laws. Freeman.

Schumacher, J. D., T. H. Kinder, D. J. Pashinski, and R. L. Charnell. 1979. A structural front over the continental shelf of the eastern Bering Sea. J. Phys. Oceanogr. **9:** 79-87.

Seuront, L., and Y. Lagadeuc. 1997. Characterisation of space-time variability in stratified and mixed coastal waters (Baie des Chaleurs, Québec, Canada): application of fractal theory. Mar. Ecol. Progr. Ser. **159:** 81-95.

Seuront, L., and Y. Lagadeuc. 1998. Spatio-temporal structure of tidally mixed coastal waters: variability and heterogeneity. J. Plankton Res. **20:** 1387-1401.

Seuront, L., F. Schmitt, D. Schertzer, Y. Lagadeuc, and S. Lovejoy. 1996*a*. Multifractal intermittency of Eulerian and Lagrangian turbulence of ocean temperature and plankton fields. Nonlinear Proc. Geophys. **3:** 236-246.

Seuront, L., F. Schmitt, Y. Lagadeuc, D. Schertzer, S. Lovejoy, and S. Frontier. 1996*b*. Multifractal analysis of phytoplankton biomass and temperature in the ocean. Geophys. Res. Lett. **23:** 3591-3594.

Seuront, L., F. Schmitt, D. Schertzer, Y. Lagadeuc, and S. Lovejoy. 1999. Universal multifractal analysis as a tool to characterize multiscale intermittent patterns: example of phytoplankton distribution in turbulent coastal waters. J. Plankton Res. **21**: in press.

Siegel, S., and N. J. Castellan. 1988. Nonparametric statistics. McGraw-Hill.

Steele, J. H., and E. W. Henderson. 1979. Spatial patterns in North Sea plankton. Deep-Sea Res. **26:** 955-963.

Strickland, J. D. H., and T. R. Parsons. 1972. A practical handbook of seawater analysis. Bull. Fish. Res. Bd. Can. **167:** 1-311.

Taylor, G. I. 1938. The spectrum of turbulence. Proc. Roy. Soc. London Ser. A **20:** 1167-1170.

Treguer, P., and P. Le Corre. 1971. Manuel d'analyse des sels nutritifs dans l'eau de mer (utilisation de l'autoanalyseur II Technicon). Université de Bretagne Occidentale.

Truffier, S., B. Hitier, R. Olivesi, R. Delesmont, M. Morel, and N. Loquet. 1997. Suivi régional des nutriments sur le littoral Nord/Pas-de-Calais/Picardie. Rapport IFREMER.

Tyler, P. J. 1977. Microbiological and chemical studies of *Phaeocystis*. PhD Thesis, University of Wales.

Weber, L. H., S. Z. El-Sayed, and I. Hampton. 1986. The variance spectra of phytoplankton, krill and water temperature in the Antarctic Ocean south of Africa. Deep-Sea Res. **33:** 1327-1343.

Werner,F.E., F. H. Page, L. R. R. Lynch, J. W. Loder, R. G. Lough, R. I. Perry, D. A. Greenberg, and M. M. Sinclair. 1993. Influences of mean advection and simple behavior on the distribution of cod and haddock early life stages on Georges Bank. Fish. Oceanogr. **2:** 43-64.

Wilcox Silver, M., A. L. Shanks, and J. D. Trent. 1978. Marine snow: microplankton habitat and source of small-scale patchiness in pelagic populations. Science **201:** 371-373.

Yamazaki, H. 1993. Lagrangian study of planktonic organisms: perspectives. Bull. Mar. Sci. **53:** 265-278.

Zar, J. H. 1984. Biostatistical analysis. Prentice-Hall.

A11

Turbulence intermittency and diffusion around small organisms: a useful approach?

Lagadeuc Y, Seuront L & Lizon F

Marine Ecology Progress Series (en révision)

Turbulence intermittency and diffusion around small organisms: a useful approach?

Y. Lagadeuc, L. Seuront, F. Lizon

Station Marine de Wimereux, Université des Sciences et Technologies de Lille, UPRES-A CNRS 8013 ELICO, BP 80, 62930 Wimereux

Abstract. Enhancement of nutrient fluxes by turbulence towards phytoplanktonic cells is estimated, and values computed from mean spectral estimates and instantaneous intermittent distributions of empirical rates of energy dissipations are compared. This approach allows specifying the frequency distribution of the flux, and show that the size of cell potentially influenced by turbulence is lowest than previously indicated. The capacity of cell to use such intermittent flux is finally discussed.

The influence of turbulence on biological production from small to meso scales have been widely described since 50 years. However, studies dedicated to the microscales are less numerous and essentially published during the last ten years (Peters & Redondo, 1997). Indeed, taking into account microscale processes implies both conceptual and technical problems (Karp-Boss et al. 1996), and the questions mainly addressed are to define the exact or real physical or biological processes implied at this scale. Subsequently, ecologist which studied such scales have to consider processes never included in previous studies at small or mesoscales such as behavioural components.

The effects of microscale turbulence on both zooplankton and ichtyoplankton have been theoretically investigated and suggested to be the result, in trophodynamics studies, of an increased of contact rates between preys and predators (Rothschild & Osborn, 1988). Subsequent numerous experimental, in situ and modelling approaches tend to confirm and specify this process (see e.g. Sunby & Fossum 1990, MacKenzie & Leggett 1991, Saiz & Kiørboe 1995, Capparoy & Carlotti 1996). For phytoplankton, even if a general relationship with turbulence has been widely recognised [see e.g. Estrada & Berdalet (1997) and Margalef (1997) for a review], the effects of microscale turbulence on phytoplankton cells is more difficult to estimate. Indeed, the size spectra of phytoplankton cells is well below the Kolmogorov scale (i.e. the viscous scale where viscosity effects cannot be neglected and start to smooth out turbulent fluctuations). Moreover most of the studies dedicated to phytoplankton and turbulence at microscale were conduced in the laboratory, and only few of them quantified turbulence levels and Reynolds number (Thomas & Gibson, 1990), which make comparisons difficult (Estrada & Berdalet, 1997). It has nevertheless been observed that turbulence could have either positive or negative effects on phytoplankton populations

(Pasciak & Gavis 1975, Thomas & Gibson 1990, Berdalet & Estrada 1993). Among the positive effects, increase of nutrient uptake have been observed (Pasciak & Gavis, 1975), leading to a turbulence induced increase of nutrient fluxes.

However, Lazier and Mann (1987) have demonstrated—on the basis of a previous study conducted by Purcell (1978) —that the effect of turbulence on nutrient fluxes, is negligible for non-motile cell under 100µm. This conclusion has recently been modified by Karp-Boss et al. (1996), and the cell size bring back to 60 µm. Those assumptions are based on estimates of the increased percentage of nutrient fluxes due to the shear induced—under the Kolmogorov scale—by an homogeneous turbulence with an average dissipation rate (ε) of 10^{-6} $m^2.s^{-3}$. However, an increase of nutrient consumption or an influence on phytoplankton growth has been observed for cells smaller than 100 µm (Savidge 1981, Thomas & Gibson 1990). Such *in vitro* observations could nevertheless be unreliable because of the lack of turbulence measurements in most of the studies, but we could hypothesise that this contradiction could also be due to the erroneous consideration of a homogeneous turbulence.

Indeed, turbulence is now known to be an extremely intermittent process exhibiting strong space-time fluctuations of the dissipation rate (Jimenez, 1997; Jou, 1997). Generally, those fluctuations are regarded to be non-efficient on plankton due to their scarcity (Estrada & Berdalet 1997, Jimenez 1997). However, Karp-Boss et al. (1996) note that one must know the probability distribution of ε (which correspond in the literature to a time average value) must be known to evaluate the fraction of the time that a cell is exposed to a given shear, and Yamazaki (1993) argue that plankton 'experienced the local flow structure of turbulence, not the average of the flow field'.

	ε1	ε2	ε3
Average current speed ($m.s^{-1}$)	0.154	0.292	0.373
Reynolds Number	30800	58400	74600
Spectral estimation ($m^2.s^{-1}$)	$6.50\ 10^{-5}$	$6.78\ 10^{-4}$	$7.09\ 10^{-4}$

Table 1. Mean current speed, Reynolds number and turbulent dissipation rate spectral estimates for our three empirical turbulent conditions

In that way, in the present paper, we investigated the potential increased rate of nutrient fluxes induced by fully developed turbulence on the basis of both basic mean spectral estimates and instantaneous intermittent distributions of turbulent energy dissipation rates of grid generated turbulence. Small-scale turbulence has been generated by means of fixed PVC grids (diameter 2mm, mesh size 1cm) in a circular flume. Considering the dimensions of the flume and the speeds used in the experiment (Tab. 1), we are then dealing with a fully developed turbulence (i.e. Re >> 2500, Tab. 1). Instantaneous horizontal turbulent velocity has been measured by high frequency (100 Hz) hot film velocimetry, and turbulent energy dissipation rate has subsequently been estimated in several ways. The average turbulent energy dissipation rate has basically been derived following Tennekes & Lumley (1972) from the turbulence spectrum obtained from Fourier analysis of time series data recorded by the hot-film probe:

$$\varepsilon = 15\nu\int_0^\infty k^2 E(k)\mathrm{d}k \qquad (1)$$

where ε is the turbulent dissipation rate ($m^2.s^{-3}$), ν the kinematic viscosity ($m^2.s^{-1}$), k the wavenumber ($k = 2\pi/\lambda$), λ the eddy wavelength (m), and $E(k)$ the turbulence spectrum ($m^2.s^{-3}$). The spectrum $E(k)$ can be thought of as the mean-square amplitude of velocity fluctuations associated with a wavenumber of turbulent motion; these turbulent motions are conveniently thought of as eddies of characteristic size corresponding to their wavelength.

In order to take into account the intermittent nature of turbulence, we now need to consider local values, ε_l, of the turbulent dissipation rate following the refined similarity hypothesis (Kolmogorov, 1962; Obukhov, 1962) as:

$$\Delta v_l = \varepsilon_l^{1/3} l^{1/3} \qquad (2)$$

where $\Delta v_l = |v(x+l) - v(x)|$ is the velocity shear at scale l. Instantaneous values of ε_l were then subsequently estimated at the smallest available resolution (i.e. 100 Hz) as a fractional differentiation of the local velocity shear Δv_l, raised to the third power [i.e. $\varepsilon_l = (\Delta v_l / l^{1/3})^3$]. Let us mention briefly that a fractional differentiation of order 1/3 corresponds to a multiplication by $k^{1/3}$ in Fourier space equivalent to power law filtering [see Schertzer and Lovejoy (1987), Schertzer et al. (1998) and Seuront et al. (1999) for more discussion and more details].

We then used the previous estimates of the turbulent energy dissipation rates (averaged and instantaneous) to derive the related increased rate of nutrient fluxes following the two calculations available in the literature: Purcell (1978) and Lazier & Mann (1989), and Karp-

Boss et al. (1996). Purcell (1978) has shown that the increased rate of nutrient fluxes is a function of a dimensionless value U defined as:

$$U = \Omega a^2 / D \quad (3)$$

where Ω the shear (units??), a the particle diameter (m), and D the molecular diffusivity ($D = 10^{-9}\ m^2.s^{-1}$). Below the Kolmogorov scale an estimate of the shear Ω is provided by (Lazier & Mann 1989) (hereafter called L & M):

$$\Omega = \sqrt{\varepsilon / 7.5\nu} \quad (4)$$

where ν is the kinematic viscosity ($\nu = 10^{-6}\ m^2.s^{-1}$) and ε the turbulent dissipation rate ($m^2.s^{-3}$). When Ω is respectively equal to 1, 2.8, 8 or 30 the flux increase is equal to 10, 25, 50 or 100% (Purcell, 1978).

Following Karp-Boss et al. (1996) (KP hereafter), the increased rate of nutrient flux can also be directly estimated using the Péclet number (*Pe*) which allows to compare advective transport with diffusive transport. In turbulent environments and with non-motile cells the Péclet number is then estimated as:

$$Pe = r^2 / D(\varepsilon / \nu)^{1/2} \quad (5)$$

where r is the cell radius (m), D the diffusivity ($D = 10^{-9}\ m^2.s^{-1}$), ε the turbulent dissipation rate ($m^2.s^{-3}$) and ν the kinematic viscosity ($\nu = 10^{-6}\ m^2.s^{-1}$). For cell smaller than η_b (which is equal to $\eta_b = (\nu D^2 / \varepsilon)^{1/4}$) and corresponds to the smallest length scale where variations of ambient concentration could be observed) or Pe <<1, Sh is equal to :

$$Sh = 1+0.29Pe^{1/2} \quad (6)$$

For cell larger than η_b and smaller than the Kolmogorov scale (Pe>>1) Sh is equal to:

$$Sh = 0.55Pe^{1/3} \quad (7)$$

For Pe between 0.01 and 100 Karp-Boss et al. (1996) propose an interpolation with lower and upper limits respectively given by $Sh = 1.014+0.15Pe^{1/2}$ and $Sh = 0.955+0.344Pe^{1/3}$. For more convenience, we used the average of these two limits as an estimate of Sh.

Results and discussion

The average values of ε obtained by spectral analysis (Tab. 1) correspond to turbulence that could be observed in coastal waters (Estrada & Berdalet 1997). Such values allow to increase flux (>25%) toward cells with size over 50µm following both L&M and KB. The sizes obtained here are smaller than those noticed in the papers of L&M or KB, this difference is due

to the lower value of ε used by these authors: 10^{-6} $m^2.s^{-3}$. Such a value, which corresponds for these authors to high value in the open ocean, corresponds to low value in a tidal coastal sea as the English Channel. In their study KB found systematically a higher value of flux compared to the result of L&M. This difference has been attributed to the Purcell's experimental result which was disturbed by boundary conditions. This lack of difference could be explained by the fact that we used an average Sh number using the upper and the lower limits of Sh; if we have had only considered the upper limit the difference observed by KB would have been found again.

The instantaneous ε exhibit strong fluctuations (Fig. 1), leading to strong fluctuations of flux toward cell (Fig. 1). The used of the instantaneous values, in comparison with the average values show, first, that the flux is very far from being a constant (Figs. 1 & 2). For instance, when the average value corresponds to an increased of 25% (Tab. 2), as observed with cells of 50μm and turbulence rate ε1, the flux is greater than 25 % during approximately 48 % of the

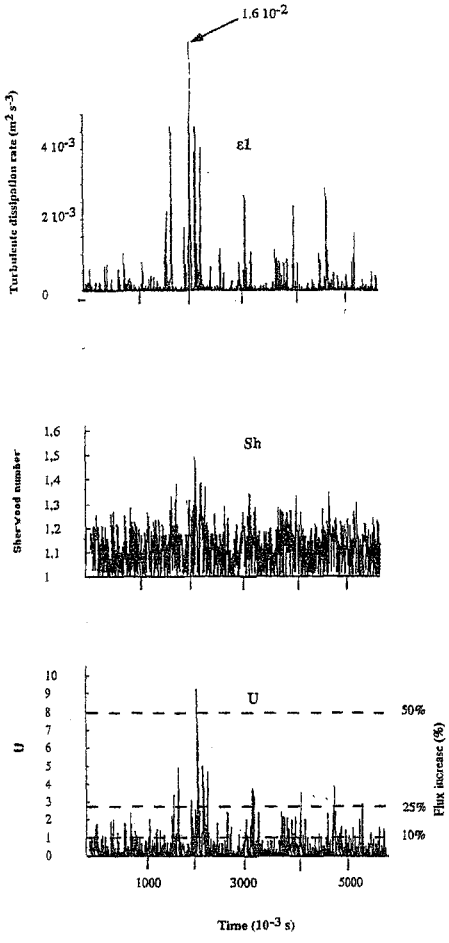

Fig. 1. Instantaneous distribution of the turbulent dissipation rate ε, the Sherwood number Sh and the dimensionless value U characterizing the increased rate of nutrient flux.

time (Fig. 2). Second, the size of the cell influenced by the turbulence is lowest than those previously observed with the average values. With the L&M approach, an increased of the flux of 25% at least could be observed for cells of 10 µm diameters during 0,2 % of the time with ε2 and ε3. With the KB approach, the same increasing flux occurs during approximately 0.08%, 1.5% and 1.6 % of the time for cells of 10µm with respectively ε1, ε2 and ε3. With cells of 20 µm this flux is greater than 25 % between approximately 2 and 30 % of the time (Fig. 2). With the instantaneous values, a slight difference, in the same way that those related

	L&M			K-B		
	ε1	ε2	ε3	ε1	ε2	ε3
5 µm	$3\ 10^{-2}$	$9\ 10^{-2}$	$8\ 10^{-2}$	1.03	1.06	1.06
10 µm	0.1	0.3	0.3	1.07	1.11	1.11
20 µm	0.5	1.5	1.4	1.12	1.20	1.19
50 µm	3.1	9.3	8.7	1.26	1.42	1.40
100 µm	12.3	37.3	34.9	1.46	1.75	1.71

Table 2. Increased of nutrient flux toward phytoplankton cells for cell size ranging from 5 to 100µm and three turbulence levels estimated following Lazier & Mann (1987) and Karp-Boss et al. (1996).

by KB, could be observed between the frequency distributions of L&M and KB estimations. Whatever the existing differences between KB and L&M estimations, it appears that instantaneous data lead to show that the effect of turbulence could exist for smaller cells than previously described. Subsequently, average value should not correspond to a good descriptor. An inadequacy of average estimate has been already shown if an adaptation of the organism took place. For instance, in studies on primary production, experiments conduced on the role of high frequencies fluctuations of light on carbon assimilation show that phytoplanktonic cells are able to respond to rapid fluctuations. Subsequently, an enhancement of production was observed under fluctuated light compared with constant light with the same average irradiance (Quéguiner & Legendre 1986). The average value of a variable is also not a good descriptor if the response of the cell is not linear. Indeed, Curry (1984) has shown—on the basis of Taylor approximation of Michaelis-Menten equation—that a heterogeneous distribution of nutrient was detrimental for phytoplankton cell absorption. This results seems to confirm that consideration of turbulence intermittency is a useful approach. However, in his approach

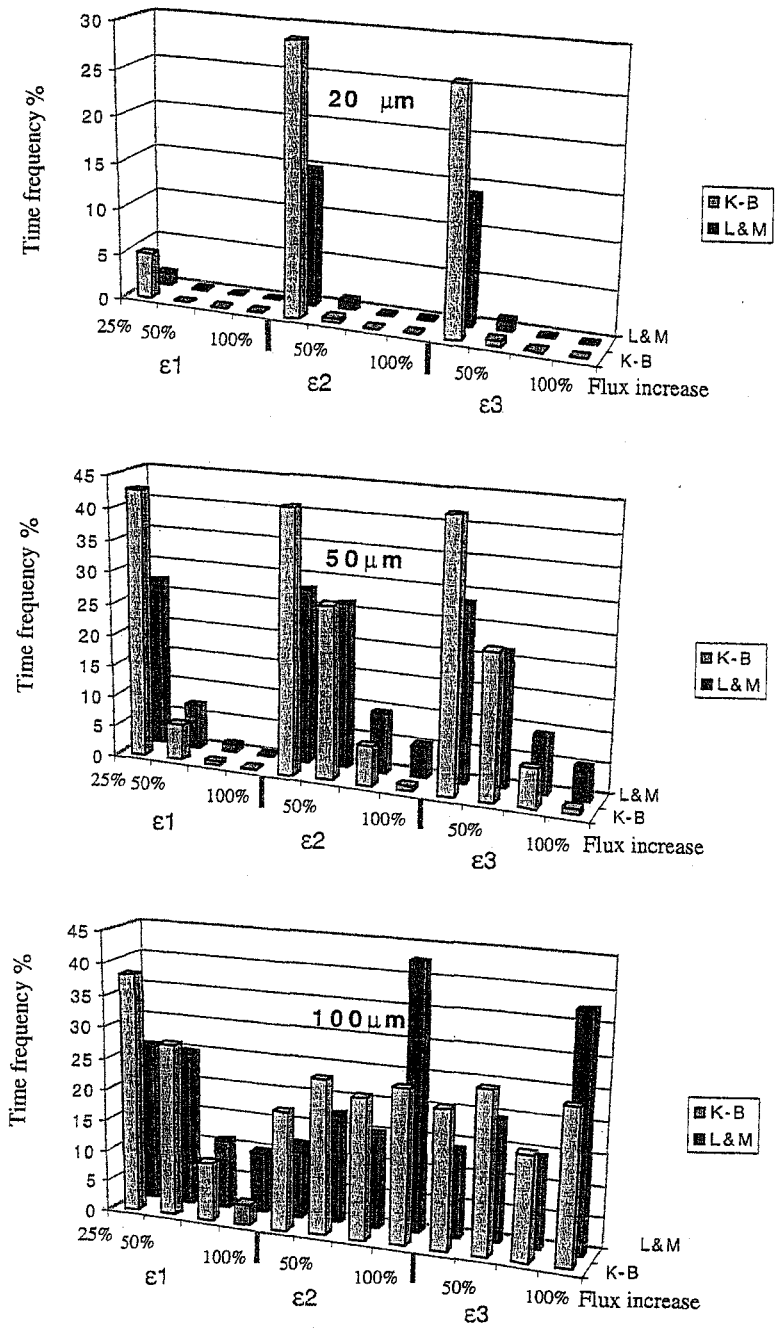

Fig. 2. Time frequency (%) of increased nutrient fluxes toward phytoplankton cells estimated following Lazier & Mann (1989) and Karp-Boss et al. (1996) for different cell size and turbulence levels.

Currie (1984) did not take into account the temporal response of cells to newly furnished nutrient. It has indeed been shown that in nutrient-depleted environments cells were able to use quickly a nutrient pulse. This event corresponds to the "surge uptake" (Collos 1983). The time scale of this rapid change in the uptake rate is typically the minute (Raimbault & Gentilhomme 1990). In the present case the time scale is however probably 1/10 of second or lower. Jou

(1997) indicates that such fluctuations induced by turbulence intermittencies are too scarce (1 second in 5 minutes) and that "the classical Kolmogorov analysis of turbulence cascade is enough to analyse most situations of biological interest". However, the techniques actually used to study nutrient uptake (transport or assimilation) do not allow to appreciate the effects of such short time flux variations. We think that at this scale it is still actually impossible to define what is a situation of biological interest, e. g. what is the minimal time required—during which the flux is increased—to influence cell production?

Moreover, the response of cells could also be nutrient-dependent: ammonium and phosphate (i.e. recycled nutrients), exhibit a rapid utilisation when they are newly furnished, while nitrate and silicate (i.e. advected nutrients), may present a lag in uptake rate (Dortch et al. 1982, Harrison et al. 1989). Consequently, capability of cells to use the intermittent increased flux could be different in regard of these two categories of nutrients, and could also conduct to a negative effect. Indeed, Savidge (1981) observed a difference in the response of diatoms to an increased of turbulence: nitrate utilisation was enhanced while phosphate utilisation was reduced. These results seem nevertheless to be in contradiction with the results of Harrison et al. (1989) and the hypothetical effect of turbulence intermittencies: the advected nutrient should be quickly used in intermittent field.

Whatever that may be, if the cell is influenced, positively or negatively, by such high frequencies fluctuations, one need to know the precise distribution of the fluctuations. The Turbulent dissipation rate distribution is generally described as being lognormal (Baker & Gibson 1987). In the present case the instantaneous ε is not log normally distributed (Kolmogorov-Smirnov test, $p < 0.05$), and the skewness of the log transformed data is negative, indicating that low unexpected values exist after the log transformation. Recent empirical and theoretical studies indicate very specific distribution of turbulent dissipation associated with scale-dependent structure described in the framework of multifractals (Schmitt et al. 1996, Schertzer et al. 1998).

Finally, one of the questions mainly addressed here is to define at what scale processes should be considered to understand the overall function of ecosystems. Numerous studies have been devoted to this question and to the knowledge of processes at the scale of individuals (Levin 1994). However, such objectives are face to the development and the use of new tools and probably new concepts. Effectively, in the present case intermittency of turbulence could affect potentially smaller cells than previously considered, but techniques allowing to study such scale or consensus n turbulent dissipation distribution are not available.

References

Baker,M.A. and Gibson,C.H. (1987) Sampling turbulence in the stratified ocean: statistical consequences of strong intermittency. *J. Phys. Oceanogr.*, **17**, 1817-1836.

Berdalet,E. and Estrada,M. (1993) Effects of turbulence on several dinoflagellate species. In Smayda,T.J. and Shimizu,Y. (eds), *Toxic phytoplankton blooms in the sea.* Elsevier, New York, pp. 737-740.

Capparoy,P. and Carlotti,F. (1996) A model for *Acartia tonsa*: effect ofturbulence and consequences for the related physiological processes. *J. Plankton Res.*, **18**, 2139-2177.

Currie,D.J. (1984) Phytoplankton growth and the microscale nutrient patch hypothesis. *J. Plankton Res.*, **6**, 591-599.

Collos,Y. (1983) Transient situations in nitrate assimilation by marine diatoms. 4. Non-linear phenomena and the estimation of the maximum uptake rate. *J. Plankton Res.*, **5**, 677-691.

Dortch,Q;, Clayton,J.R., Thoressen,S.S., Bressler,S.L. and Ahmed,S.I. (1982) Response of marine phytoplankton to nitrogen deficiency: decreased nitrate uptake vs enhanced ammonium uptake. *Mar. Biol.*, **70**, 13-19.

Harrison,P.J., Parslow,J.S. and Conway,H.L. (1989) Determination of nutrient uptake kinetic parameters: a comparison of methods. *Mar. Ecol. Prog. Ser.*, **52**, 301-312.

Jimenez,J. (1997) Oceanic turbulence at the millimeter scales. *Sci. Mar.*, **61**, 47-56.

Jou,D. (1997) Intermittent turbulence: a short introduction. *Sci. Mar.*, **61**, 57-62.

Karp-Boss,L., Boss,E. and Jumars,P.A. (1996) Nutrient fluxes to planktonic osmotrophs in the presence of fluid motion. Oceanogr. *Mar. Biol. Ann. Rev.*, **34**, 71-107.

Kolmogorov,A.N. 1962) A refinement of previous hypotheses concerning the local structure of turbulence in viscous incompressible fluid at high Reynolds numer. *J. Fluid Mech.*, 13, 82.

Laziers,J.R.N. and Mann,K.H. (1989) Turbulence and diffusive layers around small organisms. *Deep-Sea Res.*, **36**, 1721-1733.

Levin,S.A. (1994) Patchiness in marine and terrestrial systems : from individuals to populations. *Phil. Trans. R. Soc. London. B*, **343**, 99-103.

MacKenzie,B.R. and Leggett,W.C. (1991) Quantifying the contribution of small-scale turbulence to the encounter rates between larval fish and their zooplankton prey: effects of wind and tide. *Mar. Ecol. Prog. Ser.*, **73**, 149-160.

Margalef,R. (1997) Turbulence and marine life. *Sci. Mar.*, **61**, 109-123.

Obukhov,A.M. (1962) Some specific features of atmospheric turbulence. *J. Fluid Mech.*, **13**, 77.

Pasciak,W.J. and Gavis,J. (1975) Transport limited nutrient upatke in *Ditylum brightwellii*. *Limnol. Oceanogr.*, **20**, 604-617.

Peters,F. & Redondo,J.M. (1997) Turbulence generation and measurement: application to studies on plankton. *Sci. Mar.*, **61**, 205-228.

Purcell,E.M. (1978) The effect of fluid motions on the absorption of molecules by suspended particles. *J. Fluid Mech.*, **84**, 551-559.

Quéguiner,B. and Legendre,L. (1986) Phytoplankton photosynthetic adaptation to high frequency light fluctuations simualting those induced by sea surface. *Mar. Biol.*, **90**, 483-491.

Raimbault,P. and Gentilhomme,V. (1990) Short- and long-term responses of the marine diatom Phaedactylum tricornutum to spike additions of nitrate at nanomolar levels. *J. Exp. Mar. Biol. Ecol.*, **135**, 161-176.

Rothschild,B.J. & Osborn,T.R. (1988) Small-scale turbulence and plankton contact rates. *J. Plankton Res.*, **10**, 465-474.

Savidge,G. (1981) Studies of the effects of small-scale turbulence on phytoplankton. *J. Mar. Biol. Ass. U.K.*, **61**, 477-488.

Saiz,E. and Kiørboe,T. (1995) Predatory and suspension feeding of the copepod *Acartia tonsa* in turbulent environments. *Mar. Ecol. Prog. Ser.*, **122**, 147-158.

Schmitt,F., Schertser,D., Lovejoy,S. and Brunet,Y. (1996) Multifractal temperature and flux of temperature in fully developped turbulence. *Europhys. Lett.*, **34**, 195-200.

Schertzer,D. and Lovejoy,S. (1987) Physically based rain and cloud modeling by anisotropic scaling multiplicative processes. *J. Geophys. Res.*, **92**, 9693-9714.

Schertzer,D., Lovejoy,S., Schmitt,F., Chigirinskaya,Y. and Marsan,D. (1998) Multifractal cascade dynamics and turbulent intermittency. *Fractals*, **5**, 427-471.

Seuront,L., Schmitt,F., Lagadeuc,Y., Schertzer,D. and Lovejoy,S. (1999) Universal multifractal analusis as a tool to characterize multiscale intermittent patterns. Example of phytoplankton distribution in turbulent coastal waters. *J. Plankton Res.*, **21**, 877-922.

Sundby,S. & Fossum,P. (1990) Feeding conditions of Arcto-norwegian cod larvae compared with the Rothschild-Osborn theroy on small-scale turbulence and plankton contact rates. *J. Plankton Res.*, **12**, 1153-1162.

Tennekes,H. and Lumley,J.L. (1972) A first course in turbulence. MIT Press.

Thomas,W.H. and Gibson,C.H. (1990) Effects of small-scale turbulence on microalgae. *J. Appl. Phycol.*, **2**, 71-77.

Yamazaki,H. (1993) Lagrangian study of planktonic organisms: perspectives. *Bull. Mar. Sci.*, **53**, 265-278.

A12

Variability, inhomogeneity and heterogeneity: dealing with scales in marine ecology

Seuront L & Lagadeuc Y

Journal of Plankton Research (soumis)

Variability, inhomogeneity and heterogeneity: dealing with scale in marine ecology

Laurent Seuront and Yvan Lagadeuc

Station Marine de Wimereux, CNRS UPRES-A 8013 ELICO, Université des Sciences et Technologies de Lille, BP 80, F-62930 France

Abstract

Current widespread use of ecological terms such as variability, heterogeneity and homogeneity is misleading and prevents ecologists from reaching a terminological consensus on what is meant when discussing these concepts, in particular with regard to the descriptor 'heterogeneous'. We propose the use of 'inhomogeneity' to define patterns or processes exhibiting a scale-dependent structure, whether spatial or temporal. Thus, the concept of 'inhomogeneity' can be regarded as a structural ecological entity. A descriptor exhibiting different kinds of inhomogeneity, either spatially or temporally, will then only be qualified as being heterogeneous.

Basically, 'variability' in ecology indicates changes in the values of a given quantitative or qualitative descriptor; it is distinct from 'heterogeneity', which refers to a composition of different entities or kinds of elements (Kolasa and Rollo, 1991). However, this distinction is not as clear as may appear at first glance, with meanings essentially dependent on the choice of approach (Naeem and Colwell, 1991; Shashak and Brand, 1991). Even papers devoted to the synthesis of these concepts (e.g. Kolasa and Rollo, 1991; Dutilleul and Legendre, 1993) are generally misleading, in that spatial and temporal heterogeneity are used to describe spatial or temporal variability, respectively, irrespective of the basic previous definitions. Moreover, definitions themselves appear to be highly variable even within a collective synthetic work on the subject (Levin *et al.*, 1993). For instance, van Es (1993) defined spatial heterogeneity as an equivalent of spatial autocorrelation, whereas Davis (1993) proposed a clear distinction between these two concepts. Furthermore, within the framework of ecological applications of fractal geometry (see Frontier, 1987; Sugihara and May, 1990, which are becoming increasingly popular in marine ecology (Pascual *et al.*, 1995; Seuront and Lagadeuc, 1997, 1998), scale-dependent properties leading to fractal dimension estimates have also been regarded as a way to characterize space-time heterogeneity (Milne, 1991). In marine systems which are now widely recognized to be highly structured in space and time (e.g. Denman and Powell, 1984), there is a real need for additional focus placed on the knowledge of both physical and biological patterns and processes (Seuront *et al.*, 1999) which are often referred in terms of temporal intermittency and spatial heterogeneity (Platt *et al.*, 1989).

Such ambiguities should be all the more doubtful given the actual tendency for ecologists to develop more complicated theoretical frameworks for ecological processes that operate at multiple spatial and temporal scales (Maurer, 1998). Indeed, in spite of an impressive body of literature on the subject, this field of research still seems in its infancy. Arguably, one of the key factors hampering progress is the lack of a consensus on what it means for a given descriptor to be, or to be regarded as being, 'heterogeneous'. Consequently, we introduce the concept of 'inhomogeneity' which we hope could open up new horizons and help ecologists to reach a terminological consensus. The concept of 'inhomogeneity' is then regarded here as a way to describe the variability of a descriptor structured in space or in time in terms of scale-dependence. A structured descriptor will then be inhomogeneous in space or in time (Fig. 1A), whereas a non-structured descriptor cannot be distinguished from observational 'white' noise (Fig. 1B). Considering that an ecological entity can be basically regarded as patterns bounded in space and/or in time (see e.g. Cousins 1988), an inhomogeneous (as a non-inhomogeneous) descriptor can then be regarded as a structural ecological entity. Thus, 'heterogeneity' will not be applied to the variability of a given descriptor in space or in time as widely done (see Kolasa and Pickett, 1991), but rather to patterns and/or processes exhibiting different levels of structure over space or time and hence corresponding to different driving processes. However, the proposed terminological approach does not provide an absolute means with which to describe ecological patterns and processes, being that the perception, and then the characterization, of a given descriptor is intimately intertwined with grain and extent of the related sampling scheme (Wiens, 1989; Jarvis, 1995).

A few examples illustrate some of these problems. In marine ecology, Seuront *et al.* (1996) have shown on the basis of multifractal analyses [see Seuront *et al.* (1999) for a review in the framework of marine ecology] that temporal fluctuations of both phytoplankton biomass and temperature could be regarded as inhomogeneously distributed for time scales ranging from 1 second to 12 hours. Nevertheless, temperature fluctuations are similarly structured (i.e. inhomogeneous) over the entire range of available scales, while phytoplankton biomass exhibits two distinct scales of inhomogeneity. Thus, inhomogeneous temperature and phytoplankton biomass fluctuations can be regarded as being respectively homogeneously and heterogeneously distributed in time (Fig. 1C). Fractal analyses conducted on time series simultaneously recorded at different depths leads to further conclusions (Seuront and Lagadeuc, 1997). Indeed, the structure of the variables in question (i.e. temperature, salinity and phytoplankton biomass) is inhomogeneous over a large range of scales; however, these

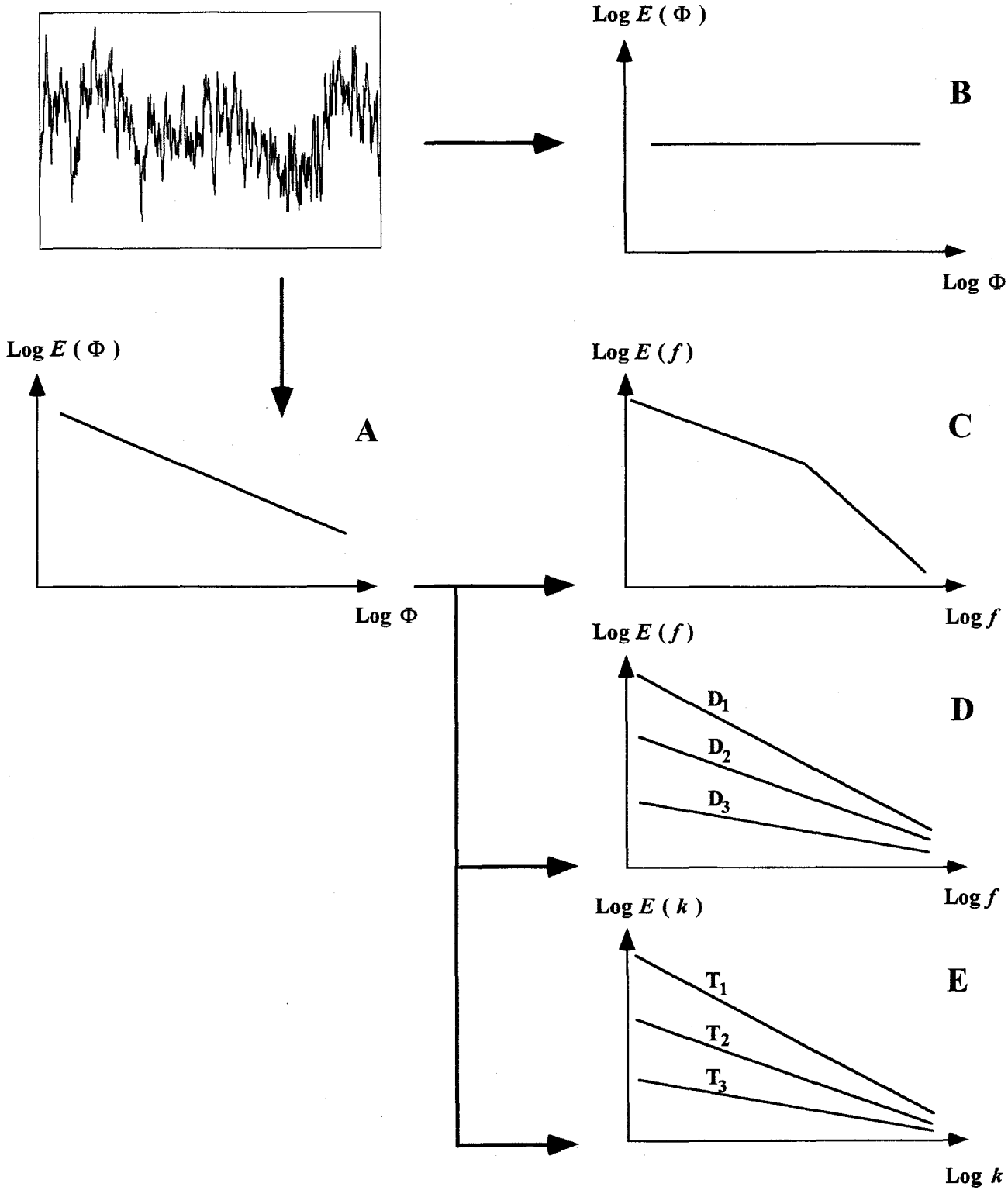

Fig. 1. Schematic illustration of the concepts of homogeneity, inhomogeneity and heterogeneity based on hypothetical power spectra, where $E(\Phi)$ is a the spectral density related to either time or space scales Φ. A homogeneous descriptor can be either structured (i.e. inhomogeneous; A) or non-structured (i.e. non-inhomogeneous; B) in time or in space. An inhomogeneous descriptor can be heterogeneous in time or in space (C), depending on the scales. Finally, an inhomogeneous descriptor over an entire range of scales can be heterogeneous either in time or in space, following that its inhomogeneous properties evolves in space S_i (D) or time T_i (E), respectively. Note that f and k are a frequency (Hz) and a wavenumber (m^{-1}), respectively.

temporal inhomogeneous structures are a function of water depth, which gives rise to spatial heterogeneity (Fig. 1D). Similar analyses conducted on the vertical fluctuations of temperature, salinity, light transmission and phytoplankton biomass in tidally mixed waters indicate that temperature, salinity and phytoplankton are inhomogeneously distributed, whereas light transmission did not exhibit any kinds of spatial inhomogeneity (Seuront and Lagadeuc, 1998). Furthermore, the spatial inhomogeneity of temperature and salinity were homogeneous over time, whereas the one of phytoplankton biomass indicates a temporal heterogeneity related with tidally induced advective processes (Fig. 1E). Light transmission, which remains non structured over time, also exhibits a form of temporal homogeneity. In summary, these previous illustrative statements clearly indicate that a descriptor inhomogeneous (or not) in space and/or in time can be either homogeneous or heterogeneous in space and/or in time.

The previous propositions suggest some terminological specifications in comparison with basic systemic approaches. For instance, hierarchical approaches, initially developed in the framework of landscape analysis, have been devoted to describe "how heterogeneity changes with scale" (Allen and Starr, 1982). On the contrary, following our approach, a system considered as being hierarchical must be viewed as a heterogeneous system presenting different scales of inhomogeneity. In that way, the main point of hierarchical theory should be rather regarded as the way to describe how inhomogeneity changes with scales. Moreover, the concepts developed in the present paper could also be regarded as a way to complement hierarchical approaches in the sense that they allow to describe how the structure of a given descriptor, hierarchical (Fig. 1C) or not (Fig. 1D, E), evolves in time and/or in space. These concepts could subsequently provide an efficient framework to reconcile space- and time-oriented approaches. Indeed, a descriptor exhibiting different inhomogeneous structure will be regarded as being heterogeneous, the inhomogeneity fluctuating either in space or in time, which is still actually not widely done (see e.g., Kolasa and Rollo, 1991; Levin *et al.*, 1993).

The challenges faced by ecology have pushed the field into a new realm of endeavor, where both theoretical and empirical ecologists need to be trained in more sophisticated sampling strategies, statistical and modeling techniques. Nevertheless, such developments should be in vain without the emergence of a general consensus on what is meant for a given pattern or process to be 'heterogeneous', which is at the core of the actual ecological thought process. One may hope that in the near future, much hard work and a terminological consensus may ensure the emergence of an ecological science that will provide effective, unified and

scientifically sound tools for analyzing the structure of ecosystems operating on different spatial and temporal scales.

Acknowledgements

We thank Christophe Luczak for stimulating discussions and comments on an earlier version of this work. We especially thank Gordon Copp for improving the English of this paper, and Joseph Davis for helpful comments and encouragements.

References

Allen,T.F.H. and Starr,T.B. (1982) *Hierarchy: Perspectives for Ecological Complexity*. University of Chicago Press , Chicago.

Cousins,S.H. (1988) Fundamental components in ecology and evolution: hierarchy, concepts and descriptions. In Wolf,W., Soeden,C.S. and Drepper,F.R. (eds), *Ecodynamics. Contribution to theoretical ecology*. Springer-Verlag, New York, pp. 60-68.

Davis, F. W. 1993. Introduction to spatial statistics. In Levin,S.A., Powell,T.M. and Steele,J.H. (eds), *Patch Dynamics*. Springer-Verlag, Berlin, pp. 16-26.

Denman,K.L. and Powell,T.M. (1984) Effects of physical processes on planktonic ecosystems in the coastal ocean. *Oceanogr. Mar. Biol. Ann. Rev.*, **22**, 125-168.

Dutilleul,P. and Legendre,P. (1993) Spatial heterogeneity against heteroscedasticity: an ecological paradigm versus a statistical concept. *Oikos*, **66**,152-171.

Frontier,S. (1987) Applications of fractal theory to ecology. In Legendre,P. and Legendre,L. (eds), *Developments in Numerical Ecology*. Springer Verlag, Berlin, pp. 335-378.

Jarvis,P.G. (1995) Scaling processes and problems. *Plant, Cell and Environment*, **18**, 1079-1089.

Kolasa,J. and Pickett,S.T.A. (1991) *Ecological Heterogeneity*. Springer-Verlag , New York.

Kolasa,J. and Rollo,D.C. (1991) The heterogeneity of heterogeneity: a glossary. In Kolasa,J. and Pickett,S.T.A. (eds), *Ecological Heterogeneity*. Springer-Verlag, New York, pp. 1-23.

Levin,S.A., Powell,T.M. and Steele,J.H. (1993) *Patch Dynamics*. Springer-Verlag, Berlin.

Maurer,B.T. (1998) Ecological science and statistical paradigm: at the threshold. *Science*, **279**, 502-503.

Milne,B.T. (1991) Heterogeneity as a multiscale characteristic of landscapes. In Kolasa,J. and Pickett,S.T.A. (eds), *Ecological Heterogeneity*. Springer-Verlag, New York, pp. 69-84.

Naeem,S., and Colwell,R.K. (1991) Ecological consequences of heterogeneity of consumable resources. In Kolasa,J. and Pickett,S.T.A. (eds), *Ecological Heterogeneity*. Springer-Verlag, New York, pp. 224-255.

Platt,T., Harrison,W.G., Lewis,M.R., Li,W.K.W., Sathyendranath,S., Smith,R.E. and Vezina,A.F. (1989) Biological production of the oceans: the case for a consensus. *Mar. Ecol. Prog. Ser.*, **52**, 77-88.

Shachak,M. and Brand,S. (1991) Relations among spatiotemporal heterogeneity, population abundance, and variability in a desert. In Kolasa,J. and Pickett,S.T.A. (eds), *Ecological Heterogeneity*. Springer-Verlag, New York, pp. 202-223.

Seuront,L. and Lagadeuc,Y (1997) Characterisation of space-time variability in stratified and mixed coastal waters (Baie des Chaleurs, Québec, Canada): application of fractal theory. *Mar. Ecol. Prog. Ser.*, **159**, 81-95.

Seuront,L. and Lagadeuc,Y. (1998) Spatio-temporal structure of tidally mixed coastal waters: variability and heterogeneity. *J. Plankton Res.*, **20**, 1387-1401.

Seuront,L., Schmitt,F., Lagadeuc,Y., Schertzer,D. and Lovejoy,S. (1999) Universal mutlifractal analysis as a tool to characterize multiscale intermittent patterns: example of phytoplankton distribution in turbulent coastal waters. *J. Plankton Res.*, **21**, 877-922.

Seuront, L., Schmitt,F., Lagadeuc,Y., Schertzer,D., Lovejoy,S. and Frontier,S. (1996) Multifractal analysis of phytoplankton biomass and temperature in the ocean. *Geophys. Res. Lett.*, **23**, 3591-3594.

Sugihara,G. and May,R. (1990) Applications of fractals in ecology. *Trends Ecol. Evol.*, **5**, 79-86.

van Hes,H.M. (1993) The spatial nature of soil variability and its implications for field studies. In Levin,S.A., Powell,T.M. and Steele,J.H. (eds), *Patch Dynamics*. Springer-Verlag, Berlin, pp. 27-36.

Wiens,J.A. (1989) Spatial scaling in ecology. *Funct. Ecol.*, **3**, 385-397.

A13

Turbulence and small-scale phytoplankton patchiness:

a new hypothesis on plankton feeding

Lagadeuc Y & Seuront L

Journal of Plankton Research (soumis)

Turbulence and small-scale phytoplankton patchiness: a new hypothesis on plankton feeding

Yvan Lagadeuc and Laurent Seuront

Station Marine de Wimereux, Université des Sciences et Technologies de Lille, UPRES-A CNRS 8013 ELICO, BP 80, F-62930 Wimereux, France

Abstract

Much of the work on effect of turbulence on plankton feeding is based on the concept of an increased of the contact rates between predator and prey. However, at the scale of mesozooplankton, the preys—the phytoplankton cells—are not homogeneously distributed under the effect of turbulence intermittency. Here, we argue that the effect of the turbulence could also be the result of the interaction between the zooplankton behaviour and the inhomogeneous distribution of the phytoplankton.

In order to understand the overall function of ecosystems, numerous studies have been devoted to the knowledge of processes at the scale of individuals (Levin, 1994). In biological oceanography, the influence of small-scale turbulence on predator-prey interactions in plankton has received much attention in recent years; this has stemmed from the seminal work of Rothschild & Osborn (1988), who proposed an enhanced rate of predator-prey contact due to small-scale turbulent shear. Thereafter, numerous studies were dedicated to this hypothesis (e.g. Dower *et al.*, 1997), and the effect of turbulence does not appear to be so simple. In particular, the zooplancton behaviours are influenced by and interact with turbulence induced increase ofpredator-prey contact rates. For instance, Saiz & Kiorboe (1985) hypothesized a major contribution of small-scale turbulence in the ambush feeding by copepods when compared to suspension feeders.

In general, all authors recognise the role of behaviour in the interaction between turbulence and plankton, and all the observed changes in behaviours are attributed to fluctuations in water motion or the motility of preys. However, no one has considered the spatial or temporal distribution of the prey, but rather that the preys, and especially the phytoplankton, are homogeneously distributed under the effect of small-scale turbulence. Yet, Yamazaki (1993) proposed that "plankton organisms, in fact, experience the local flow structure of turbulence, not the average of the flow field" because turbulence presents strong organisation in time and space. Consequently, he hypothesized that if plankton is able, with the help of their behaviour,

to use such organised flow, then it could derive some benefits. Finally, the question mainly addressed in the Yamazaki's hypothesis is that we have to know the "world" at plankton scale.

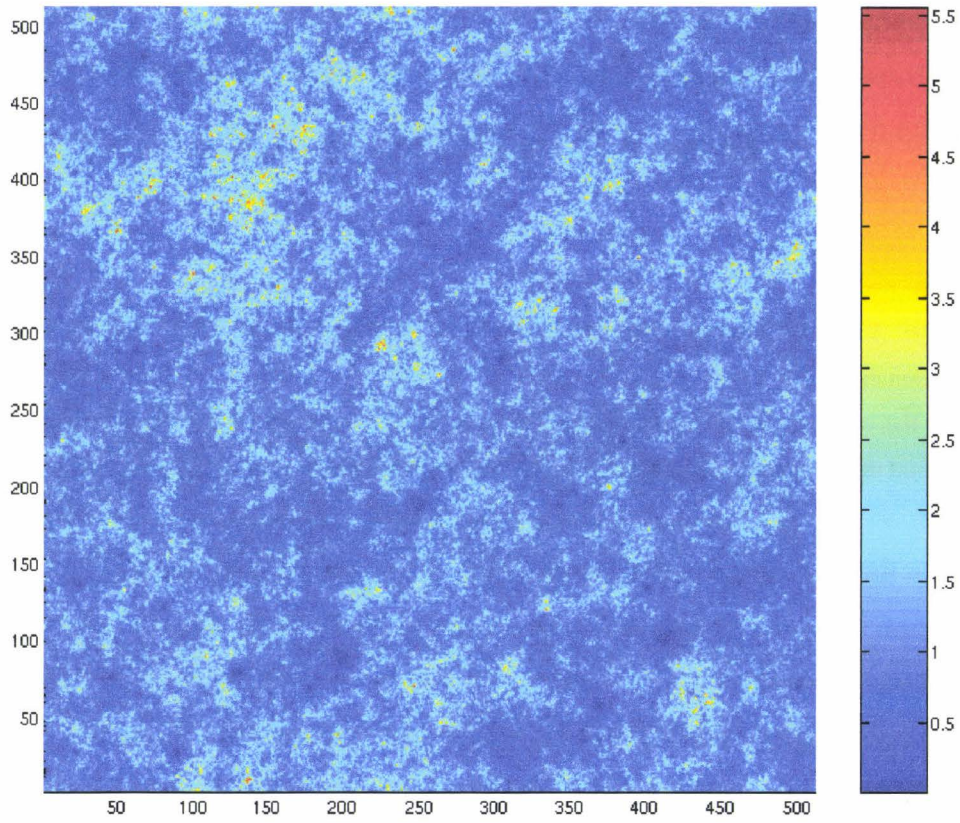

Fig. 1. Simulation of phytoplankton distribution using empirical multifractal parameters from Seuront *et al.* (1999) (arbitrary units).

In the English Channel, a highly tidally dissipative area, we have observed at microscale (Figure 1), an inhomogeneous distribution of phytoplankton (Seuront *et al.*, 1996, 1999). Moreover, the multifractal analysis, conducted on times series, has shown that the distribution of phytoplankton under 20 m is wholly controlled by the intermittency of turbulence. Consequently, copepods experience a field in which phytoplankton ditribution is not homogeneously distributed but exhibits local dense concentration values induced by turbulence. In such a context, if copepods are able to move from one dense patch to another, then they experience a local phytoplankonic field more dense than the average. Changes in copepod behaviour could thus be the response to the spatial distribution of the prey and not only to the fluctuation of turbulent water motions. Indeed, as proposed in the optimal foraging theory (Pyke 1984), zooplankton living in highly heterogeneous environments could reveal strategies used to exploit high density patches and then to optimise the energy required to

capture a given amount of food. This could be achieve, as suggested in a few laboratory studies undertaken in non-turbulent conditions, by increasing the complexity of swimming paths with increasing food densities, and/or by reducing motility in food patches (e.g. Tiselius, 1992; Bundy *et al.*, 1993; van Duren & Videler, 1995).

In following to the growing field of both theoretical and empirical studies that regard individual behaviour as a key problem to estimate the entire effect of small-scale turbulence on plankton feeding ecology, we suggest an alternative—and complementary—hypothesis to the one of Rothschild & Osborn (1988): an enhancement of feeding could also be the result of the behavioural ability of planktonic organisms to locate and exploit local dense prey patches generated by turbulent motions. This hypothesis could provide an alternative explanation to the apparent inequality observed by Saiz (1994) between empirical encounter rates and the theoretical values expected using the Rothschild & Osborn theory. Consequently, a precise description of the behaviour and distribution of both predators and prey appears to be a salient issue for the future modelling of plankton trophodynamics in turbulent environments (e.g. Osborn & Scotti 1996), supporting notably the advantage of individual based approaches (Yamazaki, 1993).

Acknowledgement

We especially thank Dr. G. Copp for improving the English of this paper, Dr. H. Yamazaki for helpful comments on the manuscript, and Dr. D. Marsan for the simulation.

REFERENCES

Bundy M.H., Gross T.F., Coughlin D.J. & Strickler J.R. (1993) Quantifying copepod searching efficiency using swimming pattern and perceptive ability. *Bull. Mar. Sci.*, **53**, 15-28.

Dower J.F., Miller T.J. & Leggett W.C. (1997) The role of microscale turbulence in the feeding ecology of larval fish. *Adv. Mar. Biol.*, **31**, 169-220.

van Duren L.A. & Videler J.J. (1995) Swimming behaviour of development stages of the calanoid copepod *Temora longicornis* at different food concentrations. *Mar. Ecol. Prog. Ser.*, **126**, 153-161.

Levin S.A. (1994) Patchiness in marine and terrestrial systems : from individuals to populations. *Phil. Trans. R. Soc. London. B*, **343**, 99-103.

Osborn T. & Scotti A. (1996) Effect of turbulence on predator-prey contact rates: where do we go from here? *Mar. Ecol. Prog. Ser.*, 139, 302-304.

Pyke J.H. (1984) Optimal foraging theory: a critical review. *Ann. Rev. Ecol. Syst.*, **15**, 523-575.

Rothschild B.J. & Osborn T.R. (1988) Small-scale turbulence and plankton contact rates. *J. Plankton Res.*, **10**, 465-474.

Saiz E. (1994) Observations of the free-swimming behavior of *Acartia tonsa*: effects of food concentration and turbulent water motion. *Limnol. Oceanogr.*, **39**, 1566-1578.

Saiz E., & Kiorboe T. (1995). Predatory and suspension feeding of the copepod Acartia tonsa in turbulent environments. *Mar. Ecol. Prog. Ser.*, **122**, 147-158.

Seuront L., Schmitt F., Lagadeuc Y., Schertzer D., Lovejoy S. & Frontier S. (1996) Multifractal structure of phytoplankton and temperature in the ocean. *Geophys. Res. Lett.*, **23**, 3591-3594.

Seuront, L., Schmitt, F., Lagadeuc Y., Schertzer, D. & Lovejoy, S. (1999) Universal multifractal analysis as a tool to characterize multiscale intermittent patterns. Exemple of phytoplankton distribution in turbulent coastal waters.*J. Plankt. Res* , **21**, 877-922.

Tiselius P. (1992) Behavior of *Acartia tonsa* in patchy food environments. *Limnol. Oceanogr.*, 37, 1640-1651.

Yamazaki H. (1993) Lagrangian study of planktonic organims: perspectives. *Bull. Mar. Sci.*, **53**, 265-278.

A14

Microscale turbulence intermittency and zooplankton dynamics: how to include behavioural components?

Lagadeuc Y, Seuront L, Ramat E, Preux P, Pitiot P, Denis V, Falk L & Vivier H

Oceanologica Acta (soumis)

Microscale turbulence intermittency and zooplankton dynamics: how to include behavioural components?

Yvan Lagadeuc[1], Laurent Seuront[1], Eric Ramat[2], Philippe Preux[2], Pascal Pitiot[3], Vanessa Denis[1], Laurent Falk[3] & Hervé Vivier[3]

1 : Station Marine de Wimereux, Université des Sciences et Technologies de Lille, UPRES-A ELICO, BP 80, 62930 Wimereux

2 : Université du Littoral, Laboratoire d'informatique du Littoral (LIL), BP 719, 62228 Calais cedex

3 : Laboratoire des Sciences du Génie Chimique, UPR CNRS 6811, BP 451, 54001 Nancy cedex

Abstract

The study of population dynamics is face to the problem of included variations existing at the scale of individual on global dynamics observed at mesoscale. The study of the influence of the turbulence, and of the intermittency of the turbulence (i.e. local strong fluctuations at all space or time scales), on the trophodynamics of zooplankton deals with this challenge. In the present case, we want to test the hypothesis that an enhancement of feeding could also be the result of the behavioural ability of plankton organisms to locate and to exploit local dense patches of phytoplankton generated by turbulent intermittent motions and exhibiting local dense concentration ranging 10 times the mean value. In this goal we have developed an experimental study of the behaviour of copepod and an individual-based model. These two kinds of approaches, which allow to study and to take into account the spatial distribution of the phytoplankton and the spatial behaviour of the zooplankton, are presented with the first results of validation.

Keywords : individual-based model, visualisation system, trophodynamic, zooplankton behaviour

Résumé:

L'étude de la dynamique des populations fait face au problème de la prise en considération des processus existants à l'échelle de l'individu dans la dynamique globale caractéristique de la mésoéchelle. L'étude de l'influence de la turbulence, et de l'intermittence de la turbulence (i.e. fortes fluctuations locales à toutes échelles d'espace et de temps), sur la dynamique trophique du zooplancton est pleinement confrontée à ce problème. Dans le cas présent, nous voulons tester l'hypothèse selon laquelle un accroissement du broutage du zooplancton peut être le résultat de la capacité comportementale des organisme planctonique à détecter et à utiliser des agrégats de phytoplancton induits par l'intermittence de la turbulence et dont la densité est parfois dix fois supérieure à la concentration moyenne. Dans ce but, nous avons développé une étude expérimentale du comportement du copépode et un modèle multi-agents. Ces deux types d'approches, qui permettent de prendre en considération la distribution spatiale du phytoplancton et le comportement spatial du zooplancton, sont présentées ainsi que les premiers résultats de validation.

Mots clés : Modèle multi-agents, système de visualisation, dynamique trophique, comportement du zooplancton

Among the objectives, or the recommendations, of the GLOBEC programme, two major axes have been underlined. The first one corresponds to a better knowledge of the interactions between physical and biological processes, the second one to a multiscale approach. These two points are generally intimately coupled because numerous physical or biological processes are multiscale [6, 21]. Such goals lead to consider simultaneously the variability or heterogeneity at each scale: e.g. from individual to community, or from the Kolmogorov scale to residual circulation. However, such objectives are face to the development and the use of new tools [14].

In such a context, a better knowledge of the population dynamics of zooplankton is tributary of a better understanding of processes implied at individual scale [23, 13]: turbulence, phytoplankton distribution, behaviour, etc. In that way, We develop studies on the effect of microscale turbulence, and more especialy on the effect of the turbulence intermittency. Indeed, if turbulence has traditionally been described as a way to create homogeneity, it is in fact a source of inhomogenity [9, 10] due to the intermittency of the flow (i.e. local strong fluctuations at all space or time scales). In a tidally dissipative environment, it appears that the phytoplankton is inhomogeneously distributed under the effect of the turbulence for scales lower than 20 meters [19]. Subsequently, the copepods experience a field where the preys, i.e. the phytoplankton cell, are not homogeneously distributed but rather exhibit local dense concentration ranging 10 times the mean value. In such a context, if copepods are able to move from one dense patch to another, they experience a local phytoplankonic field more dense than the average one. Then, We suggest an alternative–and complementary–hypothesis to the one of Rothschild & Osborn [17] : an enhancement of feeding could also be the result of the behavioural ability of plankton organisms to locate and to exploit local dense patches generated by turbulent motions. Consequently, if this hypothesis is true the copepod swimming paths should reflect the phytoplankton distribution. Numerous authors during these ten last years have studied the effect of turbulence on zooplankton, and more specifically on copepods behaviour [3, 4]. They described changes in the behavioural sequences, which generally correspond to an increased of the frequency of the fast moving behaviour. However, except the work of Bundy *et al.* [1], the technique generally used does not allow to follow the spatial location of the copepod. Modelling approach is the other way to test the effects of turbulence on trophodynamics of zooplankton [2, 24]. However, the behaviour is introduce, in existing model, by the way of the time budget spent to jump or to swim associated or not with feeding activity [2]. The mathematical expression of behaviour could also corresponds to a function

of swimming activity of both preys and predators, of the size of the prey and of the perceptive distance of the predator [11, 2]. None of these approaches allow to take into account the spatial and temporal distributions of the prey and the capacity of the predator to locate and identify areas of dense prey concentrations. In order to palliate these lacks we have developed a new technique to study experimentally the behaviour of copepods and an individual-based model. We present here these two approaches and the first results of validation.

Experimental study of the copepod behaviour

The experimental set-up was designed to track the three-dimensional displacement of a copepod in a cubic glass container (inner side 15 cm, effective volume 3.375 l). Two lamps (diffuse cold light 75W) illuminate the tank, one from the top, the other from the bottom to ensure homogeneity of the light source and thus to avoid phototropism. Reflections are minimised as much as possible and in order to produce a good contrast between the "white" copepod and the "black" background, two sides of the container were covered with black dull plastic film.

In order to reconstruct the three-dimensional motion of the copepod, two or more independent views of the system are required. Thus, two synchronised CCD cameras (HITACHI KP M1; 875*560 pixels; focal distance 17:53 mm) are placed orthogonally around the tank at a distance of about 1 m from the experimental container, so that the frame contains also a few reference points which allow a better fit of the camera. Those cameras deliver white and black frames at a rate of 12.5 frames per second. In the same conditions a grab of a ruler provides us the position of the cameras and the relation between pixels and millimetres.

The heart of the visualisation system is the encoder RGB-PAL (Enc110 (For-A)); our idea consists in using the decomposition of each colour frame in three components: one red, one green and the third blue. We only need two components in our system. Therefore, the encoder codes PAL-type colour frames from the instantaneous synchronised monochrome images from the camera called R (red) and G (green) (Figure 1). In that way each independent view gets an identity (red or green) and may be added to another at the same time t to form one single colour PAL-frame. Practically, the same copepod is filmed from two points of view and this frames superposition reduces hardware cost and provides perfect synchronisation. These colour images are digitised (image size 720*576 pixels), compressed and stored in real time thanks to a special acquisition card and an adequate software (PVR-Digital Processing Systems) on a PC. The frames-disk is able to store about 40 minutes of a series at 12.5 images per second. In this study only short movies were stored (5 minutes duration).

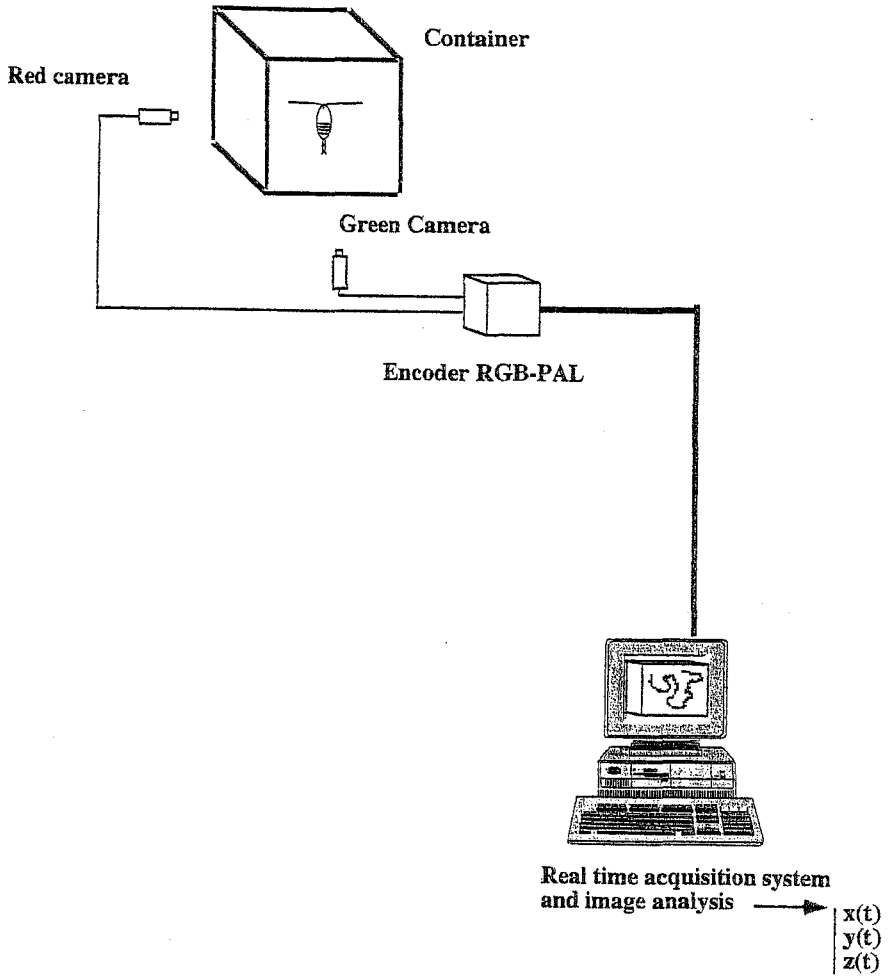

Fig. 1. Schematic representation of the visualisation system.

The three-dimensional components of the copepod motion must then be extracted from each frame using frame analysis. Because of the large field of view of the cameras, only the windows included the experimental container is kept. A pre-recorded background is removed from each frame, that leads to a coloured frame with a few objects (two, optimally: one for the red camera and one for the green camera with the same z coordinate). This later is decomposed into grey-level frames giving two binary frames by thresholding. After a morphological opening to eliminate small parasitic points, each binary frame is labelled to get the coordinates (in the image system) and the surface of the objects numbered on it. This frame processing is carried out on the acquisition PC (Pentium Pro 200 MHz) at a rate of 1.5 seconds per frame.

An identification program compares all objects found by frame analysis. After an elimination of supposed bad objects (identified as ludicrous discontinuities in the trajectory), another program takes into account spatial parallax and diffraction phenomena and gives the three coordinates of the copepod as a function of time in the container coordinates system.

In this preliminary study, we focused on the calanoid copepod *Temora longicornis* (Müller), a very abundant species in the Eastern English Channel, which is also of great ecological significance in many areas. It represent 35 to 70% of the total copepod population in the southern Bight of the North Sea [5], and in Long Island Sound, USA, *T. longicornis* has been shown to be able to remove up to 49% of the daily primary production [7].

Individuals of the copepod *Temora longicornis* were collected with a WP2 net (200 mesh size) in the offshore waters of the Eastern English Channel. Specimens were diluted in buckets and transported to the laboratory. To ensure some homogeneity in the physiological conditions of the copepods, the acclimation consisted of being held in 20 l beakers filled with 0.45 µm filtered seawater to which was added a suspension of the diatom *Skeletonema costatum* to a final concentration of 10^8 cells.l^{-1}. Prior to the filming experiment, adult females were sorted by pipette, acclimated for 24 h at 18°C and fed on a mixture of *Nannochloropsis occulata* (3 µm) and *Oxyrrhis marina* (13 µm). The larger heterotrophic flagelatte was present as an additional food source. All experiments were conducted within the same day to avoid differences in feeding history. An adult female was sorted by pipette and left in the experimental filming set-up to acclimatise for about 15 mn prior to filming. Two different concentrations of the mixture of *Nannochloropsis occulata* and *Oxyrrhis marina* were tested. One experiment (hereafter called A) has been conducted with *Nannochloropsis occulata* and *Oxyrrhis marina* at respectively 10^7 and 10^5 cells.l^{-1}, and two experiments (B and C hereafter) *Nannochloropsis occulata* and *Oxyrrhis marina* at 10^8 and 10^6 cells.l^{-1}, respectively.

The structure of the motion behaviour of *T. longicornis* was investigating by the way of spectral analysis conducted on the three components of the recorded trajectories. Roughly speaking, spectral analysis corresponds to an analysis of variance in which the total variance of a given process is partitioned into contributions arising from processes with different length scales or time scales in the case of spatially or temporally varying data, respectively. In our case (i.e. temporally recorded three-dimensional position), a power spectrum then separates and measures the amount of variability occurring in different frequency bands [8]. When all part of the spectrum $E(f)$ obeys a power-law form, i.e. $E(f) \approx f^{-\beta}$ (where f is frequency), the data are scaling in that range, i.e. the scaling regime. β is the exponent characterising spectral scale invariance. The absence of characteristic time scales and the presence of a scaling regime indicate that the same, or at least similar, process may be at the origin of the temporal structure of the observed variability.

In this preliminary results we cannot ascribe any significant effects on swimming pattern to food concentration due to the low number of experiments. However, the position plots (Figure

2) and the analyses perform show differences that will be briefly presented. In that way, one may note that within each experiment, there were significant differences between each velocity component (Kruskal-Wallis test, $p < 0.05$), the horizontal velocities being always greater than the vertical one (Dunn test, $p < 0.05$; [20]).

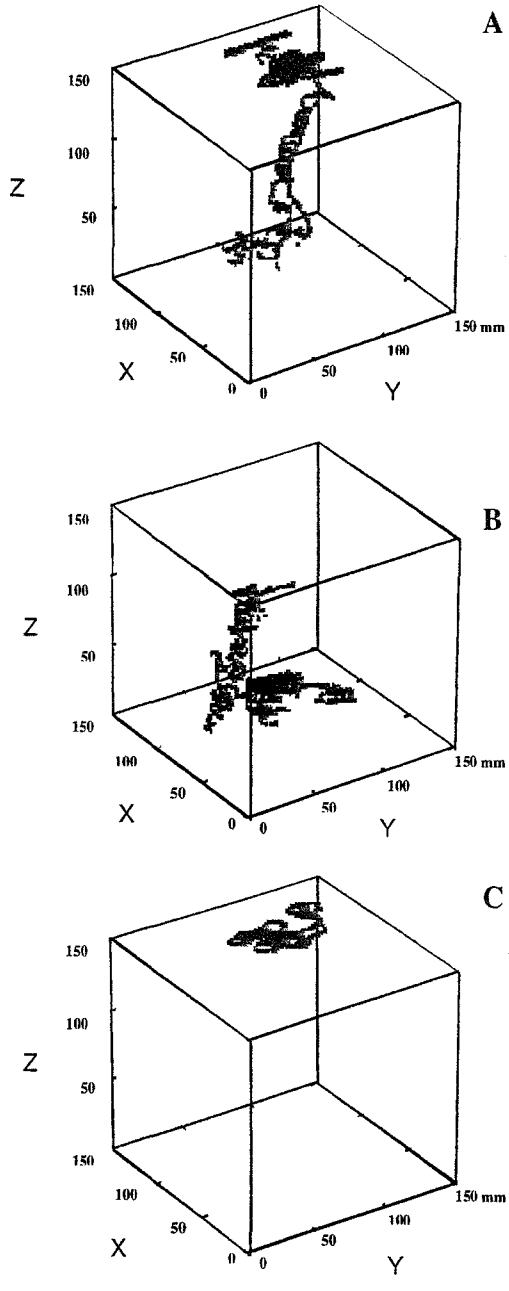

Fig. 2. Three-dimensional visualisation of the copepod location during experiments A, B and C (see text).

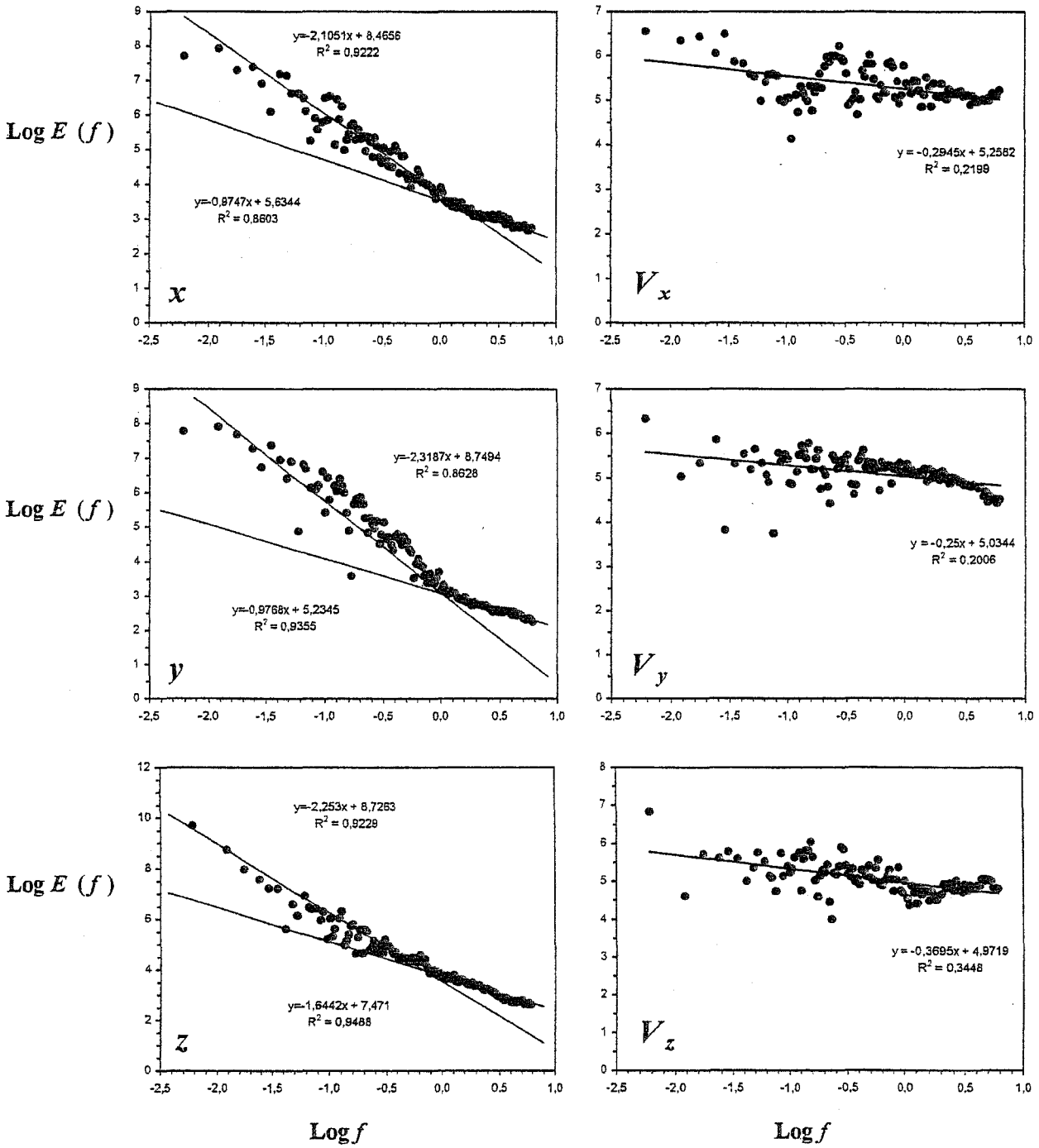

Fig. 3. Results of the spectral analyses performed on coordinates (figures on the left) and on speeds (figures on the right) for the experiment A.

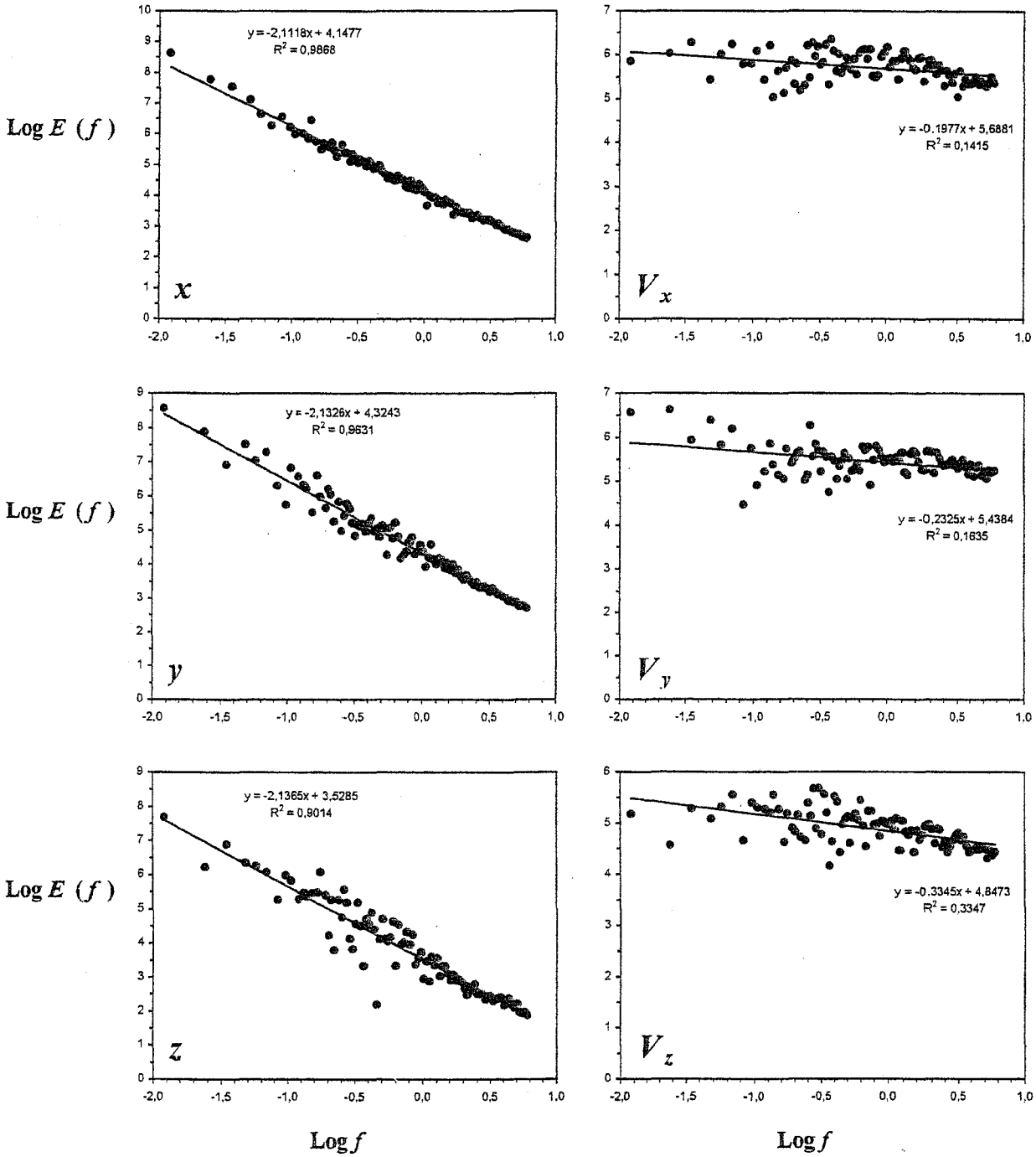

Fig. 3. Results of the spectral analyses performed on coordinates (figures on the left) and on speeds (figures on the right) for the experiment B.

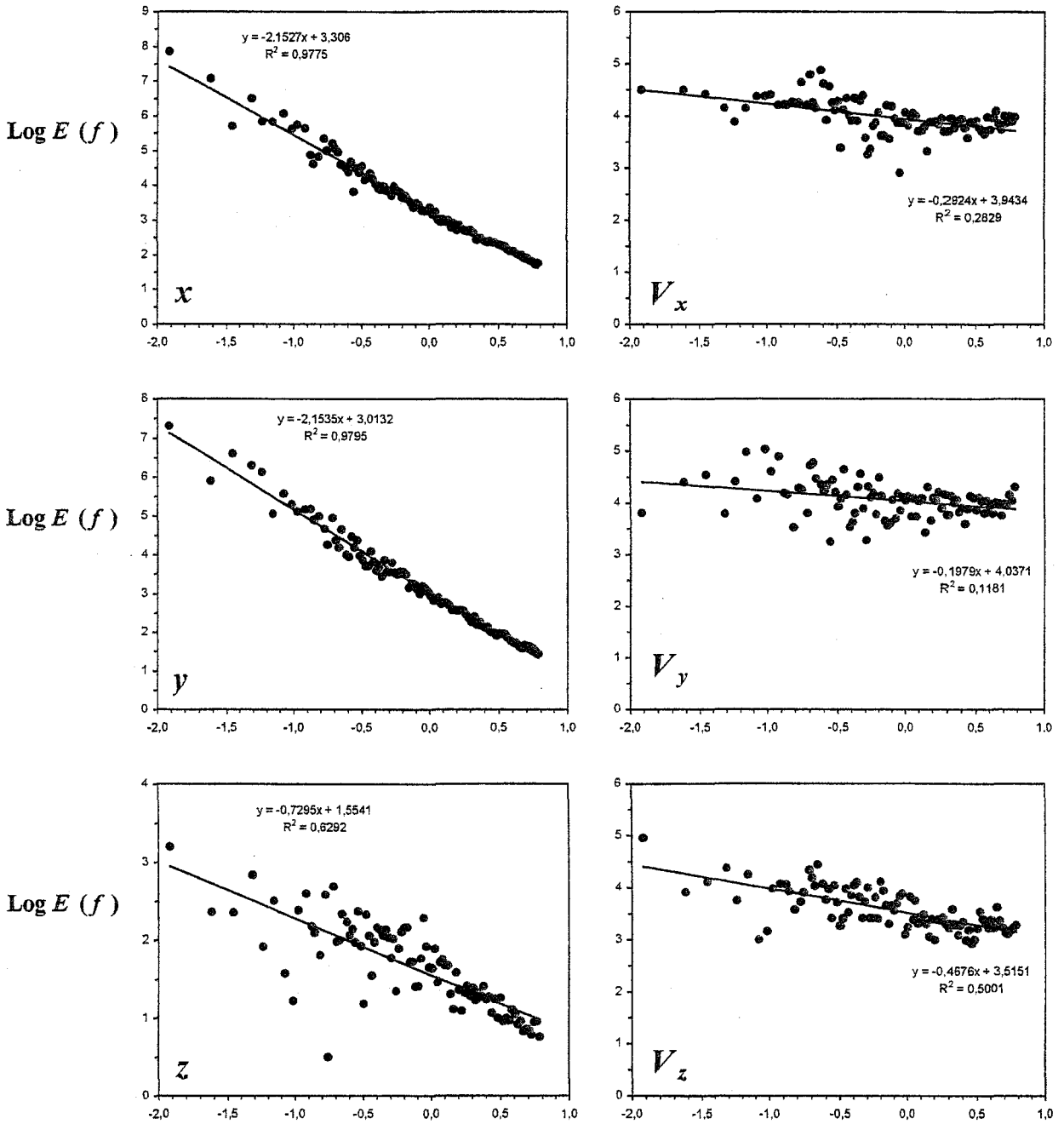

Fig. 3. Results of the spectral analyses performed on coordinates (figures on the left) and on speeds (figures on the right) for the experiment C.

The spectral analyses conducted on the different velocity components show that the spectral exponents β (Figure 3) cannot be statistically regarded as being different within a given experiment and between experiments (analyses of covariance; $p<0.05$ [25]), suggesting a relative homogeneity in the structure of the swimming speed fluctuations whatever the food concentration.

On the contrary, power spectra of the three coordinates of the swimming paths exhibit a differential behaviour related to food concentration (Figure 3). Thus, in low food concentration (experiment A), power spectra exhibit a clear scale breaking for a time scales of about one second (Figure 3 A). Moreover, the spectral exponents of the large scale scaling regime cannot be statistically distinguished ($p>0.05$), while the small scale ones exhibit significant differences. We then conducted a multiple comparison procedure based on the Tuckey test [25] to determine which β was different from the others, and showed that the spectral exponent characterising the vertical coordinate is significantly greater than the others ($p<0.05$). In high food concentration (experiments B and C), power spectra of the three coordinates of the swimming paths are obviously linear over the whole range of available scales (Figures 3B, C). The spectral exponents β of the three coordinates cannot be distinguished for the experiment B ($p>0.05$). On the contrary, there are significant differences between the spectral exponents for the experiment C ($p<0.05$), the exponent characterising the vertical coordinate being significantly smaller than the others, as indicated by a multiple comparison procedure ($p<0.05$). These results suggests, first, a differential swimming behaviour of the calanoid copepod *Temora longicornis* in the horizontal and in the vertical dimension, and second, a prey switching behaviour as a function of scales between the algae *Nannochloropsis occulata* and the flagellate *Oxyrrhis marina* in relation with food concentration. While prey switching behaviour related to food concentration has already been observed by Kiørboe *et al.* [12] for *Acartia tonsa*, further studies are still needed to test and validate these first observations.

Individual-based model

Until now, the copepod has been represented by models either of the type "black box" or analytical models. These models seek to describe in terms of input and output flows, and transfer functions each "process" of the organism. In this context, modeling of predation on phytoplankton by zooplankton includes the following processes : the copepod captures a prey

(a phytoplankton cell); then after a handling time, the prey is stored in the gut and enters the process of digestion; the gut transforms its contents in usable energy which one expresses out of nitrogen, or faecal pellets. This transformation is continuous: within each Δt, a quantity Δq of caught preys is processed (this quantity is proportional to the quantity stored in the gut). Usable energy is consumed (metabolism, digestion, or swimming activity), stored or used for reproduction.

Capparoy & Carlotti [2] proposed a model, synthesizing the various models developed until now, in which capture and ingestion processes use five coupled differential equations (Figure 4 ; Table I). This model fit well for the process of capture and metabolism functions. However, the contribution of the behaviour is partially considered. Indeed, the expression of the behaviour corresponds to a subdivision of the time into two kinds of activities: jumping or swimming. The spatial and temporal distributions of preys and predator are ignored, and our hypothesis could not be tested. To avoid this drawback we have develop an individual-based model which allows on the one hand to consider the spatial behaviour (including distribution) of prey and predator, and on the other hand to obtained emergent results without mathematical solving of coupled differential equations [16].

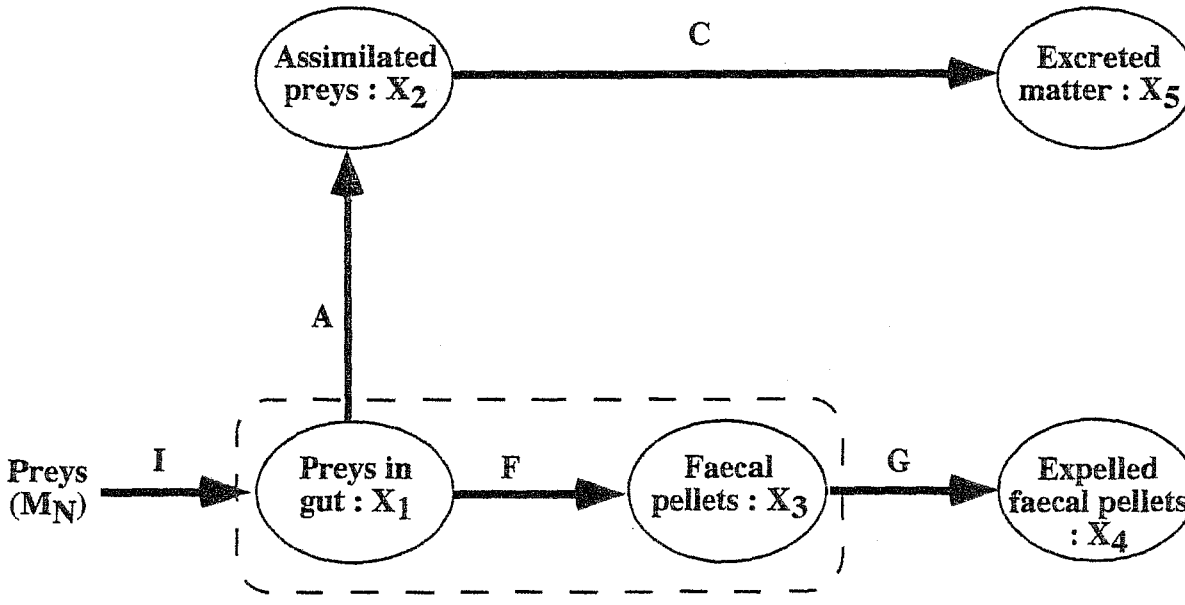

Fig. 4. Conceptual scheme of the physiological model (from [2]). X1 to X5 correspond to the state variables ; the fluxes correspond to the arrows : ingestion (I), assimilation (A), formation of faecal pellets (F), egestion (G), and excretion (C).

Prey in gut : X1	$\frac{dX_1}{dt} = I - A - F$
Assimilated prey : X2	$\frac{dX_2}{dt} = A - \left(\frac{C}{M_N}\right)$
Faecal pellets : X3	$\frac{dX_3}{dt} = F - G$
Expelled faecal pellets : X4	$\frac{dX_4}{dt} = G$
Excretted matter : X5	$\frac{dX_5}{dt} = C$

Table 1. Differential equations of the five state variables (from [2]) : X_1 (prey in the gut), X_2 (assimilated prey), X_3 (faecal pellets), X_4 (expelled faecal pellets), X_5 (excreted matter). Processes imply : ingestion (I), assimilation (A), formation of faecal pellets (F), egestion (G), excretion (C). M_N corresponds to the nitrogen mass of the prey.

The system under study is composed of a mass of water in which phytoplankton patches and copepods are immersed. Each of them, which is called agent, is located and has its properties among which its behaviour. The patches of phytoplanktons have a certain size and density, they correspond to a spatial agent. The copepod has various characteristics (its "mass" expressed in nitrogen, the volume of its gut, its swimming and jumping speeds...), and corresponds to a reactive agent. Practically, that means that its behaviour is governed by its perception and its current internal state, which, in turn, eventually induces an action and a new internal state after a stimulus. Its behaviour is defined by a Petri network [15 , 16] to allow the description of sophisticated behaviours with a standard and simple tool. Basically, Petri networks specifies the states within which an agent can be, the possible transitions between states, and the conditions to fulfill for each transition to occur. Each state is associated to a set of actions performed by the agent when the state is activated; actions may be a displacement in the space, an update of its internal state, perceiving its environment, etc. The state is activated when it is first reached. A transition actually occurs when its condition is fulfilled. In the simulation of real processes, it is crucial to take its duration into account. Hence, to each transition, a duration is assigned, which is either constant and deterministic, or stochastic. Moreover, by analogy with biological entities, any agent is endowed senses more or less developed. In this approach, senses are at the base of the network of knowledge of the agents. Dynamically, the agent builds its neighbourhood according to its position in space,

and to its senses. In our model, an agent has several senses and each them is defined by three parameters: the type of perceived agents, the sector (according to the orientation of the agent), and the distance within which the perceivable agents are actually perceived. By this way, one can test different scenarios according to possible models of perception of the copepod. In example, one agent can perceive only a part of the characteristics of another agent following specific perceived characteristics. The perception of an agent could also be modified by external factors as some environmental effect (turbidity, salinity, etc.) or internal factors (development stage, etc.).

In the present model, and in the case of those first simulations, the size of the copepod (1 mm) is used as the basic length for the discretization of the environment. The environment is considered as two dimensional and split into 1024 (32x32) chunks of $1mm^2$. Each chunk is dealt with by spatial agent and connected to the 8 neighbours. The number of cells of phytoplankton is 10^6 cells per liter. Thus, it is not conceivable to model each cell with one agent. The solution which was adopted consists in defining a property "Number of cells" at the level of spatial agents. The number of cells by chunk is defined by the multifractal parameters presented in Seuront *et al.* [18, 19]. The management of food is delegated to the spatial agent, which corresponds to the environment.

The copepod is defined by functions that control the displacement, the ingestion of food and the physiological processes. The functions governing the physiological state, or the energy budget of the copepod correspond to those used by Caparroy and Carlotti [2]. For further explanations and details concerning those functions one may then refer to this paper. The behavioural aspect of our model will be developed.

Here, We started from the assumption that the copepod adopts two distinct behaviours: a swimming behaviour associated with the search of food, and random jumps. The Petri net that models the dynamics of displacements of the copepod is divided into four parts:

- as soon as a cycle of 75 u.t.(unit of time for simulation) is elapsed, the copepod carries out a jump (one chunk in one u.t.) without considering what surrounds it, during 20 u.t. (time to cross a chunk of the environment), the copepod explores the place where it is and if food is available there it can capture a cell of phytoplankton. The handling of a cell of phytoplankton by the copepodis the quickest action in the model (1/20) and corresponds to unit time of simulation (u.t.). The captures of phytoplankton cells occur only if the copepod has not yet fed too much within the last u.t.. Indeed, the ingestion of food is control by a level of satiety, bounded, for

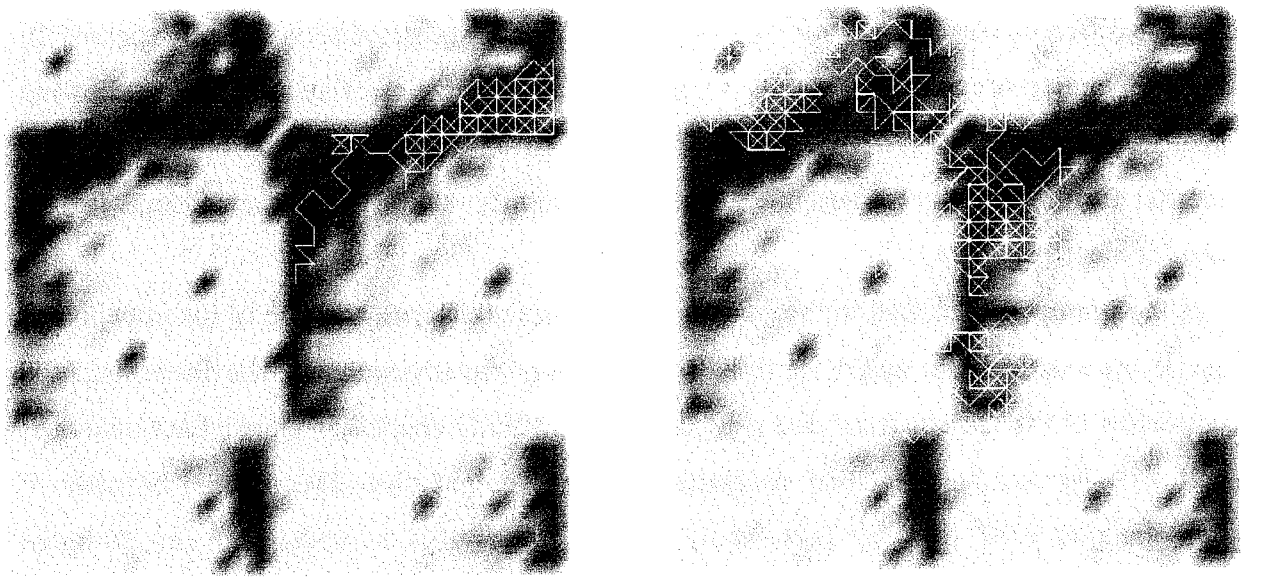

A B

Fig. 5. Visualisations of the paths followed by copepod in oriented (A) and random (B) simulations. The grey levels correspond to different phytoplankton densities.

the moment, by the number of cells of phytoplankton present in the gut. The function of satiety is [2]:

$$C_g = 1 - \frac{V_{prey} X_1}{\frac{2}{3} V_{gut}}$$

where $V_{prey}X_1$ represents the volume of the not-yet-digested preys and V_{gut} the volume of the gut of the copepod. It captures the cell according to a certain probability and, if it does not, the cell disappears from its field of vision.

- on the other hand, if there is no food, it continues to swim to reach the next chunk,
- at the end of the 20 u.t. necessary to cross a chunk, the copepod "chooses" a new chunk to be explored among the three chunks located in front of it, and proceeds there.

This last change is a function of the copepod behavioural strategy. In the case of our present work two kind of strategy have been tested. The probability that a chunk is chosen is either random or proportional to the amount of food it holds: the more food, the more likely the copepod will move to it. In the case of the oriented strategy, the densities of cells present in the three chunks are normed to one, and correspond to the probability for the copepod to move in one chunk or in the other.

Using the variables defining the internal state of copepod agents, we measure within each step of simulation: the energy, expressed in pg of nitrogen, contained in the gut, its usable energy, the number of captured phytoplankton cells and two variables of the analytical model (X3 and X4).

Visualisations of the paths followed by copepods in the oriented or random simulation show strong differences (Figure 5). These differences are well reflected by the ingestion budgets; it appears clearly that the directed stroke enhance the feeding of the copepod (Figure 6).

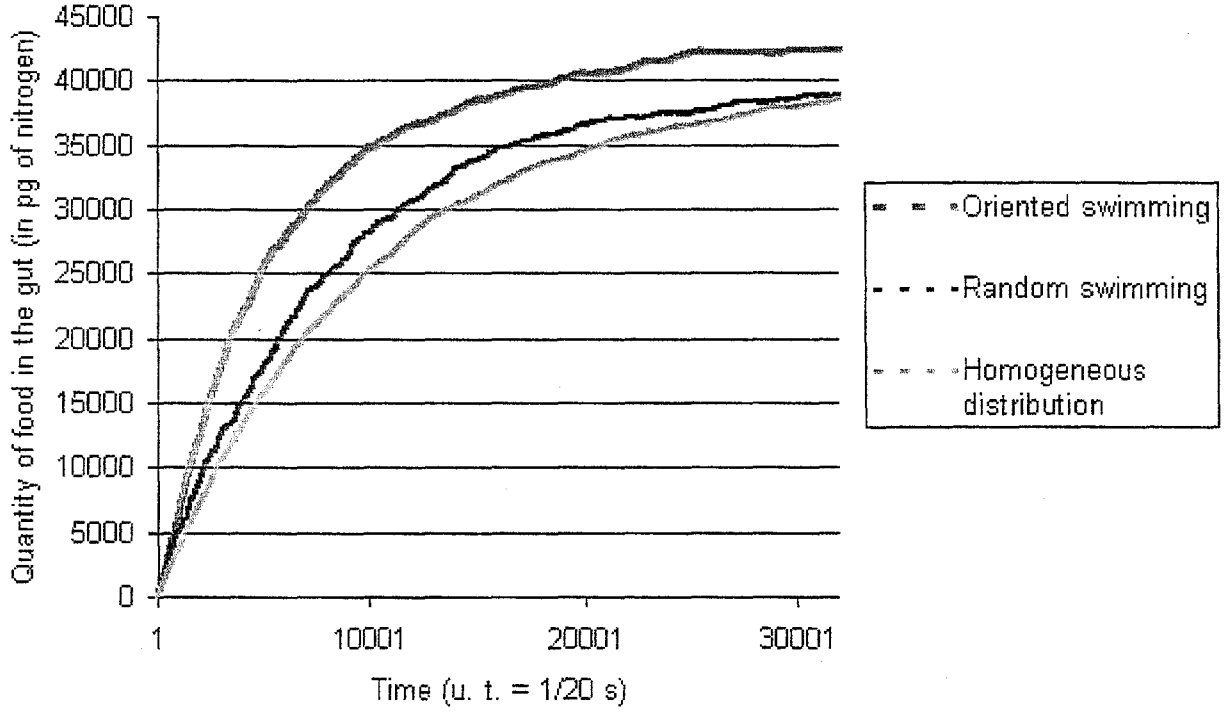

Fig. 6. Quantity of food in the gut. Results for oriented, random and « homogeneous distribution » simulations.

If the copepod is located inside a homogeneous field of phytoplankton, the swimming strategy does not have any influence on the feeding since it is able to find food in all directions in same quantity. Moreover, it will be noticed that, in a heterogeneous field, the random strategy leads the copepod to find food as it is in a homogenous field.

Conclusion

Actually, due to the low number if experiments conducted, no precise conclusion could be proposed on the effect of the turbulence intermittency on trophodynamics of zooplankton. However, we have developed two new tools, which could allow to consider the local structure of phytoplankton and turbulence on zooplankton as recommended by Yamazaki [23]. Moreover, with the double approach developed here, the individual is in the centre of our study, and the matter budget will emerge at larger scales. However, taking into account microscale and individuals also implies conceptual problems. For example, we are now interested to break up the "enigmatic" processes, such as the random jumps or the speed of constant stroke. It is obvious that behind these actions are hidden rules of decision, or more complex processes [22]. For example, the observation shows that the swimming speed is not constant and that it has been hypothesis that these variations are due to interactions with the environment. Furthermore, it is obvious that a copepod did not behave in the same way on its own, or within a colony of its kind. It remains to imagine the processes implied and subsequently specify them precisely. In addition, if one is interested in the rules of decision regarding the capture of a cell of phytoplankton, one can wonder whether elements such as the physiological state of the copepod do not come into play. For example, a female, carrying eggs, could require more food than a male.

In such context, the confrontation of the experimental observations and the model, which is able to translate simply behavioural component, will be fruitful. The results of the experiments will be translated in behavioural hypothesis and tested in the model. The model will be also used to test existing described behaviour as recently done by Kiorboe and Saiz [11].

The model could be of course developed, and one of the first step, will be the introduction of the flow induced by turbulence [24]. The second step will be the introduction of intra and inter-specific interactions.

[1] Bundy M. H., Gross T. F., Coughlin D. J., Strickler J. R., Quantifying copepod searching efficiency using swimming pattern and perceptive ability, Bull. Mar. Sci., 53(1) (1993), 15-28.

[2] Capparoy P., Carlotti F., A model for *Acartia tonsa* : effect of turbulence and consequences for the related physiological processes, J. Plankton Res., 18 (1996), 2139-2177.

[3] Capparoy P., Pérez M. T., Carlotti F., Feeding behaviour of *Centropages typicus* in calm and turbulent conditions, Mar. Ecol. Prog. Ser., 168 (1998), 109-118.

[4] Costello J. H., Strickler J. R., Marassé C., Trager G., Zeller R., Freise A. J., Grazing in a turbulent environment : Behavioral response of a calanoid copepod, *Centropages hamatus*, Proc. Natl. Acad. Sci. USA, 87 (1990), 1648-1652.

[5] Daan R., Factors controlling the summer development of the copepod populations in the southern bight of the North Sea, Neth. J. Sea. Res., 23 (1989), 305-440.

[6] Daly K. L., Smith W. O., Jr., Physical-Biological interactions influencing marine plankton production, Annu. Rev. Ecol. Syst., 24 (1993), 555-585.

[7] Dam H. G., Peterson W. T., Seasonal contrasts in the diel vertical distribution; feeding behavior and grazing impact of the copepod *Temora longicornis* in the Long Island Sound, J. Mar. Res., 51 (1993), 561-594.

[8] Fasham M. J. R., The statitical and mathematical analysis of plankton patchiness, Oceanogr. Mar. Biol. Ann. Rev., 16 (1978), 43-79.

[9] Jimenez J., Oceanic turbulence at millimeter scales, Sci. Mar., 61 (1997), 47-56.

[10] Jou D., Intermittent turbulence : a short introduction, Sci. Mar., 61 (1997), 57-62.

[11] Kiørboe T., Saiz E., Planktivorous feeding in calm and turbulent environments, with emphasis on copepods, Mar. Ecol. Prog. Ser., 15 (1995), 135-145.

[12] Kiørboe T., Saiz E., Viitasalo M., Prey switching behaviour in the planktonic copepod *Acartia tonsa*, Mar. Ecol. Prog. Ser., 143 (1996), 65-75.

[13] Levin S. A., Patchiness in marine and terrestrial systems : from individuals to populations, Phil. Trans. R. Soc. London. B, 343 (1994), 99-103.

[14] Levin S. A., Grenfell B., Hastings A., Perelson A. S., Mathematical and computational challenges in population biology and ecosystems science, Science, 275 (1997), 334-343.

[15] Peterson J. L., Petri Net Theory and the Modelling of Systems, Prentice-Hall, New Jersey, 1981, Pages pp.

[16] Ramat E., Preux P., Seuront L., Lagadeuc Y., Modélisation et simulation multi-agents en biologie marine. Etude du comportement du copépode., in , Actes du Colloque SMAGET (Système Multi-agents pour la gestion de l'environnement et des territoires), in press.

[17] Rothschild B. J., Osborn T. R., Small-scale turbulence and plankton contact rates., J. Plankton Res., 10 (3) (1988), 465-474.

[18] Seuront L., Schmitt F., Lagadeuc Y., Schertzer D., Lovejoy S., Universal multifracatla analysis as a tool to characterize multiscale intermittent patterns: example of phytoplankton distribution in turbulent coastal waters, J. Plankton Res., 21 (in press).

[19] Seuront L., Schmitt F., Lagadeuc Y., Schertzer D., Lovejoy S., Frontier S., Multifracatl analysis of phytoplankton biomass and temperature in ocean, Geophys. Res. Lett., 23 (1996), 3591-3594.

[20] Siegel S., Castellan N. J., Nonparametric Statistics for the Behavioral Sciences., McGraw-Hill, Singapor, 1988, Pages pp.

[21] Steele J. H., Henderson E. W., Coupling between phsical and biological scales, Phil. Trans. R. Soc. London B, 343 (1994), 5-9.

[22] Van Duren L. A., Videler J. J., The trade-off between feeding mate seeking and predator avoidance in copepods : behavioural responses to chemical cues, J. Plankton Res., 18 (1996), 805-818.

[23] Yamazaki H., Lagrangian study of planktonic organisms : perspectives, Bull. Mar. Sci., 53(1) (1993), 265-278.

[24] Yamazaki H., Osborn T. R., Squires K. D., Direct contact simulation of planktonic contact in turbulent flow, J. Plankton Res., 13(3) (1991), 629-643.

[25] Zar J. H., Biostatistical analysis, Prentice Hall, New Jersey, 1996, Pages pp.

A15

Small-scale mixing processes in the coastal ocean:
low order deterministic chaos or high order stochasticity?

Seuront L

Journal of Plankton Research (soumis)

Small-scale mixing processes in the coastal ocean: low order deterministic chaos or high order stochasticity?

Laurent Seuront

Station Marine de Wimereux, CNRS UPRES-A 8013 ELICO, Université des Sciences et Technologies de Lille, BP 80, F-62930 Wimereux, France

Abstract. Almost all regions of the oceans are heavily influenced by the effects of physical processes such as turbulence which in turn influence the distribution and ecology of organisms that occupy these regions. There is a real need for additional focus placed on the precise knowledge of both physical and biological processes which is often difficult using basic time series analysis. In that way, we applied non-linear analysis techniques to high frequency time series of temperature, salinity, nutrient and phytoplankton concentrations recorded in different hydrodynamical regimes related to tidal forcings in a tidally mixed coastal ecosystem. Techniques devoted to the identification of low order deterministic chaos cannot find evidence of chaos. The results rather suggest stochastic time series with many degrees of freedom: no obvious attractor in phase space trajectory, positive largest Lyapunov exponent close to zero, absence of convergence of the correlation integral. We then applied to these data specific multifractal analysis techniques and showed that these time series clearly exhibit high order stochasticity, but also that this stochasticity can be regarded as highly structured in time and space.

Introduction

Since the seminal studies of chaos in discrete time models in population ecology (May, 1974, 1975, 1976), the issue of chaotic dynamic in ecological systems has been widely controversial (Hassell *et al.*, 1976; Berryman and Millstein, 1989; Pool, 1989). Chaos in ecology has nevertheless been the subject of an increasing amount of literature. In theoretical ecology, there are many examples of temporal population models which exhibit chaos. The interaction of three variables in a predator-prey-nutrient system (Kot *et al.*, 1992) is now a well studied chaotic system, as chaotic dynamics expected through a trophic coupling of three species (Hastings and Powell, 1991). Recently, an ocean ecosystem model also exhibits chaotic properties related to the external seasonal forcings (Popova *et al.*, 1997). In particular, the issues raised by chaos theory in ecology have been the subject of several recent reviews (May, 1980, 1987; Godfrey and Blythe, 1991; Ellner, 1992; Logan and Allen, 1992; Hastings *et al.*, 1993; Little *et al.*, 1996).

The compelling reasons for the emerging chaos theory to ecology is based on the hope that complex systems could be explained by relatively low-order processes. This leads to the development of a suite of algorithms aimed at the detection of chaotic behaviour and the classification of system dynamics (see Hastings *et al.*, 1993; Ellner and Turchin, 1995 for

reviews). While such approaches have been applied to a wide variety of time series (Farmer and Sidorowich, 1987; Ellner, 1992; Theiler *et al.*, 1992), as to detect dynamic spatial chaos (Rubin, 1992; Rand, 1994; Solé and Bascompte, 1995), the development of non-linear thinking to marine ecology has a more recent history. Only a few studies have been devoted to detect chaotic signature in both marine time series and transects, and led to controversial results. Thus, Sugihara and May (1990) found evidence for chaotic dynamics in time series of weekly diatom counts, and Scheffer (1991) argued that chaotic deterministic dynamics should be commonplace in plankton communities. On the contrary, Ascioti *et al.* (1993) as Strutton *et al.* (1996, 1997) did not find any evidence of chaotic dynamics in both zooplankton and phytoplankton time series and phytoplankton transects, respectively.

More recently, a new field of marine research has been devoted to the stochastic characterization of intermittent processes in the framework of multifractals (Pascual *et al.*, 1995; Seuront *et al.*, 1996a, b, 1999; Seuront, 1997, 1999). Multifractals, which has been recently reviewed by Pascual *et al.* (1995) and Seuront *et al.* (1999), can be regarded as a generalization of fractal geometry (Mandelbrot, 1983) initially introduced to describe the relationship between a given quantity and the scale at which it is measured. While fractal geometry describes the structure of a given descriptor with the help of only one parameter (i.e. the so-called fractal dimension), multifractals characterize its detailed variability by an infinite number of sets (roughly speaking, each of them corresponds to the fraction of space where data exceed a given threshold), each with its own fractal dimension. Such approaches, which do not require any statistical preconception on the data, provide very good approximations—at all scales and all intensities—of the statistics of an intermittently fluctuating descriptor, and determine the probability description of the descriptor values (see Pascual *et al.* (1995) and Seuront *et al.* (1999) for further details). Moreover, the statistical consequence of intermittency being a strong departure from Gaussianity (Baker and Gibson, 1987), multifractals thus provide a powerful alternative to basic random walk models explicitly based on Gaussian statistics (see e.g. Peitgen *et al.*, 1992). Thus, considering that in the general background of spatio-temporal intermittency encountered in the ocean (e.g. Platt *et al.*, 1989), knowledge of the precise statistics of any intermittent fields may avoid the bias introduced by chronic undersampling of an intermittent signal (Bohle-Carbonel, 1992), a stochastic multifractal framework is particularly well suited to describe the structure of quantities that vary intermittently (Pascual *et al.*, 1995; Seuront *et al.*, 1996a, b, 1999).

Several misconceptions about chaos precisely pertain to its relationship to stochastic behaviour (Hastings *et al.*, 1993). Chaos and stochasticity are nevertheless not equivalent: not only do the underlying mechanisms differ, but the consequences for observers are very different. In purely deterministic systems, predictions made from the governing equations will be perfect. Chaotic systems are predictable over short time scales because they are deterministic; the lack of predictive power over long time scales stems from the lack of complete information about the exact location of initial conditions. In contrast, purely stochastic systems are unpredictable over any time scales because of their probabilistic nature. In such approaches, the variability of a given descriptor is driven by 'news' events, which represent exogenous variables—exogenous in the sense that they are not a part of an internal mechanism which drives the descriptor fluctuations. The branches of a tree move because of the wind, which is 'exogenous' to the tree, and therefore 'news' to it, whereas a chaotic model of the motion of trees would assume the existence of a simple deterministic 'non-linear' engine within the tree (i.e. endogenous) which generates chaotic motion by a simple mechanism of feedback of the motion of the tree upon itself. Finally, the distinction between stochastic and deterministic dynamics has important practical implications. For instance, if fluctuations in population sizes are driven primarily by deterministic factors, and if those factors are understood, then the dynamics are predictable over short time scales. Management of such populations is feasible. On the other hand, if fluctuations are driven primarily by exogenous stochastic forces, then prediction and management become much more difficult.

Thus, given that deterministic equations in a small number of variables can generate complicated behaviour, the question arises: how much of the complicated behaviour observed in nature can be describe by a small number of variables? This question has been widely addressed in the framework of turbulence. Ruelle and Takens (1971) indeed showed that near the transition to turbulence, the many degrees of freedom of turbulence are coupled coherently, and lead to an enormous reduction in dimension (i.e. low order deterministic chaos). However, both empirical and theoretical studies have demonstrated that fully developed turbulence (Schertzer and Lovejoy, 1983; Parisi and Frisch, 1985; Benzi *et al.*, 1984) was rather characterized by its multifractal properties (i.e. high order stochasticity). Moreover, let us recall that in previous empirical studies of phytoplankton patchiness in turbulent environments, Seuront *et al.* (1999) suggested a potential effects of both hydrodynamic and advective processes on the multifractal structure of both physical (i.e. temperature and salinity) and biological (i.e. phytoplankton biomass) parameters.

Herein, the goal of this paper is, first to find out whether time series of physical (temperature and salinity) and biological (phytoplankton biomass) parameters recorded in different tidal conditions during about four tidal cycles in the well-mixed waters of the Eastern English Channel are chaotic or not, and second, to test the potential effects of differential tidal forcings on the chaotic and/or stochastic nature of the variables in question. In order to identify potential chaotic signature, several complementary techniques of phase-space reconstruction were used, for the first time to our knowledge, to temporal data from the marine environment. On the other hand, the universal multifractal formalism [see Seuront *et al.* (1999) for a review in the framework of marine ecology] has been devoted to characterize the detailed stochastic structure of the data sets.

The data

Sampling experiment was conducted during 48 h (ca. four tidal cycles) in a period of spring tide, from 2 to 4 April 1996, at an anchor station (Fig. 1) located in the coastal waters of the Eastern English Channel (50°47'300 N, 1°33'500 E), a hydrodynamically dominated area characterized by its megatidal regime. Temperature, salinity and *in vivo* fluorescence intensity were simultaneously recorded at 1 Hz from a single depth (10 m) with a SBE 25 Sealogger CTD, and a Sea Tech fluorometer, respectively. Every hour, samples of water were taken at 10 meters depth to estimate chlorophyll *a* concentrations, which appear significantly correlated with *in vivo* fluorescence (Kendall's $\tau = 0.652$, $P < 0.05$; Seuront *et al.*, 1999). In the following, the latter parameter will then be regarded as a direct estimate of phytoplankton biomass. While the structure of the whole resulting temperature, salinity and *in vivo* fluorescence data sets (i.e. 167040 data points) have already been investigated in the framework of universal multifractal [see Seuront *et al.* (1999)], the main objective of this contribution is to investigate the potential effect of varying tidal forcings on the local structure of physical and biological parameters. Thus, the data analyzed here consist in 24 time series (labelled from S1 to S24) of one hour duration (ca. 3600 data points) re-sampled from the original dataset in order to be representative of the different conditions of tidal current speed and direction, taken every 5 minutes, from the sampling depth (Table I).

Method

Data pre-processing

Time series analysis requires the assumption of at least reduced stationarity, i.e. the mean and the variance of a time series depend only on its length and not on the absolute time (Legendre

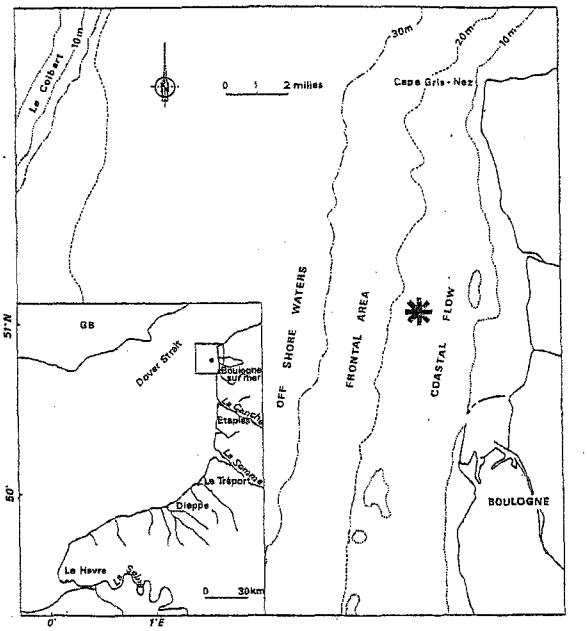

Fig. 1. Study area and location of the sampling station (*) along the French coast of the Eastern English Channel.

	Tidal current		Depth	T	S	F
	Speed ($m.s^{-1}$)	Dir (°)				
S1	0.55	240	21.56	6.55	34.60	18.32
S2	0.45	220	22.49	6.53	34.60	15.20
S3	0.10	60	27.38	6.51	34.62	10.90
S4	0.95	15	28.28	6.50	34.66	9.39
S5	0.90	10	26.21	6.49	34.70	8.23
S6	0.15	10	23.25	6.51	34.65	10.25
S7	0.32	260	21.52	6.53	34.61	15.02
S8	0.62	230	22.21	6.52	34.62	17.24
S9	0.10	85	27.19	6.50	34.65	11.45
S10	0.98	10	28.47	6.49	34.72	6.80
S11	1.00	10	26.53	6.49	34.67	7.29
S12	0.30	10	23.66	6.50	34.64	11.00
S13	0.35	290	21.38	6.53	34.62	17.40
S14	0.30	200	21.72	6.55	34.62	15.82
S15	0.11	140	26.19	6.52	34.66	13.46
S16	0.80	10	28.65	6.5	34.69	10.75
S17	1.10	10	27.15	6.49	34.70	6.64
S18	0.40	10	24.15	6.51	34.68	7.35
S19	0.35	260	21.75	6.53	34.63	12.64
S20	0.87	250	21.68	6.55	34.62	17.69
S21	0.73	230	25.23	6.55	34.61	15.16
S22	0.18	10	28.65	6.53	34.71	8.30
S23	1.04	10	27.50	6.50	34.66	5.37
S24	0.60	10	25.95	6.50	34.62	3.87

Table I. Tidal conditions, water column depth and mean values of temperature, salinity and *in vivo* fluorescence for the 24 studied data sets.

and Legendre, 1984). The existence and the significativity of any potential linear trends was testing calculating Kendall's τ autocorrelation which does not require any hypothesis about the characteristics of the original dataset distribution [Kendall's coefficient of correlation was used in preference to Spearman's coefficient of correlation ρ because Spearman's ρ gives greater weight to pairs of ranks that are further apart, while Kendall's τ weights each disagreement in rank equally, see Sokal and Rohlf (1995) for further developments]. We then eventually detrended time series fitting linear regressions to the original data by least squares and used the regression residuals in further analysis, a common remedial procedure in time-series analysis (Fuller, 1976). The purpose of this is to eliminate aliasing in further analysis due to large scale structures present in the data sets, such as in monotonically increasing or decreasing trends.

In order to provide direct comparisons between the different parameters, the time observations, y_i, were converted into normalized, dimensionless descriptors, x_i, following:

$$x_i = \frac{y_i - y_{\min}}{y_{\max} - y_{\min}} \tag{1}$$

where $y_{\max}$ and $y_{\min}$ are the maximum and minimum values of the series, respectively (Gower, 1971). Samples of the resulting time series are given in Figure 2.

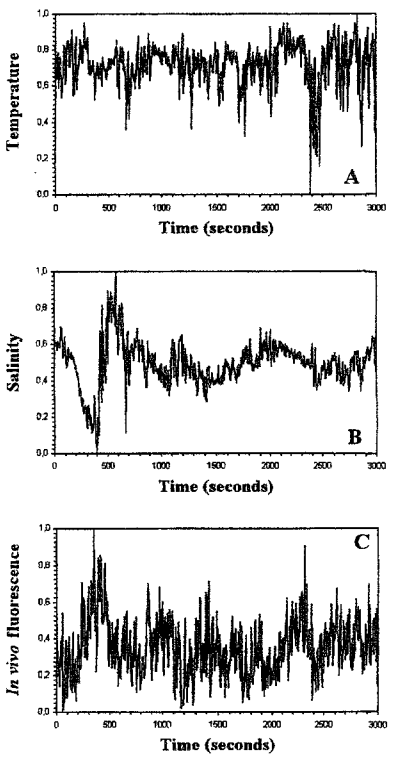

Fig. 2. Normalized temperature (**A**), salinity (**B**) and *in vivo* fluorescence (**C**) time series recorded in the Eastern English Channel, shown for data set S1.

The search for deterministic chaos

In the following our datasets are regarded as finite sets of time observations, x_i, taken at regular intervals, $\Delta t = 1$ second for temperature, salinity and *in vivo* fluorescence time series:

$$X_i = \{x(1), x(2), x(3), \ldots, x(N_{obs})\} \tag{2}$$

where N_{obs} is the total number of observations in each set. The time length of any observed period, T, is related to N_{obs} as:

$$T = N_{obs}\Delta t \tag{3}$$

More specifically, the three methods used here to investigate the properties of our sets, i.e. the Packard-Takens method (Packard *et al.*, 1980; Takens, 1981), Lyapunov exponents estimates (Wolf *et al.*, 1985), and the correlation integral method (Grassberger and Procaccia, 1983), are based on the assumption that the dynamics of any underlying dynamical systems can be described in some multidimensional phase-space from the knowledge of the time series of a single observation $x(t)$ by constructing E-dimensional vectors defined by:

$$\vec{X}(t) = (x(t), x(t-\tau), \ldots, x(t-(E-1)\tau) \tag{4}$$

where E is the embedding dimension (i.e. the dimension of the vectors), and $\tau = p\Delta t$ is the lag (i.e. the number of data points separating each of the vector's elements). As an example, one can observed that for $E = 3$ and $\tau = 1$, the vector $\vec{X}(t)$ consists of $x(t)$ and the $E-1$ immediately preceding points of the time series (i.e. the set of vectors $\{\vec{X}(3), \vec{X}(4), \ldots, \vec{X}(n)\}$ is denoted as $\{(x(3), x(2), x(1)), ((x(4), x(3), x(2)), \ldots, ((x(n), x(n-1), (x(n-2))\}$).

In the above case, the delay time τ must be chosen so as the result in points that are not correlated to previously plotted points. Thus, a first choice of τ should be in terms of the decorrelation time of the time series (Tsonis *et al.*, 1993). A straightforward procedure is to consider the decorrelation time equal to the lag at which the autocorrelation function for the first time attains the value of zero. One may also note here that no averaging nor filtering have been employed since it is known that such data manipulations can obscure the presence of chaos (Ellner, 1992).

The Packard-Takens method (PTM). Dissipative dynamical systems which exhibit chaotic behaviour often have a strange attractor in phase-space (Grassberger and Procaccia, 1983). It is for instance the case for the movements of atmospheric flows which produce a specific phase-space trajectory now widely known as the Lorentz's attractor (Lorenz, 1963). More

precisely, a strange attractor has orbits that lies within a defined region of phase-space but the orbits never intersect and never follow the same trajectory twice.

The phase-space attractor of a system is then a map of the changing conditions in the system: each point on the attractor is a summary of all the variables affecting the system at a moment in time. As the system evolves, changes in the variables result in a different location of the point in phase-space. The points in phase-space trace a trajectory that summarizes the changes of the system. Three-dimensional phase-space diagrams of the attractor describing the time series were produced using the 'time delay' method of Packard *et al.* (1980). In practice, the one-dimensional time series, and thus all the factor affecting it, can be represented by the trajectory of points in three-dimensional phase-space. The attractor is created by plotting each value as a function of its preceding value, or in other words, from the plot of $x(t+1)$ vs. $x(t)$, where x is the actual value (in our case the normalized, dimensionless descriptors) and t the index of the point. It can be noticed here that an attractor with a regular shape will also emerge in plots using $x(t+2)$ or $x(t+3)$ for example, or $x(t+n)$, with many n. This procedure was repeated for each successive point in the time series and the resultant points were connected producing the phase-space trajectory.

Largest Lyapunov exponents (LLE). The limits of predictability are set by how fast the trajectories diverge from nearby initial conditions. This feature is quantified by Lyapunov exponents which are the average exponential rates of divergence or convergence of nearby orbits in phase-space. Any systems containing at least one positive Lyapunov exponent is defined to be chaotic, with the magnitude of the exponent reflecting the time scale at which the system dynamics become unpredictable. In other words, the larger the positive exponent, the more chaotic the system, and the shorter the time scale of system predictability (Wolf *et al.*, 1985).

To define the Lyapunov exponents, imagine an infinitesimal hypersphere of initial conditions in the n-dimensional phase-space. There is one Lyapunov exponent for each degree of freedom of the system. We observe the evolution of the hypersphere as time progresses. The hypersphere will be deformed into a hyper-ellipsoid because the evolution of the system. Then the ith Lyapunov exponent can be defined in terms of the length of the ith principal axis, p_i, of the ellipsoid as:

$$\lambda_L = \lim_{\tau \to \infty} \frac{1}{\tau} \ln \frac{p_i(\tau)}{p_i(0)} \tag{5}$$

where the λ_L are ordered from largest to smallest in an algebraic sense (Wolf *et al.*, 1985; Mundt *et al.* 1991). A minimum condition for chaos is that the largest Lyapunov exponent, λ_L, is positive.

In practice, we used an algorithm developed by Wolf *et al.* (1985) to estimate the largest Lyapunov exponent, λ_L, from a time series by using a relatively simple procedure, and which has been demonstrated to be robust over a large range of input parameters and relatively accurate for small, noisy data sets (Mundt *et al.*, 1991). The delay time τ was chosen as the decorrelation time of the time series, as previously mentioned. We carried the embedding dimension E from 2 to 10.

Correlation integral algorithm (CIA). As demonstrated by Takens (1981), an attractor topologically equivalent to the attractor of the system producing the data is obtained for every value of τ and for E sufficiently greater than the fractal dimension, i.e. $E \geq (2D+1)$.

From the new multidimensional time series defined by equation (4), the correlation integral (Grassberger and Procaccia, 1983) is defined as:

$$C(r) = \lim_{N\to\infty} \frac{1}{N^2} \sum_{j=1}^{N} \sum_{i=j+1}^{N} \theta\left(r - \left|\vec{X}_i - \vec{X}_j\right|\right) \tag{6}$$

where $N = N_{obs} - p(n-1)$ is the number of distinct pairs in the embedding space, $\left|\vec{X}_i - \vec{X}_j\right|$ is the Euclidean distance operator between the *i*th and *j*th sample, r is an arbitrary time called 'lag time' (distance between vectors), and $\theta(\xi)$ is the Heaviside function, defined as follows:

$$\theta(\xi) = \begin{cases} 0 & \text{for} \quad \xi < 0 \\ 1 & \text{for} \quad \xi \geq 0 \end{cases} \tag{7}$$

The correlation integral $C(r)$ represents the probability that the distance between a pair of randomly chosen points on the E-dimensional reconstruction will be less than a distance r apart (Grassberger and Procaccia, 1983). In the case of random processes, the phase-space trajectory is directly linked to the volume of the considered E-dimensional space as:

$$C(r) \underset{r\to 0}{\propto} r^E \tag{8}$$

while for an attractor the phase-space trajectory is more compact and the correlation integral is then characterized by its following scaling properties:

$$C(r) \underset{r\to 0}{\propto} r^{\nu} \tag{9}$$

where the exponent ν is the correlation exponent (or correlation dimension); it can be estimated as the slope of the log-log plot of $C(r)$ vs. r, using a simple least square method.

For chaotic data, ν will approach a constant value as the embedding dimension E is increased. That constant value is an estimate of the correlation dimension which measures the local structure of the strange attractor. The dimension ν of the strange attractor indicates at least how many variables are necessary to describe evolution in time. For instance, $\nu = 2.5$ indicates that a given time series can be described by a system equation containing three independent variables.

High dimensionality and multifractal structure

As was implied in the introduction, high frequency fluctuations in the tidally mixed coastal waters of the Eastern English Channel are far from Gaussian. Multifractal distributions have this property, and they apply to signals with scaling characteristics (e.g. Feder, 1988; Frisch, 1995), as the one studied here may well have, see e.g. Seuront *et al.* (1996a, b) for studies of the multifractal properties of temperature, salinity and phytoplankton biomass in similar areas. Moreover, recent studies have demonstrated that multifractal processes generally lead to universal multifractals with generators characterized by only three parameters H, C_1 and α (Schertzer and Lovejoy, 1987, 1989). H $(0 \leq H \leq 1)$ characterizes the degree of non-conservation of the process (i.e. $H = 0$ for stationary process). C_1 is the codimension that characterizes the sparseness of the process, and satisfies $0 \leq C_1 \leq 1$ for time series: $C_1 = 0$ for a homogeneous process and C_1 is all the more high as the process is sparse, indicating that the field values corresponding to any given level of variability are more scarce. The index α, called the Lévy index, is the degree of multifractality bounded between $\alpha = 0$ and $\alpha = 2$ corresponding to the monofractal case and to the maximum, or log-normal, multifractal case, respectively. As α increases, the more numerous are the variability levels bounded between lower and higher values of the descriptor [see, for example, Seuront *et al.* (1999) for further details].

There are several ways to estimate the universal parameter values. The parameters H, C_1 and α can thus be estimated considering different derivation of the q^{th} order structure functions, which can be regarded as a statistical generalization of the power spectral analysis to higher order of moments (see Schmitt *et al.*, 1995, 1996a, b, 1998; Seuront *et al.*, 1996a, b, 1999), but also from the Double Trace Moment technique (Lavallée *et al.*, 1992; Schmitt *et al.*, 1992, 1993, 1994), a very specific data analysis technique which has been extensively

explained elsewhere (Seuront *et al.*, 1999). In the following, we only report the results of the analysis process, for further explanations and details one may refer to the recent review by Seuront *et al.* (1999) wholly devoted to the introduction of universal multifractal concepts and their related analysis techniques to marine ecology. More details on the universal multifractal theoretical background can also be found in Schertzer and Lovejoy (1983, 1985, 1987, 1989). Finally, for a detailed discussion of what can be ecologically concluded from the use of multifractal algorithms, one may refer to Seuront *et al.* (1999).

Results

Phase-space diagrams

The delay time τ has been chosen as the decorrelation time of the time series (Tsonis *et al.*, 1993) as 75, 105 and 25 seconds for temperature, salinity and *in vivo* fluorescence time series, respectively (Figure 3). This delay time was also used for the following calculations of Lyapunov exponents and correlation dimensions.

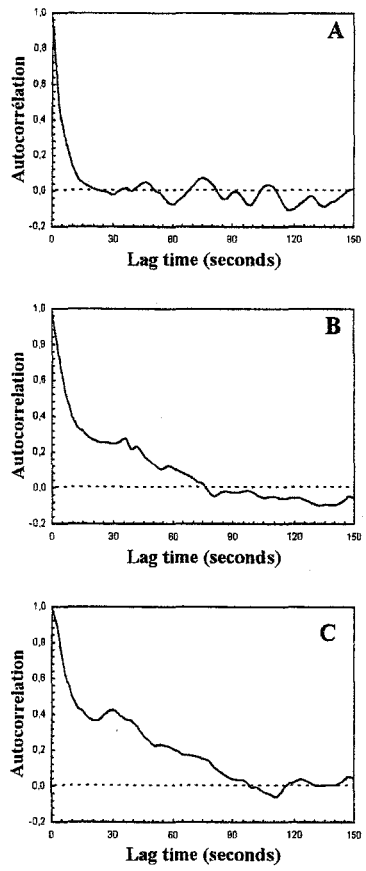

Fig. 3. Autocorrelation function for temperature (**A**), salinity (**B**) and *in vivo* fluorescence (**C**) time series, shown for data set S8.

The phase-space portraits of the attractors produced by the Packard-Takens method did not clearly exhibit any attractor (Figure 4). Nevertheless, one may note clear differences between the phase-space trajectories of *in vivo* fluorescence on the one hand and temperature and salinity on the other hand. Indeed, the phase-space trajectories for temperature and salinity appear as somewhat elongated and relatively narrow spatial distribution (Figure 4a, b). On the contrary, phase space trajectories of *in vivo* fluorescence did not exhibit any characteristic shape, suggesting a more space filling—or 'random'—behaviour (Figure 4c). Moreover, comparison of phase-space trajectories obtained from time series recorded in high and low hydrodynamic conditions leads to further results. Phase-space trajectories of temperature and salinity then appear clearly more structured in lower hydrodynamic conditions (Figure 4d, e), while the apparent randomness of *in vivo* fluorescence phase-space trajectories remains whatever the hydrodynamic conditions (Figure 4f).

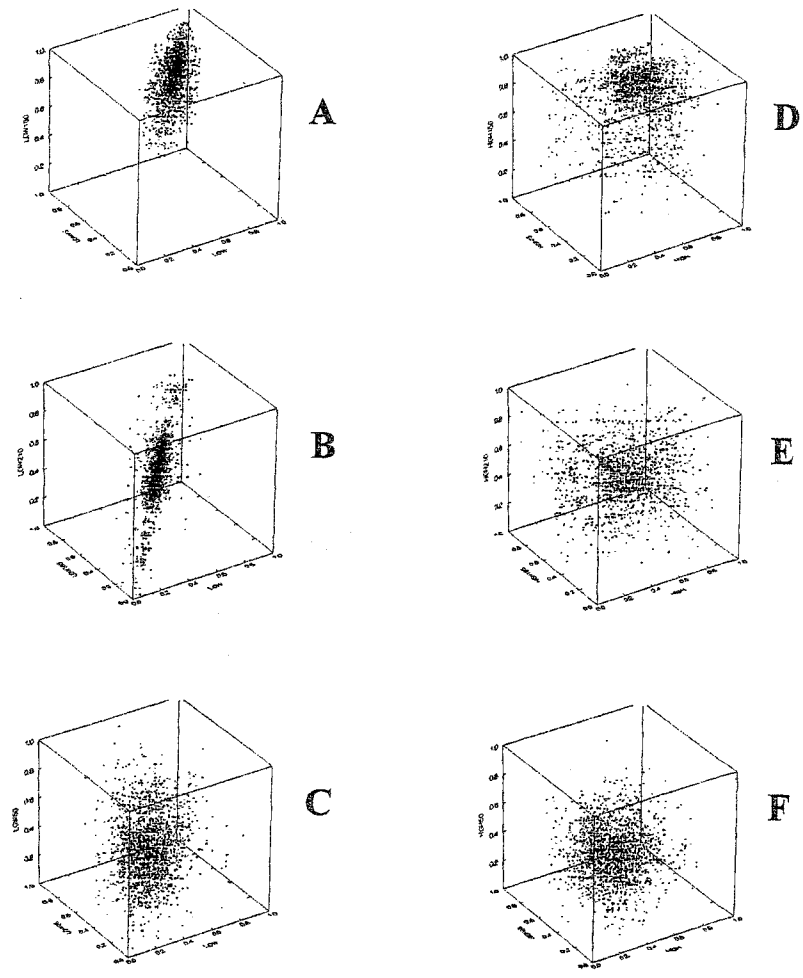

Fig. 4. Three-dimensional phase-space trajectories for temperature, salinity and *in vivo* fluorescence in low (**A**, **B**, **C**; S9) and high (**D**, **E**, **F**; S11) hydrodynamic conditions.

Largest Lyapunov exponents

The largest Lyapunov exponents, LLE, λ_L, calculated over a range of embedding dimensions E exhibit clearly different behaviours (Figure 5). By embedding dimension 8, the temperature and salinity LLE converge to positive values which are all the more large that the hydrodynamic conditions are high (Figure 5a, b). In other words, the higher are the hydrodynamic conditions, the larger the positive exponent, the more chaotic the system, and the shorter the time scale of system predictability (Wolf *et al.*, 1985). This is confirmed by the significant negative correlation between largest Lyapunov exponents of both temperature and salinity, and tidal current speed direction (Spearman's ρ, $P < 0.05$). The largest Lyapunov exponents and the associated time scale of predictability are shown in Table II.

On the contrary, whatever the hydrodynamic conditions, *in vivo* fluorescence LLE remain significantly higher than temperature and salinity LLE (Wilcoxon-Mann-Whitney U-test, $P < 0.05$), indicating more chaotic behaviour and less predictability, but never converge to any constant value, even when the embedding dimension E is increased up to 10 (Figure 5c).

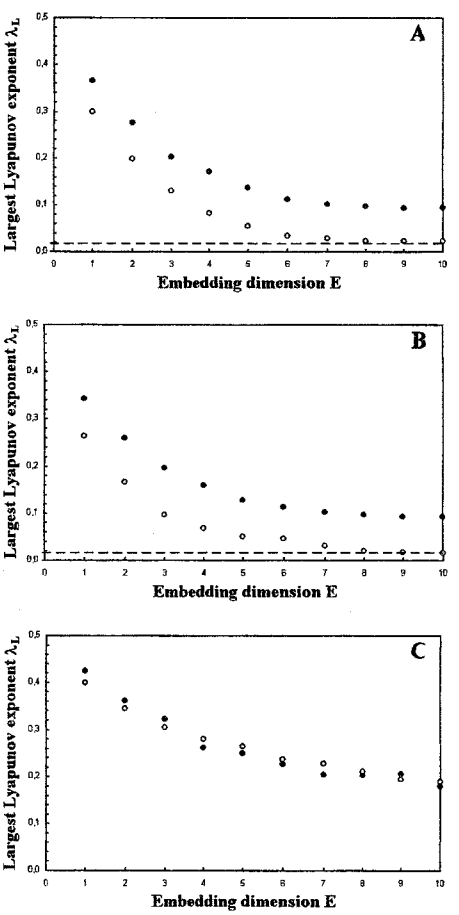

Fig. 5. The largest Lyapunov exponent λ_L estimates for temperature (**A**), salinity (**B**) and *in vivo* fluorescence (**C**) in high (black circles; S15) and low (open circles; S23) hydrodynamic conditions.

	λ_L			Predictability (second)		
	T	S	F*	T	S	F
S1	0.048	0.045	0.212	20.83	22.22	4.72
S2	0.044	0.043	0.223	22.73	23.26	4.48
S3	0.012	0.009	0.225	83.33	111.11	4.44
S4	0.098	0.105	0.243	10.20	9.52	4.12
S5	0.092	0.094	0.172	10.87	10.64	5.81
S6	0.021	0.023	0.221	47.62	43.48	4.52
S7	0.031	0.035	0.236	32.26	28.57	4.24
S8	0.055	0.057	0.198	18.18	17.54	5.05
S9	0.011	0.009	0.217	90.91	111.11	4.61
S10	0.091	0.088	0.171	10.99	11.36	5.85
S11	0.095	0.084	0.223	10.53	11.90	4.48
S12	0.038	0.039	0.181	26.32	25.64	5.52
S13	0.041	0.039	0.234	24.39	25.64	4.27
S14	0.042	0.039	0.182	23.81	25.64	5.49
S15	0.012	0.016	0.234	83.33	62.50	4.27
S16	0.076	0.079	0.172	13.16	12.66	5.81
S17	0.121	0.133	0.228	8.26	7.52	4.39
S18	0.038	0.041	0.196	26.32	24.39	5.10
S19	0.032	0.034	0.253	31.25	29.41	3.95
S20	0.085	0.088	0.228	11.76	11.36	4.39
S21	0.076	0.074	0.234	13.16	13.51	4.27
S22	0.025	0.017	0.254	40.00	58.82	3.94
S23	0.097	0.096	0.174	10.31	10.42	5.75
S24	0.071	0.075	0.187	14.08	13.33	5.35
Mean	0.056	0.057	0.212	28.53	30.06	4.79
SD	0.032	0.033	0.027	24.36	28.84	0.64
Min	0.011	0.009	0.171	8.26	7.52	3.94
Max	0.121	0.133	0.254	90.91	111.11	5.85

Table II. The largest Lyapunov exponents λ_L estimates for temperature, salinity and *in vivo* fluorescence from the 24 available data sets, and the related time scale of system predictability. * Following the absence of convergent behaviour for the fluorescence Lyapunov exponents, we reported here the λ_L estimated for $E = 10$.

Correlation integral

Figure 6 show the correlation integral $C(r)$ on logarithmic scales as a function of distance r by varying embedding dimension E from 1 to 10. Estimates of the correlation dimension ν [see equation (9)] for temperature and salinity did not converge to any constant value whatever the hydrodynamic conditions (Figure 7a, b), and indicate the lack of empirical evidence for deterministic chaos. Moreover, no significant differences can have been observed between temperature and salinity correlation dimensions (Wilcoxon-Mann-Whitney U-test, $P > 0.05$), nor between the different time series for either parameter (Kruskal-Wallis test, $P > 0.05$), suggesting very similar behaviours of temperature and salinity time series in phase-space.

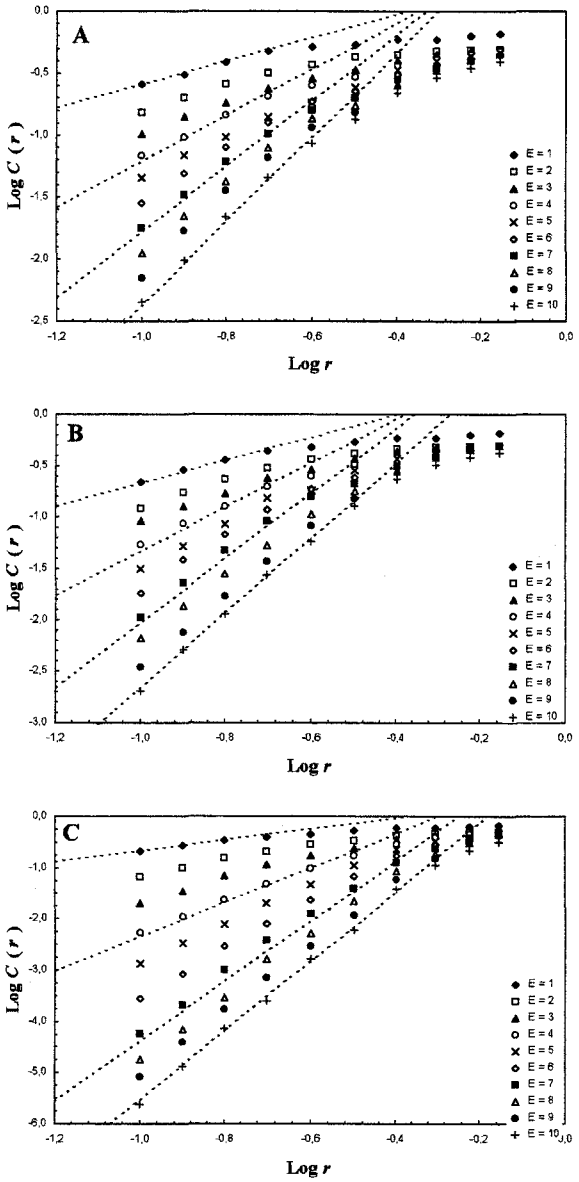

Fig. 6. Log-log plots of correlation integral $C(r)$ versus distance r for various embedding dimensions E for temperature (**A**), salinity (**B**) and *in vivo* fluorescence (**C**), shown together with their best regression lines for database S8. The slopes of the linear fits provide estimates of the correlation dimensions ν.

The results for *in vivo* fluorescence time series are very similar with those of temperature and salinity. Clearly no saturation, and therefore no evidence of low order deterministic chaos, exist whatever the hydrodynamic conditions (Figure 7c). As previously shown for temperature and salinity time series, no significant differences exist between the correlation dimensions ν (Kruskal-Wallis test, $P > 0.05$). These results confirm the previous lack of convergence of the LLE (see Figure 5c), and indicate that there is no evidence for deterministic chaos in the temporal fluctuations of phytoplankton biomass time series.

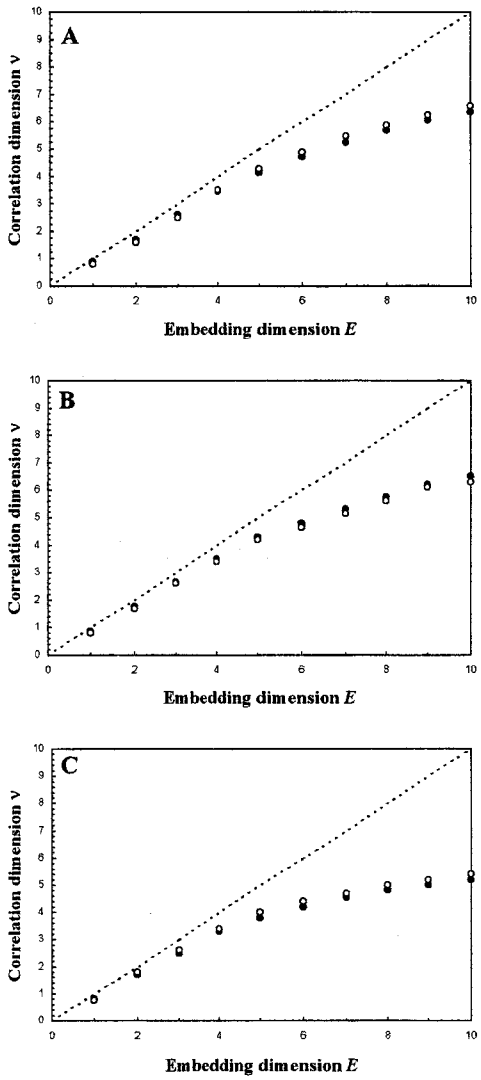

Fig. 7. Correlation dimensions ν versus embedding dimensions E for temperature (**A**), salinity (**B**) and *in vivo* fluorescence (**C**) in high (black circles; S15) and low (open circles; S23) hydrodynamic conditions. The dotted first bissectrix provides theoretical evolution of the correlation dimensions ν in case of a random noise.

Multifractal structure

Values of the universal multifractal parameters H, C_1 and α estimated for temperature, salinity and *in vivo* fluorescence time series are shown in Table III. More precisely, there were significant differences between temperature, salinity, nitrite and fluorescence H values (Kruskal-Wallis test, $P < 0.05$). A subsequent multiple comparison procedure (Dunn test; Siegel and Castellan, 1988) has shown that fluorescence parameters were significantly greater than temperature and salinity H values ($P < 0.05$) which remain indistinguishable ($P > 0.05$). The fractal codimensions C_1 lead to different results: temperature, salinity and *in vivo* fluorescence codimensions C_1 thus cannot be statistically distinguished ($P > 0.05$). Finally, the

parameters α also cannot be distinguished for temperature, salinity and *in vivo* fluorescence ($P > 0.05$; Table III).

	Temperature			Salinity			*In vivo* fluorescence		
	H	C_1	α	H	C_1	α	H	C_1	α
S1	0.38	0.040	1.90	0.37	0.049	1.88	0.38	0.042	1.84
S2	0.36	0.040	1.85	0.35	0.050	1.84	0.43	0.059	1.80
S3	0.35	0.056	1.87	0.32	0.070	1.86	0.61	0.137	1.76
S4	0.34	0.050	1.86	0.32	0.050	1.86	0.45	0.056	1.90
S5	0.37	0.050	1.84	0.36	0.060	1.85	0.45	0.052	1.88
S6	0.37	0.060	1.84	0.36	0.050	1.89	0.58	0.135	1.75
S7	0.38	0.050	1.87	0.40	0.060	1.88	0.46	0.087	1.79
S8	0.36	0.060	1.86	0.38	0.050	1.87	0.37	0.052	1.83
S9	0.38	0.050	1.83	0.39	0.060	1.85	0.50	0.098	1.76
S10	0.35	0.040	1.88	0.40	0.031	1.88	0.46	0.073	1.92
S11	0.40	0.050	1.84	0.40	0.060	1.86	0.46	0.071	1.93
S12	0.36	0.048	1.86	0.40	0.057	1.89	0.45	0.058	1.79
S13	0.35	0.040	1.86	0.37	0.050	1.88	0.45	0.054	1.79
S14	0.36	0.050	1.85	0.35	0.060	1.86	0.46	0.068	1.79
S15	0.28	0.053	1.86	0.29	0.062	1.89	0.49	0.096	1.76
S16	0.37	0.060	1.85	0.36	0.060	1.86	0.40	0.077	1.78
S17	0.38	0.040	1.84	0.36	0.050	1.87	0.38	0.068	1.96
S18	0.36	0.050	1.88	0.36	0.060	1.88	0.43	0.073	1.78
S19	0.35	0.050	1.85	0.36	0.060	1.84	0.45	0.064	1.79
S20	0.42	0.060	1.89	0.34	0.070	1.91	0.40	0.054	1.88
S21	0.41	0.070	1.91	0.39	0.060	1.90	0.41	0.055	1.86
S22	0.36	0.057	1.90	0.35	0.070	1.85	0.60	0.120	1.75
S23	0.30	0.032	1.87	0.30	0.052	1.9	0.49	0.081	1.90
S24	0.34	0.050	1.89	0.36	0.040	1.89	0.55	0.091	1.76
Mean	0.36	0.050	1.86	0.36	0.056	1.87	0.46	0.076	1.82
SD	0.03	0.008	0.02	0.03	0.009	0.02	0.07	0.026	0.06
Max	0.42	0.070	1.91	0.40	0.070	1.91	0.61	0.137	1.96
Min	0.28	0.032	1.83	0.29	0.031	1.84	0.37	0.042	1.75

Table III. Empirical estimates of the universal multifractal parameters H, C_1 and α for temperature, salinity and *in vivo* fluorescence for the 24 studied data sets.

Nevertheless, correlation analyses conducted in order to infer any potential causality between the structure of temperature, salinity and *in vivo* fluorescence time series and both physical (i.e. current speed and direction) and biological (i.e. *in vivo* fluorescence means and standard deviations) parameters (Table IV) lead to further results. It was then found that the universal parameters (i.e. H, C_1 and α) estimated for temperature and salinity time series were neither significantly correlated with current speed nor direction, indicating a relative homogeneity in the small-scale temporal structure of these purely passive scalars. On the contrary, the universal multifractal parameters characterizing *in vivo* fluorescence variability were significantly correlated with both current speed and direction. More precisely, phytoplankton biomass distributions are more conservative (i.e. low H values) and less sparse (i.e. low C_1 values) both during ebb tide and in high hydrodynamic conditions, while the Lévy

Table IV. Correlation matrix of variables relative to the structure of temperature, salinity and *in vivo* fluorescence time series. C_{Speed} and C_{Dir}: current speed and direction; SD_T, SD_S and SD_F: standard deviation of temperature, salinity and fluorescence time series; the subscript T, S and F associated to the parameters H, C_1 and α respectively identify temperature, salinity and fluorescence universal multifractal structures.

	C_{speed}	C_{Dir}	Depth	T	S	F	SD_T	SD_S	SD_F	H_T	H_S	H_F	C_{1T}	C_{1S}	C_{1F}	α_T	α_S	α_F
C_{Speed}	1.000	-	-	-	-	-	-	-	-	-	-	-	-	-	-	-	-	-
C_{Dir}	-0.251	1.000	-	-	-	-	-	-	-	-	-	-	-	-	-	-	-	-
Depth	0.315	-0.787 **	1.000	-	-	-	-	-	-	-	-	-	-	-	-	-	-	-
T	-0.350	0.824 **	-0.672 **	1.000	-	-	-	-	-	-	-	-	-	-	-	-	-	-
S	0.351	-0.746 **	0.728 **	-0.660 **	1.000	-	-	-	-	-	-	-	-	-	-	-	-	-
F	-0.330	0.893 **	-0.734 **	-0.734 **	-0.689 **	1.000	-	-	-	-	-	-	-	-	-	-	-	-
SD_T	0.576 **	-0.496 *	0.440 *	-0.455 *	0.026	-0.746 **	1.000	-	-	-	-	-	-	-	-	-	-	-
SD_S	0.690 **	-0.185	0.009	-0.213	-0.260	-0.416 *	0.833 **	1.000	-	-	-	-	-	-	-	-	-	-
SD_F	0.110	-0.140	-0.135	0.100	-0.360	-0.073	0.539 **	0.649 **	1.000	-	-	-	-	-	-	-	-	-
H_T	0.202	0.223	-0.252	0.267	-0.149	0.291	-0.398	-0.028	-0.475 *	1.000	-	-	-	-	-	-	-	-
H_S	0.048	0.102	-0.214	-0.040	-0.034	0.095	-0.306	0.015	-0.376	0.636 **	1.000	-	-	-	-	-	-	-
H_F	-0.520 **	-0.405 *	0.336	-0.187	0.123	-0.415 *	0.043	-0.330	-0.120	-0.329	-0.242	1.000	-	-	-	-	-	-
C_{1T}	-0.235	0.086	0.006	0.274	-0.107	0.230	-0.150	-0.213	-0.320	0.405 *	0.115	0.102	1.000	-	-	-	-	-
C_{1S}	-0.360	0.135	-0.037	0.330	-0.075	0.243	-0.079	-0.108	-0.146	0.240	-0.211	0.165	0.500	1.000	-	-	-	-
C_{1F}	-0.529 **	-0.408 *	0.378	-0.210	0.189	-0.364	0.174	-0.204	0.058	-0.246	-0.250	0.881 **	0.241	0.248	1.000	-	-	-
α_T	0.048	0.201	-0.058	0.492 *	-0.204	0.142	0.103	0.204	0.104	0.109	0.048	-0.019	0.212	-0.005	-0.118	1.000	-	-
α_S	0.141	0.059	-0.174	0.171	-0.196	0.067	0.391	0.168	0.089	0.012	-0.021	-0.078	0.088	-0.114	-0.047	0.507 *	1.000	-
α_F	0.901 **	-0.155	0.233	-0.287	0.313	-0.219	0.294	0.566 **	0.139	0.246	0.092	-0.501 *	-0.324	-0.296	-0.517 *	-0.021	0.118	1.000

* : 5% confidence level; ** : 1% confidence level

index α (i.e. the hierarchy of variability levels present in the phytoplankton biomass distribution) increases with current speed. Moreover, the multifractal parameters (i.e. H, C_1 and α) are not correlated to means and standard deviations (i.e. variability) for phytoplankton biomass time series.

Discussion

Searching for determinism and stochasticity in ecological time series: where do we go from here?

The Packard-Takens method. The PTM method is probably the faster and most direct method to infer the potential existence of deterministic chaos. Creating the phase-space attractor of a system with a computer is indeed a very simple task. All that is needed is the copy of the data file, paste it shifted by one, two or more places, and plot the data. Thus, a subjective assessment of the 'degree of randomness' can be reached almost instantaneously from this kind of plot. It is nevertheless evident from figure 4 that the characteristic shape of the attractor is not easy to describe in simple terms. In that way, one may note here that figure 4 shows projections of phase-space trajectories onto three-dimensional space, so that the fact that no attractors can be seen does not imply that they do not exist when embedding in higher dimensional space. However, a strange attractor of higher-dimensional space often reflects its shape onto the lower dimensional space as well. For instance, the trajectory onto the two-dimensional phase-space [embedding dimension $E = 2$ in equation (4)] reconstructed from the time series of variable x of the Lorenz equations (Lorenz, 1963; Kawamura *et al.*, 1994a, b), a well-known set of chaotic differential equations with three variables, shows a clear strange attractor. These results can then rather be regarded as a qualitative prerequisite analysis and demonstrate that inferring the existence of any deterministic structure beyond the highly fluctuating behaviour exhibiting by temperature, salinity and *in vivo* fluorescence time series (figure 2) is a far more difficult task.

Largest Lyapunov exponents. The LLE estimates quantitatively confirm the subjective results of the Packard-Takens method, i.e. a low dimensional behaviour in low hydrodynamic conditions for temperature and salinity time series, and a higher dimensional behaviour for phytoplankton biomass time series which did not exhibit any convergent behaviour of their LLE for values of the embedding dimension E up to 10 whatever the hydrodynamical conditions. Moreover, what may be regarded as being very important for ecologists is that, unlike fractal dimensions, Lyapunov exponents remain well defined in the presence of dynamical noise and can be estimated by methods that explicitly incorporate noise (Ellner *et*

al., 1991; Nychka *et al.*, 1992). This leads to consider that estimating Lyapunov exponents is the best approach for detecting chaos in ecological systems (Hastings *et al.*, 1993). One may nevertheless note some limitations of Lyapunov exponent estimates to detect deterministic chaos, lying both in estimates accuracy and the minimum number of data points required in the analysis. First, although the algorithm used in this paper (Wolf *et al.*, 1985) provides a good estimation of the largest Lyapunov exponents for noise-free synthetically generated time series from chaotic dynamics, the estimation for experimental time series is still relatively imprecise (Rodriguez-Iturbe *et al.*, 1989). Second, according to Wolf *et al.* (1985) to detect a chaotic attractor of dimension 3, at least 1000 to 30000 data points are needed, while Ramsey and Yuan (1989) found that 5000 data points is a lower bound for the detection of chaos on some simple dynamical systems known to display chaotic behaviours in certain regimes. Moreover, Vassilicos *et al.* (1993) demonstrated how the tests for chaos can give positive answers, e.g. positive Lyapunov exponents, when subsamples with smaller number of data points are used, and how these Lyapunov exponents converge to zero when the number of data points is increased. In order to confirm these results, we estimated the largest Lyapunov exponents of the larger original time series (i.e. 167040 data points) of temperature, salinity and *in vivo* fluorescence, extensively studied elsewhere in the framework of universal multifractals (Seuront *et al.*, 1999). Subsequent results (Figure 8) then indicated that LLE of temperature, salinity and phytoplankton biomass time series remain positive, but converge to zero (Binomial test, $P > 0.05$; Siegel and Castellan, 1988). As previously mentioned, positive largest Lyapunov exponent indicates chaotic dynamics, but values quite close to zero should therefore only be interpreted as an order of magnitude. Whatever that may be, the positive convergent values of the different LLE estimated for temperature and salinity time series in high and low hydrodynamic conditions could nevertheless suggest any phenomenological shift between low dimensional chaos and high dimensional stochasticity as the one observed by Ruelle and Takens (1971) near the transition to turbulence. One may also note here, as mentioned by Jeong and Rao (1996), that a positive largest Lyapunov exponents close to zero can be interpreted as having been derived from a stochastic time series with many degrees of freedom. More generally, one may note that systems with a Lyapunov exponent of zero are associated with a state called the edge of chaos, where complex behaviour is the rule. The exact meaning of the edge of chaos depends on the context within which it is used, but roughly speaking, it describes the vicinity of some instability point separating a region of more ordered (or less random) behaviour, from a region of less ordered (or more random) behaviour. The edge of

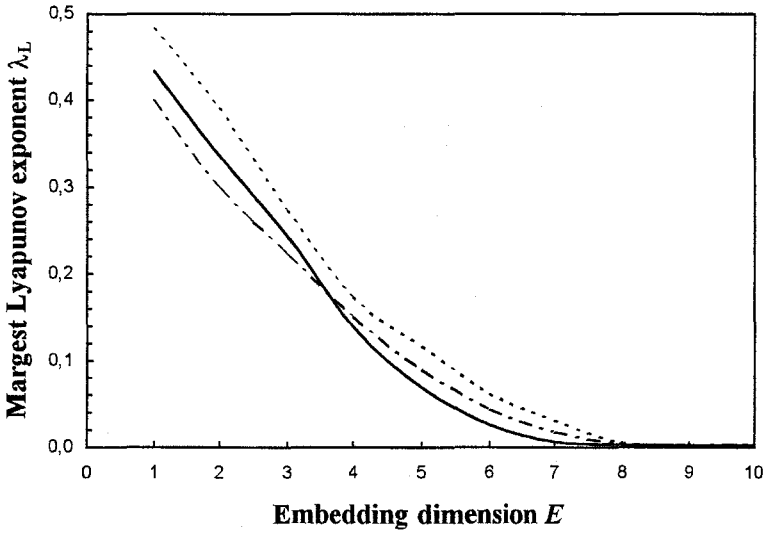

Fig. 8. The largest Lyapunov exponent λ_L estimates for temperature (continuous line), salinity (dashed line) and *in vivo* fluorescence (dotted line) from the original 167040 data set.

chaos has indeed attracted considerable interest among biologists and ecologists in the last few years because processes such as evolution or adaptative behaviour have been precisely shown to be just at the edge of chaos (Kauffman and Johnsen, 1991; Kauffman, 1993; Langdon, 1992). Such a critical state would increase the adaptative efficiency of a given system, for instance in response to fluctuating environmental conditions, and could then be of prime interest in the future understanding of ecosystems functioning.

Correlation integrals. While Smith (1988) has showed that if the data set is small, the correlation dimension ν [see equation (9)] appears to converge towards a finite value even in the absence of chaos, this is obviously not the case in our case (Figure 7). Moreover, correlation dimension ν estimates for the 167040 data points time series (Figure 9) did not converge to any constant value, and confirm the lack of empirical evidence for deterministic chaos previously shown with smaller time series (Figure 7). Our results then cannot be associated with sampling limitation. In that way, Ibanez (1986) found a correlation dimension of 2 on the basis of a 1200 values chlorophyll transect recorded in the central waters of the Ligurian Sea (NW Mediterranean Sea). This result then confirms the efficiency of the correlation algorithm to detect low deterministic chaos when applied to small data sets. Moreover, this also suggests—as previously done in this paper—that different hydrodynamical conditions might be at the origin of differential space-time structures, in terms of low order deterministic chaos or high order stochasticity. Then, high hydrodynamic conditions, as those occurring in the Eastern English Channel, could be at the origin of temperature, salinity and

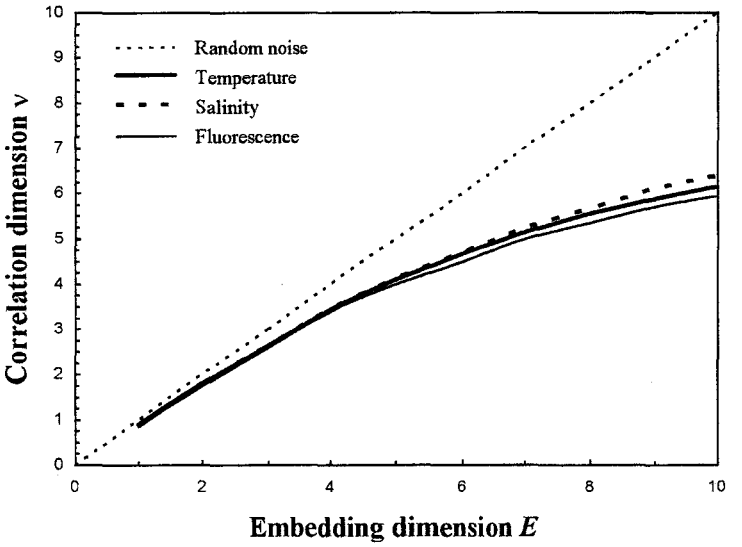

Fig. 9. Correlation dimensions ν estimates versus embedding dimensions E for temperature, salinity and *in vivo* fluorescence from the original 167040 data set. The dotted first bissectrix provides the theoretical evolution of the correlation dimensions ν in case of random noise.

phytoplankton biomass distributions characterized by their high order stochasticity, while in low hydrodynamic conditions, as those encountered in the stable waters of the Ligurian Sea, phytoplankton distribution could be rather characterized by a low order deterministic behaviour.

Whatever that may be, while our results suggest that temperature, salinity and phytoplankton biomass exhibit a higher dimensionality in high hydrodynamic conditions, we cannot conclude, on the basis on the three previously used analysis techniques, to the existence of low order deterministic chaos, but only to a lower dimensionality in low hydrodynamic conditions. In that way, the differential multifractal structures (Table III) exhibited by temperature, salinity and phytoplankton biomass time series confirm and generalize the results suggested by the analysis techniques devoted to the identification of deterministic chaos.

Towards a stochastic parametrization of turbulent processes. One needs first to note that the universal multifractal analysis techniques used in this paper have widely been shown to provide valid estimates of the whole stochastic behaviour of a given time series or transect, even when performed on small data sets (i.e. less than 1000 data points; Teissier *et al.*, 1993a, b; Schmitt *et al.*, 1995; Seuront *et al.*, 1996a, b, 1999). The multifractal parameters estimated for temperature, salinity phytoplankton biomass in this study (Table III) then clearly appear to be in the range of values previously obtained for a wide variety of tidal conditions in the

Southern Bight of the North Sea and the Eastern English Channel [see Seuront *et al.* (1999), their Table IV]. This shows that similar processes could be at the origin of both physical (i.e. temperature and salinity) and biological (phytoplankton biomass) temporal structure, and consequently that small-scale phytoplankton biomass distribution can be regarded as being passively advected by turbulent fluid motions, at least at the scale of the whole tidal cycle. However, correlation analyses have shown that temperature and salinity multifractal structures remain the same whatever the tidal conditions, while phytoplankton biomass exhibits very specific temporal patterns (Table IV). This then indicates that even in highly turbulent environments as the one experienced in the Eastern English Channel, phytoplankton biomass cannot be regarded as being a purely passive scalar even on smaller scales, but rather exhibit an altogether level of small-scale temporal structure related to the space-time scales of the tidal forcings. In particular, the observed significant negative correlation between multifractal structure of phytoplankton biomass and current speed indicate that the phytoplankton assemblages sampled in the present study are more heterogeneously distributed (i.e. high H and C_1 values) in low hydrodynamic conditions. Moreover, the values of the third multifractal parameter α ($\alpha = 1.82 \pm 0.06$ SD ; Table III) indicates that phytoplankton biomass cannot be regarded as log-normally distributed—in which case $\alpha = 2$—even in high hydrodynamic conditions. On the contrary, this value is typically in the range of α values estimated for phytoplankton biomass distribution over similar ranges of scales (Seuront *et al.*, 1996a, b, 1999; Seuront, 1997). The positive correlation between α and the current speed nevertheless indicate a differential phytoplankton biomass structure characterized by a greater complexity in the hierarchy of its variability levels in high hydrodynamic conditions. On the other hand, multifractal parameters (i.e. H and C_1; Table IV) are significantly correlated to current direction, but do not exhibit any significant correlation with mean phytoplankton biomass. This suggests that phytoplankton biomass structure cannot be regarded as resulting from any density-dependent process associated with tidal advection, but rather from the qualitative nature of phytoplankton assemblages occurring during ebb and flood, as previously suggested by Seuront *et al.* (1999). While many phenomenological hypotheses could be proposed to explain these differential temporal distributions of phytoplankton biomass—such as the differential effects of turbulence and phytoplankton composition on the formation, maintenance and structure of phytoplankton aggregates (Riebesell, 1991a, b; Kiørboe *et al.*, 1994, 1998; Kiørboe, 1997)—the resolution of this particular issue is beyond the scope of this contribution.

One can nevertheless refer to Seuront *et al.* (1999) for further comments on the potential causes and consequences of small-scale heterogeneous phytoplankton distributions.

Finally, one may note that the universal multifractal formalism can be related to the dimension formalism developed to study strange attractors. Especially, one may write (Halsey *et al.*, 1986):

$$\nu = d - K(2) \tag{10}$$

where ν is the correlation dimension defined above [see equation (9)], d is the Euclidean dimension of the observation space ($d = 1$ for time series, therefore the corresponding ν estimate is for embedding dimension $E = 2$) and $K(2)$ is the second order scaling moment $K(q)$ defined as (Schertzer and Lovejoy, 1987, 1989, 1997; Lovejoy and Schertzer, 1990; Schertzer *et al.*, 1991):

$$K(q) = \frac{C_1}{\alpha - 1}(q^{\alpha} - q) \tag{11}$$

where $K(q)$ is the scaling moment function which describes the multiscaling of the statistical moments of order q [see Seuront *et al.* (1999) for further details of equation (11) in a more general statistical framework]. Correlation dimensions ν estimated from the correlation integral algorithm [see equation (9)] and from equation (10) where $K(2)$ is reached with C_1, α (Table III) and $q = 2$ in equation (11) (Figure 10) are then very similar for temperature, salinity and *in vivo* fluorescence. The dimension formalism having been developed to describe attractors exhibiting a very high dimensionality, this result then confirms that the time series studied in the present paper are rather characterized by their high order stochasticity rather than by any kind of low order behaviour.

Non-linear dynamical systems being capable of such a variety of behaviours, these results then indicate that the use of a single technique of time series analysis should not be relied on too heavily (Casdagli, 1991). In particular, the emphasis of this paper is on supplementing techniques, rather than competing with them. When only one technique is used to analyze a time series, the results are expected to be at best incomplete, and at worst misleading. For instance, the infinite number of dimensions characterizing strange attractors (Grassberger, 1983; Grassberger and Procaccia, 1983; Hentschel and Procaccia, 1983) when specific mathematical tests, such as the correlation integral algorithm, fail to find any signs of low order deterministic behaviour could be advantageously described in the framework of universal multifractals, i.e. high order stochastic behaviour. Finally, following the behaviour of the

largest Lyapunov exponents estimates and the related concept of the edge of chaos, this study did not clearly rule out the possibility of the occurrence of both low dimensional deterministic chaos and high dimensional stochasticity in a given time series, opening very large perspectives for future modelling of marine systems.

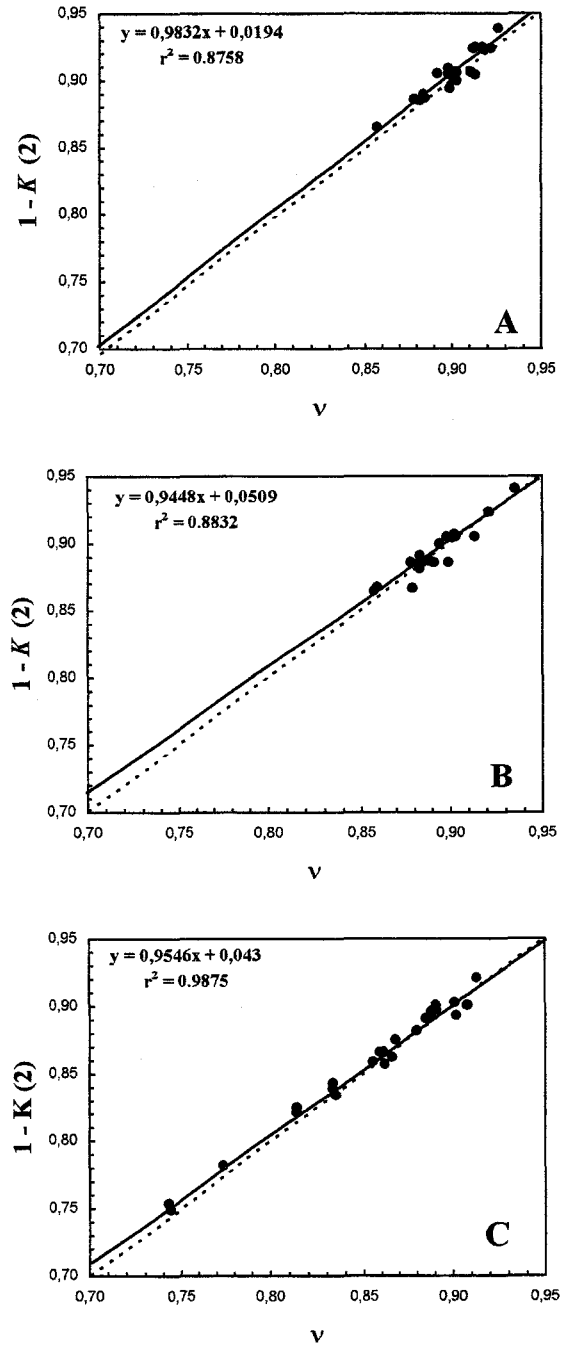

Fig. 10. Plots of the correlation dimensions ν estimated following Eq. (9) and Eq. (10), shown together with their best linear fit. The first bissectrix (dotted line) is shown for comparison.

Dealing with determinism and stochasticity: a challenge for marine ecological modelling

Following the great deal of attention recently devoted to detect and analyze chaos in plankton ecology (Sugihara and May, 1990; Scheffer, 1991; Ascioti *et al.*, 1993; Strutton *et al.*, 1996, 1997; Popova *et al.*, 1997), the results concerning the multifractal (i.e. stochastic) structure of plankton populations (Pascual *et al.*, 1995; Seuront *et al.*, 1996a, b, 1999), and more generally the increasing amount of literature providing evidence for nonlinearity in population growth and ecological interactions (e.g. Björnstad *et al.*, 1998; Grenfell *et al.*, 1998; Stenseth *et al.*, 1998) distinguishing between low dimensional deterministic chaos and high dimensional stochasticity then seems to be at the core of an emerging ecological thought process. Thus, as emphasized by Hastings *et al.* (1993), 'the study of chaos is important for ecology because the lessons of non-linear dynamics will provide very different answers than the linear models traditionally emphasized by ecologists'.

As developed above, the central tenet of deterministic chaos and stochasticity lies in their related predictive ability. Chaotic systems are predictable over short time scales because they are deterministic; the lack of predictive power over long time scales stems from the lack of complete information about the exact location of initial conditions. In contrast, systems that are stochastic are unpredictable over any time scale because of the probabilistic nature of their components. Nevertheless, systems can have endogenous dynamics that are chaotic in the presence of exogenous stochastic perturbation. Such interactions between systems with chaotic dynamics and stochasticity leads to new and interesting behaviours (Crutchfield *et al.*, 1982; Rabinovitch and Thieberger, 1988; Rand and Wilson, 1991). The number of investigations of chaos in modelling ecological systems with stochasticity has nevertheless still been quite small. Thus, investigations of a logistic model with additive noise showed that chaotic dynamics persisted (Schaffer *et al.*, 1986; Rabinovitch and Thieberger, 1988). Rand and Wilson (1991) emphasized how the interaction between the deterministic dynamics and noise can lead to a case where the average Lyapunov exponent is positive, even though the purely deterministic system with the same parameters is not chaotic. While these works provide further evidence for the ubiquity of chaos by showing that individual-based models can appear deterministic and chaotic at the level of the population, actual key challenges in the study of ecological systems involve ways to deal with the collective dynamics of various ensembles of individuals, and to understand how to relate phenomena across scales (Auger and Poggiale, 1996; Levin *et al.*, 1997; Poggiale, 1998a, b). While Denman and Powell (1984) emphasized that ecological responses could not be linked to a particular physical scale, transfers of variability across scales

have indeed been found in models for predator-prey interactions that can display variability at frequencies other than that of the periodic (i.e. seasonal) forcings (Kot *et al.*, 1992; Rinaldi *et al.*, 1993; Pascual and Caswell, 1997a, b). In that way, a direction of future research could be to focus on the responses to more realistic stochastic forcings (i.e. multifractal) of such modelling approaches in terms of determinism and/or stochasticity.

Distinguishing between chaos and stochastic processes could also have considerable implications for the design and evaluation of sampling schemes in the coastal ocean. We indeed demonstrated here that the degree of stochasticity and/or determinism exhibited by phytoplankton populations varies with both hydrodynamical and advective conditions. It has also been demonstrated over a wider range of scales (i.e. from 1 second to 48 hours) that the stochastic structure of phytoplankton biomass varies with the sampling scale (see Seuront *et al.*, 1996a, 1999). In that way, Rand and Wilson (1995) theoretically demonstrated that the optimal scale at which to measure a given process is described as the one that 'maximizes the ratio of deterministic information to stochastic fluctuations', while Pascual and Levin (1999) developed a determinism test from non-linear data analysis to describe and to identify a characteristic length scale at which to average spatio-temporal systems. Finally, one may note here that like most oceanographic data, the data analyzed here contain both spatial and temporal components, because sampling has been accomplished in the Eulerian sense, that is, in a reference frame fixed with respect to the moving fluid. While Seuront *et al.* (1996b) demonstrated that the stochastic structure of a given signal is wholly dependent on the scale of the sampling (i.e. Eulerian/Lagrangian transition), Eulerian sampling of spatially heterogeneous populations have also been suggested to obscure any deterministic signal beyond the resolving capabilities of presently available non-linear signal processing techniques (Little *et al.*, 1996). Thus, as previously suggested in a more general ecological frame (Wiens, 1989; Jarvis, 1995), the grain and extent of a given sampling experiment, as the way the samples are taken, should be regarded as being essential components to the understanding of a given time series, as precise numerical values of Lyapunov exponents, correlations dimensions and multifractals parameters might be.

Thus, in the general background of spatio-temporal intermittency encountered in the ocean (Platt *et al.*, 1989), future studies investigating the magnitude of keys fluxes such as primary production should take a great advantage to focus on the deterministic/stochastic duality to reach robust estimates and modelling of stocks and fluxes, all the more since numerical

modelling are extremely sensitive even to minor changes in parameter values (Wermer *et al.*, 1993).

Acknowledgements

The author appreciates Drs. Y. Lagadeuc and C. Luczak for their discussions and opinions. Drs. F. Schmitt and C. Nicolis offered constructive comments which greatly improved the manuscript. I also thank the captain and the crew of the N/O 'Côte d'Aquitaine' for their assistance during the sampling experiment.

References

Ascioti,F.A., Beltrami,E., Carrol,T.O., Wirrick,C. (1993) Is there chaos in plankton dynamics? *J. Plankton Res.*, **15**, 603-617.

Auger,P. and Poggiale,J.-C. (1996) Emergence of population growth models: fast migration and slow growth. *J. Theor. Biol.*, **182**, 99-108.

Baker,M.A. and Gibson,C.H. (1987) Sampling turbulence in the stratified ocean: statistical consequences of strong intermittency. *J. Phys. Oceanogr.*, **17**, 1817-1836.

Benzi,R., Paladin,G., Parisi,G. and Vulpiani,G. (1984) On the multifractal nature of fully developped turbulence and chaotic systems. *J. Phys.*, **A17**, 3521-3531.

Berryman,A. and Milstein,J. (1989) Are ecological systems chaotic—and if not, why not? *Trends Ecol. Evol.*, **4**, 26-28.

Björnstad,O.N., Begon,M., Stebseth,N.C., Falck,W., Sait,S.M. and Thompson,D.J. (1998) Population dynamics of the Indian meal moth: demographic stochasticity and delayed regulatory mechanisms. *J. Anim. Ecol.*, **67**, 110-126.

Bohle-Carbonell,M. (1992) Sampling turbulence in the stratified ocean: statistical consequences of strong intermittency. *Cont. Shelf Res.*, **12**, 3-24.

Casdagli,M. (1991) Chaos and deterministic versus stochasyic non-linear modelling. *J. R. Statist. Soc. B*, **54**, 303-328.

Crutchfield,J.P., Farmer, J.D. and Huberman,B.A. (1982) Fluctuations and simple chaotic dynamics. *Phys. Rep.*, **92**, 45-82.

Denman,K.L. and Powell,T.M. (1984) Effects of physical processes on planktonic ecosystems in the coastal ocean. *Oceanogr. Mar. Biol. Ann. Rev.*, **22**, 125-168.

Ellner,S. (1992) Detecting low dimensional chaos in population dynamic data: a critical review. In Logan,J. and Hain,F. (eds.), *Chaos and Insect Ecology* University Press of Virginia, Blacksburg, pp. 63-91.

Ellner,S. and Turchin,P. (1995) Chaos in a noisy world: new methods and evidence from time series analysis. *Am. Nat.*, **145**, 343-375.

Ellner,S., Gallant,A.R., McCaffrey,D. and Nychka,D. (1991) Convergence rates and data requirements for Jacobian-based estimates of Lyapunov exponents from data. *Phys. Let.*, **153**, 357-363.

Farmer,J.D. and Sidorowich,J.J. (1987) Predicting chaotic time series. *Phys. Rev. Lett.*, **59**, 845-848.

Feder,J. (1988) *Fractals*. Plenum, New York.

Frisch,U. (1995) *Turbulence: The Legacy of A. N. Kolmogorov*. Cambridge University Press, New York.

Fuller,W.A. (1976) An introduction to Statistical Time Series. Wiley, Chichester.

Godfrey,H.C.J. and Blythe,SP. (1991) Complex dynamics in multispecied communities. *Philos. Trans. Roy. Soc. Ser. B*, **330**, 221-233.

Gower,J.C. (1971) A general coefficient of similarity and some of its properties. *Biometrics*, **27**, 857-871.

Grassberger,I. (1983) Generalized dimensions of strange attractors. *Phys. Lett. A*, **97**, 227-230.

Grassberger,I. and Procaccia,I. (1983) Characterization of strange attractors. *Phys. Rev. Lett.*, **50**, 346-349.

Grenfell,B.T., Wilson,K., Finkenstadt,B.F., Coulson,T.N., Murray,S., Albon,S.D., Pemberton,J.M., Clutton-Brock,T.H. and Crawley,M.J. (1998) Noise and determinism in synchronized sheep dynamics. *Nature*, **394**, 674-677.

Halsey,T.C., Jensen,M.H., Kadanoff,L.P., Procaccia,I. and Shraiman,B.I. (1986) Fractal measures and their singularities: the characterization of strange sets. *Phys. Rev. A*, **33**, 443-453.

Hassell,M.P., Lawton,J.H. and May,R.M. (1976) Patterns of dynamical behaviour in single species population models. *J. Anim. Ecol.*, **45**, 471-486.

Hastings,A. and Powell,T.M. (1991) Chaos in a three species food chain. *Ecology*, **72**, 896-903.

Hastings,A., Hom,C.L., Ellner,S., Turchin,P. and Godfray,H.C.J. (1993) Chaos in ecology: is mother nature a strange attractor? *Annu. Rev. Ecol. Syst.*, **24**, 1-33.

Hentschel,H.G.E. and Procaccia,I. (1983) The infinite number of generalized dimensions of fractals and strange attractors. *Physica D*, **8**, 435-444.

Ibanez,F. (1986) Le déterminisme du chaos. *J. Rech. Océanogr.*, **11**, 66-69.

Jarvis,P.G. (1995) Scaling processes and problems. *Plant, Cell and Environment*, **18**, 1079-1089.

Jeong,G.D. and Rao,A.R. (1996) Chaos characteristics of tree ring series. *J. Hydrol.*, **182**, 239-257.

Kauffman,S. (1993) *The origins of Order*. Oxfor University Press, New York.

Kauffman,S. and Johnsen,S. (1991) Coevolution to the edge of chaos: coupled fitness landscapes, poised states, and coevolutionary avalanches. *J. Theor. Biol.*, **149**, 467-505.

Kawamura,A;, Matsumoto,M., Jinno,K. and Xu,S. (1994a) Estimation and prediction for dynamics of chaotic time series (I). On the dependence of Lorenz equation on the initial value and parameters and its prediction by nonlinear least square method. *Technology Reports of Kyushu University*, **67**, 513-521.

Kawamura,A;, Matsumoto,M., Jinno,K. and Xu,S. (1994b) Estimation and prediction for dynamics of chaotic time series (II). On the estimation and prediction for dynamics of Lorenz equation by extended Kalman filter. *Technology Reports of Kyushu University*, **67**, 523-531.

Kiørboe,T. (1997) Small-scale turbulence, marine snow formation, and planktivorous feeding. *Sci. Mar.*, **61**, 141-158.

Kiørboe,T., Lunsgaard,C., Olesen,M. and Hansen,J.L.S. (1994) Aggregation and sedimentation processes during a spring phytoplankton bloom: a field experiment to test coagulation theory. *J. Mar. Res.*, **52**, 297-323.

Kiørboe,T., Tiselius,P., Mitchell-Innes,B., Hansen,J.L.S., Wisser,A.W. and Mari,X. (1998) Intensive aggregate formation with low vertical flux during an upwelling-induced diatom bloom. *Limnol. Oceanogr.*, **43**, 104-116.

Kot,M., Sayler,G.S. and Schultz,T.W. (1992) Complex dynamics in a model of microbial system. *Bull. Math. Biol.*, **54**, 619-648.

Langdon,C.G. (1992) Life at the edge of chaos. In Langdon,C.G., Taylor,C., Farmer,J.D. and Rasmussen,S. (eds), *Artificial life II*, Addison-Wesley, Redwood City, pp. 41-91.

Lavallée,D., Lovejoy,S., Schertzer,D. and Schmitt,F. (1992) On the determination of universal multifractal parameters in turbulence. In Moffat,K., Tabor,M. and Zaslavsky,G. (eds), *Topological aspects of the dynamics of fluid and plasmas*. Kluwer, Boston, pp. 463-478.

Legendre,L. and Legendre,P. (1984) *Ecologie Numérique*, Vol. 2. Masson, Paris.

Levin,S.A., Grenfell,B., Hastings,A. and Perelson,A.S. (1997) Mathematical and computational challenges in population biology and ecosystems science. *Science*, **275**, 334-343.

Little,S., Ellner,S., Pascual,M., Neubert,M., Kaplan,D., Sauer,T., Caswell,H. and Solow,A. (1996) Detecting nonlinear dynamics in spatio-temporal systems, examples from ecological models. *Physica D*, **96**, 321-333.

Logan,J. and Allen,J.C. (1992) Nonlinear dynamics and chaos in insect populations. *Annu. Rev. Entomol.*, **37**, 455-471.

Lorenz,E.N. (1963) Deterministic nonperiodic flow. *J. Atmos. Sci.*, **20**, 130-141.

Lovejoy,S. and Schertzer,D. (1990) Multifractals, universality classes and satellite and radar measurements of cloud and rain fields. *J. Geophys. Res.*, **95**, 2021-2034.

Mandelbrot,B. (1983) *The fractal geometry of nature*. Freeman, New York.

May,R.M. (1974) Biological populations with non-overlapping generations: stable points, stable cycles and chaos. *Science*, **186**, 645-647.

May,R.M. (1975) Biological populations obeying difference equations: stable points, stable cycles and chaos. *J. Theor. Biol.*, **51**, 511-524.

May,R.M. (1976) Simple mathematical models with very complicated dynamics. *Nature*, **261**, 459-467.

May,R.M. (1980) Nonlinear phenomena in ecology and epidemiology. *Ann. N. Y. Acad. Sci.*, **357**, 267-281.

May,R.M. (1987) Chaos and the dynamics of biological populations. *Proc. Soc. London Ser. A*, **413**, 27-44.

Mundt,M.D., Maguire,W.B.II and Chase,R.R.P. (1991) Chaos in the sunspot cycle: analysis and prediction. *J. Geophys. Res.*, **96**, 1705-1716.

Nychka,D. Ellner,S., Gallant,A.R. and McCaffrey,D. (1992) Finding chaos in noisy systems. *J. Royal Stat. Soc. B*, **54**, 399-426.

Packard,N.H., Crutchfield,J.P., Farmer,J.D.and Shaw,R.S. (1980) Geometry from a time series. *Phys. Rev. Lett.*, **45**, 712-716.

Parisi,G. and Frisch,U. (1985) A multifractal model of intermittency.

Pascual,M. and Caswell,H. (1997a) From the cell-cycle to population cycles in phytoplankton-nutrient interactions. *Ecology*, **78**, 897-912.

Pascual,M. and Caswell,H. (1997b) Environmental heterogeneity and biological pattern in a chaotic predator-prey system. *J. Theor. Biol.*, **185**, 1-13.

Pascual,M. and Levin,S.A. (1999) From individuals to population densities: searching for the intermediate scale of nontrivial determinism. *Ecology*, in press.

Pascual,M., Asciotti,F.A. and Caswell,H. (1995) Intermittency in the plankton: a multifractal analysis of zooplankton biomass variabiltiy. *J. Plantkon Res.*, **17**, 1209-1232.

Peitgen,H.O., Jurgens,H. and Saupe,D. (1992) *Chaos and Fractals: News Frontiers of Science*. Springer-Verlag, New York.

Platt,T., Harrison,W.G., Lewis,M.R., Li,W.K.W., Sathyendranath,S., Smith,R.E. and Vezina,A.F. (1989) Biological production of the oceans: the case for a consensus. *Mar. Ecol. Prog. Ser.*, **52**, 77-88.

Poggiale,J.-C. (1998a) From behavioural to population level: growth and competition. *Mathl. Comput. Modelling*, **27**, 41-49.

Poggiale,J.-C. (1998b) Predator-prey models in heterogeneous environments: emergence of functional response. *Mathl. Comput. Modelling*, **27**, 63-71.

Pool,R. (1989) Is it chaos or is it just a noise? *Science*, **243**, 310-313.

Popova,E.E., Fasham,M.J.R., Osipov,A.V. and Ryabchenko,V.A. (1997) Chaotic behavior of an ocean ecosystem model under seasonal external forcing. *J. Plankton Res.*, **19**, 1495-1515.

Rabinovitch,A. and Thieberger,R. (1988) Biological populations obeying a stochastically perturbed logistic difference equation. *J. Theor. Biol.*, **131**, 509-514.

Ramsey,J.B. and Yuan,H.J. (1989) Bias and error bars in dimension calculations and their evaluations in some simple models. *Phys. Lett. A*, **134**, 287-297.

Rand,D.A. (1994) Measuring and characterizing spatial patterns, dynamics and chaos in spatially extended dynamical systems and ecologies. *Phil. Trans. R. Soc. London Ser. A*, **348**, 497-514.

Rand,D.A. and Wilson,H.B. (1991) Chaotic stochasticity: a ubiquitous source of unpredictability in epidemics. *Proc. Roy. Soc. Lond. Ser. B*, **246**, 179-184.

Rand,D.A. and Wilson,H.B. (1995) Using spatio-temporal chaos and intermediate-scale determinism to quantify spatially extended ecosystems. *Proc. Roy. Soc. London Ser. B*, **259**, 111-117.

Riebesel,U. (1991a) Particle aggregation during a diatom bloom. I. Physical aspects. *Mar. Ecol. Prog. Ser.*, **69**, 273-280.

Riebesel,U. (1991b) Particle aggregation during a diatom bloom. II. Biological aspects. *Mar. Ecol. Prog. Ser.*, **69**, 281-291.

Rinaldi,S., Muratori,S. and Kuznetzov,Y. (1993) Multiple attractors, catastrophes, and chaos in seasonally perturbed predator-prey communities. *Bull. Math. Biol.*, **55**, 15-36.

Rodriguez-Iturbe,I., de Power,B.F., Sharifi,M.B. and Georgakakos,K.B. (1989) Chaos in rainfall. *Wat. Resour. Res.*, **25**, 1667-1675.

Rubin,D.M. (1992) Use of forecasting signatures to help distinguishing periodicity, randomness and chaos in ripples and other spatial patterns. *Chaos*, **2**, 525-535.

Ruelle,D. and Takens,F. (1971) On the nature of turbulence. *Communs Math. Phys.*, **20**, 167-192.

Schaffer,W.M., Ellner,S. and Kot,M. (1986) Effects of noise on some dynamical models in eclogy. *J. Math. Biol.*, **24**, 479-523.

Scheffer,M. (1991) Should we expect strange attractors behind plankton dynamics—and if so, should we bother? *J. Plankton Res.*, **13**, 1291-1305.

Schertzer,D. and Lovejoy,S. (1983) The dimension and intermittency of atmospheric dynamics. In Launder,B. (ed.), *Turbulent Shear Flows 4*, Springer-Verlag, Karlsruhe, pp. 7-33.

Schertzer,D. and Lovejoy,S. (1985) Generalised scale invariance in turbulent phenomena. *Physico-Chem. Hydrodyn. J.*, **6**, 623-635.

Schertzer,D. and Lovejoy,S. (1987) Physically based rain and cloud modeling by anisotropic multiplicative turbulent cascades. *J. Geophys. Res.*, **92**, 9693-9714.

Schertzer,D. and Lovejoy,S. (1989) Nonlinear variability in geophysics: multifractal analysis and simulation. In Pietronero,L. (ed.), *Fractals: physical origin and consequences*. Plenum, New York, pp. 49-79.

Schertzer,D. and Lovejoy,S. (1997) Universal multifractals do exist! *J. Appl. Meteorol.*, **36**, 1296-1303.

Schertzer,D., Lovejoy,S., Lavallée,D. and Schmitt,F. (1991) Universal hard multifractal turbulence, theory and observations. In Sagdeev,R.Z., Frisch,U., Hussain,F., Moiseev,S.S. and Erokhin,N.S. (eds), *Nonlinear Dynamics of Structures*. World Scientific, Singapore, pp. 213-235.

Schmitt,F., Lavallée,D., Shertzer,D. and Lovejoy,S. (1992) Empirical determination of universal multifractal exponents in turbulent velocity fields. *Phys. Rev. Lett.*, **68**, 305-308.

Schmitt,F., Schertzer,D., Lovejoy,S. and Brunet,Y. (1993) Estimation of universal multifractal indices for atmospheric turbulent velocity fields. *Fractals*, **1**, 568-575.

Schmitt,F., Schertzer,D., Lovejoy,S. and Brunet,Y. (1994) Empirical study of multifractal phase transitions in atmospheric turbulence. *Nonlin. Proc. Geophys.*, **1**, 95-104.

Schmitt,F., Lovejoy,S. and Schertzer,D. (1995) Multifractal analysis of the Greenland ice-core project climate data. . *Geophys. Res. Lett.*, **22**, 1689-1392.

Schmitt,F., Schertzer,D., Lovejoy,S. and Brunet,Y. (1996a) Multifractal temperature and flux of temperature in fully developped turbulence. *Europhys. Lett.*, **34**, 195-200.

Schmitt,F., Schertzer,D., Lovejoy,S. and Brunet,Y. (1996b) Multifractal properties of temperature fluctuations in turbulence. In Giona,M. and Biardi,G. (eds), *Fractals and Chaos in Chemical Engineering*. World Scientific, Singapore, pp. 464-475.

Schmitt,F., Schertzer,D. and Lovejoy,S. (1998) Multifractal modeling of turbulent fluctuations in finance. In Marsella,F. and Salvadori,G. (eds), *Chaos, Fractals and Models*. Italian University Press di Giovanni Iuculano, Pavia, pp. 150-157.

Seuront,L. (1997) Distribution inhomogène multiéchelle de la biomasse phytoplanctonique en milieu turbulent. *J. Rech. Océanogr.*, **22**, 9-16.

Seuront,L. (1999) Fractals et multifractals: nouveaux outils de caractérisation de l'hétérogénéité spatio-temporelle en écologie marine. *Océanis*, in press.

Seuront,L., Schmitt,F., Lagadeuc,Y., Schertzer,D., Lovejoy,S. and Frontier,S. (1996a) Multifractal analysis of phytoplankton biomass and temperature in the ocean. *Geophys. Res. Lett.*, **23**, 3591-3594.

Seuront,L., Schmitt,F., Lagadeuc,Y., Schertzer,D. and Lovejoy,S. (1996b) Multifractal intermittency of Eulerian and Lagrangian turbulence of ocean temperature and plankton fields. *Nonlin. Proc. Geophys.*, **3**, 236-246.

Seuront,L., Schmitt,F., Lagadeuc,Y., Schertzer,D. and Lovejoy,S. (1999) Universal multifractal analysis as a tool to characterise multiscale intermittent patterns. Example of phytoplankton distribution in turbulent coastal waters. *J. Plankton Res.*, in press.

Siegel,S. and Castellan,N.J. (1988) *Nonparametric Statistics*. McGraw-Hill, New York.

Smith,L.A. (1988) Intrinsic limits on dimension calculations. *Phys. Lett. A*, **133**, 283-288.

Sokal,R.R. and Rohlf,F.J. (1995) *Biometry. The Principles and Practice of Statistics in Biological Research*. Freeman, San Francisco.

Solé,R.V. and BAscompte,J. (1995) Measuring chaos from spatial informations. *J. Theor. Biol.*, **175**, 139-147.

Stenseth,N.C., Chan,K.S., Framstad,E. and Tong,H. (1998) Phase- and density-dependent dynamics in Norwegian lemmings: interaction between deterministic and stochastic processes. *Proc. Roy. Soc. London Ser. B*, **265**, 1957-1968.

Strutton,P.G., Mitchell,J.G. and Parslow,J.S. (1996) Non-linear analysis of chlorophyll a transects as a method of quantifying spatil structure. *J. Plankton Res.*, **18**, 1717-1726.

Strutton,P.G., Mitchell,J.G. and Parslow,J.S. (1997) Using non-linear analysis to compare the spatial structure of chlorophyll with passive tracers. *J. Plankton Res.*, **19**, 1553-1564.

Sugihara,G. and May,R.M. (1990) Nonlinear forecasting as a way of distinguishing chaos from measurement error in time series. *Nature*, **344**, 734-741.

Takens, F. (1981). Detecting strange attractors in turbulence. *Lect. Notes Math.*, **898**, 366-381.

Teissier,Y., Lovejoy,S. and Schertzer,D. (1993a) Universal multifractals: theory and observations of rain and clouds. *J. Appl. Meteor.*, **32**, 223-250.

Tessier,Y., Lovejoy,S., Schertzer,D., Lavallée,D. and Kerman,B. (1993b) Universal multifractal indices for the ocean surface at far red wavelengths. *Geophys. Res. Lett.*, **20**, 1167-1170.

Theiler,J., Eubank,S., Longtin,A., Galdrikian,B. and Farmer,J.D. (1992) Testing for nonlinearity in time series: the method of surrogate data. *Physica D*, **58**, 77-94.

Tsonis,A.A., Elsner,J.B. and Georgakakos,K.P. (1993) Estimating the dimension of weather and climate attractors: important issues about the procedure and interpretation. *J. Atmos. Sci.*, **50**, 2549-2555.

Vassilicos,J.C., Demos,A. and Tata,F. (1993) No evidence of chaos but some evidence of multifractals in the foreign exchange and stock markets. Crilly,A.J., Eranshaw,R.A. and Jones,H. (eds), *Applications of Fractals and Chaos. The Shape of Things.* Springer-Verlag, Berlin, pp. 249-265.

Werner,F.E., Page,F.H.,Lynch,D.R., Loder,J.W., Lough,R.G., Perry,R.I., Greenberg,D.A. and Sinclair,M.M. (1993) Influences of mean advection and simple behavior on the distribution of cod and haddock early life stages on Georges Bank. *Fish. Oceanogr.*, **2**, 43-64.

Wiens,J.A. (1989) Spatial scaling in ecology. *Funct. Ecol.*, **3**, 385-397.

Wolf,A., Swift,J.B., Swinney,H.L. and Vastano,J.A. (1985) Determining Lyapunov exponents from a time series. *Physica*, **16D**, 285-317.

A16

Eulerian and Lagrangian spatio-temporal patterns in a tidally mixed coastal ecosystem: a multiscale approach

Seuront L, Schmitt F & Lagadeuc Y (manuscrit)

Eulerian and Lagrangian spatio-temporal patterns in a tidally mixed coastal ecosystem: a multiscale approach

Laurent Seuront[1,3], François Schmitt[2] and Yvan Lagadeuc[1,4]

[1] *Station Marine de Wimereux, Université des Sciences et Technologies de Lille, CNRS-UPRESA 8013 ELICO, BP 80, F-62930 Wimereux, France*

[2] *Department of Fluid Mechanics, VUB, Pleinlaan 2, 1050 Brussels, Belgium*

[3] *Present adress: Department of Ocean Science, Tokyo University of Fisheries, 4-5-7 Konan, Minato-ku, Tokyo 108, Japan*

[4] *Present address: University of Caen, IUT, Bd du Maréchal Juin, F-14032 Caen cedex, France*

Abstract. In the Eastern English Channel, a tidally mixed coastal ecosystem, the multifractal nature of physical and biological parameters such as temperature, salinity, light transmission and *in vivo* fluorescence have been investigated on the basis of 22 high frequency time series randomly recorded both in space and time adrift during a 30 months sampling experiment. Time series analysis have been conduced both on the resulting Eulerian and Lagrangian scales (i.e. the lengths scales respectively smaller and greater than the size of the sampling boat) in the spectral and multifractal frameworks. Over Eulerian scales, temperature and salinity exhibit very similar behaviours, mainly associated with the gradients characterizing the studied area. Phytoplankton biomass exhibits a clear density-dependence related with biological seasonal cycle, while particles distributions is wholly dependent on the qualitative nature of the suspended sediment. Over Lagrangian scales, the structure of temperature and salinity appear quite constant both in space and time, whereas phytoplankton biomass and particles distributions are wholly dependent on the seasonal phytoplankton concentration. The results show that the whole structure of the studied coastal ecosystem can be viewed as the result of multiplicative cascade processes which exhibit very specific features both in space and time in relation with sampling scales, but also with the biological and physical nature of the studied parameters. The implications of these space-time patterns on sampling processes and ecosystem functioning are also discussed.

Introduction

The perception and the understanding of the space-time structure of marine plankton set the priority of the biological oceanographers of the early 20th century, so that by about 1930 many investigators have shown that planktonic organisms are neither uniformly nor randomly distributed in the ocean (Hardy, 1926, 1939; Hardy and Gunther, 1935). Subsequently, marine systems have been shown to exhibit intimate relationships between physical and biological processes (Legendre and Demers, 1984), as shown by the coupling between the distribution of phytoplankton populations and the structure of their physical environment over a wide range of spatial and temporal scales (Haury *et al.*, 1978). However, in spite of an impressive body of literature on the subject (e.g. Mackas *et al.*, 1985 ; Daly and Smith, 1993), little is finally

known about the multiscale space-time couplings between physical and biological processes, especially on smaller scales (Seuront *et al.*, 1999) and, as recently stated by Pascual *et al.* (1995), this field of research still seems in its infancy. Two major interrelated limitations hampering progress are indeed associated to the intermittent nature of turbulent processes and to sampling schemes.

Thus, in the ocean, strong intermittency has been found in physical quantities such as the dissipation rates of turbulent velocity and temperature fluctuations (Baker and Gibson, 1987), and leads to biased estimates of means and confidence limits (Bohle-Carbonel, 1992). Moreover, while the intermittent distributions of phytoplankton and zooplankton have also been described (Pascual *et al.*, 1995; Seuront *et al.*, 1996a, b, 1999), such results are still too scarce to lead to some generalizations, even in a given ecosystem which needs to be sampled as fully as possible both in space and time (Platt *et al.*, 1989). In that way, the implications of such distributions for sampling strategy still remain to be explored. In particular, sampling is most easily accomplished in the Eulerian sense, that is, in a reference frame fixed with respect to the moving fluid, such as moored buoy or a pier. For an externally advected population, this effectively means that temporally successive samples are not taken from the same spatial location with respect to the spatial pattern of the population, so that the data contain both spatial and temporal components. However, the environment is sampled not only by oceanographers but by the organisms that live in the ocean. The small-scale variability experienced by individual organisms may indeed have important implications for foraging, growth and populations dynamics, leading to the development of Lagrangian concepts (e.g. Yamazaki, 1993).

In that way, in a preliminary study, Seuront *et al.* (1996b) have shown that both intermittency of Eulerian and Lagrangian turbulence of ocean temperature and plankton fields simultaneously recorded from a drifter in the mixed coastal waters of the Eastern English Channel, a hydrodynamically dominated ecosystem, could be efficiently characterized in terms of multifractals. Thus, these results lead to very specific features of turbulent processes when viewed as being Eulerian or Lagrangian. However, these results are based on an unique high resolution time series, and then cannot provide precise informations on the space-time structure of both Eulerian and Lagrangian small-scale physical and biological structures. Thus, in the Eastern English Channel, the fluvial supplies, distributed from the Bay of Seine to Cape Griz-Nez, generate a coastal water mass drifting nearshore, separated from the open sea by a frontal area (Brylinski and Lagadeuc, 1990; Lagadeuc *et al.*, 1997a). This coastal flow ('fleuve

côtier'; Brylinski *et al.*, 1991) is characterized by its freshness, turbidity (Dupont *et al.*, 1991) and phytoplankton richness (Brylinski *et al.*, 1984; Quisthoudt, 1987). Moreover, in this coastal ecosystem, phytoplankton populations are known to be highly fluctuating both in time and space, from a quantitative as qualitative point of view (e.g. Truffier *et al.*, 1997; Peta *et al.*, 1998). In that way, the knowledge of such a coastal ecosystem functioning obviously requires informations relevant to the space-time scales of both biological and physical processes occurring in its waters.

Herein, the goal of this paper is to focus on the space-time structure of both Eulerian and Lagrangian variability on the basis of high resolution time series of both physical and biological parameters simultaneously recorded in a Lagrangian frame in order to generalize previous results by Seuront et al. (1996b). In that way, our computations required (i) a comprehensive data set representing as fully as possible the different physical (i.e. both inshore/offshore and spring/neap tide tidal conditions) and biological (phytoplankton seasonality) conditions occurring in the coastal waters of the Eastern English Channel, (ii) analysis techniques that allow to describe the precise structure of the variability present in the dataset and (iii) an efficient algorithm to discriminate between the extreme intricacy of space-time scales in our sampling experiment and then to resume the space-time organization of the system under considerations. Moreover, these requirements had to be met regularly both in time and space at a sufficient number of data points to capture the details of the small-scale variability revealed in the data sets.

Physical-biological data, multiscale and spatio-temporal analysis

Study area and sampling

Sampling was carried out between March 1995 and December 1996 adrift in the coastal waters of the Eastern English Channel (Figure 1) at different depths, and in different tidal and meteorological conditions (Table I) aboard the N/O 'Sepia II (CNRS-INSU), and on the 2 of April 1998 aboard the N/O 'Côte de la Manche' (CNRS-INSU). During each sampling experiment (Table I), physical parameters (temperature, salinity and light transmission) and *in vivo* fluorescence (i.e. an index of phytoplankton biomass) were simultaneously recorded at high frequency (see Table I) from a single depth with a SBE 25 Sealogger CTD and a Sea Tech fluorometer, respectively. Our analysis are based on 22 time series labeled from S1 to S22 (Table I), which contain temperature, salinity, light transmission and *in vivo* fluorescence data, i.e. 1431084 data points.

Every 15 minutes, measurement of physical parameters (temperature and salinity) were taken from the surface to the bottom with a SBE 19 Seacat Profiler to ascertain the structure of the water column, except for the sampling experiment S22. Moreover, water samples were

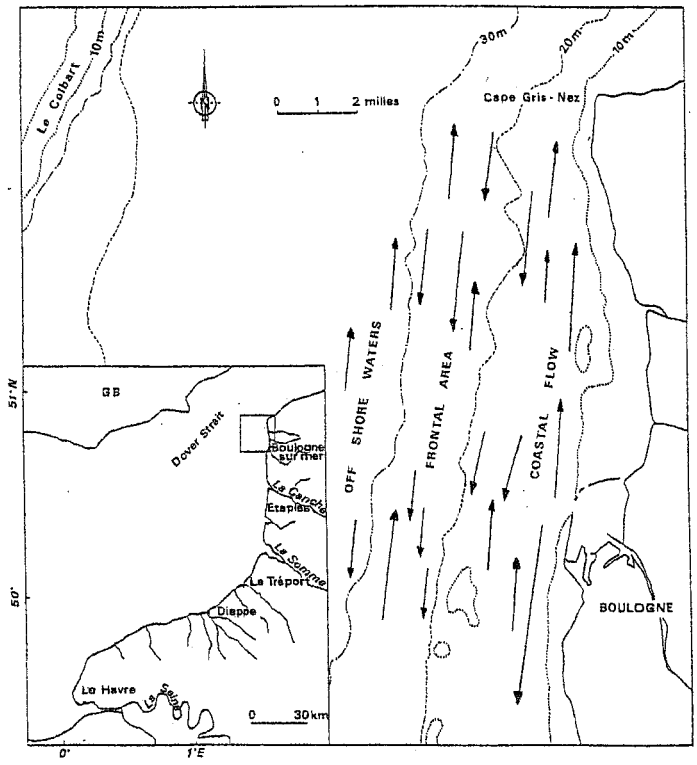

Fig. 1. Study area and location of the drifting experiments along the French coast of the Eastern English Channel; the arrows indicate the direction of the drift.

taken from the sampled depth with Niskin bottles and chlorophyll *a* concentrations were estimated following Strickland and Parson (1972) on the basis of 1 l filtered frozen samples, extracted with 90% acetone and assayed in a spectrophotometer.

Multiscale time series characterization

Spectral analysis. Roughly speaking, a spectral analysis corresponds to an analysis of variance in which the total variance of a given process is partitioned into contributions arising from processes with different time scales. A power spectrum then separates and measures the amount of variability occurring in different frequency bands. When all or parts of the spectrum follow a power law:

$$E(f) \approx f^{-\beta} \tag{1}$$

where f is frequency, and β is the exponent characterizing spectral scale invariance (e.g. $\beta = 5/3$ and $\beta = 2$ in Eulerian and Lagrangian turbulence, respectively; see Seuront *et al.*

Code	Date	Latitude	Longitude	*f*	Depth	Tidal current		Wind	
						Speed	Direction	Speed	Direction
S1	March 30, 1995	50°40'00	1°31'00	2	15.7	1.00	180	7	120
S2	November 29, 1995	50°48'56	1°29'45	2	14.7	0.22	90	5	22
S3	January 19, 1996	50°52'24	1°34'93	1	7.6	1.12	0	6	230
S4	February 1, 1996	50°42'73	1°27'49	1	15.8	0.60	0	3	220
S5	February 22, 1996	50°43,09	1°32'30	1	6.2	0.88	180	4	90
S6	March 28, 1996	50°45'56	1°33'82	2	10.4	0.28	180	8	90
S7	April 26, 1996	50°55'26	1°32'64	2	16.8	0.45	90	3	170
S8	May 28, 1996	50°49'93	1°32'93	2	15.6	0.75	0	3	90
S9	June 3, 1996	50°49'35	1°31'62	2	16.1	1.50	0	6	130
S10	June 19, 1996	50°42'42	1°28'51	2	10.5	1.01	180	1	260
S11	June 25, 1996	50°51'21	1°29'65	2	21.2	0.91	180	1	330
S12	September 4, 1996	50°40'53	1°30'63	2	5.9	0.99	180	5	310
S13	September 25, 1996	50°44'73	1°33'05	2	6.2	0.39	0	5	210
S14	September 25, 1996	50°44'91	1°33'19	2	11.2	0.39	0	5	210
S15	September 25, 1996	50°45'39	1°33'45	2	15.8	0.39	0	5	210
S16	October 2, 1996	50°42'08	1°32'90	2	6.6	0.69	180	1	100
S17	October 2, 1996	50°42'08	1°32'90	2	6.0	0.69	180	1	100
S18	October 2, 1996	50°42'08	1°32'90	2	6.2	0.69	180	4	40
S19	October 8, 1996	50°47'79	1°33'68	2	6.3	0.50	0	1	220
S20	December 5, 1996	50°45'50	1°32'85	2	6.6	0.30	0	2	190
S21	December 18, 1996	50°45'46	1°32'87	2	5.9	0.60	0	6	210
S22	April 2, 1998	50°45'00	1°33'50	2	6.0	0.60	0	2	100

Table I. Summary of the date, locations, sampling frequency f (Hz) and environmental variables of the 22 sampling experiments.

1996b for further details), the data are scaling in that range, that is, the scaling regime. The absence of characteristic time scales and the presence of a scaling regime indicate that a multifractal analysis may prove to be successful. One may note here that for time series, the exponent β and the fractal dimension D can be related according to $D = 2-(\beta-1)/2$ (Feder, 1988; Schroeder, 1991). In that way, following the terminology defined by Seuront and Lagadeuc (1997, 1998) in the monofractal frame, low and high fractal dimensions D (i.e. high and low β values) then characterize patterns exhibiting strong and weak temporal dependence, respectively.

Multifractal analysis. Since a multifractal process is characterized by a (fractal) dimension that varies continuously (e.g. Feder, 1988; Falconer, 1993), this quantity ceases to be a unique parameter that characterizes the scaling behaviour. However, recent studies have shown that multifractal processes generally lead to universal multifractals with generators characterized by three basic parameters (see e.g. Schertzer and Lovejoy, 1987, 1989). This greatly simplifies the analysis and modeling of multifractals by replacing the infinite number of dimensions by a few dynamically significant parameters. We will follow this line of reasoning in the present study and determine the whole statistical structure of our empirical time series with the help of only three basic parameters, H, C_1 and α in the framework of universal multifractals. In this paper, we only briefly present the analysis techniques used to estimate the universal multifractal parameters, for further details one may refer to a recent review devoted to the introduction of these concepts and their related analysis techniques to marine ecology (Seuront *et al.*, 1999).

The previous power spectral approach (i.e. based on a second order moment) is then generalized with the help of the q^{th} order structure functions $\left\langle [\Delta Q(\tau)]^q \right\rangle = \left\langle |Q(t+\tau)-Q(\tau)|^q \right\rangle$ where for a duration τ the fluctuations of the quantity Q are averaged over all the available values, angle brackets indicating a statistical average. For multifractal processes the scale invariant structure function exponent $\zeta(q)$ is defined by:

$$\left\langle [\Delta Q(\tau)]^q \right\rangle \approx \tau^{\zeta(q)} \tag{2}$$

More precisely, in the universal multifractal framework, the Eulerian relation for structure function exponent $\zeta(q)$ is given by (Seuront *et al.*, 1996b):

$$\zeta(q) = qH - \frac{C_1}{\alpha-1}(q^\alpha - q) \tag{3}$$

where $K(q)=\frac{C_1}{\alpha-1}(q^\alpha-q)$, $K(q)$ being the scaling function describing the multiscaling properties of the statistical moments of order q [see Seuront *et al.* (1999) for a detailed derivation of equation (3) in a more general statistical framework]. The first moment gives the scaling exponent $H=\zeta(1)$ corresponding to the degree of non-conservation of the process (i.e. $H=0$ for stationary process), and the second moment is linked to the power spectrum by $\beta=1+\zeta(2)$. The second term expresses a deviation from homogeneity (in which case $\zeta(q)=qH$), and represents the intermittency corrections. C_1 is the fractal codimension that characterizes the sparseness of a given descriptor, and satisfies $0\leq C_1\leq 1$ for time series: $C_1=0$ for a homogeneous descriptor and C_1 is all the more high as the descriptor is sparse, indicating that the values corresponding to any given level of variability are more scarce. The Lévy index α is the degree of multifractality bounded between $\alpha=0$ and $\alpha=2$ corresponding to the monofractal case and to the maximum, or log-normal, multifractal case, respectively. As α increases, the more numerous are the variability levels bounded between lower and higher values of the descriptor (i.e. the more complex is the structure of the descriptor; see Seuront *et al.*, 1999, their figure 15 for more details on the precise meaning of C_1 and α). Let us recall that in the Lagrangian frame, equation (3) writes (Seuront *et al.*, 1996b):

$$\zeta(q)=\frac{q}{2}-\frac{C_1}{\alpha-1}\left(\left(\frac{q}{2}\right)^\alpha-\frac{q}{2}\right) \tag{4}$$

The parameters C_1 and α can be estimated considering different derivation of equations (3) and (4) (see e.g. Schmitt *et al.*, 1995; Seuront *et al.*, 1996a, b, 1999), but also from the Double Trace Moment Technique (Lavallée, 1991; Lavallée *et al.*, 1992), a very specific data analysis technique which has been extensively explained elsewhere (Seuront *et al.*, 1999). More details on the universal multifractal theoretical background can be found in Schertzer and Lovejoy (1983, 1985, 1987, 1989) and related analysis techniques such as Double Trace Moment and structure functions have been extensively described respectively in Lavallée *et al.* (1992), Schmitt *et al.* (1992, 1993, 1994), and in Schmitt *et al.* (1995, 1996a, b, 1998) and Seuront *et al.* (1996a, b, 1999).

Because an objective criterion is needed for deciding upon an appropriate range of scales to include in the regressions to determine both the spectral exponents β and the structure function scaling exponents $\zeta(q)$ respectively from equations (1) and (2), we used the values of

the frequencies and the time scales which maximized the coefficient of determination (r^2) and minimized the total sum of the squared residuals for the regression, as proposed by Seuront and Lagadeuc (1997). Before performing the calculations, the measured time series must be detrended and normalized. This is done, first, by calculating Kendall's coefficient of rank correlation, τ, between time series and the x-axis values in order to detect the presence of a linear trend (Kendall and Stuart, 1966). We thus eventually detrended the time series by fitting linear regressions to the original data by least squares and used the regression residuals in further analysis, a common remedial procedure in time series analysis (Fuller, 1976). Second, the measured time series were normalized (nondimensionalized) by dividing all values by the average of the total series.

Spatio-temporal analysis (STA)

In order to estimate the space-time properties of the whole sampling experiment, we applied a spatio-temporal analysis (STA) initially introduced by Ibanez (1973) to characterize sampling processes in plankton ecology, and recently used by Seuront and Lagadeuc (1998) to describe the space-time structure of a coastal ecosystem. We selected variables related to the space-time scales of our sampling experiment and a principal component analysis (PCA) was performed on the observations (Q mode) and the variables (R mode, *sensu* Legendre and Legendre, 1984). These variables are latitude, longitude, depth, tidal current speed and direction, nature of the superficial sediment, mean chlorophyll *a* concentration and temperature. We take as an arbitrary origin for latitude and longitude a point located at the entrance of the fishing port of Boulogne/Mer (Figure 1). Depth is expressed in meters, current speed is estimated as the mean drift speed during each sampling experiment, and current direction is expressed as an

Superficial sediment	Code
Bedrock	0
Gravels and pebbles	1
Coarse sand	2
Bioclastic medium sand	3
Medium sand	4
Grey fine sand	5
Muddy sediment	6

Table II. Codes used in the PCA to represent the qualitative nature of the bottom superficial sediment.

alternance between northerly and southerly drifts during flood and ebb tides, respectively. The nature of the superficial sediment (Table II) is coded following the classification of Augris *et al.* (1995). Chlorophyll *a* and temperature estimated from the sampling depth were averaged over the whole dataset for each sampling experiment. While the effect of wind events have been demonstrated to be of main interest in structuring the whole water column (Raby *et al.*, 1994; Lagadeuc *et al.*, 1997b; Seuront and Lagadeuc, 1997), one may note here that we did not introduce wind speed and direction as variables in our analysis because the effect of wind on turbulent kinetic energy dissipation rates is clearly smaller than the effect of tide. Indeed, the dissipation rates of wind-generated turbulent kinetic energy, estimated for each sampled depth following the boundary layer model used by MacKenzie and Leggett (1991) as $\varepsilon_w = 7.4\times10^{-8} \pm 8.1\times10^{-8}$ $m^2.s^{-3}$ ($\bar{x} \pm SD$), were always about one order a magnitude lower than the dissipation rate of turbulent energy induced by tide expected in shallow coastal waters which are typically in the range 10^{-6}-10^{-4} $m^2.s^{-3}$ (MacKenzie and Leggett, 1991). Furthermore, the identification of the components of the multivariate analysis was carried out using the factor loadings of the variable in the R mode of PCA analysis since the factor loadings of a given factor could be related to the variance explained by such a factor (Legendre and Legendre, 1984). Because a criterion is needed for deciding upon appropriate observations to group in the data space, a cluster analysis based on an unweighted centroid algorithm (Sokal and Michener, 1958) has been carried out on a (Euclidean) distance matrix calculated from the first three principal components of the multivariate analysis. Afterwards, we introduced additional variables related to mean, variability (expressed as the sum of a given power spectra, i.e. an estimate of the total variation in a given record; Bendat and Piersol, 1986) and structure (i.e. spectral exponent β, and the universal multifractal parameters H, C_1 and α) of temperature, salinity, light transmission and *in vivo* fluorescence in order to characterize their organization in the spatio-temporal space associated with the whole sampling experiment. The concentration of Prymnesiophyceae *Phaeocystis* sp.—known for its highly developed swarming capacities in the coastal waters of the Eastern English Channel (Tyler, 1977; Lennox, 1979)—has also been introduced as a potential source of increased patchiness for phytoplankton populations. Wind speed and direction were also introduced as additional variables related to external (atmospheric) physical forcing.

Results

Environmental conditions

In the Eastern English Channel, characterized by its megatidal regime, the dissipation of tidal energy is basically regarded to be responsible for the vertical homogenization of inshore and shallow water masses (50 m maximum depth), except in very specific tidal conditions (i.e. a vertical stratification associated to a moving of the coastal lighter waters over heavier offshore waters during ebb tide in neap tide conditions; Brylinski and Lagadeuc, 1990; Lagadeuc *et al.*, 1997a) which has never been reached during our sampling experiment. In that way, one may note that a density gradient has never been observed in any sampling experiment, indicating vertical homogeneity of the water column. Thus, our sampling experiments can be regarded as having been conducted in well mixed waters.

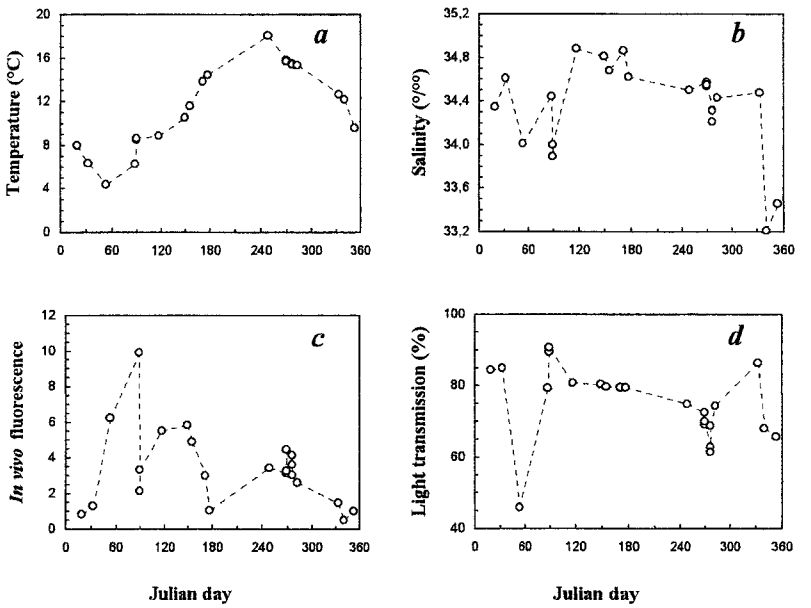

Fig. 2. Mean values of temperature (**a**), salinity (**b**), *in vivo* fluorescence (**c**) and light transmission (**d**) for the 22 sampling experiments.

Mean values and variability of temperature, salinity, *in vivo* fluorescence and light transmission did not show any characteristic temporal patterns (Figure 2), except in the case of mean temperature data which exhibit a clear seasonal cycle (Figure 2a). A correlation analysis (Table III) nevertheless leads to further conclusions. Indeed, while mean values of the studied parameters did not exhibit significant correlations, standard deviations of *in vivo* fluorescence and light transmission were respectively correlated ($P < 0.05$) and non correlated ($P > 0.05$) with standard deviations of physical parameters (i.e. temperature and salinity). Considering the space-time scales of the whole sampling experiment, this suggests a potential

phenomenological link between phytoplankton biomass distribution and small-scale physical variability. Moreover, the highly significant positive and negative correlations ($P < 0.01$) occurring respectively between means and standard deviations of *in vivo* fluorescence and light transmission indicate a differential density-dependent control of small-scale variability for these parameters. Finally, chlorophyll *a* concentration and *in vivo* fluorescence being highly correlated (Spearman's $\rho = 0.870, P < 0.01$), *in vivo* fluorescence fluctuations can be related to the fluctuations of phytoplankton biomass.

	Chloro	S	T	Trans	SD_F	SD_S	SD_T	SD_{Tr}
Chloro	1,00							
S	0,29	1,00						
T	-0,02	0,18	1,00					
Trans	-0,17	0,34	-0,40	1,00				
SD_F	0,82 **	0,21	0,04	-0,34	1,00			
SD_S	-0,55 **	-0,39	-0,26	0,15	-0,42 *	1,00		
SD_T	-0,65 **	-0,19	-0,19	0,09	-0,50 *	0,88 **	1,00	
SD_{Tr}	-0,01	-0,45 *	-0,02	-0,57 **	0,05	-0,12	-0,03	1,00

*: 5% significance level
** : 1% significance level

Table III. Correlation matrix of mean values and standard deviations (SD) of temperature, salinity, *in vivo* fluorescence and light transmission.

Spectral analysis and Eulerian/Lagrangian scale breaking

Samples of the double logarithmic power spectra for the studied time series together with their best fitting lines are given in figure 3. The power spectra present a mixed behaviour with two scaling tendencies, the change of behaviour of the power spectra occurring for frequencies f ranging from 0.02 to 0.11 Hz (i.e. $\bar{x} \pm \mathrm{SD}: 0.06 \pm 0.03$ Hz) which are associated with characteristic time scales t ranging from about 9 to 54 seconds (i.e. $\bar{x} \pm \mathrm{SD}: 23.3 \pm 12.9$ sec). Within each data set, the transition scales are very similar whatever the variables in question, as shown by the weak dispersion of the estimates of the transition frequencies f ($\mathrm{SD}_f = 0.005 \pm 0.001$ SD).

Those temporal transition scales can be associated with spatial scales using probably the most cited and widely used method of relating time and space in the frame of turbulence studies, 'Taylor's hypothesis of frozen turbulence' (Taylor, 1938), which basically states that temporal and spatial averages t and l, respectively can be related by a constant velocity V,

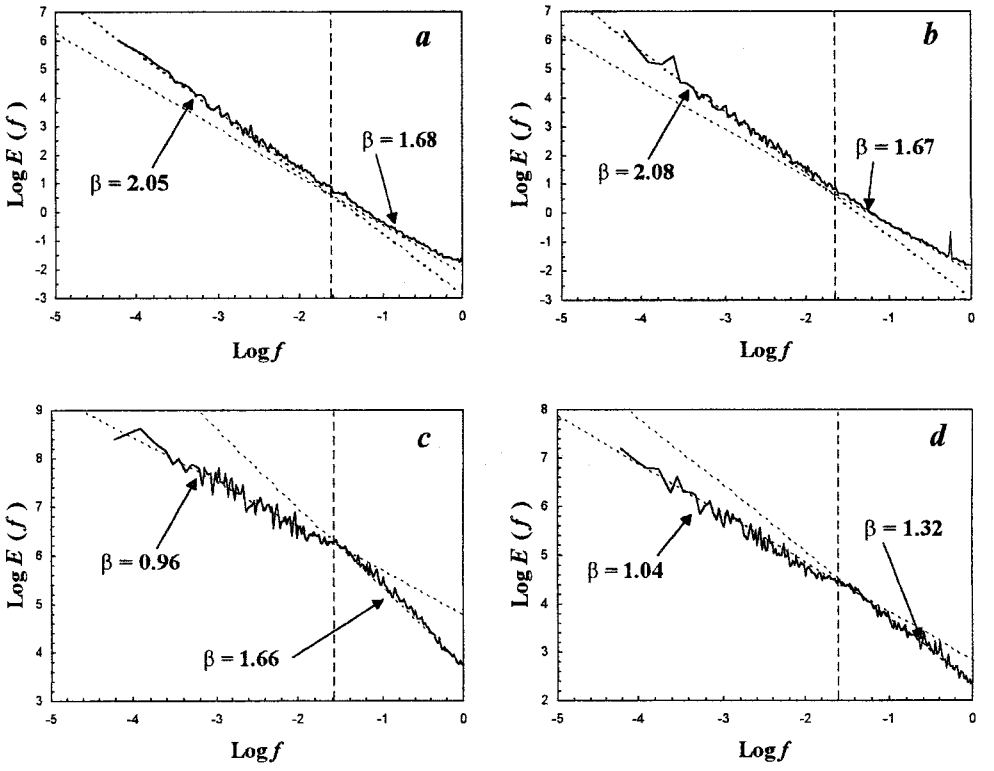

Fig. 3. The power spectra $E(f)$ (f is frequency) of temperature (**a**), salinity (**b**), *in vivo* fluorescence (**c**) and light transmission (**d**), shown in log-log plots, for time series S22. The power spectra exhibit a mixed behaviour with two scaling tendencies, the change of behaviour of the power spectra occurring for frequency $f = 2.5\ 10^{-2}$ Hz.

$l = V \cdot t$. Then, using the mean tidal drift observed during each field experiment (Table I), we estimate that the associated length scales were ~12 meters ($\bar{x} \pm \mathrm{SD}$: 12.1 ± 1.6 m) for sampling experiments S1 to S21 and 24.6 meters for sampling experiment S22. These length scales are close to the size of the ships used during the sampling experiment, i.e. 12.5m and 24.9m for N/O 'Sepia II' and N/O 'Côte de la Manche', respectively. These results thus confirm and generalize the results obtained by Seuront *et al.* (1996b) from a single sampling experiment conducted at the end of March 1995 during a period of spring tide (Table IV; Figure 4).

In order to interpret this change of behaviour of the power spectra, let us recall that the measurements were taken from a boat adrift in the Channel. This means that for the high frequency range of the measurements we can consider the boat as not moving, so the measurements correspond to a fix-point procedure, i.e. Eulerian sampling. This is confirmed by the slopes of the small-scale temperature, salinity and *in vivo* fluorescence power spectra (Table V) which were not significantly different (Kruskal-Wallis test, $P > 0.05$), and cannot be statistically distinguished from the theoretical spectral value $\beta = 5/3$ (Binomial test,

Time series	Time (s)[1]	Time (s)[2]	Space (m)[1]	Space (m)[2]
*	12.30	12.70	12.30	12.70
S1	12.59	12.70	12.59	12.70
S2	53.70	54.00	11.81	11.88
S3	10.23	10.50	11.46	11.76
S4	21.38	21.00	12.83	12.60
S5	12.88	44.50	11.34	39.16
S6	44.67	44.00	12.51	12.32
S7	25.70	26.00	11.57	11.70
S8	16.22	16.50	12.16	12.38
S9	8.91	9.00	13.37	13.50
S10	12.30	12.00	12.43	12.12
S11	14.13	14.00	12.85	12.74
S12	12.30	12.50	12.18	12.38
S13	33.33	33.50	13.00	13.07
S14	30.90	31.00	12.05	12.09
S15	33.88	34.00	13.21	13.26
S16	18.62	19.00	12.85	13.11
S17	17.78	18.00	12.27	12.42
S18	19.50	20.00	13.45	13.80
S19	26.92	27.00	13.46	13.50
S20	40.74	41.00	12.22	12.30
S21	19.50	19.50	11.70	11.70
S22	44.68	44.50	24.58	24.48
Mean	*23.62*	*25.08*	*12.96*	*14.25*
SD	*12.81*	*13.24*	*2.61*	*6.00*

*: Seuront *et al*. (1996b), [1]: spectral analyses and [2]: structure functions

Table IV. Temporal and spatial transition scales obtained from power spectra and structure functions. The association between temporal and spatial transition scales has been done *via* the 'Taylor's hypothesis of frozen turbulence' (see text).

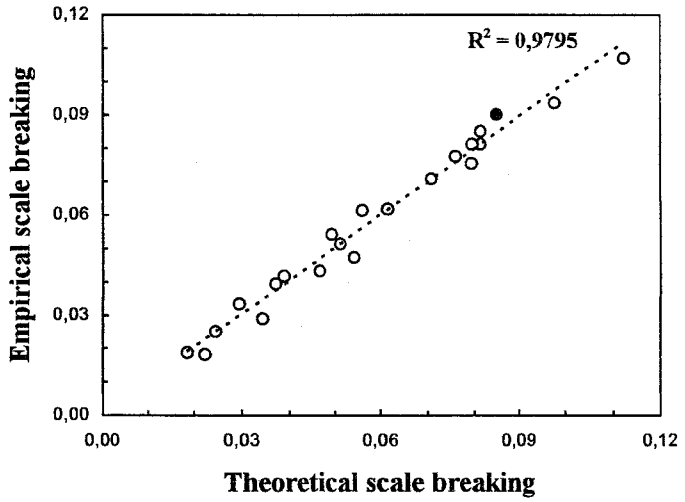

Fig. 4. Theoretical versus empirical scale breakings (Hz) between Eulerian and Lagrangian scales. Theoretical scale breaking has been estimated multiplying the size of the boat used during the sampling experiment by the mean tidal drift observed during each experiment. Empirical scale breaking has been estimated as the mean transition scale from the power spectra of temperature, salinity, *in vivo* fluorescence and light transmission. The result obtained by Seuront *et al.* (1996b) is shown for comparison (black dot).

$P > 0.05$; Siegel and Castellan, 1988) expected in the case of an isotropic three-dimensional homogeneous turbulence (Obukhov, 1949; Corrsin, 1951). Nevertheless, for each sampling experiment, an analysis of covariance (Zar, 1984) has been conduced for the slopes of the power spectra for temperature, salinity and *in vivo* fluorescence. It is found that the chlorophyll *a* concentration exhibits highly significant positive correlation ($P < 0.01$) with the F-statistic, used here as a measure of any significant difference between the slope of temperature, salinity and fluorescence power spectra for a given sampling experiment. Subsequent multiple comparison procedures based on the Tuckey test (Zar, 1984) conducted to determine which β was different from the others then confirm and specify the previous results. Thus, these analyses indicate that rejection of the null hypothesis was always due to β values for *in vivo* fluorescence significantly higher than those for temperature and salinity. On

	Eulerian scales			
	β	H	C_1	α
Temperature	1.70 (0.05)	0.39 (0.03)	0.042 (0.005)	1.75 (0.05)
Salinity	1.72 (0.06)	0.40 (0.03)	0.044 (0.006)	1.74 (0.04)
Fluorescence	1.69 (0.03)	0.38 (0.02)	0.038 (0.003)	1.84 (0.03)
Transmission	1.31 (0.36)	0.30 (0.09)	0.162 (0.110)	1.73 (0.13)

	Lagrangian scales			
	β	H	C_1	α
Temperature	2.03 (0.05)	0.52 (0.02)	0.052 (0.001)	1.86 (0.04)
Salinity	2.03 (0.04)	0.52 (0.02)	0.052 (0.001)	1.86 (0.04)
Fluorescence	1.03 (0.24)	0.27 (0.15)	0.343 (0.067)	1.62 (0.13)
Transmission	1.02 (0.24)	0.27 (0.15)	0.301 (0.056)	1.63 (0.12)

Table V. Mean values and standard deviation of the spectral exponent β universal multifractal parameters H, C_1 and α estimated from the 22 time series considered in the Eulerian frame and the 13 time series considered in the Lagrangian frame.

the contrary, light transmission power spectra (Table V) appear significantly smaller than the theoretical $\beta = 5/3$ value ($P < 0.05$). Finally, one may also note here that analyses of covariance showed that the 22 spectral exponents β were not all equal for each parameter, indicating potential differential spectral structure of the variables in question at the space-time scales of the whole sampling experiment.

On the other hand, for frequencies smaller than the observed scale breakings, the inertia of the boat becomes negligible and the measurements are effectively taken following the flows, i.e. in a Lagrangian framework. One may note here that we had to average the original time

series up to the Eulerian/Lagrangian transition scale (Table IV), in order to be in the Lagrangian scales. In that way, our characterization of the Lagrangian behaviour of time series of temperature, salinity, light transmission and *in vivo* fluorescence is based on time series exhibiting at least 256 data points (i.e. the lower bound for a dataset to lead to efficient multifractal analysis; Teissier *et al.*, 1993a, b; Seuront *et al.*, 1999). In the following, we then focused on 13 time series S1-S3, S5, S7, S9, S10-S12, S14, S19 and S21-S22. The previously described transition is also confirmed by the similar scaling behaviours exhibited by temperature and salinity time series (Table V), which cannot be statistically distinguished from the theoretical slope $\beta = 2$ (Binomial test, $P > 0.05$) expected in the case of purely passive scalars advected by Lagrangian fluid motions (Monin and Yaglom, 1975). On the contrary, *in vivo* fluorescence and light transmission spectral exponents show very specific behaviours (Table V) which cannot be statistically distinguished (Wilcoxon-Mann-Whitney U-test, $P > 0.05$). Moreover, analyses of covariance concluded that the 13 spectral exponents β were not all equal ($P < 0.05$) for both light transmission and fluorescence power spectra.

Eulerian scales

Multifractal analysis. The computations of the temperature, salinity, *in vivo* fluorescence and light transmission structure functions [i.e. $\langle[\Delta T(\tau)]^q\rangle$, $\langle[\Delta S(\tau)]^q\rangle$, $\langle[\Delta F(\tau)]^q\rangle$, and $\langle[\Delta Tr(\tau)]^q\rangle$] confirm and generalize to higher orders of moment the scaling regimes previously shown by spectral analysis (Figure 5; Table IV). We subsequently plotted the structure function scaling exponent $\zeta(q)$ whose non-linearity indicate that the variables in question can be considered as multifractals. Figure 6 shows that within a given time series (here time series S22), the three curves corresponding to temperature, salinity and *in vivo* fluorescence are always very close to each other, and cannot be qualitatively considered as being different. On the contrary, light transmission exhibit a very specific behaviour for time series S1-S5, S7-S11, S18 and S22 (Figure 6). Finally, one may note that the correspondence between the empirical estimates and the theoretical curves is excellent until critical moment order after which the empirical curves are linear (Figure 6). This linear behaviour of the structure function scaling exponent $\zeta(q)$ is well-known for sufficiently high order moments (Schertzer and Lovejoy, 1989) and, as demonstrated and studied by Seuront *et al.* (1996b, 1999), is due to sampling limitations. In particular, this problem has been extensively studied in Seuront *et al.* (1999) in the general framework defined by equation (3).

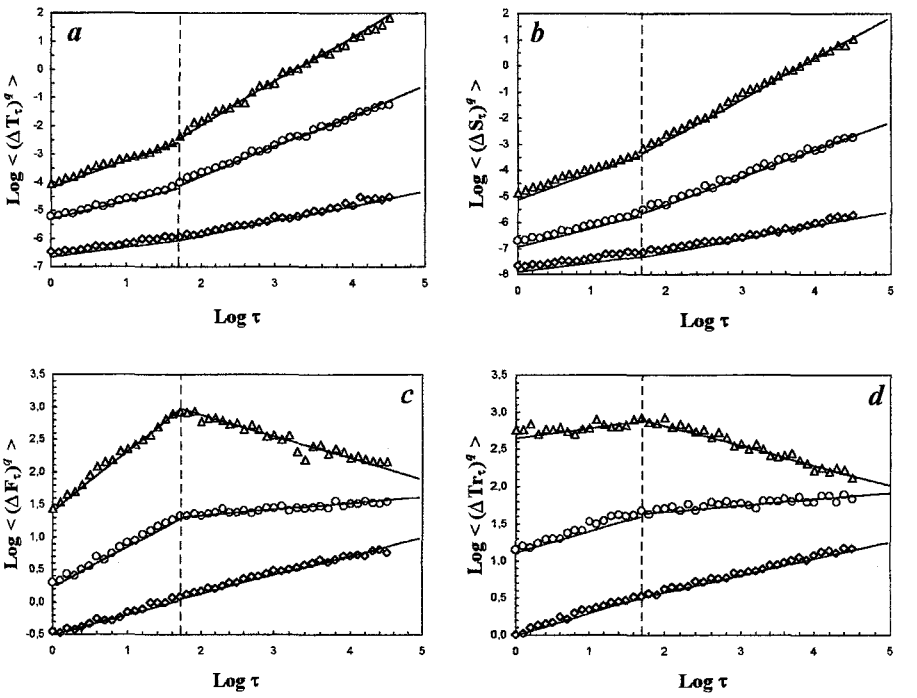

Fig. 5. The structure functions of temperature $\langle[\Delta T(\tau)]^q\rangle$ (**a**), salinity $\langle[\Delta S(\tau)]^q\rangle$ (**b**), *in vivo* fluorescence $\langle[\Delta F(\tau)]^q\rangle$ (**c**) and light transmission $\langle[\Delta Tr(\tau)]^q\rangle$ (**d**) vs. τ, shown in log-log plots for q = 1, 2 and 3 (from bottom to top) for time series S22. Linear trends are clearly visible for all order of moments for Eulerian scales (less than 40 seconds) and Lagrangian scales (greater than 40 seconds). The straight lines indicate the best regression over each range of scales for each value of q.

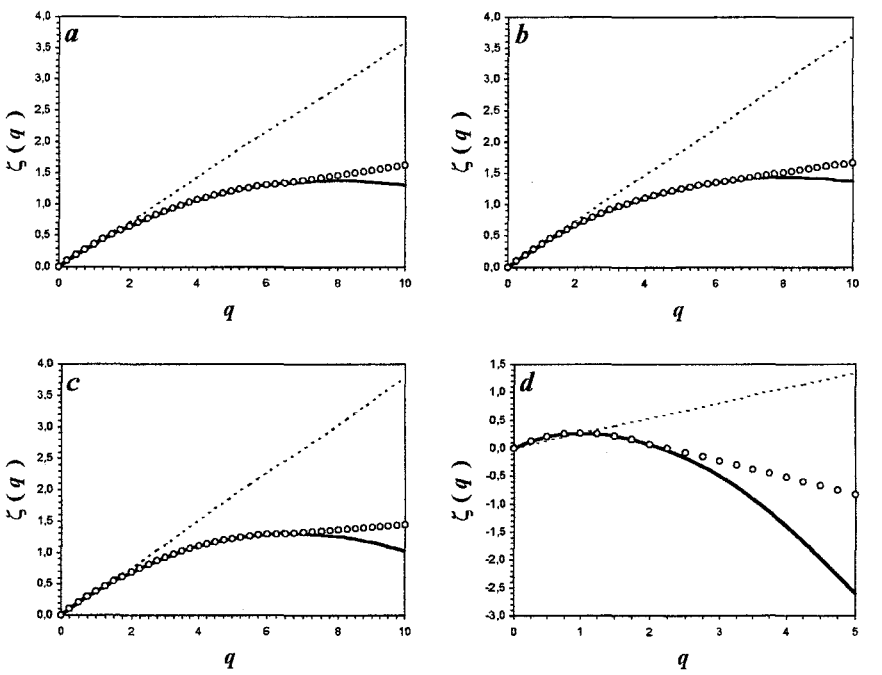

Fig. 6. The Eulerian structure function scaling exponent $\zeta(q)$ empirical curves (dots), compared to the monofractal curves $\zeta(q) = qH$ (dashed line), and to the universal multifractal curves (continuous curve) obtained with C_1 and α in equation (3) for temperature (**a**), salinity (**b**), *in vivo* fluorescence (**c**) and light transmission (**d**) for time series 22. The empirical curves are clearly non-linear, indicating multifractality.

Estimates of the three universal multifractal parameters H, C_1 and α provide a quantitative confirmation of the previously described multifractal statistics. We then showed that there were significant differences between temperature, salinity, fluorescence and transmission exponents H (Table V; Kruskal-Wallis test, $P < 0.05$), the light transmission exponents being significantly smaller than the others (Dunn test, $P < 0.05$). Moreover, as previously shown for the spectral exponents β, analyses of covariance indicated that the H values were not all equal for each parameter ($P < 0.05$). The fractal codimensions C_1 lead to similar results: temperature, salinity and *in vivo* fluorescence codimensions cannot be statistically distinguished ($P > 0.05$), while light transmission codimension C_1 is significantly smaller than the others ($P < 0.05$; Table V). Finally, the parameters α cannot be statistically distinguished for temperature, salinity and light transmission ($P > 0.05$; Table V), but the Lévy index of *in vivo* fluorescence is significantly greater than the others ($P < 0.05$).

		Eulerian scales			Lagrangian scales		
	Code	**PC-1**	**PC-2**	**PC-3**	**PC-1**	**PC-2**	**PC-3**
Latitude	λ	-0.43	-0.82	-0.08	-0.93	-0.14	0.23
Longitude	φ	0.57	-0.62	-0.33	0.20	-0.90	-0.25
Depth	**Depth**	-0.87	-0.20	0.18	-0.79	0.36	0.31
Tidal current speed	C_{Speed}	-0.44	0.49	-0.12	-0.03	0.20	-0.40
Tidal current direction	C_{Dir}	0.18	0.56	-0.47	0.41	0.66	-0.11
Sediment quality	**Sed**	0.93	-0.04	0.23	0.73	-0.27	0.34
Chlorophyll *a*	**Chl. *a***	0.20	-0.08	-0.86	0.21	0.14	-0.71
Temperature	**T**	0.55	0.04	0.53	0.43	0.11	0.72

Table VI. The first three spatio-temporal eigen vectors (standardized after multiplication by the square root of the eigen vector's corresponding eigen values) associated with the eight spatio-temporal variables.

Spatio-temporal analysis. The results of the PCA showed that three components explain 72.58% of the total variance. The first component (hereafter called PC-1), which explains 33.87% of the variance is positively correlated to longitude, temperature and superficial sediment quality, and negatively correlated to latitude, depth and tidal current speed (Figure 7a, b; Table VI). This component can nevertheless be mainly considered representative of superficial sediment quality and depth. The second component (PC-2 hereafter), which explains 20.52% of the total variance, was positively correlated to current speed and direction, and negatively correlated to latitude and longitude (Figure 7a; Table VI). This component can then be considered representative of tidal and geographical effects. The third component (PC-3 hereafter) explaining 18.19% of the total variance is positively correlated to temperature, and negatively correlated to chlorophyll *a* concentration and tidal current direction (Figure 7b;

Table VI). The significance of the latter component is first linked to the seasonal physical forcing of temperature and, second, to the biological features of chlorophyll *a* concentrations and tidal current direction, the association of these two variables being related to the increase in chlorophyll *a* concentration occurring during ebb tide.

The projections of the observations in the two-dimensional planes defined by the three first components seem to indicate that the observations are mainly distributed following the first two principal components (Figure 7c, d). Nevertheless, the unweighted centroid clustering showed five groups of observations (Table VII; Figure 7c, d). These clusters (numbered from C-I to C-V) were indeed related to the space-time discrimination shown by the PCA: C-I characterizes high current speed and ebb tides sampling, C-II deeper and northern position, C-III highest chlorophyll *a* concentration, C-IV the association of fine sediment and ebb tide sampling, while C-V only characterizes fine superficial sediment.

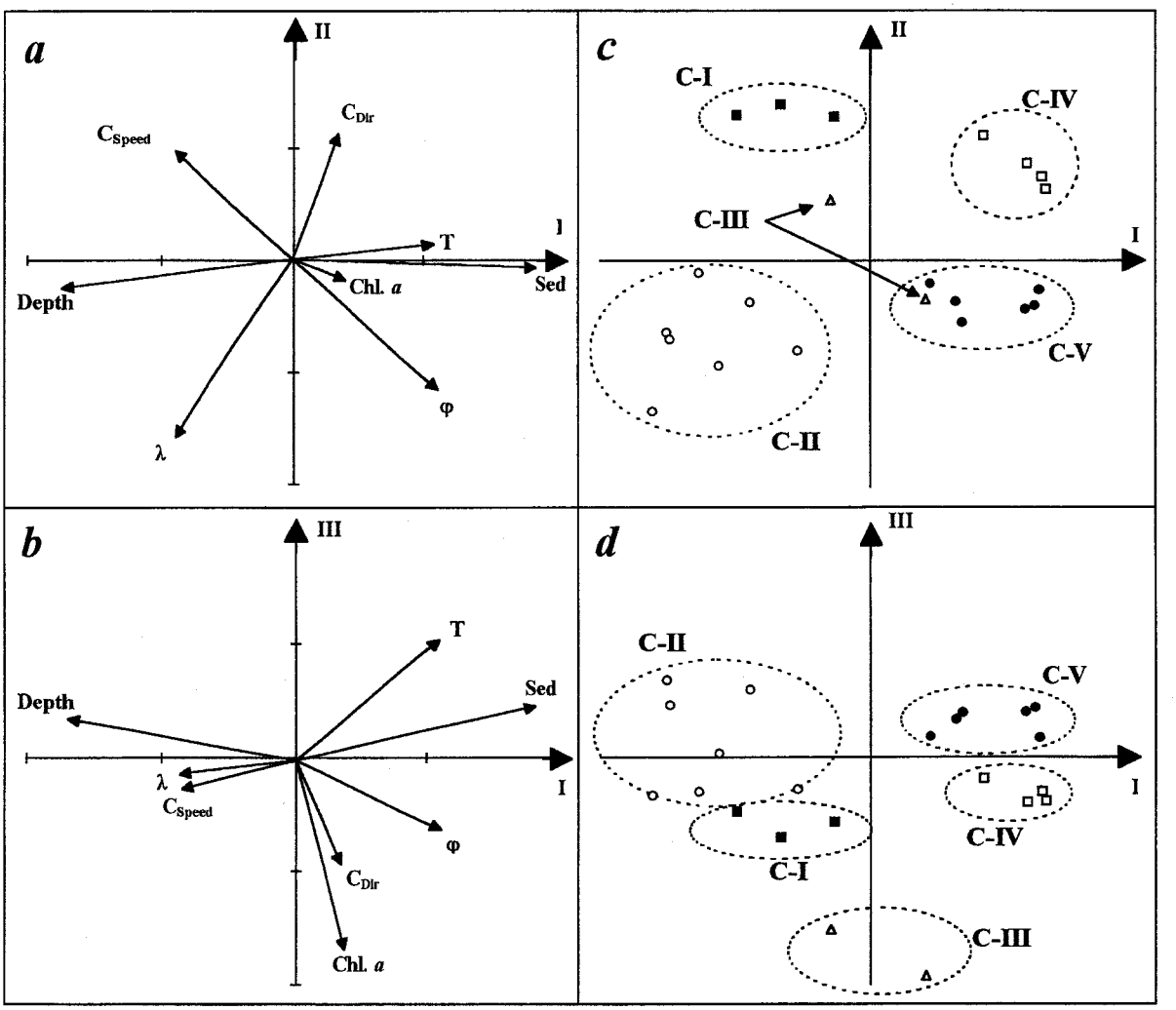

Fig. 7. Correlation plots showing (**a**) the position of the initial variables, and the projection of the observations in the bidimensional spaces defined by the three first principal components (**b**) in the Eulerian frame.

The additional variables (Table VIII), shown in the space defined by the three first components, have been plotted considering their correlation with these axes as coordinates; a central square indicates the 95% confidence limits (Figure 8). The coordinates of the initial eight spatio-temporal variables were also plotted considering the values of their corresponding eigen vectors (Table VI).

The observed means, variability (i.e. sums of power spectra) and spectral exponents β exhibit very specific behaviours (Figure 8a, b; Table VIII). Mean values of salinity and light transmission are negatively correlated with PC-2 and PC-1, respectively. This indicates an increase in salinity from southern to northern locations, and an increase in light transmission in deeper locations, whatever the tidal current directions. The mean concentration of *Phaeocystis* is positively correlated with PC-3, indicating a seasonal effect of climatic forcing rather than any biological density-dependent effect. Temperature and salinity spectral sums both exhibit positive and negative correlation with PC-1 and PC-3. This indicates an increased variability in coastal waters and during ebb tide. The spectral sum of light transmission is positively correlated with PC-1 (fine sediment), while the one of *in vivo* fluorescence is negatively correlated with PC-3 (high chlorophyll *a* concentration).

Temperature and salinity spectral exponents β exhibit very similar spatio-temporal patterns. Thus, their significant negative correlation with PC-2 indicates an increase temporal dependence (i.e. high β values) in northern and coastal locations. As previously shown for their spectral sums, spectral exponents of fluorescence and light transmission are respectively negatively and positively correlated with PC-3 and PC-1. These results then indicate that *in vivo* fluorescence temporal dependence (i.e. β value) is greater when the chlorophyll concentration is high, while light transmission temporal dependence is greater when the bottom sediment is finer. One may nevertheless note the positive and negative correlation of *in vivo* fluorescence with PC-1 and PC-2, suggesting an increase in the β values in coastal waters (Figure 8a).

The space-time structuration of the universal multifractal parameters H, C_1 and α lead to further results (Figure 8c, d; Table VIII). First, as previously demonstrated in the case of the spectral exponent β, temperature and salinity multifractal parameters exhibit very similar behaviours. In particular, H and C_1 are negatively correlated with PC-2, indicating an increased non stationarity (i.e. high H value) and sparsity (i.e. high C_1 value) of temperature and salinity fields both in northern and coastal locations. On the contrary, the Lévy index α do

not exhibit any significant correlation in the space defined by the three principal components. This parameter can then be regarded as remaining constant in the space-time of the whole sampling experiment. Second, the space-time structure of light transmission appears to be wholly characterized by the first principal component. The parameters H, C_1 and α are then positively correlated with PC-1, indicating an increased non stationarity, sparsity and complexity of the light transmission field as the superficial bottom sediment becomes finer. Finally, the space-time structure of *in vivo* fluorescence exhibit a more complex behaviour. Thus, the parameter H, C_1 and α are positively correlated with PC-1 and negatively

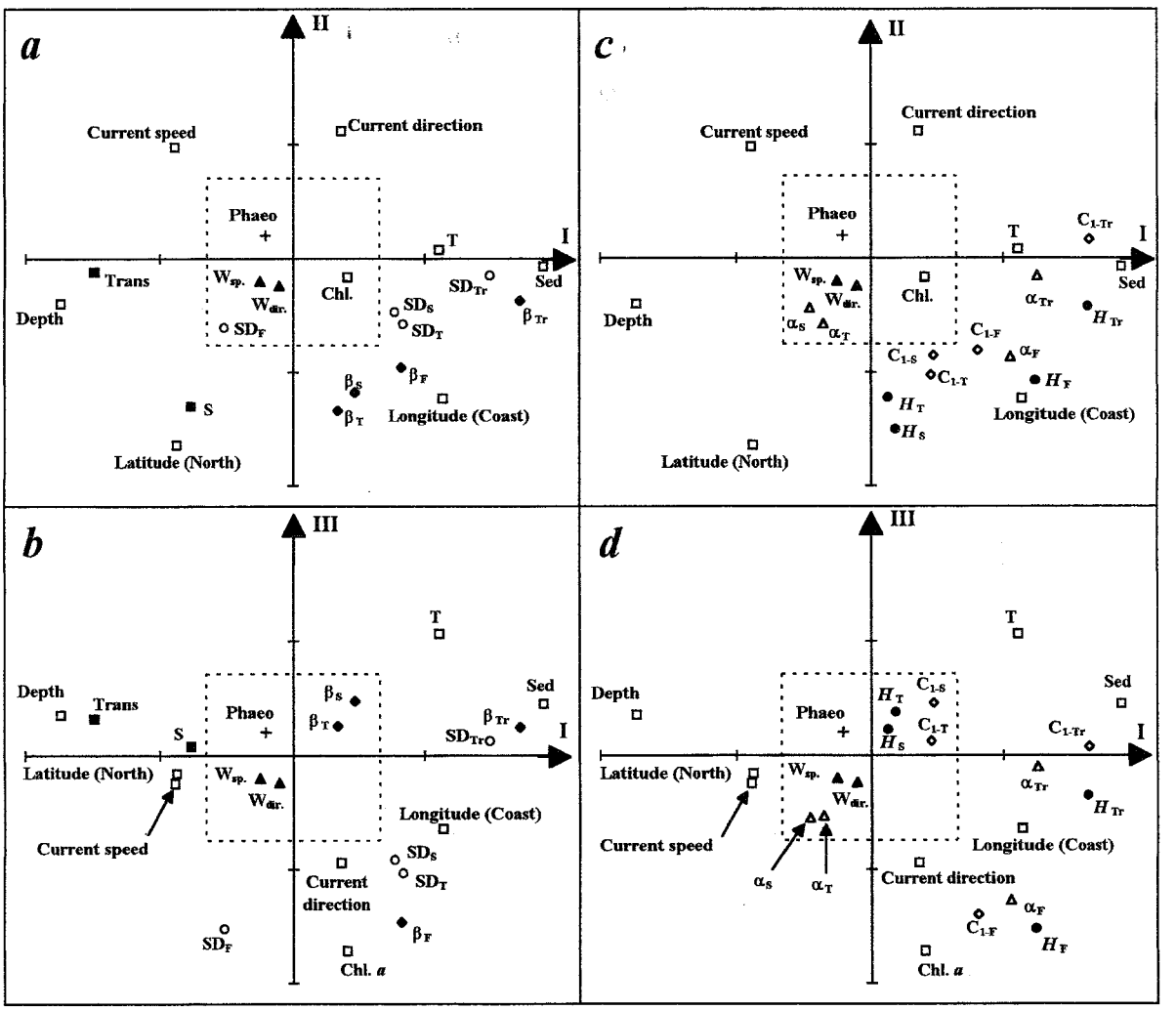

Fig. 8. Position of the additional variables (for codes, see Table 8) in the bidimensional spaces of the three first principal components in the Eulerian frame. The coordinates are the correlation coefficients with these axes. The eight initial variables are placed with the corresponding elements of the eigen vectors (standardized after multiplication by the square root of the corresponding eigen values). Factors significantly correlated with the principal components are located outside the central square, corresponding to the 95% confidence interval.

correlated with both PC-2 and PC-3. This leads to consider a differential space-time structure of phytoplankton population associated with inshore-offshore gradient and chlorophyll *a* concentration (i.e. higher values of H, C_1 and α in coastal waters and in high chlorophyll *a* concentration).

(a)

Eulerian scales				
C-I	C-II	C-III	C-IV	C-IV
S1-S2 S11	S3-S5 S8-S10 S12	S6-S7	S13 S17-S19	S14-S16 S20-S22

(b)

Lagrangian scales			
C-I	C-II	C-III	C-IV
S2-S3 S7-S9 S11	S12-S14 S19-S21	S1 S10	S5 S22

Table VII. Clusters of stations using the first three components of the PCA. Cluster analysis has been carried out on a Euclidean distance matrix calculated from the three first components of the PCA. C, cluster; S*i*, time series number (*i*).

Lagrangian scales

Multifractal analysis. As with Eulerian data above, we estimated the scaling exponent $\zeta(q)$ from the structure function of the Lagrangian temperature, salinity, *in vivo* fluorescence and light transmission which also exhibit a characteristic nonlinear behaviour (Figure 9). In that way, one may note here that while temperature and salinity multifractal parameters H, C_1 and α have been estimated in the theoretical Lagrangian frame of equation (4), this framework appears unsuited in the case of fluorescence and light transmission. Thus, following the very specific behaviours shown by fluorescence and light transmission scaling exponents $\zeta(q)$ (Fig. 9c, d), which significantly differ from the expected behaviour for purely passive scalars advected by Lagrangian turbulence [in which case equation (4) holds, with in particular $\beta = 1+\zeta(2) = 2.0$ and $H = \zeta(1) = 0.5$], the parameter H, C_1 and α for fluorescence and light transmission have then been estimated in the general frame provided by equation (3). This relation is indeed not specific to the Eulerian frame, but can be applied to characterize any multifractal processes in the absence of well defined theoretical framework [see Seuront *et al.* (1999) for further details]. As shown in the Eulerian frame, the linear behaviour exhibited by the empirical scaling exponent $\zeta(q)$ can be associated with sampling limitations [see Seuront *et al.* (1996b, 1999) for further details].

		Eulerian scales			Lagrangian scales		
Additional data	Code	PC-1	PC-2	PC-3	PC-1	PC-2	PC-3
Mean value							
Salinity	S	-0.38	-0.65	0.04	-0.62	-0.08	0.21
Light transmission	Tr	-0.74	-0.06	0.16	-0.53	0.16	0.39
Standard deviation							
Temperature	SD_T	0.42	-0.29	-0.52	0.22	-0.70	0.30
Salinity	SD_S	0.39	-0.24	-0.46	-0.08	-0.65	0.31
Fluorescence	SD_F	-0.25	-0.30	-0.76	-0.10	-0.30	-0.76
Light transmission	SD_{Tr}	0.74	-0.08	0.06	0.30	-0.08	-0.61
Spectral exponent β							
Temperature	β_T	0.17	-0.67	0.13	-0.07	0.41	0.18
Salinity	β_S	0.23	-0.59	0.24	-0.18	0.46	0.24
Fluorescence	β_F	0.41	-0.48	-0.73	-0.19	-0.36	0.75
Light transmission	β_{Tr}	0.85	-0.19	0.12	-0.26	-0.19	0.62
Scaling exponent H							
Temperature	H_T	0.06	-0.61	0.11	-0.09	0.36	0.41
Salinity	H_S	0.09	-0.75	0.19	-0.18	0.42	0.32
Fluorescence	H_F	0.62	-0.54	-0.76	-0.35	-0.09	0.83
Light transmission	H_{Tr}	0.81	-0.21	-0.18	-0.28	0.10	0.71
Codimension C_1							
Temperature	C_{1T}	0.23	-0.51	0.06	-0.16	0.36	0.26
Salinity	C_{1S}	0.24	-0.43	0.23	-0.04	0.44	0.40
Fluorescence	C_{1F}	0.41	-0.41	-0.70	-0.08	-0.12	0.78
Light transmission	C_{1Tr}	0.81	0.08	0.04	0.24	-0.13	0.64
Lévy index α							
Temperature	α_T	-0.17	-0.29	-0.27	0.08	-0.34	-0.41
Salinity	α_S	-0.22	-0.22	-0.27	0.22	-0.22	-0.32
Fluorescence	α_F	0.53	-0.43	-0.64	0.34	0.27	-0.64
Light transmission	α_{Tr}	0.62	-0.08	-0.05	0.42	0.36	-0.57
Phaeocystis	***Phaeo***	-0.10	0.10	0.10	0.12	0.30	0.10
Wind speed	***Wsp.***	-0.12	-0.10	-0.10	0.11	-0.39	-0.10
Wind direction	***Wdir.***	-0.05	-0.12	-0.12	0.36	-0.36	-0.12

Table VIII. Names and codes of the 25 additional variables used in the PCA, together with their correlation with the three first components of the PCA. The codes are used on the graphs.
PC-1, first principal component; PC-2, second principal component; PC-3, third principal component.

Temperature and salinity scaling exponents H are not significantly different (Wilcoxon-Mann-Whitney U-test, $P > 0.05$) for the whole dataset, and cannot be distinguished from the theoretical value $H = 0.5$ expected in the Lagrangian frame (Binomial test, $P > 0.05$). On the contrary, *in vivo* fluorescence and light transmission scaling exponents H remain indistinguishable (Wilcoxon-Mann-Whitney U-test, $P > 0.05$), but are significantly smaller that the $H = 0.5$ value (Binomial test, $P < 0.05$). Moreover, analyses of covariance indicated that the H values were indistinguishable for temperature and salinity ($P > 0.05$), while there are significant differences between the H values for both light transmission and *in vivo* fluorescence ($P < 0.05$). Finally, both fractal codimension C_1 and Lévy index α for temperature and salinity time series in the one hand, and for *in vivo* fluorescence and light transmission on the other hand are indistinguishable ($P > 0.05$) for the whole dataset. Light transmission and fluorescence fractal codimension and Lévy index are nevertheless respectively greater and smaller than those of temperature and salinity ($P < 0.05$).

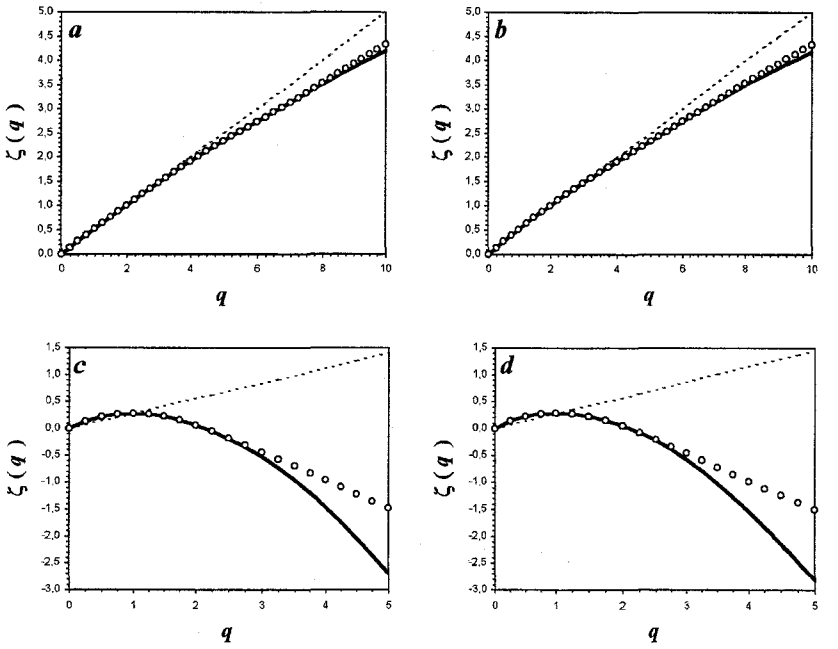

Fig. 9. The Lagrangian structure function scaling exponent $\zeta(q)$ empirical curves (dots), compared to the monofractal curves $\zeta(q) = q/2$ (dashed line), and to the universal multifractal curves (continuous curve) obtained with C_1 and α in equation (4) for temperature (**a**) and salinity (**b**) for time series 22. The Lagrangian exponent $\zeta(q)$ empirical curves (dots), compared to the monofractal curves $\zeta(q) = qH$ (dashed line), and to the universal multifractal curves (continuous curve) obtained with C_1 and α in equation (3) for *in vivo* fluorescence (**c**) and light transmission (**d**) for time series 22.

Spatio-temporal analysis. The results of the PCA showed that three components explain 75.50 % of the total variance. The first component (PC-1), which explains 32.51% of the variance is positively correlated to superficial sediment nature, and negatively correlated to latitude and depth (Figure 10a, b; Table VI). The meaning of this component is then slightly different from the one displayed in the Eulerian case where the first principal component was representative of superficial bottom sediment quality and water column depth. In the present Lagrangian frame, it is also representative of a geographical effects associated to latitude (i.e. northern locations). The second component (PC-2), which explains 22.72% of the total variance, is respectively positively and negatively correlated to tidal current direction and longitude (Figure 10a; Table VI). This component can then be related to the tidal effects associated with advective processes—while in the Eulerian frame it was also representative of hydrodynamical forcing (i.e. current speed)—and to the geographical effects associated with sampling conducted in coastal waters. The third component, which explains 20.27% of the total variance, is positively and negatively correlated to temperature and chlorophyll *a* concentration, respectively (Figure 10b; Table VI). As previously shown in the Eulerian case, this axe is then mainly representative of physical and biological seasonal forcings.

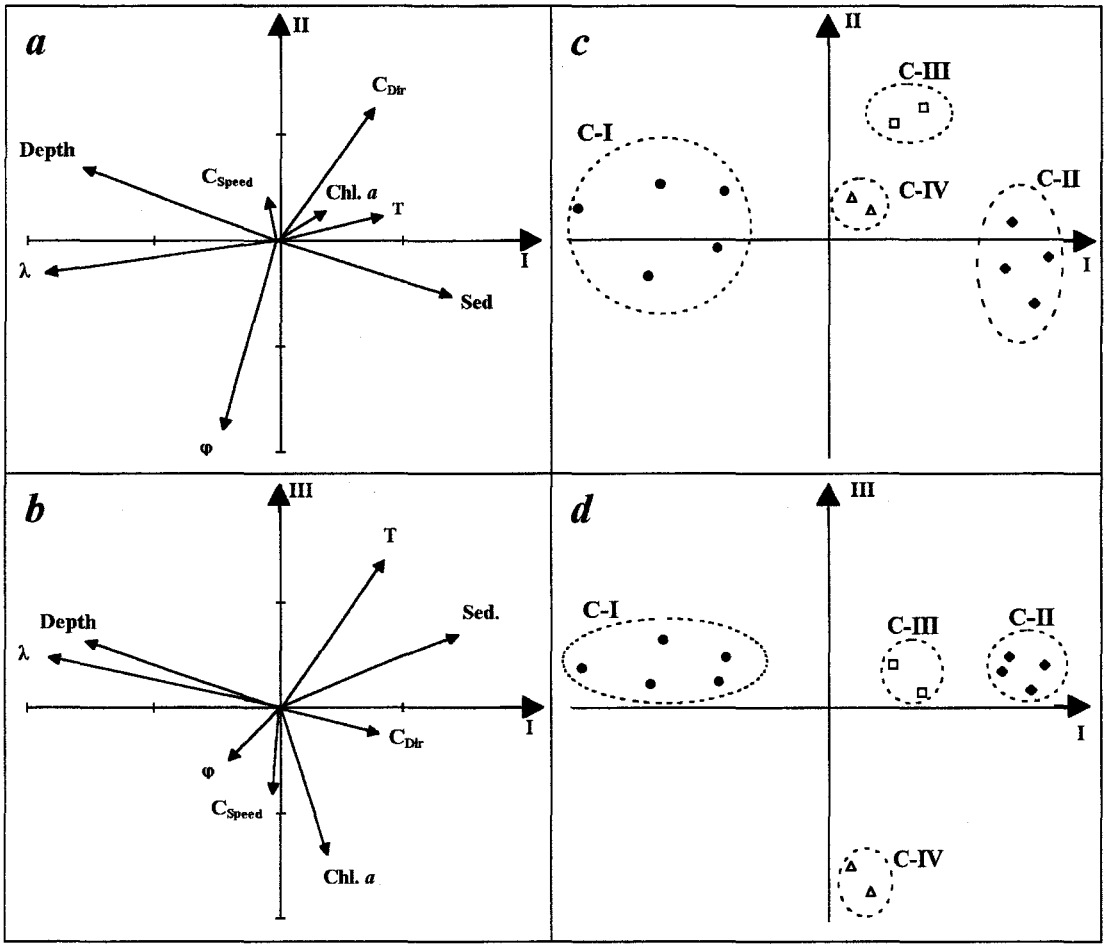

Fig. 10. Correlation plots showing the position of the initial variables (**a**, **b**), and the projection of the observations in the bidimensional spaces defined by the three first principal components (**c**, **d**) in the Lagrangian frame.

The projections of the observations in the two-dimensional planes defined by the three first components exhibit a clearer space-time patterns than in the Eulerian case (Figure 10c, d). Indeed, the observations are mainly distributed following the first principal component. This is confirmed and specified by the unweighted centroid clustering which showed four clusters of observations (numbered from C-I to C-IV): C-I characterizes deeper and northern sampling experiments, C-II fine superficial sediment, C-III ebb tide sampling and C-IV high chlorophyll *a* concentration (Table VII).

While the space-time pattern exhibited by the variables of the PCA is similar to those displayed in the Eulerian case, the additional variables leads to further comments in the Lagrangian frame (Figure 11; Table VIII). Thus, mean values of salinity and light transmission are both negatively correlated with PC-1 (Figure 11a, b), indicating an increased salinity and

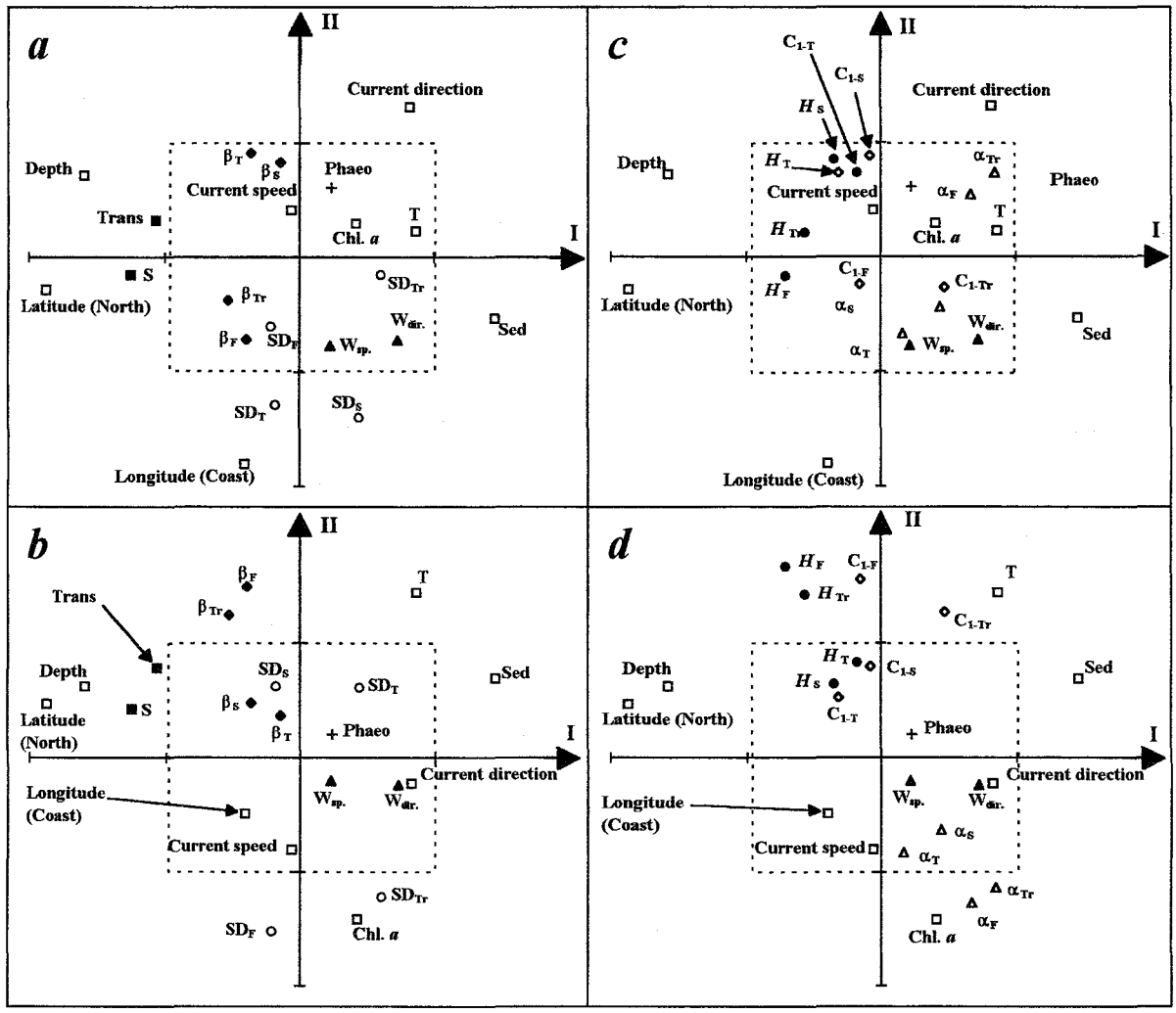

Fig. 11. Position of the additional variables (for codes, see Table 8) in the bidimensional spaces of the three first principal components in the Lagrangian frame. The coordinates are the correlation coefficients with these axes. The eight initial variables are placed with the corresponding elements of the eigen vectors (standardized after multiplication by the square root of the corresponding eigen values). Factors significantly correlated with the principal components are located outside the central square, corresponding to the 95% confidence interval.

light transmission in northern and deeper locations. On the contrary, the mean concentration of *Phaeocystis* exhibit no significant correlation to any principal component. Temperature and salinity spectral sums are both negatively correlated to PC-2 (i.e. increased variability in coastal waters; Figure 11a, b), while those of light transmission and fluorescence are both negatively correlated to PC-3 (i.e. high chlorophyll concentration).

Finally, the space-time patterns exhibited by the monofractal parameter β, and the multifractal parameters H, C_1 and α can be described in very simple terms when compared with the Eulerian case. Thus, one may note that none of these parameters exhibit any significant correlation in the two-dimensional planes defined by the three first principal components in the case of temperature and salinity (Figure 11). On the contrary, light transmission and phytoplankton biomass space-time structure exhibits a slightly more complex behaviour (Figure 10) which is nevertheless wholly related to PC-3. Then, contrary to what has been observed in the Eulerian case (Figure 8), parameters β and H exhibit a very similar space-time pattern for both light transmission and phytoplankton biomass. They are indeed both positively correlated with PC-3 (Figure 11b, d). Furthermore, C_1 and α are positively and negatively correlated with PC-3 (Figure 11d), respectively. Phytoplankton and light transmission then exhibit greater temporal dependence (i.e. high β values), lower stationarity (i.e. high H values), more sparse (i.e. high C_1 values) and complex (i.e. high α values) distributions when chlorophyll concentration is high. This suggests that the space-time structural homogeneity of the Lagrangian turbulent processes, while light transmission and phytoplankton biomass structures rather seem to be wholly density-dependent.

Discussion

Eulerian and Lagrangian multiscale structures in the coastal ocean

The values of both spectral exponents β and universal multifractal parameters H, C_1 et α obtained in the Eulerian frame (Table V) are in the range of values previously estimated from temperature, salinity and *in vivo* fluorescence time series in the Eastern English Channel (Seuront *et al.*, 1996a, b, 1999; Seuront, 1997). Furthermore, the weak dispersion of both spectral and multifractal parameters values (cf. Table V) suggests that the same process, or at least similar processes, can be regarded as being responsible for the observed variability. On the other hand, the spectral and multifractal parameters estimated for the very first time to our knowledge for light transmission time series clearly indicate that particles distributions were most of the time characterized by smaller values of the parameters β, H and α, and higher values of the parameter C_1 than temperature, salinity and *in vivo* fluorescence distributions. More precisely, this shows that light transmission is less scale-dependent (lower β values), more conservative (lower H values), more sparse (higher C_1 values) and less complex (lower α values) than simultaneously recorded temperature, salinity and fluorescence. Light

transmission could then be mainly linked to very specific phenomenons related to the qualitative nature of particles, but also to their quantitative properties such as their size, sedimentation speed, density or stickiness. All these properties are now recognized to play a major role in aggregation processes of marine particles (e.g. Li *et al.*, 1998; Milligan and Hill, 1998), and can then be regarded as a potential source of small-scale variability leading to flatter power spectra for light transmission distributions (Table V; Figure 3). More generally, the fact that 22 time series recorded in different water masses, in different hydrodynamical conditions and during a sampling experiment conducted over a period of 3 years can be characterized in terms of multifractals then could indicate that such structure could be the rule in turbulent coastal ecosystems such as the Eastern English Channel.

Such a general conclusion can also be drawn in a Lagrangian frame following the multifractal structure shown for the 13 analyzed time series of temperature, salinity, *in vivo* fluorescence and light transmission. However, one may note that contrary to the Eulerian frame, fluorescence and light transmission—which have been characterized in a Lagrangian frame for the very first time in this study—both exhibit very similar structure, in terms of spectral and multifractal parameters (Table V). In particular, the distribution of phytoplankton biomass and particles are always less scale-dependent (lower β values), more conservative (lower H values), more sparse (higher C_1 values) and less complex (lower α values) than temperature and salinity. Such structures could be related, as previously shown by Seuront *et al.* (1996a, 1999) for phytoplankton biomass, to any aggregative behaviours of both phytoplankton cells and suspended particles leading to very specific "active" distribution as revealed by the flattening of the power spectral exponents β when compared to those of temperature and salinity (Table V). In that way, one may note here that the general multifractal formalism $\zeta(q)$ used in the Lagrangian frame for *in vivo* fluorescence and light transmission [equation (3)] can be compared to the structure function scaling exponent theoretical expression $\zeta_F(q)$ derived by Seuront *et al.* (1996b) from the previous theoretical results of Denman and Platt (1976) to describe the scales of phytoplankton biological activity:

$$\zeta_F(q) = -K(q/2) = -\frac{C_1}{\alpha - 1}\left(\left(\frac{q}{2}\right)^{\alpha} - \frac{q}{2}\right) \tag{5}$$

In that way, we show that equation (5) does not provide good estimates of the empirical function $\zeta(q)$ (Figure 12a) except for the time series characterized by spectral exponents β which cannot be distinguished from the theoretical value $\beta = 1$ (Binomial test, $P > 0.05$) proposed by Denman and Platt (1976) to characterize the scaling behaviour of phytoplankton

for scales where the biological activity has time to develop and is not destroyed by turbulent motions (Figure 12b). These results then provide the first empirical validation of the theoretical expression $\zeta_F(q)$ [cf. equation (5)] proposed by Seuront *et al.* (1996b) as a multifractal generalization of the early work of Denman and Platt (1976) in a Lagrangian framework.

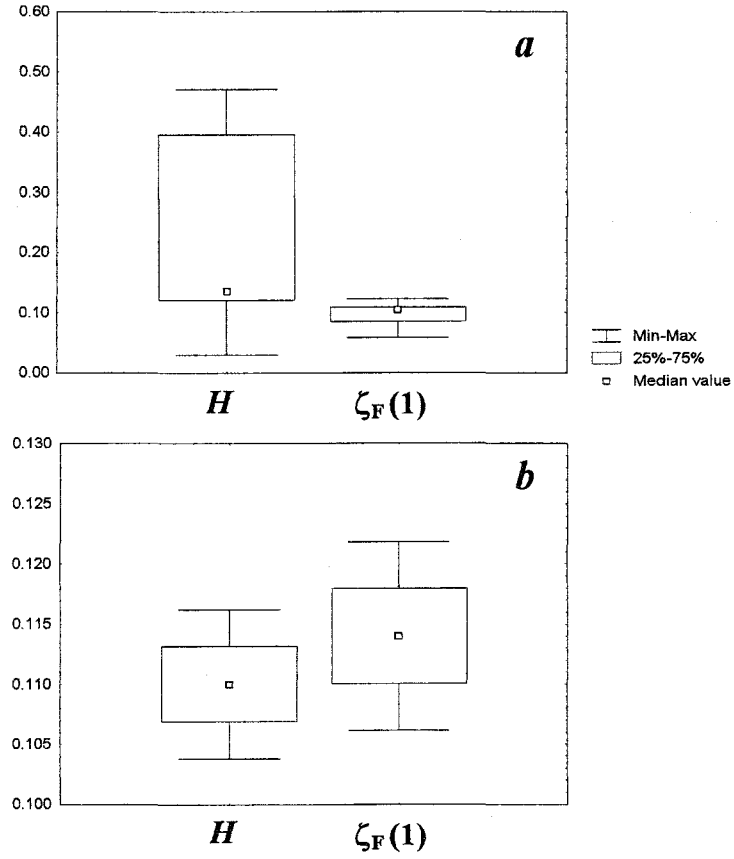

Fig. 12. Comparisons between the empirical structure function scaling exponents $\zeta(1) = H$ and the theoretical exponents $\zeta_F(1)$ obtained with C_1 and α in equation (5) for the 13 time series used in the Lagrangian frame (**a**), and for the time series which presents a spectral exponent statistically indistinguishable from the theoretical value $\beta = 1$ proposed by Denman and Platt (1976) (**b**). The central square represents the median of the distribution, the upper and lower limits of the box the first and third quartiles, and the upper and lower bars the maximum and minimum of the distribution.

Space-time patterns of Eulerian and Lagrangian multiscale structures

In the Eulerian frame, mean values of salinity and light transmission appear to be higher respectively in northern and in deeper locations. This suggests first a progressive integration of the fluvial supplies distributed from the Bay of Seine to Cape Griz-Nez in the marine waters of the Eastern English Channel, and second that particles concentrations depend on the water column depth, whatever the tidal current directions. In particular, this could be linked with

both resuspension processes and hydrodynamical conditions which can be regarded as main factors in regulating the particles abundance in the water column, but also to a pure dilution process if we consider that the processes responsible for the quantity of suspended particles in the water column can be regarded as being equivalent in both inshore and offshore waters. On the other hand, the space-time pattern of the variability (i.e. the spectral sum) of the studied parameters exhibit two distinct patterns. First, the variability of temperature and salinity are always higher in coastal waters, while *in vivo* fluorescence variability is higher in coastal locations and during periods of high phytoplankton concentrations. These results then confirms and generalizes in space and time first the basic space-time pattern shown by Seuront and Lagadeuc (1998) for the vertical structure of temperature and salinity expressed in terms of fractal dimension, and second the density-dependence hypothesis of phytoplankton biomass variability. On the contrary, light transmission variability being all the more high since the bottom sediment is finer, this suggests a qualitative control of particles distribution variability by the nature of the superficial bottom sediment. Finally, we demonstrated that the spectral and multifractal structures of purely passive scalars (i.e. temperature and salinity) are both associated with South-North and inshore-offshore gradients (Figure 8). This indicates that the structure of these parameters could not be regarded as being purely driven by three-dimensional turbulence but also by larger scale mixing processes occurring between different waters masses corresponding to a progressive integration of fluvial supplies in marine waters along a South-North gradient and to a progressive integration of offshore waters in the coastal flow along a inshore-offshore gradient. On the other hand, phytoplankton biomass structure appears to be dependent on both inshore-offshore gradient and phytoplankton concentrations (Figure 8). This leads to view phytoplankton biomass structure as being mainly density-dependent. In particular, the spectral exponents β being linked to fractal dimension D as $D = 2 - (\beta - 1)/2$ (Schroeder, 1991), the higher spectral exponent values as the higher multifractal parameters H, C_1 et α observed for inshore waters and during periods of high phytoplankton concentrations confirms the hypothesis of a density-dependent control of phytoplankton biomass structure in both fractal (Seuront and Lagadeuc, 1998) and multifractal frames (Seuront *et al.*, 1999). The space-time pattern of light transmission spectral and multifractal structure appears to be very specific. Thus, the spectral exponent β and the multifractal parameters H, C_1 et α are wholly dependent on the nature of the superficial sediment (Figure 8). Particles distributions in the water column, expressed in terms of

multifractal structure, are then dependent on the qualitative nature of the bottom superficial sediment resulting of the differential properties of qualitatively different suspended sediments.

In the Lagrangian frame, while the space-time patterns exhibited by salinity and light transmission means values and temperature and salinity variability confirm the results shown in the Eulerian frame (Figure 8), the space-time patterns of both spectral and multifractal structures leads to further comments. Thus, temperature and salinity structures do not exhibit any significant space-time pattern at the space-time scales relevant to our analyses (Figure 11). In that way, the perception of its surrounding physical environments is constant in space and time for pelagic organisms. On the contrary, both *in vivo* fluorescence and light transmission structures only exhibit a temporal pattern related to phytoplankton concentrations. Then, in a Lagrangian frame, phytoplankton and particles distributions are clearly density-dependent (Figure 11). However, this density-dependence is expressed differently following the parameters considered. Thus, the spectral exponent β and the multifractal parameters H et C_1 are all the more high since the phytoplankton concentrations are low, whereas the multifractal parameter α is all the more high since the phytoplankton concentrations are high. In particular, considering the importance of food particles distributions for foraging (e.g. Davis *et al.*, 1991; Rothschild, 1992), these results have considerable implications for future studies devoted to estimate key fluxes such as carbon or nitrogen fluxes between primary and secondary producers, which should take advantage to focus on the ecological consequences of the Lagrangian structure of resources in the ocean.

Finally, the different space-time patterns shown in the Eulerian and Lagrangian frames, especially the shift between a control by superficial sediment nature and a control by phytoplankton density for light transmission, should nevertheless be interpreted with caution following the differences in terms of input data points in the Eulerian and Lagrangian spatio-temporal analysis (STA), i.e. 22 time series in the Eulerian frame and only 13 in the Lagrangian frame. Thus, the absence of temporal heterogeneity in the biological structure at the scales of both high/low and spring/neap tidal cycles in the Lagrangian frame—demonstrated elsewhere (Seuront and Lagadeuc, 1998) in the same area—could then also be associated with the weaker number of time series used in the spatio-temporal analysis and not only to pure phenomenological differences between Eulerian and Lagrangian frames.

Whatever that may be, the ramification of these results to uncovering space-time dynamics in the ocean are severe. They imply that the usual Eulerian sampling of the ocean may be a very poor method to collect data for analyzing the structure of the pelagic environment, both in

terms of physical and biological processes. A more general conclusion may also be drawn for experiments in for related oceanographic fields. When it is not possible to compensate for the movement of a spatio-temporal system in relation to the measurement point—as it is usually the case—it may be better to take fixed spatial averages rather than moving individual point samples. For oceanographic data, this amounts to obtaining spatial averaging of large sections of populations, for example using remote sensing images of plankton populations. Alternatively, Lagrangian measurements should be obtained, where the sample is always taken from approximately the same point in the population at each time step.

Acknowledgements

We thank the captain and the crew of the N/O 'Sepia II' and N/O 'Côte de la Manche' for their assistance during the whole sampling experiment. We also thank those who contributed to the work at sea and the extraction of chlorophyll *a*: Stéphanie Courty, Natacha Esquerre, Ludovic Férrière, Vincent Pécheux and Didier Saïu. Valérie Gentilhomme offered very helpful suggestions, we also enjoy very constructive discussions with Shaun Lovejoy and Daniel Schertzer and we are grateful to them for their assistance.

References

Augris,C., Clabaut,P., Tessier,B. and Carré,D. (1995) *The coastal area of Nord-Pas de Calais (France) superficial geology map*. Ifremer, Plouzané.

Baker,M.A. and Gibson,C.H. (1987) Sampling turbulence in the stratified ocean: statistical consequences of strong intermittency. *J. Phys. Oceanogr.*, **17**, 1817-1836.

Bendat,J.S. and Piersol,A.G. (1986) *Random Data: Analysis and Measurement Procedures*. Wiley.

Bohle-Carbonel,M. (1992) Pitfalls in sampling, comments on reliability and suggestions for simulation. *Cont. Shelf Res.*, **12**, 3-24.

Brylinski,J.M. and Lagadeuc,Y. (1990) L'interface eau côtière/eau du large dans le Pas-de-Calais (côte française): une zone frontale. *C. R. Acad. Sci. Paris Sér. II*, **311**, 535-540.

Brylisnki,J.M., Dupont,J. and Bentley,D. (1984) Conditions hydrologiqes au large du cap Griz-Nez (France): premiers résultats. *Oceanol. Acta*, **7**, 315-322.

Brylinski *et al.* (1991) Le 'fleuve côtier': un phénomène hydrologique important en Manche orientale. Exemple du Pas-de-Calais. *Oceanol. Acta*, **11**, 197-203.

Corrsin,S. (1951) On the spectrum of isotropic temperature in an isotropic turbulence. *J. Appl. Phys.*, **22**, 469.

Daly,K.L. and Smith,W.O. (1993) Physical-Biological interactions influencing marine plankton production. *Annu. Rev. Ecol. Syst.*, **24**, 555-585.

Denman,K.L. and Platt,T. (1976) The variance spectrum of phytoplankton in a turbulent ocean. *J. Mar. Res.*, **34**, 593-601.

Dupont,J.P., Lafite,R., Huault,M.F., Lamboy,M., Brylisnki,J.M. and Guéguéniat,P. (1991) La dynamique des masses d'eau et matière en suspension en Manche orientale. *Oceanol. Acta*, **11**, 177-186.

Falconer,K. (1993) *Fractal Geometry. Mathematical Foundations and Applications*. Wiley.

Feder,J. (1988) *Fractals*. Plenum.

Fuller,W.A. (1976) *An Introduction to Probability Theory and its Application*. Wiley.

Hardy,A.C. (1926) A new method of plankton research. *Nature*, **18**, 630-632.

Hardy,A.C. (1939) Ecological investigation with Continuous Plankton Recorder: object, plan and methods. *Hull. Bull. Mar. Ecol.*, **1**, 1-57.

Hardy,A.C. and Gunther,E.R. (1935) The plankton of the South Georgia whaling grounds and adjacent waters, 1926-1927. *Discovery Rep.*, **11**, 1-456.

Haury,L.R., McGowan,J.A. and Wiebe,P.H. (1978) Patterns and processes in the time-space scales of plankton distributions. In Steele,J.H. (ed.), Spatial pattern in plankton communities. Plenum, New York, pp. 277-327.

Ibanez,F. (1973) Méthode d'analyse spatio-temporelle du processus d'échantillonnage en planctonologie, son influence dans l'interprétation des données par l'analyse en composantes principales. *Ann. Inst. Océanogr.*, **49**, 83-111.

Kendall,M. and Stuart,A. (1966) *The Advanced Theory of Statistics*. Hafner.

Lagadeuc,Y., Brylinski,J.M. and Aelbrecht,D. (1997a) Temporal variability of the vertical stratification of a front in a tidal Region of Freshwater Influence (ROFI) system. *J. Mar. Syst.*, **12**, 147-155.

Lagadeuc,Y., Boulé,M. and Dodson,J.J. (1997b) Effect of vertical mixing on the vertical distribution of copepods in coastal waters. *J. Plankton Res.*, **19**, 1183-1204.

Lavallée,D., Lovejoy,S., Schertzer,D. and Schmitt,F. (1992) On the determination of universal multifractal parameters in turbulence. In Moffat,K., Tabor,M. and Zaslavsky,G. (eds), *Topological aspects of the dynamics of fluid and plasmas*. Kluwer, Boston, pp. 463-478.

Legendre,L. and Demers,S. (1984) Towards dynamic biological oceanography and limnology. *Can. J. Fish Aquat. Sci.*, **41**, 2-19.

Legendre,L. and Legendre,P. (1984) *Ecologie numérique*, Vol. 2. Masson, Paris.

Lennox,A.J. (1979) Studies of the ecology and physiology of *Phaeocystis*.PhD Thesis, University of Wales.

Li,X., Passow,U. and Logan,B.E. (1998) Fractal dimensions of small (15-200 μm) particles in Eastern Pacific coastal waters. *Deep-Sea Res. I*, **45**, 115-131.

MacKenzie,B.R. and Leggett,W.C. (1991) Quantifying the contribution of small-scale turbulence to the encounter rates between larval fish and their zooplankton prey : effects of wind and tide. *Mar. Ecol. Prog Ser.*, **73**, 149-160.

Mackas,D.L., Denman,K.L., Abbott,M.R. (1985) Plankton patchiness: biology in the physical vernacular. *Bull. Mar. Sci.*, **37**, 652-674.

Milligan,T.G. and Hill,P.S. (1998) A laboratory assessment of the relative importance of turbulence, particle composition, and concentration in limiting maximal floc size and settling behaviour. *J. Sea Res.*, **39**, 227-241.

Obukhov,A.M. (1949) Structure of the temperature field in a turbulent flow. *Izv. Akad. Nauk. SSSR Geogr. I Geofiz.*, **13**, 55.

Pascual,M., Ascioti,F.A. and Caswell,H. (1995) Intermittency in the plankton: a multifractal analysis of zooplankton biomass variability. *J. Plankton Res.*, **17**, 1209-1232.

Peta,O., Hitier,B., Olivesi,R., Delesmont,R., Morel,M. & Loquet,N. (1998) *Suivi régional des nutriments sur le littoral nord/Pas-de-Calais/Picardie. Bilan de l'année 1997.* IFREMER, Boulogne-sur-Mer.

Platt,T., Harrison,W.G., Lewis,M.R., Li,W.K.W., Sathyendranath,S., Smith,R.E. and Vezina,A.F. (1989) Biological production of the oceans: the case for a consensus. *Mar. Ecol. Prog. Ser.*, **52**, 77-88.

Quisthoudt,C. (1987) Production primaire phytoplanctonique dans le détroit du Pas-de-Calais (France): variations spatiales et annuelles au large du cap Griz-Nez. *C. R. Acad. Sci. Paris Sér. II*, **304**, 245-250.

Raby,D., Lagadeuc,Y., Dobson,J.J., Mingelbier,M. (1994) Relationship between feeding and vertical distribution of bivalve larvae in stratified and mixed waters. *Mar. Ecol. Prog. Ser.*, **103**, 275-284.

Scherrer,B. (1984) *Biostatistiques.* Morin, Boucherville.

Schertzer,D. and Lovejoy,S. (1983) The dimension and intermittency of atmospheric dynamics. In Launder,B. (ed.), *Turbulent Shear Flows 4*, Springer-Verlag, Karlsruhe, pp. 7-33.

Schertzer,D. and Lovejoy,S. (1985) Generalised scale invariance in turbulent phenomena. *Physico-Chem. Hydrodyn. J.*, **6**, 623-635.

Schertzer,D. and Lovejoy,S. (1987) Physically based rain and cloud modeling by anisotropic multiplicative turbulent cascades. *J. Geophys. Res.*, **92**, 9693-9714.

Schertzer,D. and Lovejoy,S. (1989) Nonlinear variability in geophysics: multifractal analysis and simulation. In Pietronero,L. (ed.), *Fractals: physical origin and consequences.* Plenum, New York, pp. 49-79.

Schertzer,D. and Lovejoy,S. (1992) Hard and soft multifractal processes. *Physica A*, **185**, 187-194.

Schmitt,F., Lavallée,D., Shertzer,D. and Lovejoy,S. (1992) Empirical determination of universal multifractal exponents in turbulent velocity fields. *Phys. Rev. Lett.*, **68**, 305-308.

Schmitt,F., Schertzer,D., Lovejoy,S. and Brunet,Y. (1993) Estimation of universal multifractal indices for atmospheric turbulent velocity fields. *Fractals*, **1**, 568-575.

Schmitt,F., Schertzer,D., Lovejoy,S. and Brunet,Y. (1994) Empirical study of multifractal phase transitions in atmospheric turbulence. *Nonlin. Proc. Geophys.*, **1**, 95-104.

Schmitt,F., Lovejoy,S. and Schertzer,D. (1995) Multifractal analysis of the Greenland ice-core project climate data. . *Geophys. Res. Lett.*, **22**, 1689-1392.

Schmitt,F., Schertzer,D., Lovejoy,S. and Brunet,Y. (1996a) Multifractal temperature and flux of temperature in fully developped turbulence. *Europhys. Lett.*, **34**, 195-200.

Schmitt,F., Schertzer,D., Lovejoy,S. and Brunet,Y. (1996b) Multifractal properties of temperature fluctuations in turbulence. In Giona,M. and Biardi,G. (eds), *Fractals and Chaos in Chemical Engineering.* World Scientific, Singapore, pp. 464-475.

Schmitt,F., Schertzer,D. and Lovejoy,S. (1998) Multifractal modeling of turbulent fluctuations in finance. In Marsella,F. and Salvadori,G. (eds), *Chaos, Fractals and Models.* Italian University Press di Giovanni Iuculano, Pavia, pp. 150-157.

Schroeder,M. (1991) *Fractals, Chaos power laws.* Freeman San Francisco.

Seuront,L. (1997) Distribution inhomogène multiéchelle de la biomasse phytoplanctonique en milieu turbulent. *J. Rech. Océanogr.*, **22**, 9-16.

Seuront,L. (1999) Fractals et multifractals: nouveaux outils de caractérisation de l'hétérogénéité spatio-temporelle en écologie marine. *Océanis*, in press.

Seuront,L. and Lagadeuc,Y. (1997) Characterisation of space-time variability in stratified and mixed coastal waters (Baie des Chaleurs, Québec, Canada): application of fractal theory. *Mar. Ecol. Prog. Ser.*, **259**, 81-95.

Seuront,L. and Lagadeuc,Y. (1998) Spatio-temporal structure of tidally mixed coastal waters: variability and heterogeneity. *J. Plankton Res.*, **20**, 1387-1401.

Seuront,L., Schmitt,F., Lagadeuc,Y., Schertzer,D., Lovejoy,S. and Frontier,S. (1996a) Multifractal analysis of phytoplankton biomass and temperature in the ocean. *Geophys. Res. Lett.*, **23**, 3591-3594.

Seuront,L., Schmitt,F., Lagadeuc,Y., Schertzer,D. and Lovejoy,S. (1996b) Multifractal intermittency of Eulerian and Lagrangian turbulence of ocean temperature and plankton fields. *Nonlin. Proc. Geophys.*, **3**, 236-246.

Seuront,L., Schmitt,F., Lagadeuc,Y., Schertzer,D. and Lovejoy,S. (1999) Universal multifractal analysis as a tool to characterise multiscale intermittent patterns. Example of phytoplankton distribution in turbulent coastal waters. *J. Plankton Res.*, in press.

Siegel,S. and Castellan,S.J. (1988) *Nonparametric Statistics for the Behavioural Sciences*. McGraw-Hill, New York.

Sokal,R.R. and Michener,C.D. (1958) A statistical method for evaluating systematic relationships. *Univ. Kansas Sci. Bull.*, **38**, 1409-1438.

Strickland,J.D.H. and Parson,T.R. (1972) A practical handbook of seawater analysis. *Bull. Fish. Res. Bd. Can.*, **167**, 1-311.

Taylor,G.I. (1938) The spectrum of turbulence. *Proc. R. Soc. London Ser. A*, **164**, 476-490.

Truffier,S., Hitier,B., Olivesi,R., Delesmont,R., Morel,M. & Loquet,N. (1997) *Suivi régional des nutriments sur le littoral nord/Pas-de-Calais/Picardie. Bilan de l'année 1996.* IFREMER, Boulogne-sur-Mer.

Tyler,P.J. (1977) Microbiol and chemical studies of *Phaeocystis*. PhD Thesis, University of Wales.

Yamazaki,H. (1993) Lagrangian study of planktonic organisms : perspectives. *Bull. Mar. Sci.*, **53**, 265-278.

Zar,J.H. (1984) *Biostatistical Analysis*. Prentice-Hall.

A17

Turbulence intermittency, small-scale phytoplankton patchiness and encounter rates in plankton: where do we go from here?

Seuront L, Schmitt F & Lagadeuc Y

Deep-Sea Research I (soumis)

Turbulence intermittency, small-scale phytoplankton patchiness and encounter rates in plankton: where do we go from here?

Laurent Seuront[1], François Schmitt[2] and Yvan Lagadeuc[1,3]

[1] Station Marine de Wimereux, CNRS UPRES-A 8013 ELICO, Université des Sciences et Technologies de Lille, BP 80, F-62930 Wimereux, France

[2] Department of fluid Mechanics, VUB, Pleinlaan 2, B-1050 Brussels, Belgium

[3] Present adress: Université de Caen, IUT, Bd du Maréchal Juin, F-14032 Caen cedex, France

Abstract. Turbulence is widely recognized to enhance contact rates between planktonic predators and their preys. However, previous estimates of contact rates are implicitly based on homogeneous distributions of both turbulent kinetic energy dissipation rates and phytoplanktonic preys, while turbulent processes as phytoplankton cells distributions have now been demonstrated to be highly intermittent even on smaller scales. Moreover, turbulent kinetic energy dissipation rates and phytoplankton intermittent (i.e. patchy) distributions can be wholly parametrized in the frame of universal multifractals. In that way, we propose to evaluate the effect of turbulence intermittency on predator-prey encounter rates in an intermittent frame, and to investigate conceptually the potential effects on encounter rates of zooplankton behavioral responses to the related small-scale phytoplankton patchiness. Our results then indicate that the effects of turbulence on predator-prey encounter rates is about 30-35% less important when considering intermittently fluctuating turbulent dissipation rates instead of a mean dissipation value, and that taking into account zooplankton behavioral adaptations to phytoplankton patchiness can increased encounter rates of a factor that can go up to a value of 60.

INTRODUCTION

The influence of small-scale turbulence on predator-prey interactions in plankton has received a great deal of attention in recent years. Much of this attention stems from the seminal work of Rothschild and Osborn (1988), who proposed an enhanced rate of predator-prey contact due to small-scale turbulent shear. Subsequently, much has been written about the positive influences of turbulence on predator-prey encounter and the potential negative influences of turbulence on organism behavior (MacKenzie et al. 1994, Dower et al. 1997). In any cases, small-scale turbulent processes being basically regarded as a great factor of homogenization, modeling approaches of predator-prey contact rates under turbulent conditions, and subsequent studies of plankton trophodynamics, implicitly assumed that both zooplanktonic or phytoplanktonic preys are randomly distributed in space and time (e.g. Sundby and Fossum 1990, MacKenzie and Leggett 1991, Kiørboe and Saiz 1995, Caparroy and Carlotti 1996).

However, an intriguing aspect of small-scale turbulence is that it may promote small-scale patchiness rather than uniformity (Jimenez 1997, Jou 1997). Instantaneous gradients of scalar such as temperature, salinity or nutrients are indeed greatest at scales similar to the Kolmogorov microscale, i.e. the viscous scale where viscosity effects cannot be neglected and start to smooth out turbulent fluctuations (Gargett 1997, Sanford 1997). Thus we occasionally should expect stronger bursts, more often than in the Gaussian case, leading to skewed distributions reflecting heterogeneous distributions with a few dense patches and a wide range of low density patches (Seuront et al. 1999). Recent empirical studies conducted in highly turbulent environments have thus shown that both physical and biological parameters such as temperature, salinity, and phytoplankton biomass were nor homogeneously nor randomly distributed but rather exhibit very specific heterogeneous distributions, even on smaller scales (Seuront et al. 1996a, b, 1999).

Such heterogeneous distribution could be a salient issue for the general understanding of pelagic ecosystem functioning. Davis et al. (1991) thus showed that the feeding and growth rates of larval fish increased when the larvae were capable of finding and remaining in food patches, perhaps via some kind of area-restricted searching strategy (i.e. increased rate of turning once food has been encountered). Subsequently, Yamazaki (1993) propounded that "plankton organisms experience the local flow structure of turbulence, not the average of the flow field" because turbulence presents strong organization both in space and time. In such a context, if copepods are able to move from one dense patch to another, then they experience a local phytoplanktonic field more dense than the average. Changes in copepod behavior could thus be the response to the spatial distribution of the prey and not only to the fluctuation of turbulent water motions. Indeed, as proposed in the frame of optimal foraging theory (Pyke 1984), zooplankton living in highly heterogeneous environments could reveal strategies devoted to exploit high density patches and then to optimize the energy required to capture a given amount of food. This could be achieve, as suggested in a few laboratory studies undertaken in non-turbulent conditions, by increasing both the swimming speed and the complexity of swimming paths with increasing food densities, and/or by reducing motility in food patches (e.g. Tiselius 1992, Bundy et al. 1993, van Duren and Videler 1995). Consequently, in order to estimate an average encounter rates between predators and preys, one needs first to consider very carefully the distributions of both physical and biological parameters we are dealing with, and second the potential effect of these distributions on the average encounter rate, and thus, on zooplankton behavior.

Herein, in this study we derive in the multifractal frame simple equations from classical encounter theory that take into account both turbulence and behavior contributions to the encounter rates between predator and prey. Our conceptual approach is somewhat similar to that of Kiørboe and Saiz (1995), but our results are more general in that they provide for the very first time an objective way to examine direct and indirect effects of an intermittent turbulence on predator-prey encounter rates. We then first evaluate the effect of turbulence on predator-prey encounter rates in an intermittent frame and, finally we conceptually investigate the potential effects of zooplankton behavioral responses to the related small-scale phytoplankton patchiness.

TURBULENCE AND ENCOUNTER RATES IN PLANKTON: MODEL FORMULATION

Following the theory of Rothschild & Osborn (1988), the encounter rate E (encounters.s^{-1}) between planktonic predators and preys is expressed as (Evans 1989):

$$E = C\pi R^2 (u^2 + v^2 + 2w^2)^{1/2} \quad (1)$$

where C is the number of preys per unit volume (preys.m^{-3}), R is the perceptive distance of the predator (m), u (m.s^{-1}) and v (m.s^{-1}), are respectively the velocity of preys and predators, and w (m.s^{-1}) is the root-mean-square turbulent velocity contributing to enhance the relative motion between predator and prey. The rms turbulent velocity w is directly related to the intensity of turbulence, characterized by the turbulent kinetic energy dissipation rate ε (m^2.s^{-3}), and the following Rothschild & Osborn (1988):

$$w = 1.9(\varepsilon d)^{1/3} \quad (2)$$

where d is the separation distance between predator and prey when the encounter takes place, i.e. $d = R$ (Denman & Gargett 1995, Kiørboe & Saiz 1995, Kiørboe & MacKenzie 1995, MacKenzie & Kiørboe 1995). Because water motion differs below and above Kolmogorov length scale λ_k ($\lambda_k = (\nu^2/\varepsilon)^{0.25}$) where ν is the kinematic viscosity, ca 10^{-6} m^2.s^{-1}), the scale where viscous effect cannot be neglected and start to smooth out turbulent fluctuations, the equations relating turbulent velocity w and ε are different, and the encounter rates due to turbulence also differ. The rms velocity w should then be expressed as $w = 1.37(\varepsilon R)^{1/3}$ for $R > \lambda_k$ (Delichatsios and Probstein 1975), and $w = 0.42(\varepsilon/\nu)^{1/2}$ for $R < \lambda_k$ (Jackson and Lochman 1993), where $(\varepsilon/\nu)^{1/2}$ is the sub-Kolmogorov scale shear fluid rate (γ, s^{-1}). In an intermittent turbulence, this distinction is, however, not as sharp as may appear at first glance,

and the Kolmogorov length scale cease to be a reference frame (Frisch 1995). Moreover, Hill et al. (1992) have demonstrated that Eq. (2) is valid well below the Kolmogorov length scale. Thus in the following, we will consider that application of Eq. (2) is warranted at the spatial scales relevant to planktivorous predators such as copepods.

In order to evaluate for what types of predators turbulence is likely to be of importance, Kiørboe & Saiz (1995) rewrite Eq. (1) as:

$$E = E_{\text{behaviour}} + E_{\text{turbulence}} \tag{3}$$

where $E_{\text{behaviour}}$ and $E_{\text{turbulence}}$ are the encounter rates due to the behavior of the organisms and to turbulent water motions, respectively. Considering that both predators and preys swim along straight lines in random directions, the behavioral encounter rate $E_{\text{behaviour}}$ is defined as (Gerritsen and Strickler 1977):

$$E_{\text{behaviour}} = C\pi R^2 \left(\frac{u^2 + 3v^2}{3v} \right) \tag{4}$$

Assuming that $u = 0$ for phytoplankton cells, Eq. (4) can be simplified as:

$$E_{\text{behaviour}} = C\pi R^2 v \tag{5}$$

On the other hand, the encounter rate due to turbulence is expressed following Rothschild & Osborn (1988) as:

$$E_{\text{turbulence}} = C\pi d^2 w \tag{6}$$

Inserting the expression for the rms turbulent velocity w (Eq. 2) yields:

$$E_{\text{turbulence}} = 1.9 C\pi R^{7/3} \varepsilon^{1/3} \tag{7}$$

Different expressions of the previous equations that yield slightly different results have been widely applied to both copepods and fish larvae (e.g. Sundby & Fossum 1990, MacKenzie & Leggett 1991, Saiz 1994, Kiørboe & Saiz 1995, Kiørboe & MacKenzie 1995, Caparroy & Carlotti 1996). All these approaches implicitly assumed that both zooplanktonic or phytoplanktonic preys are randomly—with random we mean independent random variables expressing a lack of correlation between successive fluctuations—distributed in space and time, and we are not aware of any theoretical nor empirical attempt to deal simultaneously with the potential effects of microscale turbulence intermittency and the associated phytoplankton patchiness on encounter rates in plankton. This is ,however, now feasible following the recent advent of multifractal concepts in marine ecology (Pascual et al. 1995, Seuront et al. 1996a, b, 1999).

INTERMITTENCY AND MULTIFRACTAL FORMALISM

A new field of marine research has recently been devoted to the stochastic characterization of marine intermittent processes in the framework of multifractals (e.g. Pascual et al. 1995, Seuront et al. 1996a, b, 1999). In particular, Seuront et al. (1996a, b, 1999) empirically demonstrated on the basis of temperature, salinity and *in vivo* fluorescence high resolution time series recorded in the Eastern English Channel and the Southern Bight of the North Sea, both highly dissipative areas, that these parameters cannot be regarded as homogeneously distributed, but rather exhibit a very specific kind of skewed distribution—far from the Gaussian hypothesis—wholly characterized in the frame of multifractals.

Multifractals, which have been recently reviewed by Pascual et al. (1995) and Seuront et al. (1999) in the marine ecological framework, can be viewed as a generalization of fractal geometry (Mandelbrot 1983) initially introduced to describe the relationship between a given quantity and the scale at which it is measured. While fractal geometry describes the structure of a given descriptor with the help of only one parameter (i.e. the so-called fractal dimension), multifractals characterize its detailed variability by an infinite number of sets (roughly speaking, each of them corresponds to the fraction of space where data exceed a given threshold), each with its own fractal dimension. More precisely, multifractal approaches, which do not require any statistical preconception on the data, provide very good approximations—at all scales and all intensities—of the statistics of an intermittently fluctuating descriptor, and determine the probability distribution of the descriptor values (see Pascual et al. (1995) and Seuront et al. (1999) for further details). Moreover, the statistical consequence of intermittency being a strong departure from Gaussianity (Baker and Gibson, 1987), multifractals thus provide a powerful alternative to basic random walk and spectral methods implicitly based on Gaussian statistics (see e.g. Peitgen and Saupe 1988). Thus, considering that in the general background of spatio-temporal intermittency encountered in the ocean (e.g., Platt *et al.*, 1989), knowledge of the precise statistics of any intermittent fields may avoid the bias introduced by chronic undersampling of an intermittent signal (Bohle-Carbonel, 1992), a stochastic multifractal framework is particularly well suited to describing the structure of quantities that vary intermittently (Pascual et al. 1995, Seuront et al. 1996a, b, 1999).

Under fairly general conditions, the properties of the probability distribution of a random variable are equivalently specified by its statistical moments. In the multifractal frame, the probability distribution of a (multifractal) variable can thus be conveniently described

introducing the function $K(q)$ depending on the statistical moment q of the variable that describes how the statistical properties of each moment behave under isotropic dilatations and contractions; $K(q)$ is non-linear and concave with in particular, $K(0) = 0$ and $K(1) = 0$ (see Seuront et al. (1999) for further details on the properties of the function $K(q)$). That is, given a multifractal quantity Q at a scale ratio λ, the statistical properties of Q are given by (Schertzer and Lovejoy 1987):

$$\left\langle (Q_\lambda^q) \right\rangle = Q_0^q \lambda^{K(q)} \tag{8}$$

where '$\langle . \rangle$' indicates statistical or spatial averaging, and $Q_0 = \langle Q \rangle$ is the mean of the multifractal quantity Q. The scale ratio λ is the ratio between the larger outer scale L and the smallest resolution of the measurements l over which the data exhibit any scaling behavior, i.e. $\lambda = L / l$ (Fig. 1).

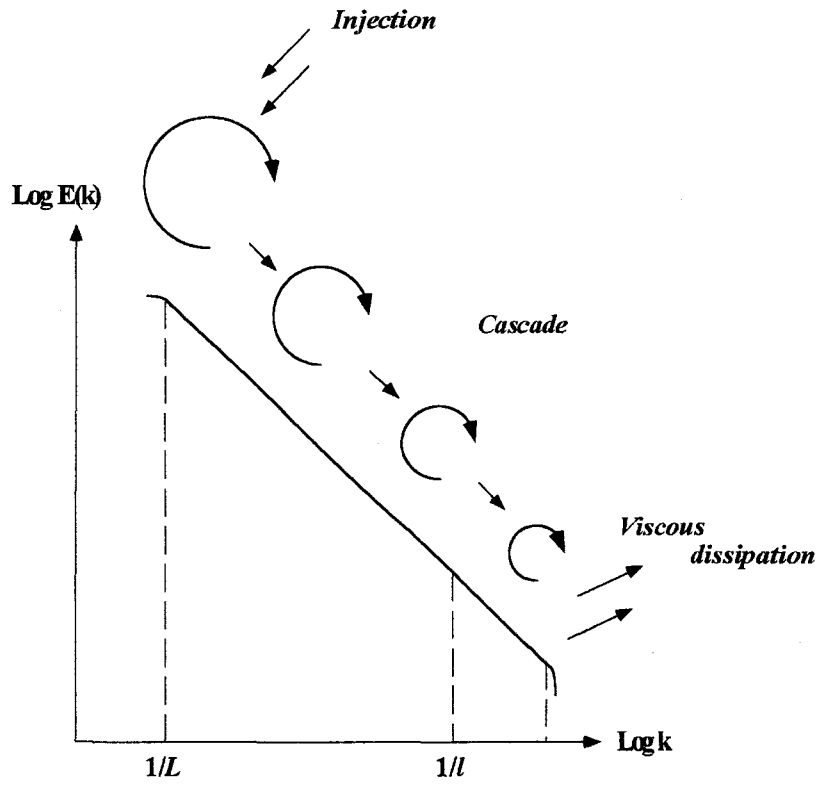

Fig. 1. Schematic representation showing the form of the frequency spectrum of turbulent velocity cascade, where $E(k)$ is the spectral density and k is a wavenumber (m^{-1}). The kinetic energy generated at large-scale L cascades through a hierarchy of eddies of decreasing size to the viscous subrange where it is dissipated into heat. Practically, this cascade is observed between the outer scale L, and the resolution scale, l, of the measurements (often limited by the size of the sampling apparatus), leading to the scale ratio $\lambda = L / l$.

Finally, Eq. (8) can be used to consider the average value of a function $f(Q)$ of a multifractal variable Q when considering a Taylor development of this function:

$$f(Q) = \sum_{p=0}^{N} a_p Q^p \tag{9}$$

where a_p are constants, Q is a multifractal variable as defined above and p the order of the Taylor development. Then, inserting the expression for the statistics of the variable Q (Eq. 8) yields:

$$f(Q) = \sum_{p=0}^{N} a_p Q_0^p \lambda^{K(p)} \tag{10}$$

Finally, for a detailed discussion of what can be ecologically conclude from the use of multifractal algorithms, one may refer to the recent review by Seuront *et al.* (1999) wholly devoted to the introduction of multifractal concepts and their related analysis techniques to marine ecology.

SIGNIFICANCE OF INTERMITTENCY FOR ENCONTER RATES

To evaluate the potential significance of intermittency for predator-prey encounter rates we need to compare the encounter rates expected in the case of homogeneous and intermittent (i.e. multifractal) turbulence and phytoplankton fields, i.e. introducing the precise statistical distributions of turbulent dissipation rates and phytoplankton biomass in predator-prey equations defined above instead of their average values. In the following we shall apply the concepts related to the statistical properties of intermittently distributed turbulence kinetic energy dissipation rate and phytoplankton biomass to the encounter rates due to turbulence and behavior.

Effect of turbulence intermittency

Let the phytoplankton cell concentration C and the turbulent kinetic energy dissipation rate ε be multifractal variables characterized by the scaling moment functions $K_C(q)$ and $K_\varepsilon(q)$ defined above, and by their means $\langle C \rangle = C_0$ and $\langle \varepsilon \rangle = \varepsilon_0$, respectively. Here as below, $E_{turbulence}$ and $E_{behaviour}$ will be regarded as estimates of encounter rates due to turbulence and behavior under the hypothesis of homogeneous turbulence and prey distributions, i.e. $E_{turbulence} = E(C_0, \varepsilon_0)$ and $E_{behaviour} = E(C_0)$. On the other hand, $E'_{turbulence}$ and $E'_{behaviour}$ will

estimate encounter rates due to turbulence and behavior when C and ε are regarded as multifractal variables, i.e. $E'_{turbulence} = E(C,\varepsilon)$ and $E'_{behaviour} = E(C)$. The scale ratio λ introduced to describe the statistical behavior of a multifractal variable in Eqs. (8) & (10) will be denoted as λ_ε and λ_C for turbulence and phytoplankton distributions, respectively.

Under the general hypothesis of independence of the variables C and ε, Eq. (7) is rewritten as:

$$E'_{turbulence} = \langle E(C,\varepsilon)\rangle = 1.9\pi R^{7/3}\langle C\rangle\langle \varepsilon^{1/3}\rangle \tag{11}$$

and then:

$$E'_{turbulence} = \langle E(C,\varepsilon)\rangle = 1.9\pi R^{7/3} C_0 \varepsilon_0^{1/3} \lambda_\varepsilon^{K_\varepsilon(1/3)} \tag{12}$$

now $E(C_0,\varepsilon_0) = 1.9\pi R^{7/3} C_0 \varepsilon_0^{1/3}$ $[E(C_0,\varepsilon_0) = E_{turbulence}\lambda_\varepsilon^{K(1/3)}]$, $\lambda_\varepsilon >> 1$ and $K_\varepsilon(1/3) < 0$, therefore:

$$E'_{turbulence} < E_{turbulence} \tag{13}$$

This yield to consider that taking into account the intermittent nature of turbulent energy dissipation rates ε leads to smaller estimates of the encounter rates between zooplankton and phytoplankton due to turbulence than previous estimates.

In order to quantify the demonstrated negative effect of the intermittent nature of turbulent energy dissipation rates ε on the encounter rate due to turbulence, we need to compare the relative magnitudes of $E_{turbulence}$ and $E'_{turbulence}$. First, one need to note that this effect depends on the scale ratio λ_ε of large and small turbulent scales. Nevertheless, the power $K_\varepsilon(1/3)$ acts as a moderator of this effect, since it is usually quite small, e.g. $K(1/3) = -0.05$, as extrapolated from atmospheric turbulence (Schmitt et al. 1992a, b, 1993, 1994) with a scale ratio $\lambda_\varepsilon = 1000$, this would yield $E'_{turbulence} = 0.70E_{turbulence}$. More specifically, we investigated this potential decrease in the encounter rate due to turbulence induced by fully developed intermittent turbulence on the basis of both basic spectral estimates and instantaneous intermittent distributions of turbulent energy dissipation rates of grid generated turbulence. Micro-scale turbulence has been generated by means of fixed PVC grids (diameter 2mm, mesh size 1 cm) in a circular flume. Instantaneous horizontal turbulent velocity has been measured by high frequency (100 Hz) hot-film velocimetry, and turbulent energy dissipation rate has subsequently been estimated in several ways. The average turbulent energy dissipation rate has basically been derived following Tennekes and Lumley (1972) from the turbulence spectrum obtained from Fourier analysis of time series data recorded by the hot-film probe:

$$\varepsilon = 15\nu\int_0^\infty k^2 E(k)\mathrm{d}k \quad (14)$$

where ε is the turbulent dissipation rate ($m^2.s^{-3}$), ν the kinematic viscosity ($m^2.s^{-1}$), k the wavenumber ($k = 2\pi/\lambda$), λ the eddy wavelength (m), and $E(k)$ the turbulence spectrum ($m^2.s^{-3}$). The spectrum $E(k)$ can be thought of as the mean-square amplitude of velocity fluctuations associated with a wavenumber of turbulent motion; these turbulent motions are conveniently thought of as eddies of characteristic size corresponding to their wavelength.

In order to take into account the intermittent nature of turbulence, we now need to consider local values, ε_l, of the turbulent dissipation rate following the refined similarity hypothesis (Kolmogorov, 1962; Obukhov, 1962) as:

$$\Delta v_l = C\varepsilon_l^{1/3} l^{1/3} \quad (15)$$

where C is a constant nearly equal to 1 (Table 1), $\Delta v_l = |v(x+l) - v(x)|$ is the velocity shear at scale l. Instantaneous values of ε_l were then subsequently estimated at the smallest available resolution (i.e. 100 Hz) as a fractional differentiation of the local velocity shear Δv_l, raised to the third power (i.e. $\varepsilon_l = (\Delta v_l / l^{1/3})^3$). Let us mention briefly that a fractional differentiation of order 1/3 corresponds to a multiplication by $k^{1/3}$ in Fourier space equivalent to power law filtering (see Schertzer and Lovejoy (1987) and Schertzer et al. (1998) for more discussion and more details). We then estimated both $E_{turbulence}$ and $E'_{turbulence}$ on the basis of 40

v (cm.s^{-1})	**ε**	**ε_l (SD)**		**$\varepsilon/\varepsilon_l$**	**$(E_\varepsilon - E\varepsilon_l) / E_\varepsilon$**
10	9.12E-07	9.55E-07	(2.40E-07)	0.95	32.26
20	1.31E-06	1.26E-06	(3.12E-07)	1.04	36.52
30	2.01E-06	2.11E-06	(4.89E-07)	0.95	39.87
40	4.87E-06	4.79E-06	(1.38E-06)	1.02	35.59
50	8.08E-06	7.80E-06	(2.12E-06)	1.03	38.59
60	1.14E-05	9.62E-06	(2.49E-06)	1.19	33.48
70	1.40E-05	1.31E-05	(3.37E-06)	1.07	33.88
80	2.35E-05	2.28E-05	(6.12E-06)	1.03	36.59
90	7.50E-05	7.11E-05	(2.18E-05)	1.05	37.68
100	1.05E-04	9.28E-05	(2.45E-05)	1.13	38.12

Table 1. Comparison between the turbulent energy dissipation rates estimated from power spectra (ε) and from fractional differentiation of order 1/3 (ε_l), and the related differences in the estimated predator-prey encounter rates due to turbulence.

experiments conducted for mean velocity fields ranging from 10 to 100 cm.s^{-1} (Table 1). Thus, considering a mean value of the turbulent kinetic energy dissipation rates ε instead of the

instantaneous values ε_I (Fig. 2) leads to overestimate the encounter rates due to turbulence of about $36.3 \pm 2.5\%$ (a value similar to the 30% estimated above) for values of the kinetic energy dissipation rate ranging between from 10^{-6} to 10^{-4} $m^2.s^{-3}$, values characterizing highly turbulent areas such as coastal and frontal areas (MacKenzie & Leggett 1991).

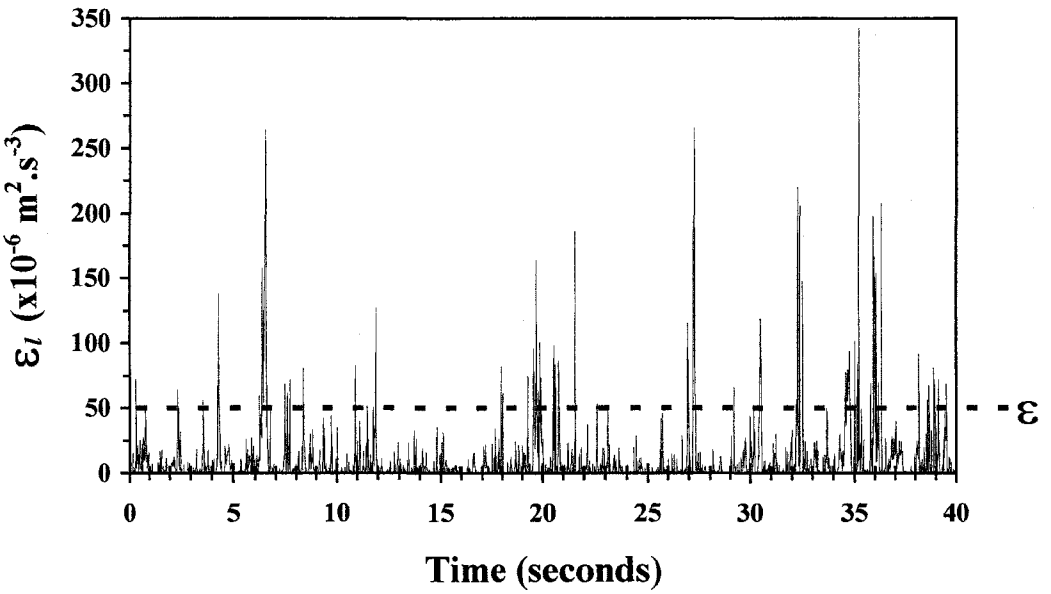

Fig. 2. Comparison between the instantaneous distribution of turbulent energy dissipation rates (ε_I) estimated from fractional differentiation of order 1/3 and the mean value (ε) estimated from power spectra.

Effect of small-scale phytoplankton intermittent distribution

Consider a situation with a planktonic predator searching for phytoplanktonic preys intermittently distributed in a multifractal frame; in this simple situation, following the parametrization described by Seuront et al. (1996a, b, 1999) a copepod will experience a very heterogeneous phytoplankton field exhibiting local concentrations reaching up to 10 time the average field value (Fig. 2). Moreover, previous laboratory experiments—while conduced in non-turbulent conditions—have suggested some zooplankton behavioral adaptations related to food densities and/or food patchiness. Thus, some studies have shown a reduced motility in high food concentrations and in food patches, both for ciliate (e.g. Buskey and Stoecker 1988, Fenchel and Jonsson 1988, Jonsson 1989, Jonsson & Johansson 1997) and copepods (e.g. Tiselius 1992, Bundy et al. 1993, Saiz et al. 1993, Tiselius et al. 1993), while others indicated an increasing swimming speed with increasing food densities (Bundy et al. 1993, van Duren & Videler 1995).

We then examine here the relative importance of phytoplankton patchiness for the behavioral component of the predator-prey encounter rate defined by Eq. (5). Four type of behavioral adaptations have been considered: (i) a constant swimming speed basically used to mimic the straight swimming behavior of cruising predators, (ii) an increasing swimming speed with increasing food concentration, (iii) both a constant swimming speed and an increasing swimming path complexity with increasing food concentration, and finally (iv) both an increasing swimming speed and swimming path complexity with increasing food concentrations.

Case 1: Constant swimming speed.

As stated above, the phytoplankton distribution is regarded as a multifractal variable characterized by its mean density $\langle C \rangle = C_0$, and the scaling moment function $K_C(q)$. In this case, Eq. (5) is simply rewritten as:

$$E'_{behaviour} = \langle E(C) \rangle = \pi R^2 v C_0 \lambda_C^{K_C(1)} \tag{16}$$

now $E(C_0) = \pi R^2 v C_0$, and $K_C(1) = 0$ as defined above, therefore:

$$E'_{behaviour} = E_{behaviour} \tag{17}$$

This clearly demonstrate that small-scale phytoplankton patchiness cannot have any effect on the behavioral predator-prey encounter rate if predator are basically regarded as 'passive' particles only characterized by their swimming velocity, unable to adapt their behavior to the ambient conditions. This is, however, all the more unlikely following the large amount of literature demonstrating the great chemo- and mecanoreception abilities of planktonic copepods (e.g. Buskey 1984, Strickler 1982, 1985, Paffenhöffer and Lewis 1990, Yen and Fields 1992, Bundy et al. 1998). We then consider a more likely hypothesis based on a differential swimming speed regarded as a function of food density.

Case 2: Density-dependent swimming speed

For simplicity, we will assume that the swimming speed of the predator, v, is a linear function of the phytoplankton density C following $v = aC + b$, where a and b are constants, with $a > 0$ and $b > 1$. Thus, Eq. (16) yield (Eqs. 8, 9 & 10):

$$E'_{behaviour} = \langle E(C) \rangle = \pi R^2 (a C_0^2 \lambda_C^{K_C(2)} + b C_0) \tag{18}$$

Considering $E(C_0) = \pi R^2 (a C_0^2 + b C_0)$, Eq. (18) yields:

$$E'_{behaviour} > E_{behaviour} \tag{19}$$

In both cases, we find that such a simple behavioral adaptation to phytoplankton patchiness can have salient consequences on the behavioral encounter rate initially defined by Eq. (5). Thus, a positive effect could be expected when the swimming speed increases with increasing phytoplankton densities, which has been experimentally demonstrated on two copepod species, *Centropages velificatus* (Bundy et al. 1993) and *Temora longicornis* (van Duren & Videler 1995) for phytoplankton concentrations within the range of cell densities found in waters where those species are abundant. On the other hand, a negative effect could be expected when the swimming speed decreases with increasing phytoplankton densities. This particular situation has, however, only been observed to our knowledge in one laboratory experiment conduced on female *Temora longicornis* at very high food concentrations (van Duren & Videler 1995). Moreover, from this particular point of view, the effect of phytoplankton patchiness is most significant for cruising than for ambush feeding predators, and also for fast swimming predators (high v). In any case, the effect of phytoplankton patchiness is here quite important. Indeed, $K(2) = \mu$ is usually denoted as the intermittency parameter which has already been estimated as being in the range 0.1-0.3 for passive scalars—as phytoplankton cells are—distributions in turbulent flows (Prasad et al. 1988, Seuront et al. 1996a, b, 1999). Scale ratios of $\lambda_C = 100$ (Seuront et al. 1996a) and $\lambda_C = 20$ (Seuront et al. 1999) thus respectively give enhancing factors of 1.6-4 and 1.4-2.5 of the encounter rate due to intermittency of phytoplankton distribution. In the two previous empirical studies, phytoplankton cells have been shown to behave as a purely passive scalar over spatial scales ranging from 0.2 m (the smallest resolution of the measurement) and 20 m. One may thus hypothesize that such a behavior could still be observed to the smallest scales (i.e. Batchelor scales) and a potential scale ratio of $\lambda_C = 1000$ can be reasonably suggested for phytoplankton distribution in the ocean, leading to enhancing factors of the behavioral encounter rate defined in Eq. 18 in the range 2.0-8.0.

Case 3: Constant swimming speed and patch exploitation

This hypothesis has been drawn following empirical results demonstrated the ability of zooplanktonic organisms to detect and to remain in food patches. This could be achieve following different strategies such as an increase in the swimming path complexity (e.g. Bundy et al. 1993), but can be generally summed up considering that the time spend by a copepod in a food patch is all the more important that the associated food density is elevated.

So, let $C_{\min}$ be an hypothetical minimal food patch density in which case the time, t, spent in the considered patch is set to be unity (i.e. $t=1$). For a given food quantity C, such as $C > C_{\min}$, the time spent in a food patch will be expressed as $t = \frac{C}{C_{\min}}$. Finally, the biological encounter rate $E'_{behaviour}$ is expressed as an addimensional expansion of Eq. (5) as:

$$E'_{behaviour} = \langle E(C) \rangle = \frac{\pi R^2 v}{C_{\min}} C_0^2 \lambda_C^{K_C(2)} \tag{20}$$

now $E(C_0) = \frac{\pi R^2 v}{C_{\min}} C_0$, and $K_C(2) > 0$, therefore

$$E'_{behaviour} > E_{behaviour} \tag{21}$$

Thus, predators able to develop strategies to remain in a given high food density patch will substantially increase—up to a factor $C_0^2 \lambda_C^{K_C(2)} / C_{\min}$—their effective encounter rate with phytoplankton cells. Following the previously chosen formalism, this effect will be all the more important that the prey density is high (see Eq. 20). Finally, this could be the most likely behavioral adaptation to resources patchiness, because this strategies has been found for a wide variety of organisms and prey patchiness (Coughlin et al. 1992, Larsson & Kleiven 1996, Bascompte & Vila 1997, Jonsson & Johansson 1997, Kostylev et al. 1997, Ritchie 1998).

Case 4: Density-dependent swimming speed and patch exploitation

The equation is now obtained introducing the previous density-dependent swimming speed, $v = aC + b$, in Eq. (20) yielding:

$$E'_{behaviour} = \langle E(C) \rangle = \frac{\pi R^2}{C_{\min}} (aC_0^3 \lambda_C^{K_C(3)} + bC_0^2 \lambda_C^{K_C(2)}) \tag{22}$$

With $E(C_0) = \pi R^2 / (C_{\min}(aC_0^3 + bC_0^2))$, and as previously stated when we tested the effect of a density-dependent swimming speed alone, $b > 0$, it comes:

$$E'_{behaviour} > E_{behavioour} \tag{23}$$

This particular situation can be regarded as a generalization of Eq. (18) to a more complete and complex behavioral response to phytoplankton patchiness. In particular, for $a > 0$, we have Eq. (18) < Eq. (22), indicating an increased behavioral contribution to predator-prey encounter rates. The effect is here becoming very important. Indeed, the scale ratio λ_C is usually quite large and $K_C(3)$ is in the range 0.3-0.6 for passive scalars advected by fully turbulent flows (Schmitt et al. 1996, Seuront et al. 1996a, b, 1999), giving for $\lambda_C = 100$ and $\lambda_C = 20$

enhancing factors in the range 3.0-16 and 2.5-6.0, respectively. Here our test-case $\lambda_C = 1000$ would lead to an enhancing factor in the range 8.0-63.0.

While further investigations could have been conduced in order to provide further insight into the analytical properties of the previous equations, the resolution of this particular issue is beyond the scope of this contribution. Let us nevertheless recall that, as demonstrated by Kiørboe & Saiz (1995) and Kiørboe & MacKenzie (1995), the swimming speed of planktonic predators is very dependent on their size, suggesting that the previously demonstrated effect of behavior will be all the more important that the predators are large (i.e. high v values in Eqs. 16 & 18, and high b values in Eqs. 18 & 23). Moreover, Eqs. (16, 18, 21 & 23) are also sensitive to the perceptive distance of the predator (R), which is decreased in high hydrodynamic conditions (Kiørboe & Saiz 1995), leading to a an increase in the behavioral contribution to the predator-prey encounter rates in low hydrodynamic conditions. Moreover, these features could also provide an alternative explanation to the apparent inadequation observed by Saiz (1994) between empirical encounter rates and the theoretical values expected following the basic particle encounter theory.

CONCLUSIONS

The general result here—based on multifractal parametrisation of intermittent distributions of both turbulent kinetic energy dissipation rates and phytoplankton biomass—is first that the effect of turbulence on predator-prey encounter rates is less important than previously thought on the basis of the basic hypothesis of homogeneous turbulence. Nevertheless, a numerical estimate of this effect in a test-case with $\lambda_\varepsilon = 1000$ leads to a moderate effect of intermittency, due to small value of the exponent $K_\varepsilon(1/3)$. Afterwards, the contribution of behavioral components is obviously more developed than when phytoplankton preys are regarded as being homogeneously distributed. An increase in encounter rates cannot thus be any longer regarded as a simple direct consequence of an increase in the relative velocity of the predator and the prey induced by turbulent velocity, but rather as both direct and indirect consequences of intermittent small-scale turbulence which generates very heterogeneous phytoplankton distributions. Indeed, the scale ratio of the turbulent cascades (cf. Fig. 1) is here of salient importance. With a test-case of $\lambda_C = 1000$, an intermittent (i.e. multifractal) phytoplankton distribution can thus lead to enhance the behavioral component of the predator-prey encounter rate of a factor that can go up to a value of 60 in our last case study. Since this enhancing

factor depends on the scale ratio λ_c, it appears to be a determinant factor for the encounter rate estimates.

The previous approaches have been developed with copepods in mind, but the equations can be easily generalized so that they apply to other planktivorous predators as well. Indeed, considering the recently demonstrated very specific heterogeneous distribution of zooplankton (Pascual et al. 1995, Tsuda 1995), similar approaches could be conduced on the effects of both turbulence and intermittent zooplankton distributions on the larval fish feeding behavior, which has widely been shown to exhibit very complex patterns [see e.g. Dower et al. (1997) for a review]. This also suggests reconsidering the effects of small-scale turbulence on estimates of plankton food requirements, and energy gain-and-loss for foraging. Indeed, following studies related to optimal foraging theory (Pyke 1984), zooplankton living in highly heterogeneous environments could develop strategies to exploit high density patches and then to optimize the energy required to capture a given amount of food. This could be achieved, as previously suggested, by increasing the complexity of swimming pathes with increasing food densities, and/or reducing motility in food patches. Recent papers (Marguerit et al. 1998) dealing with grazing in heterogeneous (i.e. multifractal) phytoplankton fields have thus demonstrated that very simple behavioral strategies related to food quantity perceived by a predator could lead to very specific results in terms of swimming behavior and ingestion rates in comparison with what would have been obtained in homogeneous environments. A precise description of the behavior of both predators and preys then appears to be a salient issue for the future modeling of plankton trophodynamics in turbulent environments (Browman and Skiftesvik 1996, Osborn and Scotti 1996), propounding notably the advantage of individual based approaches (Yamazaki 1993, Levin 1994).

In reviewing the available literature on turbulence and larval fish feeding, Dower et al. (1997) pointed out that future research would do well to include non-homogenous prey distributions and predator behaviors that more realistically mimic field conditions. Indeed, in the field patchiness is present at both temporal and spatial scales. Systematic studies of simplified mimics and real plankton organisms of widely varying nature and behavioral properties in a diversity of steady and unsteady flows are then still needed to dissect the multiple adaptative strategies of real organism in a real ocean. In that way, both the analytical model and the multifractal frame [see Seuront et al. (1999) for a review], may be a starting point to investigate the precise effects of the real nature of the physical and biological surrounding environments on both plankton behaviors and distributions.

References

Baker MA, Gibson CH (1987) Sampling turbulence in the stratified ocean: statistical consequences of strong intermittency. J Phys Oceanogr 17: 1817-1836

Bascompte J, Vila C (1997) Fractals and search paths in mammals. Landsc Ecol 12: 213-221

Bird JL, Kitting CL (1982) Laboratory studies of a marine copepod (Temora turbunata Dana) tracking dinoflagellate migrations in a miniature water column. Contrib Mar Sci 25:27-44

Bohle-Carbonel M (1992) Pitfalls in sampling, comments on reliability and suggestions for simulation. Cont Shelf Res 12: 3-24

Browman HI, Skiftesvik AB (1996) Effects of turbulence on the predation cycle of fish larvae: comments on some of the issues. Mar Ecol Prog Ser 139:309-312

Bundy MH, Gross TF, Coughlin DJ, Strickler JR (1993) Quantifying copepod searching efficiency using swimming pattern and perceptive ability. Bull Mar Sci 53: 15-28

Bundy MH, Gross TF, Vanderploeg HA, Strickler JR (1998) Perception of inert particles by calanoid copepods: behavioral observations and a numerical model. J Plankton Res 20:2129-2152

Buskey EJ (1984) Swimming patterns as an indicator of copepod sensory system in the recognition of food. Mar Biol 79:165-175

Buskey EJ, Stoecker DK (1988) Locomotory patterns of the planktonic ciliate *Favella* sp.: adaptations for remaining within food patches. Bull Mar Sci 43:783-796

Caparroy P, Carlotti F (1996) A model for Acartia tonsa: effect of turbulence and consequences for the related physiological processes. J Plankton Res 18:2139-2177

Coughlin DJ, Strickler JR, Sanderson B (1992) Swimming and search beheviour in clowfish, *Amphiprion perideraion*, larvae. Anim Behav 44: 427-440

Davis CS, Flierl GR, Wiebe PH, Franks PJS (1991) Micropatchiness turbulence and recruitment in plankton. J Mar Res 49:109-151

Denman KL, Gargett AE (1995) Biological-physical interactions in the upper ocean: the role of vertical and small scale transport processes. Annu Rev Fluid Mech 27:225-255

Delichatsios MA, Probstein RF (1975) Coagulation in turbulent flow: theory and experiment. J Coll Interf Sci 51:394-405

Dower JF, Miller TJ, Leggett WC (1997) The role of microscale turbulence in the feeding ecology of larval fish. Adv Mar Biol 31:169-220

Evans GT (1989) The encounter speed of moving predator and prey. J Plankton Res 11:415-417

Fenchel T, Jonsson PR (1988) The functional biology of *Strombinium sulcatum*, a marine oligotrich ciliate (Ciliophora, Oligotrichina). Mar Ecol Prog Ser 48:1-15

Frisch U (1995) Turbulence. Cambridge University Press

Gargett AE (1997) "Theories" and techniques for observing turbulence in the euphotic zone. Sci Mar 61:25-45

Gerritsen J, Strickler JR (1977) Encounter probabilities and community structure in zooplankton: a mathematical model. J Fish Res Bd Can 34:73-82

Hill PS, Nowell ARM, Jumars PA (1992) Encounter rate by turbulent shear of particles similar in diameter to the Kolmogorov scale. J Mar Res 50:643-668

Jackson GA, Lochmann S (1993) Modeling coagulation of algae in marine ecosystems. In: Buffle J, van Leeuwen HP (eds) Environmental analytical and physical chemistry series, Vol 2, Environmental particles. Lewis Publishers, Boca Raton, p 387-414

Jimenez J (1997) Oceanic turbulence at millimeter scales. Sci Mar 61:47-56

Jonsson PR (1989) Vertical distribution of planktonic ciliates—an experimental analysis of swimming behaviour. Mar Ecol Prog Ser 52:39-53

Jonsson PR, Johansson M (1997) Swimming behaviour, patch exploitation and dispersal capacity of a marine benthic ciliate in flume flow. J Exp Mar Biol Ecol 215: 135-153

Jou D (1997) Intermittent turbulence: a short introduction. Sci Mar 61:57-62

Kiørboe T, Saiz E (1995) Planktivorous feeding in calm and turbulent environments, with emphasis on copepods. Mar Ecol Prog Ser 122:135-145

Kiørboe T, MacKenzie BR (1995) Turbulence-enhanced prey encounter rates in larval fish: effects of spatial scale, larval behaviour and size. J Plankton Res 17:2319-2331

Kolmogorov AN (1962) A refinement of previous hypotheses concerning the local structure of turbulence in viscous incompressible fluid at high Reynolds number. J Fluid Mech 13:82

KostylevV, Erlandson J, Johannesson K (1997) Microdistribution of the polymorphic snail *Littorina saxatilis* (Olivi) in a patchy rocky shore habitat. Ophelia 47: 1-12

Larsson P, Kleiven OT (1996) Food search and swimming speed in Daphnia. In: Lenz PH, Hartline DK, Purcell JE, Macmillan DL (eds) Zooplankton: sensory ecology and physiology. Gordon & Breach, Amsterdam.

Levin SA (1994) Patchiness in marine and terrestrial systems: from individuals to populations. Phil Trans R Soc London B 343:99-103

MacKenzie BR, Kiørboe T (1995) Encounter rates and swimming behavior of pause-travel and cruise larval fish predator in calm and turbulent laboratory experiments. Limnol Oceanogr 40:1278-1289

MacKenzie BR, Leggett WC (1991) Quantifying the contribution of small-scale turbulence to the encounter rates between larval fish and their zooplankton prey: effects of wind and tide. Mar Ecol Prog Ser 73:149-160

MacKenzie BR, Miller, TJ, Cyr S, Leggett WC (1994) Evidence of a dome-shaped relationship between turbulence and larval fish ingestion rates. Limnol Oceanogr 39: 1790-1799

Mandelbrot B (1983) The fractal geometry of nature. Freeman, New York

Marguerit C, Schertzer D, Schmitt F, Lovejoy S (1998) Copepod diffusion within multifractal phytoplankton fields. J Mar Syst 16:69-83

Obukhov AM (1962) Some specific features of atmospheric turbulence. J Flui Mech 13:77

Osborn T, Scotti A (1996) Effects of turbulence on predator-prey contact rates: where do we go from here? Mar Ecol Prog Ser 139: 302-304

Paffenhöffer GA, Lewis KD (1990) Perceptive performance and feeding behavior of calanoid copepods. J Plankton Res 12:933-946

Pascual M, Ascioti FA, Caswell H (1995) Intermittency in the plankton: a multifractal analysis of zooplankton biomass variability. J Plankton Res 17:1209-1232

Peitgen HO, Saupe D (1988) The science of fractal image. Springer-Verlag, New York

Platt T, Harrison WG, Lewis MR, Li WKW, Sathyendranath S, Smith RE, Vezina AF (1989) Biological production of the oceans: the case for a consensus. Mar Ecol Prog Ser 52: 77-88

Prasad,R.R., Meneveau,C. and Sreenivasan,K.R. (1988) The multifractal nature of the dissipation field of passive scalars in fully turbulent flows. Phys. Rev. Lett. 61:74-77

Pyke JH (1984) Optimal foraging theory: a critical review. Ann Rev Ecol Syst 15:523-575

Ritchie ME (1998) Scale-dependent foraging and patch choice in fractal environments. Evol Ecol 12: 309-330

Rothschild BJ, Osborn TR (1988) Small-scale turbulence and plankton contact rates. J Plankton Res 10:465-474

Saiz E (1994) Observations of the free-swimming behavior of Acartia tonsa: effects of food concentration and turbulent water motion. Limnol Oceanogr 39:1566-1578

Saiz E, Tiselius P, Jonsson PR, Verity P, Paffenhöfer GA (1993) Experimental records of the effects of food patchiness and predation on egg production of *Acartia tonsa*. Limnol Oceanogr 38: 280-289

Sanford LP (1997) Turbulent mixing in experimental ecosystem studies. Mar Ecol Prog Ser 161:265-293

Schertzer D, Lovejoy S (1987) Physically based rain and cloud modeling by anisotropic multiplicative turbulent cascades. J Geophys Res 92:9693-9714

Schertzer D, Lovejoy S, Schmitt F, Chigirinskaya Y, Marsan D (1998) Multifractal cascade dynamics and turbulent intermittency. Fractals 5:427-471

Schmitt F, Lavallée D, , Schertzer D, Lovejoy S (1992a) Empirical determination of universal mutlifractal exponents in turbulent velocity fields. Phys Rev Lett 68:305-308

Schmitt F, Lavallée D, Lovejoy S, Schertzer D, Hooge C (1992b) Estimations directes des indices de multifractals universels dans le champ de vent et de température. C R Acad Sci Paris Série II, 314: 749-754

Schmitt F, Schertzer D, Lovejoy S, Brunet Y (1993) Estimation of universal multifractal indices for atmospheric turbulent velocity fields. Fractals 1: 568-575

Schmitt F, Schertzer D, Lovejoy S, Brunet Y (1994) Empirical study of multifractal phase transition in atmospherc turbulence. Nonlin Processes Geophys 1:95-104

SchmittF, Schertzer D, Lovejoy S, Brunet Y (1996) Multifractal temperature and flux of temperature in fully developped turbulence. Europhys Lett 34: 195-200

Seuront L, Schmitt F, Lagadeuc Y, Schertzer D, Lovejoy S, Frontier S (1996a) Multifractal analysis of phytoplankton biomass and temperature in the ocean. Geophys Res Lett 23:3591-3594

Seuront L, Schmitt F, Schertzer D, Lagadeuc Y, Lovejoy S (1996b) Multifractal intermittency of Eulerian and Lagrangian turbulence of ocean temperature and plankton fields. Nonlin Proc Geophys 3:236-246

Seuront L, Schmitt F, Lagadeuc Y, Schertzer D, Lovejoy S (1999) Universal multifractal analysis as a tool to characterize multiscale intermittent patterns: example of phytoplankton distribution in turbulent coastal waters. J Plankton Res 21:877-922

Strickler JR (1982) Calanoid copepods, feeding currents and the role of gravity. Science 218:158-160

Strickler JR (1985) Feeding currents in calanoid copepods: two new hypothesis. Symp Soc Exp Biol 89:459-485

Sundby S, Fossum P (1990) Feeding conditions of Arcto-norwegian cod larvae compared with the Rothschild-Osborn theroy on small-scale turbulence and plankton contact rates. J Plankton Res 12: 1153-1162

Tennekes H, Lumley JL (1972) A first course in turbulence. MIT Press.

Tiselius P (1992) Behavior of *Acartia tonsa* in patchy food environments. Limnol Oceanogr 37:1640-1651

Tiselius P, Jonsson PR, Verity PG (1993) A model evaluation of the impact of food patchiness on foraging strategy and predation risk in zooplankton. Bull Mar Sci 53: 247-264

Tsuda A (1995) Fractal distribution of the oceanic copepod *Neocalanus cristatus* in the subarctic Pacific. J Oceanogr 51:216-266.

van Duren LA, Videler JJ (1995) Swimming behaviour of development stages of the calanoid copepod *Temora longicornis* at different fod concentrations. Mar Ecol Prog Ser 126: 153-161

Yamazaki H (1993) Lagrangian study of planktonic organisms: perspectives. Bull Mar Sci 53:265-278

Yen J, Fields DM (1992) Escape response of *Acartia hudsonica* (Copepoda) nauplii from the flow field of *Temora longicornis* (Copepoda). Arch Hydrobiol Beith Ergebn Limnol 36:123-134

A18

Multi-agent modeling of the physical/biological coupling

A case study in marine ecology

Ramat E, Preux P, Seuront L & Lagadeuc Y

ECAL (soumis)

Multi-agent modeling of the physical/biological coupling — A case study in marine ecology

Eric Ramat[1], Philippe Preux[1], Laurent Seuront[2], and Yvan Lagadeuc[2]

[1] Laboratoire d'Informatique du Littoral (LIL)
BP 719,
62228 Calais, France
{ramat, preux}@lil.univ-littoral.fr
http://www-lil.univ-littoral.fr
[2] Station marine de Wimereux,
ELICO UPRES A8013,
28 avenue Foch - BP 80,
62930 Wimereux, France
{seuront, yvan}@loalit.univ-littoral.fr

Abstract. Within the framework of a pluridisciplinar research project gathering biologists, mathematicians, and computer scientists, we propose a multi-agent modeling of an ecosystem. We justify the use of a multi-agent modeling for the study of the behavior for such a system which can not be suitably modeled analytically to guarantee its relevancy. Such a modeling focusses on the behavior of the living being rather than on emergent properties of the dynamics of the system. By the way, we present the concepts (such as Petri networks [11], perception of agents, simulation of concurrent living processes) and the platform that we have developed in a generic way, using the application in ecology as a case study.

1 Introduction

The main objective of this work is to identify the behavioral rules of a small crustacean, part of the family of zooplanktons named "copepod" (see Fig. 1). A keypoint in this modeling is the study of the influence of the environment on its behavior: our assumption is that the copepod has an active behavior of search for food (phytoplanktons). By "active", we mean that the copepod has an individual behavior rather than being merely transported as a particule by the turbulences of water. (At its millimetric scale, the oceans are extremely turbulent.) We aim at showing that the fact that the behavior of the copepod is active implies important consequences on its viability and its success for survival, and reproduction. Being a very important link within the food chain in oceans, a more accurate knowledge of the copepod will finally bring us a more accurate and sounder understanding of the way the marine eco-system works, as well as its dynamics. To that purpose, the project develops itself along three complementary directions that are continuously interacting with each others: *in*

vivo observations, analytical models, and modeling of the individual behavior of copepods using agents. Our research has shown that the distribution of phytoplankton is strongly heterogeneous in the environment of the copepod [10]. Current results show that this heterogeneity influences the energy assessment of the copepod. By measuring the quantity of nitrogen absorption during nutrition, the observations show that the output of the behavior of the copepod (the ratio of the energy that is spent and the energy that is ingested) varies according to the type of distribution of food. For example, a turbulent environment, favourable to an overall mixing, increases the rate of meeting of the copepod with the particles of phytoplankton and thus increases the energetic ratio. It now remains to study the influence of the behavior of the copepod in such situations. The study of this behavior is incompatible with an analytical approach, as we will see it. So, we use a multi-agent system (MAS) approach [4].

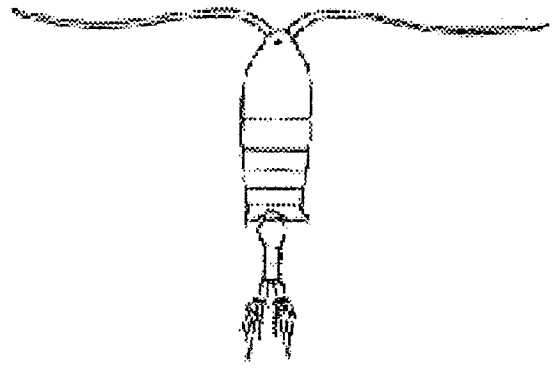

Fig. 1. Copepode *Centropages hamatus*

Using a MAS approach is a considerable change in the mode of thinking in biology which relies on models using equations, statements, and statistical analyses [5]. The researcher, in our case the biologist, has to formulate the studied individual behavior and its interactions with its environment. In section (2), we state the problem (just to give its flavor!). Section (3) is devoted to the presentation of our modeling tool. We show how the dynamics of agents is formalized with Petri nets, as well as the modeling of agents' perception of their environment. Some results are then presented in section (4).

2 The system under study

At present, the copepod is represented by models either of the type "black box" (see Fig. 2), or analytical models [1]. These models seek to describe in terms of input flow, output flow and transfer function each "process" of the organism.

Let us describe the process of ingestion of preys in the case of the phytoplankton (see Fig. 2). The copepod captures a prey (a particle of phytoplankton). After

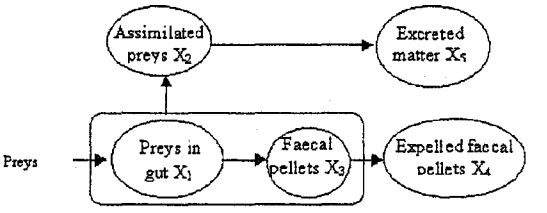

Fig. 2. Model of the process of ingestion

a handling time, the prey is stored in the gut and enters the process of digestion. The gut transforms its contents in usable energy (comparable preys) which one expresses out of nitrogen, or wastes (fecal balls). This transformation is continuous: within each Δt, a quantity Δq of caught preys is processed (this quantity is proportional to the quantity stored in the gut). Usable energy is either consumed (metabolism, digestion, or stroke), or stored (egg production for females, for example). As for wastes, it is expelled.

There are analytical models which have the ambition to represent, as well as possible, the biological processes which govern the copepods. [1] proposes a model synthesizing the various models developed until now. It captures the activities of capture and ingestion using five coupled differential equations.

This model suits for the process of capture. However, from our point of view, the contribution of the behavior is partially neglected. Indeed, one can put into equations the fact that the activity of nutrition of copepod as a function of the density of preys, the level of turbulence of the environment, the mode of hunting and the quantity of food in the gut; however, it is much more difficult to take into account various factors within the behavior such as the way copepods perceive their environment, the size of preys, and the speed of stroke of copepod relatively with that of its prey.

3 The multi-agent modeling

The system under study is composed of a mass of water in which "patches" of phytoplankton and copepods are immersed. Each agent is located and has its properties among which its behavior. The patches of phytoplanktons have a certain size and are subject to currents and turbulence. The copepod has various characteristics (its "weigth" expressed in nitrogen, the volume of its gut, its speed of stroke...). Its behavior, object of the study for the biologist, is defined by a Petri network to allow the description of sophisticated behaviors with a standard and simple tool. Agents are reactive which means that their behavior is governed by their perception and their current internal state, which, in turn, eventually induces an action and a new internal state (see Fig. 3).

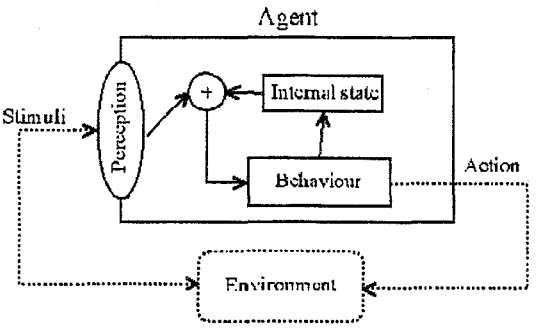

Fig. 3. Reactive agent

3.1 Modeling tool

There is a large number of modeling tools more or less general (Swarm [9], Manta [8]...). In the majority of the cases, they are platforms either adapted to one or a family of problems, or generic. To our knowledge, the generics involves, in all the cases, a dependence with respect to a data-processing environment or of a language of development but especially these platforms is containing reusable primitives and thus should be written code ! All these reasons pushed us to design a new tool of modeling and simulation of reactive, perceptive and located agents.

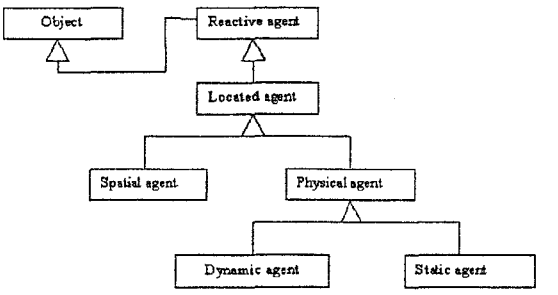

Fig. 4. Hierarchy of agent familly

We use an object language (Java) in which we find all the concepts of the paradigm object as well as a set of advanced classes (thread, stream...). These classes enabled us to define our classes of agents. Initially, these classes of agents were accessible by a language with which one can describe a category of agents via their behavior, their properties and their means of communication. A second language makes possible the description of the environment. These two languages composes a platform where one can describe the agents, to create them and activate them. At present, these two languages are encapsulated in a graphic

interface written in Java (thus portable and accessible on Internet - http://www-lil.univ-littoral.fr/ ramat) and are accompanied by tools for the definition of the environment, tools for the representation of moves of located agents and layout of the variations of the properties of the agents.

Dynamics. The dynamics of agents is modeled using Petri networks. Each agent can have several Petri networks and each net perform, in parallel with others, a process. The Petri networks can model process including changes of states, moves, message exchanges... Basically, Petri networks specifies the states within which an agent can be, the possible transitions between states, and the conditions to fulfill for each transition to occur. To each state is associated a set of actions performed by the agent when the state is activated; actions may be a displacement in the space, an update of its internal state, perceiving its environment... The state is activated when it is first reached. A transition actually occurs when its condition is fulfilled.

In the simulation of real processes, it is crucial to take its duration into account. Hence, each transition is assigned a duration which is either constant and deterministic, or stochastic.The introduction of the time allows to construct dynamically a schedule. At every time t, each active Petri net checks if it has activable transitions. If it is the case then they are occur. Two cases of figure are then to consider : either the crossed transitions are not temporized or they are it. In the second case, the activation of following states put in the schedule. This mechanism supposes that all active Petri nets reach either a temporized transition or a state from which no transition can be activated.

Perception. By analogy with biological entities, any agent is endowed senses more or less developed. In our model, an agent has several senses and each one of them is defined by three parameters: the type of perceived agents, the sector (according to the orientation of the agent), and the distance within which the perceivable agents are actually perceived. By this way, one can test different scenarios according to possible models of perception of the copepod. Moreover, one agent can perceive only a part of the characteristics of another agent. One specifies in this case the perceived characteristics. Furthermore, an agent perception of a certain feature of an other agent may not be a carbon copy of the perceived agent actual feature but somehow blurred by some perception bias, or some environmental effect (turbulence...). An agent can also have several senses. The sense to be used as a certain stage of the behavior of the agent has to be specified.

In this approach, senses are at the base of the network of knowledge of the agents. Dynamically, the agent builds its neighborhood according to its position in space, and to its senses.

3.2 The model

We started from the assumption that the copepod adopts two distinct behaviors: a stroke directed in the search of food and random jumps. These behaviors have

a direct influence on the process of ingestion of the cell of phytoplankton. Thus, we focus exclusively on this process and we leave aside the digestion which is not to disregard to obtain a complete model.

General information. The system is composed of three entities: a mass of water, cells of phytoplankton and copepods. Initially, we consider only one copepod at a time since the aim of this study is the hunting behavior of copepods. The mass of water constitutes the environment in which evolves and moves the other entities. The size of the copepod (1 mm) is used as the basic length for the discretization of this environment. For the moment, the environment is considered as two dimensional and split into chunks of $1mm_2$. Each chunk is dealt with by spatial agent. The cells of phytoplankton are very numerous (from 10 cells per liter to 10^8 cells per liter which yields a maximum of 10^2 cells per chunk). Thus, it is not conceivable to model each cell with one agent. The solution which was adopted consists in defining a property "Number of cells" at the level of spatial agents. One delegates the management of food to the spatial agents, that is to the environment. As the copepod, the environment is represented by a dynamic agent which behavior is described in the subsequent part.

The unit of time of simulation is noted u.t. It is fixed by the duration corresponding to the time necessary to perform the quickest action, i.e. the handling of a cell of phytoplankton by the copepod, 1/20 s.

The dynamics of the copepod. The Petri network that models the dynamics of displacements of the copepod is divided into four parts:

- as soon as a cycle of $t1$ u.t., for example 75 u. t., is elapsed, the copepod carries out a jump without considering what surrounds it,
- during $t2$ u.t. (time to cross a chunk of the environment), the copepod explores the place where it is and if food is available there; within each unit of time, it can capture a cell of phytoplankton,
- on the other hand, if there is no food, it continues to swim to reach the next chunk,
- at the end of the $t2$ u.t. necessary to cross a chunk, the copepod "chooses" a new chunk to be explored and proceeds there.

Let us take a closer look at the active phase dealing with the capture of food. With the exception of the random jumps, the copepod strokes and traverses a chunk at each $t2$ u.t. When this time amount of time has elapsed, the copepod changes its location. This change is a function of the copepod behavioral strategy. In the case of our present work, the probability that a chunk is chosen is proportional to the amount of food it holds: the more food, the more likely the copepod will move to it.

Locally, the copepod captures the cells of phytoplankton if it has not yet eaten too much within the last u.t. Indeed, the copepod decreases the quantity of food which it absorbs according to its level of satiety, itself directly bounded, for the moment, with the number of cells of phytoplankton present in the gut. The function of satiety is:

$$C_g = 1 - \frac{V_{prey} X_1}{\frac{2}{3} V_{gut}} \quad (1)$$

where $V_{prey}X_1$ represents the volume of the not-yet-digested preys and V_{gut} the volume of the gut of the copepod. It captures the cell according to a certain probability and, if it does not, the cell disappears from its field of vision.

4 Experimental Results

We define two types of copepods according to their strategy of stroke: random or directed towards food. The environment is composed of a 2D grid of 1024 square chunks (32x32). Each chunk is a spatial agent and is connected to its 8 neighbors. The cells of phytoplankton are distributed either by patches (see Fig. 5 and Fig. 6 - the distribution is multifractal [10]), or uniformly. In both cases, the total density is identical (2 cells by chunk). For patches, various densities of phytoplankton are used (represented by different levels of gray).

Using the variables defining the internal state of copepod agents, we measure within each step of simulation: the energy, expressed in pg of nitrogen, contained in the gut, its usable energy, the number of captured cells of phytoplankton and two variables of the analytical model (X_3 and X_4, see Fig. 2).

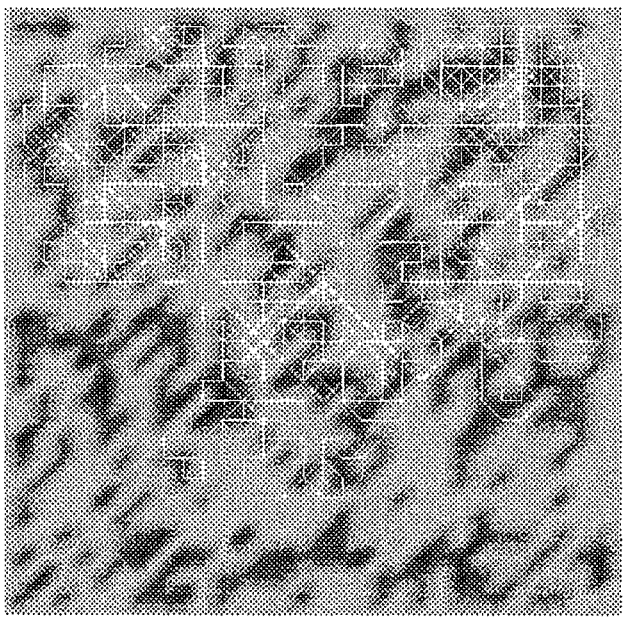

Fig. 5. Path of the copepod swimming at random

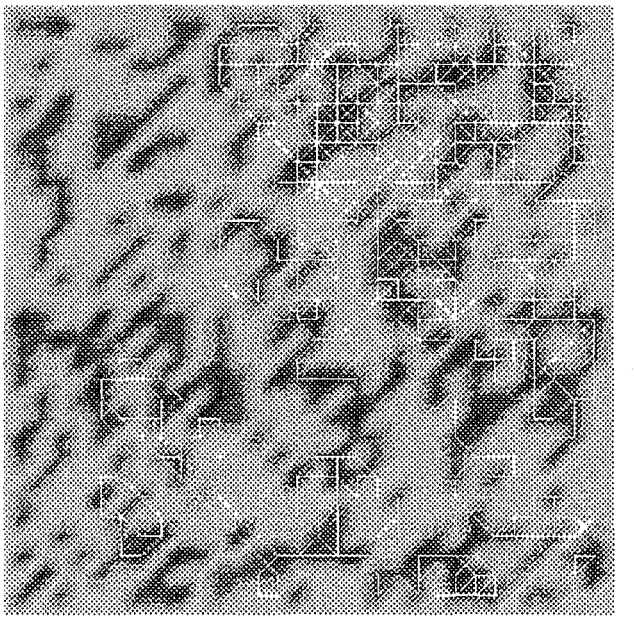

Fig. 6. Path of the copepod swimming towards food

We use a graphical tool to visualize the paths followed by copepods. By superimposing the path of the studied copepod and the distribution of cells of phytoplankton, one shows that in the case of a non homogeneous distribution of the cells of phytoplankton, the strategy of the directed stroke is more effective.

If one compares the curves representing the quantity of food in the gut of the copepod along the time (see Fig. 7), according to the distribution of the cells of phytoplankton and the strategy of stroke, it appears clearly that the directed stroke is favorable to the feeding of the copepod from the point of view of energy.

If the copepod is located inside a homogeneous field of phytoplankton, the strategy of stroke does not have any influence on the feeding since it is able to find food in all directions in same quantity. On the other hand, in a heterogeneous field, the random strategy leads the copepod to find food at random, and especially to leave chunks with food without seeking to benefit from it. Therefore this strategy is less effective.

In conclusion, we find the principal results stated in [1] for a uniform configuration of field and random stroke. It remains to carry out comparisons in vivo with results of experiments. However, these in vivo remain difficult to realize for the moment. The only points of possible comparison relates to the aspect of the paths according to the density of food [3].

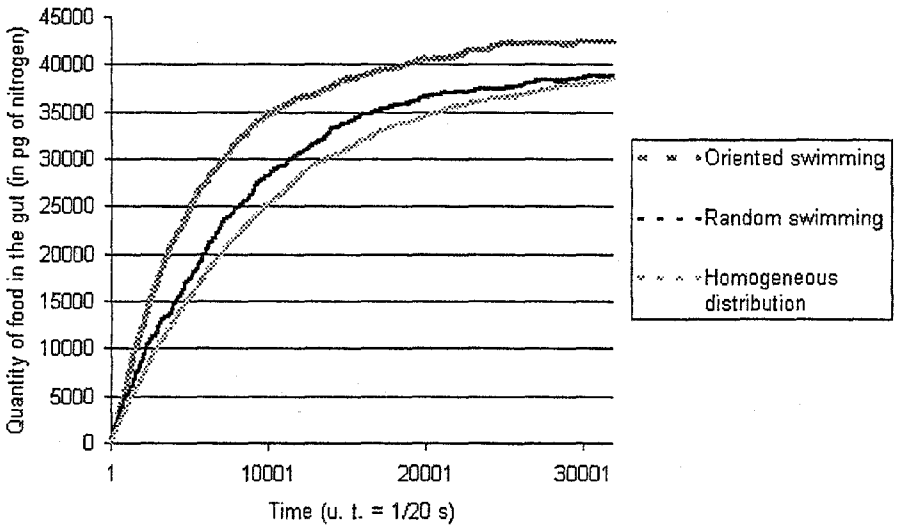

Fig. 7. Quantity of food (pg of nitrogen) in the gut of the copepod against time

5 Conclusion

As part of a joint project gathering biologists, mathematicians, and computer scientists, we have presented the modeling of the behavior of an animal pertaining to the family of zooplanktons, namely the copepod. The goal of our work is to study the coupling between the behavior of the animal and its environment. We use multi-agent systems to obtain an executable model with which a wide variety of behavioral dynamics can be expressed. Using MAS, we are also able to make the behavior of agents evolved during time, and co-adapts to its changing environment. We obtain results of simulation that are compatible with *in vivo* observations and which are based on a model of the behavior of the copepod rather than an analytical description using abstract quantities and parameters. Owing to this behavioral model, we are able to assess many assumptions about it, something which does not seem to be able to be done within the usual analytical framework.

Basically, the model presented in this paper is a translation of the analytical model into algorithm. Thus, we end-up with averaged measures resulting from assessments and random processes, such as that of satiety. The same remark is valid for the digestion part. The only new element is taking into account the behavior at the level of the stroke. We emphasize that the definition of the agents is definitely simpler and uses a reduced number of parameters compared to the analytical model.

We are now interested into breaking up the "enigmatic" processes, such as the random jumps, and the speed of constant stroke. It is obvious that these actions hides complex processes. For example, the observation shows that the

speed of stroke is not constant and that these variations are due to interactions with the environment. It remains to imagine them and subsequently specify them precisely.

In addition, if one is interested in the rules of decision regarding the capture of a cell of phytoplankton, one can wonder whether elements such as the physiological state of the copepod does not come into play. For example, a female, carrying eggs, has significantly more requirements in food than a male. Furthermore, it is obvious that a copepod did not behave in the same way on its own, or within a colony of its kind.

References

1. Caparroy, P., Carlotti, F.: A model for Acartia tonsa : effect of turbulence and consequences for the related physiological processes. Journal of Plankton Research, vol. 18, n° 11, pp. 2139-2177 (1996)
2. Tiselius, P., Jonsson, P. R.: Foraging behaviour of six calanoid copepods : observations and hydrodynamic analysis. Marine ecology progress series, vol. 66, pp. 23-33 (1990)
3. Bundy, M. H., Gross, T. F., Coughlin, D. J., Strickler J. R.: Quantifying copepod searching efficiency using swimming pattern and perceptive ability. Bulletin of Marine Science, vol. 53, n° 1, pp. 15-28 (1993)
4. Ferber, J.: Les systèmes multi-agents, vers une intelligence collective. InterEditions (1995)
5. Pavé, A.: Modèlisation en biologie et en écologie. ed. Aléas, 559 p. (1994)
6. Cambier, Ch., Perrier, E., Treuil, J-P., Preux, Ph.: Action physique et géométrique, Contribution à une réflexion sur l'utilisation des processus physiques, Application RIVAGE. Poster, 5th JFIADSMA (1997)
7. Marcenac, P.: Modèlisation de systèmes complexes par agents. Techniques et Sciences Informatiques (TSI), vol. 16, n° 8, pp. 1013-1037 (1997)
8. Drogoul, A., Ferber, J.: Multi-Agent Simulation as a Tool for Modeling Societies: Application to Social Differentiation in Ant Colonies. Proceedings of Workshop MAA-MAW'92, Viterbo (1992)
9. Minar, N., Burkhart, R., Langton, C., Askenazi, M.: The SWARM simulation system : a toolkit for building multi-agent simulations. Report (1996)
10. Seuront, L., Schmitt, F., Lagadeuc Y., Schertzer, D. Lovejoy, S.: Universal multifractal analysis as a tool to characterize multiscale intermittent patterns. Example of phytoplankton distribution in turbulent coastal waters. J. Plankton Res. (1999)
11. James L. Peterson: Petri Net Theory and the Modelling of Systems. Prentice-Hall, Englewood Cliffs, New Jersey (1981)

A19

Space-time heterogeneity of phytoplankton biomass in tidally mixed coastal waters: implication on primary production estimates

Seuront L, Lizon F & Lagadeuc Y (manuscrit)

Space-time heterogeneity of phytoplankton biomass in tidally mixed coastal waters: implications on primary production estimates

L. Seuront[1,2], F. Lizon[1], Y. Lagadeuc[1,3]

[1] Station Marine de Wimereux, Université des Sciences et Technologies de Lille, CNRS UPRES-A 8013, BP 80, F-62930 Wimereux, France

[2] Present address: Departement of Ocean Science, Tokyo University of Fisheries, 4-5-7 Konan, Minato-ku, Tokyo 108, Japan

[3] Present address: University of Caen, IUT, Bd du Maréchal Juin, F-14032 Caen cedex, France

Abstract. In the tidally mixed coastal waters of the Eastern English Channel, the vertical structure of temperature, salinity and *in vivo* fluorescence have been characterised in terms of fractal dimensions, while light transmission did not exhibit such structures. Thus, on the basis of a sampling strategy conduced during five years in both offshore and inshore waters of the Eastern English Channel, we showed that, while temperature and salinity fractal structure is tidally and geographically independent, fluorescence fractal dimensions are (i) significantly higher in offshore locations, (ii) dependent on the current direction at the scale of the high-low tidal cycle, (iii) dependent on the current speed at the scale of the neap-spring tidal cycles, and (iv) dependent on phytoplankton concentration at the biological annual cycle. Finally, a fractal modelling approach showed that the impact of this space-time structure of phytoplankton biomass vertical structure on primary production estimates could be potentially very important, essentially for inshore waters and in high phytoplankton density conditions. Moreover, the relative importance of vertical phytoplankton distribution on primary production estimates has been demonstrated to lie in the occurrence and persistence of small-scale phytoplankton layers, opening new perspectives on the understanding of structure and functioning of marine systems.

Introduction

Marine systems exhibit intimate relationships between physical and biological processes (Legendre & Demers 1984, Mackas et al. 1985), as shown by the coupling between the distribution of phytoplankton populations and the structure of their physical environment over a wide range of spatial and temporal scales (Haury et al. 1978).

In particular, in tidally mixed coastal waters such as the Eastern English Channel, the dissipation of tidal energy is basically regarded to be responsible for the vertical homogenisation of the shallow (50 m maximum depth) inshore and offshore water masses. However, recent investigations have shown that the variability perceived in temperature, salinity and phytoplankton biomass fluctuations can be wholly characterised in terms of heterogeneity over a wide range of scales (Seuront et al., 1996a, b, 1999) and that this heterogeneity cannot be neglected (Seuront et al., 1999). In particular, Seuront & Lagadeuc

(1998) demonstrated that the vertical distribution of phytoplankton biomass, basically regarded as vertically homogenised by vertical mixing—and then characterised by a mean concentration and its associated variability (i.e. the variance S^2)—should also be regarded as being vertically structured in terms of fractal dimension. Moreover, this fractal structure appears to be both space and time-dependent, in relation respectively with the inshore-offshore hydrological gradient and the tidal advective processes. However, these results, based on the analysis of the data recorded along an inshore-offshore transect, and characterised by an extreme intricacy of space-time scales and processes and to severe limitations in terms of sampling temporal resolution, led to a lack of generality concerning the processes responsible for the observed structure for both inshore and offshore locations.

Herein, the goal of this paper is to provide a precise quantification of the vertical structure of phytoplankton distribution at the scale of the high-low tidal cycles and at the scale of neap-spring tidal cycles for both inshore and offshore waters of the Eastern English Channel in order to specify and generalise preliminary results by Seuront & Lagadeuc (1998). Moreover, considering that vertical mixing could control daily primary production rates at the scale of the high-low tidal cycles at spring tide and at the scale of neap-spring tidal cycles in shallow coastal waters, leading to increased primary production estimates from 40 to 100% (Lizon et al. 1995, Lizon 1997, Lizon & Lagadeuc 1998), we also explore a modelling hypothesis based for the very first time on fractal simulations of the vertical fractal structure of phytoplankton biomass on primary production estimates.

	Sampling date	Tidal conditions	Sampling site	Chl. *a* ($\mu g.l^{-1}$)	Profiles
S1	29/04/93 - 01/05/93	NT	OW	1.50	36
S2	20/03/94 - 21/03/94	NT	CW	1.50	36
S3	07/09/94 - 08/09/94	ST	CW	7.50	24
S4	02/04/96 - 04/04/96	ST	CW	13.80	47
S5	06/04/1996	ST	CW	15.00	15
S6	07/04/1996	ST	OW	3.00	13
S7	21/06/1998	ST	CW	8.40	24

Table 1. Main characteristics of the seven sampling experiments considered in the present study including tidal conditions (NT: neap tide; FT: flood tide), sampled water masses (IW: inshore waters; OW: offshore waters), mean chlorophyll a concentration (averaged over the whole water column) and the number of recorded profiles

Material and methods

The data. The data set studied in this paper consists in hourly measurements of physical parameters (temperature, salinity and light transmission) and *in vivo* fluorescence (i.e. an index of phytoplankton biomass) taken from the surface to bottom with an SBE 25 Sealogger CTD and a Sea Tech fluorometer during seven sampling experiment (numbered from S1 to S7) conduced between 1993 and April 1997 in different tidal conditions both in offshore and inshore waters of the Eastern English Channel (Fig. 1; Table 1). Current speed and direction were recorded with Aanderaa current meter every 5 minutes at different depths (Table 1). Water samples were collected from each sampled depth at 2 h intervals for data sets S1 to S4 and at 1 h intervals for data sets S5 to S7, and chlorophyll *a* concentrations [1 l filtered frozen samples, extracted with 90% acetone, assayed in a spectrophotometer and the chlorophyll *a* concentration calculated following Strickland & Parson (1972)] were estimated for each sampled depth.

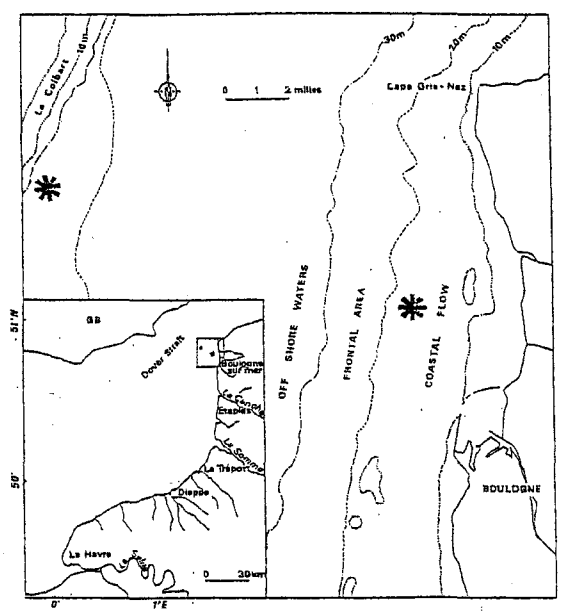

Fig. 1. The study area showing the two sampling stations, and the inshore and offshore waters of the Eastern English Channel

Fractal analysis. Fractal dimensions, whose applicability to planktonology has recently been demonstrated (Seuront & Lagadeuc 1997, 1998), were estimated using a method based on geostatistics and regionalised variables (RV) theory (Journel & Huijbregts 1978). The variations between measurements of RV is expressed by the semivariogram $\gamma(h)$, defined as:

$$\gamma(h) = \frac{1}{2N(h)} \sum_{i=1}^{N(h)} [Z(x_i) - Z(x_i + h)]^2 \qquad (1)$$

where $z(x_i+h)$ is the value of the observation $z(x_i)$ at a point separated from point i $(i=1,2,\ldots,N)$ by distance, or lag, h, and $N(h)$ is the number of pairs of observations separated by the lag h. The function $z(x_i)$ is said to be intrinsically stationary if its expectation $E\{z(x_i)\}$ is constant (i.e. $\mu(x)=\mu$), and the variance of the difference between $z(x_i)$ and $z(x_i+h)$ is finite. At the same time both the expectation and the variance are assumed to be independent of the position x (i.e. for a vertical profile, expectation and variance depend only on its length and not of the absolute location). In this paper stationarity was not intrinsically assumed, but was tested by calculating Kendall's coefficient of rank correlation, τ, between the profile and the x-axis values in order to detect the presence of a linear trend (Kendall & Stuart 1966; see Seuront & Lagadeuc (1997) for further details). We thus eventually detrended the time series by fitting linear regressions to the original data by least squares and used the regression residuals in further analysis, a common remedial procedure in time series analysis (Fuller 1976).

The fractal dimension D can thus be estimated from the slope m of a log-log plot of the semivariogram of $z(x_i)$ as:

$$D=(4-m)/2 \tag{2}$$

Furthermore, the appropriate range of h values to include in the regression was determined using the values of h which maximised the coefficient of determination (r^2) and minimised the total sum of the squared residuals for the regression (Seuront & Lagadeuc 1997). For vertical profile, the fractal dimension D takes values between 1 and 2. A low D value means that the heterogeneity is high (strong autocorrelation both in weak and high values of h) and there may be dominant log-range effects, while high D value indicates that the variable is randomly distributed in space (weak or no autocorrelation) and that only weak short-range effects exist [e.g. Seuront & Lagadeuc (1997) for further details]. In this paper, the fractal dimension is regarded as a measure of the degree of spatial dependence of a variable. So the relation of D to the sampling scale indicates the trend of the spatial structure of the variable.

Primary production estimates and fracatl model. Primary production rate can be predicted by the empirical model of Platt et al. (1980), as a function of the light incident I, photosynthetic parameters P_m^B, α^B and β^B, and chlorophyll a concentration B:

$$P(I;P_m^B;\alpha^B;\beta^B)=B\cdot P_m^B(1-e^{(-\alpha^B I/P_m^B)}).e^{(-\beta^B I/P_m^B)} \tag{3}$$

where P_m^B is the photosynthetic capacity [maximum of the photosynthesis-irradiance curve], α^B is the photosynthetic efficiency (slope of the photosynthesis-irradiance curve at low light

intensity, and β^B a photoinhibition indice (slope of the photosynthesis-irradiance curve at high irradiance) [see Lizon et al. (1998) for further details].

Rather than considering the chlorophyll *a* concentration B of a single cell or a vertical mean value of phytoplankton biomass as usually done (Montagnes & Berger 1994, Lizon et al. 1998), we simulate heterogeneous vertical distributions of phytoplankton biomass $B(z)$ (z is the depth) on the basis of a random midpoint displacement algorithm (Saupe 1988) based on our previous empirical estimates of fluorescence fractal dimension. While this algorithm have been shown to diverge slightly from a true fractional Brownian motion (Mandelbrot 1982), it has nevertheless been included as a part of some computer graphics reference text books (Hearn & Baker 1986, Harrington 1987). Moreover, we preferred this algorithm to the straight forward spectral methods (Yaglom 1962, Priestley 1981) because, due to the nature of Fourier transforms [see e.g. Peitgen & Saupe (1988) for further details], the generated samples are periodic.

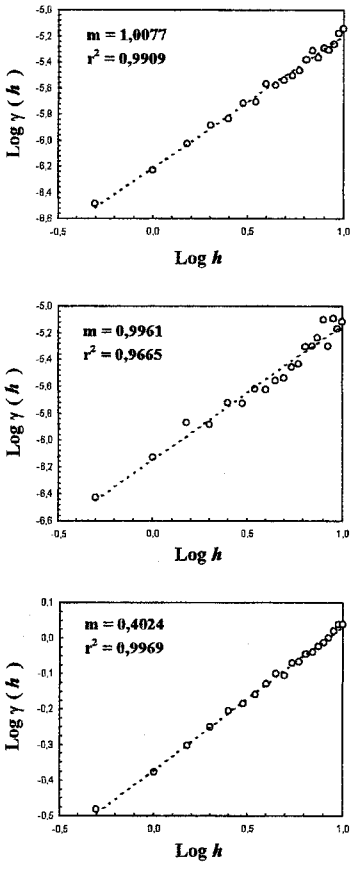

Fig. 2. Double logarithmic semivariograms of temperature, salinity and *in vivo* fluorescence (from top to bottom) for sampling experiment S1, shown together with their best fitting line. m is the slope of the empirical semivariance $\gamma(h)$ versus the lag h , in a log-log plot

Results

Fractal dimensions were estimated for *in vivo* fluorescence, temperature and salinity which exhibited a scaling behaviour over the whole range of studied scales, for the whole data set (Fig. 2). Their linearity over the whole range of spatial scales illustrates spatial dependence, suggesting that the same process, or at least similar processes, can be regarded as the source of physical and biological patterns, whatever the sampling locations or the hydrodynamical conditions. However, the mean fractal dimensions of temperature, salinity and *in vivo* fluorescence, estimated for the whole data set as 1.52 (±0.02 SD), 1.53 (±0.02 SD) and 1.63 (±0.14 SD), respectively, were significantly different (Kruskal-Wallis test, $p < 0.05$), the temperature and salinity fractal dimensions being not significantly different (Dunn test, $p > 0.05$; Siegel & Castellan 1988). At the scale of the whole sampling experiment, the vertical distribution of phytoplankton cells then cannot be regarded as being wholly driven by vertical mixing. Finally, as previously shown by Seuront & Lagadeuc (1998), it must be added that light transmission did not exhibit even a partial scaling behaviour (i.e. its variability is independent of scale), and therefore could not have been subjected to fractal analysis.

	Temperature	**Salinity**	***In vivo* fluorescence**
S1	1.50 (0.05)	1.52 (0.04)	1.82 (0.07)
S2	1.52 (0.06)	1.53 (0.05)	1.63 (0.09)
S3	1.54 (0.03)	1.50 (0.04)	1.57 (0.09)
S4	1.52 (0.04)	1.54 (0.06)	1.46 (0.12)
S5	1.53 (0.05)	1.53 (0.04)	1.54 (0.10)
S6	1.49 (0.03)	1.52 (0.05)	1.82 (0.06)
S7	1.53 (0.04)	1.55 (0.06)	1.56 (0.10)

Table 2. The mean fractal dimension of temperature, salinity and *in vivo* fluorescence for the seven sampling experiments, shown together with their standard deviation

The mean empirical estimates of the fractal dimensions D of temperature, salinity and *in vivo* fluorescence estimated for each sampling experiment lead to further results (Table 2). Thus, we showed that there were no significant differences between salinity and temperature between each sampling experiment (Kruskal-Wallis test, $p > 0.05$). On the contrary, *in vivo* fluorescence fractal dimensions were significantly different ($p < 0.05$) and exhibited very specific behaviours. Thus, fluorescence fractal dimensions were significantly lower for inshore than for offshore locations (Wilcoxon-Mann-Whitney U-test, $p < 0.05$), with values ranging

from 1.54 (±0.12 SD) to 1.82 (±0.07 SD), respectively. Moreover, correlation analysis demonstrated that fluorescence fractal dimensions were significantly correlated ($p < 0.05$) with current direction for each sampling experiment (i.e. at the scale of the high-low tidal cycle) for both inshore and offshore waters (Table 3), except for sampling experiment S1 and S2 characterised by their very low chlorophyll *a* concentrations (cf. Table 1). On the contrary, there were no significant correlations between fluorescence fractal dimension and current speed, nor between fluorescence fractal dimension and phytoplankton biomass at the scale of the high-low tidal cycles.

	D / $C_{Direction}$	D / C_{Speed}	D / Chl. *a*
S1	0.22	0.22	0.10
S2	0.19	-0.10	0.20
S3	0.76 **	-0.33	0.01
S4	0.79 **	-0.14	-0.19
S5	0.95 **	-0.12	0.36
S6	0.80 **	-0.20	-0.37
S7	0.89 **	-0.13	0.28

*: 5% significance level

**: 1% significance level

Table 3. Spearman's rank correlation coefficients between *in vivo* fluorescence fractal dimensions D and current direction (D / $C_{Direction}$), current speed (D / C_{Speed}), and mean chlorophyll *a* concentration (D / Chl. *a*)

However, at the scale of the neap-spring tidal cycles, fluorescence fractal dimension exhibited highly significant ($p < 0.001$) and significant ($p < 0.05$) positive correlations with current speed for inshore and offshore waters, respectively. *In vivo* fluorescence fractal dimensions were then all the more high as the hydrodynamical conditions were high. Moreover, there was also a significant ($p < 0.05$) correlation between mean fractal dimensions and mean chlorophyll *a* concentrations (Fig. 3), suggesting a density-dependent control of the vertical fractal structure of phytoplankton biomass distribution.

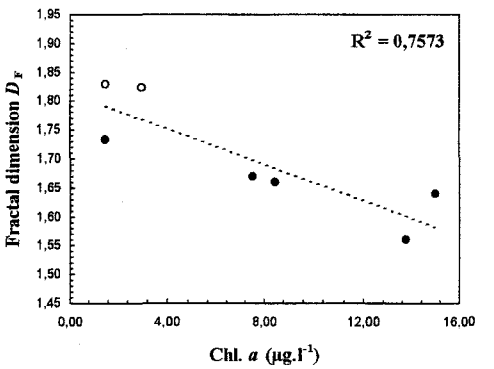

Fig. 3. Mean values of *in vivo* fluorescence fractal dimension D_F versus mean chlorophyll *a* concentrations, estimated for sampling experiments conduced both in offshore (open dots) and inshore (black dots) waters

In order to test the effect of the previously demonstrated space-time variability of the fractal phytoplankton distributions on primary production estimates, we simulated the vertical distributions of phytoplankton biomass for fractal dimensions ranging from 1.27 to 1.75 for inshore waters and from 1.70 to 1.95 for offshore waters (i.e. the lower and upper bounds of our empirical estimates) in order to reproduce the conditions encountered in the seven sampling experiments considered here. The resulting simulations were then systematically submitted to semivariogram analysis to ensure that their efficiency was optimal. Thus, the simulated heterogeneous phytoplankton distributions were very similar to the empirical ones (Fig. 4; Table 4). The primary production rates were subsequently estimated on the basis of

D	D_{RMD}
1.25	1.22 (0.03)
1.30	1.31 (0.05)
1.35	1.36 (0.04)
1.40	1.42 (0.02)
1.45	1.47 (0.02)
1.50	1.54 (0.06)
1.55	1.52 (0.04)
1.60	1.58 (0.03)
1.65	1.64 (0.06)
1.70	1.70 (0.02)
1.75	1.72 (0.02)
1.80	1.81 (0.03)
1.85	1.85 (0.02)
1.90	1.89 (0.03)
1.95	1.98 (0.05)

Table 4. Comparisons between the fractal dimension inputs of our simulations (D) and the fractal dimension estimated from our random midpoint displacement (RMD) simulations on the basis of semivariogram analysis (D_{RMD}). The mean dimension D_{RMD} results from 100 simulated phytoplankton distribution for each of the 15 conditions considered here and are shown together with their standard deviation

100 phytoplankton distributions $B(z)$ for each conditions (i.e. fractal dimension) considered. Finally, the primary production outcomes have been estimated as the percentage difference between primary production estimates obtained with homogeneous and heterogeneous (i.e. fractal) phytoplankton distribution, i.e. respectively P_{Homo} and P_D (Fig. 5). Thus, whatever the water masses and the tidal conditions considered, the primary production outcomes cannot be statistically regarded as being different (Kruskal-Wallis test, $p < 0.05$), nor statistically distinguished from a zero value (Binomial test, $p > 0.05$; Siegel & Castellan 1988). However, the amplitude of primary production outcome obtained in flood conditions for inshore waters is significantly higher than those obtained both for offshore waters and inshore waters ebb conditions (Siegel-Tuckey test for scale differences, $p < 0.01$; Siegel & Castellan 1988).

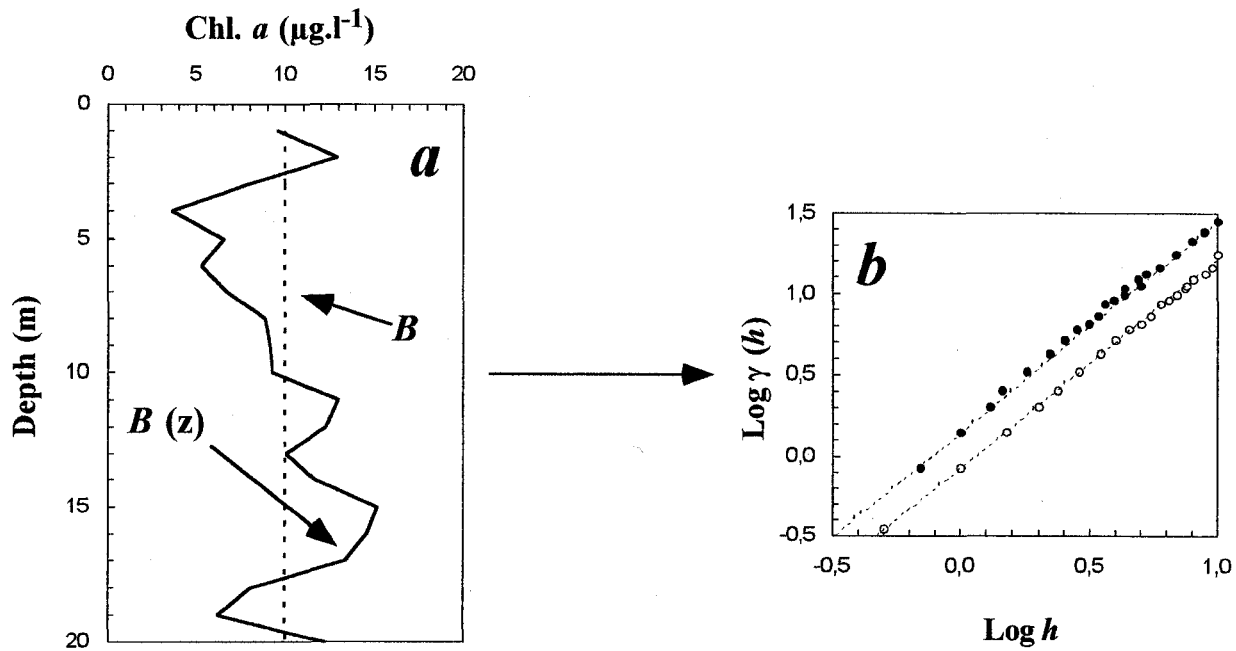

Fig. 4. Heterogeneous phytoplankton distribution $B(z)$ simulated on the basis of a fractal dimension of 1.35 in the random midpoint displacement algorithm and homogeneous phytoplankton distribution B in relation to depth (**a**), and (**b**) comparison between semivariograms computed from empirical data (open dots) and from simulated data (black dots). Both homogeneous and heterogeneous phytoplankton distributions have a mean of 10 $\mu g.l^{-1}$.

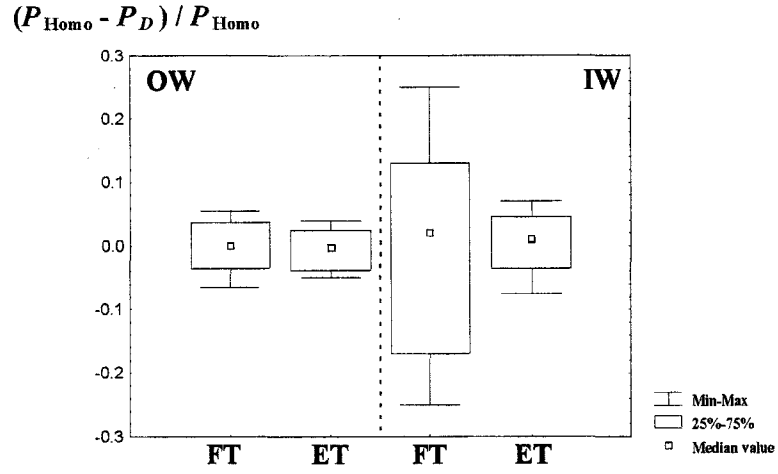

Fig. 5. Primary production outcomes estimated as the percentage difference between primary production estimates obtained with homogeneous (P_{Homo}) and heterogeneous (P_D) phytoplankton distributions for ebb and flood tide conditions in offshore (OW) and inshore (IW) waters.

Discussion

Biological-physical vertical structure

The empirical fractal dimensions, estimated over the whole range of available spatial scales suggest that the scales of spatial dependence are very similar for *in vivo* fluorescence, salinity and temperature, indicating similar sources of physical and biological patterns. However, the differences shown between fractal dimensions of temperature, salinity and fluorescence fractal dimensions suggest that the vertical distribution of phytoplankton cells is very specific and cannot be regarded as being passively advected by mixing processes, even when chlorophyll *a* concentrations are very low as it is the case for sampling experiment S1 and S2 (cf. Table 2). Thus, as shown by the correlation analysis, fractal dimension of temperature and salinity are tidally and geographically independent, in opposition to fluorescence fractal dimensions which are (i) significantly higher in offshore locations, (ii) dependent on the current direction at the scale of the high-low tidal cycle, (iii) dependent on the current speed at the scale of the neap-spring tidal cycles, and (iv) dependent on phytoplankton concentration at the biological annual cycle. The vertical structure of phytoplankton biomass is then more homogeneous, or less structured, in offshore locations and during flood, but also when hydrodynamical conditions are high and phytoplankton concentrations are low, showing that the structure of the vertical distribution of phytoplankton biomass is determined by different processes following the implied temporal scales.

These results then confirm and generalise previous studies conduced in the same environment (Seuront & Lagadeuc, 1998). In particular, fluorescence fractal dimensions being higher for offshore than for inshore waters, these differences could be associated to a purely

density-dependent effect (Seuront & Lagadeuc, 1998), to a qualitative effect relative to the specific composition of phytoplankton assemblages (Truffier et al. 1997, Peta et al. 1998), or to a combination of the two previous hypothesised phenomenologies. Whatever that may be, an increased in fluorescence fractal dimensions should have been expected during flood, because of the offshore waters advection associated with the semidiurnal M2 tidal component, instead of the significant decrease generally observed. At the scale of the high-low tidal cycles it can then be suggested that the observed differential tidal structure of phytoplankton distribution could be rather associated to the differential mixing occurring during a tidal cycle between water masses qualitatively and quantitatively different in terms of phytoplankton populations which could then be regarded as a secondary source of heterogeneity. On the other hand, at the scale of the neap-spring tide cycles phytoplankton distributions appear controlled by hydrodynamical conditions, high hydrodynamical conditions leading to more homogeneous distributions characterised by high fractal dimensions. Finally, comparisons between mean fractal dimensions of fluorescence and mean chlorophyll *a* concentrations for each sampling experiment confirm the density-dependent control of phytoplankton structure proposed by Seuront & Lagadeuc (1998) as a potential explanation of the different fractal dimensions observed for the vertical distribution of phytoplankton biomass between inshore and offshore waters. In particular, this means that the heterogeneity of phytoplankton is all the more high as its density is high, and the observed density-dependence could be a consequence of the aggregation processes of phytoplankton cells, mainly driven by phytoplankton density and hydrodynamism (e.g. Kiørboe 1997).

Whatever that may be, given the previously demonstrated control of phytoplankton distribution at the scales of the high-low and neap-spring tidal cycles and at the seasonal scale, the question is now to estimate the effect of these vertical phytoplankton distribution variations on the primary production rates.

Primary production rates versus vertical heterogeneity

While the previously estimated primary production outcomes were very similar and close to zero whatever the water masses and the tidal conditions, the highly fluctuating primary production outcome obtained in flood conditions for inshore waters nevertheless implies some comments on the approaches used in the present paper. Thus, if one considers two vertical phytoplankton distributions obtained from the same fractal dimensions, the related primary production estimates will be extremely dependent on the depth at which high and low

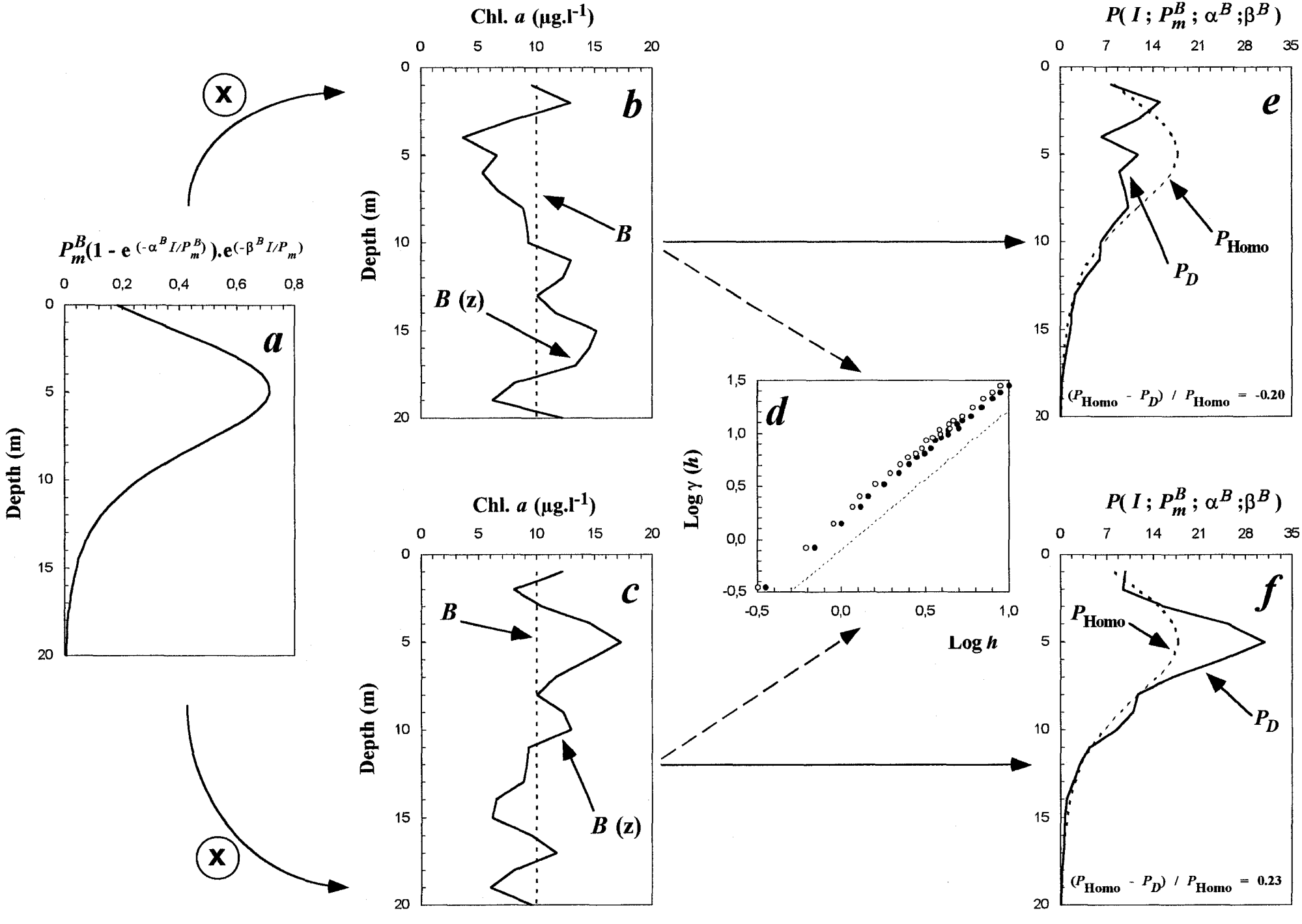
Chl. a (µg.l-1)
0 5 10 15 20
Depth (m)
b
B
B (z)
P(I ; PmB ; αB ;βB)
0 7 14 21 28 35
e
PHomo
PD
(PHomo - PD) / PHomo = -0.20
PmB(1 - e (-αB I/PmB)).e(-βB I/Pm)
0 0,2 0,4 0,6 0,8
a
Depth (m)
x
x
Chl. a (µg.l-1)
0 5 10 15 20
Depth (m)
c
B
B (z)
d
Log γ (h)
1,5
1,0
0,5
0,0
-0,5
-0,5 0,0 0,5 1,0
Log h
P(I ; PmB ; αB ;βB)
0 7 14 21 28 35
f
PHomo
PD
(PHomo - PD) / PHomo = 0.23

Fig. 6. The non-linear function of the photosynthetic parameters P_m^B, α^B and β^B (**a**) [shown here at solar midday for the typical coastal waters values of P_m^B, α^B and β^B given by Lizon et al. (1998), their table 1] multiplied by homogeneous and heterogeneous distributions of phytoplankton B and $B(z)$ (**b**, **c**) [see Eq. (3)] can lead to very different primary production outcomes (**e**, **f**) depending on the depth at which the high and low phytoplankton concentration layers occurs (**b**, **c**). Heterogeneous phytoplankton distributions $B(z)$ leading to different primary production estimates have nevertheless exactly the same fractal characteristics, shown here by open and black dots and compared with the empirical slope (dashed line) of the empirical semivariance $\gamma(h)$ versus the lag h, in a log-log plot (**d**)

concentration phytoplankton layers occur, leading to significant differences in the primary production outcome which range from a 25% decrease to a 25% increase when compared with the results obtained with a homogeneous distribution of phytoplankton biomass from surface to bottom (Fig. 6). This approach is conceptually different from previous works devoted to estimate primary production rates on the basis of Lagrangian simulations of individual phytoplankton cells photoadaptation processes in relation with vertical mixing intensity (Lizon et al. 1998). Our results are nevertheless roughly compatible with the high-low tide and neap-spring tide control of primary production via vertical mixing intensity (Lizon et al. 1998). In that way, such approaches could be advantageously coupled with some Lagrangian model of aggregation (Yamazaki & Haury 1993, Yamazaki & Okubo 1995) in order to provide a more precise phenomenological basis to the existing model of fractal simulations, such as the random midpoint displacement algorithm used in the present paper, and then to deal with more realistic features of phytoplankton distributions.

More generally, these results raised a critical problem for primary production estimates in turbulent coastal waters. Thus, following the potential importance of small-scale phytoplankton layers in primary production estimates, the question is now to estimate the number of persistent layers and how long they persist. Both being dependent on physical and biological processes (Cowles et al. 1998), this opens very large perspectives for future studies devoted to the understanding of the formation and persistence of phytoplankton layers, and more generally to the understanding of the physical-biological couplings in the ocean.

Concluding remarks

Recent studies have revealed that the phytoplankton and zooplankton distributions are particularly complex and structured even in high hydrodynamic conditions (e.g. Pascual et al. 1995, Seuront et al. 1996a, b, 1999, Seuront & Lagadeuc 1997, 1998). Moreover, the

knowledge of the precise distribution of organisms in the ocean is now widely recognised to be a critical problem in understanding ecosystems structure and functioning, and in obtaining robust estimates of stocks and fluxes (Platt et al. 1989). In that way, our data demonstrate that the vertical distribution of phytoplankton biomass can be regarded as being highly structured (in terms of fractal structure), and is far from being homogenised by vertical tidal mixing in the coastal ocean. Furthermore, our simulations show the potential importance of the vertical distribution of phytoplankton biomass in the primary production estimates, especially for inshore waters at the scale of the high-low tidal cycles and at the scale of the neap-spring tidal cycles and when phytoplankton density is high.

The present work finally demonstrated that primary production in coastal seas—such as the Eastern English Channel—would not be only a function of light intensity and nutrient concentrations (e.g. Moloney et al. 1986, Hoch & Ménesguen 1995, Ménesguen & Hoch 1995), or photoadaptation processes related with vertical mixing intensity (Lizon et al. 1995, Lizon & Lagadeuc 1998), but also of phytoplankton biomass vertical distribution. In that way, the scheme proposed in the present work could not be only limited to the Eastern English Channel but following recent results concerning the microscale vertical structure of phytoplankton (e.g. Cowles et al. 1998, Jaffe et al. 1998) would also be applicable to aquatic systems over wide geographical range, and then have considerable applications on primary production rates estimation procedures.

Acknowledgements. We greatly acknowledge the captains and the crews of the NO 'Pluteus II', 'Côte d'Aquitaine' and 'Côte de la Manche' for their assistance during the sampling experiments.

References

Cowles TJ, Desiderio RA, Carr MA (1998) Small-scale planktonic structure: persistence and trophic consequences. Oceanography 11:4-9

Harrington S (1987) Computer graphics. A programming approach. McGraw-Hill, New York

Haury LR, McGowan JA, Wiebe PH (1978) Patterns and processes in the time-space scales of plankton distributions. In: Steele JH (ed) Spatial pattern in plankton communities. Plenum, New York, p 277-327

Hearn D, Baker MP (1986) Computer graphics. Prentice-Hall, Englewood Cliffs

Hoch T, Ménesguen A (1995) Modelling the biogeochemical cycles of elements limiting primary production in the English Channel. II. Sensitivity analyses. Mar Ecol Prog Ser 146:189-205

Fuller WA (1976) An introduction to statistical time series. Wiley

Jaffe J, Franks PJ, Leising AW (1998) Simultaneous imaging of phytoplankton and zooplankton distributions. Oceanography 11:24-29

Journel AG, Huijbregts CJ (1978) Mining geostatistics. Academic Press, London

Kendall M, Stuart A (1966) The advanced theory of statistics. Hafner, New York

Kiørboe T (1997) Small-scale turbulence, marine snow formation, and planktivorous feeding. Sci Mar 61:141-165

Legendre L, Demers S (1984) Towards dynamic biological oceanography and limnology. Can J Fish Aquat Sci 41:2-19

Lizon F, Lagadeuc Y (1998) Comparisons of primary production values estimated from different incubation times in a coastal sea. J Plankton Res 20:371-381

Lizon F, Seuront L., Lagadeuc Y. (1998) Photoadaptation and primary production study in tidally mixed coastal waters using a Lagrangian model. Mar Ecol Prog Ser 169: 43-54

Lizon F, Lagadeuc Y, Brunet C, Aelbrecht D, Bentley D (1995) Primary production and photoadaptation of phytoplankton in relation with tidal mixing in coastal waters. J Plankton Res 17:1039-1055

Mackas DL, Denman KL, Abbott MR (1985) Plankton patchiness: biology in the physical vernacular. Bull Mar Sci 37:652-674

Mandelbrot B (1977) Fractals. Form, chance and dimension. Freeman, London

Mandelbrot B (1982) Comment on computer rendering of fractal stochastic models. Comm. of the ACM 25: 581-583

Mandelbrot B (1983) The fractal geometry of nature. Freeman, New York

Ménesguen A, Hoch T (1995) Modelling the biogeochemical cycles of elements limiting primary production in the English Channel. I. Role of thermocline stratification. Mar Ecol Prog Ser 146:173-188

Moloney CL, Bergh MO, Field JG, Newell RC (1986) The effect of sedimentation and microbial nitrogen regeneration in a plankton community: a simulation investigation. J Plankton Res 8:427-445

Montagnes DJS, Berger JA (1994) Estimating carbon, nitrogen, protein, and chlorophyll *a* from volume in marine phytoplankton. Limnol Oceanogr 39:1044-1060

Pascual M, Ascioti FA, Caswell H (1995) Intermittency in the plankton: a multifractal analysis of zooplankton biomass variability. J Plankton Res 17:1209-1232

Peitgen HO, Saupe D (1988) The science of fractal image. Springer-Verlag, New-York

Peta O, Hitier B, Olivesi R, Delesmont R, Morel M, Loquet N (1998) Suivi régional des nutriments sur le littoral nord/Pas-de-Calais/Picardie. Bilan de l'année 1997. IFREMER, Boulogne-sur-Mer

Platt T, Gallegos CL, Harrison WG (1980) Photoinhibition of photosynthesis in natural assemblages of marine phytoplankton. J Mar Res 38:687-701

Priestely MB (1981) Spectral analysis and time series, univariate series. Academic Press, London

Saupe D (1988) Algorithms for random fractals. In: Peitgen HO, Saupe D (eds) The science of fractal images. Springer-Verlag, New York, p 71-136

Seuront L, Lagadeuc, Y (1997) Characterisation of space-time variability in stratified and mixed costal waters (Baie des Chaleurs, Québec, Canada): application of fractal theory. Mar Ecol Prog Ser 159: 81-95

Seuront L, Lagadeuc, Y (1998) Spatio-temporal structure of tidally mixed coastal waters: variability and heterogeneity. J Plankton Res 20: 1387-1401

Seuront L, Schmitt F, Lagadeuc, Y, Schertzer D, Lovejoy S (1999) Universal multifractal analysis as a tool to characterize multiscale intermittent patterns: example of phytoplankton distribution in turbulent coastal waters. J Plankton Res 21: 877-922

Siegel S, Castellan NJ (1988) Nonparametric statistics. McGraw-Hill

Strickland JDH, Parsons TR (1972) A practical handbook of seawater analysis. Bull Fish Res Bd Can 167:1-311

Truffier S, Hitier B, Olivesi R, Delesmont R, Morel M, Loquet N (1997) Suivi régional des nutriments sur le littoral nord/Pas-de-Calais/Picardie. Bilan de l'année 1996. IFREMER, Boulogne-sur-Mer

Yaglom A (1962) An introduction of the theory of stationary random functions. Prentice-Hall, Englewood Cliffs

Yamazaki H, Haury LR (1993) A new Lagrangian model to study animal aggregation. Ecol. Model 69:99-111

Yamazaki H, Okubo A (1995) A simulation of grouping: an aggregating random walk. Ecol. Model 79:159-165

A20

Multiscale horizontal distribution of the calanoid copepod *Temora longicornis* in a turbulent coastal sea

Seuront L & Lagadeuc Y (manuscrit)

Multiscale horizontal distribution of the calanoid copepod *Temora longicornis* in a turbulent coastal sea

Laurent Seuront[1,2] and Yvan Lagadeuc[3]

[1] *Station Marine de Wimereux, Université des Sciences et Technologies de Lille, CNRS UPRES-A 8013 ELICO, BP 80, F-62930 Wimereux, France*

[2] *Present address: Department of Ocean Science, Tokyo University of Fisheries, 4-5-7 Konan, Minato-ku, Tokyo 108, Japan*

[3] *Université de Caen, IUT, Bd du Maréchal Juin, F-14032 Caen cedex, France*

Abstract. We present the evidence that intermittent variability in zooplankton abundance can be characterized in terms of multifractals. A 3-min resolution time series of the abundance of the calanoid copepod *Temora longicornis*, taken from a fixed mooring on the coastal waters of the Eastern English Channel during 66 hours, provided the data for our analysis. The multifractal nature of the abundance distribution of *T. longicornis* appears to be very specific in comparison with those of purely passive scalars (i.e. temperature and salinity), or phytoplankton biomass over similar range of scales in similar environments. Finally, we show that the multifractal distribution of *T. longicornis* can be wholly parametrized with the help of only three basic parameters in the frame of universal multifractals, opening very large perspectives for future modeling of pelagic ecosystem structures and functions.

Introduction

Heterogeneity in the distribution of zooplankton has been recognized for many years (e.g. Hardy, 1936) and has received considerable amount of attention since (Mackas *et al.*, 1985; Davis *et al.*, 1991). The phenomenon, however, has seldom been described precisely, although zooplankton patchiness is relevant to many aspects of biological oceanography (Daly and Smith, 1993). Quantitative analyses of zooplankton spatial patterns in the ocean using time series analysis and power spectral analysis (Mackas and Boyd, 1979 ; Tsuda *et al.*, 1993) and more recently fractal analysis (Tsuda, 1995) have generated a large body of observational and theoretical works (e.g. Powell and Okubo, 1994). However, a new field of marine research has recently been devoted to the characterization of marine intermittent patterns in the frame of multifractals (Pascual *et al.*, 1995; Seuront *et al.*, 1996a, b, 1999).

Multifractals can be viewed as a generalization of fractal geometry (Mandelbrot, 1983) initially introduced to describe the relationship between a given quantity and the scale at which it is measured. While fractal geometry describes the structure of a given pattern with the help of only one parameter (i.e. the so-called fractal dimension), multifractals characterize its detailed variability by an infinite number of sets, each with its own fractal dimension. More

precisely, multifractal approaches, which do not require any statistical preconception on the data, provide very good approximations—at all scales and all intensities—of the statistics of intermittently fluctuating patterns, and determine the probability distribution of the pattern values [see Pascual *et al.* (1995) and Seuront *et al.* (1999) for further details]. Moreover, the statistical consequence of intermittency being a strong departure from Gaussianity (Baker and Gibson, 1987), multifractals thus provide a powerful alternative to basic random walk and spectral methods implicitly based on Gaussian, or quasi-Gaussian, statistics (see e.g. Peitgen *et al.*, 1992). Thus, considering that in the general background of spatio-temporal intermittency encountered in the ocean (e.g. Platt *et al.*, 1989), knowledge of the precise statistics of any intermittent fields may avoid the bias introduced by chronic undersampling of an intermittent signal (Bohle-Carbonel, 1992), a stochastic multifractal framework is particularly well suited to describing the structure of quantities that vary intermittently such as phytoplankton and zooplankton distributions (Pascual *et al.* 1995, Seuront *et al.* 1996a, b, 1999).

The knowledge of the distribution of particles is thus essential in understanding the trophic transaction mechanisms that regulate the flows of energy and matters in the ocean (Davis et al., 1991). Indeed, both phytoplankton and zooplankton biomass are concentrated in numerous zones of continuously varying sizes and concentrations, and the food-signal generated by such complex structures has characteristics that traditional approaches using statistics based on spatial or temporal homogeneity are unable to resolve (Rothschild, 1992). Moreover, previous observations conducted on zooplankton distributions indicate that generally, larger life forms show more extreme spatial scale aggregations than do smaller and less mobile organisms (Mackas and Boyd, 1979; Mackas *et al.*, 1985; Daly and Smith, 1993). The understanding of pelagic ecosystem structure and function then requires the precise estimates of both predators and preys, i.e. phytoplankton and zooplankton, spatial patterns.

In particular, the calanoid copepod *Temora longicornis*, which is very abundant in temperate waters of the northern hemisphere, also appears to be of great ecological significance. Indeed, it represents 35 to 70% of the total population in the Southern Bight of the North Sea (Daan, 1989), and in Long Island Sound (USA), *T. longicornis* is able to remove up to 49% of the daily primary production (Dam and Peterson, 1993). In that way, following the recent empirical investigations conduced on phytoplankton distributions in the highly dissipative waters of the Eastern English Channel and the Southern Bight of the North Sea (Seuront *et al.*, 1996a, b, 1999), the aim of this paper is to investigate the distribution of the calanoid copepod *Temora longicornis*—a dominant species in these waters—in order to

provide further insights into the trophic interactions occurring in such turbulent coastal ecosystems.

Method

Study area and sampling

Sampling was conducted from 1 to 3 April 1997 in the Eastern English Channel during 66 hours (ca. 5.5 tidal cycles). The tidal range in this system is one of the highest in the world (ranging from 3 to 9 m). Tides generate a residual circulation parallel to the coast, drifting nearshore coastal waters from the English Channel to the North Sea. Coastal waters are influenced by freshwater runoff from the Seine estuary to the Strait of Dover, and then separated from offshore waters by a tide-controlled frontal area (Brylinski and Lagadeuc, 1990; Lagadeuc *et al.*, 1997; Figure 1). Sampling location has been chosen because its physical and hydrological properties are representative of the coastal water flow encountered in the Eastern English Channel (Lizon *et al.*, 1995; Lizon and Lagadeuc, 1998) where *Temora longicornis* is known to be very abundant and dominate zooplankton composition (Brylinski and Lagadeuc, 1988).

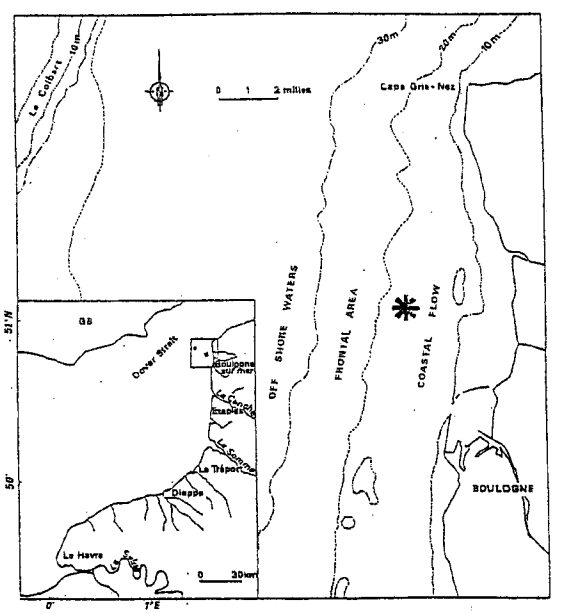

Fig. 1. Study area and location of the sampling station (*) along the French coast of the Eastern English Channel.

Since our aim was to investigate the horizontal distribution of *Temora longicornis*, water was continuously taken from a depth of 10 meters through a weighted down sea-water intake, and directly brought through a 200 µm mesh size plankton net by means of a Flight pump with

an output of 300 $l.mn^{-1}$, connected to 10 cm diameter plastic tubing. Every 3 minutes, filtered organisms were collected and immediately preserved in a 10% formaldehyde solution. The adult males and females were subsequently counted under a dissecting microscope from the 1321 collected samples. Figure 2 shows the resulting time series of the abundance of adults *Temora longicornis* which shows a significant 12.5 hours cycles, but exhibits a very intermittent 'background'.

Data analysis

After detrending, the scaling properties of empirical fields are usually tested using Fourier power spectral analysis, leading to a characteristic power-law form:

$$E(f) \approx f^{-\beta} \tag{1}$$

where f is frequency. This indicates absence of characteristic time-scale in the range of the power-law, i.e. a scaling behavior. The power-law form will manifests itself as an approximately straight-lined behavior of the power spectrum when plotted in a double-logarithmic diagram. One may note that for time series, the exponent β and the fractal dimension D are relating according to (Feder, 1988):

$$D = d + 1 - (\beta - 1)/2 \tag{2}$$

where d is the Euclidean dimension of the observation space (i.e. $d = 1$ for time series). However, power spectral analysis, implicitly assuming "quasi-Gaussian" statistics and limited to a second order statistic (i.e. the variance) characterizes very poorly quantities that vary

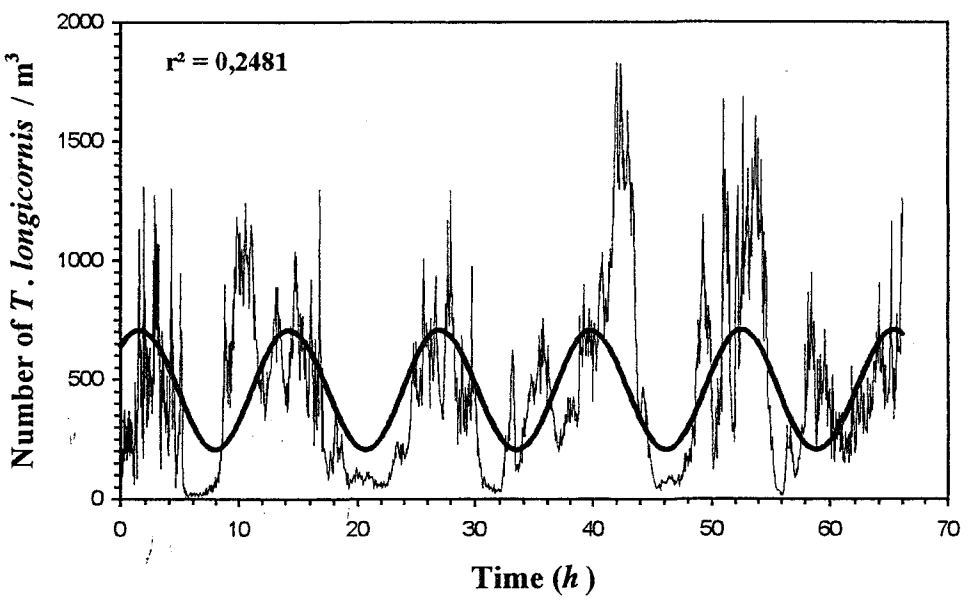

Fig. 2. Time series of *Temora longicornis* abundance ($ind.m^{-3}$) recorded at 10 m depth in the Eastern English Channel, shown together with the best tidal sinusoidal fit.

intermittently (i.e. occasional and unpredictable large peaks separated by very low values). We then adopt an empirical generalization of the widely used power spectral approach with the help of the q^{th} order structure functions:

$$\left\langle (\Delta Zoo_\tau)^q \right\rangle \approx \tau^{\zeta(q)} \tag{3}$$

where ΔZoo_τ is the fluctuations of the abundance of *Temora longicornis* at scale τ and angle brackets "$<.>$" indicate a statistical average, which is performed for all points of the *T. longicornis* abundance time series separated by a distance τ [i.e. $\left\langle (\Delta Zoo_\tau)^q \right\rangle$ are the statistical moments of the fluctuations $(\Delta Zoo_\tau) = |Zoo(t+\tau) - Zoo(t)|$]. The scaling exponent $\zeta(q)$ is estimated by the slope of the linear trends of $\left\langle (\Delta Zoo_\tau)^q \right\rangle$ vs. τ in a log-log plot. Eq. (3) gives the scale invariant structure functions exponent $\zeta(q)$, which characterizes all the statistics of the field. In particular, the first moment gives the scaling exponent $H = \zeta(1)$ corresponding to the scale dependency of the average fluctuations (ΔZoo_τ) : if $H \neq 0$ the latter will depend on the time scale τ, it therefore characterizes the degree of stationarity of the process. The second moment is linked to the slope, β, of the power spectrum by $\beta = 1 + \zeta(2)$. For simple scaling (fractal) processes, the scaling exponent of the structure function $\zeta(q)$ is linear [$\zeta(q) = q/2$ for Brownian motion, and $\zeta(q) = q/3$ for non-intermittent turbulence]. For multifractal processes, this function in nonlinear and concave (Seuront *et al.*, 1999).

A priori, the function $\zeta(q)$ could depend on a very large number—even an infinity—of parameters, therefore a very large number of its estimates for different values of q would be necessary. However, in the frame of universal multifractals (Schertzer and Lovejoy, 1987, 1989), $\zeta(q)$ is determined by only three parameters:

$$\zeta(q) = qH - \frac{C_1}{\alpha - 1}(q^\alpha - q) \tag{4}$$

where H is still given by $H = \zeta(1)$; the second term [i.e. the scaling moment function $K(q)$ characterizing the statistical behavior of a given intermittent process]:

$$K(q) = \frac{C_1}{\alpha - 1}(q^\alpha - q) \tag{5}$$

expresses the intermittent correction from homogeneity [in which case $\zeta(q) = qH$] of the process. C_1 is a codimension that characterizes the sparseness of the process, and is bounded between $C_1 = 0$ for a homogeneous space-filling process and $C_1 = d$ (d is the dimension of the space supporting the considered process, $d = 1$ for time series). With low C_1 value (i.e. close to

0), the field is almost everywhere close to its mean value; a large C_1 is characteristic of a field that has very low values almost everywhere except in some rare and sparse locations where it takes large values much greater than its mean value. The Lévy index α varies between 0 (a minimum value corresponding to a monofractal pattern) to a maximum of 2 (log-normal multifractal case) and indicates the degree of multifractality. As α increases, the more numerous are the variability levels bounded between lower and higher values of the process.

There are several ways to estimate the universal multifractal indices C_1 and α (see Seuront *et al.*, 1996a, b, 1999). However, we can easily estimate C_1 and α from Eq. (4): if Eq. (4) is differentiated and evaluated at $q = 0$, simple algebra shows that:

$$q\zeta'(0) - \zeta(q) = \frac{C_1 q^{\alpha}}{\alpha - 1} \tag{6}$$

Thus a log-log plot of $[q\zeta'(0) - \zeta(q)]$ vs. q will yield a straight line. The slope of the line is given by α and the corresponding C_1 value can be estimated by the intercept (Schmitt *et al.*, 1995). Once we know the parameter values, we can completely characterize the underlying multifractal process in a spatial or temporal variation. Finally, for a detailed discussion of what can be ecologically conclude from the use of multifractal algorithms, one may refer to Seuront *et al.* (1999).

Results

The estimation of the zooplankton power spectrum $E(f) \approx f^{-\beta}$ with $\beta = 1.42$ in a log-log plot shows an unique scaling regimes from smaller to larger scales (Figure 3). This indicates that the same process, or at list similar processes can be regarded as responsible for the scaling structure of the abundance of *Temora longicornis* from time scales ranging from 6 minutes to 66 hours. This range of temporal scales can be converted into spatial scales using the 'Taylor's hypothesis of frozen turbulence' (Taylor, 1938), which basically states that temporal and spatial averages t and l, respectively, can be related by a constant velocity v, $l = v.t$. Then using the mean instantaneous tidal circulation of 0.509 $m.s^{-1}$ observed during the field experiment at the sampling depth, the associated spatial scales ranges between 92 meters and 120 kilometers. Finally, the estimated power spectral exponent β estimated over this range of scales can be converted to a fractal dimension following Eq. (2) as $D = 1.79$.

This result can be confirmed and generalized in the frame of the q^{th} order structure functions (Figure 4). Thus, it clearly appears that for values of q ranging from 1 to 3, $\left\langle \left(\Delta Zoo_{\tau}\right)^{q} \right\rangle$ exhibits linear trends over the whole range of available time scales. The different

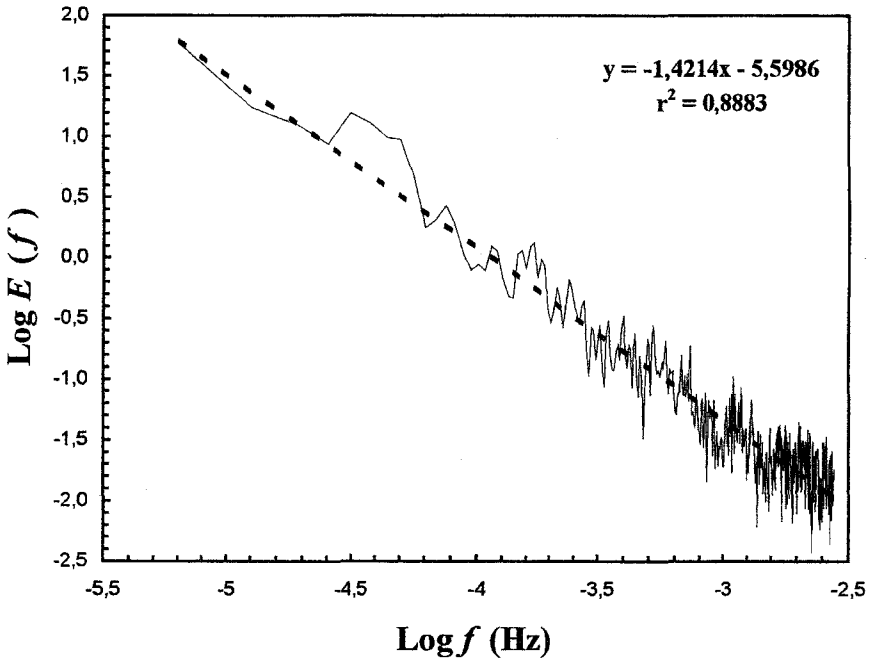

Fig. 3. The power spectrum of the *Temora longicornis* abundance data, shown in a log-log plot. The global straight line $f^{-1,42}$ is an indication of scaling for frequencies ranging from (6 min^{-1}) to (66 h^{-1}).

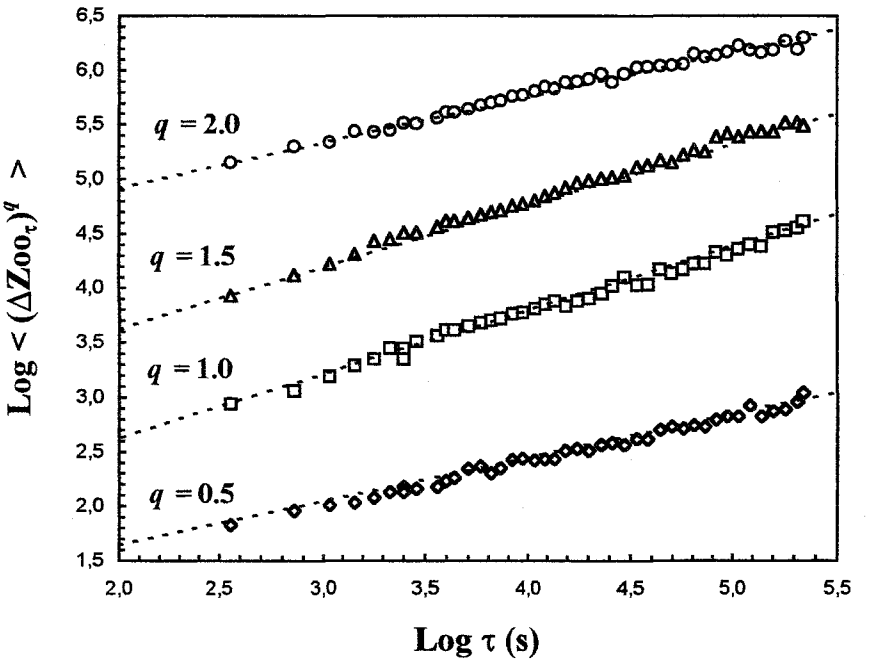

Fig. 4. The structure functions $\left\langle \left(\Delta Zoo_\tau\right)^q \right\rangle$ vs. τ in a log-log plot for q = 0.5, 1, 1.5, and 2. Linear trends are clearly visible for all order of moments, for a range of scales ranging from 6 min to 66 hours. The straight lines indicate the best linear regression over this range of scales for each value of q. This gives in particular $H = \zeta(1) = 0.58$, and $\zeta(2) = 0.41$.

values of the empirical exponent $\zeta(q)$ were estimated for a range of q values from 0 to 3 with a 0.1 increments. The empirical curve is clearly nonlinear, even for moments $q < 1$, showing that the abundance fluctuations of *T. longicornis* can be regarded as multifractal over the time scales ranging from 6 min to 66 h (Figure 5). In particular, the scaling of the first moment gives $H = \zeta(1) = 0.58$, indicating that the temporal distribution of *T. longicornis* is far from conservative, or stationary (in which case $H = 0$). The scaling of the second order moment confirms the estimate from the power spectrum: $\zeta(2) = 0.41$ (i.e. $\beta = 1 + \zeta(2)$).

We now estimate the universal parameters α and C_1 from Eq. (6). Figure 6 shows that $\alpha = 1.6 \pm 0.1$ and $C_1 = 0{,}44 \pm 0.02$, the error bars come from comparison between these α and C_1 estimates and those obtained from the Double Trace Moment technique (Lavallée, 1991; Lavallée *et al.*, 1992), which we also applied to the data and which has extensively been described elsewhere (see Seuront *et al.*, 1999). The theoretical curve corresponding to these values in Eq. (4) is shown in Figure 4 by a thick continuous line. The universal multifractal fit is excellent until moment order $q_{max} = 1.7$ after which the empirical curve (dots) is linear. This linear behavior of the empirical scaling exponent structure function $\zeta(q)$ for sufficient high order moments is well-known (Schertzer & Lovejoy, 1989) and is due to sampling limitations.

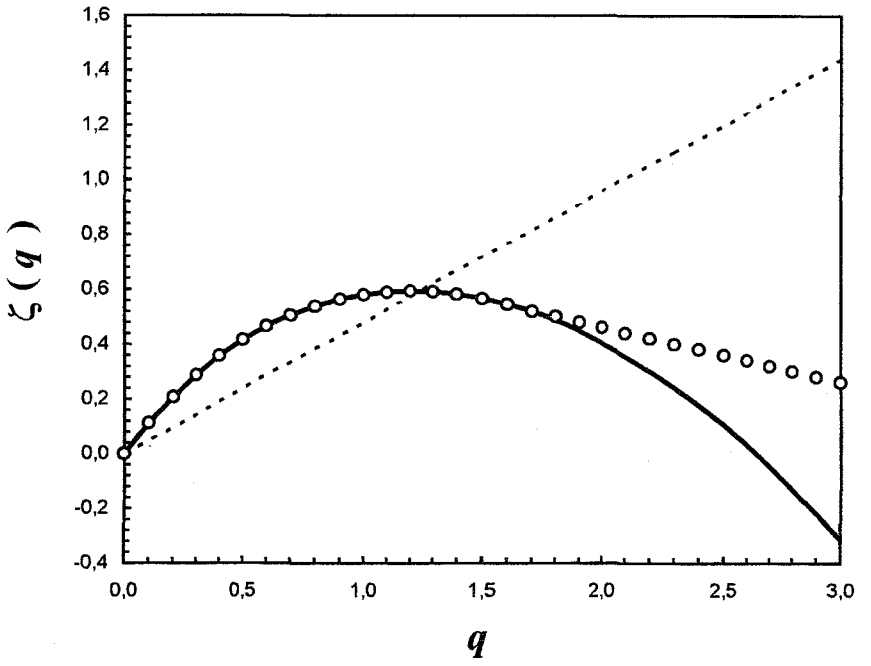

Fig. 5. The scaling exponent structure function $\zeta(q)$ empirical curves (dots) compared to the monofractal curve $\zeta(q) = qH$ (dashed line), and to the universal multifractal function (thick continuous line) obtained with $\alpha = 1.6$ and $C_1 = 0.44$ in Eq. (4). The universal multifractal fit is excellent until moment order $q_{max} = 1.7$, corresponding to a multifractal phase transition occurring because of sample limitations.

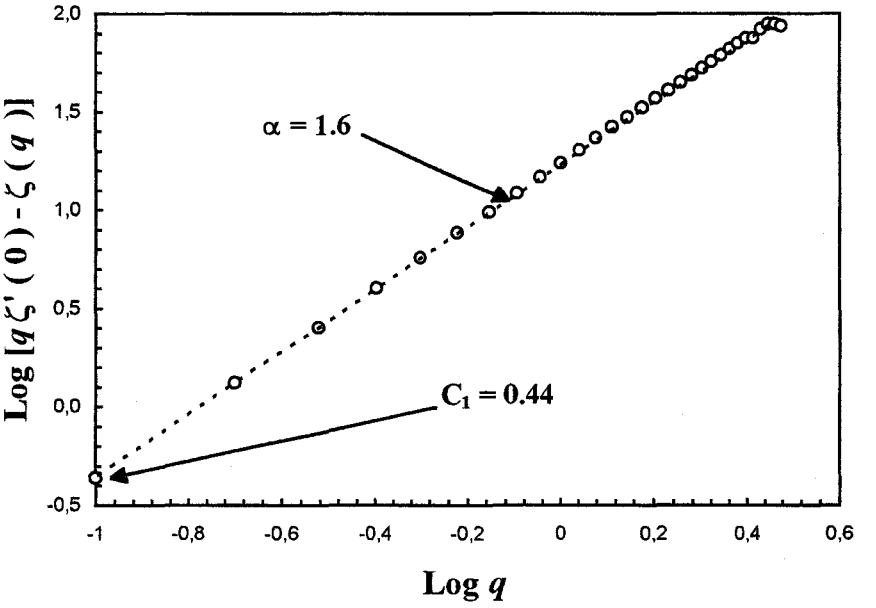

Fig. 6. Empirical curve $[q\zeta'(0)-\zeta(q)]$ vs. q in a log-log plot providing direct estimates of the universal multifractal parameters C_1 and α: α is the slope of the straight line and C_1 is estimated by the intercept, therefore $\alpha \approx 1.6$ and $C_1 \approx 0.44$.

Discussion

The recognition of patchiness is hardly new to plankton ecology; it was described within zooplankton communities over a century ago (Hackael, 1891). However, if a distribution is patchy, then conventional statistical methods become less useful as analytical tools due to violations in basic assumptions such as randomness. In that way, the main point of our multifractal approach is that it does not require any preconception on the data. In an intermittent framework, it should then be regarded as an alternative to the widely used spectral methods, implicitly based on Gaussian statistics (e.g. Platt and Denman, 1975), but also to the more recently developed one-dimensional neighbor techniques devoted to estimate zooplankton patch size and based on an untenable assumption of a regular distribution of patches (Shiyomi and Yamamura, 1993; Currie *et al.*, 1998). In particular, both the fractal and universal multifractal frames used here characterize the structure of the whole variability of a given intermittent pattern with respectively one and three basic parameters, and then allow direct comparisons to be made between biological and physical fields.

Our fractal dimension estimates of the *Temora longicornis* distribution can then be compared with those estimated from oceanic turbulence and both phytoplankton and zooplankton distributions. Reported fractal dimensions of two dimensional oceanic turbulence

then range from 1.2 to 1.4 (Osborne *et al.*, 1989; Osborne and Caponio, 1990; Sanderson and Booth, 1991), while the theoretical spectral exponent $\beta = 3$ (Kraichnan, 1967) of two dimensional turbulence leads to a fractal dimension $D = 1.50$. On the other hand, in three dimensional turbulence, the fractal dimension related to the theoretical spectral exponent $\beta = 5/3$ expected in the case of purely passive scalar (Kolmogorov, 1941) is $D = 5/3$. Therefore, the estimated fractal dimensions for *T. longicornis* distribution ($D = 1.79$) are significantly higher than those of oceanic turbulence. This fractal dimension is also higher than those of phytoplankton distributions estimated from *in vivo* fluorescence time series in the Southern Bight of the North Sea and the Eastern English Channel which range between 1.61 and 1.67 (Seuront *et al.*, 1996a, b, 1999). Higher fractal dimension corresponds with weaker wavenumber dependence in the power spectrum. Indeed, copepods and zooplankton differ in their size and motility. We then speculate that copepod behaviors such as diel migration, phototaxis, rheotaxis, and social behaviors should cause the larger fractal dimensions (i.e. flatter power spectrum) in comparison with phytoplankton. Indeed, Steele and Henderson (1992) suggested that a zooplankton mortality term given as a stochastic variant and random redistribution associated with diel vertical migration combined with vertical shear could lead to a flatter spectrum for zooplankton in a numerical experiment based on the Lotka-Volterra equations with diffusion terms. In other words, because zooplankton are subjected to more stochastic processes determining their distribution than phytoplankton, zooplankton show a more fragmented and space-filling distribution. Finally, one may note that the fractal distribution estimated here from the distribution of *T. longicornis* is very similar to the one estimated for the oceanic copepod *Neocalanus cristatus* abundance transects from the subarctic Pacific, i.e. $D = 1.80$, over a similar range of scales (i.e. between tens of meters and over 100 kilometers), suggested that the distribution of zooplankton species could be very similar whatever their surrounding environments.

Comparisons of the universal multifractal parameters estimated in the present study with those of other phytoplankton and zooplankton dataset lead to further results. The values of the parameter H ($H = 0.58$) and C_1 ($C_1 = 0.44$), are then obviously higher than those of phytoplankton biomass over similar ranges of scales, i.e. $H \in [0.12 - 0.34]$ and $C_1 \in [0.02 - 0.05]$ (Seuront *et al.*, 1996a, b). That leads to view zooplankton distribution as being less conservative and more sparse (i.e. characterized by low values except in some rare and sparse location where it takes large values much greater than its mean value) than those of phytoplankton. On the contrary, the parameter $\alpha = 1.60$ is within the range of α values

estimated for phytoplankton distributions (Seuront *et al.*, 1996a, b, 1999). These high values indicate that singularities of all magnitudes contribute significantly to the multifractal processes underlying our measured *T. longicornis* abundance. In other words, we are very far from the monofractal case. The differences found between the values of the parameters H and C_1 for zooplankton and phytoplankton then confirms the observations conducted in the monofractal frame concerning the influence of mobility of zooplankton on their spatial distribution. These differences also confirm that generally, larger life forms show more extreme spatial scale aggregations than do the smaller and less mobile organisms, which in the multifractal sense corresponds to larger C_1 values. One may also note that the D_q multifractal formalism used by Pascual *et al.* (1995) can be related with our scaling moment function $K(q)$ formalism as:

$$D_q = d - K(q) \tag{7}$$

where d is the Euclidean dimension of the observation space (i.e. $d = 1$ for time series and transects). In particular, we have $D_2 = 1 - K(2)$, leading to $D_2 \approx 0.38$ from Pascual *et al.* (1995) and $D_2 = 0.24$ from the present study. This suggests that the intermittency perceptible in the present dataset is higher than in the former dataset. However, this difference might be due to the better quality and resolution of the present dataset as so far as the acoustic data analyzed by Pascual *et al.* (1995) were constructed by averaging measurements vertically and hourly, and corresponds to a multispecies zooplankton biomass.

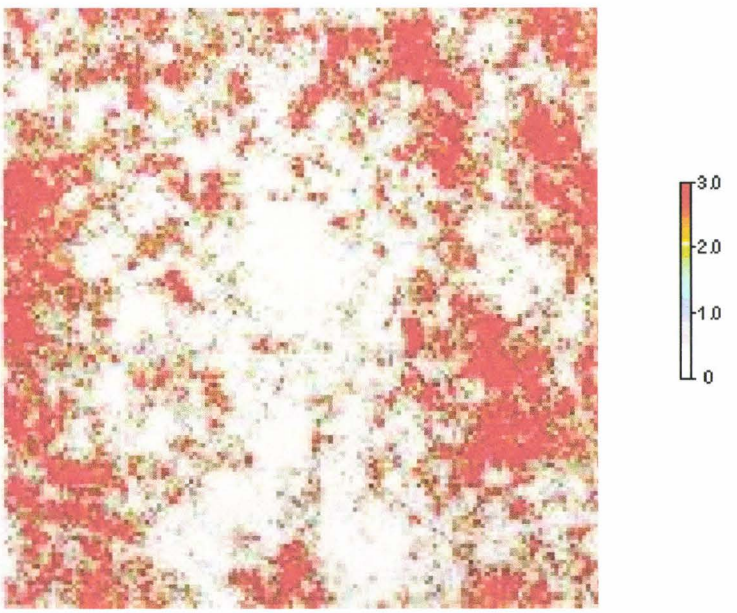

Fig. 7. A two dimensional simulation of *T. longicornis* abundance using the empirical estimates of the universal multifractal parameters $H = 0.58$, $C_1 = 0.44$ and $\alpha = 1.6$ (arbitrary units).

Multifractals, and in particular universal multifractals, leading to a very precise characterization of the whole statistical structure of any given intermittent pattern (with the help of the three basic empirical parameters), appears to be an efficient descriptive tool which should also allow the modeling of the multiscale detailed variability of intermittently fluctuating biological fields as the global properties of their surrounding environment [see Seuront *et al.* (1999) for further discussions]. In particular, using the modeling techniques detailed in Pecknold *et al.* (1993), a simulation of the copepod horizontal distribution based on the estimated multifractal parameters $H = 0.58$, $C_1 = 0.44$ and $\alpha = 1.60$ has been performed (Figure 7). Figure 7 shows a two dimensional simulation of the *Temora longicornis* distribution which clearly exhibits a very intermittent behavior associated with the occurrence of a few high density patches over a wide range of low density patches. Multifractal modeling should then be suggested as a potential powerful alternative to physical models of turbulence which lead to the parametrisation of the effects of turbulence on plankton distribution. Indeed, these models, incorporating diffusive processes (e.g. Okubo, 1980), non diffusive advection (Abraham, 1998), or coupling fluid-dynamic models of quasi-geostrophic turbulence, multi-compartment ecosystem dynamics and seasonal forcing (Smith *et al.*, 1996), can describe certain, but not all, aspects of turbulence and are often far from comprehensive (Visser, 1997). The advantages of universal multifractal simulation techniques are essentially the weak number of input parameters (only the three basic parameters H, C_1 and α), the low computation time involved (only a few seconds on a Pentium II for a 512×512 field) and their stochasticity, allowing to avoid numerical artifacts linked for instance to the sensitivity to initial conditions as encountered with models dealing with Navier-Stockes equation or with systems of differential equations.

The precise knowledge of the distribution of pelagic organisms is indeed of main importance to understand the trophic relationships between organisms and then the related matter fluxes. For instance, the distribution of preys is very important for predators, because the food availability changes depending on the dimension. Low fractal dimension means smooth and predictable distribution of particles gathered in small number of patches, and high dimension means rough, fragmented, space-filling and unpredictable distribution. Therefore, when a predator has some information on the location of the preys and can remotely detect them, foods with low dimension should be more efficient. In contrast, when a predator has no information or detection ability, foods with high dimension should be relatively better, because available food quantity or encounter rate approaches proportional to searched volume with

increase of fractal dimension. Moreover, the very complex patchy structure related with a multifractal distribution may also change the nature of the food signal, usually regarded as homogeneously distributed in space and time in models of predator-prey encounter rates [see Dower *et al.* (1997) for a review]. Indeed, planktonic animals have been shown to remain within patches when feeding (Price, 1989), or exhibit more fine-scale movements in areas of higher food concentration (Bundy *et al.*, 1993). Thus encounter rates might be very different when organisms feed within patches (intensive search) and during the search for new patches (extensive search) as has been described in the foraging behavior of beetles (Ferran and Dixon, 1993). In that way, foraging models will likely to incorporate switching between feeding and searching behaviors as scaled to the organism size, in order to effectively simulate these complex physical-biological relationship (Noda *et al.*, 1992).

Heterogeneity of zooplankton distribution has been a complicated problem to study and patchy distributions are often very difficult to parametrize. The descriptive analysis and modeling tools shown in the present study, however, demonstrates that only three parameters are sufficient for accurately describing and reconstructing the patchy structure of the horizontal distribution of copepods. As shown by recent studies in different fields of geophysical sciences (Schertzer *et al.*, 1997; Schmitt *et al.*, 1998; Seuront *et al.*, 1999), we believe that multifractals are the most accurate expression of irregular distribution of some objects in ecological models.

Acknowledgments

We thank J. Harlay, A. Lefebvre and D. Saïu for their help during the sea experiment, and F. Berreville, O. Borot, S. Coulomb, J. Harlay, D. Hilde and S. Jaskulski for their help in copepods countings. Thanks are also extended to the captain and the crew of the NO 'Côte de la Manche' for their assistance, and to V. Gentilhomme for nice discussions during the cruise.

References

Abraham,E.R. (1998) The generation of plankton patchiness by turbulent stirring. *Nature*, **391**, 577-580.

Baker,M.A. and Gibson,C.H. (1987) Sampling turbulence in the stratified ocean: statistical consequences of strong intermittency. *J. Phys. Oceanogr.*, **17**, 1817-1836.

Bohle-Carbonel,M. (1992) Pitfalls in sampling, comments on reliability and suggestions for simulation. *Cont. Shelf Res.*, **12**, 3-14.

Brylisnki,J.M. and Lagadeuc,Y. (1988) Influence du coefficient de la marée sur la répartition côte-large d'une espèce planctonique à affinités côtières: temora longicornis (Crustacé, Copépode). *C. R. Acad. Sci. Paris Sér. II*, **307**, 183-187.

Brylinski,J.M. and Lagadeuc,Y. (1990) L'interface eau côtière/eau du large dans le Pas-de-Calais (côte française): une zone frontale. *C. R. Acad. Sci. Paris Sér. 2*, **311**, 535-540.

Bundy,M.H., Gross,T.F., Coughlin,D.J. and Strickler,J.R. (1993) Quantifying copepod searching efficiency using swimming pattern and perceptive ability. *Bull. Mar. Sci.*, **53**, 15-28.

Currie,W.J.S., Claereboudt,M. and Roff,J.C. (1998) Gaps and patches in the ocean: a one-dimensional analysis of planktonic distributions. *Mar. Ecol. Prog. Ser.*, **171**, 15-21.

Brylinski,J.M. and Lagadeuc,Y. (1988) Influence du coefficient de marée sur la répartition côte/large d'une espèce planctonique à affinités côtières: Temora longicornis (Crustacés, Copépode). *C. R. Acad. Sci. Paris Sér. 3*, **307**, 183-187.

Bundy,M.H., Gross,T.F., Coughlin,D.J. and Strickler,J.R. (1993) Quantifying copepod searching efficiency using swimming pattern and perceptive ability. *Bull. Mar. Sci.*, **53**, 15-28.

Currie,W.J.S., Claereboudt,M. and Roff,J.C. (1998) Gaps and patches in the ocean: a one-dimensional analysis of planktonic distributions. *Mar. Ecol. Prog. Ser.*, **171**, 15-21.

Daan,R. (1989) Factors controlling the summer development of the copepod populations in the southern bight of the North Sea. *Neth. J. Sea Res.*, **23**, 305-322.

Dam,H.G. and Peterson,W.T. (1993) Seasonal contrasts in the diel vertical distribution feeding behavior and grzing impact of the copepod Temora longicornis in Long Island Sound. *J. Mar. Res.*, **51**, 561-594.

Davis,C.S., Flierl,G.R., Wiebe,P.H. and Franks,P.J.S. (1991) Micropatchiness, turbulence and recruitment in plankton. *J. Mar. Res.*, **49**, 109-151.

Daly, K. L. and Smith, W. O. (1993) Physical-Biological interactions influencing marine plankton production. *Annu. Rev. Ecol. Syst.*, **24**, 555-585.

Dower, J.F., Miller, T.J. and Leggett, W.C. (1997) The role of microscale turbulence in the feeding ecology of larval fish. *Adv. Mar. Biol.*, 31, 169-220.

Feder,J. (1988) *Fractals*. Plenum, New York.

Ferran,A. and Dixon,A.F.G (1993) Foraging behaviour of ladybird larvae (Coleoptera: Coccinellidae). *Eur. J. Entomol.*, **90**, 383-402.

Hardy,A.C. (1936) Observation on the uneven distribution of oceanic plankton. *Discovery Rep.*, **11**, 511-538.

Haeckel,E. (1891) Plankton studien. *Jena Zt. Naturwissensch*, **25**, 232-336.

Kolmogorov,A.N. (1941) The local structure of turbulence in incompressible viscous fluid for very large Reynolds numbers. *Dokl. Akad. Nauk SSSR*, **30**, 299-303.

Kraichnan,R.H. (1967) Inertial ranges in two-dimensional turbulence. *Phys. Fluids*, **9**, 1937-1943.

Lagadeuc,Y., Brylinski,J.M. and Aelbrecht,D. (1997) Temporal variability of the vertical stratification of a front in a tidal Region of Freshwater Influence (ROFI) system. *J. Mar. Syst.*, **12**, 147-155.

Lavallée,D. (1991) Multifractal techniques: analysis and simulation of turbulent fields. Ph.D. thesis, McGill University, Montréal, Canada.

Lavallée,D., Lovejoy,S., Schertzer,D. and Schmitt,F. (1992) On the determination of universal multifractal parameters in turbulence. In Moffat,K., Tabor,M. and Zaslavsky,G. (eds.), Topological aspects of the dynamics of fluid and plasmas. Kluwer, Boston, pp. 463-478.

Lizon,F. and Lagadeuc,Y. (1998) Comparisons of primary production values estimated from different incubation times in a coastal sea. *J. Plankton Res.*, **20**, 371-381.

Lizon,F., Lagadeuc,Y., Brunet,C., Aelbrecht,D. and Bentley,D. (1995) Primary production and photoadaptation of phytoplankton in relation with tidal mixing in coastal waters. *J. Plankton Res.*, **17**, 1039-1055.

Mackas,D.L. and Boyd,C.M. (1979) Spectral analysis of zooplankton spatial heterogeneity. *Science*, **204**, 62-64.

Mackas,D.L., Denman,K.L. and Abbot,M.R. Plankton patchiness: biology in the physical vernacular. *Bull. Mar. Sci.*, **37**, 652-674.

Mandelbrot,B. (1983) *The Fractal Geometry of Nature*. Freeman, New York.

Noda,M., Kawabata,K., Gushima,K. and Kakuda,S. (1992) Importance of zooplankton patches in foraging ecology of the planktivorous fish Chromis chrysurus (Pomacentridae) at Kuchinoerabu Island, Japan. *Mar. Ecol. Prog. Ser.*, **87**, 251-263.

Okubo,A. (1980) *Diffusion and ecological problems: mathematical models*. Springer-Verlag, New York.

Osborne,A.R. and Caponio,R. (1990) Fractal trajectories and anomalous diffusion for chaotic pattern motions in 2D turbulence. *Phys. Rev. Lett.*, **64**, 1733-1736.

Osborne,A.R., Kirwan,A.D., Provenzale,A. and Bergamasco,L. (1989) Fractal drifter trajectories in the Kuroshio extension. *Tellus*, **41A**, 416-435.

Pascual,M., Ascioti,F.A. and Caswell,H. (1995) Intermittency in the plankton: a multifractal analysis of zooplankton biomass variability. *J. Plankton Res.*, **17**, 1209-1232.

Pecknold,S., Lovejoy,S., Schertzer,D., Hooge,C. and Malouin,J.F. (1993) The simulation of universal multifractals. In Perdang,J.M. and Lejeune,A. (eds.), *Cellular automata: Prospects in Astrophysical Applications*. World Scientific, Singapore, pp. 228-267.

Peitgen,H.O., Jürgens,H. and Saupe,D. (1992) *Chaos and Fractals. New Frontiers of Science*. Springer-Verlag, New York.

Platt,T. and Denman,K.L. (1975) Spectral analysis in ecology. *Ann. Rev. Ecol. Syst.*, **6**, 189-210.

Platt,T., Harrison,W.G., Lewis,M.R., Li,W.K.W., Sathyendranath,S., Smith,R.E. and Vezina,A.F. (1989) Biological production of the oceans: the case for a consensus. *Mar. Ecol. Prog. Ser.*, **52**, 77-88.

Powell,T.M. and Okubo,A. (1994) Turbulence, diffusion and patchiness in the sea. *Phil. Trans. R. Soc. Lond. B*, **343**, 11-18.

Price,H.J. (1989) Swimming behavior of krill in response to algal patches: a mesocosm study. *Limnol. Oceanogr.*, **34**, 649-659.

Rothschild,B.J. (1992) Applications of stochastic geometry to problems in plankton ecology. *Phil. Trans. R. Soc. Lond. B*, **336**, 225-237.

Sanderson,L.F. and Booth,D.A. (1991) The fracatal dimension of drifter trajectories and estimates of horizontal eddy-diffusivity. *Tellus*, **43A**, 334-349.

Schertzer,D. and Lovejoy,S. (1987) Physically based rain and cloud modeling by anisotropic multiplicative turbulent cascades. J. Geophys. Res., 92, 9693-9714.

Schertzer,D. and Lovejoy,S. (1989) Nonlinear variability in geophysics: multifractal analysis and simulation. In Pietronera,L. (ed.), *Fractals: Physical Origin and Consequences*. Plenum, New York, pp. 49-79.

Schertzer,D., Lovejoy,S., Schmitt,F., Chigirinskaya,Y. and Marsan,D. (1997) Multifractal cascade dynamics and turbulent intermittency. *Fractals*, **5**, 427-471.

Schmitt,F., Lovejoy,S. and Schertzer,D. (1995) Multifractal analysis of the Greenland ice-core project climate data. . *Geophys. Res. Lett.*, **22**, 1689-1392.

Schmitt,F., Vannitsem,S. and Barbosa,A. (1998) Modeling of rainfall time series using two-state renewal processes and multifractals. *J. Geophys. Res.*, **103**, 23181-23193.

Seuront,L., Schmitt,F., Lagadeuc,Y., Schertzer,D., Lovejoy,S. and Frontier,S. (1996a) Multifractal analysis of phytoplankton biomass and temperature in the ocean. *Geophys. Res. Lett.*, **23**, 3591-3594.

Seuront,L., Schmitt,F., Lagadeuc,Y., Schertzer,D. and Lovejoy,S. (1996b) Multifractal intermittency of Eulerian and Lagrangian turbulence of ocean temperature and plankton fields. *Nonlin. Proc. Geophys.*, **3**, 236-246.

Seuront,L., Schmitt,F., Lagadeuc,Y., Schertzer,D. and Lovejoy,S. (1999) Universal multifractal analysis as a tool to characterise multiscale intermittent patterns. Example of phytoplankton distribution in turbulent coastal waters. *J. Plankton Res.*, **21**, 877-922.

Shiyomi,M. and Yamamura,K. (1993) Spatial pattern indices based on distances between individuals on a line-segment with finite length. *Res. Popul. Ecol.*, **34**, 321-330.

Smith,C.L., Richards,K.J. and Fasham,M.J.R. (1996) The impact of mesoscale eddies on plankton dynamics in the upper ocean. *Deep Sea. Res. I*, **43**, 1807-1832.

Steele,J.H. and Henderson,E.W. (1992) A simple model for plankton patchiness. *J. Plankton Res.*, **14**, 1397-1403.

Taylor,G.I. (1938) The spectrum of turbulence.*Proc. R. Soc. Lond. A*, **164**, 476-490.

Tsuda,A. (1995) Fractal distribution of the oceanic copepod *Neocalanus cristatus* in the subarctic Pacific. *J. Oceanogr.*, **51**, 261-266.

Tsuda,A., Sugisaki,H., Ishimaru,T., Saino,T. and Sato,T. (1993) White-noise-like distribution of the oceanic copepod *Neocalanus cristatus* in the subarctic North Pacific. *Mar. Ecol. Prog. Ser.*, **97**, 39-46.

Visser,A.W. (1997) Using random walk models to simulate the vertical distribution of particles in a turbulent water column. *Mar. Ecol. Prog. Ser.*, **158**, 275-281.

UNIVERSITÉ DES SC ET TECHN
BIBLIOTHÈQUE UNIVERSITAIRE
LILLE